LBL-8151 c.1
UC-34

NUCLEAR SCIENCE

ANNUAL REPORT
1977-1978

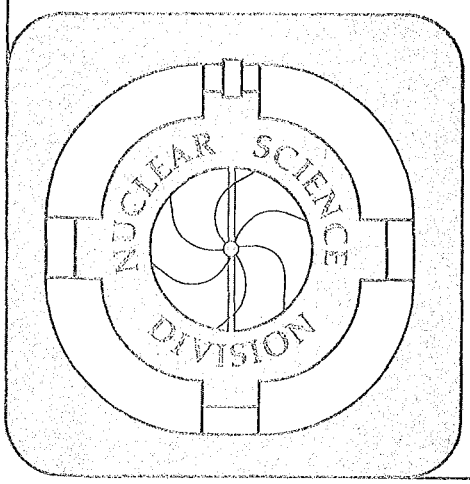

LAWRENCE BERKELEY LABORATORY
UNIVERSITY OF CALIFORNIA/BERKELEY

Prepared for the U.S. Department of Energy under Contract W- 7405-ENG-48

Printed in the United States of America
Available from
National Technical Information Service
U.S. Department of Commerce
5285 Port Royal Road
Springfield, VA 22161
Price Code: A13

LBL-8151

NUCLEAR SCIENCE

Annual Report
for the period
July 1, 1977 — June 30, 1978

B. G. HARVEY
Director

L. S. SCHROEDER
R. A. GOUGH
M. J. NURMIA
Editors

Lawrence Berkeley Laboratory
University of California/Berkeley

GENERAL INTRODUCTION

B.G. Harvey

This is the third Annual Report of the Nuclear Science Division. I believe that its contents will give the reader an excellent overview of the large body of work that has been accomplished in the past twelve months.

During this year we have seen several events that give us great cause for optimism about the future. The seventh edition of the Table of Isotopes has been completed. Through funding in FY '78 we have made a start on the construction of the superconducting spectrometer HISS, a machine that will add enormously to our ability to mount the complex experiments that are needed to investigate high energy nucleus-nucleus collisions. We have been fortunate in bringing to Berkeley a group of Postdoctoral Fellows and visitors of enormous talent and energy. Our fruitful collaborations with our German and Japanese colleagues continue to flourish to the mutual benefit of all of us. Perhaps of greatest importance, we have made a vote of confidence in our future and that of our field by adding to our staff two young nuclear theorists and, we hope, a young experimentalist. Their presence here will, we are sure, guarantee many more years of exciting research.

Without the help of many people in other disciplines and Divisions we would accomplish very little. I take this opportunity to draw the reader's attention to the largely hidden but nevertheless essential contributions that are made by our friends and colleagues who design, build, operate and maintain all sorts of complex devices that range in size from Bevalac, SuperHILAC and the 88" Cyclotron down to the smallest semiconductor components. It is one of the experimentalist's great joys to be at the nerve center, and to assemble all these disparate parts into a complex system in which everything must function at one and the same time for the purpose of investigating aspects of nature that have never been studied before.

It is in this spirit that the members of Nuclear Science Division offer to the reader this summary of their work.

CONTENTS

C. Relativistic Heavy Ions

1. Projectile and Target Fragmentation

2. Central Collisions

D. Table of Isotopes Project, Atomic Physics, and Magnetic Monopoles

II. THEORY OF NUCLEAR COLLISIONS

A. Microscopic

B. Macroscopic

C. Relativistic

III. APPARATUS

A. Accelerator Operations and Development

B. Nuclear Instrumentation

I. EXPERIMENTAL RESEARCH

A. NUCLEAR STRUCTURE

(HEAVY ION, 2p) REACTIONS ON LIGHT NUCLEI

A.N. Bice, R.J. de Meijer,* D.P. Stahel, and J. Cerny

The known limit of particle stability of neutron-excess nuclei extends far beyond the region accessible to nuclear spectroscopy by conventional light-ion—induced reactions.[1] With the (t,p) and (α,^{2}He) reactions, only nuclei two neutrons removed from stable targets can be studied. With heavy ion stripping reactions, for instance the (^{11}B, ^{8}B) reaction,[2] nuclei removed by three or four neutrons from stability may be examined. However, another way to produce very neutron-rich nuclei, such as ^{29}Mg and ^{34}Si, is to use reactions initiated by neutron-rich heavy ions on targets also rich in neutrons. Then, with emission of protons from the resulting compound nucleus, one may achieve the formation of these exotic nuclei. Recent reports of successful (heavy ion, 2p) reactions[3] suggested the possibility of extending the ^{2}He detection method to studying exotic nuclei via such reactions, in spite of related unsuccessful attempts.[4] Indeed Panagiotou et al.[3] have claimed detection, with their single counter system, of correlated proton pairs, emitted as an unbound ^{2}He system from the compound nucleus.

Studies were initiated at the 88-inch cyclotron to observe a variety of (heavy ion, 2p) reactions at several different energies in preparation for investigating highly neutron-rich nuclei with this experimental technique. Self-supporting targets of ^{12}C, ^{13}C and ^{28}Si approximately 25-, 200- and 40-μg/cm^2 thick, respectively, were bombarded with a 40 MeV ^{16}O beam. In addition the ^{12}C + ^{20}Ne reaction was examined utilizing the same carbon target with a 50 MeV ^{20}Ne beam. Reaction products, including two-proton coincidences, were detected by three separate counter telescopes intercepting similar solid angles. Two of the telescopes were mounted vertically and comprised the usual ^{2}He detection system. The third telescope was located on the opposite side of the beam axis from the ^{2}He detection system and was capable of being positioned independently of the other two telescopes. Coincidence timing of less than 2 ns was established between each possible pair of the three telescopes utilizing fast electronics. The third telescope system was employed in conjunction with the ^{2}He detection system to investigate the anticipated compound nuclear behavior of the (heavy ion, 2p) reaction and to serve as a comparative method (with a different, wide angle geometry) for detecting proton pairs as opposed to the close angle ^{2}He system.

Figure 1 shows two spectra obtained by detecting two proton coincidences with a) a small angle, two-telescope configuration (^{2}He system) and b) a wide separation angle, two-telescope system (opposite sides of the beam axis). As can be seen, the ^{12}C(^{16}O, 2p) ^{26}Mg reaction yielded quite similar populations of several final states at the excitation energies E_x = g.s., 1.81, 2.94, 3.94, (4.32 + 4.33 + 4.35) and (4.84 + 4.90 + 4.97) MeV for both the narrow and wide telescope separation configurations.

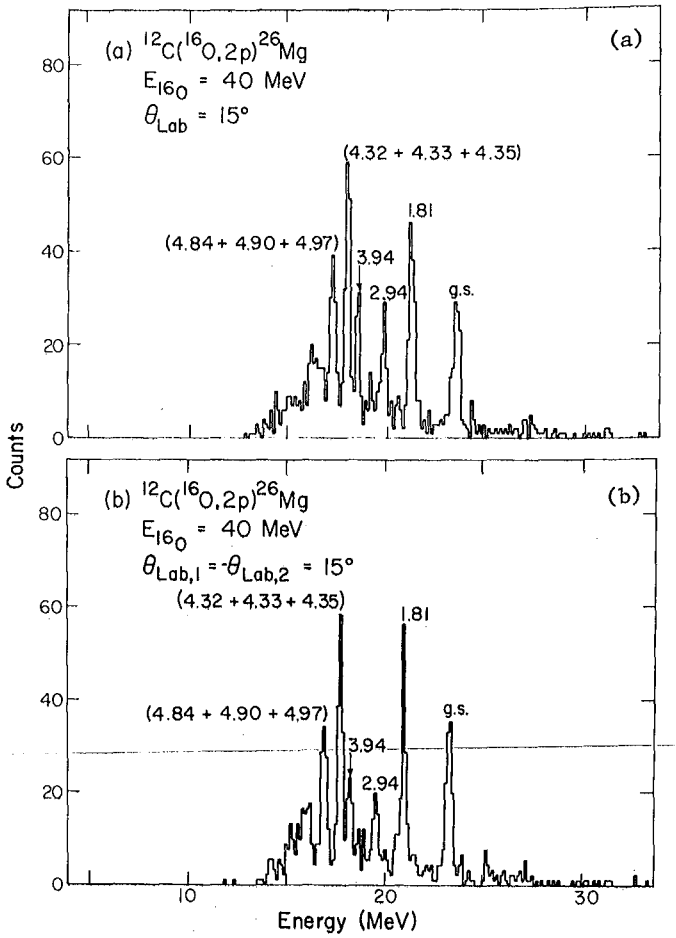

Fig. 1. Two proton coincidence spectra of ^{12}C(^{16}O, 2p)^{26}Mg reaction at 40 MeV: (a) 10° vertical telescope separation, $\theta_{lab,1} = \theta_{lab,2}$ = 15° and (b) 30° telescope separation, $\theta_{lab,1}$ = 15°, $\theta_{lab,2}$ = -15°. (XBL 788-1455)

This observed similarity between the wide geometry and narrow geometry spectra suggests that ^{26}Mg is produced from a two-proton sequential decay process via a compound nucleus reaction. However, the production of the unbound ^{2}He

system via an evaporation process or some form of direct reaction should be considered. If the reaction proceeded via ^{2}He emission, proton energy spectra projected on one axis would show, given sufficient statistics, a final state interaction enhancement around $E_{p1} \approx E_{p2}$ for the narrow geometry detector configuration. If, however, a majority of the two-proton coincidences resulted from sequential proton decay through a few intermediate states in ^{27}Al, sharp peaks corresponding to the proton transitions should appear in the projected energy spectra.

Figure 2 displays typical projections onto the E_p axis of proton-proton coincidences such that their energies sum to that of the 1.81 MeV state in ^{26}Mg. Although the statistics are poor, Fig 2 shows little evidence for a relative proton energy distribution characteristic of a two-proton final state interaction (FSI) (cf., Ref. 5) or little indication of peaks which could correspond to sequential transitions through definite intermediate states in ^{27}Al. Analysis of the other states indicated in Fig. 1 does not give clear evidence for ^{2}He emission or for sequential decay via specific intermediate states either.

Interestingly, the reaction ^{28}Si + ^{16}O, ^{13}C + ^{16}O and ^{12}C + ^{20}Ne yielded no discernible isolated states in the 2p coincidence spectra in any of the detector combinations: only the ^{12}C + ^{16}O system produced observable states via 2p coincident events. An additional experiment at an ^{16}O bombarding energy of 45 MeV on a ^{12}C target was investigated yielding results similar to the ^{12}C + ^{16}O reaction at 40 MeV but with higher background. The fact that no 2p spectra were collected containing discernible states (as in ^{26}Mg) for the reactions ^{28}Si (^{16}O, 2p)^{42}Ca, ^{13}C(^{16}O,2p)^{29}Si and ^{12}C(^{20}Ne,2p)^{30}Si is explainable perhaps with arguments similar to those of Ref. 6 if one assumes a compound nuclear type of reaction. For instance, the reaction ^{13}C(^{16}O,2p)^{29}Si would produce a compound nucleus of excitation energy over 4 MeV higher than that from the ^{12}C(^{16}O,2p)^{28}Si reaction at the same bombarding energy and this provides more decay channels through which the system may de-excite. Similar arguments apply to the reactions ^{28}Si(^{16}O,2p) and ^{12}C(^{20}Ne,2p), which were examined. In addition, angular momentum effects need to be considered.

Such unsuccessful reactions as those listed previously reflect the difficulties inherent in attempting to utilize this method of observing the spectroscopy of very neutron-rich nuclei, but they do not preclude its applicability to such studies.

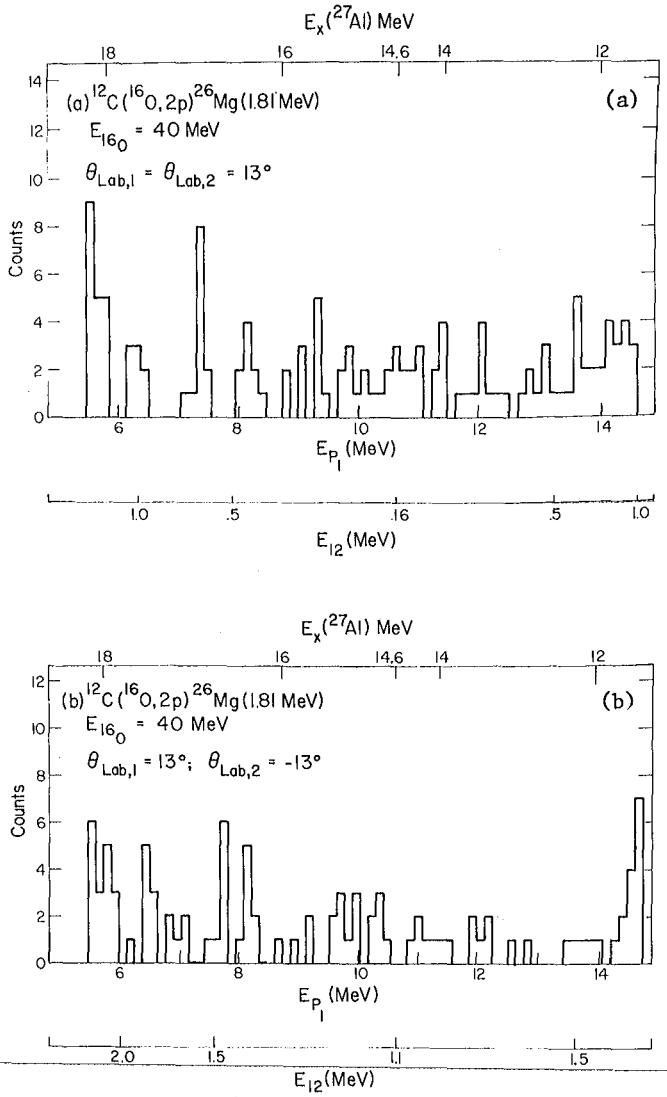

Fig. 2. Projected proton energy spectra of coincident protons yielding ^{26}Mg (1.81 MeV) via ^{12}C(^{16}O,2p) reaction at 40 MeV: (a) 10° vertical telescope separation, θ_{lab} = 13° both telescopes, and (b) 26° telescope separation, $\theta_{lab,1}$ = 13°, $\theta_{lab,2}$ = -13°. (XBL 788-1460)

Footnotes and References

*On leave from Kernfysisch Versneller Instituut, University of Groningen, Groningen 8002, The Netherlands.

1. J. Cerny, in Proceedings of the Conference on Reactions Between Complex Nuclei, Nashville, Tennessee, 1974, R. L. Robinson et al., eds. (North-Holland, Amsterdam, 1974).

2. D. K. Scott, B. G. Harvey, D. L. Hendrie, L. Kraus, C. F. Maguire, J. Mahoney, Y. Terrien and K. Yagi, Phys. Rev. Lett. 33, 1343 (1974).

3. A. D. Panagiotou, P. Kakanis, E. N. Gazis, E. Kossionides and N. Xiromeritus, J. Phys. G: Nucl. Phys. 3, L85 (1977) and references therein.

4. J. Cerny, in Proceedings, 3rd Conf. on Nuclei Far from Stability (Cargese, Corsica 1976).

5. D. P. Stahel, R. J. de Meijer, A. N. Bice, and J. Cerny, elsewhere in this report.

6. R. G. Stokstad, in Proceedings of the Conference on Reactions Between Complex Nuclei, Nashville, Tennessee, 1974, R. L. Robinson et al., eds. (North-Holland, Amsterdam, 1974), p. 327.

HIGH SPIN STATES OF ^{20}O

A.N. Bice, D.P. Stahel, R.J. de Meijer,* and J. Cerny

A recent study of the $(\alpha, {}^2He)$ reaction on 2sld-shell target nuclei[1] has demonstrated a pronounced selectivity for populating two-neutron states of high-spin, e.g., $(d_{5/2})^2_{4+}$ and $(f_{7/2})^2_{6+}$. This selectivity is not unlike that observed in the (α,d) reaction on light nuclei at E_α = 50 MeV where large angular momentum transfers are favored and hence the population of high spin states in the residual nucleus is enhanced due to the kinematical conditions.[2] As has previously been shown[1,3] the $(\alpha,{}^2He)$ reaction provides a convenient spectroscopic tool for investigating $\Delta S = 0$, $\Delta T = 1$ transfers to such states of light nuclei that are inaccessible by the (t,p) reaction due to the lack of sufficiently high energy triton beams.

Because relatively little is known about excited states in the $T_z = 2$ nuclide ^{20}O, the $^{18}O(\alpha,{}^2He)^{20}O$ reaction was utilized to study the higher excited, high spin states of ^{20}O which are kinematically favored and hence preferentially populated. A 65-MeV alpha beam produced by the 88-inch cyclotron was employed along with a gas cell containing approximately 18 cm Hg of 99.7% pure ^{18}O gas at ~25°C. Under such conditions the excitation of several previously uncharacterized states was observed at several angles, determining angular distributions which have been fit with zero-range DWBA calculations.

The counter system employed in these measurements has been described in detail elsewhere.[1] Since ^2He is unbound it must be detected by means of a coincidence measurement of the two breakup protons. Therefore the detection system consisted of two (vertically arranged) counter telescopes. Each telescope was comprised of 200-μm thick phosphorus diffused Si transmission ΔE and a 5-mm Si(Li) E detector. In addition, two 5-mm thick counters were mounted behind the E detectors in order to reject events that traversed the ΔE-E system. Typical detection efficiencies of ^2He's with such a system ranged around 1%.

Figure 1 shows a spectrum of the $^{18}O(\alpha,{}^2He)^{20}O$ reaction at 15°. The experimental energy resolution of ~400 keV was due mainly to kinematic broadening and the gas cell, with Havar windows. The high selectivity of the $(\alpha,{}^2He)$ reaction is clearly demonstrated by Fig. 1. The spectrum shows transitions to three previously known states in ^{20}O of the $(d_{5/2})^2$ configuration: the ground state $J^\pi = 0^+$, the $J^\pi = 2^+$ state at 1.67 MeV, and the $J^\pi = 4^+$ state at 3.57 MeV excitation. In addition, strong transitions to previously uncharacterized states at 7.78, 8.78, 10.2 and 11.3 MeV were observed. Since the angular momentum mismatch for this $(\alpha,{}^2He)$ reaction is ~5ħ, states with relatively large spin are favored in the stripping reaction as indeed is borne out by the dominance of the $E_x = 3.57$, $J^\pi = 4^+$ state in the spectrum. The relatively large cross section for states at higher excitation suggest high spin character also for their configurations.

Figures 2a shows the angular distributions for the $(\alpha,{}^2He)$ reaction leading to the $J^\pi = 0^+, 2^+, 4^+$ low lying states of ^{20}O along with DWBA fits obtained from the program DWUCK4. For the DWBA analysis the following optical model parameters, taken essentially from the (α,d) reaction at a comparable bombarding energy, was employed:[4] V = 200 MeV, r_0 = 1.2 fm, a = 0.61 fm, W = 26.9 MeV, r_0' = 1.5 fm, a' = 0.515 fm and V = 93 MeV, r_0 = 1.2 fm, a = 0.75 fm, $4W_0$ = 85 MeV, r_0' = 1.25 fm, a' = 0.75 fm for α and ^2He, respectively. Since reasonably good fits to the 0^+, 2^+ and 4^+ states were obtained, the same parameters were used to fit the angular distributions of the higher excited states in an attempt to deduce the L-transfer involved in the $(\alpha,{}^2He)$ reaction to these previously unknown states. In these reactions the spin transfer S is zero, thus the final spin and parity is given by $J = L$ and $\pi = (-1)^L$. Those L-values which corresponded to expected transitions in ^{20}O and yielded predictions resembling the data are shown in Fig. 2b. Due to the rather structureless experimental angular distributions (a characteristic of high spin states), definitive L-transfers and thus J assignments cannot be deduced.

It is possible, however, to suggest very general assignments for these new states. Simple shell model calculations with a surface-delta residual nuclear interaction indicate that several high spin states should indeed be found in this higher excitation energy region of ^{20}O. One expects states of $(d_{5/2}d_{3/2})_{4+}$ and $(d_{5/2}f_{7/2})_{5^-}$ character (coupled to an inert ^{18}O core) around 8 and 9 MeV, respectively, and a pair of $J^\pi = 3^-$ states are expected 1-2 MeV higher. Also, an extrapolation of the experimentally-deduced Bansal-French lines of binding energy versus mass number for the $(\alpha,{}^2He)$ data[1] would predict a state of configuration $(d_{3/2}f_{7/2})_{5^-}$ to be around 8.1 MeV and also predicts one of $(f_{7/2})^2_{6+}$ configuration around 11 MeV excitation.

Although several new high-spin states of ^{20}O have been observed via the $(\alpha,{}^2He)$ reaction, clearly further studies are necessary to completely deduce the associated nuclear configurations.

Footnote and References

*On leave from Kernfysisch Versneller Instituut, University of Groningen, Groningen 8002, The Netherlands.

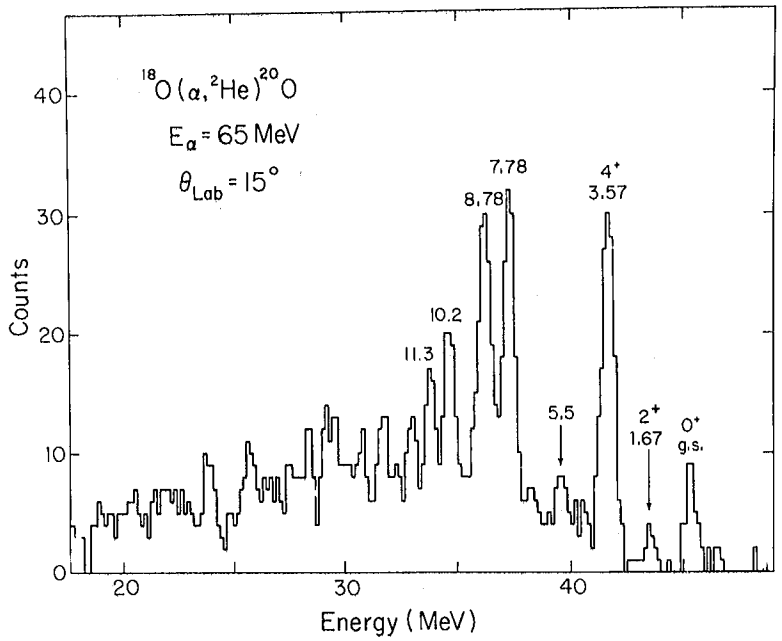

Fig. 1. A spectrum of the $^{18}O(\alpha,^2He)^{20}O$ reaction at $\theta_{Lab} = 15°$. (XBL 783-455A)

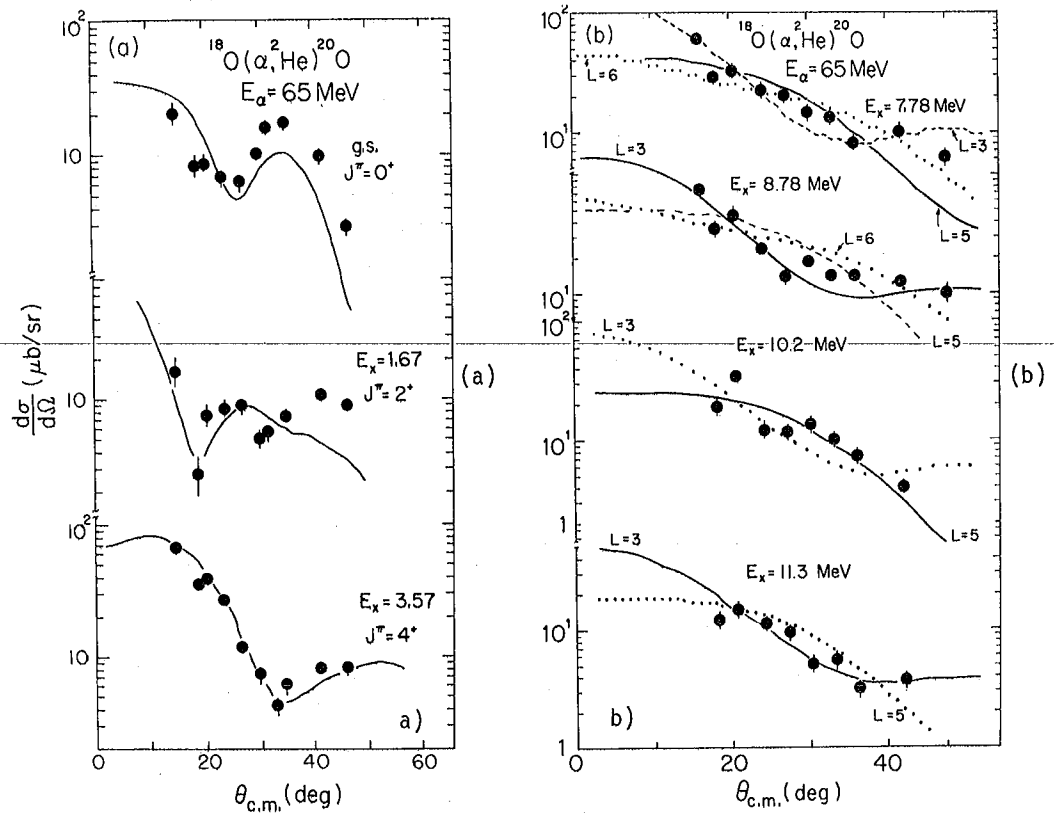

Fig. 2. The angular distributions for transitions to states observed in $^{18}O(\alpha,^2He)^{20}O$ reaction at $E_\alpha = 65$ MeV. The solid dots represent experimental points, curves represent DWUCK4 calculations. a) Angular distributions and calculations for $J^\pi = 0^+$, 2^+, and 4^+ states at E_X = g.s., 1.67 and 3.57 MeV in ^{20}O. b) E_X = 10.2 and 11.3 MeV in ^{20}O. (XBL 783-454A)

1. R. Jahn, D. P. Stahel, G.J. Wozniak, R. J. de Meijer and J. Cerny, Phys. Rev. C. 18, 9 (1978).

2. See, for instance, E. Rivet, R.H. Pehl, J. Cerny and B. G. Harvey, Phys. Rev. 141, 1021 (1966).

3. R. Jahn, G. J. Wozniak, D. P. Stahel and J. Cerny, Phys. Rev. Lett., 37, 812 (1976).

4. R. J. de Meijer, R. Kamermans, J. van Driel, and H. P. Morsch, Phys. Rev. C 16, 2442 (1977).

INVESTIGATION OF HIGH SPIN STATES IN 1p AND 2s1d SHELL NUCLEI VIA THE (α,^{2}He) REACTION

R. Jahn,† D.P. Stahel, G.J. Wozniak, R.J. de Meijer,‡ and J. Cerny

A recent study[1] of the (α,^{2}He) reaction on 1p shell targets has demonstrated that this reaction selectively populates two-neutron states of high spin. This feature is similar to that observed in (α,d) reactions on light nuclei.

The unbound ^{2}He was identified by measuring its two breakup protons in fast coincidence in two separate ΔE-E counter telescopes. A detection geometry was chosen such that the vertical acceptance angle of the system matches the size of the breakup cone of the two protons with a tighter horizontal acceptance for good energy resolution.

The (α,^{2}He) reaction has been measured on targets of ^{12}C, ^{13}C, ^{14}N, ^{15}N, ^{16}O, ^{18}O, ^{20}Ne, ^{22}Ne, ^{24}Mg, ^{26}Mg, ^{28}Si, ^{29}Si, ^{32}S, ^{36}Ar, ^{38}Ar, and ^{40}Ca using 65 and 55 MeV alpha beams from the 88-inch cyclotron in order to obtain an initial survey of this reaction. Large cross sections were found for transitions to states of $(d_{5/2})^2_4$, $(d_{3/2}f_{7/2})_5$ and $(f_{7/2})^2_6$ character, resulting in the location of a number of 2n states, many of which were previously unknown.

Figure 1 shows spectra from the ^{28}Si, ^{26}Mg and ^{29}Si(α,^{2}He) reactions. In addition to the marked selectivity of this reaction, one notes a specific similarity among these spectra. Reactions

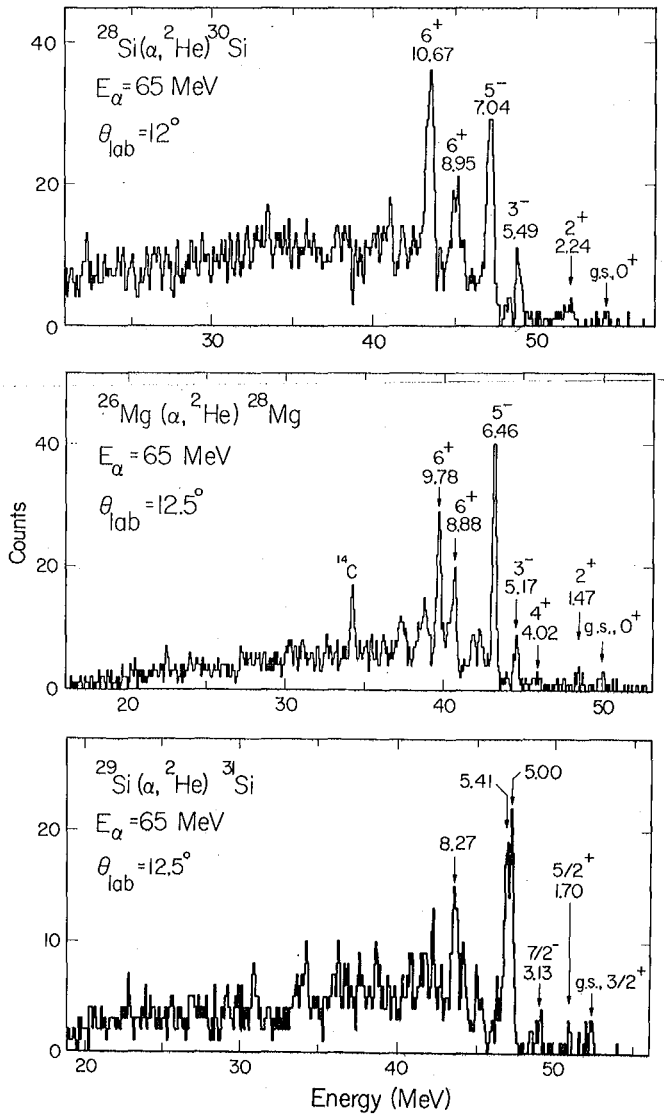

Fig. 1. The spectra of the (α,^{2}He) reaction on ^{28}Si, ^{26}Mg and ^{29}Si. (XBL 783-7773)

on the isotopes ^{28}Si and ^{26}Mg might be expected to be similar with strong population of the

$(d_{3/2}f_{7/2})_5$ $(f_{7/2})^2_6$ and $(f_{7/2}f_{5/2})_6$ states

(in order to increasing excitation energy). This indicates the importance of the closed neutron subshell. The ^{31}Si spectrum then shows the effects of the weak coupling of the $s_{1/2}$ neutron in ^{29}Si to these 2n transfers, in that two of these transitions appear in ^{31}Si and doublets at 5.00 and 5.41 MeV and 8.27 MeV (unresolved).

In Fig. 2 the experimental binding energies, B, for several configurations are plotted versus the mass number A of the final nucleus. The solid lines represent Bansal-French weak coupling model calculations using the values a = -0.30 MeV and b = 2.6 MeV. These values are very similar to the ones found in the analysis of the binding energies of np states with $(f_{7/2})^2$ character.[2]

Predicated on the observed selectivity of the $(\alpha,^2He)$ reaction, simple shell-model calculations have been carried out to further establish the character of the strongly populated states. The T_z = 0 target nuclei from ^{24}Mg to ^{40}Ca were assumed to be an inert core and the two neutrons were allowed to occupy the valence orbits in the 2s1d and 1f2p shell. The single particle energies were taken to be the separation energies of the single particle levels in the A_{core} + 1 nucleus. The two-body matrix elements of Kuo and Brown[3] and Erné[4] have been used or, if not available, calculated from the modified surface delta interaction. Hamiltonian matrices were truncated to, at most, a simple 2 x 2 matrix by neglecting higher configurations.

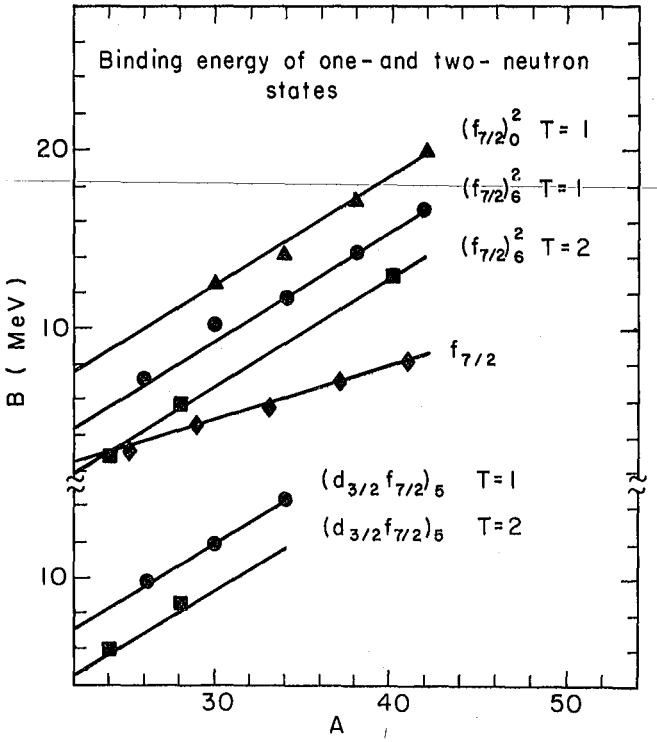

Fig. 2. Binding energies, B, for several configurations as a function of the mass of the final nucleus A. (XBL 782-247)

Figure 3 compares the calculations for ^{30}Si, ^{34}S, ^{42}Ca with energy spectra observed in the present experiment. Except for the energies of the ground states, which are very sensitive to the limitations of the above approach, the calculations are in good agreement with the experiment and are additional support for the suggested assignments.

Footnotes and References

*Condensed from LBL-7157, Phys. Rev. C 18, 9 (1978).

†Present address: Institut für Strahlen und Kernphysik der Universität Bonn, Nussallee 14-16, 53 Bonn, West Germany.

‡On leave from Kernfysisch Versneller Instituut, University of Groningen, Groningen 8002, The Netherlands.

1. R. Jahn, G. J. Wozniak, D. P. Stahel, and J. Cerny, Phys. Rev. Lett. 37, 812 (1976).

2. R. Sherr, R. Kouzes, and R. Del Vecchio, Phys. Lett. B 52, 401 (1974).

3. T. T. S. Kuo and G. E. Brown, Nucl. Phys. A 114, 271 (1968).

4. F. C. Erné, Nucl. Phys. 84, 91 (1966).

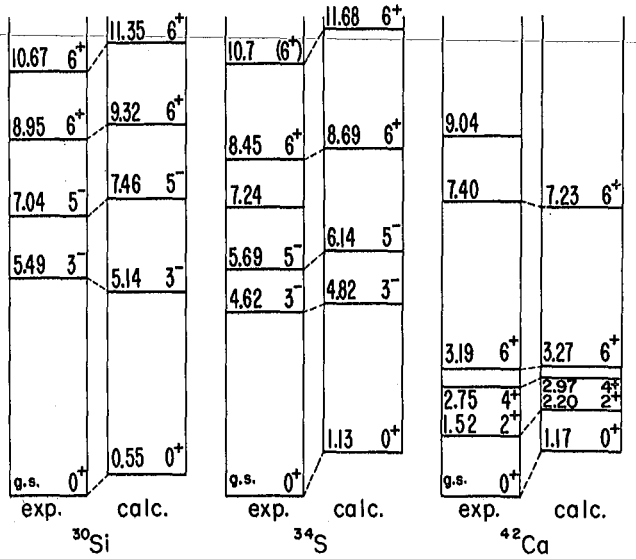

Fig. 3. Comparison of the calculated and experimental level schemes of ^{30}Si, ^{34}S, and ^{42}Ca. Above the ground states only the states observed in these experiments are presented. (XBL 782-250)

OBSERVATION OF ^{18}N VIA THE ^{18}O (d, ^{2}He)^{18}N REACTION

R.J. de Meijer,* D.P. Stahel, A.N. Bice, R. Jahn and J. Cerny

A ^{2}He-detection system, consisting of two ΔE-E counter telescopes, has been used to investigate the low lying states in ^{18}N via the (d,^{2}He) reaction at E_d = 50 and 55 MeV from the 88-inch cyclotron using a gaseous ^{18}O target.

Although the detection efficiency is rather low (~1%) due to the geometry for detecting the two breakup protons, and the energy resolution is not as good with a single counter telescope as can be found in (t,^{3}He) reactions, high energy deuteron beams are readily available. Presently, therefore, the (d,^{2}He) reaction is potentially a most suitable reaction for obtaining mass and excitation energies of nuclei that are only accessible by charge exchange reaction and for which the (t,^{3}He) Q-value is too negative to be studied with the present triton beams.

Two experiments have been reported on the mass of ^{18}N, the most accurate being the ^{18}O(t,^{3}He)^{18}N reaction studies by Stokes et al.[1] at a bombarding energy of 22 MeV. The negative Q-value for this reaction results in low energy ^{3}He reaction products and, due to the straggling in the gas and the exit window, the resolution is on the order of 300 keV. Stokes et al. observed a broad peak whose centroid is attributed to the ground state of ^{18}N and which yields a mass excess for ^{18}N of 13.274 ± 0.030 MeV. In an earlier experiment the ^{18}N mass was determined to be 13.1 ± 0.4 MeV from the ^{18}O(n,p)^{18}N reaction in a measurement[2] of the β-end point energies in coincidence with the subsequent γ-decay of the 1$^-$, 4.45 MeV state in ^{18}O. From the allowed nature of the β-decay, it was concluded that the ^{18}N ground state has $J^\pi = (0,1,2)^-$.

The cross section for the ^{18}O(d,^{2}He)^{18}N reaction was found to be on the order of 5μb/sr, similar to the values of the ^{18}O(t,^{3}He)^{18}N reaction at 22 MeV. This low cross section combined with the 1% efficiency and the breakup of the incoming deuterons in the gas cell makes it difficult to carry out the experiment since the accidental coincidence rate is proportional to the beam current squared, whereas the "real" count rate increases only linearly. In order to kinematically identify the ^{18}N peaks, experiments were carried out at E_d = 50 MeV and θ = 25° and 35°, and E_d = 55 MeV and θ = 25°, 35° and 45°. Calibration spectra were taken from the ^{12}C(d,^{2}He)^{12}B reaction at the same energies and a wider range of angles and with CO_2 and C_4H_{10} gas targets at pressures such that the calculated energy losses matched the losses in the ^{18}O(d,^{2}He)^{18}N reaction. Each of the ^{2}He energy spectra was converted to a Q-value spectrum and added to the spectrum taken at E_d = 50 MeV and θ = 25° in order to improve the statistics. The result of the combined run is shown in Fig. 1.

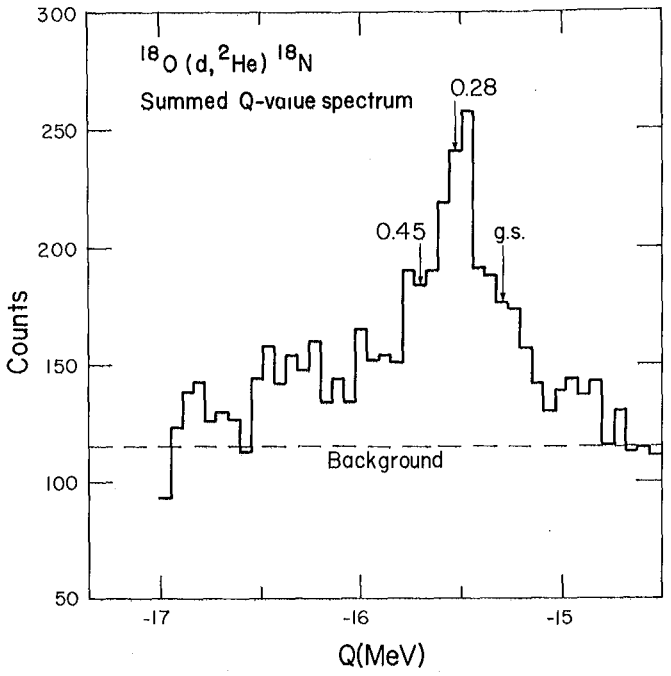

Fig. 1. A composite energy spectrum from the ^{18}O(d,^{2}He)^{18}N reaction. (XBL 788-1454)

As seen from Fig. 1, the centroid of the broad peak is in agreement with the Q-value of -15.499 ± 0.030 MeV as follows from the mass excess reported in Ref. 1. However, at all angles and energies there seems to be evidence for "shoulders" on both sides of the strongest peak. If one interprets shoulders as states in ^{18}N, their Q-values would be -15.27 ± 0.10 and 15.72 ± 0.10 MeV, with the error estimated from the uncertainty in the peak positions and energy calibration. This interpretation then leads to the suggestion that the broad peak consists of at least three peaks corresponding to the ground state and two new excited states of ^{18}N at 0.28 ± 0.10 and 0.45 ± 0.10 MeV, respectively. The ground state Q-value would then lead to a mass excess of ^{18}N of -13.04 ± 0.10 MeV, a value closer to the numerical value found in Ref. 2, but 240 keV lower than the one obtained in Ref. 1. These results must remain preliminary until this experiment can be repeated with lower background.

Footnotes and References

*On leave from Kernfysisch Versneller Instituut, University of Groningen, Groningen 8002, The Netherlands.

†Present address: Institut für Strahlen und Kernphysik der Universität Bonn, Nussallee 14-16, 53 Bonn, West Germany.

1. R. H. Stokes and P. G. Young, Phys. Rev. 178, 1789 (1969).

2. L. F. Chase, H. A. Grensch, R. E. McDonald and F. J. Vaughn, Phys. Rev. Lett. 13, 665 (1964).

OBSERVATION OF ^{2}He AND α^* AS INTERMEDIATE STATES IN THREE-BODY REACTIONS

D.P. Stahel, R.J. de Meijer,† A.N. Bice, and J. Cerny

A nuclear reaction producing three particles in its final state of the type p+t → 1+2+3 where p and t stand for the projectile and target nuclei, respectively, and 1, 2, and 3 denote the three final nuclei, often proceeds through an intermediate state of the nuclei (1-2), (1-3) or (2-3). Such a process can be symbolized as p+t → (1-2)+3 → 1+2+3 for the first case, and similarly for the other two cases. These intermediate states can be identified in kinematically complete experiments in which both particles 1 and 2 are measured in coincidence.

Figure 1 shows a two-dimensional spectrum of the energies E_{p1} vs E_{p2} of the reaction $\alpha+^{12}C \rightarrow p_1+p_2+^{14}C$ at E_α = 65 MeV performed at the 88-inch cyclotron. The solid lines represent the kinematic loci for the reaction leaving ^{14}C in its ground, 0^+; 6.73-MeV, 3^-; and 10.72-MeV, 4^+ states; calculated using the three-body kimematics formalism of Ohlsen.[1] Any intermediate state through which the reaction proceeds can be observed as a peak on these loci.

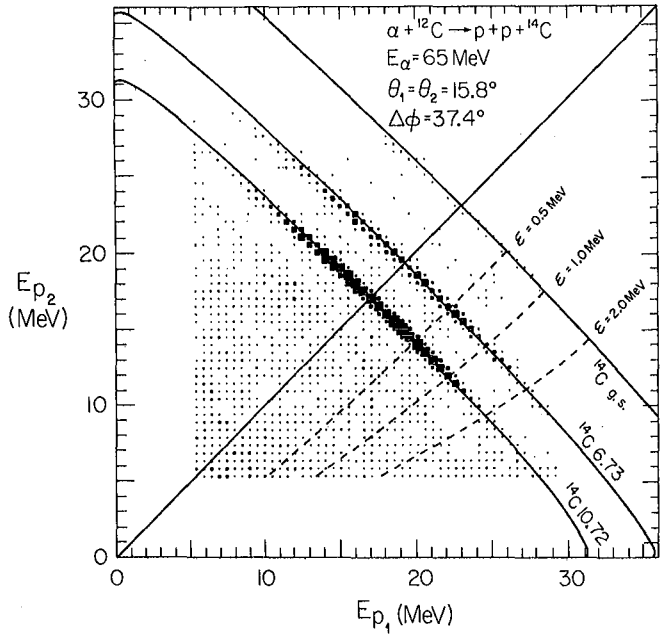

Fig. 1. Two-dimensional spectrum of E_{p1} vs E_{p2} of the reaction $^{12}C(\alpha,pp)^{14}C$ at E_α = 65 MeV. (XBL 787-1275)

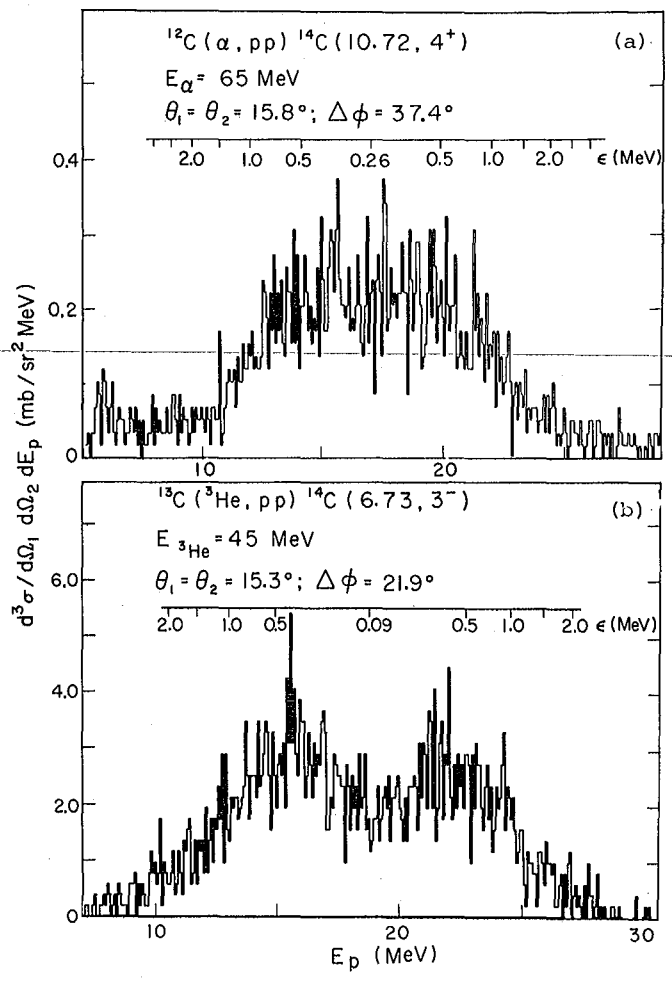

Fig. 2. Projected energy spectrum Ep of the (a) $^{12}C(\alpha,pp)^{14}C$(10.72 MeV, 4^+) at E_α = 65 MeV, and (b) $^{13}C(^3He,pp)^{14}C$(6.73 MeV, 3^-) at $E_{^3He}$ = 45 MeV. (XBL 788-1458)

In analyzing such two-dimensional spectra it is convenient to project the locus for a given state in ^{14}C onto one E_p axis. Figure 2a shows such a projected spectrum $d^3\sigma/d\Omega_1 d\Omega_2 dEp1$ for the reaction to the 10.72-MeV, 4^+ state. This reaction can only go through states in ^{15}N above the ^{14}C + p threshold at 10.2 MeV or through states in the pp-system. The kinematics restricts the intermediate ^{15}N states to those that lie at excitation energies between about 12 and 30 MeV and no evidence for transitions through such states is observed in agreement with the quite small cross section for the (α,p) reaction on ^{12}C to these states. In fact, the structure of the spectrum in Fig. 2a can be attributed to transitions via the pp system (^2He). Thus, the reaction proceeds essentially as a two-neutron stripping reaction $\alpha+^{12}C \rightarrow {}^2He+^{14}C \rightarrow p+p+^{14}C$ and not as a sequential reaction $\alpha+^{12}C \rightarrow {}^{15}N^*+p \rightarrow p+p+^{14}C$. This is consistent with the observed selective population of two-neutron states in this and other (α,^{2}He) reactions.[2]

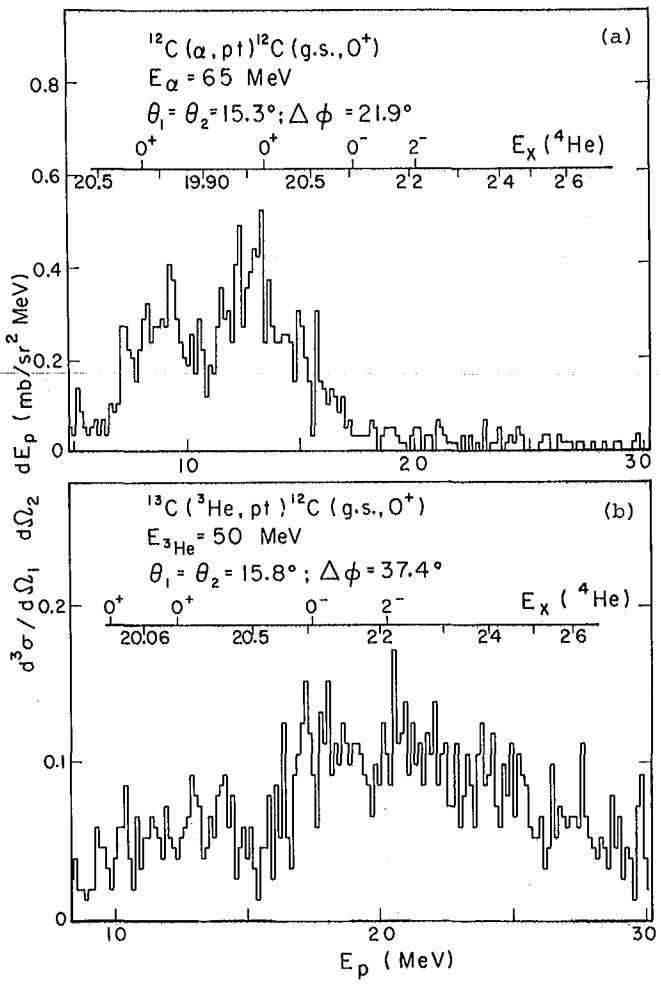

Fig. 3. Projected energy spectrum Ep of the (a) $^{12}C(\alpha,pt)^{12}C(g.s.,0^+)$ at E_α = 65 MeV, and (b) $^{13}C(^3He,pt)^{12}C(g.s.,0^+)$ at $E_{^3He}$ = 50 MeV. (XBL 788-1459)

A similar projected Ep1 energy spectrum from the (^{3}He,^{2}He) reaction on ^{13}C to the 6.73 MeV, 3^- state in ^{14}C at $E_{^3He}$ = 45 MeV is shown in Fig. 2(b). The observed enhancement of the cross section at small relative pp energies, ε, is caused by the pp final-state interaction (FSI) of the virtual $^1S_0$, T = 1 state of ^2He, whereas the central dip in the spectra at E < 400 keV arises from the Coulomb repulsion between the two protons. The spectra in Fig. 2 were fitted with FSI calculations based on the model of Watson and Migdal.[3] It was found, however, that the calculations using the known p-p scattering length did not reproduce the data and only a larger value could give agreement with the observed shape of the spectra. Such an effect has been observed before[4] and can be explained as a result of the complete separation of the FSI effects from the primary reaction process in the Watson-Migdal theory.

In the same way as the projected E_p spectra have demonstrated that the (α,pp) reaction on ^{12}C at E_α = 65 MeV proceeds as an (α,^{2}He) reaction, it can also be shown that the $^{12}C(\alpha,pt)^{12}C$ reaction at the same incident energy takes place as an (α,α*) reaction,[5] where α* is the 0^+ first excited state of ^4He at 20.1 MeV. As shown in Fig. 3a, the $^{12}C(\alpha,\alpha^*)^{12}C(g.s.)$ reaction proceeds entirely through the first excited state of ^4He with no evidence for transition through higher excited states of ^4He below 25 MeV; all these other states possess unnatural parity and can therefore not be populated in a simple inelastic scattering process $\alpha \rightarrow \alpha^*$. In contrast, the $^{13}C(^3He,pt)^{12}C$ reaction at $E_{^3He}$ = 50 MeV has no such restriction and can therefore go through many of the excited states in ^4He, as shown in Fig. 3b for the $^{13}C(^3He,pt)^{12}C(g.s.)$ reaction. Due to the large width of the higher excited states of ^4He, only transitions to the 20.1 MeV, 0^+ state are resolved. It is apparent that only a small fraction of the transitions proceeds through the first excited state of ^4He, whereas the main part of the cross section goes into the higher lying states. A detailed analysis of the angular distributions of the (^{3}He,α*) reaction in comparison with the (^{3}He,α) reaction is in progress; it may yield important information on the structure of the excited states of ^4He.

Footnote and References

†On leave from Kernfysisch Versneller Instituut, University of Groningen, Groningen 8002, The Netherlands.

1. G. G. Ohlsen, Nucl. Instrum. Methods 37, 240 (1965).

2. R. Jahn, G. J. Wozniak, D. P. Stahel, and J. Cerny, Phys. Rev. Lett. 37, 812 (1976). R. Jahn, D. P. Stahel, G. J. Wozniak, R. J. de Meijer, and J. Cerny, Phys. Rev. C 18, 9 (1978).

3. K. M. Watson, Phys. Rev. 88, 1163 (1952); A. B. Migdal, Soviet Phys. JETP 1, 2 (1955).

4. R. M. Haybron, Nucl. Phys. A 112, 594 (1968).

5. R. Jahn, D. P. Stahel, G. J. Wozniak, J. Cerny, and H. P. Morsch, Phys. Lett. B 65, 339 (1976).

USE OF HEAVY-ION MULTI-NEUTRON PICK-UP REACTIONS TO MEASURE NUCLEAR MASSES

G. Kekelis,* M.S. Zisman, D. Scott, R. Jahn,† D. Vieira,‡ and J. Cerny

Spallation reactions such as $^{238}U + p$ effectively produce nuclei with large neutron excesses that are stable to particle decay.[1] It is important to determine the masses of these nuclei because the various models that are used to calculate nuclear mass excesses do not agree in their predictions for nuclei with $T_z \geq 3$.[2] However, nuclear reactions that are capable of producing these nuclei in their ground states appear to be characterized by minute cross sections that decrease as one produces nuclei further and further from the valley of beta stability. Therefore, if these masses are to be measured, the amount of information obtainable in a given run period must be maximized.

A scheme which appears to be an efficient method for observing these exotic nuclei is to use a large solid angle spectrometer in conjunction with multiple neutron pick-up reactions. Using this approach one finds that as more neutrons are picked up, reaction Q-values become more negative and resulting magnetic rigidities ($B\rho \propto \sqrt{ME/q}$) remain constant to within a few percent for three or four successive neutron-rich isotopes. For example, for a ^{11}B beam at 115 MeV on a ^{48}Ca target, the relative rigidities for ejectiles emitted at angles near zero degrees vary by only 6% for the boron isotopes from ^{11}B to ^{17}B. Similar results are obtained for ^{18}O to ^{25}O and ^{13}C to ^{20}C at appropriate beam energies. Using the QSD spectrometer at the 88-inch cyclotron, which has an acceptance of 12% in rigidity, we can in principle simultaneously observe the ground state transitions produced by ejectiles from ^{11}B to ^{17}B (excluding the known particle, unstable ^{16}B).

A serious complication occurs in the detection of neutron-rich isotopes in a magnetic spectrometer due to the overlap in time-of-flight (TOF) and differential energy loss (ΔE) for different charge states of various isotopes. For example, $^{15}B^{+5}$ has an identical TOF ($\propto M/q$) and $\Delta E[\propto (MZ/q)^2]$ to that of $^{12}B^{+4}$. Therefore, they are only separable by an energy measurement ($\propto q^2/M$), which requires an energy resolution of $<<20\%$.

The detector used in the present experiment has been described in detail elsewhere.[3] Basically, it provides a double position measurement (trajectory), energy loss in a 10-cm ion chamber (resolution 3%), time-of-flight, and residual energy in a plastic scintillator (resolution 15%). For this experiment the plastic scintillator was replaced by a set of four solid state counters, each with a diameter of 5 cm and resolution of 2%. This system provided unambiguous identification for all the isotopes and charge states of boron.

The experiment was performed at a beam energy of 115 MeV with a 200 $\mu g/cm^2$ target of ^{48}Ca (as a carbonate). Ejectiles of interest were detected at 8° using the full 2 msr solid angle of the QSD spectrometer. The main field of the magnetic

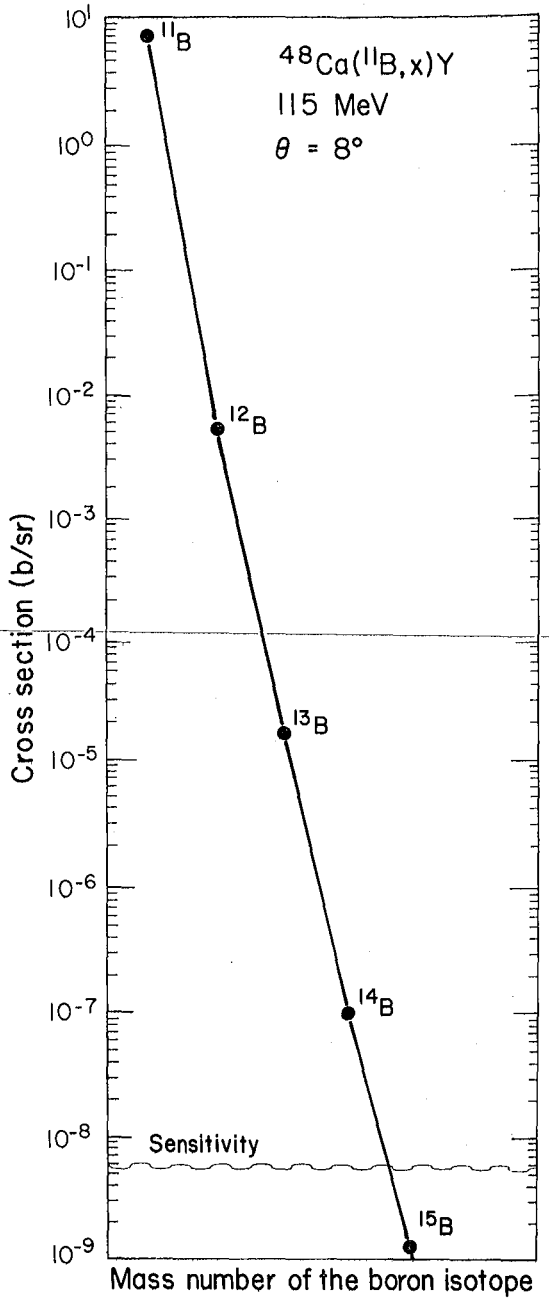

Fig. 1. Observed and predicted cross sections for ^{11}B-induced multi-neutron pickup reactions on ^{48}Ca. (XBL 788-1453)

spectrometer was adjusted so as to obtain ground states of the $^{48}Ca(^{11}B,^{12}B$ to $^{17}B)$ reactions simultaneously. Ground state cross sections were obtained for each additional neutron picked up by the ^{11}B beam. As shown in Fig. 1, an approximately exponential decrease in cross section was observed as a function of ejectile mass. The $(^{11}B,^{14}B)$ reaction was observed with a ground state cross section of roughly 100 nb/sr and the extrapolated ^{15}B production cross section was about 1 nb/sr. Since the sensitivity of the present experiment was limited to about 7 nb/sr, no estimate of the ^{15}B mass could be obtained. In fact, although ejected ^{15}B particles leading to states from the ground state to 8 MeV excitation in the product nucleus should have been detectable, not a single count attributable to $^{15}B+5$ was observed. Although the detection system was capable of producing particularly clean spectra, the reaction cross sections of interest are well below its present sensitivity.

Footnotes and References

*Present address: Williams College, Williamstown, Mass. 01267.

†Present address: Institut für Strahlen und Kernphysik der Universität Bonn.

‡Present address: CNC Division, Los Alamos Scientific Lab., Los Alamos, New Mexico.

1. G. W. Butler, D. G. Perry, L. D. Remsberg, A. M. Poskanzer, J. B. Natowitz, and F. Plasil, Phys. Rev. Lett. 38, 1380 (1977).

2. Atomic Data and Nuclear Data Tables 17, 411 (1975).

3. B. G. Harvey, J. Mahoney, and R. F. Burton, 1975 Nuclear Science Annual Report, Lawrence Berkeley Laboratory Report LBL-5075, p. 354.

SOME INITIAL RESULTS WITH THE ON-LINE MASS SEPARATOR—RAMA*

D.M. Moltz, H.C. Evans,† D.J. Vieira,‡ R.F. Parry, J. M Wouters, R.A. Gough, M.S. Zisman, and J. Cerny

We have for some time been interested in developing a reasonably fast and universal (having little or no chemical selectivity) on-line mass analysis system to expand our capabilities in studying nuclei far from stability. The system selected was originally proposed by Nitschke[1] and is termed RAMA, an acronym for Recoil Atom Mass Analyzer. Basically, this system utilizes the helium-jet method to transport activity to a Sidenius hollow-cathode ion source which is coupled to a mass spectrometer. A discussion of RAMA has appeared elsewhere.[2,3]

After some initial test experiments with ^{20}Na and ^{211}At activity, one sequence of experiments was performed to confirm the mass assignments of a number of the short-lived, high-Z rare-earth alpha-particle emitters produced by (HI,xn) reactions on various targets. The initial reaction studied was $^{142}Nd(^{12}C,xn)^{154-x}$ Dy with the intention of observing the alpha emitters ^{150}Dy and ^{151}Dy, which are made in high yield (>500 mb). Further experiments confirmed the mass assignments of other N = 84, 85 rare-earth alpha-particle emitters from terbium through ytterbium with half-lives ranging from 4.1 h to 400 msec. Figure 1 is an example of these alpha-particle emitters and Table 1 summarizes our observations compared to the literature assignments.[4]

Some of the odd-Z rare-earth alpha emitters were also investigated. These nuclides exhibit substantial isomerism, with the excitation functions for the low-spin isomers shifted relative to the high-spin isomers by as much as 18 MeV, much more than is usually observed in excitation function shifts for isomer production in other mass regions. This is particularly noticeable

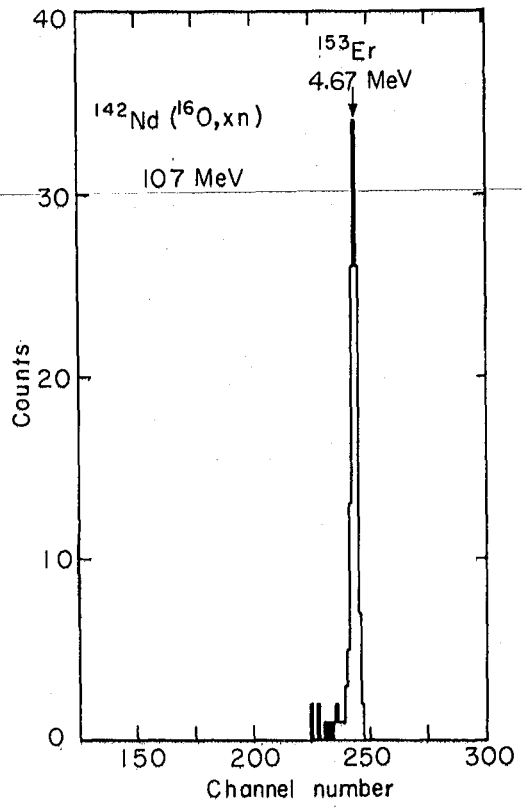

Fig. 1. ^{153}Er alpha spectrum at the mass 153 focal plane position produced by the $^{142}Nd(^{16}O,5n)$ reaction. (XBL 776-1484)

Table 1. Rare-earth alpha-particle emmiter mass confirmations.

Nuclide	Z	E_α Observed[a] (MeV)	E_α Literature[b] (MeV)	$t_{1/2}$ Observed	$t_{1/2}$ Literature[b]
^{149}Tbg	65	3.95	3.95	4.07±0.1 h	4.1 h
^{151}Dy	66	4.07	4.07	17.5±0.5 m	17.7 m
^{150}Dy	66	4.23	4.23	7.1±0.7 m	7.2 m
^{152}Ho(High Spin)	67	4.45	4.46	53±4 s	52 s
^{151}Ho(High Spin)	67	4.51	4.52	36±2 s	35.6 s
^{153}Er	68	4.68	4.67	35±4 s	36 s
^{152}Er	68	4.82	4.80	-	9.8 s
^{154}Tmm	69	5.02	5.04	-	3 s
^{155}Yb	70	5.19	5.21	-	1.65 s
^{154}Yb	70	5.32	5.33	-	400 ms

[a]Typical errors are ±0.03 MeV.

[b]Reference 4.

for ^{151}Ho, when produced by the ^{141}Pr(^{16}O,6 n) reaction, has a peak yield for the high-spin isomer at 123 MeV relative to 105 MeV for the low-spin isomer.[5] This situation was investigated with the RAMA system to clarify the mass assignments of these isomers because the excitation function for ^{151}Ho(LOW SPIN) peaks very near that for ^{152}Ho(HIGH SPIN), and thus could conceivably have been an isomer of ^{152}Ho. Our experiments did, however, confirm the earlier mass assignments.

A more recent experiment has verified the mass assignment of ^{111}Te through the observation of the beta-delayed protons associated with its decay. The mass of this neutron-deficient Te nuclide was originally controversial with Macfarlane and Siivola[6] assigning the 19 sec β-delayed proton activity to ^{110}Te and Bogdanov et al.[7] assigning it to ^{111}Te. Figure 2 shows that the known proton spectrum appears at the mass 111 position so that the observed protons can be attributed to the decay of ^{111}Te; this has been separately confirmed by recent work reported from UNILAC.[8]

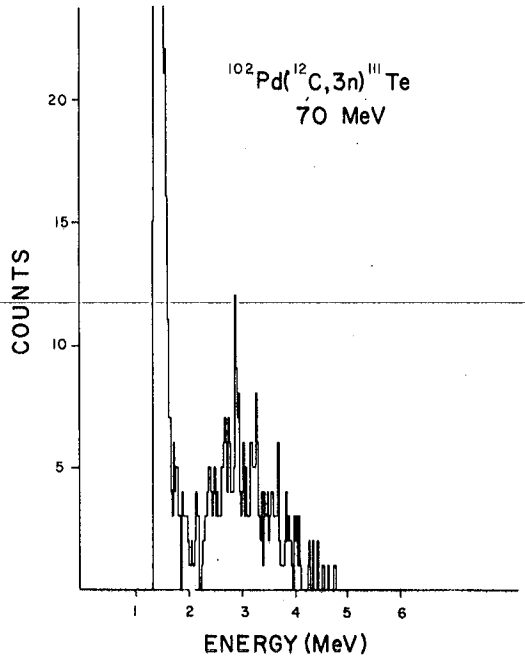

Fig. 2. Proton spectrum at the mass 111 position from ^{111}Te produced by the ^{102}Pd(^{12}C,3n) reaction at 70 MeV. (XBL 7711-10433)

Footnotes and References

*Condensed from LBL-7156.

†Permanent address: Queen's University, Kingston, Ontario.

‡Permanent address: Los Alamos Scientific Lab., Los Alamos, New Mexico.

1. J. M. Nitschke, in Proc. of the Intern. Conf. on the Properties of Nuclei Far from the Region of Beta-Stability, Leysin, Switzerland, 1970 (ERN Report 70-30, Geneva, 1970), vol. 1, p. 153.

2. Nuclear Science Division Annual Report for 1975, Lawrence Berkeley Laboratory Report LBL-5075, p. 351.

3. Nuclear Science Division Annual Report for 1976-77, Lawrence Berkeley Laboratory Report LBL-6575, p. 236.

4. H. Gauvin, Y. Le Beyec, J. Livet, and J. L. Reyss, Ann. Phys. 9, 241 (1975).

5. R. D. Macfarlane and R. D. Griffioen, Phys. Rev. 130, 149 (1963).

6. R. D. Macfarlane and A. T. Siivola, Phys. Rev. Lett. 14, 114 (1964).

7. D. D. Bogdanov, I. Bacho, V. A. Karnaukhov, and L. A. Petrov, Sov. J. Nucl. Phys. 6, 650, 807 (1968).

8. R. Kirchner, O. Klepper, G. Nyman, W. Reisdorf, E. Roeckl, D. Schardt, N. Kaffrell, P. Peuser, and K. Schneeweiss, Phys. Lett. B 70, 150 (1977).

IMPROVEMENTS IN THE RAMA-88 SYSTEM

D. M. Moltz, J.M. Wouters, J. Äystö, R.F. Parry, H.C. Evans,* R. von Dincklage, M.D. Cable, and J. Cerny

During the past year three major innovations have been successfully introduced on the Recoil Atom Mass Analyzer (RAMA) system to (1) improve its overall transport efficiency, (2) increase the yield of radioactive nuclei, and (3) improve the half-life measurement capability to include short-lived nuclides (~100 msec). These innovations were partly motivated by the experimental requirements of our anticipated studies of the $T_z = -2$ nuclides ^{20}Mg, ^{24}Si, and ^{28}S. They included redesigning the entire ion source region to optimize its geometry and permit the use of a higher extraction potential, the introduction of a multiple capillary system in conjunction with the Helium-jet technique,[1] and the development of a set of electrostatic plates for rapid vertical switching of the RAMA beam between two detector stations.

The entire ion source region of the RAMA system was replaced in January 1978 with a new, more versatile system. The reasons for reconstruction included the need to (1) increase the extraction potential from a maximum of 12 kV, to 20 kV, (2) better align the ion source, and (3) eliminate the unnecessary length in the ion source owing to an ineffective, large focusing solenoid. The new ion source holder can be adjusted in all three dimensions and accommodates an ion source having less than half the original length. The critical internal dimensions surrounding the plasma region, however, were left unchanged. At an extraction potential of 18 kV a minimal amount of sparking was observed to the grounded skimmer caused by a pressure rise from the incoming helium-jet. Unlike the old system, the new system has an extractor that can be moved while the ion source is operating.

The new ion source has been tested with ^{153}Er, a high-melting-point, rare-earth alpha-particle emitter produced via the ^{142}Nd(^{16}O,5n) reaction. By increasing the extraction potential from 10.5 kV to 18 kV, the ^{153}Er yield on the RAMA focal plane was increased by a factor of 4. Subsequent tests using ^{10}Na, a β-delayed alpha-emitter produced via the ^{20}Ne(^{3}He,p2n) reaction, indicated a factor of 3 increase in the yield under similar operating conditions.

A recently installed multiple capillary system for gas targets has been extremely successful. The beam from the 88-inch cyclotron passes through a cooled copper cylinder containing the target gas (see Fig. 1). The radioactive recoils stop in the gas and are swept from the collection cylinder by 12 short stainless steel capillaries (1.0 mm-i.d.) to a single, larger, 6-meter-long capillary (1.4 mm-i.d.) that transports the recoils to the RAMA ion source. Tests using ^{20}Na yielded a factor of 10 increase over a single capillary system in the number of radioactive recoils reaching the ion source. (The target and transport gas is actually spark chamber gas, consisting of 90% Ne and 10% He). Combining the new capillary system with the improved ion source results in a factor of 30 overall increase in the yield (see Table 1). In fact, during a recent experiment over a million counts of mass separated ^{20}Na were detected on the focal plane.

Tests have been conducted on the above multiple capillary system to measure the sweep out and transit times of the radioactive nuclides from the target chamber to the first of two skimmers (positioned just before the ion source). With spark chamber gas the average elapsed time was 280 msec, while for pure helium it is expected to be only 140 msec. In the case of spark chamber gas, the multiple capillary system has about a 100-msec longer elapsed time than with a single capillary.

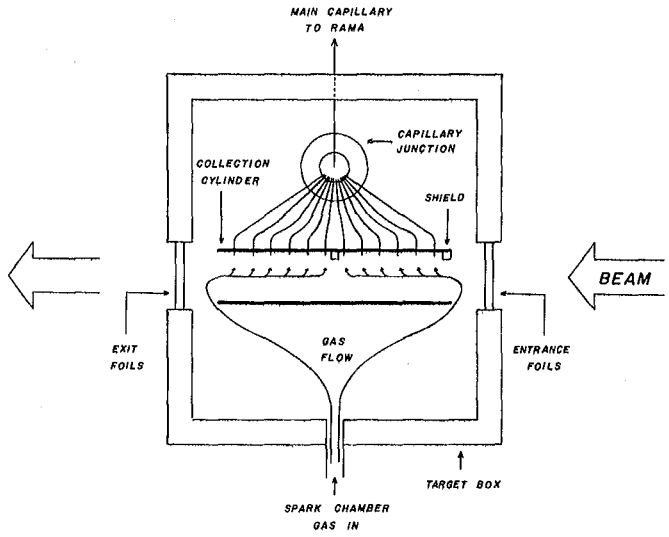

Fig. 1. The multiple capillary system. (XBL 787-9660)

Table 1. Examples of yield improvements in the RAMA-system.

Nuclide	^{20}Na	^{21}Mg	^{153}Er
He-jet yield	10	10	1[a]
Ion source efficiency	3	—	20
Overall improvement	30	—	20

[a]No multiple capillary system.

In order to obtain half-life data for short-lived nuclides a rapid beam switching system has been installed on RAMA. The beam can be rapidly flipped vertically from one detector station on the focal plane to another. While the beam is positioned on the first of the two stations, a multiple event TAC records the exponential decay from the second. This system has been successfully tested with ^{21}Mg, a β-delayed proton emitter having a 122-msec half-life.[2] The flip rate was set at 350 msec. Two standard ΔE-E telescopes were employed in these tests since they will also be necessary in the experiments seaching for ^{20}Mg. In this mass-20 case it is imperative to distinguish between the β-delayed proton activity of ^{20}Mg and the β-delayed alpha activity of ^{20}Na.

The feasibility of detecting the unknown $T_z = -2$ β-delayed proton emitters ^{20}Mg and ^{28}S was determined by a series of test runs on ^{21}Mg and ^{29}S. They were produced via the ^{20}Ne(^{3}He,2n) and ^{28}Si(^{3}He,2n) reactions, both at 41.5 MeV. In the former case spark chamber gas was used in conjunction with the multiple capillary system and the two ΔE-E telescopes on the focal plane.

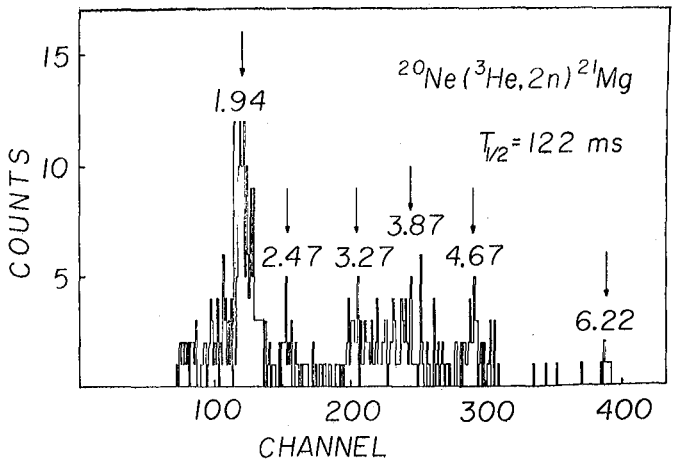

Fig. 2. Energy spectrum of β-delayed protons from ^{21}Mg. Energies are taken from Ref. 2. (XBL 787-9688)

An energy spectrum from the decay of ^{21}Mg is shown in Fig. 2.

In anticipation of our future experimental work, several new systems are being planned. These include a solid target multiple capillary system and a fast tape transport system which will be used with x-ray, γ-ray, and β-ray counters.

Footnote and References

*Permanent address--Queen's University, Kingston, Ontario.

1. Nuclear Chemistry Division Annual Report for 1973, Lawrence Berkeley Laboratory Report LBL-2366, p. 443.

2. R. G. Sextro, R. A. Gough, and Joseph Cerny, Phys. Rev. C 8, 258 (1973).

SHELL EFFECTS AT HIGH SPIN IN THE γ CONTINUUM FROM Te EVAPORATION RESIDUES*

R.S. Simon,† R.M. Diamond, Y. El Masri,‡ J.O. Newton,§ P. Sawa,‖ and F.S. Stephens

The liquid-drop model of the nucleus is a simple and convenient representation capable of explaining many of the macroscopic properties of nuclei, but it cannot give all details. Only the addition of shell corrections[1,2] brings the energysurface calculations into good agreement with experimental results. This shell structure is related to the spacing or bunching of the single-particle levels at the Fermi surface, and it plays a major role in determining the properties of nuclei near the ground state.

As angular momentum is added to a nucleus, the various Nilsson orbitals are expected to move with respect to each other depending upon their Ω values.[2] Thus the level density at the Fermi surface changes as a function of the angular momentum. This variation in the bunching of the single-particle levels will shift the shell closures and many cause marked shape changes in the nucleus at certain (higher) spins. In fact, it is thought that shell effects will continue to occur up to high spins with comparable magnitudes, but there has been little experimental evidence on this point.

In this paper we report on an investigation of the γ-continuum from the decay of Te evaporation residues, in which we observe additional finer structure. This structure may be interpreted as evidence for shell effects in these nuclei at high angular momentum and is compared to results from recent microscopic calculations.

The ^{122}Te system was produced via ^{110}Pd + ^{12}C and ^{82}Se + ^{40}Ar reactions with ~7 mg/cm^2 self-supporting and ~1 mg/cm^2 lead-backed targets, respectively. The initial projectile energies were 53, 78, and 105 MeV for the ^{12}C bombardments and 161, 174, and 185 MeV for the ^{40}Ar ones. The decay γ-radiation was observed in four 7.5 cm x 7.5 cm NaI (Tl) detectors placed at 0°, 30°, 60° and 90° to the beam direction and 60 cm from the target. These detectors were gated by coincident pluses in a Ge detector in order to select continuum γ-spectra associated with individual xn reaction channels as described previously.[3,4]

From the raw NaI spectra corresponding to the individual xn channels the true γ-distributions were obtained by unfolding.[4,5] As an example, the pulse-height and unfolded spectra obtained in the ^{82}Se(^{40}Ar,4n)^{118}Te reaction at 181 MeV are shown in Fig. 1.

The three components of the γ-spectrum seem to be well established in these spectra: (1) the sharp peaks around 600 and 800 keV arise from the lowest seven discrete transitions in the ground band of ^{118}Te; (2) the large bump above 1.2 MeV with an upper edge around 2.3 MeV represents the collective cascades along the yrast region; and (3) the roughly exponentially decreasing tail at still higher energies is interpreted as part of the statistical cascade. But the yrast bump appears to be much reduced or missing altogether at the lower angular momenta brought in with the ^{12}C bombardments, as shown for the 4n channelin Fig. 2. The changes in the yrast bump region for the 4n, 5n, and 6n channels are shown in Fig. 3 for both the 157- and 181-MeV ^{40}Ar reactions.

The anisotropy of the γ-radiation, plotted above the unfolded spectrum in Fig. 1, confirms the stretched-E2 character of the bump region. Integration of the total spectrum gives the average γ-ray multiplicity, $\bar{N}_\gamma$, after taking into account the gating transition in the Ge detector and correcting for multiple coincidences that have been suppressed electronically.

Tellurium nuclei are spherical or weakly deformed near the ground state as a result of nuclear shell structure, namely the closed proton shell at Z = 50. However, at high spins the classical liquid-drop effects are predicted to drive these nuclei oblate, though one must keep in mind the possible effect of shell corrections. Experimentally, information about the high-spin states observed in the Te nuclei produced in the present study is contained in the continuum spectra in the ^{82}Se + ^{40}Ar reaction at 181 MeV (Fig. 1). It is compared with those for other reaction channels in Fig. 3, and with those for the 4n channel from the ^{40}Ar and from the ^{12}C reactions at several projectile energies in Fig. 2.

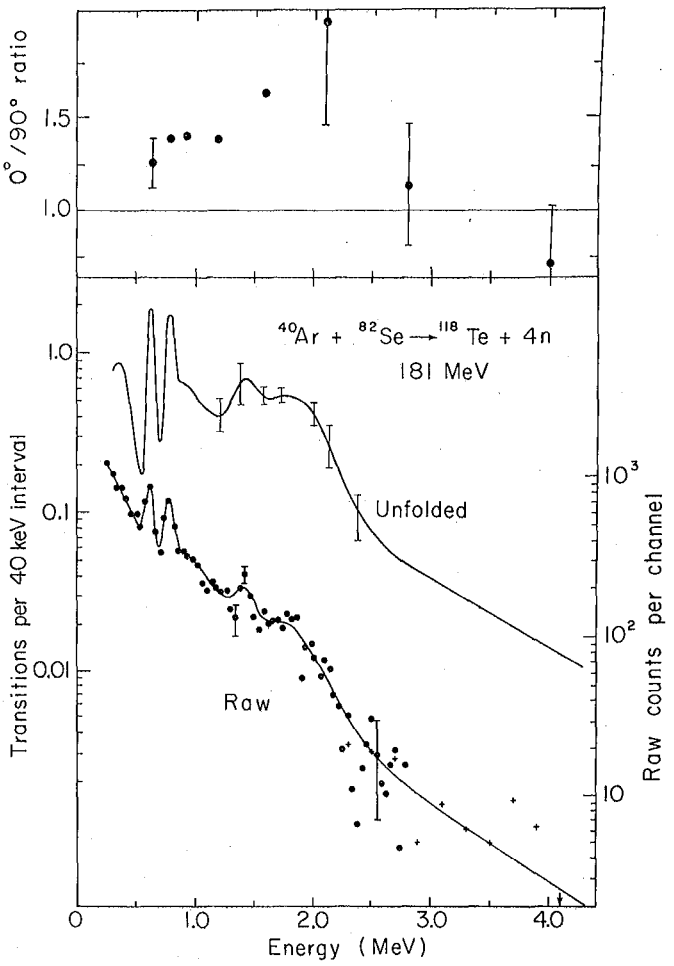

Fig. 1. NaI pulse-height spectrum for ^{40}Ar + ^{82}Se → ^{118}Te + 4n at 118 MeV, and the corresponding unfolded spectrum. The pulse-height spectrum is the sum from all four detectors at 0°, 30°, 60° and 90° and is close to the isotropic average. We have used no additional absorbers in front of the NaI detectors. The unfolded spectrum is given as number of transitions per 40 keV transition-energy interval. At the top of the figure the 0°/90° ratio, the anisotropy, is plotted as a function of transition energy. This ratio was obtained from the separately unfolded spectra at 0° and 90°. (XBL 7610-4989)

When comparing the spectra from the ^{12}C reactions with that from the 157 MeV ^{40}Ar irradiation it is clear that the size of the yrast bump in the spectrum develops with increasing angular momentum input to the compound system. This suggests that these transitions arise from rotational cascades, as recently suggested in studies of the continuum γ-rays from Yb nuclei produced in a wide range of angular momenta by ^{16}O, ^{40}Ar, and ^{86}Kr reactions).[4] But while the bump increased regularly with angular momentum in all Yb cases the situation seems to be somewhat different for Te.

First of all, the yrast bump in Te appears only after a certain amount of angular momentum (~30ħ) is brought into the system (as shown by

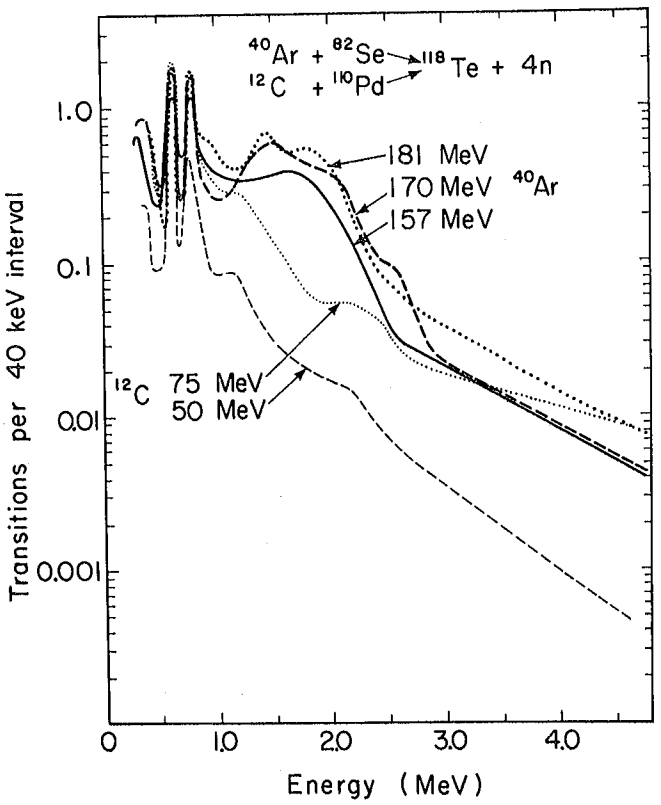

Fig. 2. Unfolded NaI spectra from ^{118}Te produced via the 4n channel in the reactions $^{40}Ar + ^{82}Se$ at 157, 170 and 181 MeV and $^{12}C + ^{110}Pb$ at 50 and 75 MeV. The spectra are given as the number of transitions per 40 keV transition-energy interval. (XBL 771-149)

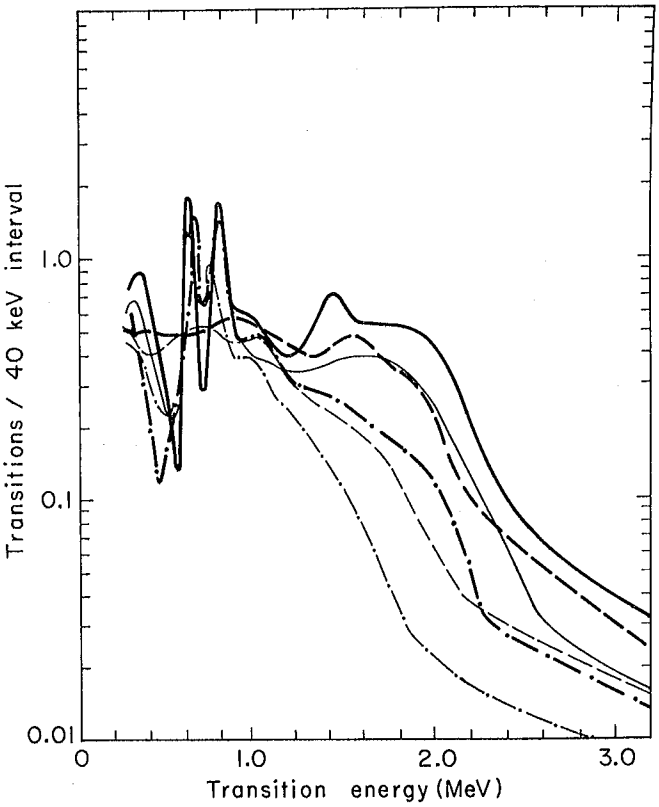

Fig. 3. For $^{82}Se + ^{40}Ar$ at 157 MeV (light lines) and 181 MeV (heavy lines), unfolded spectra for the 4n (——), 5n(- - -) and 6n (-·-·-) reactions, given as the number of transitions per 40 keV transition-energy interval. (XBL 765-2847)

the ^{12}C, 4n spectra in Fig. 2). Then with increasing angular-momentum uptake, the bump develops regularly at first. In Fig. 3 its upper edge is seen to move to higher transition energies if one follows the sequence from the 6n channel spectrum to the 5n one at 157 MeV, to the 6n and 5n channel spectra at 181 MeV, and the 4n channel spectrum at 157 MeV. This corresponds to the behavior previously observed in Yb nuclei and suggests (as discussed there) the existence of regular rotational bands in this spin region.

At still higher input angular momenta the energy of the edge of the yrast bump no longer moves much. This can be seen in Fig. 2 if one compares the ^{40}Ar, 4n spectra at 157, 170, and 181 MeV average bombarding energy. Since the 4n reaction at 157 MeV already corresponds to a maximum angular momentum of ~55ħ, and the maximum spin that can be held in the compound nucleus is of the order of 60ħ, little more angular momentum can be brought to the γ-ray cascades with increasing ^{40}Ar energy. So, little further movement of the edge is expected; additional input angular momentum will lead to other exit channels (these are likely to involve α-particle emission). This is in agreement with the observed increasing population of αxn channels as the bombarding energy is raised, and is also plausible from the reduction in γ-ray multiplicity observed for the sum of all reactions at 181 MeV ^{40}Ar compared to 170 MeV. However, another possible explanation for the limited movement of the edge at these high spins is that a back-bend is taking place. At present we cannot say much about this from our data, so that we cannot decide between these possibilities.

In contrast, the behavior of Te at moderate spins seems to be more readily understood. Thus the two peaks observed at γ-ray energies of ~600 and ~800 keV in the even-n spectra represent peculiarities in the nuclear structure that lead to the existence of several levels, roughly equally spaced at those energies. In addition, there appears to be a minimum in the ^{40}Ar spectra between the 800 keV peak and the yrast bump. These factors argue against the existence of deformed rotational bands as the collective mode of excitation at spins much below 30ħ. A relationship between transition energy and spin different from the rigid-rotor one is necessary to explain these data. The appearance of the pump then indicates a change to collective rotational behavior and is a reflection of changes in nuclear structure (shell effects) caused by the increasing angular momentum.

Recently, shell effects have been included in theoretical calculations[2,6,7] for nuclei at very high angular momentum by using a Strutinsky-smearing type of approach. The results for ^{118}Te with I > 20 from Ragnarsson and Soroka[7] are shown in a plot of transition energy vs spin in Fig. 4,

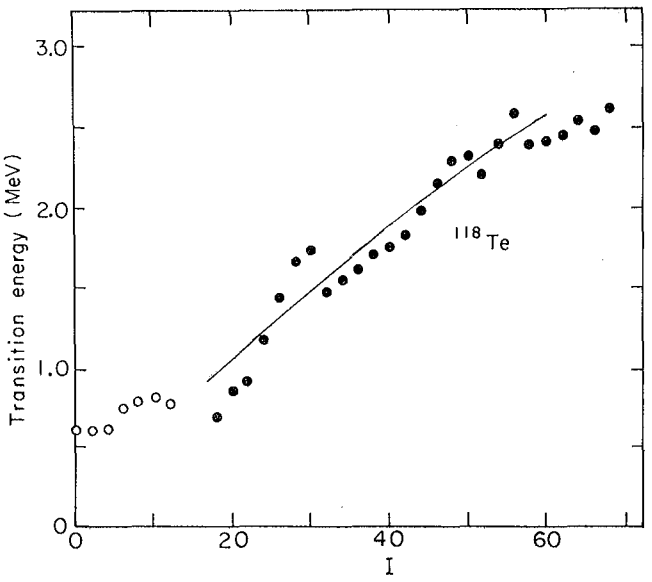

Fig. 4. Plot of transition energy vs spin as given by the liquid-drop model (——) and as calculated by Ragnarsson and Soroka[7] with shell corrections added (· · ·). The results of Faessler and Ploszajcak[6] also show the distinct increase in transition energy just below spin 30.
(XBL 767-3134A)

along with a curve representing the liquid-drop values for an A = 118 nucleus and the lowest known transitions in ^{118}Te. It is the slope in such a plot that should compare inversely with the height of the Te spectrum of Fig. 3, if the feeding into the yrast region is mainly complete. It is not clear whether the correspondence between the experimental spectra and the results from the calculations is real or fortuitous, but it does appear that the accuracy and sensitivity of both experiment and calculation are approaching the point where meaningful comparisons can be made.

Footnotes and References

*Condensed from LBL-6531.

†Gesellschaft für Schwerionenforschung, Darmstadt, Germany.

‡Institut de Physique Corpusculaire, Louvain-la-Neuve, Belgium.

§The Australian National University, Canberra, A. C. T. 2600, Australia.

‖Research Institute for Physics, Stockholm, Sweden.

1. V. M. Strutinsky, Nucl. Phys. A 95, 420 (1967).

2. G. Andersson, S. E. Larson, G. Leander, P. Möller, S. G. Nilsson, I. Ragnarsson, S. Åberg, R. Bengtsson, J. Dudek, B. Nerlo-Pomorska, K. Pomorski, and Z. Symanski, Nucl. Phys. A 262, 205 (1976). A. Bohr and B. R. Mottelson, Physica Scripta 10A, 13 (1974).

3. P. Tjøm, F. S. Stephens, R. M. Diamond, J. de Boar, and W. E. Meyerhof, Phys. Rev. Lett. 33, 593 (1974); M. V. Banaschik, R. S. Simon, P. Colombani, D. P. Soroka, F. S. Stephens, and R. M. Diamond, Phys. Rev. Lett. 34, 892 (1975); R. S. Simon, M. V. Banaschik, P. Colombani, D. P. Soroka, F. S. Stephens, and R. M. Diamond, Phys. Rev. Lett. 36, 359 (1976).

4. R. S. Simon, M. V. Banaschik, R. M. Diamond, J. O. Newton, and F. S. Stephens, Nucl. Phys. A 290, 253 (1972).

5. J. F. Mollenauer, Phys. Rev. 127, 867 (1962).

6. A. Faessler and M. Ploszajcak, private communication (1977).

7. I. Ragnarsson and D. P. Soroka, private communication (1976).

AVERAGE LIFETIMES OF COLLECTIVE TRANSITIONS IN THE SPIN 30-50 REGION

H. Hübel,* U. Smilansky,† R.M. Diamond, F.S. Stephens, and B. Herskind‡

The de-excitation γ-ray spectra of nuclei produced at very high angular momenta in heavy-ion compound-nucleus reactions are composed of three parts.[1] A statistical region ($E_\gamma \gtrsim 1.5$ MeV for deformed nuclei in the heavy rare-earths); a low-energy region of the spectrum ($\lesssim$0.7 MeV) dominated by discrete lines; and an intermediate range of γ-ray energies where the spectrum shows a broad structure (the "bump"). The latter region has the following characteristics: (a) The multiplicity of transitions at the high-energy edge of the bump is higher than the average multiplicity associated with either the statistical or discrete parts of the spectrum--indicating that these transitions come from the highest spin states populated. (b) Angular distribution measurements show predominantly a stretched quadrupole component in these decays. These characteristics can be explained by a model which assumes that the quadrupole bump is composed of collective transitions within rotational bands parallel to the yrast line. However, until now no measurements

have shown that these transitions are indeed very highly collective. In the present experiment an attempt is made to measure average lifetimes in the bump region by a Doppler-shift method.

The experimental setup is similar to the one described in Ref. 2, with six 7.6 x 7.6 cm NaI detectors serving as a multiplicity filter. Two 7.6 x 7.6 cm NaI detectors were located at 0^o and 90^o with respect to the beam direction at a distance of 60 cm from the target to allow for neutron discrimination. Average lifetimes of the continuum γ-rays were deduced by comparing the Doppler shift for the spectra measured in the 0^o detector with a ~1 mg/cm^2 self-supporting target and with a target from the same thickness on a thick backing. The beams of 700-MeV ^{136}Xe ions were from the LBL SuperHILAC and are listed in Table 1.

As an example of our data, Fig. 1a shows the sum of the two- to six-fold spectra obtained in the 0^o detector for self-supporting ^{27}Al and ^{27}Al on Au targets. Below ~600 keV the displacement of the two spectra results mainly from lifetimes of the discrete lines. In the region of 750-1500 keV, the lifetimes of the continuum γ-rays were responsible for the difference between the two spectra. At still higher γ-ray energies, the lifetimes are much shorter than the characteristic stopping time, hence, no difference is observed between the backed and unbacked targets, and this is a means of normalization of the spectra. The different effects in these three regions are accentuated in the ratio of the two spectra which is displayed in Fig. 1b. The ratio for a different target, ^{28}Si, is shown in Fig. 1d.

The data were analyzed in the following way. First the pulse height spectra were unfolded[3] to give the primary photon spectra. The spectrum for recoil into vacuum was then folded with the response function calculated for a doppler-shifted distribution, and the calculated ratio of spectra for recoil into vacuum and for recoil into backing was compared to the experimental ratio. The response function that generates the Doppler-broadened spectrum was obtained by following the population of the decaying levels during the slowing down of the emitting nuclei. The population of levels in the continuum was calculated using a model in which the continuum is described by a series of rotational bands with an average moment of inertia $\mathcal{J}$. To each energy bin at a median energy E_γ a spin I is assigned using the relationship

$$E_\gamma = \frac{\hbar^2}{2\mathcal{J}}(4I - 2)$$

with the empirical[2,4,5] value

$$\frac{2\mathcal{J}}{\hbar^2} = (150 \pm 20)\ \mathrm{MeV}^{-1} \quad .$$

We assume that the level decays to the next member of the band by an E2 transition. The feeding of each level consists of two parts: the prompt feeding, and the cascading from upper members of the band. The prompt part is approximated by a σ_I = distribution of initial populations, $\sigma_I \propto I/\{1 + \exp[(I - I_{max})/2.5]\}$, where I_{max} is the maximum angular momentum brought into the compound nucleus, determined for this case as $I_{max} = 50$.[4] For the cascading part, the transition lifetimes are determined according to the rotational model with a constant intrinsic quadrupole moment Q_o,

$$\tau = 8 \cdot 10^2 E_{(keV)}^{-5} \frac{1}{\langle I_i\ 2\ K\ 0 | I_i\ 2\ I_f K\rangle^2 e^2 Q_{o(b)}^2} \quad \mathrm{sec} \cdot$$

Table 1. Intrinsic quadropule moments Q_o, enhancement factors $B(E2)/B(E2)_W$, and deformation parameters β_2 for the ^{163}Ho* and ^{164}Er* compound systems.

Target	Compound nucleus	Stopper	$\lvert Q_o \rvert$ a)	$\lvert Q_o \rvert$ b)	$\lvert Q_o \rvert$ Average	$\frac{B(E2)}{B(E2)_W}$	β_2
^{27}Al	^{163}Ho*	Au	9.3(2.5)	8.0(2.3)	8.2(2.2)	270(100)	0.37(11)
^{27}Al	^{163}Ho*	Pb	7.0(2.6)	8.6(3.0)			
^{28}Si	^{164}Er*	Au	8.5(3.0)	8.6(3.0)	9.8(3.3)	380(180)	0.43(15)
^{28}Si	^{164}Er*	Au	12.2(4.9)	10.2(4.3)			

a) Determined from ratios of spectra at 0^o as described in the text.

b) Determined from double ratios of spectra at 0^o and 90^o as described in the text.

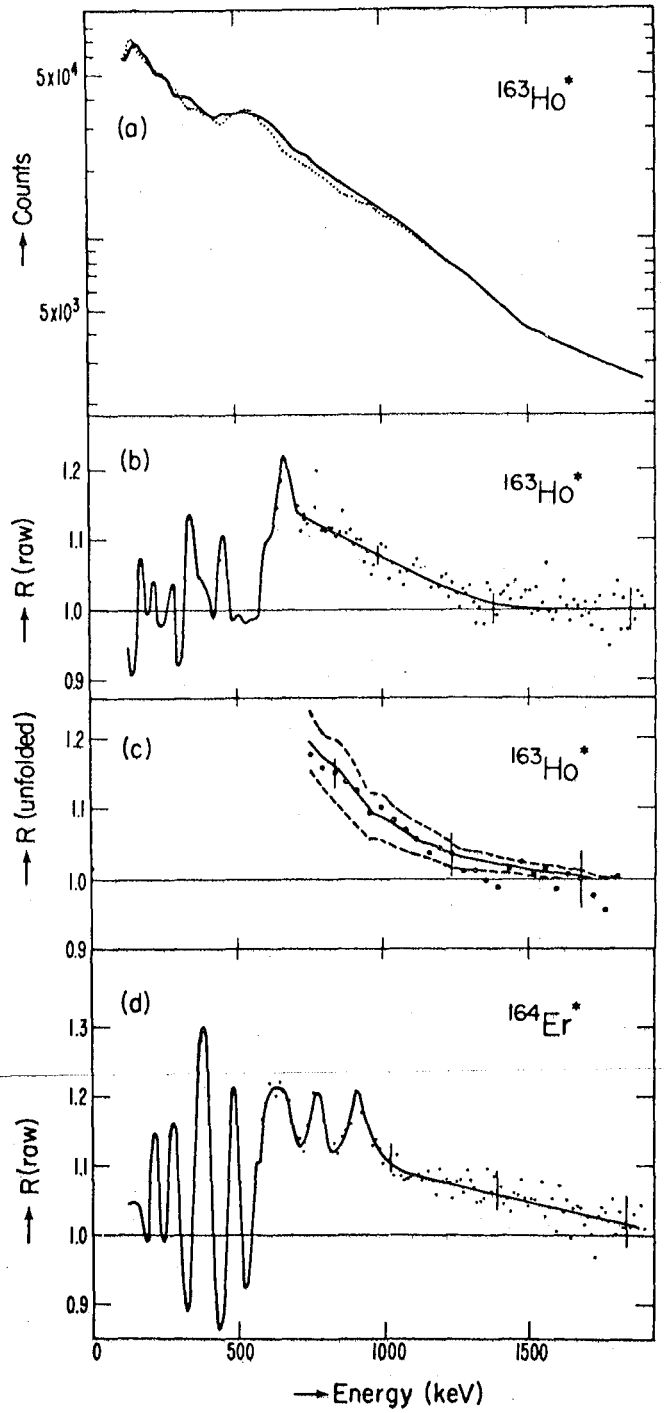

Fig. 1. (a) Sum of two- to six-fold coincidence γ-ray spectra (raw data) measured at 0° for a self-supporting ^{27}Al target (solid curve) and for a ^{27}Al target on a Au backing (dotted curve).
(b) Ratio of the raw (not unfolded) spectra measured at 0° for a self-supporting ^{27}Al target on a Au backing (the curve is drawn to guide the eye).
(c) Ratio of the unfolded spectra (dots) measured at 0° for a self-supporting ^{27}Al target and for a ^{27}Al target on Au backing. The solid curve represents the best fit of the calculated ratio to the data. The dashed lines show the ratios calculated for the two extreme values of Q_0 allowed by the errors given in Table 1.
(d) Same as Fig. 1b, but for a ^{28}Si target. (XBL 7810-12110)

The population equations are solved for all members of the band which contribute to the feeding. To solve this system of 10-30 coupled linear equations, we derived a fast algorithm which made the analysis of the experiment tractable. The slowing-down process was calculated using the Northcliffe and Schilling[6] electronic stopping power and the nuclear contribution was treated according to Blaugrund.[7]

The average Q_0 is obtained by fitting the calculated ratios of the spectra for the backed and unbacked targets to the experimental ratio with Q_0 as the only free parameter. The Q_0 values, corresponding enhancement factors (in Weisskopf units[8]), and deformation parameters obtained for the two systems investigated are given in Table 1. Figure 1c shows the ratio of the unfolded spectra measured at 0° for a Au-backed and unbacked ^{27}Al target in the region of interest. The solid line is the best fitting calculated curve. The dashed lines show the ratios calculated for the two extreme values of Q_0 allowed by the errors given in Table 1.

The uncertainties assigned to the results contain estimates of the following systematic errors: (a) neglect of terms higher than first order in v/c, of angular distribution effects due to hyperfine interaction (the deorientation effect is calculated to be insignificant), and of finite target thickness (we assume no transverse velocity even at the range of nuclear stopping); (b) uncertainty from insufficient knowledge of the stopping power; (c) an estimated five-fold increase in the statistical errors from unfolding the raw data.

We derive from the data that the transitions between the high-spin states of I ~ 30-50 show an enhancement of ~300 s.p.u. and a rather large deformation of $\beta_2 = 0.4$. As can be seen from Fig. 1c there is good agreement in both magnitude and slope for the calculated and measured curves. This indicates that for the investigated nuclei the model provides a satisfactory description of their behavior, suggesting no abrupt change in structure in the investigated region. We conclude that the transitions in the E2 bump are of strongly collective nature, with as high or higher a degree of collectivity as in the ground-state rotational bands of deformed nuclei.

Acknowledgement

We would like to thank Dr. D. Ward for helpful discussions on the stopping power calculations.

Footnotes and References

*Permanent address: Institute für Strahlen und Kernphysik, D-5300 Bonn, W. Germany, Supported by a Max Kade Foundation Fellowship.

†Permanent address: Department of Physics, The Weizmann Institute of Science, Rehovot, Israel.

‡Permanent address: The Neils Bohr Institute, University of Copenhagen; supported in part by the Danish Natural Science Research Council.

1. R. S. Simon, M. V. Banaschik, R. M. Diamond, J. O. Newton and F. S. Stephens, Nucl. Phys. A 290, 253 (1977).

2. M. A. Deleplanque, Th.Byrski, R. M. Diamond, H. Hübel, F. S. Stephens, B. Herskind and R. Bauer, to be published in Phys. Rev. Lett.

3. J. F. Mollenauer, Phys. Rev. 127, 867 (1962).

4. M. A. Deleplanque, I. Y. Lee, F. S. Stephens, R. M. Diamond and M. M. Aleonard, Phys. Rev. Letters 40, 629 (1978).

5. D. Hillis, B. Fernandez, F. Folkmann, J. Garrett, G. B. Hagemann and B. Herskind, to be published in Nucl. Phys.

6. L. C. Northcliffe and R. F. Schilling, Nucl. Data A 7, 233 (1970).

7. A. E. Blaugrund, Nucl. Phys. 88, 501 (1966).

8. A. Bohr and B. R. Mottelson, Nuclear Structure, Vol. I (W. A. Benjamin, New York and Amsterdam, 1969), p. 389.

OBLATE AND PROLATE STRUCTURE IN ^{187,189}Tl

L. L. Riedinger,* A.C. Kahler,† C.R. Bingham,* M.W. Guidry,* I.Y. Lee,‡ M.M. Aleonard,§ R.M. Diamond, Y. El-Masri,‖ J.O. Newton,¶ R.S. Simon,** and F.S. Stephens

The purpose of this experiment was to study rotational bands of levels built on $h_{9/2}$ and $i_{13/2}$ proton states in ^{187,189}Tl. The cores for these particle states are ^{186,188}Hg, the yrast states of which are known to undergo changes in shape at I = 4 and I = 6, respectively. This experiment was designed to test the importance of the $h_{9/2}$ and $i_{13/2}$ orbitals in causing these shape changes by looking for similar changes in the bands of these particles in Tl. Another purpose was to trace the positions of the $h_{9/2}$ and $i_{13/2}$ bandheads with mass number to see if their minimum excitation energies occur at the same Tl isotope.

In-beam γ-ray measurements were made last year on ^{189}Tl by the ^{165}Ho (^{28}Si,4nγ) reaction. As in the heavier odd-mass Tl isotopes[1] rotational bands built on the $h_{9/2}$ and $i_{13/2}$ proton particle states were observed. However, unlike the heavier Tl nuclei, the nature of both bands in ^{189}Tl changes from strongly coupled to decoupled at approximately 1.2 MeV above the respective bandheads, reflecting the known oblate-prolate shape change in ^{188}Hg. Moreover, the decoupled bands match very well with the sequence of states in the prolate band of the ^{188}Hg core. We thus conclude that the formation of this prolate minimum in Hg is neither hindered nor enhanced by the presence of a $h_{9/2}$ or $i_{13/2}$ proton. While studies of the light odd-neutron Hg isotopes are still required, there does not appear to be any neutron orbitals which are rapidly changing as a function of deformation and which could greatly change the structure of light Hg nuclei. Therefore, it appears that the prolate minimum seen in Hg for A $<$ 188 is truly a collective phenomenon and does not result from alignment effects of a few selected high j, low Ω particles.

Another interesting feature of the data is the excitation energies of the $h_{9/2}$ and $i_{13/2}$ bandheads. These intruder states have energies which decrease with decreasing A for odd Tl nuclei above A = 189. These data, as well as UNISOR decay data,[2] reveal that the $h_{9/2}$ state has reached its minimum value in ^{189}Tl, whereas the $i_{13/2}$ state continues its rapid decrease in energy. These decreasing energies cannot be explained in terms of changing deformations since the bands built on these states are very similar for A $\geq$ 191, and thus must result from nucleon-nucleon residual interactions. These observed differences in the two shell states hopefully provide theorists with information needed for the understanding of these residual interactions.

In order to strengthen our case with regard to the onset of deformation and to trace the descent of the $i_{13/2}$ excitation energies one step further, measurements were recently made on ^{187}Tl by the ^{156}Gd (^{35}Cl,4n) reaction. Our preliminary analysis of the data indicates that one band was observed which switches from dipole to quadrupole transitions above the third state. A few other gamma-ray cascades were observed to have the correct excitation function but do not appear to be strongly in coincidence with any of the lines in the first band mentioned. While the presence of the changing band is analogous to the $h_{9/2}$ band observed in ^{189}Tl, the absence of feeding of the low lying members of this band by the $i_{13/2}$ band is not understood. Further analysis of the data is required before definite conclusions can be drawn.

Footnotes and References

*The University of Tennesse, Department of Physics, Knoxville, Tennessee 37916, and Oak Ridge National Laboratory.

†Graduate student from the University of Tennessee. Present address: Texas A&M University Cyclotron Institute, College Station, Texas 77840.

‡Present address: Oak Ridge National Laboratory, Oak Ridge, Tennessee 37830.

§Present address: Centre d'Etudes Nucléaires de Bordeaux-Gradignan, 33130 Gradignan, France.

‖ Present address: Université de Louvain, Louvain-la-Neuve, Belgium.

¶ Present address: The Australian National University, Canberra, A.C.T. 2600, Australia.

**Present address: Gesellschaft für Schwerionenforschung, Darmstadt, West Germany.

1. A. C. Kahler, L. L. Riedinger, P. Hubert, N. R. Johnson, E. Eichler, R. L. Robinson, and G. J. Smith, Bull. Am. Phys. Soc. 21, 976 (1976).

2. A. G. Schmidt, R. L. Mlekodaj, E. L. Robinson, F. T. Avignone, J. Lin, G. M. Gowdy, J. L. Wood, and R. W. Fink, Phys. Lett. B 66, 133 (1977).

NUCLEAR SHAPES AT HIGH ANGULAR MOMENTUM*

M.A. Deleplanque,† I.Y. Lee,‡ F.S. Stephens, R.M. Diamond, and M.M. Aleonard§

The study of nuclear structure at angular momenta above 30ħ presently requires measurements of the continuum γ-ray spectrum. Previous studies[1] have shown this continuum to be composed usually of a lower-energy stretched-E2 bump and a higher-energy tail interpreted as a statistical cascade. Also some measurements[2] of the total delay time to reach the ground-state band imply the occurrence of collective γ-transitions during the deexcitation process. The aim of the present work is to learn more about nuclear structure at these high angular momenta. The method developed consists of studying the number of γ-rays (multiplicity) associated with each transition energy in the continuum γ-ray spectrum. There is no restriction on the reaction channel, so that the whole range of angular momenta produced in the reaction is considered.

In order to recognize possible systematic features, a number of targets, ranging from ^{12}C to ^{174}Yb, have been bombarded at the LBL 88-inch cyclotron and SuperHILAC with either ^{40}Ar or ^{48}Ca projectiles which induce high angular momentum in the compound nucleus.

A set of six 3" x 3" NaI counters (halo) was placed symmetrically around the beam axis, upstream from the target in order to minimize the number of neutrons detected. A seventh NaI detector was located at 40° to the beam direction, and 60 cm away from the target in order to discriminate against neutrons by time-of-flight. The unfolded spectra from the seventh detector in coincidence with one to six of the halo counters were used to obtain the multiplicity spectrum. In the following, three examples will be discussed as representative of the characteristic features observed.

The system $^{124}Sn+^{40}Ar$ leads to the compound nucleus ^{164}Er and the possible residual nuclei are known to be rotational at angular momenta up to around 20ħ. The multiplicity spectra are shown in Fig. 1a for 158, 170, and 185 MeV bombarding energies. For all the bombarding energies, the multiplicity has a peak at lower γ-ray energies, and then drops to a roughly constant value for the statistical part of the spectrum. This latter value is expected to be near the average multiplicity for all the reaction channels as the statistical γ-rays are thought to occur at all angular momenta. If some kind of rotational behavior is involved in the bump region, the spin, and hence the multiplicity, will increase with the γ-ray transition energy ($I \propto E_\gamma$) until the highest angular momentum is reached. This could give rise to the multiplicity peaks observed, and indeed, not only does the height of the whole multiplicity spectrum increase as more angular momentum is brought in, but also the upper edge of the peak moves toward higher energies in agreement with the rotational hypothesis.

An attempt to explain the data more quantitatively has been made by calculating the energy and multiplicity spectra, and the model used is discussed in LBL-7145 and in the Phys. Rev. Letters. The calculation for the $^{124}Sn + ^{40}Ar$ case (Fig. 1b) reproduces the experimental features remarkably well, considering that no adjustment is allowed except that of I_{er}, the critical angular momentum for evaporation residues, and $\mathcal{J}$. The I_{er} value obtained by fitting the relative height of the two upper multiplicity curves (60ħ) is reasonably consistent with the angular momentum value corresponding to an upper limit for the fusion of the two incoming nuclei (calculated before particle emission) based[3] on the fission barrier (67ħ), and also that deduced[3] from other experiments (65ħ) The moment of inertia value corresponds to 95% of $\mathcal{J}$ for a rigid sphere, also in excellent agreement with previous experience.

The $^{82}Se+^{40}Ar$ case, which leads to Te nuclei near the Z = 50 closed shell, is quite different (Fig. 1c). There is no significant structure in the multiplicity spectrum for the two lowest bombarding energies. A multiplicity peak only begins to appear at 138 MeV and then develops for higher bombarding energies, suggesting the onset of rotational motion only at the higher angular momenta. The lower multiplicities at 185 MeV are due to the onset of fission and deep-inelastic events. The non-structured multiplicity spectra observed at low ^{40}Ar energies correspond to a cascade where there is no strong correlation between the transition energy and the spin. We have tried to reproduce this feature in the calculation by assuming that up to a certain

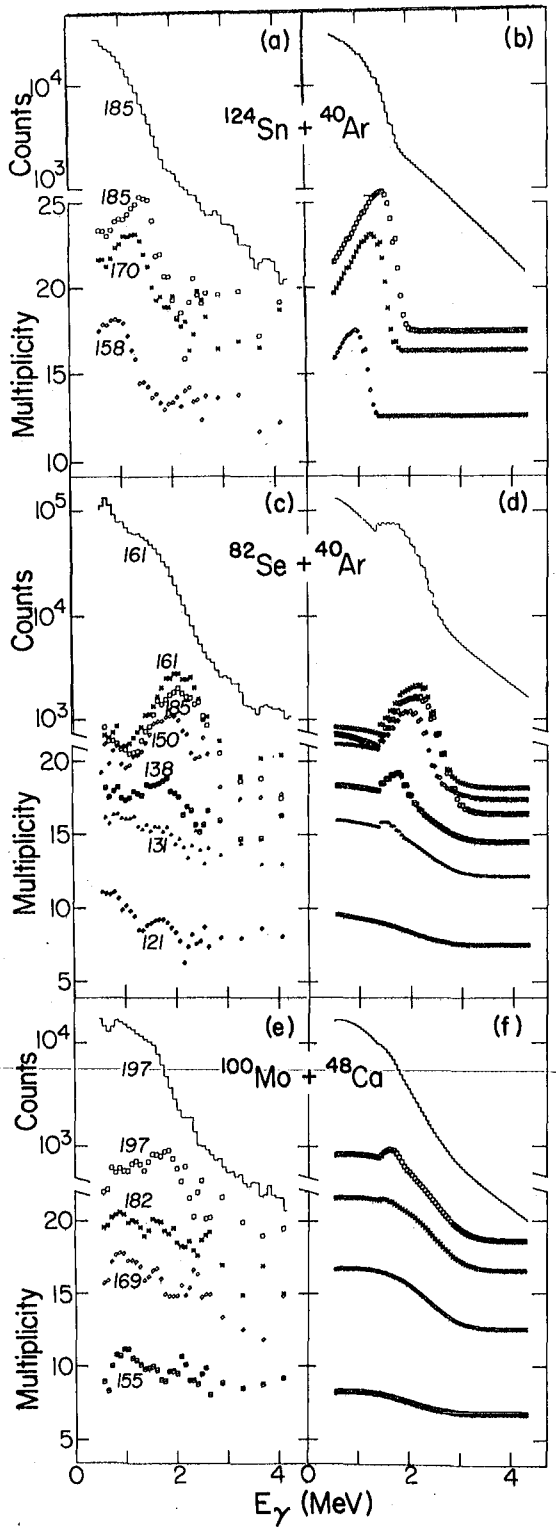

Fig. 1. Observed and calculated multiplicity spectra for the systems and bombarding energies indicated. One γ-ray spectrum is also compared for each system. (XBL 7712-11406)

spin, I_1, the γ-ray spectrum is given by $N(E_\gamma) = E_\gamma \exp(-E_\gamma^2/\sigma^2)$, with σ = 1.13 MeV independently of the spin value of the emitting state. This noncorrelated cascade may contain other than pure stretched-E2 transitions, so that the multiplicity is (I/2)(1+P) where P is fit to the data. Between I_1 and another spin I_2, there is a competition between this cascade and a rotational cascade, and above I_2 the cascade is rotational. Figure 1d shows that the characteristic features are reproduced, with the parameter values: I_1 = 27ħ, I_2 = 38ħ, I_{er} = 53ħ, $\mathcal{I} = 0.85\,\mathcal{I}_{rig}$ and P = 0.17.

In the ^{100}Mo + ^{48}Ca case, which leads to nuclei in the N = 82 closed-shell region, it is immediately apparent that the absence of structure remains up to high spins; indeed, the rotational competition starts only around spin 50.

Since almost any type of collective motion would lead to a strong correlation between transition energy and spin, the non-correlated cascade very likely indicates non-collective motion. Non-collective high-spin states are expected to lie lowest in oblate or spherical nuclei, since the largest moment of inertia in these cases corresponds to rotation (non-collective) around the symmetry axis. On the other hand, collective high-spin states are expected to be lowest in basically prolate (including somewhat triaxial) nuclei, since in this case the largest moment of inertia corresponds to rotation (collective) around an axis perpendicular to the symmetry axis. Thus the interpretation of the ^{82}Se+^{40}Ar → Te data would be that the residual Te nuclei are nearly spherical or oblate at low spins, and then between spins 27 and 38 deform to a basically prolate shape. This change seems to occur only around 50 ħ for the ^{100}Mo+^{48}Ca → Sm system.

Thus these multiplicity spectra appear to contain rather detailed information about the nuclear shape at spins up to 60. In particular, we are able to recognize rotational motion as a characteristic peak in the multiplicity spectrum, to determine the spin regions where it occurs, and to deduce the moment of inertia of the nucleus in these regions.

Footnotes and References

*Condensed from LBL-7145.

†On leave from Institut de Physique Nucléaire, 91406 Orsay, France; supported by Centre National de la Recherche Scientifique and National Science Foundation.

‡Present address: Oak Ridge National Laboratory, Oak Ridge, Tennessee.

§Permanent address: Centre d'Etudes Nucléaires de Bordeaux-Gradignan, Domaine du Haut-Vigneau, 33170 Gradignan, France.

1. R. S. Simon, M. V. Banaschik, P. Colombani, D. P. Soroka, F. S. Stephens, and R. M. Diamond, Phys. Rev. Lett. 36, 359 (1976), and references therein.

2. J. O. Newton, F. S. Stephens, R. M. Diamond, W. H. Kelly, and D. Ward, Nucl. Phys. A 141, 631 (1970).

3. H. C. Britt et al., Phys. Rev. Lett. 39, 1458 (1977).

MULTIPOLARITY OF CONTINUUM γ-RAYS FROM ENHANCED ANGULAR CORRELATION MEASUREMENTS*

M.A. Deleplanque,† Th. Byrski,‡ R.M. Diamond, H. Hubel,§ F.S. Stephens, B. Herskind,‖ and R. Bauer‖

At the present time it appears that most of the information on nuclear structure at high angular momentum is contained in the low-energy bump observed in γ-ray spectra from evaporation residues following heavy-ion compound-nucleus reactions. The high-energy exponential tail in these spectra seems to be statistical in nature and thus contains less-detailed information. The bump very likely consists mainly of stretched E2 transitions, as indicated by previous studies[1] of its systematic behavior and by measurements of the γ-ray anisotropy. However, the latter measurements have been only qualitative, since there has been no proper calculation of the angular correlations expected in the cases where one or more additional γ-rays are detected following the compound-nucleus formation. This work reports on experiments designed to determine the multipolarity of the continuum γ-ray spectrum making use of a multiple-counter array to preferentially select the axis of alignment of the de-exciting nuclei so that the sensitivity to different types of radiation is increased. At the same time the selection of high-multiplicity events enriches the spectrum in γ-rays from states with high angular momentum.

The experimental setup is shown in the inset of Fig. 1. The angular-momentum vectors of the compound nuclei are initially oriented in the plane (XY) perpendicular to the beam direction. A particular alignment direction is selected out by requiring coincidences in a set of six 7.6 x 7.6 cm NaI counters (multiplicity counters) located around the target in a plane (XZ) containing the beam direction. Thus, for example, stretched quadrupole γ-rays detected in these six counters will select preferentially nuclei which are aligned along the Y axis. The angular correlation has been measured in four 7.6 x 7.6 NaI detectors placed along the X axis (θ=90°, ϕ=180°; "up" counter) and the remaining three in the YZ plane (θ = 0, 45, 90°, ϕ = 90°, "0", "45", "90" counters). These "angle detectors" were located 60 cm away from the target in order to discriminate against neutrons by time-of-flight. Six spectra ("folds"), determined by the number of multiplicity counters in coincidence, were obtained for each angle detector and then unfolded[2] to give the primary photon spectra. These were used to obtain the multiplicity and multipole spectra described below.

The multiplicity spectra have been calculated[3] from the sixfold spectra summed over the four angle detectors. A remaining ~3% correction to the multiplicity for angular correlation effects has been made. Some of the multiplicity spectra are shown in Fig. 2a. We present the results only in terms of ΔI = 2 quadrupoles and ΔI = 1 dipoles, because: a) though I = 0 dipoles cannot be distinguished very well here from ΔI = 2 quadrupoles,

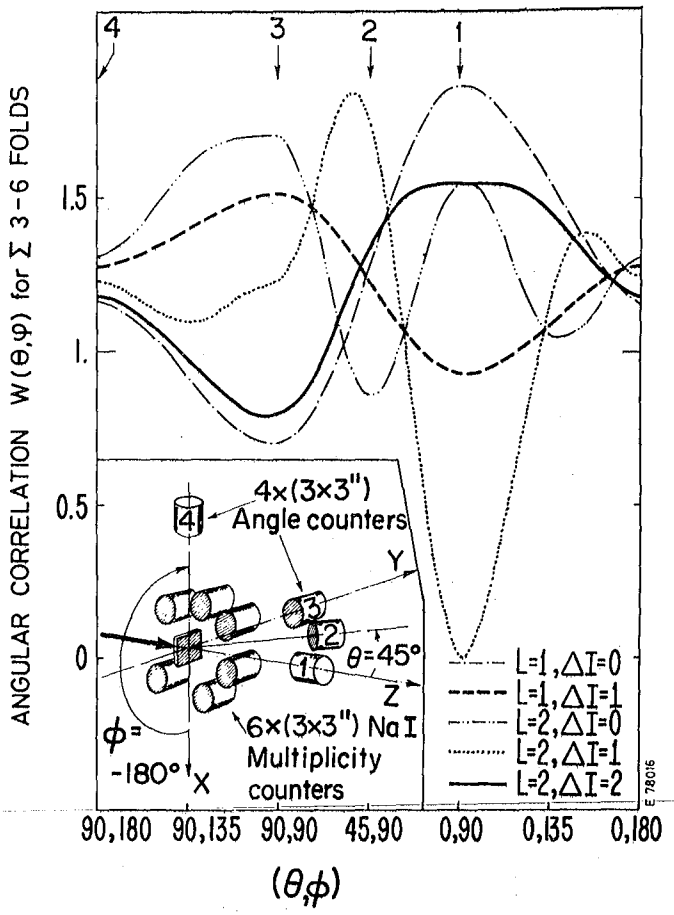

Fig. 1. The angular correlation functions are shown versus angle for the five transition types considered, with the assumption that three or more of the multiplicity counters fired. The numbers 1-4 indicate the actual counter position. The inset shows the experimental arrangement.
(XBL 784-8204A)

the initial spins and observed multiplicities do not allow many ΔI = 0 dipoles; and b) whereas the ΔI = 0 and 1 quadrupoles are similar to ΔI = 1 dipoles in the 0/90 ratios, the results from the 45° detector indicate very little of these ($\lesssim$ 5%). Only ΔI = 2 quadrupoles and ΔI = 1 dipoles were considered in the multiplicity counters since the intensities observed in the angle detectors are not very sensitive to this choice.

Figure 1 shows an example of the sensitivity of the angular correlation functions for the three- and higher-fold coincidences calculated by a semi-classical method.[4] The 0/90 ratio has been used to determine the multipole ratios,

but in several cases we have also calculated them from the 0/up, 45/90, and 45/up ratios; all gave similar results. From these multipole ratios and any angle detector spectrum, we can reconstruct the stretched quadrupole and dipole spectra, and when the integral of these two spectra is normalized to the (average) multiplicity, the resulting spectra give the number of transitions of each type per channel (160 keV interval). Some of these spectra are shown in Fig. 2b.

Previous studies[1] of multiplicity spectra have shown different behavior in strongly and weakly deformed nuclei. Based on this experience we have studied the following systems: ^{116}Cd + ^{48}Ca and ^{124}Sn + ^{40}Ar leading to rotational Er residual nuclei; ^{130}Te + ^{48}Ca and ^{122}Te + ^{48}Ca leading to rotational Hf nuclei; ^{106}Cd + ^{48}Ca, ^{82}Se + ^{40}Ar, and ^{110}Pd + ^{40}Ar leading to residual nuclei near closed shells. Three or four different bombarding energies were used for each system.

Three general properties are clearly established. These are: 1) the quadrupole bump, 2) the dipole bump, and 3) the tail region. The multipole spectra in Fig. 2b confirm that in the rotational nuclei, the low-energy bump is composed of $\Delta I = 2$ quadrupole transitions. The multiplicity spectra of Fig. 2a show that in these cases there is a correlation between γ-ray energy and spin (multiplicity), and both types of spectra (Fig. 2a and 2b) show that the γ-ray energies increases with increasing spin (higher bombarding energies). The ^{116}Cd + $^{48}Ca \rightarrow$ $^{164}Er^*$ and ^{124}Sn + $^{40}Ar \rightarrow$ $^{164}Er^*$ systems have these rotational properties.

In the ^{82}Se + $^{40}Ar \rightarrow$ $^{122}Te^*$ system, the evolution of the $\Delta I = 2$ part of the spectrum with increasing bombarding energies confirms[1] that the rotation-like behavior sets in only at rather high spin (~35$\hbar$). The dipole part of the multipole spectrum is a much newer feature, whose occurrence in rotational nuclei has recently been suggested.[5] In the rotational nuclei we do find evidence for a weak low-energy ($\lesssim$0.6 MeV) bump of mainly $\Delta I = 1$ dipole transitions (sizeable amounts of $\Delta I = 1$ quadrupole cannot be excluded). On the whole, this feature seems consistent with a contribution of $\Delta I = 1$ (E2, M1, or mixed) rotational cascade transitions. A completely new feature, however, is the large amount of $\Delta I = 1$ dipole transitions in the ^{110}Pd + $^{40}Ar \rightarrow$ $^{150}Gd^*$ and ^{82}Se + $^{40}Ar \rightarrow$ $^{122}Te^*$ cases. The overall percentage of $\Delta I = 2$ quadrupoles is around 80% for the rotational nuclei, 70% for the ^{106}Cd target, 60% for the ^{82}Se target, and 50% for the ^{110}Pd target. Thus the systems leading to products near closed shells have strong $\Delta I = 1$ dipole radiation, which the variation with bombarding energies shows to be concentrated at lower spins. This radiation gives little or no structure in the multiplicity spectra and corresponds to the "non-correlated" component previously identified.[1] The main difference between the ^{82}Se and ^{110}Pd systems seems to be the presence of $\Delta I = 1$ transitions at the lowest spins in the Pd system instead of the $\Delta I = 2$ quadrupoles (0.7 MeV) observed in the ^{82}Se system. Thus a pattern seems to emerge where we find, with increasing collectively, first, many $\Delta I = 1$ transitions (^{110}Pd system); later, mostly $\Delta I = 2$ transitions but uncorrelated (^{82}Se at 131 MeV); and finally, highly correlated

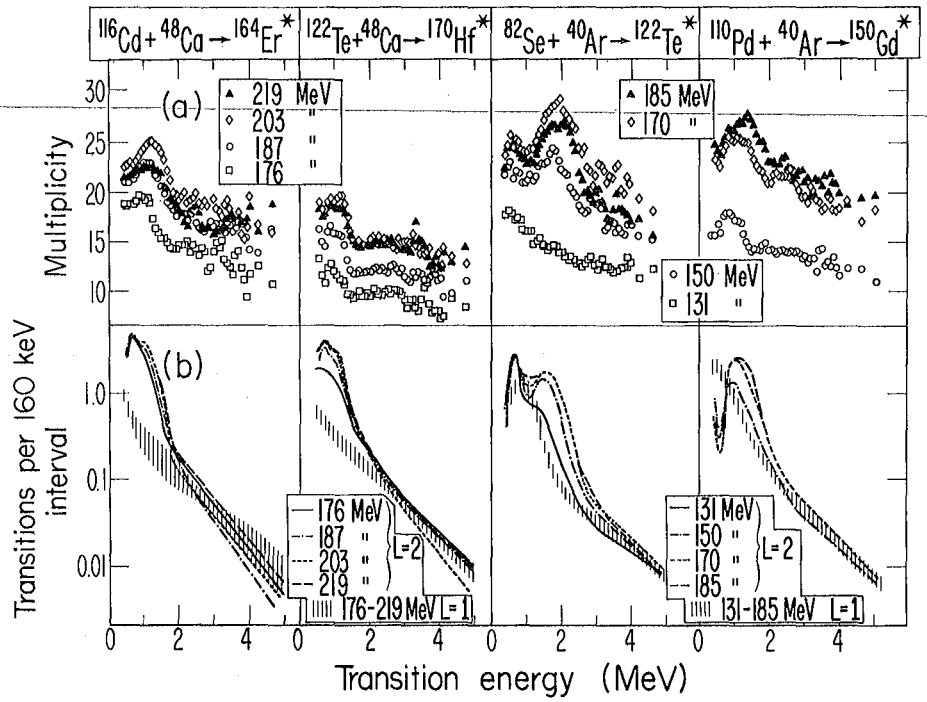

Fig. 2. (a) The multiplicity spectra are shown for the four indicated systems at several bombarding energies.
(b) The corresponding multipole spectra are shown for stretched quadrupole and dipole components. Each hatched area covers the full range of the dipole spectra for all bombarding energies listed.
(XBL 785-2522)

$\Delta I = 2$ transitions--no doubt the rotational electric quadrupoles.

In summary, we have developed methods to study the angular correlations of continuum γ-rays following heavy-ion compound-nucleus reactions and to evaluate these angular correlations in terms of the transition types present. The most striking new feature observed is the presence of intense $\Delta I = 1$ (mostly dipole) transitions at relatively low-spin values in the nuclei near closed shells. These transitions appear to be an alternative to collective transitions at lower spins, and their study should teach us something about the competition of collective and non-collective motion in such nuclei.

Footnotes and References

*Condensed from LBL-7726.

†Permanent address: Institut de Physique Nucléaire, B.P. No. 1, 91406 Orsay, France. Sponsored by the National Science Foundation and Centre National de la Recherche Scientifique.

‡Permanent address: Centre de Recherche Nucléaires, 67037 Strasbourg Cedex, France.

§Permanent address: Institut für Strahlen und Kernphysik, D-5300 Bonn, W. Germany. Supported by a Max Kade Foundation Fellowship.

‖Permanent address: Niels Bohr Institute, University of Copenhagen; supported in part by the Danish Natural Science Research Council.

1. M. A. Deleplanque, I. Y. Lee, F. S. Stephens, R. M. Diamond, and M. M. Aleonard, Phys. Rev. Lett. 40, 629 (1978).

2. J. F. Mollenauer, Phys. Rev. 127, 867 (1962).

3. O. Andersen, R. Bauer, G. B. Hagemann, M. L. Halbert, B. Herskind, M. Neiman, H. Oeshler, and H. Ryde, Nucl. Phys. A 295, 163 (1978).

4. R. Bauer, to be published.

5. J. O. Newton, S. H. Sie, and G. D. Dracoulis, Phys. Rev. Lett. 40, 625 (1978).

COULOMB-NUCLEAR INTERFERENCE FOR HIGH-SPIN STATES EXCITED BY ^{86}Kr, ^{40}Ar, AND ^{16}O PROJECTILES*

M. W. Guidry,† P.A. Butler, R. Donangelo, E. Grosse,‡ Y. El Masri,§ I.Y. Lee,‖ F.S. Stephens, R.M. Diamond, L.L. Riedinger,† C.R. Bingham,† A.C. Kahler,† J.A. Vrba,† E.L. Robinson,¶ and N.R. Johnson‖

Inelastic excitation in the Coulomb-nuclear interference (CNI) region has been studied extensively for ions such as helium,[1] carbon,[2] and oxygen.[3] However, little attention has been given to CNI in the scattering of very heavy projectiles from highly deformed nuclei. We have studied the systems ^{86}Kr + ^{232}Th and ^{40}Ar + ^{238}U, at the Berkeley SuperHILAC, and ^{16}O + ^{162}Dy at the Oak Ridge isochronous cyclotron. In all cases the de-excitation γ-ray cascade was detected in coincidence with backscattered particles, using standard Ge(Li) and annular silicon-detector arrangements. The annular geometry yielded average particle scattering angles of $\theta_{c.m.} \sim 165^{o}$.

Thick targets were used, and γ-ray spectra as a function of incident beam energy were generated by taking coincidence cuts in the heavy-ion spectrum, each corresponding to a different effective beam energy. The relation of incident beam energy (checked by time-of-flight measurements) to detected particle energy was determined using elastic kinematics and theoretical stopping powers. With these methods we obtained spectra simultaneously at several different energies.

The number of particle-γ coincidences, N_γ, was determined from the areas of the γ-ray peaks corrected for efficiencies, γ-ray angular distributions, conversion coefficients, and cascade feeding. The number of heavy ions, N_p, detected at a given angle was determined from the relevant energy cut of the singles heavy-ion spectrum, and the excitation probability was defined by $P_\gamma = N_\rho/N$.

The excitation functions for various states are displayed in Fig. 1, along with an example representative of results obtained in α-particle experiments.[1] The solid line in each figure represents the result expected for pure Coulomb excitation, calculated as described in Ref. 4, with use of the best experimental values of B(E2, $0 \rightarrow 2$) and B(E4, $0 \rightarrow 4$) and the rotational model. Calculations with the Winther-de Boer method[5] yield the same probabilities to $\pm 10\%$. Several things should be noted concerning these examples: (1) The probabilities agree well with Coulomb excitation calculations at low energies. (2) The interference effects are large. (3) In contrast to the usual α-particle results, there are a variety of constructive and destructive interferences in the regions where CNI first begins. (4) The sign, strength, and energy for onset and extrema of the interference are state dependent.

The general features of these data are explained by the simple model underlying the calculations of Ref. 4. To conserve space, we assume some familiarity with that model in the following discussion. The excitation probability for backward scattering from a deformed rotor can be written as

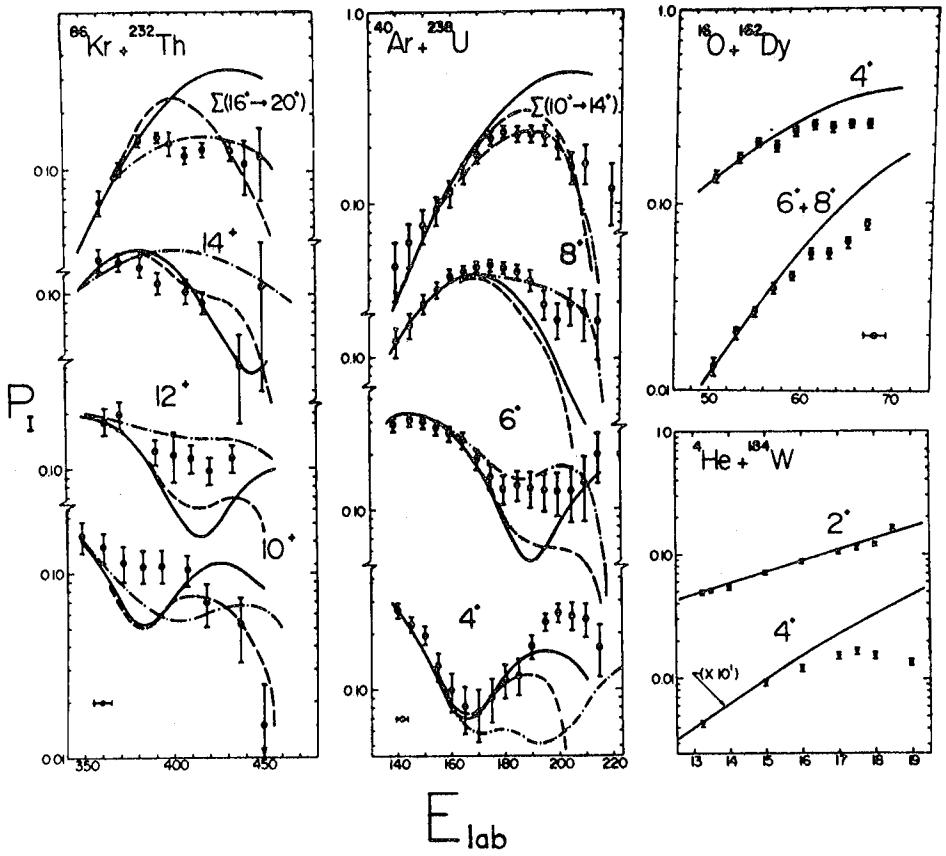

Fig. 1. Excitation functions in the CNI region. The solid line is a calculation for pure Coulomb excitation. ^{4}He data are from Ref. 1. The approximate energy uncertainty is indicated by the horizontal bars at the bottom corners. Dashed and dash-dotted lines are calculations using a nuclear potential described in Ref. 4. (XBL 7810-11914)

$$P \approx p_1 + p_2 + 2(p_1 p_2)^{1/2} \sin(\mathrm{Re}(\phi_2 - \phi_1)) \quad \text{("allowed states")} \quad (1)$$

$$P \approx p e^{-2\,\mathrm{Im}\phi} \quad \text{("forbidden states")} \quad (2)$$

where the three terms in Eq. (1) arise from the coherent contribution of two different initial rotor orientation angles for a particular state. The classical action in units of $\hbar$ is denoted by ϕ, and the lower-case p's are the purely classical probabilities for a given initial orientation. Only a single exponentially damped term contributes to P for classically forbidden states (the highest-spin states).

We assume that the nuclear interaction can be approximated by a smooth complex potential which is largely real in the surface region. Then, the initial effect of the potential is mainly confined to the phases of Eqs. (1) and (2), decreasing the real phase difference in Eq. (1), and increasing the imaginary phase of Eq. (2); with the small p's not affected very much. Therefore, in this region the effect of the CNI can be predicted from the effect of the nuclear potential on the sine term in Eq. (1), and the exponential damping factor in Eq. (2). Remembering that the oscillations in the pure Coulomb excitation probabilities for allowed states arise from the sine term and that the forbidden states (highest spins) are characterized by steeply rising excitation functions, the following general rule emerges: The initial Coulomb-nuclear interference will be constructive (destructive) if the excitation function for pure Coulomb excitation is approaching or at a minimum (maximum). Consulting Fig. 1, we note that this simple prediction holds for every case displayed except for the 4^+ state in the ^{40}Ar + ^{238}U reaction. This is probably associated with the interference beginning in this case at a higher energy (~195 MeV), where p_k's are also affected, and the conditions for the above rule are not fulfilled.

From the rule and Fig. 1 it is apparent why only destructive initial interferences are seen for α-particle rotational excitation of 2^+ and 4^+ states. For sub-barrier scattering, the monopole-quadropole interaction is not sufficient with α particles for either the 2^+ or 4^+ probability to have passed its first maximum, and the CNI is always destructive. That is, a critical value of the quadrupole coupling strength $\bar{q}_2$ is necessary for constructive initial interference when the simple rule applies. In practical terms, for well-deformed targets the Z of the projectile must exceed a value lying roughly in the region between Ne

and Ar projectiles, before the initial interference may be constructive. It follows that the seemingly different qualitative behavior of α-particle and ^{16}O CNI compared to heavier-particle CNI actually arises from the same physics. This does not preclude the possibility of quantitative differences, to be discussed shortly.

We emphasize that the simple rule discussed here becomes less valid for deeper penetration into the complex nuclear potential. In that case, one must rely on detailed calculations.[4] Experiments of this type are expected to be delicate probes of the surface nuclear potential, due to the sensitivity of inelastic excitation to the phases in Eqs. (1) and (2). Some preliminary calculations using a variety of potentials suggest the following: (1) Nuclear potentials determined from experiments in which elastic and inelastic components are not cleanly separated are not adequate to describe inelastic excitation in deformed nuclei. (2) The fact that these potentials fit some states but not offers suggests that all states are not equivalent for determining nuclear potentials, and that inelastic excitation may carry information about the nuclear potential beyond that contained in the elastic scattering. (3) The success of the experimental method described here, and the calculations of Ref. 4, demonstrate that it is now possible to probe the nuclear surface by studying excitation of collectively coupled states directly, rather than by approximating their effect on the elastic channel. In our opinion, this is necessary to describe properly the scattering of heavy ions from deformed nuclei.

Footnotes and References

*Condensed from Phys. Rev. Lett. 40(15), 1016 (1978).

†Present address: Department of Physics, University of Tennessee, Knoxville, Tennessee 37916.

‡Present address: Gesellschaft für Schwerionenforschung, Darmstadt, Germany.

§Present address: Université de Louvain, Louvain-la-Neuve, Belgium.

‖Oak Ridge National Laboratory, Oak Ridge, Tennessee 37830.

¶Department of Physics, University of Tennessee, Knoxville, Tennessee 37916.

1. I. Y. Lee et al., Phys. Rev. C 12, 1483 (1975) and references therein.

2. D. L. Hillis et al., Phys. Rev. Lett. 36, 304 (1976), and references therein.

3. C. E. Thorn et al., Phys. Rev. Lett. 38, 384 (1977).

4. M. W. Guidry et al., Nucl. Phys. A 274, 183 (1976).

5. A. Winther and J. de Boer, in Coulomb Excitations, K. Alder and A. Winther, eds. (Academic, New York, 1966), p. 303.

MULTIPLE BAND CROSSINGS IN ^{164}Er

N.R. Johnson,* D. Cline,† S.W. Yates,‡ F.S. Stephens, L.L. Riedinger,§ R.M. Ronningen‖

From the amassing experimental evidence it is now generally concluded that the "backbending" phenomenon is caused by the intersection of the ground state rotational band with a second rotational band possessing an appreciably larger moment of inertia. In the rotation-alignment model[1] the structure of this band corresponds to two quasiparticles whose angular momenta are aligned with the rotating core. Studies of the properties of both even- and odd-mass nuclei in the erbium region show behavior in reasonable agreement with predictions of the rotation-alignment model.[1] The rotation-alignment model predicts a series of rather similar rotation-aligned bands, which we shall call superbands. The structure of the superbands can be probed by studying their interactions with the ground, β- and γ-vibrational bands. Thus far, only the interaction of the lowest superband with the ground and β bands has been observed. The γ band would appear to be a better probe of the superbands since here one can study the interactions with both even and odd-spin states. In this work we present the first evidence for higher superbands, and also the first example of intersections between the γ band and these superbands.

A beam of 69.6-MeV ^{18}O ions from the Oak Ridge Isochronous Cyclotron was used to bombard a 2.4 mg/cm^2 metallic neodymium foil enriched to 96% in mass 150. Both γ-ray singles and γ-γ-time coincidence data (total of 3.5×10^7 coincidence events) were stored simultaneously in the experiment at a γ-ray resolution of 2.3 keV for 1.33 MeV. A level scheme which includes the positive parity states is shown in Fig. 1.

The plot of the experimental excitation energies versus I (Fig. 2a) cleary shows several intersecting rotational bands. To understand these results a calculation was made using typical parameters to illustrate the general features predicted by the rotation-alignment model.[1] Both zero and two-quasineutron configurations within

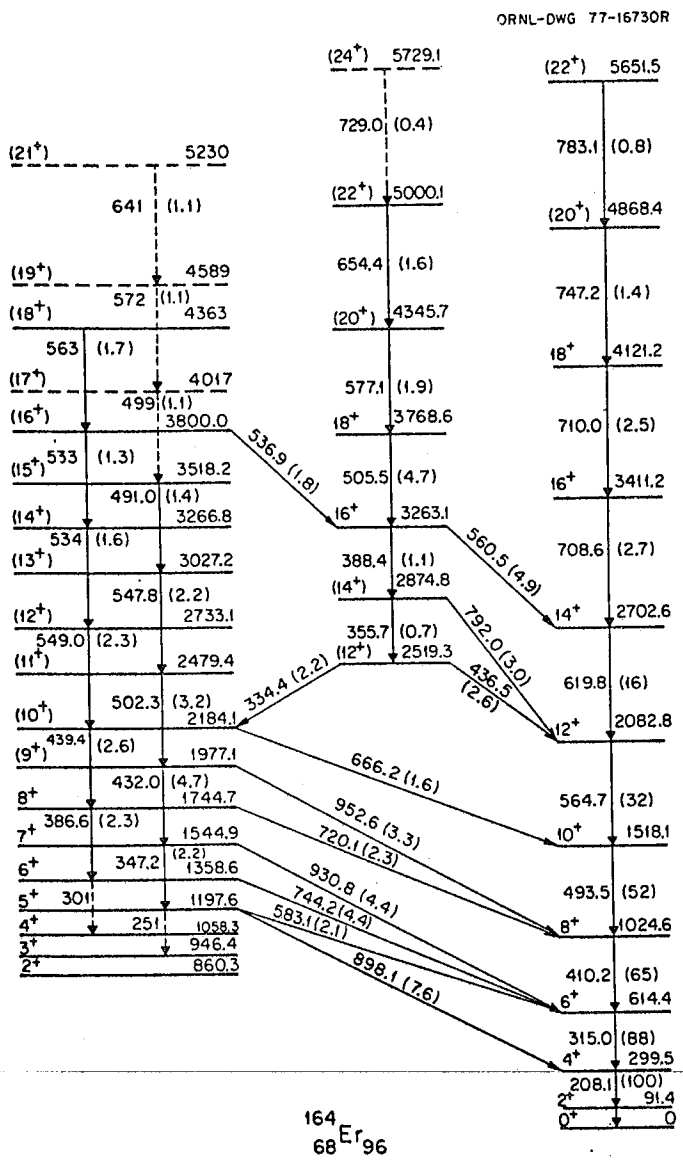

Fig. 1. Level scheme of ^{164}Er showing the ground band, the yrast superband and the γ-vibrational band populated in the $^{150}Nd(^{18}O, 4n)^{164}Er$ reaction. Shown on each transition is the energy and in parentheses, the relative intensity. Uncertanties range from less than 10% for the intensities of the stronger transitions up to 30-40% for some of the very weak ones. (XBL 789-11458)

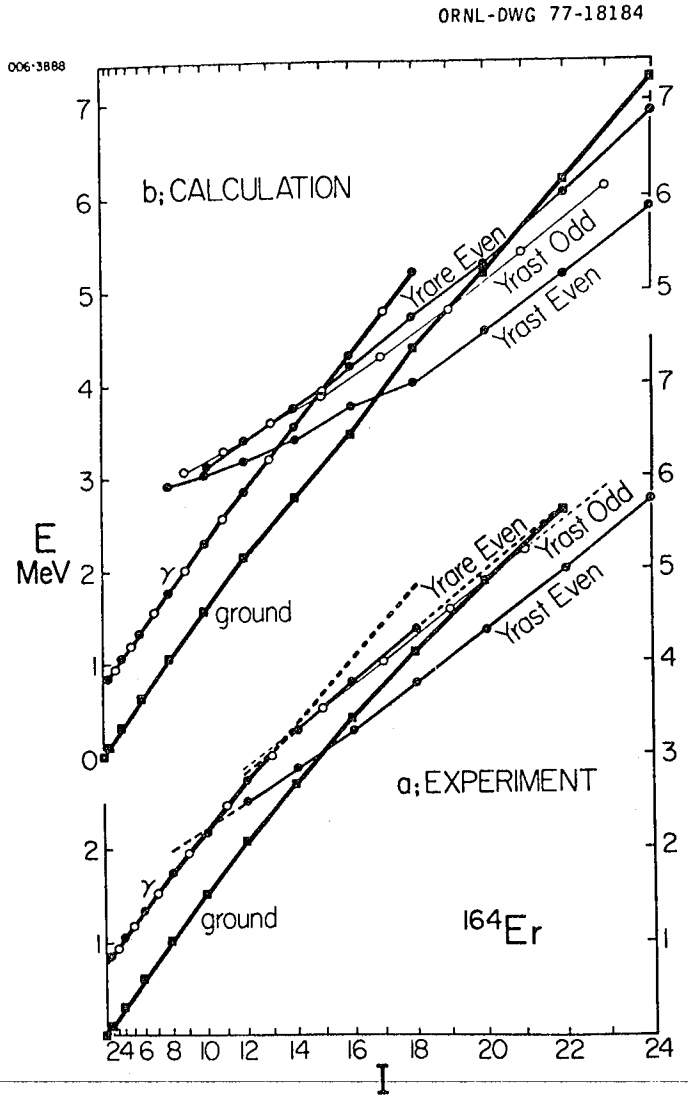

Fig. 2. Plot of the level excitation energies for various bands in ^{164}Er from a) experiment and b) the rotation-alignment model. The solid points correspond to even-spin states and the open circles to odd-spin states. (XBL 789-11460)

the complete $i_{13/2}$ orbit were included. The excitation energies from these calculations are shown in Fig. 2b. The γ band is shown for illustration but was not explicitly included in the calculations. The correspondence between experiment and theory is indeed striking.

The interaction between the intersecting bands is most clearly illustrated using the backbending plot of the data shown in Fig. 3. From the present data and previous work[2,3] it is found that near the intersection of the ground band and lowest yrast superband, both the level energies and γ-ray branching ratios indicate about 45 - 50 keV interaction matrix elements between these bands. A small value is typical of interaction matrix elements observed between both the ground and β bands with the lowest superband. Although the calculation predicts small interaction matrix elements, they still appear to be around a factor of two or three larger than this experimental value.

If a 45-keV interaction is used, then the unperturbed groundband energies lie on a smooth extension of the lines up through the 18^+ state and the yrast even-I superband energies likewise vary smoothly, as shown by the open circles in the left half of Fig. 3. However, the 20^+ and 22^+ members of the ground band are affected very little by this interaction. Interestingly, if we extrapolate the yrare even superband, as shown by the dashed line in Fig. 2a, and assume H_C = 45 keV,

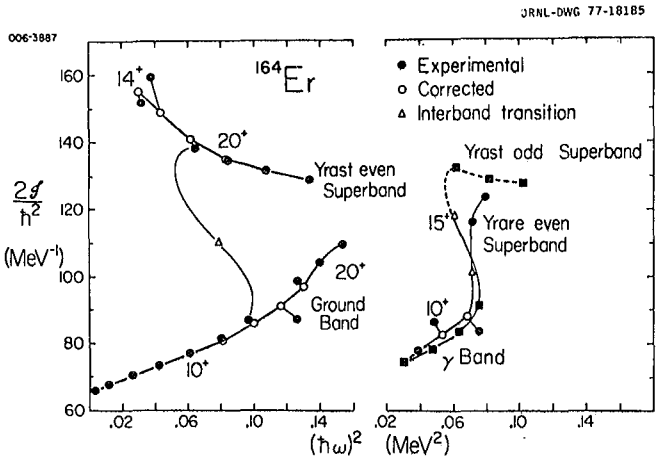

Fig. 3. Plot of $2\mathcal{J}/\hbar^2$ vs $(\hbar\omega)^2$ for members of the ground band, γ-vibrational band and superbands in ^{164}Er. The open circles on the ground and yrast even superbands are corrections for a 45-keV interaction matrix element. Open circles on the γ band result from a 25-keV shift in the 10^+_γ energy. The circles represent even spin and the squares odd-spin states. (XBL 789-11459)

then the upward kink in the ground band for the 20^+ and 22^+ states is largely removed.

On the right hand side of Fig. 3 we show a plot for the transitions in the γ-vibrational band. We have made a 25-keV shift in the 10^+_γ level energy, which produces equal but opposite shifts in the $10^+_\gamma \to 8^+_\gamma$ and $12^+_\gamma \to 10^+_\gamma$ transition energies. Such an energy shift is expected, due to a crossing of the γ band and the lowest (yrast) superband, provided there is an interaction matrix element around 45 keV. The odd-spin state energies in the γ band are smooth in this spin region without such a shift, providing the first direct evidence that the odd-spin states in the yrast superband lie considerably higher than the even-spin states.

In Fig. 3 backbends of both the even- and odd-spin members of the γ band are apparent around spins 13 and 14. A marked reversal in the odd-even staggering occurs through the backbend region in the γ band. This is rather clear even without the very tentative 17^+ and higher odd-spin states. The direction of this staggering is that the odd-spin states lie high relative to the even-spin ones below the backbend, and low after the backbend. The lower-spin behavior in the (true) γ band might be caused by the interaction with the β band, whereas the higher-spin behavior (in the superbands) is exactly what is expected from the calculations (Fig. 2). This reversal in the staggering is the strongest evidence that these higher superbands indeed correspond to the higher $i_{13/2}$ bands coupled to the ground band.

In summary, we have found additional even-spin and odd-spin superbands lying above the well known superband which produces the backbend for the yrast states. We have observed the intersection of the γ band with all three superbands and this provides evidence that all these superbands consist of two quasineutron $i_{13/2}$ bands coupled to the quasiparticle vacuum (ground state).

References

*Oak Ridge National Laboratory, Oak Ridge, Tennessee 37830.

†University of Rochester, Rochester, NY 14627.

‡University of Kentucky, Lexington, KY 40506.

§University of Tennessee, Knoxville, TN 37916.

‖Vanderbilt University, Nashville, TN 37207.

1. F. S. Stephens and R. S. Simon, Nucl. Phys. A 183, 257 (1972).

2. I. Y. Lee, D. Cline, R. S. Simon, P. A. Butler, P. Colombani, M. W. Guidry, F. S. Stephens, R. M. Diamond, N. R. Johnson and E. Eichler, Phys. Rev. Lett. 37, 420 (1976).

3. N. R. Johnson, S. W. Yates, R. M. Ronningen, R. D. Hichwa, L. L. Riedinger, and A. C. Kahler, Bull. Am. Phys. Soc. 21, (8), 984 (1976).

153 MeV ^{6}Li SCATTERING TO ISOSCALAR GIANT QUADRUPOLE RESONANCES*

K.T. Knöpfle,† G.J. Wagner,† P. Doll, D.L. Hendrie, and H. Wieman

Inelastic ^{6}Li scattering on ^{12}C, ^{14}N, ^{16}O, ^{40,44,48}Ca, ^{90}Zr, and ^{118}Sn has been studied using the 153-MeV ^{6}Li beam of the LBL 88-inch cyclotron. Spectra (Fig. 1) taken with dE-E telescopes clearly show in all nuclei, except ^{12}C,[1] the existence of an isoscalar giant resonance (GR) the location of which agrees with that of the isoscalar giant quadrupole resonance (GQR) as identified by inelastic α scattering.

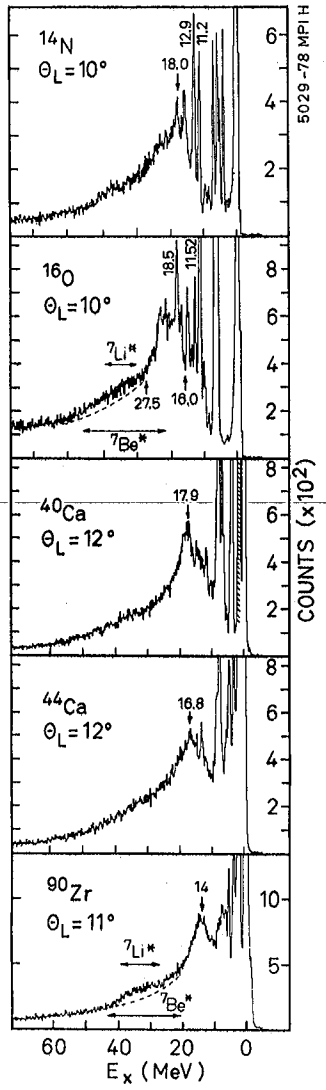

Fig. 1. Spectra of ^{6}Li particles scattered inelastically by ^{14}N, ^{16}O, ^{40,44}Ca and ^{90}Zr at 153-MeV incident energy. (XBL 789-11112)

Compared to other A≤4 hadron scattering data these spectra, however, reveal a strongly improved peak to continuum ratio in the GR region[2] and the shape of the continuum resembles that observed in heavy-ion scattering.[3] The experimental angular distributions of the GR's show a distinct diffraction pattern which is much better developed than at E(^{6}Li) = 74 MeV[4] and which agrees well with L = 2 DWBA fits. Centroids and widths of the up-to-now unexplored GQRs in ^{44,48}Ca exhibit a most interesting behavior: the GQR centroid energy ⟨E_x⟩ decreases much more quickly from ^{40}Ca (⟨E_x⟩ = 17.9 MeV) to ^{44}Ca(⟨E_x⟩ = 16.8 MeV) than expected (~$A^{-1/3}$) and the width increases from 3.4 MeV to about 5.2 MeV. In ^{48}Ca, however, the centroid energy and the width are nearly identical with those in ^{40}Ca.

All spectra exhibit additional broad structures around E_x ~ 30 to 40 MeV which fall within the kinematic limits (arrows in Fig. 1) of the [^{6}Li,^{7}Li* (7.5, ~9.6 MeV) → ^{6}Li+n][4] and [^{6}Li,^{7}Be* (7.2, ~9.3 MeV) → ^{6}Li+P] break up processes.

Figure 2 shows a ^{24}Mg(^{6}Li,^{6}Li') spectrum taken at 4.4° with the magnetic spectrograph in comparison with ^{24}Mg(α, α') data[5] (inset) after subtraction of a large α-continuum. The good agreement of both spectra confirms the conclusion from the data of Ref. 5, i.e., the fact of an extremely strong splitting of the giant quadrupole strength in ^{24}Mg.

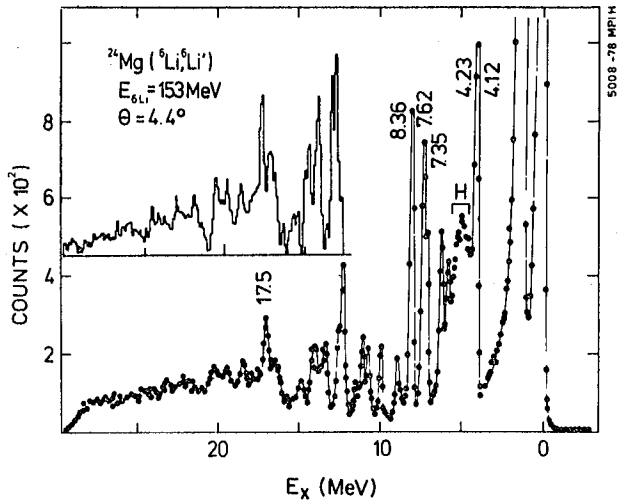

Fig. 2. The ^{24}Mg(^{6}Li,^{6}Li') spectrum taken at 4.4° with the magnetic spectrograph, compared with ^{24}Mg(α,α') data[5] (inset) after subtraction of a large α-continuum. (XBL 789-11113)

Footnotes and References

*Contribution to the Intern. Conf. on Nuclear Interactions, Canberra, Australia, 1978.

†Max-Planck-Institut für Kernphysik, 69 Heidelberg, Germany.

1. Knöpfle, K. T., et al., Phys. Lett. B 64, 263 (1976).

2. Gils, H. J., et al., Phys. Lett. B 68, 427 (1978).

3. Buenerd, M., et al., Phys. Rev. Lett. 40, 1482 (1978).

4. Pardo, R., et al., Phys. Lett. B 71, 301 (1977).

5. Youngblood, D. H., et al., Phys. Rev. C 15, 1644 (1977).

THE NEW BERKELIUM ISOTOPE—^{242}Bk

K.E. Williams and G.T. Seaborg

A new isotope of berkelium, ^{242}Bk, has been produced with a cross section of ~10 μb in reactions of boron on uranium and nitrogen on thorium. It decays by electron capture with a half-life of 7 ± 1.3 minutes. The alpha branching ratio for this isotope is less than 1% and for spontaneous fission is less than 0.03%.

Evidence for a short-lived (<10 min) component in the curium Kα1 and Kα2 x rays was found in the first experiment, ^{235}U(^{11}B,xn)$^{246-x}$Bk, even though the time from the end of bombardment to the detector was ~25 minutes. Subsequent bombardments using a shorter chemistry confirmed this component as having a $t_{1/2}$ = 7±1.3 minutes. A typical decay curve is shown in Fig. 1. The short-lived component stands out quite strongly and is easily resolved from the longer-lived activity of ^{243}Bk ($t_{1/2}$ = 4.5 hours).

The excitation function for this activity from ^{11}B + ^{235}U, shown in Fig. 2, agrees quite well in peak energy and width (FWHM = 5 MeV) with the Alonso calculations[1] for the 4n reaction. The experimental cross section of ~10 ± 2 μb, however, is approximately a factor of 20 below that calculated.

As a further check on the mass number and the cross section for production of this 7-minute activity, ^{232}Th was bombarded with ^{15}N. Once more, the experimental FWHM (10.1 MeV) and peak energy agree well with the calculations for the 5n reaction, but the cross section (9 ± 1 μb) is again ~25 times lower than predictions.

One of the best ways to confirm the mass number (and Z) of an isotope is to identify positively its daughter in the original parent chemical fraction. While long term alpha counting of the various berkelium fractions gave hints (i.e., 7 counts expected in 4 days, 6 seen) of the presence of ^{242}Cm, the electron capture daughter of ^{242}Bk, it was decided to milk a number of separate bombardments for the ^{242}Cm daughter.

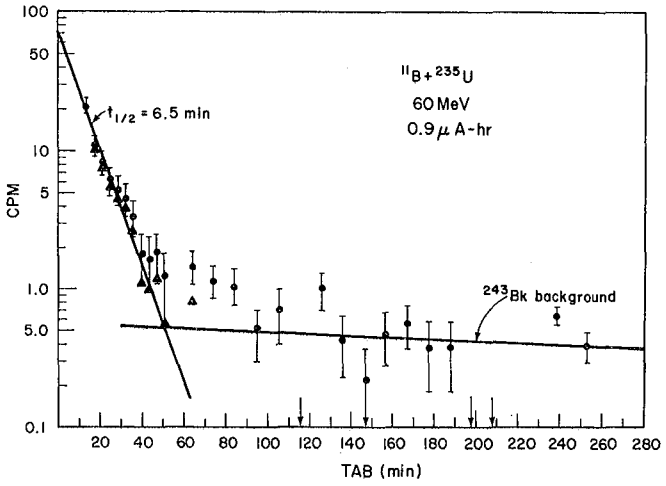

Fig. 1. Decay of curium Kα1 and the Kα2 x rays from a berkelium sample from the reaction ^{11}B + ^{235}U. (XBL 786-1078)

A total of twelve 25-minute bombardments was carried out using ^{11}B on ^{235}U at 59.5 MeV. Berkelium was immediately separated (~4.5 minutes from end bombardment) from the dissolved aluminum catcher foil and the final berkelium fractions for each run were pooled. A day or so later, ^{244}Cm tracer was added and a curium fraction was removed from this combined berkelium fraction. From the amount of ^{242}Cm present, a cross section for ^{242}Bk of 9.3 ± 1.5 μb was found, in excellent agreement with the direct measurement of 10 ± 2 μb.

Table 1 lists the various target/projectile combinations and the beam energies used to produce ^{242}Bk as well as the pxn and αxn products, curium and americium, respectively, and Table 2 summarizes the cross sections observed.

Since it now appeared that the cross sections for the compound nucleus, xn reactions, were indeed much lower than expected, the question was raised as to what products were being produced It was decided to examine the pxn and αxn products, curium and americium respectively, produced directly in the same reaction and at the same energies used to produce ^{242}Bk.

In 1967 Fleury et al.[2,3] measured the production of ^{240}Cm and ^{242}Cm from $^{10,11}B$ on ^{238}U. They interpreted the excitation functions

Table 1. Summary of bombardments.

System	Reaction	Lab Energy (MeV)	Product(s)
$^{10}B + ^{238}U$	5n,4n	60	$^{243,244}Bk$
$^{10}B + ^{238}U$	6n	67	^{242}Bk
	p7,5n	67	$^{240,242}Cm$
$^{10}B + ^{235}U$	4n	52-60	none observed
$^{11}B + ^{235}U$	4n	55-65	^{242}Bk
	4n	60	milked ^{242}Cm
	p5,3n	60	$^{240,242}Cm$
	α4,3,2n	60	$^{238,239,240}Am$
$^{14}N + ^{232}Th$	4n	77	^{242}Bk
	p5,3n		$^{240,242}Cm$
	α2n		^{240}Am
$^{15}N + ^{232}Th$	5n	76-93	^{242}Bk

Table 2. Yield of pxn and αxn products.

Target/ Projectile	Energy (MeV)	Product	Reaction	Cross Section
$^{11}B + ^{235}U$	60	^{242}Bk	4n	10 μb
		^{243}Bk	3n	1 μb
		^{242}Cm	p3n; $^{242}Bk \xrightarrow{EC}$ $^{242}Am \xrightarrow{\beta^-}$	78 μb
			p3n; $^{242}Am \xrightarrow{\beta^-}$	69 μb
		^{240}Cm	p5n	0.035 μb
		^{240}Am	α2n	1500 μb
		^{239}Am	α3n	410 μb
		^{238}Am	α4n	<1.6 μb
$^{10}B + ^{238}U$	67	^{242}Bk	6n	8.9 μb
		^{242}Cm	p5n; $^{242}Bk \xrightarrow{EC}$ $^{242}Am \xrightarrow{\beta^-}$	60 μb
			p5n; $^{242}Am \xrightarrow{\beta^-}$	51 μb
		^{240}Cm	p7n	0.12 μb
$^{14}N + ^{232}Th$	77	^{242}Bk	4n	0.48 μb
		^{242}Cm	p3n; $^{242}Bk \xrightarrow{EC}$ $^{242}Am \xrightarrow{\beta^-}$	1.00 μb
			p3n; $^{242}Am \xrightarrow{\beta^-}$	0.52 μb
		^{240}Cm	p5n	0.055 μb
		^{240}Am	α2n	200 μb

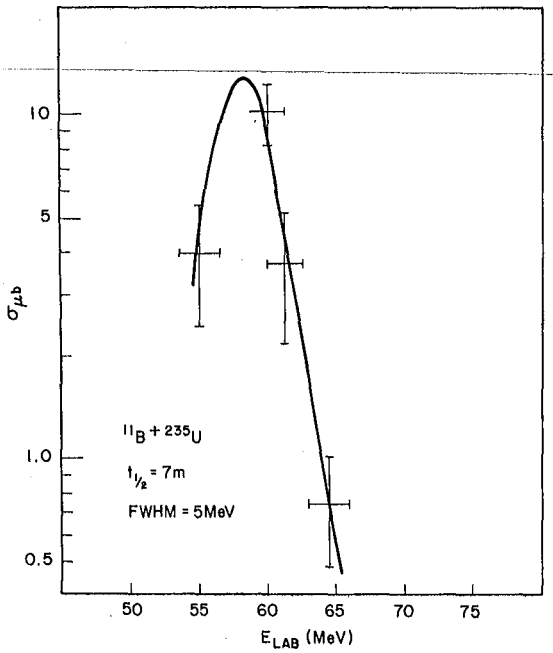

Fig. 2. Experimental excitation function for the reaction $^{11}B + ^{235}U$. The solid curve represents the Alonso-calculated cross sections lowered by approximately a factor of 25.
(XBL 786-9223)

to be due to a compound nucleus mechanism. Presumably, ^{242}Bk and ^{240}Bk were produced which then decayed to their curium daughters (prior to the chemical separations). The cross sections they reported were significantly higher than those measured in this work for ^{242}Bk. It did not seem reasonable that cross sections as high as several hundred microbarns for ^{242}Cm could have come only from the decay of ^{242}Bk. Indeed, this work has shown that such is not the case. Only a small contribution to the curium cross section comes from the decay of berkelium. The primary yield of ^{242}Cm (and presumably ^{240}Cm) has been shown to be due to either direct production of ^{242}Cm (^{240}Cm) or to the evaporation of a proton and 3(5) neutrons from the compound nucleus. The latter seems extremely unlikely due to the high Coulomb barrier to charged particle emission from a nucleus with a Z as high as 97.

This work further demonstrates the high yield of pxn and αxn products in heavy ion reactions in the actinide region. The reaction showing the highest yield is the α2n followed by the α3n. Again, it is unlikely that these products result from alpha evaporation, but rather, they are most probably the result of direct formation. To this effect, Hahn et al.[4] have demonstrated that the αxn products from ^{12}C + ^{239}Pu are indeed the result of a transfer mechanism rather than a compound nucleus (with subsequent particle evaporation) mechanism. They found, as well, in agreement with the present work, that the yield of α2,3n products are equal to or higher than the 2-4n compound nucleus product. Actually, this is not too surprising since the probability of neutron emission to fission (Γ_n/Γ_f) is so highly Z dependent. The pxn and xn products have Z's lower than the xn products and, therefore, higher Γ_n/Γ_f ratios. While more compound nuclei may be formed initially, few of them are able to survive fission competition due to their lower Γ_n/Γ_f ratios.

These findings point out the dangers in assuming that the yields of αxn and/or pxn products in the actinide region are negligible. While charged particle evaporation most certainly is of little consequence, one cannot neglect the production of the same products by a direct mechanism. Before a new element or isotope may be claimed, therefore, it must be shown that such directly produced products are not responsible for the new observations.

References

1. J. R. Alonso, Gmelin, Handbuch der Anorganischen Chemie, Band 7b, Teil A1 II. 28 (1973).

2. A. Fleury, F. Minvielle, G. N. Semonoff, Phys. Lett. B 24, 576-577 (1967).

3. A. Fleury and F. Hubert, J. de Physique 10, 855-868 (1970).

4. R. L. Hahn, P. F. Dittner, K. S. Toth and O. L. Keller, Phys. Rev. C 10, 1889-1903 (1974).

THE PRODUCTION OF TRANSPLUTONIUM ELEMENTS IN HEAVY ION REACTIONS WITH URANIUM TARGETS

P.A. Baisden and G.T. Seaborg

Experiments have continued to investigate the possibility that deep inelastic collisions may result in the synthesis of very heavy elements in heavy ion reactions with heavy targets. The extent of mass transfer from the projectile to the target nucleus was studied by radiochemically measuring the production of transplutonium elements in the reaction of ^{40}Ar, ^{48}Ca, ^{86}Kr and ^{136}Xe with thick, enriched ^{238}U targets. The production and survival of isotopes of Es, Fm and Md were of particular interest since their presence would indicate that fairly large mass transfers had occurred at relative low excitation energies.

After irradiation chemical separations were performed on the targets which included standard cation and anion exchange column and precipitation techniques. The procedure, which has been previously reported,[1] included steps for the rapid removal of α-emitting nuclides below the target which were formed either directly in the reaction or were present as a result of decay chains. In some cases an α-hydroxyisobutyrate cation column was added which served to separate Es, Fm and Md. A summary of experimental conditions is given in Table 1.

The cross sections for the isotopes observed in these reactions are given in Table 2. Also listed in the table are upper limits which were calculated for several short-lived transcalifornium isotopes. Within experimental error the cross sections obtained for the curium isotopes and ^{246}Cf for the ^{40}Ar and ^{136}Xe reactions agree with those reported by Wolf et al.[2] Even though the incident energy in the ^{40}Ar + ^{238}U reaction carried out by Wolf et al. was some 50 MeV lower than that used in our experiments, we did not see any notable difference in the measured cross sections. A similar observation can be made when comparing the cross section for the production of ^{254}Cf in the reaction of ^{238}U with ^{136}Xe

Table 1. Summary of irradiations with ^{238}U

Projectile	E_L(lab) MeV	V_{cb}(lab) MeV	Total Beam Particles	Range (mg/cm^2)
^{136}Xe	1150	707	3.2×10^{15}	20
			8.3×10^{14}	
^{86}Kr	731	432	7.2×10^{15}	23
			1.3×10^{15}	
^{48}Ca	404	226	1.2×10^{15}	30
^{40}Ar	340	202	3.4×10^{15}	28

ions at three different bombarding energies as shown in Table 3.

The calculated upper limits for the short-lived, high Z transfer products are consistent with cross sections or upper limits reported for the longer-lived isotopes by Wolf et al. for the $^{136}Xe + ^{238}U$ reaction at the same bombarding energy. In the same reaction at an incident energy of 7.5 MeV/A, no isotopes with Z > 98 were observed by Kratz et al. with beam intensities of the order of 10^{12} particles/sec.[5] With increasing number of transferred protons, the cross sections for these transfer products fall off quite rapidly. Our inability to observe products that require a transfer of greater than six protons appears to be limited by low cross sections and the available beam intensity.

Table 3. $^{136}Xe + ^{238}U$ reaction to produce ^{254}Cf

	σ	MeV	MeV/A	Reference
^{254}Cf	2×10^{-34}	840	6.2	3
^{254}Cf	6×10^{-35}	1020	7.5	4
^{254}Cf	1.7×10^{-34}	1130	8.3	2

Qualitatively in the context of a transfer reaction, the observed decrease in cross section with increasing ΔZ above the target can be understood in terms of a number of factors. First, from counter-telescope studies of heavy ion reactions it has been shown that the probability of charge (mass) transfer decreases with increasing proton transfer.[6] It has been further shown that the transfer of charge and the dissipation of the initial kinetic energy occur simultaneously. In the language of a diffusion model, mass transfer and energy dissipation are relaxation processes with the mass transfer being the slower of the two. Thus on the average a product which is formed as a result of a large proton transfer will be produced in a highly excited state. The probability of its survival is expected to be diminished due to increased fission competition, particularly if the final product is a very heavy element such as an actinide.

A direct comparison of our measured cross sections for the ^{86}Kr induced reaction and those of Wolf for the ^{84}Kr induced reaction is not possible due to the differences in the mass-to-

Table 2. Cross sections for production of selected transplutonium elements

Isotope	$T_{1/2}$	^{40}Ar (cm^2)	^{48}Ca (cm^2)	^{86}Kr (cm^2)	^{136}Xe (cm^2)
^{240}Cm[a]	27 d	$5.1\pm0.3 \times 10^{-31}$	$2.1\pm0.3 \times 10^{-31}$	$6.4\pm0.2 \times 10^{-31}$	$3.7\pm0.3 \times 10^{-32}$
^{242}Cm	163 d	$1.95\pm0.04 \times 10^{-29}$	$4.7\pm0.5 \times 10^{-30}$	$8.53\pm0.04 \times 10^{-30}$	$2.3\pm0.1 \times 10^{-30}$
243-244Cm	24 y	$2.5\pm0.3 \times 10^{-29}$	$4.0\pm0.4 \times 10^{-29}$	$1.9\pm0.3 \times 10^{-29}$	$6.0\pm0.3 \times 10^{-30}$
^{246}Cf[a]	36 h	$1.8\pm0.3 \times 10^{-32}$	$1.5\pm0.6 \times 10^{-32}$	$3.0\pm0.4 \times 10^{-32}$	$8.9\pm0.8 \times 10^{-33}$
^{253}Es	20.5 d	$<1 \times 10^{-32}$	$<4 \times 10^{-32}$	$<3 \times 10^{-32}$	$<2 \times 10^{-33}$
^{254m}Es	39 h	$<9 \times 10^{-34}$	$<4 \times 10^{-33}$	$<2 \times 10^{-33}$	$<4 \times 10^{-33}$
^{256}Es	37.6 h	$<1 \times 10^{-34}$	$<5 \times 10^{-34}$	$<4 \times 10^{-34}$	$<6 \times 10^{-34}$
^{254}Fm	3.24 h	$<2 \times 10^{-34}$	$<6 \times 10^{-34}$	$<5 \times 10^{-34}$	$<9 \times 10^{-34}$
^{256}Fm	2.6 h	$<8 \times 10^{-34}$	$<3 \times 10^{-34}$	$<3 \times 10^{-34}$	$<5 \times 10^{-34}$
^{256}Md	77 m	$<1 \times 10^{-34}$	$<5 \times 10^{-34}$	$<4 \times 10^{-34}$	$<1 \times 10^{-33}$

(a) Isotope identification checked with half-life measurement. Upper limits were calculated assuming 1 atom produced.

charge ratios for the respective composite systems. On the basis of counter studies of deep inelastic collisions it has been shown that the A/Z ratio is equilibrated on a very fast time scale, much faster than the time required for mass transfer. As a result, the A/Z ratio of the composite system is reflected in the final products. Thus a reaction with a high A/Z ratio favors the production of more neutron rich products with the other factors, such as excitation energy and angular momentum, being the same. With respect to the A/Z ratios, the reactions we have studied fall into two classes. The first class, which represents relatively low mass to charge ratios, includes the ^{40}Ar and ^{86}Kr induced reactions. For these reactions the maxima in the measured isotopic distribution for the curium isotopes occur roughly at the same mass number. For the second class, due to the relatively higher A/Z values for the ^{48}Ca and ^{136}Xe induced reaction, the isotopic distribution for curium isotopes are displaced toward higher mass number.

On the basis of this work it seems unlikely that the multi-nucleon transfer process will lead to the production of new elements with detectable cross sections with A $\leq$ 136 projectiles on uranium targets. This is a direct consequence of the magnitude of energy transfer required for the necessary mass transfer and the high fissility of these elements. However, in principle lower excitation energies can be achieved in deep inelastic collisions, as opposed to compound nucleus reactions, due to a finite probability that in some collisions sufficient mass transfers will occur in which only a small amount of the initial kinetic energy is damped into internal degrees of freedom. However, the consequence of angular momentum may considerably reduce the probability of survival even if the product is formed in a relatively cold state.

References

1. P. A. Baisden, K. E. Thomas, and G. T. Seaborg, Lawrence Berkeley Laboratory Report, LBL-7585, p. 38 (1976).

2. K. L. Wolf, J. P. Unik, E. P. Horwitz, C. A. A. Bloomquist, and W. Delphin, Abstract, American Physical Society Meeting (Chicago 1977), 25, 7.

3. G. N. Flerov, and Y. T. Oganessian, J.I.N.R. E7, 6838 (1972).

4. H. Gäggeler, W. Brüchle, M. Schädel, and N. Trautmann, GSI Report (1977).

5. J. V. Kratz, M. Schädel et al., Phys. Rev. Lett. 41, 469 (1978).

6. J. R. Huizenga, J. R. Birkeland, W. U. Schroder, K. L. Wolf, and V. E. Viola, Phys. Rev. Lett. 37, 885 (1976).

ISOMERIC STATES IN ^{212}Bi*

P. W. Baisden, R.E. Leber, M. Nurmia, J.M. Nitschke, M. Michel, and A. Ghiorso

During a search for superheavy elements via the reaction of ^{48}Ca with ^{248}Cm we discovered several alpha lines around 10 MeV with a half-life of 25 ± 1 min.[1] In addition, a line at 11.66 MeV was observed and found to contain a longer-lived component of 9 ± 1 min in addition to the expected 45-sec half-life of ^{212m}Po.[2] Both activities could be produced by the bombardment of ^{208}Pb with ^{40}Ar, and also from ^{238}U with a variety of projectiles such as ^{40}Ar, ^{48}Ca and ^{136}Xe.

A spectrum of a source obtained by irradiating ^{238}U with ^{40}Ar followed by electrolytic dissolution and extraction of the Bi-Po-At fraction into diphenylthiocarbazone-CCl_4 at pH 2.5 is shown in Fig. 1; the doublet at 6.3 MeV was found to decay with the same 25-min half-life as the group at 10 MeV.

The 25-min activity was found to follow the chemistry of Bi through the technique of residue adsorption or chemisorption[3] and its mass number was found to be 212 in three isotope

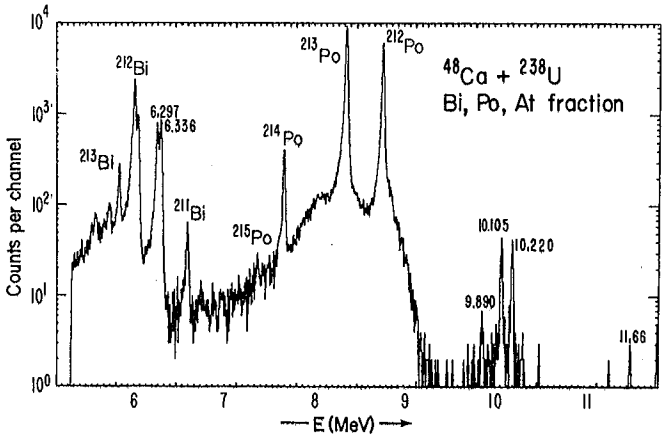

Fig. 1. Alpha spectrum of the Bi, Po and At fraction from ^{48}Ca + ^{238}U. Geometry 20%, resolution, FWHM = 25 keV. (XBL 783-332)

separation runs made with chemically separated samples using the LBL Isotope Separator. Our studies indicate that this isomeric state, ^{212m1}Bi, decays both by alpha emission to ^{208}Tl and by beta emission to excited levels in ^{212}Po, followed by the emission of "long-range" alpha particles to the ground state of ^{208}Pb.

The fact that an isomeric state should exist in ^{212}Bi is suggested by analogy with the 9$^-$ isomeric state in ^{210}Bi.[4-7] The configuration of ^{212}Bi, $(\pi h_{9/2})(\nu g_{9/2})^3$, differs from that of ^{210}Bi, $(\pi h_{9/2})(\nu g_{9/2})$, in that ^{212}Bi has two additional $g_{9/2}$ neutrons. Shell-model studies have been carried out on the ground state and low-lying states of the configuration $(\pi h_{9/2})(\nu g_{9/2})$ of ^{210}Bi by Kim and Rasmussen.[8] Their calculations, which are in excellent agreement with the experimental observations of Motz et al.,[9] indicate the level responsible for the isomeric state is a 9$^-$ state located at 268 keV. Therefore, we suggest an analogous 9$^-$ spin for the isomeric state in ^{212m1}Bi.

Detailed shell-model calculations of the excited levels of ^{212}Po have been made by several authors. In one such calculation Glendenning and Harada, allowing for configuration mixing, predicted a state with $J^\pi = 18^+$ to explain the 45-second ^{212m}Po.[10] Their results also indicate the possibility of another isomeric state J = 10-12 at an excitation energy of 1.2 MeV. On the other hand, calculations by Auerbach and Talmi, assuming no configuration mixing, indicate a spin of 16 for ^{212m}Po.[11] Likewise, their calculations also suggest a second isomeric state, however, of lower spin, around J = 8-10.

It is reasonable to assume that since the first excited state of ^{208}Pb is 2.6 MeV above the ground state, the 10-MeV group decays to the ground state of ^{208}Pb. This would place the levels in ^{212}Po responsible for the 10-MeV transitions at an excitation energy of 1.1 to 1.5 MeV. These levels are consistent with either of the shell-model calculations mentioned.

As a test for the assumption of a 9$^-$ isomeric level in ^{212}Bi, one would expect a log ft value of 6-9 (first forbidden transition) for a beta decay from a 9$^-$ to either an 8$^+$ or 10$^+$ state in ^{212}Po. In view of the possibility of gamma decay the ratio of alpha transitions from the 9$^-$ state yields a lower limit of 7% for the beta branch to ^{212}Po. The resulting upper limit of 6.8 for the log ft value is then compatible with the spin assignment of 9$^-$ for ^{212m1}Bi.

We were unable to obtain a definite elemental or mass assignment of the 9-min activity in the chemisorption and isotope separation experiments but we did find out that it is coprecipitated with CuS from an acidic solution. Since our ^{48}Ca + ^{248}Cm work showed that it is genetically related to the 45-sec ^{212m}Po, it could, in principle, be an isomer in ^{212}At, ^{212}Po or ^{212}Bi. The first possibility was eliminated when we observed that we could volatilize the ^{211}At-^{211}Po activity away from our sources while the 9-min and 25-min activities remained.

In their discovery work on ^{212m}Po, Perlman et al.[2] irradiated a lead oxide target with 116-MeV ^{11}B ions and separated a Po fraction by a combination of volatilization and cation exchange. They found that ratio of the ^{211}Po and ^{212m}Po activities was not changed by the chemical procedure if the latter was assumed to have a half-life of 45 seconds; this apparently rules out the possibility that the 9-min ute activity is another isomer in ^{212}Po feeding the 45-second state. It is also difficult to postulate a second isomer in ^{212}Po that would decay into the known ^{212m}Po and yet have the required long half-life against alpha decay.

The remaining possibility, that the 9-min activity is another isomeric state in ^{212}Bi which beta decays into ^{212m}Po, appears quite plausible. If one breaks the pair of $g_{9/2}$ neutrons in ^{212}Bi and recouples the four particles outside the ^{208}Pb core to maximum spin, a 15$^-$ state is obtained.[12] We consider this state in ^{212}Bi the most likely explanation of the 9-min activity; a consequence of this assignment would be that the spin of ^{212m}Po would be 16 as suggested by Auerbach and Talmi.[11] A decay scheme of the two isomers is shown in Fig. 2.

In conclusion we have shown evidence for the existence of two isomeric states in ^{212}Bi. Since

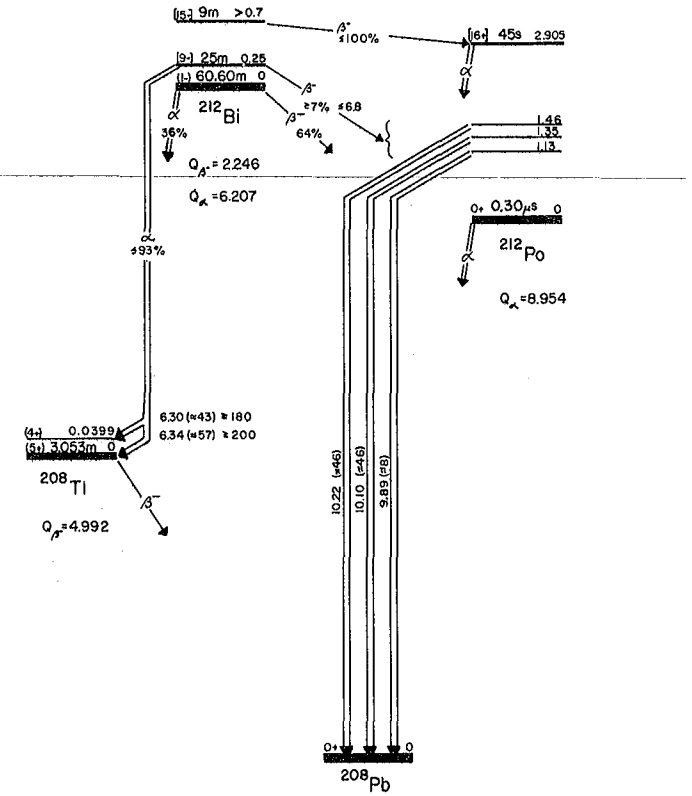

Fig. 2. Tentative decay scheme for isomeric states in ^{212}Bi. Relative alpha intensities are given in parentheses after the alpha energies. Other pertinent information shown, which was not explicitly determined in this work, was taken from Ref. 13. (XBL 783-330)

these isomers are made in a variety of heavy reactions with heavy targets, the high energy alpha particles associated with their decay may be present in experiments aimed at the synthesis of superheavy elements. The possibility is accentuated by the fact that Bi is a homolog of element 115 and will follow the chemistry of the eka-Pb group of the superheavy elements.

Acknowledgments

The authors would like to thank Dr. R. Eggers for his help in the more recent phases of this work. We would also like to thank Mrs. Diana Lee and Miss Bonner Nishida for their help with the data acquisition.

Footnote and References

*Condensed from LBL-7708; also, published in Phys. Rev. Lett. 41, 738 (1978).

1. A. Ghiorso, 173rd American Chemical Society, National Meeting (New Orleans, Louisiana, March 1977).

2. I. Perlman, F. Asaro, A. Ghiorso, A. Larsh and R. Latimer, Phys. Rev. 127, 917 (1962).

3. H. W. Kirby, J. Inorg. Nucl. Chem. 35, 2043 (1973).

4. J. R. Erskine, W. W. Buechner and H. A. Enge, Phys. Rev. 128, 720 (1962).

5. E. H. Spejewski, Nucl. Phys. A 100, 236 (1967).

6. R. C. Lange, G. R. Hagee and A. R. Campbell, Nucl. Phys. A 133, 273 (1969).

7. D. G. Tuggle, Ph. D. Thesis, University of California, LBL-4460.

8. Y. E. Kim and J. O. Rasmussen, Nucl. Phys. 47, 184 (1963).

9. H. T. Motz, E. T. Jurney, E. B. Shera and R. K. Sheline, Phys. Rev. Lett. 26, 854 (1971).

10. N. K. Glendenning and K. Harada, Nucl. Phys. 72, 481 (1965).

11. A. Auerbach and J. Talmi, Phys. Lett. 10, 297 (1964).

12. This was also independently pointed out to us by C. M. Lederer, Lawrence Berkeley Laboratory.

13. C. M. Lederer, J. M. Hollander and I. Perlman, eds., Table of Isotopes, 7th Edition (John Wiley and Sons, Inc., New York, 1978).

PRODUCTION OF ^{235m}Pu FISSION ISOMER AND ^{234}Pu IN THE REACTIONS α + ^{233}U and ^{3}He + ^{234}U

L.P. Somerville, M.J. Nurmia, A. Ghiorso and G.T. Seaborg

The known spontaneous fission isomer ^{235m}Pu has been produced in bombardments of ^{3}He + ^{234}U at the 88-inch cyclotron. An annular detector concentric with the 3/16-in. diameter target and located 4 mm downstream from the target was used to detect spontaneous fissions from recoils decaying in flight (Fig. 1). By fitting the calculated radial track distributions, assuming compound nuclear recoil velocity, we are able to estimate, very roughly, the half-life for this isomer to be 23 ns from the α + ^{233}U bombardment and 10-27 ns from the ^{3}He + ^{234}U bombardments. The cross section forproduction of this isomer is ~137 nb for 36.1 MeV α + ^{233}U, assuming a calculated 15% geometry for detection of a spontaneous fission event. This result is within 10% of previous work.[1] In a calibration experiment we had produced the well-known 3.8-ns fission isomer ^{240m}Pu in the reaction ^{238}U(α,2n) ^{240m}Pu and found excellent agreement between the calculated and observed radial track distribution and number of events.

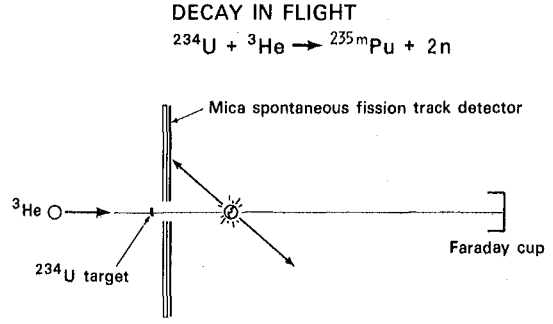

Fig. 1. Experimental setup for measuring spontaneous fissions from recoils decaying in flight. (XBL 784-689)

An excitation function (Fig. 2) has been measured for the reaction 21.5-31.4 MeV ^{3}He + ^{234}U (99% pure) with σ = 46 nb at the maximum. Identification of this activity as ^{235m}Pu in the reaction ^{3}He + ^{234}U is based primarily on the flat excitation function, characteristic of the direct reactions observed in other bombardments of ^{3}He + ^{207}Pb and ^{3}He + ^{181}Ta.[2] In the direct reaction mechanism it is assumed that the two protons amalgamate with the target and the neutron flies on.

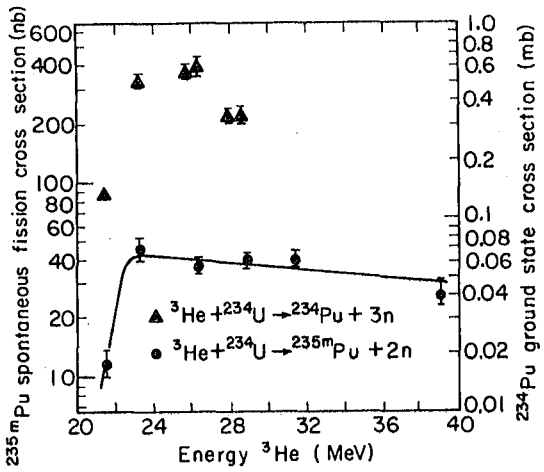

Fig. 2. Excitation function for production of ^{235m}Pu and ^{234}Pu in the reaction of ^{3}He + ^{234}U. The left scale refers to the ^{235m}Pu cross section in nb, the right one to ^{234}Pu in mb. (XBL 788-1650)

A second neutron may then be evaporated. In the case of α + ^{233}U the ~23-ns half-life obtained is close to the previous measurement of 30 ns for ^{235m}Pu[1] (Fig. 3). Furthermore, Lark et al.[3] have established low upper-limit cross sections

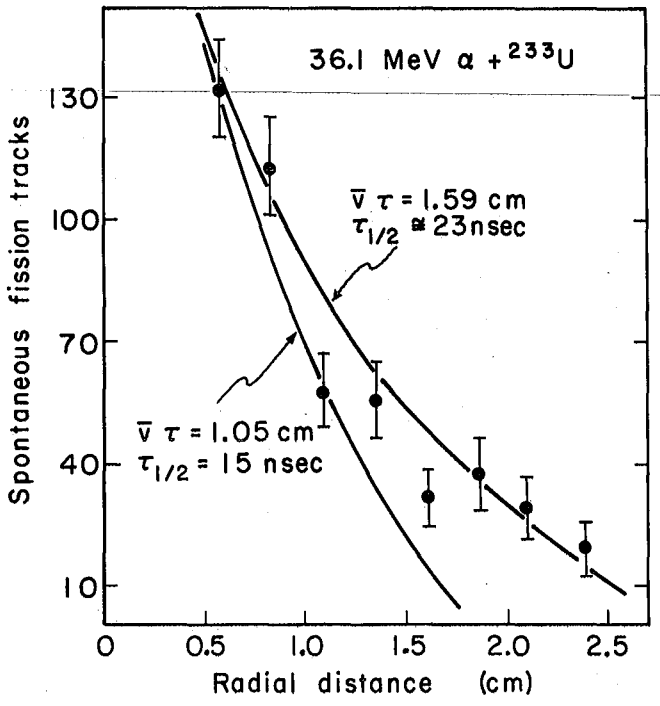

Fig. 3. Radial track distribution on mica taking the number of tracks in uniformly spaced concentric rings around the target for the reaction 36.1 MeV α + U. (XBL 7180-11516)

for production of fission isomers of $^{234-235}$U and $^{233-236}$Np isotopes, which might be produced here in non-compound nucleus reactions. In a bombardment of 23.2-MeV ^{3}He + ^{233}U an upper limit of 2.6 nb was estimated for spontaneous fission activities with half-lives between 10 ns and 1 μs. Since ^{235m}Pu would have to be produced in a (^{3}He,n) reaction with low probability, this result supports the assignment of ^{235m}Pu for the fissions produced in the α + ^{233}U and ^{3}He + ^{234}U bombardments.

The half-life measurements are very rough due to the continuous spread of recoil velocities from thick ^{233}U and ^{234}U targets, in most cases thicker than the compound nucleus recoil range. Recoil ranges were calculated using the empirical formulas of Liukkonen et al.[4]

The prompt fission cross section was also measured for each of the ^{3}He energies by measuring the number of fissions in mica facing the target. At the peak of the excitation curve the ratio of isomer to prompt fission cross sections was found to be $1.9 \pm 0.7 \times 10^{-7}$.

During some of the ^{3}He + ^{234}U and α + ^{233}U runs we proved that the fissions were not due to target material sticking to the mica and fissioning under the intense neutron flux. We proved this by using mica to measure the number of neutron-induced fission events from alpha decay calibrated samples of ^{234}U or ^{233}U exposed to the same neutron flux. Then by measuring the alpha decay rate on the mica surface at the end of the experiment (usually 0-1 ct/min) we found that possible neutron-induced fission of uranium stuck to the mica could not account for the number of fissions we observed. To prove instead that the fissions came from recoils decaying in flight from the ^{3}He + ^{234}U reaction, we placed a thin 30-μg/cm^2 aluminum stopper foil over the target. The foil was selected just thick enough to stop the recoils. We observed 5% of the number of fission as were observed without the foil.

The excitation curve for the ^{234}Pu ground state was also measured by catching the recoils in a thin 50-μg/cm^2 carbon foil and measuring the alpha spectrum from the foil in ~2π geometry. The yield at the peak energy was found to be only x2 lower than the 1.2 mb result predicted by JORPLE code. If ^{234}Pu has a fission isomer in the nanosecond region, these experiments allow us to quote an upper limit for ^{234}Pu isomer to ground state ratio of $\sigma_i/\sigma_g \leq \sim 2 \times 10^{-4}$.

References

1. Yu. P. Gangrskii et al., Atomnaya Energiya 33(4), 829-833 (1972).

2. N. E. Scott et al., Nucl. Phys. A 119, 131-145 (1968).

3. N. L. Lark et al., Nucl. Phys. A 139, 481-500 (1969).

4. E. Liukkonen et al., Nucl. Instr. Methods 125, 113-117 (January 1975).

A NEW METHOD FOR CALIBRATING THE PULSE HEIGHT DEFECT IN SOLID STATE DETECTORS*

J.B. Moulton, E.J. Stephenson,† R.P. Schmitt, and G.J. Wozniak

As the capability of heavy ion accelerators expands to include heavior and heavier nuclei at ever greater energies, a greater need develops for accurate calibration of the energy and mass non-linearity of solid-state detectors. These non-linearities are defined relative to the detector response to alpha particles. In general terms, the pulse height defect (PHD) is the difference between the detector response to a heavy ion and to an alpha particle of the same energy.

In the present work we present PHD measurements made at Lawrence Berkeley Laboratory's 88-inch cyclotron. These measurements cover a larger mass and energy range than previously reported work and use a direct irradiation technique that avoids some errors inherent in recoil scatter measurements and that provides fragments with unit atomic number and mass resolution.

Since the cyclotron can be tuned very precisely to select one value of the charge-to-mass ratio, it provides just one specific isotope at a time to the experimental area in nearly all cases.[1] The extremely low backgrounds obtained for several Au beams are illustrated in Fig. 1.

To obtain such heavy ion beams, a Penning Ion Gauge (PIG) source was fed with a mixture of noble gases (Ne, Ar, Kr, Xe). In addition, either Au or a combination of rare earths was mixed with Ta and used in the ion source as a mixed pellet at the edge of the ion discharge, opposite the anode opening. In this way many charge states of elements over a large mass range were produced by the ion source and injected into the cyclotron. Tuning of the cyclotron frequency, the dee voltage and electrostatic deflector voltages allowed quick selection of a particular isotope and charge state. Low intensity beams of 45 different ions were accelerated and extracted from the cyclotron during a typical 16-hour run. Typical beam currents ranged from tens to thousands of particles per second impinging on the detector. Ion energies from 5 to 160 MeV were achieved, without exhausting the potential of the machine.

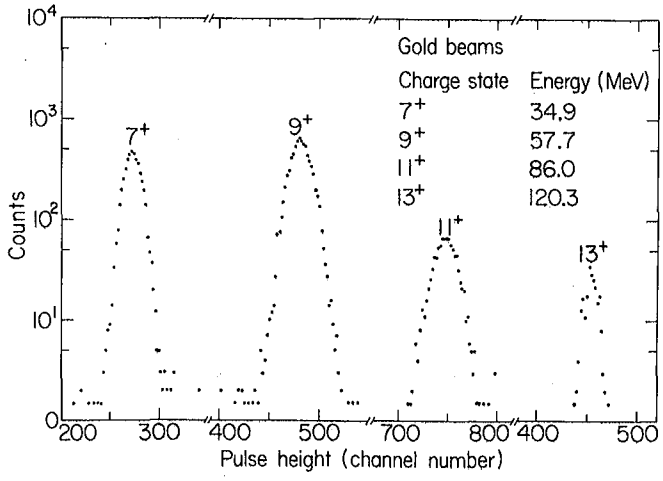

Fig. 1. Pulse height spectrum of counts vs energy for Au^{7+}, Au^{9+}, Au^{11+}, and Au^{13+} beams. Note the near absence of background events. (XBL 7710-2090)

Because the cyclotron parameters are known for each ion and because no intermediate scattering in a target occurs, the true energy incident at the detector is known quite accurately.

The pulse height response of the detector to alpha particles was measured using a thin ^{212}Pb source, which emits two alpha particles of substantially different energies in its decay chain. This calibration was extrapolated to higher energies using a mercury pulser. The alpha particle calibration defines an "alpha energy," E_α, for the centroid of each spectrum. The true total energy, E_T, minus the energy loss E_W of the heavy ion in the detector window, yields the "deposited energy," E_d. The PHD is then defined as the difference between the deposited energy and the alpha energy:

$$PHD = (E_T - E_W) - E_\alpha = E_d - E_\alpha \quad . \qquad (1)$$

The accuracy of the PHD data is limited by the accuracy to which three different quantities can be measured or calculated: the total ion energy e_T, the "alpha energy" E_α, and the energy loss in the surface dead layer E_W. Experience with measuring the absolute energies[2] of beams from the 88-inch cyclotron using a magnetic analysis system[3] has lead to an upper limit on the error of E_T of ±0.5%. The accuracy of E_α depends on the measurement of the energy centroids of the two alpha particle peaks and the extrapolation to higher energies with a linear pulser. The error in this extrapolation has been estimated to be ±0.36% of E_α. The error of E_W arises from the uncertainties in the dead layer thickness and in the range-energy relations.[4] The error of E_W has been estimated as ±2.5% of E_W based on the reproducibility of the dead layer measurements. The window correction is comparable to the PHD only for lighter masses, and in all cases makes only a negligible contribution to the PHD error. The net uncertainty in the PHD is less than the size of the data points shown in Fig. 2.

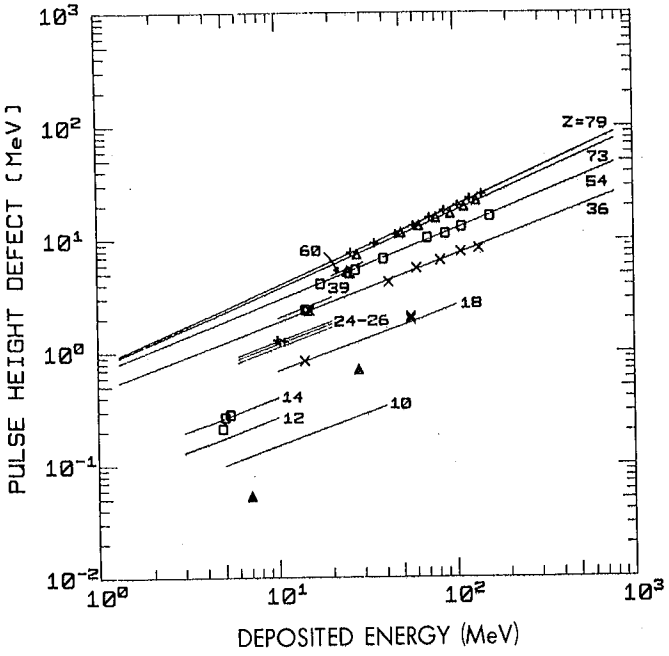

Fig. 2. PHD of a silicon surface barrier detector vs deposited energy. The PHD is defined to exclude the energy loss in the surface window (see text). Long lines are linear least-square fits to the data with equal weights; short lines are extrapolations using method described in the text. Errors are less than the size of the data points (see discussion in text).
(XBL 783-7655)

PHDs have been measured for elements ranging from Ne to Au, for energies from about 5 to 160 MeV. The PHD data for one counter is shown in Fig. 2 in MeV units and log-log format. Two important features should be noticed: that log PHD is linear with log E_d for each element, and different elements lie on different lines. The four long solid lines represent linear least-square fits to the Au, Ta, Xe and Kr data. The good agreement with the data reveals the utility of a simple power-law fitting function:

$$\text{PHD} = 10^{b} E_d^{a} \quad , \tag{2}$$

where a is the slope and b is the y-intercept of a plot of log PHD vs log E_d. Both the slopes and the intercepts increase with atomic number (Z) and a typical value for the slope is 0.6.

Since the data for each element cluster on separate lines, it is desirable to have a procedure for mathematically generating calibration lines for all elements from lines measured for just a few. This has been done by fitting the slope and intercept parameters of Eq. (2) to simple functions of the atomic number (Z) and mass number (A). Figure 3 shows linear fits of the slope, a, to the square of Z and A for the Au, Ta, Xe and Kr data shown in Fig. 2. The fitting functions are:

$$a(Z) = 0.02230\left(\frac{Z^2}{10^3}\right) + 0.5682 \quad , \tag{3}$$

$$a(A) = 0.03486\left(\frac{A^2}{10^4}\right) + 0.5728 \quad . \tag{4}$$

Using one of these correlations for the a parameter, a value of intercept, b, can be calculated from the measured PHD and the deposited energy (E_d) according to the following equation:

$$b = \log\left(\frac{\text{PHD}}{E_d^{a}}\right) \quad . \tag{5}$$

With the exception of the lightest elements (Ne and Mg), where the PHD is very small and the percent error is large, the calculated intercepts are accurately represented by a straight line. The fitting equations are

$$b(Z) = -0.1425\left(\frac{100}{Z}\right) + 0.0825 \quad , \tag{6}$$

$$b(A) = -0.2840\left(\frac{100}{A}\right) + 0.0381 \quad . \tag{7}$$

The slope and the intercept calculated from

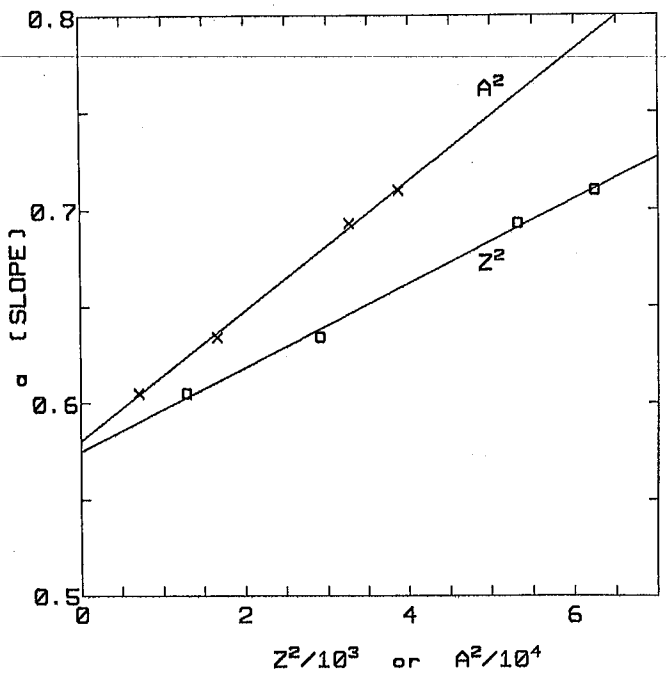

Fig. 3. Measured values of the parameter a [of Eq. (2)] for Au, Ta, Xe and Kr, plotted vs Z^2 and A^2. Lines are linear least-square fits to the data with equal weights.
(XBL 783-7427)

Eqs. (3) or (4) and (6) or (7) can be used in Eq. (2) to compute the PHD for any element.

As a test of the scheme, the PHD lines were calculated from Eq. (2) for the remaining elements in Fig. 2. The slope and intercept were calculated from Eqs. (3) and (6). The results, shown by the short lines in Fig. 2, provide good agreement with the observed PHD. This calibration scheme is valid for elements from Ne to Au and energies from 5 to 160 MeV.

Footnotes and References

*Condensed from an article submitted to Nucl. Instr. and Methods.

†Present address: Physics Division, Argonne National Laboratory, Argonne, IL 60439.

1. E. J. Stephenson, D. J. Clark, R. A. Gough, W. R. Holley and A. Jain, Lawrence Berkeley Laboratory Report LBL-6591, to be published.

2. R. E. Hintz, F. B. Selph, W. S. Flood, B. G. Harvey, F. G. Resmini and E. A. McClatchie, NIM 72, 61 (1969); and A. D. Bacher, E. A. McClatchie, M. S. Zisman, T. A. Weaver, and T. A. Tombrello, Nucl. Phys. A 181, 453 (1972).

3. R. A. Gough, private communication.

4. L. C. Northcliffe and R. F. Schilling, Nuclear Data Table A7, 233 (1970).

B. NUCLEAR REACTIONS AND SCATTERING

1. Microscopic

SYSTEMATIC STUDY OF COULOMB ABSORPTION IN HEAVY ION SCATTERING*

P. Doll,† A.J. Baltz,‡ M. Bini,§ D.L. Hendrie, S.K. Kauffmann, J. Mahoney, A. Menchaca-Rocha,‖ D.K. Scott, T.J.M. Symons, K. Van Bibber, Y.P. Viyogi,¶ and H. Wieman

Recent investigations of elastic scattering of heavy ions, with sufficient resolution to separate the ground state from low-lying target and projectile states, reported a strong damping of the elastic scattering cross section below the Rutherford value even at angles smaller than the grazing angle.[1,2] We present a systematic investigation of ^{20}Ne scattering on ^{148,150,152}Sm below the Coulomb barrier to study deviations from pure Rutherford scattering as a function of the deformation of the target nucleus, and to test an analytical Coulomb absorption model,[3] which was derived to overcome time consuming coupled channel calculations.

The measurements were performed with a 70-MeV $^{20}Ne^{4+}$ beam from the 88-inch cyclotron; scattered ^{20}Ne particles were detected in the focal plane of the QSD magnet spectrometer by Borkowski-Kopp type position detectors and an ionization chamber measuring the residual energy loss.

The spectrometer was operated with a solid angle of 1 msr typically. Under these conditions the energy resolution was sufficient to resolve the 551 keV, 2^+ state in ^{148}Sm, the 334 keV, 2^+ level in ^{150}Sm, and at a few angles the 122 keV, 2^+ level in ^{152}Sm (see Fig. 1). A peak fitting procedure was applied to all spectra, and errors in the cross sections represent uncertainties in this procedure. Systematic effects due to energy dependent charge state distributions were measured up to 80° in the laboratory system and extrapolated to be 5% for backward angles.

Position spectra from the focal-plane detector taken at 90° and 140° in the laboratory system are shown for the different target nuclei in Fig. 1. A comparison with energy spectra taken at the most forward angles shows an increasing enhancement of the inelastic yields when approaching the backward angles, which become larger than the elastic yield for the ^{152}Sm target.

In Fig. 2 we compare the measured angular distributions for elastic scattering with the predictions of the analytical closed form for the cross section ratio $\sigma_{el}/\sigma_R = \exp[-a\cdot f(\theta)]$, based on a long range imaginary potential.[3] All reaction parameters are contained in the sum

$$a = 0.223 \frac{k^4}{\eta^2}\left[\frac{B_T(E2,\ 0^+ \to 2^+)}{Z_T^2\, e^2}\, g_T(\xi) + \frac{B_p(E2,\ 0^+ \to 2^+)}{Z_p^2\, e^2}\, g_p\right](\xi)$$

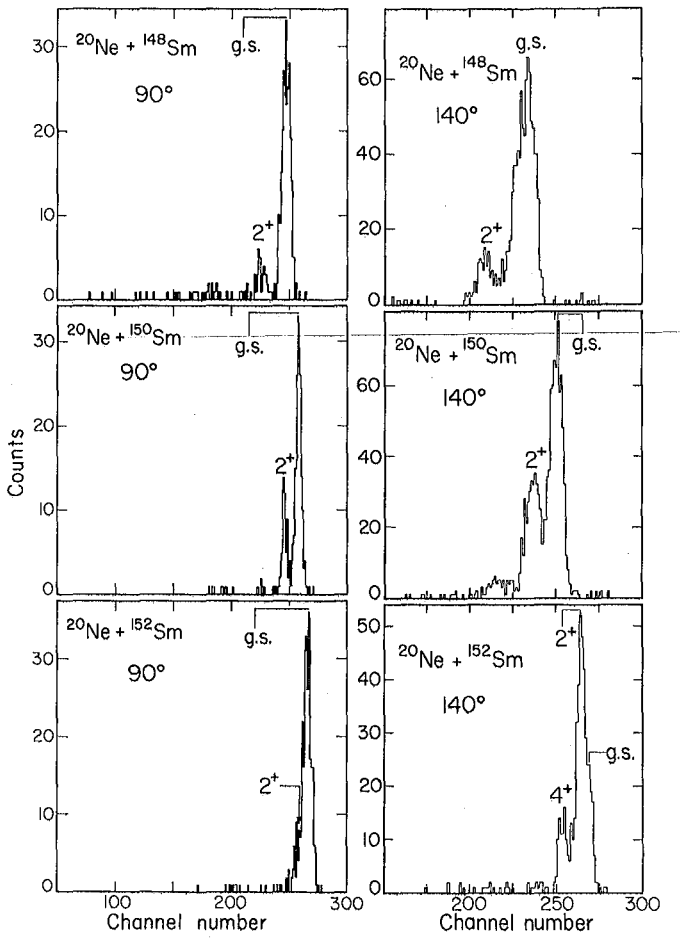

Fig. 1. Energy spectra of $^{20}Ne^{9+}$ after scattering from 148, 150, 152Sm at θ_{lab} = 90° and θ_{lab} = 140°. (XBL 782-253A)

and $f(\theta)$ is a function only of the scattering angle θ in the center of mass system. The $B_T(E2, 0 \rightarrow 2^+)$, $B_p(E2, 0^+ \rightarrow 2^+)$ values for the target and projectile respectively, were taken from the compilation of Christy and Häusser.[4] The Sommerfeld parameter is $\eta = 52$ in the present experiment. The semi-classical model applies a correction factor $g(\xi)$ to the potential in order to take some account of the energy loss during the 2^+ excitation process.

The model (dashed curves in Fig. 2) gives a satisfactory description of the measured angular distributions up to 100° in the c.m. system. Some discrepancies occur at more backward angles, especially for ^{148}Sm and ^{150}Sm. For comparison, coupled channel calculations were performed using the code CHORK with the same $B(E2, 0^+ \rightarrow 2^+)$ transition probabilities as in the semi-classical model, and with quadrupole moments derived in the rotational limit from these values. Coupling to both low-lying 2^+ states in target and projectile and including reorientation effects in both channels result in distributions given by the solid curves in Fig. 2.

The lower solid curve for ^{152}Sm shows the calculation, without reorientation coupling. For ^{148}Sm and ^{150}Sm, non-reorientation coupling calculations (not given in Fig. 2) are only 6% and 16% lower at extreme backward angles, respectively, indicating the decreasing importance of this coupling mode for the lighter Sm nuclei. While direct coupling to additional target states at incident energies above the Coulomb barrier is known to reduce further the elastic scattering flux, their influence is assumed to be small in the present experiment.

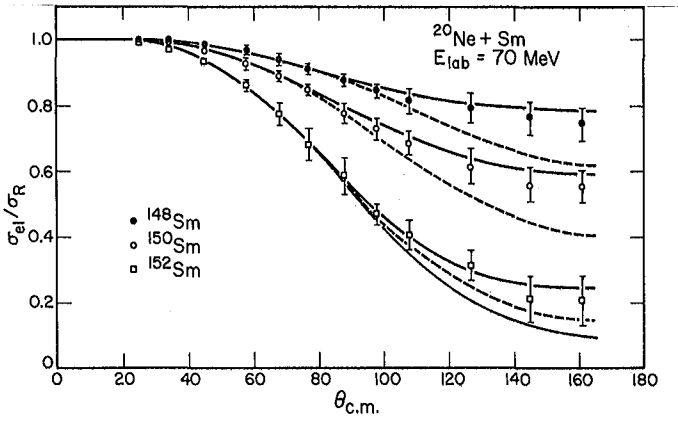

Fig. 2. Angular distributions from elastic scattering of ^{20}Ne on samarium nuclei. Dashed curves show calculations in a Coulomb absorption model, solid curves represent coupled channel calculations (see text). (XBL 782-251)

We have demonstrated that the elastic scattering flux is depleted by 30% to 80% at backward angles in sub-Coulomb heavy ion scattering, systematically increasing with the collectivity of low-lying target states. From a comparison with the semi-classical Coulomb absorption model and coupled channel calculations it becomes clear that the present model does not account for a) reorientation effects and b) trajectory dependent energy loss corrections, which seem to be required for ^{148}Sm and ^{150}Sm by the remaining difference between non-reorientation calculations and the model calculations at backward angles. Nevertheless the development of this analytical approach is useful for giving physical insight into the process, and for surveys of much heavier systems, such as ^{84}Kr + ^{209}Bi,[5] for which the exact calculations are difficult to perform.

Footnotes and References

*Condensed from anarticle to be published in Phys. Lett. and LBL-7195.

†Nato Fellow, on leave from MPI, Heidelberg, Germany.

‡Brookhaven National Laboratory, Upton, N.Y. 11973.

§Permanent address: University of Florence, Italy.

‖Permanent address: Instituto de Fisica, UNAM, Mexico, partially supported by CONACYT (PNCB-0022).

¶IAEA Fellow on deputation from Bhabha Atomic Research Centre, Calcutta, India.

1. C. E. Thorn, M. J. Levine, J. J. Kolata, C. Flaum, P. D. Bond, and J. S. Sens, Phys. Rev. Lett. 38, 384 (1977).

2. D. L. Hillis, E. E. Gross, D. C. Hensley, C. R. Bingham, F. T. Baker, and A. Scott, Phys. Rev. C 16, 1467 (1977).

3. A. J. Baltz, S. K. Kauffmann, N. K. Glendenning, and K. Pruess, Phys. Rev. Lett. 40, 20 (1978).

4. A. Christy and O. Hausser, Nucl. Data Table 11, 281 (1973). $B(E2, 0^+ \rightarrow 2^+)$ [e^2b^2] used: 0.048, 0.73, 1.44, 3.40 for ^{20}Ne, ^{148}Sm, ^{150}Sm, ^{152}Sm, respectively, and Q^{2+}_{ROT} [eb] =- 0.9059 $\sqrt{B(E2, 0^+ \rightarrow 2^+)}$.

5. J. R. Birkelund, J. R. Huizenga, H. Freiesleben, K. L. Wolf, J. P. Unik, and V. E. Viola, Jr., Phys. Rev. C 13, 133 (1976).

EXCITATION OF GIANT RESONANCES IN ^{208}Pb BY INELASTIC SCATTERING OF ^{16}O*

A. Guterman,† D. Ashery,† J. Alster,† D.K. Scott, M.S. Zisman, C.K. Gelbke,‡ H.H. Wieman, and D.L. Hendrie

Giant resonances in general, and those in ^{208}Pb in particular, have been extensively investigated in recent years.[1] A variety of different projectiles is helpful for understanding the details of the observed states such as their structure, multipolarity, and strength distribution. The interest in using heavy ions for the excitation of giant resonances is twofold. First, these experiments provide additional information on the structure of the giant resonances--for instance, the stronger excitation of components populated through large angular momentum transfer. In addition, it has been proposed[2] that the giant resonances could play an important role as doorway states for heavy-ion deeply-inelastic collisions. In the present work we report the excitation of giant resonances in ^{208}Pb by the inelastic scattering of ^{16}O ions at 140 MeV.

A ^{208}Pb target of 1.4 mg/cm^2 thickness was bombarded with a 140-MeV ^{16}O beam. The target was a self-supporting foil covered on both sides with 150-μg/cm^2 carbon layers to prevent the evaporation of the lead. The scattered ions were momentum-analyzed with a magnetic spectrometer where their time-of-flight and energy loss were also measured. All these parameters were recorded by a computer and stored event-by-event on magnetic tape. The presence of light contaminants on the target was not a problem since they gave rise to very low energy particles at the angles covered in the experiment. Data were taken at nine laboratory angles between 31° and 50° in 2°-3° steps. The energy resolution of 450 keV FWHM was mainly due to the target thickness. Energy calibration was done by using elastic scattering and inelastic scattering to low-lying states in ^{208}Pb, and by the transfer reaction ^{208}Pb(^{16}O,^{15}O)^{209}Pb populating the ground state and 1.45-MeV excited states, equivalent to Q-values of -11.72 and -13.17 MeV.

The energy spectrum of ^{16}O ions detected at 35° is shown in Fig. 1. The spectrum shows several features common to all spectra. The giant resonances (9-15 MeV) sit on top of a background which is not flat and which is probably due to excitation of the continuum in ^{208}Pb and to tails of bound states--mainly that of the 6.1-MeV state in ^{16}O. The figure also shows the assumed background, the unfolding of the resonance, and the total fit to the data as discussed below.

In order to obtain the angular distribution for the resonances, a systematic subtraction of the background is very important. The background was assumed to be composed of two parts--a straight line at the high excitation energy region (17-22 MeV), a part of which is shown in Fig. 1, and a tail from the bound states at lower excitation energy. Parameters of the straight line were obtained by a least squares fit, and parameters of the Gaussians which describe the bound states were obtained by the minimum χ^2 method. The background defined in this way is shown in Fig. 1. After background subtraction, the most consistent results for all the data were obtained by decomposing the spectra into four Gaussians at excitation energies of 9.2, 11.0, 13.0 and 14.3 MeV with full widths at half maximum of 1.1, 3.0, 1.75, and 1.1 MeV respectively. An example of such a decomposition is shown in Fig. 1.

Projectile excitation cannot contribute to the observed spectrum at these excitation energies, which are well above the threshold for particle emission from ^{16}O. Combined excitation of the target and projectile is expected to be negligible since the cross sections for excitation of the relevant bound states in ^{208}Pb (4.1 and 5.4 MeV) are about 5 mb/sr at 40°, compared to 8 mb/sr for the resonances. We therefore conclude that the observed spectrum is predominantly due to excitation of resonances in ^{208}Pb. This conclusion is strengthened by the observation of similar structures in ^{197}Au, for which the excitation of discrete states is not observed.[3]

The angular distribution of the sum of the four peaks is shown in Fig. 2, with only statistical errors (including background subtraction) indicated. The absolute errors, including systematic errors in background subtraction, are estimated to be 20%. The results of DWBA calculations for an L = 2 transition, normalized to the data

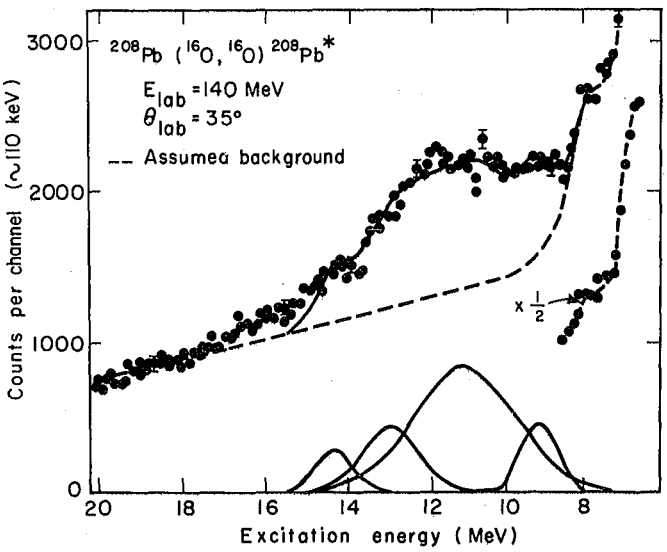

Fig. 1. Energy spectrum for ^{208}Pb(^{16}O,^{16}O)^{208}Pb. The unfolding of the spectrum into four Gaussian peaks and a background is indicated. (XBL 787-1417)

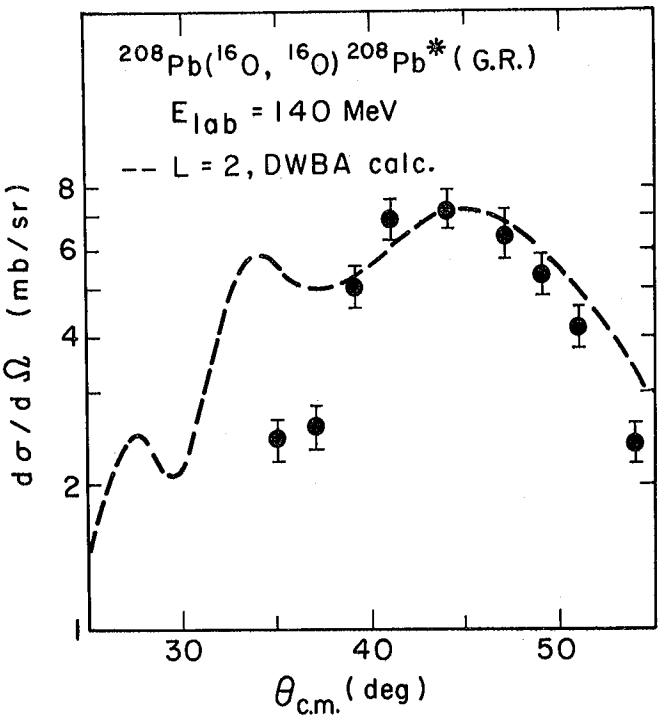

Fig. 2. Angular distribution of the sum of all peaks in the giant resonance region in ^{208}Pb. The errors do not include systematic ambiguities in background subtraction. The dashed line is the result of a DWBA calculation for a L = 2 transition. (XBL 787-1418)

at the grazing angle, are also shown in the figure. The question of the multipolarity of the various components of the giant resonances region in ^{208}Pb and in particular the question of the breathing mode (the giant monopole resonance) is still open. In a recent paper[4] the results from previous experiments, in which several different projectiles were used to excite the giant resonances in ^{208}Pb, are discussed in detail. The conclusion drawn is that the (L = 0) breathing mode is located mainly at the excitation energy of 8.9 ± 0.2 MeV, exhausting 50% of the energy-weighted sum rule (EWSR). Another recent paper,[5] in which a similar analysis is done and RPA calculations are carried out, comes to the conclusion that the breathing mode is located at the excitation energy of 14 MeV, exhausting 80% of the EWSR. The 9-MeV resonance, according to this paper, is proposed to be a component of the split T = 0 quadrupole resonance. Both papers assign the broad peak centered at 11 MeV as mainly a T = 0 giant quadrupole resonance.

In order to help resolve this problem we have carried out DWBA calculations for the 9.2- and 14.3-MeV states excited in the present work, assuming both L = 0 and L = 2 transitions. The results are summarized in Table 1, and indicate that the 14.3-MeV resonance is unlikely to be a monopole excitation since this assumption would imply at excitation strength of 250% of the EWSR. The results of these calculations for the 9.2-MeV resonance are consistent with an L = 0 assignment,[4] but the possibility of L = 2 is not excluded. Calculations assuming an L = 2 transition for the whole resonance region show that about 150% of the EWSR for E2 excitation is exhausted (see Table 1). The large percentage observed may be reconciled with the experimental systematic errors and ambiguities in the DWBA calculations. Of course it cannot be ruled out that other multipolarities are excited in the same energy region.

Although the cross section measured in the present work for excitation of the giant resonances (≈10 mb) is small, it still exhausts a large fraction of the EWSR. The giant resonances appear to be excited with the maximum allowed strength for inelastic scattering. Therefore it is difficult to conclude that significant flux is removed by multistep excitation into the deeply inelastic continuum.[6] For this system of ^{16}O + ^{208}Pb at 140 MeV the giant resonances do not appear to act as doorway states for deeply inelastic scattering, and it will be interesting to see if this conclusion is supported by detailed calculations, which predict that the observed strength of the direct excitation depends on the system.[2,6]

Footnotes and References

*Condensed from LBL-7758, submitted to Phys. Rev. Lett.

†Physics Department, Tel Aviv University, Israel.

‡Physics Department, Michigan State University, East Lansing, Michigan 48824.

1. F. E. Bertrand, Ann. Rev. Nucl. 26, 457 (1967).

2. R. A. Broglia, C. H. Dasso, and A. Winther, Phys. Letters B 61, 113 (1976).

Table 1. Values of B(E2) and $|M(0)|^2$ and the percentage of the T = 0 sum rule limit.[a]

Excitation Energy (MeV)	L^π	B(E2) or $\|M(0)\|^2$	Percentage of T = 0 sum rule
9.2	0^+	4.4 x 10	66%
	2^+	0.13 x 10	10%
10-14	2^+	1.54 x 10	140%
14.3	0^+	10.5 x 10	250%
	2^+	0.45 x 10	54%

[a]The sum rule limits are defined as follows:

$$S_L = E_x B(EL) = \frac{3A\hbar^2 L R^{2L-2}}{8m\pi} \qquad L \geq 2$$

$$S_0 = E_x |M(0)|^2 = \frac{6A\hbar^2 R^2}{5m}$$

where A is the mass number of the nucleus, and m is the nucleon mass.

3. D. Ashery, M. S. Zisman, R. B. Weisenmiller, A. Guterman, D. K. Scott and C. Maguire, LBL Nuclear Sciences Annual Report, 1975, p. 97.

4. R. Pitthan and F. R. Buskirk, Phys. Rev. C 16, 983 (1977).

5. J. Wamback, V. A. Madsen, G. A. Rinker, Phys. Rev. Lett. 39, 1443 (1977). See also: N. Marty, M. Morlet, A. Willis, V. Comparat, and R. Frascaria, Int. Symp. on Highly Excited States in Nuclei (Julich, 1975), Vol. 1, p. 17; D. H. Youngblood, C. M. Rozsa, J. M. Moss, D. R. Brown, and J. D. Bronson, Phys. Rev. Lett. 39, 1188 (1977).

6. R. A. Broglia, O. Civitarese, C. H. Dasso, and A. Winther, Phys. Lett. B 73, 405 (1978).

A NEW TYPE OF GIANT RESONANCE IN HIGH ENERGY HEAVY ION SCATTERING

P. Doll,* D.L. Hendrie, J. Mahoney, A. Menchaca-Rocha,† D.K.Scott, T.J.M. Symons, K. Van Bibber, Y.P. Viyogi,‡ and H. Wieman

The excitation of giant resonances as the mechanism by which two nuclei lose part of their relative kinetic energy in a collision has been discussed frequently in the past.[1,2] In a theoretical picture[2] it is suggested that giant resonance states are possible doorway states through which energy and angular momentum is dissipated into intrinsic degrees of freedom of the colliding nuclei. To investigate this problem we have performed survey studies at the 88-inch cyclotron by scattering 312 MeV ^{16}O from ^{12}C, ^{58}Ni and ^{208}Pb targets. At the focal plane of the QSD spectrometer we looked simultaneously at inelastically scattered ^{16}O particles and ions near the projectile mass to compare nucleon transfer cross sections with the amount of cross section exhausted by giant resonance excitations. We discovered that the $(^{16}O,^{15}O)$ reaction has a g.s. Q-value comparable with the energy loss due to excitation of high-lying multipolarities.

Spectra were taken around the grazing angles for ^{16}O on ^{58}Ni and ^{208}Pb to study the transition from large impact parameters, where the two nuclei interact rather gently, to small impact parameters where the two ions become highly excited. With the exception of ^{12}C, the heavier target nuclei exhibit pronounced structures in the continuum region near their grazing angles. We may interpret the 10.7-MeV bump in ^{208}Pb and the comparatively broader structure at 14.7 MeV in Ni as the known[3] giant quadrupole resonance, and the 13.5-MeV and 20.6-MeV structure in lead and nickel, respectively, we identify tentatively with the giant monopole resonance. Hardly any structure was found in ^{12}C around 26 MeV of excitation energy even at angles forward of 6° in the laboratory system; future investigations near the grazing angle (~3°) in the ^{16}O + ^{12}C system will be undertaken. There seems to be an increasing transfer probability compared to the multipole excitation probability in going to lighter target nuclei.

One of the most striking features is the observation of an additional gross structure peak at around 20 MeV of excitation energy in ^{208}Pb (see Fig. 1). No light ion or hadron scattering experiment has revealed any resonance structure at this excitation energy so far. However, several theoretical calculations predict a strong concentration of strength for the ℓ=3 and ℓ=5 response function of Pb in this region. It is well known in heavy-ion scattering that angular momentum matching conditions favor large ℓ-transfers and can therefore be used to search for new collective modes. Angular distributions have been taken for dominant transitions revealing a peak around the grazing angle. In

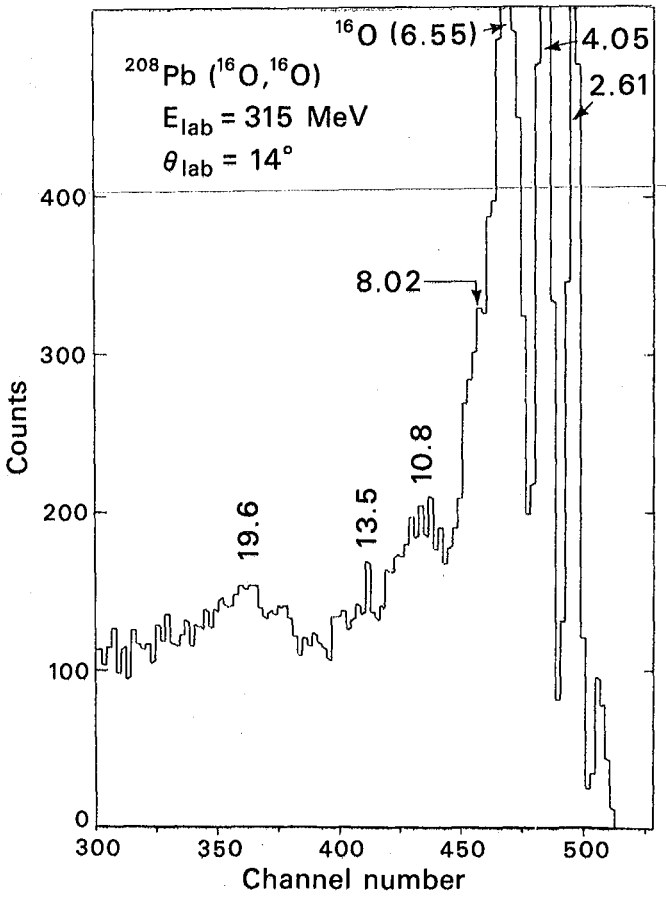

Fig. 1. Energy spectrum of inelastically scattered ^{16}O particles on ^{208}Pb. (XBL 786-1055)

^{16}O scattering on ^{208}Pb the energy integrated cross section for $(^{16}O,^{15}O)$ turned out to be comparable to that of the high multipole transition, which is indicative of the role the latter may play as doorway states in deep-inelastic processes. This comparison is less obvious for lighter nuclear systems due to the faster damping of the giant resonance modes in light nuclei.

Footnotes and References

*NATO Fellow, on leave from MPI, Heidelberg, Germany.

†Permanent address: Instituto de Fisica, UNAM, Mexico. Partially supported by CONACYT (PNCB-0022).

‡IAEA Fellow on deputation from Bhabha Atomic Research Centre, Calcutta, India.

1. M. Buenerd, D. Lebrun, J. Chauvin, T. Gaillard, J. M. Loiseaux, P. Martin, G. Perrin, and P. de Saintignon, Phys. Rev. Lett. 40, 1782 (1978).

2. R. A. Broglia, O. Civitarese, C. H. Dasso and A. Winther, Phys. Lett. B 73, 405 (1978).

3. D. H. Youngblood, J. M. Moss, C. M. Rozsa, J. D. Bronson, A. D. Bacher, and D. R. Brown, Phys. Rev. C 13, 994 (1976).

THE RAPID ONSET OF FRAGMENTATION IN PERIPHERAL HEAVY ION COLLISIONS*

D.K. Scott, M. Bini,† P. Doll,‡ C.K. Gelbke,§ D.L. Hendrie, J.-L. Laville,‖ J. Mahoney, A. Menchaca-Rocha,¶ M.C. Mermaz,** C. Olmer,†† T.J.M. Symons, Y.P. Viyogi,‡‡ K. Van Bibber, H. Wieman, and P.J. Siemens§§

Our knowledge of collisions between complex nuclei comes mainly from two extremes of incident energy, each dominated by characteristic reaction processes. Below 10 MeV/nucleon, the collision time is longer than the transit time of nucleons at the Fermi level; consequently the whole nucleus responds coherently to the collision, and the dominant phenomena are characteristic of the mean field.[1] At relativistic energies of GeV/nucleon, on the other hand, the reaction processes are dominated by independent collisions of individual nucleons. The transition between the two regimes is expected to occur when the incident energy allows the complete disjunction of the two nuclei in momentum space, at a few tens of MeV/nucleon.[1]

Our approach to the study of this transition is to measure the production cross sections and energy spectra of projectile-like fragments from ^{16}O-induced reactions on targets of Pb, Au and Ni as a function of incident energy. Typical spectra for outgoing ^{12}C products at incident energies of 140, 218, 250 and 315 MeV are shown in Fig. 1. The spectra peak at an energy corresponding to a velocity close to that of the projectile (E_p). The widths of the spectra increase rapidly with energy, which is a manifestation of the transition in the nature of the reaction mechanism.

First we use the concept of temperature to find systematic trends in the data. At low energies ($\lesssim$10 MeV/nucleon), the production cross sections of isotopes in reactions of the type reported here have an exponential dependence,[2] $\sigma \propto \exp(Q_{gg}/T)$, which is explained by a statistical model of partial equilibration in the dinuclear system at temperature T. The two-body, ground state Q-value, Q_{gg}, determines the relevant excitation energy. For our data the associated temperatures are shown as a function of the incident energy (top scale) in Fig. 2 by filled circles. The variation of the temperature initially follows the trend of the Fermi gas equation of state, $(E_c\text{-}V) = aT^2$, where E_c is the center of mass energy and V the Coulomb barrier in the incident channel (Q-values are neglected); the level density parameter, a, is set equal to A/8, with A the mass number of the intermediate complex. Hence, T is proportional to $\sqrt{E_c\text{-}V}$, the variable appearing on the bottom scale. Data from the analysis[3] of ^{16}O, ^{15}N + ^{232}Th reactions, at incident energies similar to the present work, are included with square symbols.

At relativistic energies the concept of temperature has also been useful in explaining isotope production cross sections, where the "emitter" is the projectile rather than the dinuclear complex.[2,4] Then $\sigma \propto \exp(Q_F/T)$, with Q_F equal to the appropriate fragmentation Q-value, and T is the projectile temperature. This approach was previously adopted for the data at 315 MeV[2] ($\approx$20 MeV/nucleon) and at 2.1 GeV/nucleon.[5] These values of T are also shown in Fig. 2 by the filled circles. Following the initial trend of the Fermi gas equation, a rapid rise sets in between 10 and 20 MeV/nucleon, after which the temperature appears to remain constant in the region of 8 MeV. Above 15 MeV/nucleon, where the curve departs from the prediction of the Fermi gas for heating the entire intermediate complex, only a part of the total system can be heated.

Although temperature is a useful concept for understanding the limiting behavior in the high-energy region, an alternative interpretation comes from the abrasion model[6] in which the primary fragments emerge by the sudden shearing of the projectile without prior excitation. We show that the dependence $\sigma \propto \exp(Q_F/T)$ can

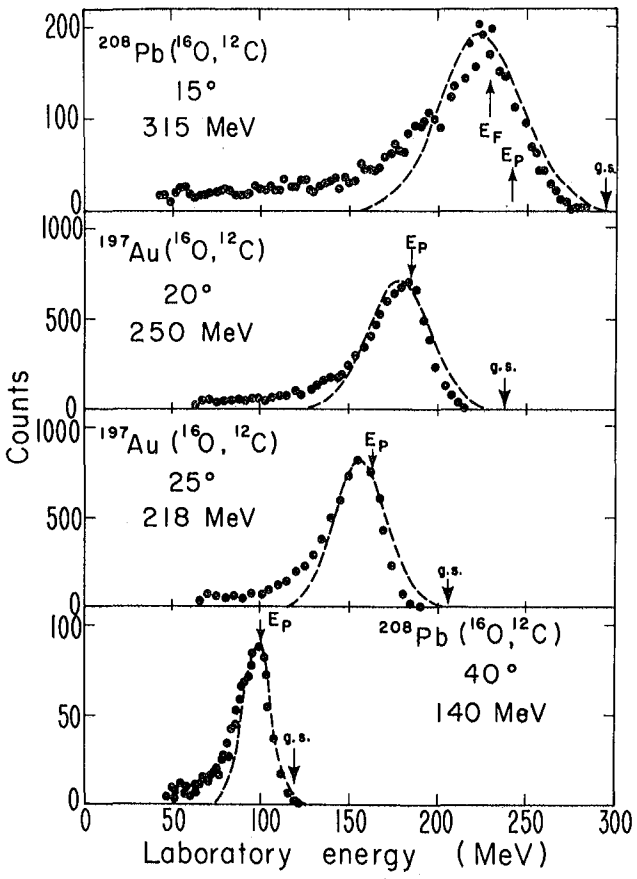

Fig. 1. Energy spectra of ^{12}C fragments produced in the collision of ^{160} + ^{208}Pb and ^{197}Au at several energies. The arrow g.s. corresponds to a two-body reaction forming residual nuclei in the ground state. If two-body processes are dominant, the spectra imply high excitation energies. The arrow E_p denotes the energy of a fragment travelling with beam velocity. This energy is characteristic of two-body processes at low energy and of fragmentation at high energy. The dashed curves are theoretical predictions using Eq. 3, as discussed in the text.
(XBL 7711-11041A)

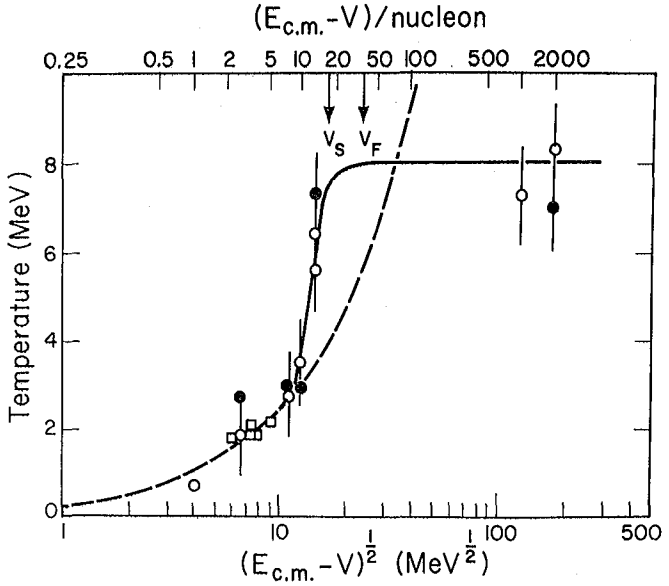

Fig. 2. The variation of temperature with incident energy in the collision of ^{160} with ^{208}Pb, ^{197}Au, ^{58}Ni and Ta (the lowest energy point). The open circles correspond to the widths of momentum distributions. The filled circles and square blocks are derived from isotope production systematics. The hatched line is the prediction of a statistical equilibrium model, based on the Fermi gas equation of state. The arrows v_s and v_F mark the characteristic velocity of sound and the Fermi velocity in nuclear matter. The solid line is drawn to guide the eye. (XBL 785-948)

also be derived analytically with this model. For the primary distribution of fragments in neutron number N about the mean N_0, we use the formulation of the abrasion model in Ref. 7:

$$\sigma \propto \exp\left[-(N-N_0)^2\left(\frac{1}{2\sigma_a^2}+\frac{1}{8\sigma_{t_3}^2}\right)\right] = \exp\left[-\frac{(N-N_0)^2}{\alpha}\right], \quad (1)$$

where σ_a, σ_{t_3} are the dispersions in particle number and isospin, which are derived from a model[7] with correlations built into the nuclear ground state, viz., $\sigma_{t_3} \approx 0.24\ A^{1/3}$, $\sigma_a \approx 4.9\ \sigma_{t_3}$. In the production of a series of isotopes, the changes in Q_F are determined primarily by the N-dependent terms in the liquid drop mass formula. For small excursions in N from the mean, it follows that the sum of the fragment masses exceeds that of a symmetric division ($N=N_0$) by the amount:

$$Q_F \approx 4\left(\frac{a_s}{A}-\frac{a_{ss}}{A^{4/3}}\right)(N-N_0)^2 = \beta(N-N_0)^2 \quad (2)$$

where a_s and a_{ss} are the symmetry and surface symmetry coefficients, respectively. From Eqs. (1) and (2) we get $\sigma \propto \exp(Q_F/\alpha\beta)$, which is equivalent to the result of the thermal excitation model, with T replaced by $\alpha\beta$. By inserting the values[7] σ_a,σ_t and the mass formula coefficients, we deduce that T = 9 MeV (or 32 MeV with values of σ_a,σ_{t_3} neglecting correlations. This value of 9 MeV is close to the required saturation value of 8 MeV shown in Fig. 2. The parameter in the exponential dependence of σ on Q_F is, however, identified with the onset of the fast abrasion mechanism, rather than with the saturation of nuclear temperature in the slower process of local equilibration.

In the saturation region above 20 MeV/nucleon, the abrasion model also accounts consistently for the momentum distribution of fragments in the projectile rest frame.[5] For the energy distribution in the laboratory frame at angle θ, the model predicts[8]:

$$\frac{d^2\sigma}{dEd\Omega} \propto \sqrt{2A_FE}\ \exp\left[-\frac{A_F}{\sigma^2}\left(E-2\varepsilon E^{1/2}\cos\theta+\varepsilon 2\right)\right], \quad (3)$$

where $\varepsilon^2 = 1/2\ M_F v_p^2$, v_p is the velocity corresponding to the peak of the energy distribution,

$$\sigma^2 = \sigma_0^2\ \frac{A_F(A_p-A_F)}{A_p-1},$$

A_F and A_p are the mass numbers of the observed fragment and the projectile, and $\sigma_0 = P_F/\sqrt{5}$, where P_F is the Fermi momentum of the projectile. The value σ_0 = 86 MeV/c, appropriate[5,8] for the data at 20 MeV/nucleon, 1.05 GeV/nucleon and 2.1 GeV/nucleon, corresponds to P_F = 192 MeV/c (0.97 fm^{-1}) which is close to the measured Fermi momentum of a nucleus as light as ^{16}O. The predicted energy distribution at 20 MeV/nucleon is shown in Fig. 1.

The energy distribution in Eq. 3 is also expected from a statistical model of fragment emission.[5] Therefore, the formula can be applied equally well to the lower energy spectra in Fig. 1, where we have already shown that equilibration processes at temperature T are relevant. By consideration of energy and momentum, T and σ_0 are related[5] by

$$\sigma_0^2 = Tm\ \frac{A_p-1}{A_p},$$

where m is the nucleon mass in MeV. The value of T required to fit the data at all energies are shown in Fig. 2 by the open circles. At low energies (<10 MeV/nucleon), the temperatures extracted from the momentum (open circles) and isotope yield distributions (filled circles and square symbols) are in agreement, supporting the temperature model. At high energies (>20 MeV/nucleon), the saturation of the widths of the momentum and isotope distributions with T = 8 MeV is consistent with a fast abrasion mechanism.

If we adopt the abrasion model for the description of the high energy data, then the sudden transition from equilibration to fragmentation must contain information on characteristic properties of nuclear matter, such as the relaxation time for spreading the localized deposition of energy, or "hot-spot,"[9] over the nucleus. The initial excitation may be in the form of uncorrelated particle-hole excitations, in which case this relaxation time is related to the Fermi velocity. On the other hand, if the initial excitation is carried by coherent, collective compressional modes, then this time is related to the frequency of these modes, which in turn depends on the speed of sound in nuclear matter[10] and can be evaluated from the compressibility coefficient K ≈ 300 MeV, as $v_s = \sqrt{K/9m}$, i.e., 0.19c (m is the nucleon rest mass). This velocity and the Fermi velocity in nuclear matter (equivalent to 36 MeV/nucleon) are marked in Fig. 2, but it would be premature to specify which defines the change of mechanism without a detailed model.

Our study of single-particle inclusive peripheral reactions over a broad range of incident energy demonstrates the rapid transition from equilibration to abrasion or fragmentation above 20 MeV/nucleon. This transition implies an increased localization of the nuclear response as the time scale of the reaction becomes faster. If a quantitative treatment of this behavior can be developed, it may be possible to extract interesting information on the tensile strength of nuclear matter,[11] as the healing properties of the nucleus disappear under the stress of the collision.

Footnotes and References

*Condensed from LBL-7729, submitted to Phys. Rev. Letters.

†Nato Fellow, on leave from University of Florence, Florence, Italy.

‡Nato Fellow.

§Present address: Physics Dept., Michigan State University, East Lansing, Michigan 48824.

‖On leave from CNRS, Caen, France.

¶On leave from Instituto de Fisica, UNAM, Mexico.
Partially supported by CONACYT (PNCB 0022).

**On leave from CEN, Saclay, France.

††Present address: Physics Division, Argonne National Laboratory, Argonne, Illinois.

‡‡IAEA Fellow, on deputation from Bhabha Atomic Research Centre, Calcutta, India.

§§On leave from Niels Bohr Institute, DK-2100, Copenhagen, Denmark.

1. G. Bertsch, Lecture Notes for the Les Houches Summer School, 1977.

2. M. Buenerd, C. K. Gelbke, B. G. Harvey, D. L. Hendrie, J. Mahoney, A. Menchaca-Rocha, C. Olmer, and D. K. Scott, Phys. Rev. Lett. 37, 1191 (1976).

3. V. V. Volkov, Sov. J. Nucl. Phys. 6, 240 (1976).

4. V. K. Lukyanov and A. I. Titov, Phys. Lett. B 57, 10 (1975).

5. A. S. Goldhaber, Phys. Lett. B 53, 306 (1974).

6. J. Hüfner, C. Sander, and G. Wolschin, Phys. Lett. B 73, 289 (1978).

7. J. P. Bondorf, G. Fai, and O. B. Nielsen, Phys. Rev. Lett. 41, 391 (1978).

8. C. K. Gelbke, D. K. Scott, M. Bini, D. L. Hendrie, J.-L. Laville, J. Mahoney, M. C. Mermaz, and C. Olmer, Phys. Lett. B 70, 415 (1977).

9. P. A. Gottschalk and M. Weström, Phys. Rev. Lett. 39, 1250 (1977).

10. P. J. Johansen, P. J. Siemens, A. S. Jensen, and H. Hofmann, Nucl. Phys. A 288, 152 (1977).

11. G. Bertsch and D. Mundinger, Phys. Rev. C 17, 1646 (1978).

MEASUREMENT OF THE $^{6}Li(^{3}He, d)^{7}Be$ AND $^{7}Li(^{3}He, t)^{7}Be$ CROSS SECTIONS*

R.V. Pyle,† L. Ruby,† and J.W. Sterbentz†

A suggestion[1] has been made that a lithium waterfall could have an ameliorating effect on the first-wall radiation damage and radioactivation problems in an inertial fusion reactor. However, radioactivation of the lithium itself may present a new problem, making it desirable to know the cross sections for the reactions:

$$^{3}He + {}^{6}Li \rightarrow {}^{7}Be + {}^{2}H + 0.1144 \text{ MeV}$$

$$^{3}He + {}^{7}Li \rightarrow {}^{7}Be + {}^{3}H - 0.8807 \text{ MeV}, E_{th} = 1.258 \text{ MeV}.$$

These cross sections have been measured with the aid of $^{3}He^{+}$ beams of 2.0, 3.0, and 6.0 MeV from the Lawrence Berkeley Laboratory 88-inch cyclotron. Thin targets of 99.32% ^{6}LiF, 99.99% ^{7}LiF, and normal LiF were evaporated onto aluminum backings and irradiated in the cyclotron beam. The ^{7}Be activity in the targets was subsequently counted absolutely by integrating the 477-keV photopeak as recorded by a Ge(Li) detector. Preparation and irradiation of the targets proceeded as described previously[2] in connection with the measurement of the $^{6}Li(^{6}Li, {}^{5}He)^{7}Be$ cross section. Calibration of the detector was accomplished by measuring the photopeak efficiency for several gamma-ray standards, both above the below 477 keV. Interpolation to the 477-keV efficiency was accomplished by a least-squares fitting procedure. A final correction for the fact that gamma rays are emitted in only 10.3% of the ^{7}Be decays permitted the activity to be computed from the measured counting rate. The error made in assuming that the relatively large (2.9 cm) ^{7}Be targets, with possible non-uniform irradiation, had the same efficiency as a point source of ^{7}Be was investigated experimentally by moving one of the calibration standards progressively off axis. As a result, a non-uniformity error of $\pm 1.25\%$ was assigned, which considerably exceeds the statistical error of typically $\pm 0.8\%$. The largest error assigned to the resultant cross sections $\pm 5.0\%$ is ascribed to the measurement of the target thickness by successive weighings, before and after evaporation. Some of the additional uncertainties which were also considered are the $\pm 1.5\%$ stated error in the calibration standards, and $+0.52\%$ as determined experimentally for the beam-current integrator.

Since the targets contain fluorine, an investigation was undertaken to determine whether ^{7}Be could be made by the reaction:

$$^{3}He + {}^{19}F \rightarrow {}^{7}Be + {}^{15}N - 2.424 \text{ MeV}, E_{th} = 2.806 \text{ MeV}.$$

Some initial tests were done using teflon (C_2F_4) targets, but a more satisfactory material was found in the form of MgF_2, which, like LiF, is a relatively insoluble, high-melting-point salt. The threshold energies for production of ^{7}Be in the isotopes of either carbon or magnesium are all about 6.0 MeV. Although, at 6.0 MeV, activity was found in both the teflon and MgF_2 targets, the gamma emission turned out to be annihilation radiation whose half life was characteristic of 1.82-hour ^{18}F. The latter was presumably made in the reaction:

$$^{3}He + {}^{19}F \rightarrow {}^{18}F + {}^{4}He + 10.15 \text{ MeV}.$$

No detectable photopeak in the teflon or MgF_2 targets was observed at 477 keV, and to make sure that the presence of ^{18}F in the LiF targets did not interfere with the counting of ^{7}Be, the targets were always stored for a few days after irradiation to allow for decay of the former.

As a check on the cross sections determined for ^{6}Li and ^{7}Li, an irradiation of normal LiF was made at 6.0 MeV. The resulting value of 206 ± 12 mb per lithium atom compares well with the constructed value of 218 ± 26 mb based on the isotopic cross sections.

The resultant cross sections and other pertinent data are shown in Table 1. Because the targets were relatively thin, the effective energy of the beam was taken as the average energy in the target. The adjusted cross section is a weighted average for all of the targets exposed under the same conditions. It is seen that to the extent that 0.8-MeV ^{3}He ions will be present in fusion reactors, as a result of $^{2}H(d,n)^{3}He$ reactions, the ^{6}Li cross section for production of ^{7}Be will be appreciable.[3] Further details are available.[4]

Acknowledgments

This work was supported by a grant from the National Science Foundation.

Table 1. Results of cross section calculations.

Target	LiF target thickness ($\mu g/cm^2$)	Incident beam energy (MeV)	Statistical countering error (%)	"Effective" energy in target (MeV)	Measured cross section (mb)	Adjusted cross section (mb)
^6LiF	446	2.0	0.63	1.7	290 ± 16	
	462	2.0	0.83	1.7	278 ± 16	283 ± 16
	464	2.0	0.83	1.7	282 ± 16	
	467	3.0	0.67	2.8	387 ± 22	
	473	3.0	0.65	2.8	380 ± 21	384 ± 22
	509	6.0	0.63	5.9	397 ± 22	
	509	6.0	0.62	5.9	375 ± 21	
	487	6.0	2.51	5.9	391 ± 24	389 ± 23
	505	6.0	0.53	5.9	403 ± 23	
	520	6.0	0.57	5.9	379 ± 23	
^7LiF	544	2.0	8.20	1.7	7.2 ± 0.7	6.9 ± 0.7
	540	2.0	9.20	1.7	6.5 ± 0.7	
	568	2.0	1.10	2.8	92 ± 5	95 ± 6
	547	3.0	1.00	2.8	98 ± 6	
	509	6.0	0.85	5.9	199 ± 11	204 ± 12
	505	6.0	0.88	5.9	208 ± 12	
^{NAT}LiF	519	6.0	0.86	5.9	208 ± 12	206 ± 12
	526	6.0	0.88	5.9	203 ± 11	

Footnotes and References

*Submitted to the November 12-17, 1978, meeting of the American Nuclear Society, Washington, D.C.

†Department of Nuclear Engineering, University of California, Berkeley.

1. W. Meier and J. A. Maniscalco, Reactor Concepts for Laser Fusion, Lawrence Livermore Laboratory, Report UCRL-79654, 1977.

2. Y-C. Wong, R. V. Pyle, and L. Ruby, Trans. Am. Nucl. Soc. 27, 863 (1977).

3. We wish to acknowledge a communication from D. W. Barr at Los Alamos whose prior unpublished work on these cross sections is in excellent agreement with ours.

4. James W. Sterbentz, Cross Sections for the $^6Li(^3He,d)\ ^7Be$ and $^7Li(^3He,t)^7Be$ Reactions, M.S. Thesis presented to the Department of Nuclear Engineering, University of California, Berkeley (1978).

CHARGE SYMMETRY IN THE NUCLEON-NUCLEON SYSTEM*

H.E. Conzett

The polarization analyzing-power theorem[1] for (p,n) transitions between charge-symmetric nuclear states B and B', i.e., B(p,n) B', establishes the equality

$$A_y(\vec{p},n) = p_y(p,\vec{n}) \quad .$$

That is, the proton analyzing power is equal to the neutron polarization produced in the (p,n) transition. Recently, Plattner[2] has made a very interesting and timely proposal for an experimental check of charge-symmetry in the nucleon-nucleon interaction. Taking the states B and B' to be the neutron and proton, respectively, it follows that

$$A_y\,[n(\vec{p},n)p] \;=\; p_y[n(p,\vec{n})p] \quad ,$$

so that the proton analyzing power, A_p, is equal to the neutron polarization, pn, in n+p scattering for a charge-symmetric N-N interaction. The proposal is particularly timely because the time-honored test for basic charge-symmetry, i.e. the comparison of the neutron-neutron scattering length with the Coulomb-corrected proton-proton scattering length, is presently in disrepute. The comparison of the scattering lengths, a, has been attractive because of the amplification factor involved. That is, for a square well of depth V and range b, the relative change in scattering length for a relative change in the interaction strength is given by

$$\frac{\Delta a}{a} \simeq \frac{a}{b}\frac{\Delta V}{V} \quad , \quad \text{with} \quad \frac{a}{b} \simeq 8 \qquad (1)$$

because of the large scattering length, $a_{nn} = -17$ fm. Thus, with

$$a_{nn} = a^c_{pp} \pm 0.5 \text{ fm}$$

determined experimentally, Eq. (1) gives

$$\frac{\Delta V}{V} = \frac{1}{8}\left(\frac{0.5}{17}\right) = 0.4\% \quad , \qquad (2)$$

so that it was believed that charge-symmetry of the N-N interaction had been verified at the level of a few parts per thousand. However, Sauer[3] showed that all the previous local potential model calculations of the Coulomb-corrected scattering length, a^c_{pp}, were suspect. He showed that a^c_{pp} was strongly dependent on the form of the nuclear interaction at small distances, where it is really unknown, and this had been ignored in the model calculations. He parameterized the short range (non-local) behavior of the potential, and from his calculation he found values of a^c_{pp} ranging from -34 to -17 fm, so there was no longer any value with which to compare a_{nn} for a test of charge symmetry. The range of uncertainty in the calculated value of a^c_{pp} has since been reduced to 3 to 8 fm., but this is still very large compared to the experimental uncertainty in a_{nn} of 0.5 fm.

The proposal for an experimental verification of charge-symmetry is to test the equality of $A_p = p_n$ in n + p scattering. Time-reversal invariance makes $p_n = A_n$. Thus, one looks experimentally from $A_p \neq A_n$ as direct evidence for a charge-symmetry breaking component of the N-N interaction. Theoretically, one expects small deviations from exact charge symmetry due to one-photon exchange and ρ-ω mixing,[4] and these have been estimated to give values of $\Delta A \equiv A_p - A_n$ in the range 0.005 to 0.015. Clearly, an experimental comparison of A_p and A_n to this level of accuracy would be very difficult, if even possible, from using an ordinary method of comparing the A_p and A_n values derived in separate experiments, where the complete equivalence of the experimental conditions cannot be guaranteed. I have recently found a solution to this particular aspect of the problem whereby an experimental determination of <u>both</u> A_p and A_n can be made from a <u>single</u> <u>experiment</u>. It requires the combination of a polarized neutron beam and a polarized proton target, for which the scattered yield is given by

$$I_{++}(\theta) = I_o(\theta)\ 1 + P_n A_n + P_p A_p + p_n p_p A_{yy} \quad , \qquad (3)$$

where p_n, p_p, and A_{yy} are, respectively, the neutron polarization, the proton polarization, and the np spin-correlation parameter. $I_o(\theta)$ is the scattered yield for unpolarized beam and target, and $I_{++}(\theta)$ is that for positive values of both p_n and p_p. Changing the signs of p_n and/or p_p gives the other yields $I_{+-}(\theta)$, $I_{-+}(\theta)$, and $I_{--}(\theta)$. From Eq. (3) one finds that

$$\frac{(I_{++}+I_{+-}) - (I_{--}+I_{-+})}{4I_o} = p_n A_n \quad , \qquad (4a)$$

$$\frac{(I_{++}-I_{+-}) - (I_{--}-I_{-+})}{4I_o} = p_p A_p \quad . \qquad (4b)$$

Thus, from these various combinations of experimental yields with the different signs of beam and target polarizations, both A_n and A_p can be determined from a single experiment.

Footnotes and References

*Excerpted from an invited talk at the Gordon Conference on Few Body Problems in Chemistry and Physics, Kimball Union Academy, Meriden, N.H, Aug. 15-19, 1977.

1. H. E. Conzett, Phys. Lett. B <u>51</u>, 445 (1974).

2. G. R. Plattner, private comunication.

3. P. U. Sauer, Phys. Rev. Lett. <u>32</u> 626 (1974).

4. C. Y. Cheung, E. M. Henley, and G. A. Miller, to be published.

RECENT POLARIZATION RESULTS IN THE TWO- AND THREE-NUCLEON SYSTEMS*

H.E. Conzett

Because the "exact" three-nucleon theory calculates the three-nucleon observables from the (presumed known) two-nucleon interaction via the Faddeev equations, it follows that there is interest in the latest developments in the N-N system below, say, 100 MeV. New N-N results within the past year are: (a) precise measurements of the neutron analyzing power in $\vec{n}$-p scattering between 14 and 17 MeV,[1] and (b) recent work on the determination of the np $^3S_1$-$^3D_1$ mixing parameter, ε_1, at 50 MeV.[2] The absolute errors in the measurements of the $\vec{n}$-p analyzing power are below ±0.002. These data are reasonably consistent with the previous data in this energy region, but also are finally of sufficient precision to show that the analyzing powers calculated from the presently accepted n-p phase shifts are too large in the backward hemisphere. Thus, these data will cause some changes in the phase shifts in the region of 10-20 MeV. Since the analyzing power is determined by the spin-orbit splitting of the partial-wave phase shifts, an analysis was made in terms of the spin-orbit phase parameters which are linear combinations of the phase shifts, δ_{LS}, for each value of L. A clear requirement for the inclusion of an L = 3 spin-orbit phase parameter, in addition to the previously determined L = 1,2 contributions, was demonstrated.

The next new result concerns the determination of the n-p mixing parameter ε_1 for the coupled $^3S_1$-$^3D_1$ state, the deuteron channel. Just a few years ago Binstock and Bryan[3] showed that the then available n-p data near 50 MeV, consisting of σ_{TOTAL}, $\sigma(\theta)$ and $p_n(\theta)$, were not sufficient to determine ε_1. They also examined the sensitivity of other observables to changes in ε_1, and they found that the spin correlation coefficient A_{yy} was a good one to measure for a determination of ε_1. This $A_{yy}(\theta)$ measurement was a difficult experimental task, because it required the preparation of both a polarized neutron beam and a polarized proton target.[2] For this arrangement, the scattered neutron yield for both neutron p_n and proton p_p positive polarizations is

$$I_{++}(\theta) = I_0(\theta)[1 + p_n A_n + p_p A_p + p_n p_p A_{yy}] .$$

From this and the three other yields for the other possible combinations of p_n and p_p, the values of $A_{yy}(\theta)$ can be determined as

$$A_{yy}(\theta) = \frac{(I_{++} - I_{+-}) + (I_{--} - I_{-+})}{4 p_n p_p I_0(\theta)} .$$

Four values of $A_{yy}(\theta)$ were determined between θ_{cm} = 109 and 174 degrees, and when these data were included in a phase shift analysis,[2] the value of ε_1 = 2.9 ±1.0 degrees was obtained, in excellent agreement with Bryan's theoretical prediction.

The only new results in the three-nucleon system are measurements of the neutron analyzing-power in $\vec{n}$-d scattering at 12 MeV[4] and measurements of deuteron tensar analyzing powers in $\vec{d}$-p scattering at 45.4 MeV.[5] The 12-MeV $\vec{n}$-d data again are characterized by a considerably improved accuracy over previous neutron results. There is agreement with the 12-MeV $\vec{p}$-d analyzing power data within the experimental errors of 1%-2% and this is in good accord with the expectation based on charge symmetry of the N-N interaction.

The $\vec{d}$-p deuteron analyzing powers measured recently at Berkeley are shown in Fig. 1. These now establish a rather complete set of data in nucleon-deuteron scattering at E_N = 22.7 MeV, consisting of cross section, proton analyzing powers, deuteron vector and tensor analyzing powers, and vector polarization transfer measurements as well. A primary goal of the three-body theory has certainly been to reproduce the three-nucleon data from exact calculations that use the known two-nucleon forces. During the past few years, considerable success has been achieved in that direction.[6] The principal remaining discrepancy has been the failure to provide a quantitative fit to both the nucleon and deuteron vector analyzing powers at scattering angles forward of θ_{cm} = 120°. Doleschall's calculation[7] showed the vector analyzing powers to be quite sensitive to the details of the input nucleon-nucleon ($^3S_1$-$^3D_1$) tensor interaction, so it seemed likely that this discrepancy was coupled to the difficulty in providing a separable tensor interaction which simultaneously reproduces the $^3S_1$,$^3D_1$ phase shifts and the corresponding mixing parameter ε_1. Since the calculations at E_N = 22.7 MeV also show a significant sensitivity of the deuteron tensor polarizations to changes in the nucleon-nucleon tensor interaction, we have made measurements of the tensor analyzing powers T_{20} and T_{22} in $\vec{d}$-p scattering at E_d = 45.4 MeV for direct comparison with the calculated results at the equivalent nucleon energy of 22.7 MeV.

Doleschall[8] has recently noted that his two-nucleon tensor interaction had an unreasonably long range; and, when this feature was corrected, a dramatic improvement was obtained in the calculated fits to the analyzing-power data. Both the nucleon and deuteron vector analyzing powers are in almost perfect agreement with experiment as is demonstrated by his calculation labelled 2T4 in Fig. 2. The fits to our tensor analyzing power results in Fig. 1 are not as good. Even though the best fit curves, labelled 3T4, result from a tensor force which correctly represents

ε_1, it was still of the type with the poor long-range behavior. So, a correction of that deficiency could very well result in a corresponding improvement in the calculations of T_{20} and T_{22}. If that should be the case, the goal of reproducing the three-nucleon data from these exact calculations will have been achieved.

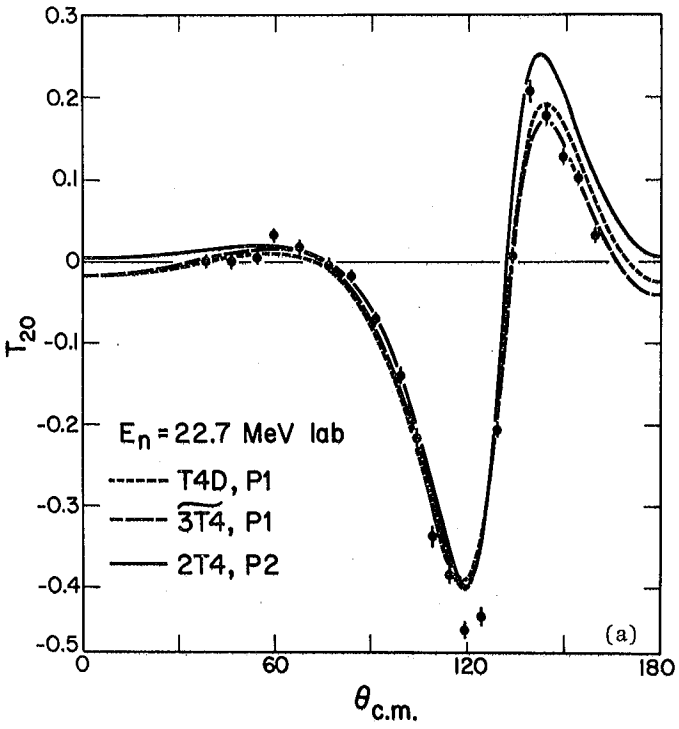

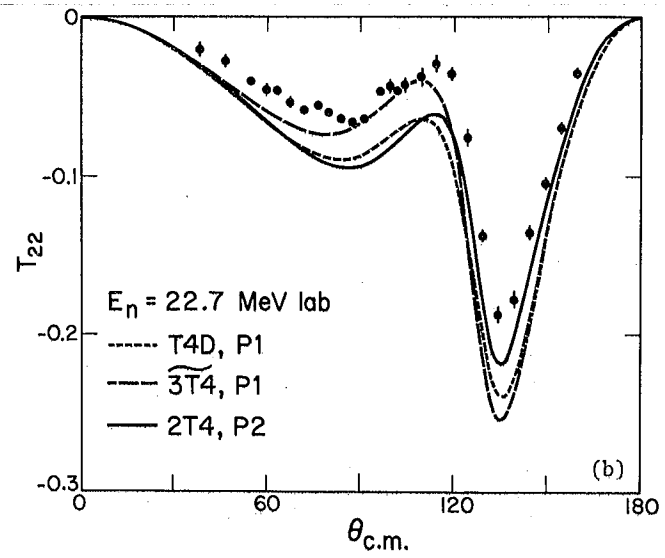

Fig. 1. (a) Tensor analyzing power component T_{20} in d-p scattering at E_d = 45.4 MeV. The calculated curves are from Ref. 8.
(b) Tensor analyzing power component T_{22} in d-p scattering at E_d = 45.4 MeV. The calculated curves are from Ref. 8.
[(a) XBL 778-1575; (b) XBL 778-1576]

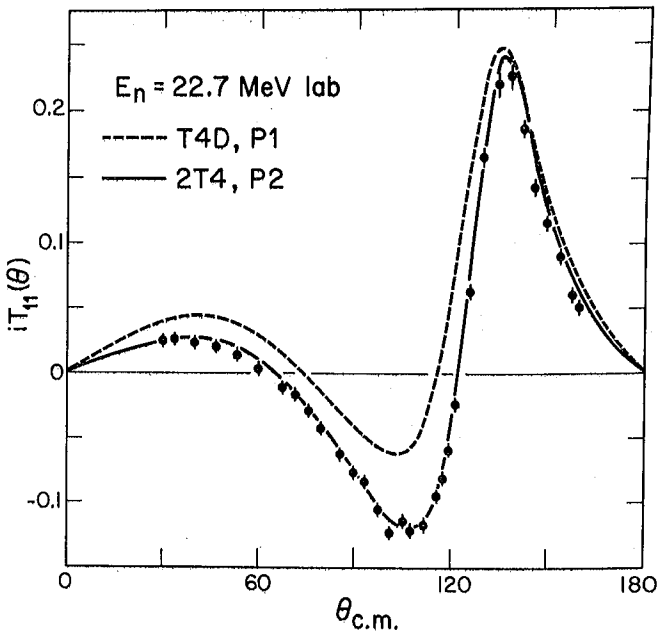

Fig. 2. Deuteron vector analyzing power iT_{11} in d-p scattering at E_d = 45.4 MeV. The calculated solid curve is from Ref. 8. (XBL 778-1574)

Footnotes and References

*Excerpted from invited talks given at the Symp. on Few Body Problems, Science University of Tokyo, Japan, 2-3 September 1977 and at the Symp. on Highly Excited States and Polarization Phenomena, Osaka University, Osaka, Japan, 14-17 September 1977.

1. W. Tornow et al., Phys. Rev. Lett. 39, 915 (1977).

2. D. H. Fitzgerald et al., Nucleon-Nucleon Interactions--1977, AIP Conf. Proc. No. 41, D. F. Measday, H. W. Fearing, and A. Strathdee, eds. (Amer. Inst. of Physics, NY, 1978), p. 91.

3. J. Binstock and R. Bryan, Phys. Rev. D 9, 2528 (1974).

4. R. L. Walter, private communication.

5. R. Roy et al., Proc. Intl. Conf. on Nuclear Structure, Organizing Committee, eds. (Intl. Academic Printing Co., Japan, 1977), p. 4.

6. H. E. Conzett, in Few Body Problems in Nuclear and Particle Physics, R. J. Slobodrian et al., eds. (Les Presses de L'Université Laval, Québec, 1975), p. 566.

7. P. Doleschall, Nucl. Phys. A 220, 491 (1974).

8. P. Doleschall, private communication.

TENSOR ANALYZING POWER IN $\vec{d}$ + p SCATTERING AND THE DEUTERON D-STATE

H.E. Conzett, P. von Rossen, E.J. Stephenson,* B.T. Leemann, and R.M. Larimer

Although it has been known for more than 35 years that the deuteron has a small D-wave component, the D-state probability has not been determined within a factor of 2, with values ranging from 3.3 to 9%.[1] Since its value is always deduced from an experimental result via a model-dependent calculation, it is in fact not an experimental observable of the deuteron.

In a recent paper, Amado et al.[2] advocate the use of a different quantity to specify the deuteron D-state, i.e., the ratio, ρ_D of the asymptotic D-wave to S-wave parts of the deuteron wave function. They show how ρ_D can be determined in a model-independent fashion from precise measurements in d+p elastic-scattering at backward angles. The back-angle scattering amplitude is dominated by the neutron-exchange amplitude, which has a pole (in the momentum-transfer variable) whose position in the complex θ_{cm} plane is given by

$$\cos\theta_p = -\left(\frac{5}{4} + \frac{9}{4}\ B/E\right) \quad , \qquad (1)$$

where B is the deuteron binding energy and E is the deuteron laboratory kinetic energy. At the pole, the calculation of Ref. 2 yields an exact and simple relationship between ρ_D and the tensor-analyzing power component $T_{22}(\theta)$:

$$\rho_D = -(T_{22}(\theta)/\sin^2\theta)(0.2495E)^{-1} \quad , \qquad (2)$$

at $\cos\theta_p$. The procedure, then, is to measure $T_{22}(\theta)$ precisely, with particular emphasis on data at angles approaching $\theta = 180^0$ where $\cos\theta = -1.0$. An extrapolation of the measured $T_{22}(\theta)/\sin^2\theta$ to the pole at $\cos\theta_p$ then gives a direct determination of ρ_D from Eq. (2).

From Eq. (1), it is important to measure $T_{22}(\theta)$ in $\vec{d}$ + p scattering at the higher energies that are available with polarized deuteron beams, since the pole position then moves closer to the physical region at $\cos\theta = -1.0$. Thus, we have measured $T_{22}(\theta)$ at E = 45 MeV, for which $\cos\theta_p = -1.36$. Our data are shown in Fig. 1, where the errors indicated are from counting statistics alone. An additional overall normalization error of 3%-5% is present. A preliminary extrapolation to the pole via a Legendre polynomial fitting of $T_{22}(\theta)/\sin^2$ revealed a problem connected with the fitting procedure. That is, the deduced value of ρ_D is rather strongly dependent on the maximum L-value of the Legendre polynomial fit, so it is clear that the extrapolation procedure must be investigated in an attempt to find a procedure that has a better convergence behavior.

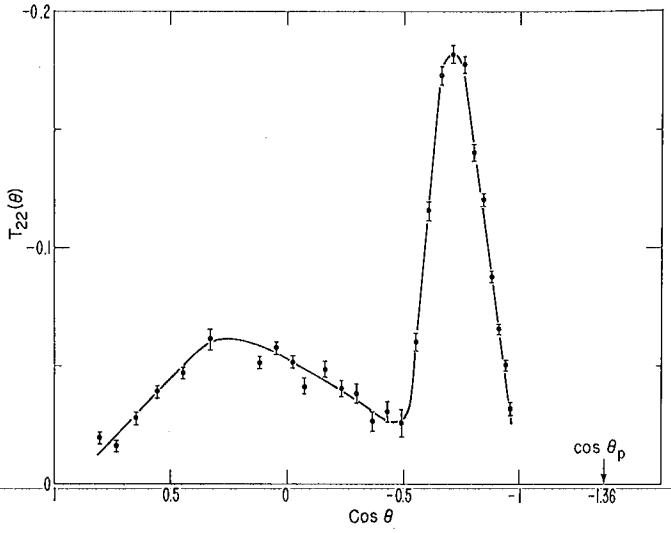

Fig. 1. Tensor-analyzing power, $T_{22}(\theta)$, in $\vec{d}$ + p elastic-scattering at 45 MeV. The arrow marks the position of the neutron exchange pole at $\cos\theta_p = -1.36$. (XBL 788-2623)

Footnotes and References

*Present address: Physics Division, Argonne National Laboratory, Argonne, Illinois.

1. D. W. L. Sprung, in Few Body Problems in Nuclear and Particle Physics, R. J. Slobodrian et al., eds. (Les Presses de L' Université Laval, Québec 1975), p. 475.

2. R. D. Amado, M. P. Locher, and M. Simonius, Phys. Rev. Lett. 17, 403 (1978).

CROSS SECTION AND VECTOR ANALYZING POWER iT_{11} IN THE PROCESSES $^3He(\vec{d}, d)^3He$ AND $^3He(\vec{d}, p)^4He$ BETWEEN 15 AND 40 MeV

R. Roy,* F. Seiler,† H.E. Conzett, F.N. Rad,‡ and R.M. Larimer

The mass-5 system has been the object of numerous experimental and theoretical studies in the past several years. The $^3He(d,p)^4He$ reaction is a particularly suitable process for both theoretical and experimental investigations. Its spin structure is already quite complex, but polarized beams or targets can be prepared for all reactants with spin, making a large number of observables available for a detailed comparison of theory and experiment. The present work extends the range of vector polarization studies of the processes $^3He(\vec{d},d)^3He$ and $^3He(\vec{d},p)^4He$ from 15 to 40 MeV in 5 MeV intervals. Complete differential cross sections $\sigma_0(\theta)$ and angular distributions of the vector analyzing power $iT_{11}(\theta)$ have been measured at all energies. Cross sections and angular-distributions of polarization for both processes were analyzed in terms of Legendre polynomials. The resulting coefficients were investigated for energy-dependent features such as those predicted by some analyses and models. In addition, the elastic scattering data were fitted with an optical model analysis.

A purely vector polarized deuteron beam of the Berkeley 88-inch cyclotron impinged on a ^3He gas target in a 36 in. scattering chamber. The beam polarization was monitored in a $^4He(\vec{d},d)^4He$ polarimeter located further downstream. Typically about 80% of the maximum possible value ($P_y = 2/3$) was found. During a run the polarization usually remained constant to within 0.01.

The present data, summarized in Figs. 1 and 2, show few and only gradual changes in the angular distributions of both observables. The vector analyzing power reaches relatively large fractions of the maximum possible values ($iT_{11} = \pm(1/2)\sqrt{3}$), mostly at rear angles for elastic scattering but at forward angles for the proton reaction. In the latter the angular distribution of iT_{11}, which is essentially antisymmetric with regard to 90^0 at 11.5 MeV and below, changes to a more symmetric appearance between 20 and 30 MeV. The elastic scattering data, on the other hand, show little change over the entire energy region.

Both the cross sections $\sigma_0(\theta)$ and the quantities $-2iT_{11}(\theta)\cdot\sigma_0(\theta)$, derived from the vector analyzing power, were parametrized by expansions in terms of appropriate Legendre polynomials. The normalized expansion coefficients $d_{00}(L)$ and $d_{11}(L)$, respectively, have been defined elsewhere.[1] The maximum degree L_m of the polynomials used was determined in the usual manner, except in cases where a generally nonzero coefficient crosses zero as a function of energy. In these circumstances, that particular coefficient was also allowed to vary freely. The values of maximum degree L_m, determined in this manner, varied between 8 and 12. With 25 to 35 data points per angular distribution, the resulting degrees of freedom of the fits were sufficiently large for a reliable determination of the coefficients. The resulting fits are shown as the solid lines in Figs. 1 and 2.

The cross section $\sigma_0(\theta)$ for elastic scattering of the deuterons shows a strong energy-dependent structure of the coefficients $d_{00}(L)$ near 35 MeV and a weaker one near 20 MeV. While almost all coefficients are strongly affected at the higher energy, the structure near 20 MeV shows best in the coefficients of higher degree L. A similar situation obtains for the cross section of the $^3He(d,p)^4He$ reaction. The structure at higher energies, however, is not nearly as dominant, while the one at the lower energy affects again all coefficients.

The expansion coefficients $d_{11}(L)$ show quite generally less structure. In elastic scattering they are small and do not vary strongly with energy, although they show perturbations near both 20 and 35 MeV. In the $^3He(\vec{d},p)^4He$ reaction, almost no corresponding structure can be discerned at 35 MeV, while the one at 20 MeV is very weak. In this process, however, the main energy dependent features are shown by the coefficients $d_{11}(1)$ and $d_{11}(2)$. At low energies the L = 2 term is large and dominates all others. As the energy increases toward 20 MeV, it goes to small values, while the initially unimportant L = 1 coefficient becomes large enough to determine the gross structure of the angular distribution.

This change can be interpreted in terms of intermediate states in the ^5Li system. An expansion coefficient $d_{kq}(L)$ is a linear combination of a set of interference terms $R_1R_2^*$ of reaction amplitudes

$$R_i \equiv \langle \ell_i', s_i', J_i^\pi | R | \ell_i, s_i, J_i^\pi \rangle \quad .$$

A restriction required by parity conservation for all first-order and some second-order polarization observables[1] is that the interference term must satisfy the condition $\ell_1+\ell_2+L$ = even. Thus the L = even terms involve combinations of reaction matrix elements with equal parity, while opposite parities lead to contributions to the L = odd coefficients. Thus the predominance of the coefficient $d_{11}(2)$ supports the result of calculations by Heiss and Hackenbroich[2] which lead to strong interference terms between members of a quartet of d-wave resonances. Correspondingly, the rise in importance of the L = 1 coefficient with increasing energy is due to terms involving matrix elements of opposite parity, such as the d-wave amplitudes and a large f-wave $7/2^-$-state proposed recently[1] at deuteron energies above 11.5 MeV.

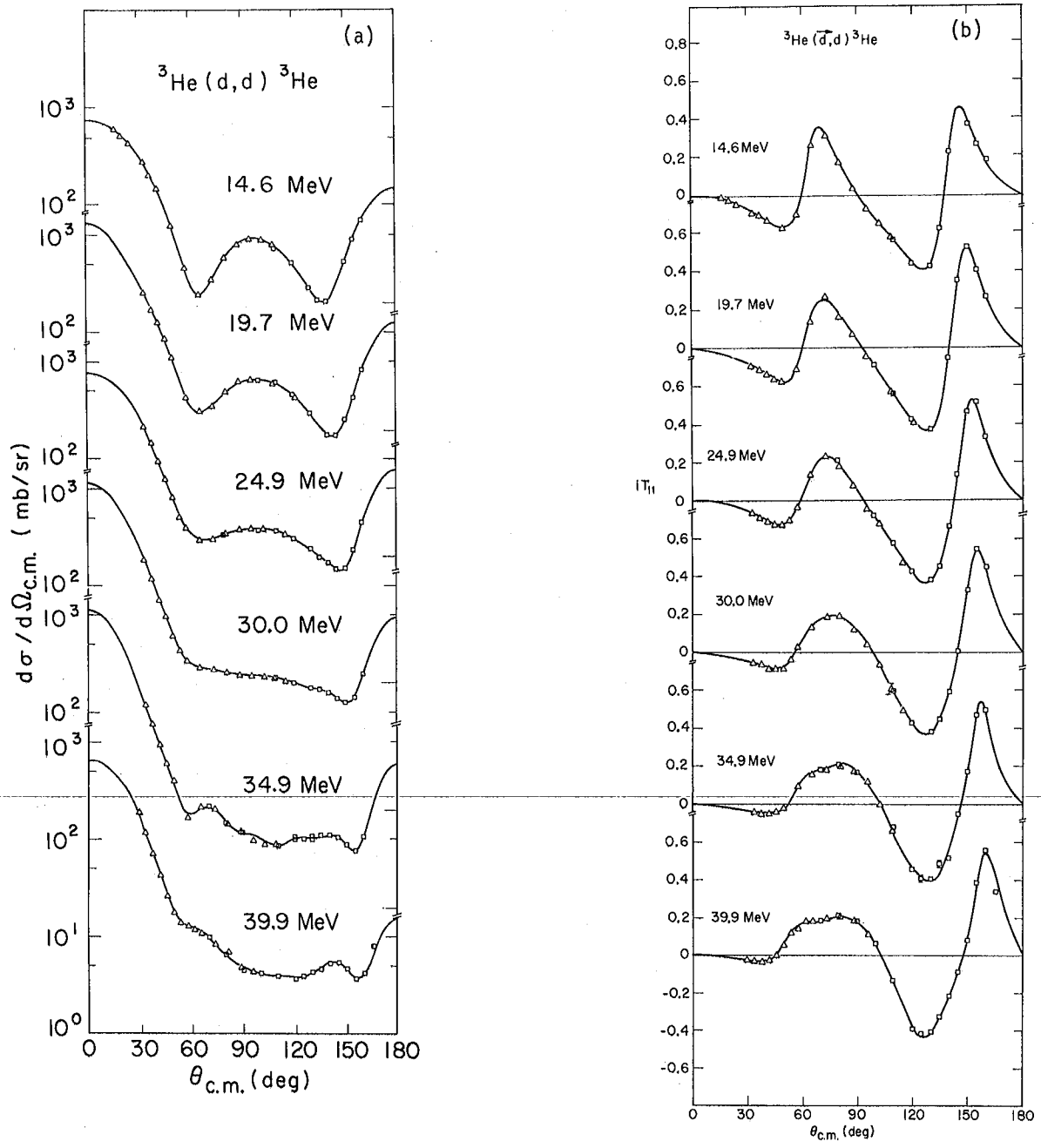

Fig. 1. ^{3}He($\vec{d}$,d)^{3}He: (a) differential cross sections, and (b) vector analyzing powers. The solid lines are Legendre polynomial fits to the data. [(a) XBL 763-2524; (b) XBL 7512-9210]

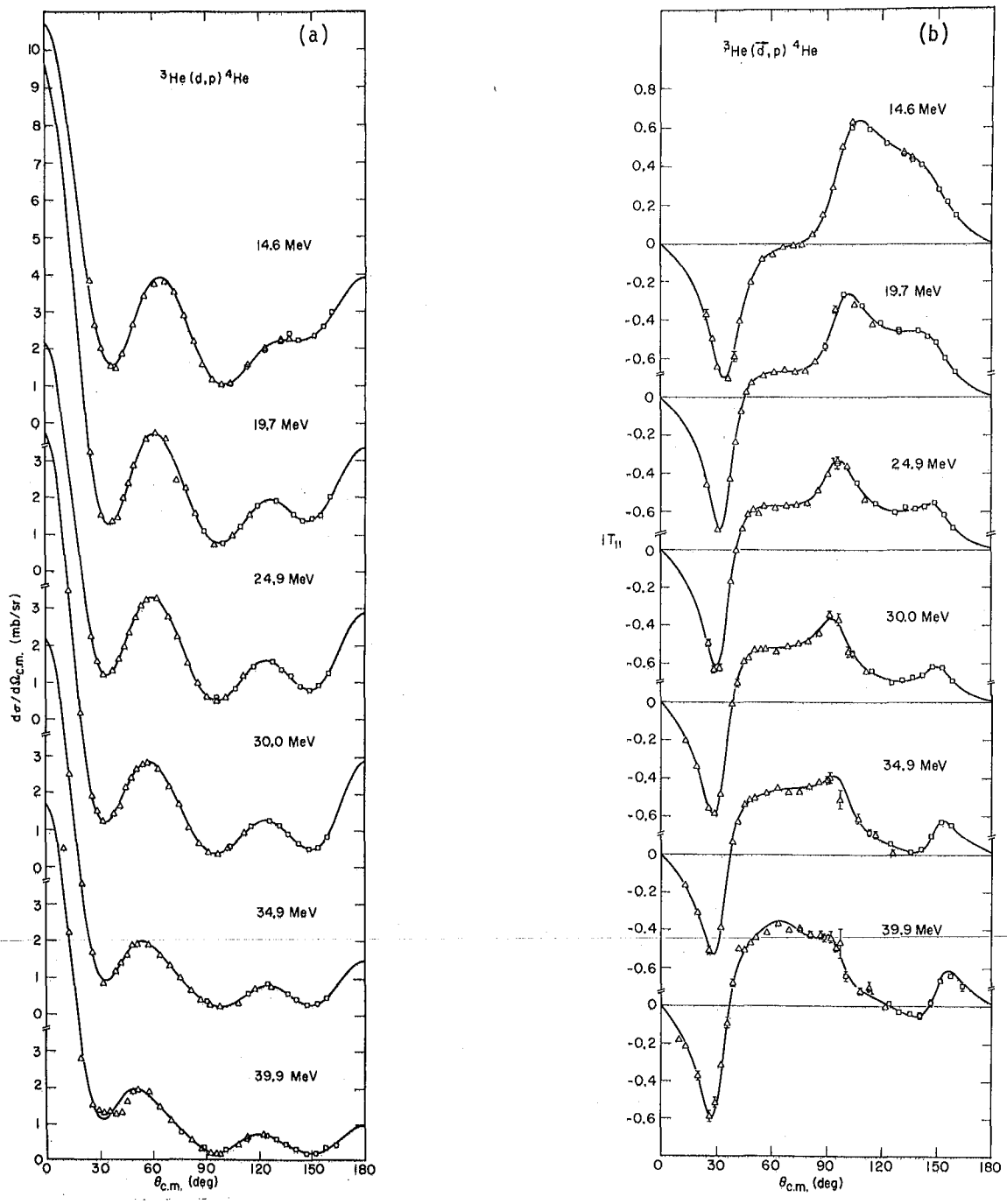

Fig. 2. ^{3}He(d⃗,p)^{4}He: (a) differential cross sections, and (b) vector analyzing powers. The solid lines are Legendre polynomial fits to the data.
[(a) XBL 7512-9207; (b) XBL 7512-9209]

Footnotes and References

*Research Council of Canada, Postdoctoral Fellow. Present address: Universite Laval, Québec, Canada.

†Present address: Physics Department, University of Basel, Switzerland.

‡Present address: Laboratory for Nuclear Science, MIT, Cambridge, Massachusetts.

1. F. Seiler, Nucl. Phys. A 187, 379 (1972), and A 244, 236 (1975).

2. P. Heiss and H. H. Hackenbroich, Nucl. Phys. A 162, 530 (1971).

ELASTIC SCATTERING OF $\vec{p}$ + ^{28}Si IN THE GIANT RESONANCE REGION

C.R. Lamontagne,* B. Frois,† R.J. Slobodrian,* H.E. Conzett, and Ch. Leemann

We have measured angular distributions of the differential cross section and of the analyzing power in the scattering of polarized protons from ^{28}S at eight energies between 17 and 29 MeV. Our experimental results are shown in Fig. 1. The analyzing power shows a strong energy dependence of the negative maximum (near $\theta_{cm} = 40^{o}$) through this energy region. An optical model (OM) analysis of these data yields a corresponding energy dependence of the spin-orbit interaction strength, V_{SO}, shown in Fig. 2. Since this energy interval spans the giant dipole resonance region of the

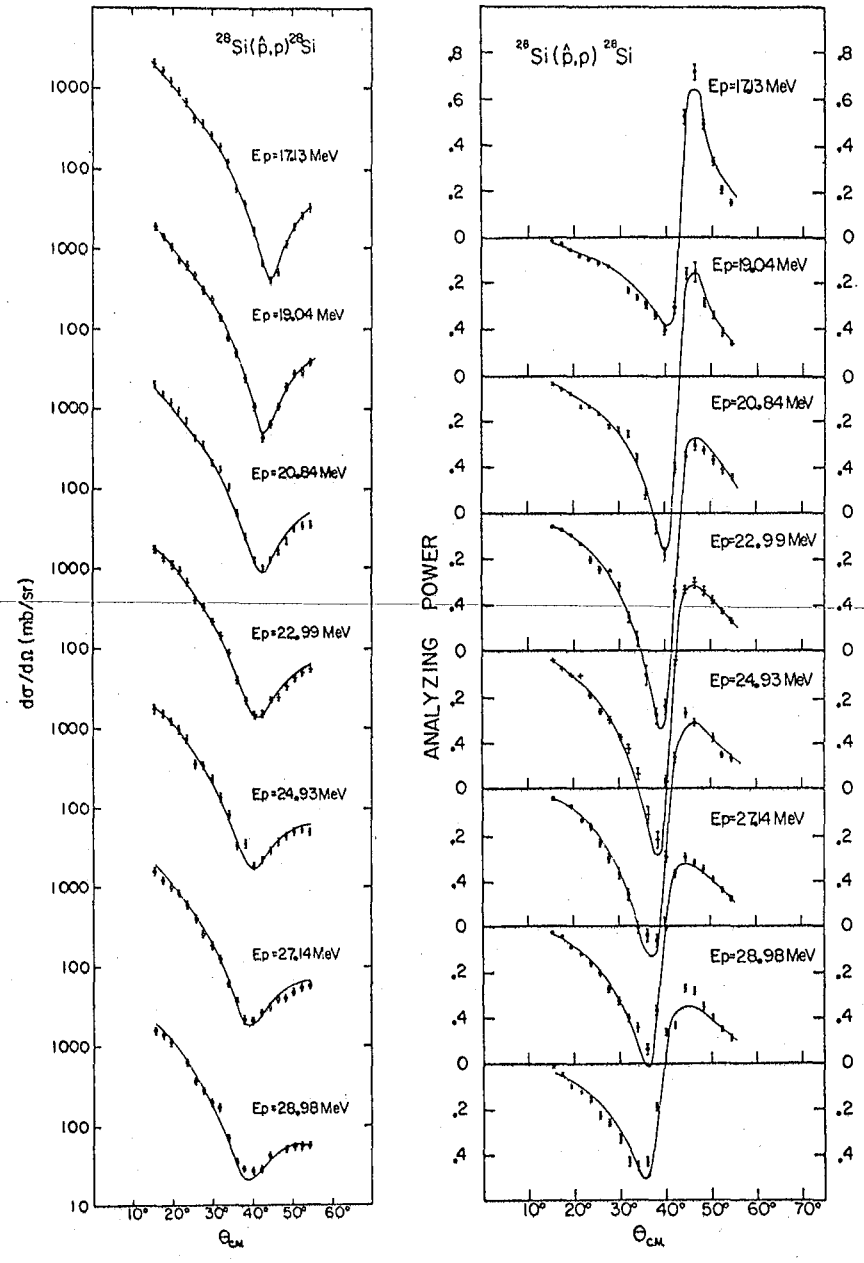

Fig. 1. Differential cross sections and analyzing powers in $\vec{p}$ + ^{28}Si elastic scattering between 17 and 29 Mev. The solid line are optical model fits to the data. (XBL 788-2626)

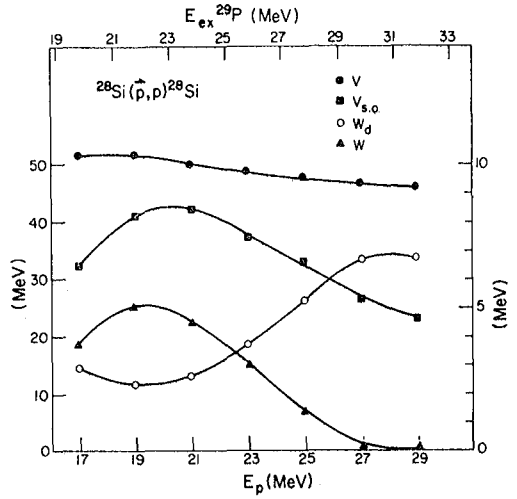

Fig. 2. Optical model potential parameters derived from fitting the data. The absorptive potential, W + W_D, is an approximately constant function of energy. (XBL 788-2627)

composite system, ^{29}P, it is natural to try to explain the energy dependence of our experimental results in terms of the coupling of the giant resonance to the elastic proton channel. Other studies have been carried out in such regions for $\vec{p}$ + ^{24}Mg, $\vec{p}$ + ^{27}Al, and $\vec{p}$ + ^{32}S.[1] Weller et al.[2,3] have studied $\vec{p}$ + ^{14}C and p + ^{56}Fe. It has been established through inelastic proton scattering from a broad range of nuclei that just below the giant dipole there are also quadrupole and monopole resonances. The proton widths of these resonances imply that they should affect the proton elastic scattering.

Since the standard OM calculation does not include contributions to the scattering from other than the shape-elastic resonances, it is possible that the anomalous behavior found for $V_{SO}(E)$ is due to a giant resonance contribution to the scattering which is not specifically included in the calculation. In their investigations over the giant resonance regions of ^{15}N and ^{57}Co via $\vec{p}$ + ^{14}C and $\vec{p}$ + ^{56}Fe elastic scattering, Weller et al. carried out phase shift analyses of their data, and they found in each case an energy dependence of a single partial-wave amplitude that showed a broad resonance behavior which they interpreted to be consistent with the effect of a giant dipole resonance. Weller and Divadeenam[4] had also examined the phase shifts derived from the OM analysis of our data,[5] and they concluded that the $g_{9/2}$ partial wave exhibited an energy dependence appropriate to a J^π = 9/2* resonance at E_{LAB} = 23 MeV, with a proton width of 1.62 MeV and a total width of 6.0 MeV. This clearly had no connection with the giant dipole resonance in ^{29}P, which is restricted to J^π = 1/2$^-$ or 3/2$^-$ components since only these can decay to the 1/2$^+$ ground state via an E1 transition. Then, on the basis of a 2p - 1h doorway state calculation, they concluded that a strong 9/2$^+$ resonance, with an energy and a width appropriate to account for the data, was indeed predicted by the calculation.

We find an alternate, more plausible explanation for the behavior of the $g_{9/2}$ phase shifts in p + ^{28}Si scattering between 17 and 29 MeV, and we raise the question as to whether or not the resonance behavior seen in the $\vec{p}$ + ^{14}C and the p + ^{56}Fe studies[2,3] can be attributed unambiguously to the giant dipole resonances of those systems. We have examined the energy dependence of the partial wave amplitudes,

$$f_{lj} = [\eta_{lj}\exp(2i\delta_{lj}) - 1]/2i \quad ,$$

and it is seen that the anomalous behavior of V_{SO} (Fig. 2) does not result in a resonant behavior of $f_{g\ 9/2}$ between 17 and 29 MeV which is not already present for the potential with a linearly interpolated V_{SO}, i.e., a shape elastic effect. It is also not clear that the energy dependence of $f_{g\ 9/2}$ can be described as resonant. Its trajectory certainly does not trace an approximate circle in a counter-clockwise direction in an Argand diagram. Thus, the ascription of the $g_{9/2}$ phase shift behavior to a doorway state resonance is questionable. In order to investigate whether the giant dipole resonance of ^{29}P was in some way connected with the anomalous behavior of $V_{SO}(E)$ in our OM analysis, we performed a constrained phase-shift analysis of our data. That is, we searched on the p-wave phase shifts while constraining the other phase shifts to their OM values for the potential with the linearly interpolated values of $V_{SO}(E)$. The p-wave amplitudes determined in this manner were less smooth functions of energy, but their general trends were similar. Thus, no evidence for a p-wave resonance was found, so an effect due to the ^{29}P giant dipole resonance is not seen in our analysis.

Footnotes and References

*Université Laval, Québec, Canada.

†Present address: CEN SACLAY, SPNHE, Gif-sur-Yvette, France.

1. J. Birchall, H. E. Conzett, C. R. Lamontagne, R. M. Larimer, R. Roy, and R. J. Slobodrian, to be published.
2. H. R. Weller et al., Phys. Rev. Lett. 33, 657 (1974).

3. H. R. Weller et al., Phys. Rev. C. 13, 1055 (1976).

4. H. R. Weller and M. Divadeenam, Phys. Lett. B 55, 41 (1975).

5. C. R. Lamontagne et al., Phys. Lett. B 45, 465 (1973.

EXTREME VALUES OF THE SPIN POLARIZATION ANALYZING POWER IN NUCLEAR REACTIONS*

F. Seiler,† F.N. Rad,‡ H.E. Conzett, and R. Roy§

Large values of the polarization have been known in p-α and n-α scattering for some time. Analytically the existence of absolute values of unity was first proven by Plattner and Bacher[1] for several elastic scattering processes with the particularly simple spin space $\vec{1/2} + 0 \to 1/2 + 0$. Subsequently, Gruebler and collaborators[2] proved the existence of several extreme values for the spin-1 polarization in d-α elastic scattering ($\vec{1} + 0 \to 1 + 0$). In both cases a single linear relation between transition amplitudes must be satisfied. Proof is therefore simple if an analysis of the process is available.

In a nuclear reaction, as opposed to elastic scattering, the possibility of an extreme value of a polarization observable was first proposed[3] for the process $^3\mathrm{He}(\vec{d},p)^4\mathrm{He}$. The proof of existence used above for the cases of elastic scattering with a simple spin space can no longer be applied, since two conditions have to be satisfied simultaneously. Recently, these linear conditions for elements of the transition matrix were derived quite generally[4] for the analyzing power of the four-particle reaction $\vec{A} + B \to C + D$ with spins $\vec{a} + b \to c + d$. In this paper, we provide a more general discussion of extreme values of analyzing powers. States of maximum polarization (analyzing power) are described, and their usefulness in the calibration of polarization measurements and in the analysis of data for the determination of the M-matrix amplitudes is discussed. Known and proposed points of extreme values in elastic scattering and in reactions, respectively, are reviewed, and the required values of the other polarization observables are listed.

The description of a state of maximum polarization for an ensemble of spin-1/2 particles is straightforward. Therefore consideration will be given here only to the less obvious case of spin-1 polarization. It is usually described in terms of tensor moments of an irreducible set of spherical tensors τ_{kq} or of the set of corresponding Cartesian tensors p_i, p_{ij} as defined by the Madison convention.[5] Since the Cartesian tensors do not form an irreducible set, there exists a condition requiring that

$$p_{xx} + p_{yy} + p_{zz} = 0 \quad . \tag{1}$$

Therefore the second rank quantities usually given are p_{zz}, p_{xz} and p_{xx}-p_{yy}, in direct correspondence to the spherical tensors t_{2q}. An equivalent situation exists for the analyzing power T_{kq} or A_{ij}, so that again the quantity A_{yy} often does not appear directly, but only in the combination $A_{xx} - A_{yy}$. This probably is the reason why extreme values of the analyzing power A_{yy} went unnoticed in some instances even though experimental data indicating such values were available.

The limits of the values for the usual polarization parameters are

$$-1/2\sqrt{3} \leq it_{11} \leq 1/2\sqrt{3} \quad , \quad -1 \leq p_y \leq 1 \tag{2a}$$

$$-\sqrt{2} \leq t_{20} \leq 1/2\sqrt{2} \quad , \quad -2 \leq p_{zz} \leq 1 \tag{2b}$$

$$-1/2\sqrt{3} \leq t_{21} \leq 1/2\sqrt{3} \quad , \quad -3/2 \leq p_{xz} \leq 3/2 \tag{2c}$$

$$-1/2\sqrt{3} \leq t_{22} \leq 1/2\sqrt{3} \quad , \quad -3 \leq p_{xx}-p_{yy} \leq 3 \quad . \tag{2d}$$

For the polarization efficiencies T_{kq} and A_i, A_{ij}, also defined according to the Madison convention, the same range of values apply. For the components p_{xx} and p_{yy} that appear only in combination in Eq. (2d), the individual limits are the same as for p_{zz}.

Limits for the polarization attainable by an ensemble of spin-1 particles produced in a nuclear reaction were discussed very early in Lakin.[6] These maximum possible values were derived using the fact that the density matrix of the ensemble is positive semi-definite. This imposes restrictions on the tensor moments t_{kq}, derived from the expansion of the density matrix of the outgoing particles in terms of the set of irreducible operators τ_{kq}. Invoking time reversal invariance, identical limitations can be shown to apply to the polarization efficiencies T_{kq}.

Since the conditions due to parity conservation assume a particularly simple form in a transverse coordinate system S', this was the frame of reference chosen by Lakin. The z'-axis of this coordinate system lies perpendicular to the reaction plane, along $k_{in} \times k_{out}$, while the y'-axis is chosen along the direction k_{out} of the polarized particles. The positivity conditions turn out to be considerably more simple in the traverse system S' than in the Madison frame. They yield the inequalities[6]

$$\varepsilon^2 \equiv 1/2\{(T'_{10})^2 + (T'_{20})^2 + 2|T'_{22}|^2\} \leq 1 \tag{3}$$

and

$$\varepsilon^2 \equiv (T'_{20} + \sqrt{2})^2 - 3(T'_{10})^2 - 6|T'_{22}|^2 \geq 0 \quad . \tag{4}$$

In the space $(T'_{10}, T'_{20}, \sqrt{2}|T'_{22}|)$ the condition $\varepsilon^2 \leq 1$ defines the interior of a sphere, and the inequality $\varepsilon^2 \geq 0$ the interior of an inscribed cone. Clearly, condition (4) is more restrictive than inequality (3). This situation is shown graphically in Fig. 1, where the coordinate axes have been relabelled with the Cartesian observables according to the Madison convention.

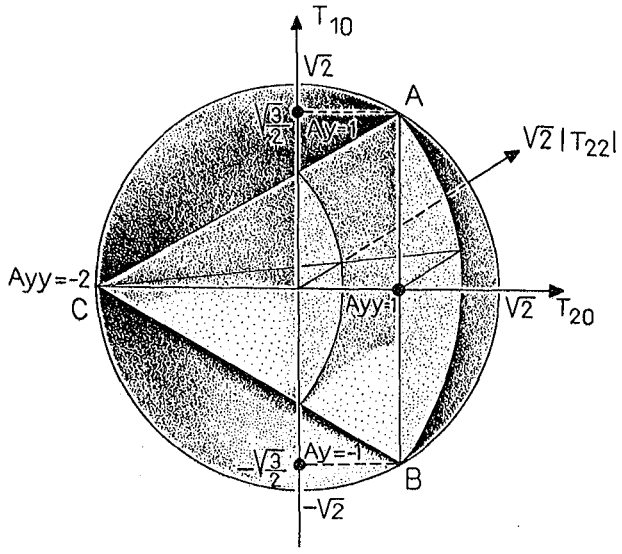

Fig. 1. The polarization sphere with the inscribed Lakin cone. Points A and B correspond to $A_y = \pm 1$, point C to $A_{yy} = -2$ and the base of the cone to $A_{yy} = 1$. The axes of the transverse polarization quantities T_{kq} have been partly labeled with the usual Cartesian tensors. (XBL 788-2624)

Extreme points $A_{yy} = 1$ lie anywhere on the bases of the cone, and condition (4) yields the restriction

$$1 \geq (A_y)^2 + 4/9(A_{xz})^2 + 1/9(A_{zz} - A_{xx})^2 \quad . \qquad (5)$$

Extreme values $A_y = \pm 1$ are only possible at the points A and B of Fig. 1, respectively. The necessary conditions are

$$A_{yy} = 1 \quad , \quad A_{xx} = A_{zz} = -1/2 \quad , \quad A_{xz} = 0 \quad . \qquad (6)$$

They are not sufficient, however, since they only define a point somewhere on the line AB. Equations (6) thus show that the condition $A_{yy} = 1$ is a prerequisite for an extreme value $A_y = \pm 1$, and that all the other efficiencies are numerically determined. This was demonstrated for $^4He(\vec{d},d)^4He$ elastic scattering by Grüebler et al.,[2] using the properties of that particular M-matrix. From the derivation given here, it is obvious that Eqs. (6) are valid for any process

$$\vec{1} + b \rightleftharpoons c + d \quad , \qquad (7)$$

where b, c and d are arbitrary spins and $\vec{1}$ stands for the only polarization (spin-1) determined in or by the experiment. The requirement that both A_y and A_{yy} reach their peak values at the same point (θ_0, E_0) is therefore also a general condition, which may be useful in experimental and theoretical work. Near the point $A_y = \pm 1$, the relations between the values of A_{yy} and A_y may be of use. Noting that the slope of the Lakin cone is $\pm 1/3$, it follows that

$$A_y = 1 - \eta \rightarrow A_{yy} \gtrsim 1 - 3\eta \quad . \qquad (8)$$

Despite the singular nature of points A and B, a curve representing the values of polarization

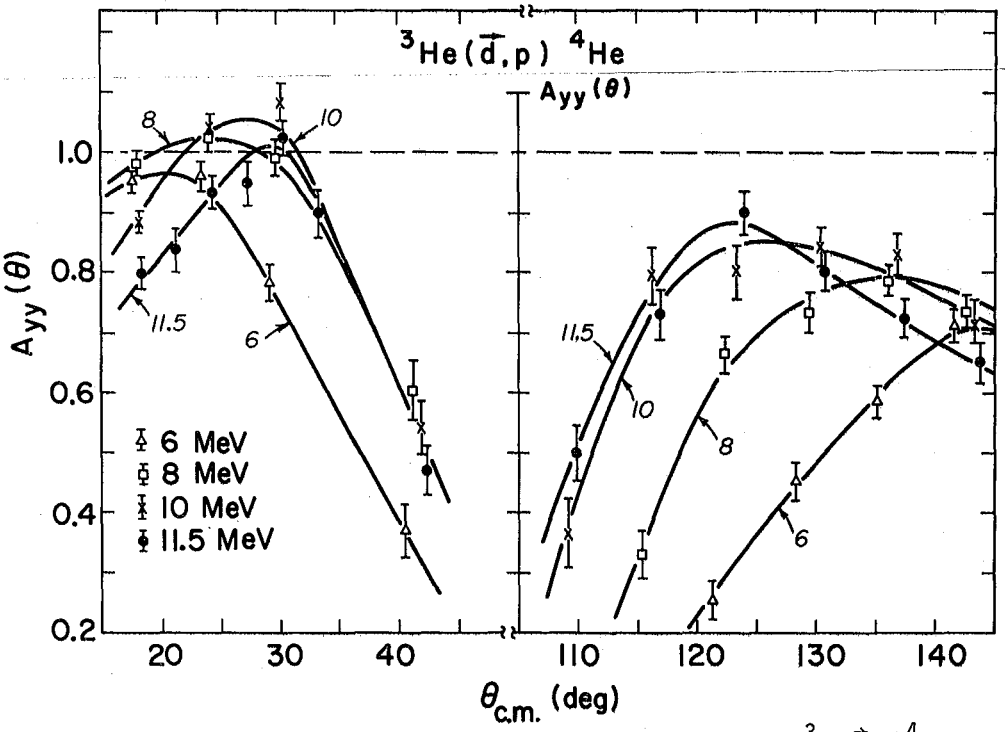

Fig. 2. The component A_{yy} of the analyzing power of the $^3He(\vec{d},p)^4He$ reaction, calculated from the data obtained by Grüebler et al.[8] Clearly an extreme point is reached near 9 MeV and $\theta_{cm} = 27^o$. At angles near 120^o another point might be found at energies above 12 MeV. (XBL 753-2495)

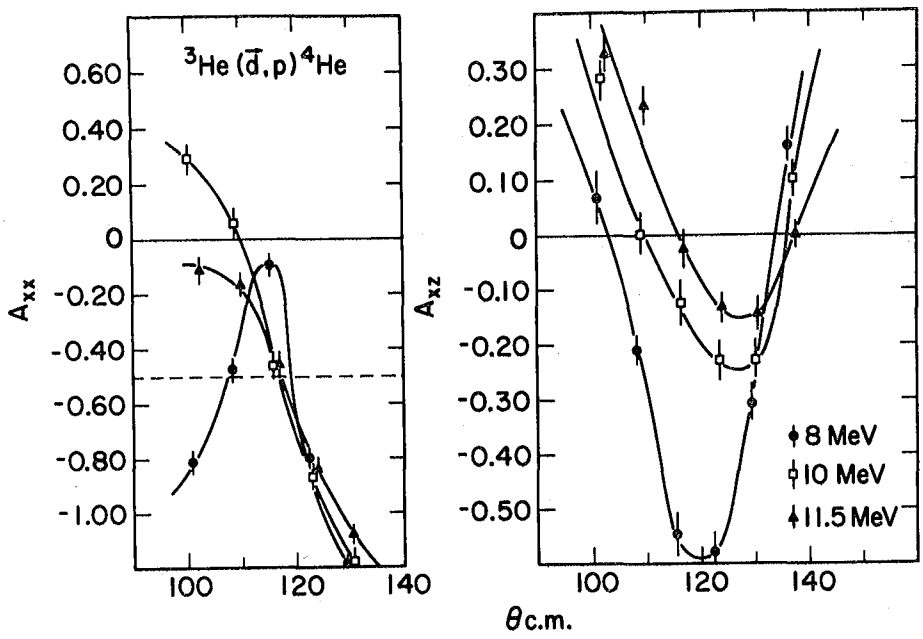

Fig. 3. Values of the components A_{xx} and A_{xz} of the analyzing power of the ^{3}He($\vec{d}$,p)^{4}He reaction near 10 MeV. For a point $A_y = \pm 1$ the values $A_{xx} = -1/2$ and $A_{xz} = 0$ are needed. With increasing energy these values may be obtained near 120°. (XBL 754-2663)

as a function of angle for a given energy may touch these points, with the trajectory starting and ending somewhere within the Lakin cone.

As an example, we consider extreme values of the analyzing power components for a reaction with the spin structure $\vec{1} + 1/2 \rightarrow 1/2 + 0$. The best known reaction of this type, ^{3}He($\vec{d}$,p)^{4}He, was the first process other than elastic scattering for which a point (θ_0, E_0) with maximum possible tensor analyzing power $A_{yy} = 1$ was proposed.[3] This extreme value has recently been confirmed within the experimental error.[7] In addition, an inspection of the complete polarization data of Grüebler et al.[8] at 11.5 MeV and of the measurements of iT_{11} at 15 MeV by Roy et al.[9] indicates the possibility of large absolute values near $\theta_{cm} = 120°$ for both components A_y and A_{yy} of the analyzing power. As the energy increases, so does A_{yy} near 120° (see Fig. 2) and the rest of conditions (6) are nearly fulfilled at 11.5 MeV (see Fig. 3), a prerequisite for values of A_y close to unity. Thus a point (θ_0, E_0) between 12 and 15 MeV with $A_y = A_{yy} = 1$ is a possibility. It should be noted that for large values of A_y the component A_{yy} has to be large also due to restriction (8). Also conditions (6) have to be more or less fulfilled. However, a circle is not very restrictive for lateral movement away from a diameter, even close to the periphery. Thus a close approach of the measured data to the required values may be indicative of an extreme point $A_y = \pm 1$.

Extreme values of the analyzing power have been used very successfully for the calibration of polarizations. In practice, however, problems have arisen with the transfer of the calibration to energies different from that of the extreme point. Clearly, the identification of as many extreme values as possible is therefore of importance. Of particular interest are those points that have in addition near-extreme values over a large range of energy and angle.

Perhaps the most important application of extreme values of polarization observables may be found in the analyses of the processes in which they occur. Similar to the invariance conditions of parity and time reversal, the conditions imposed[4] are linear in the elements of the M-matrix. Unlike the former, they are not valid independent of energy and angle, but hold only for the extreme point (θ_0, E_0). There, however, they lead to severe restrictions on the solution space. Thus the measurements made to extablish the presence of an extreme value have another important application. Introduced into the data base of an analysis, they directly impose these linear conditions on the set of bilinear equations. This may be of importance even in those cases where the existence of an extreme point can be proven analytically, since the quality of the solution required for that kind of proof is not very high. With a few additional measurements, it can thus be improved considerably. Measurements on or near points of extreme values of polarization observables should help to reduce decisively the effort necessary to analyze processes with a non-trivial spin-space.

Footnotes and References

*Condensed from Nucl. Phys. A 296, 205 (1978).
†Present address: Physics Department, University of Basel, Switzerland.
‡ Present address: Laboratory for Nuclear Science, Department of Physics, MIT, Cambridge, Mass., USA.
§Research Council of Canada, Postdoctoral fellow. Present address: Université Laval, Québec, Canada.

1. G. R. Plattner and A. D. Bacher, Phys. Lett. B 36, 211 (1971).

2. W. Grüebler et al., Nucl. Phys. A 242, 285 (1975).

3. F. Seiler, Phys. Lett. B 61, 144 (1976).

4. H. E. Conzett and F. Seiler, Nucl. Phys. A 290, 93 (1977).

5. Polarization Phenomena in Nuclear Reactions, H. H. Barschall and W. Haeberli, eds. (University of Wisconsin Press, 1971).

6. W. Lakin, Phys. Rev. 98, 139 (1955).

7. W. Grüebler et al., Phys. Lett. B 63, 273 (1976); Nucl. Phys. A 271, 29 (1976).

8. W. Grüebler et al., Nucl. Phys. A 176, 631 (1971).

9. R. Roy et al., Proc. of the 4th Intern. Symp. on Polarization Phenomena in Nuclear Reactions, W. Grüebler and V. Konig, eds. (Birkhäuser, Basel, 1976).

STUDY OF THE (^{3}He, t) REACTION MECHANISM*

G. Bruge,† M.S. Zisman, A. Bacher,‡ R. Schaeffer,† C.J. Zeippen,§ and J.M. Loiseaux‖

The present work is concerned with the "charge-exchange" reaction ^{38}Ar(^{3}He,t)^{38}K at 40 MeV. In recent years, increasing use has been made of the (^{3}He,t) reaction as a spectroscopic tool.[1] In fact, it is a very powerful method of reaching nuclei which could otherwise be obtained only through transfer reactions. The charge-exchange reaction is generally described in terms of a microscopic model. In this framework, the (^{3}He,t) reaction is very similar to a reaction involving inelastic scattering of a light projectile. However, in the case of (^{3}He,t) charge exchange, the cross sections are very small, and multistep processes can be a very important part of the reaction mechanism.[2,3]

Great progress has been made in our knowledge concerning the (^{3}He,t) reaction mechanism. Usually an effective force interacting between the projectile center-of-mass and the excited nucleon in the target is used.[4] It seems that enough information has been gathered in the case of nuclei with simple structures to enable one to make a reasonable choice of the force parameters and to start a spectroscopic study of more complex nuclei.[1,4-10]

In particular, the existence of new codes allowing for coupled-channel calculations[11] makes it possible to investigate the effect of two-step processes, such as [(^{3}He,α) + (α,t)], on the usual one-step microscopic description of the (^{3}He,t) reaction mechanism. We have concentrated here on the first five levels of ^{38}K since they are well separated in our experiment and their spins and parities are well known.

The experiment was performed using a 40 MeV ^{3}He beam from the Berkeley 88-inch cyclotron. The target was argon gas (enriched to 94.4% ^{38}Ar) at a pressure of 120 Torr which was contained in a cell having a thin (0.68 mg/cm^2) nickel entrance foil and a 2.1 mg/cm^2 Havar exit foil. Tritons were detected by telescopes consisting of 0.25-mm ΔE and 3-mm E detectors which fed a Goulding-Landis particle identifier.[12] Triton groups corresponding to 26 states in ^{38}K up to an excitation energy of about 8 MeV have been observed with an overall energy resolution of 75 keV FWHM; angular distributions have been measured from $\theta_{c.m.}$ = 11° to 50°.

The transitions occurring via the [(^{3}He,α) + (α,t)] channel can be included in a way which is now rather well known.[13-15] We have not solved the whole set of coupled equations, but we have taken into account only the contributions up to second order. The intermediate states were assumed to be obtained by simply picking up a particle from the ^{38}Ar ground state without disturbing the others. The spectroscopic amplitude for the (^{3}He,α) process: $S = \langle {}^{37}\mathrm{Ar} | a_n | {}^{38}\mathrm{Ar} \rangle$ is then unity, since $|{}^{37}\mathrm{Ar}\rangle = a_n |{}^{38}\mathrm{Ar}\rangle$ except for small corrections. Also, the spectroscopic amplitude for the (α,t) process:

$S_p = \langle {}^{38}\mathrm{K} | a_p^+ |{}^{37}\mathrm{Ar}\rangle = \langle {}^{38}\mathrm{K} | a_p^+ a_n |{}^{38}\mathrm{Ar}\rangle$ is then proportional to the same configuration mixing amplitudes as those which enter into the direct, one-step transition.

All the calculations of the present part of our study were done using the coupled channels code CHUCK.[11]

If one considers the magnitude of the second-order transition for each of the levels studied, one realizes that it is rather sensitive (the variation can be a factor of 2, in some cases) to the choice of optical parameters. Obviously the parameter set which gave the best overall agreement with the experimental angular distributions of the five lowest levels of ^{38}K in a one-step calculation is not necessarily the best choice if second-order effects are included. We have had problems in finding optical parameters consistent with the known value of D_0 since large cross sections are usually obtained. The expla-

Table 1. Parameters used in the present calculation which allow for two-step processes.

Set	Particle	V	r_V	a_V	W	r_W	a_W	V_{so}	r_{so}	a_{so}
B + T	^{3}He(a)	150.7	1.22	0.7	23.5	1.5	0.8	-0.96	1.5	0.8
	t(a)	143.7	1.22	0.7	23.5	1.5	0.8	0.96	1.5	0.8
	α(b,c)	198.6	1.458	0.502	19.8	1.51	0.79			
	α(b,d)	183.7	1.4	0.56	26	1.48	0.56			
Boulder	^{3}He(e)	149.0	1.2	0.72	32.2	1.4	0.88	10	1.2	0.72
	t(e)	159.2	1.2	0.72	41.5-0.32E	1.4	0.84	10	1.2	0.72
	α(e)	200	1.4	0.57	55.2-0.6E	1.4	0.57			

(a)Ref. 5.

(b)Rev. 2.

(c)A = 38.

(d)A = 48.

(e)D. C. Weisser, J. S. Lilley, R. K. Hobbie, and G. W. Greenlees, Phys. Rev. C 2, 544 (1970).

nation for this behavior can probably be found in Ref. 16. As it is commonly accepted that the optical model V_R should be close to 200 MeV for α particles and as the parameter $D_0 \approx 480$ MeV-fm$^{3/2}$ is fairly well known, we shall restrict ourselves to the parameters listed in Table 1. One should note that our ^{3}He and triton optical parameter sets are very similar to the ones used by Toyama[2] and indeed they give comparable results.

Whatever optical parameters are chosen, the second-order transition dominates the 3^+ state when the tensor strength is adjusted to fit the ^{48}Ca → ^{48}Sc 3^+ transition. Using the parameters of Table 1, the second-order contribution has about the right magnitude for the 3^+ state of ^{38}K. This gives us a prediction for the two-step process which shall no longer be modified. Figure 1 shows the theoretical results for the direct, two-step and combined processes, as well as experimental measurements for each of the five lowest levels of ^{38}K. One can see that, in the case of the 0^+ and 2^+ levels, the second-order contribution alone is a factor of 2 too small at forward angles, but has the correct magnitude at angles beyond 30°, where the calculations involving a direct mechanism fit poorly. Also, if a central force $V_\tau = 12.5$ MeV is used for both levels, one-step contributions provide just the missing strength at forward angles, and the interference between the two amplitudes leads to angular distributions in which both forward-and backward-angle experimental patterns are qualitatively reproduced. Thus, in the case of natural-parity states, it is possible to describe both levels using exactly the same parameters. In particular, one should notice that the lack of structure and the slope of the 2^+ level are well reproduced. [The theoretical results which are shown in the case of the 2^+ level have been obtained by using the wave functions of Dieperink and Glaudemans;[17] this leads to better agreement than that obtained by simply assuming a $(d^{-2}_{3/2})$ configuration.] As far as the unnatural-parity states are concerned, the two-step contribution alone explains the observed strength of both the 0.458 MeV 1^+_1 and 3^+ ground state, which could not be reproduced by a one-step calculation; on the other hand the second-order effect is too small by an order of magnitude for the 1.704 MeV (1^+_2) state. If one uses a tensor force $V_{T\tau} = 7$ MeV for the 3^+ and both 1^+ levels, all these unnatural-parity states can be reproduced quite well. In this case also, it is possible to describe all the levels by using the same parameters. It should nevertheless be acknowledged that while the magnitude of the 0.458 MeV (1^+_1) level is quite satisfactory and the shape is qualitatively reproduced, the precise form remains a problem. In brief, it seems we are fully justified to conclude that two-step processes including an intermediate α particle are essential to explain the experimental results concerning the ^{38}Ar(^{3}He,t)^{38}K reaction at 40 MeV. However, a more elaborate treatment of the second-order process still seems necessary.[16,18]

As the specific choice of the different parameters has been shown to be crucial, we felt it was important to test the various values we

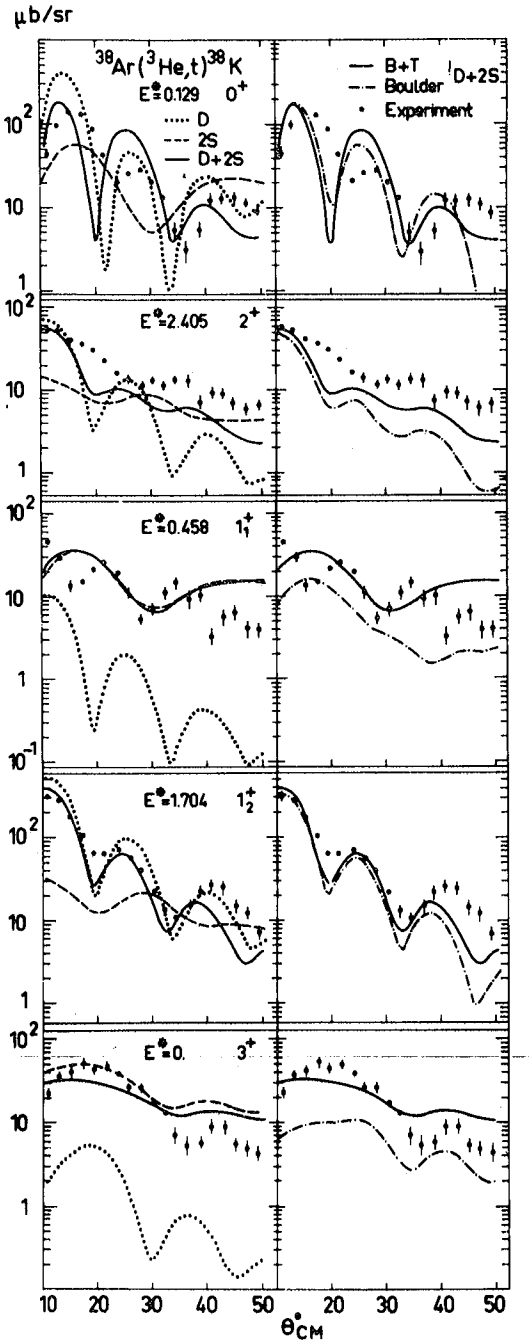

Fig. 1. Microscopic calculations (V_T = 12.5 MeV, V_{T_T} = 7 MeV) for the lowest five levels of ^{38}K, allowing for two-step transitions. Curves for the direct, two-step and combined processes are shown. The optical parameters are given in Table 1.
(XBL 777-9742)

used for A = 38 in the case of A = 48. Figure 2 shows the theoretical curves for direct, two-step and combined transitions, together with experimental data. We show results for all

$(f_{7/2} \rightarrow f_{7/2})_{0^+ \rightarrow 7^+}$ transitions in the

^{48}Ca(^{3}He,t)^{48}Sc reaction. Toyama[2] discussed this reaction previously, but restricted himself to natural-parity levels and to separate two-step and direct transitions. In our case, the strengths we have used to describe the (^{3}He,t) mechanism for A = 38 are consistent with the requirements for A = 48. The theoretical cross sections are in satisfactory agreement with the experimental ones and the shapes of the theoretical curves are quite good. Our results are correct within a factor of 2: the natural-parity transitions are somewhat too weak, whereas the unnatural-parity transitions are slightly too strong. If

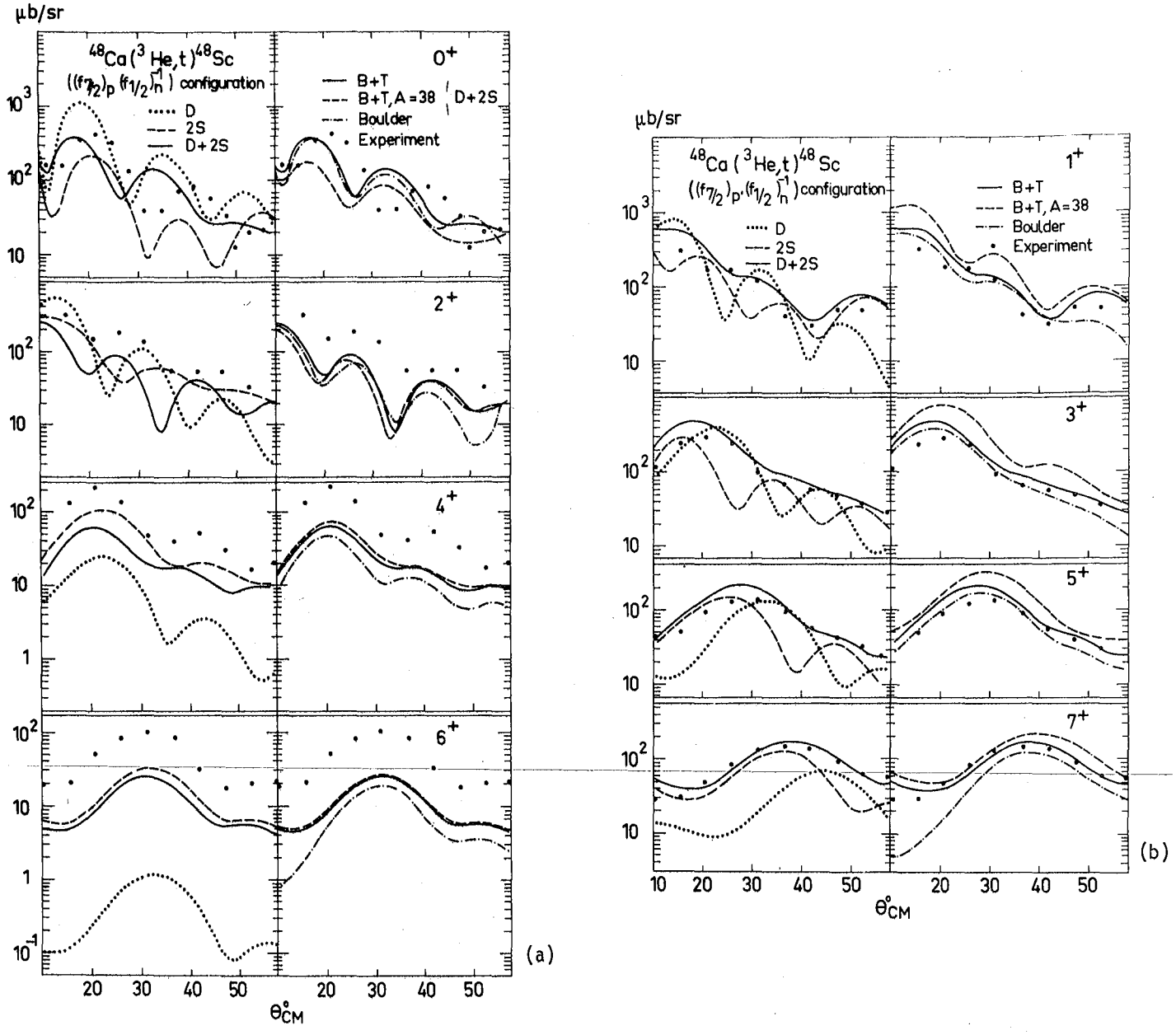

Fig. 2. Microscopic calculations (V_T = 15 MeV, V_{T_T} = 5 MeV) for the $f_{7/2}$ multiplet $0^+ \rightarrow 7^+$ of ^{48}Sc, allowing for two-step transitions: (a) natural parity states; (b) unnatural parity states. Curves for direct, two-step and combined processes are shown, together with experimental data taken from A. Richter, J. R. Comfort, V. Anantaraman, and J. P. Schiffer, Phys. Rev. C 5, 821 (1972). The optical parameters are given in Table 1. [(a) XBL 777-9741; (b) 777-9740]

we made the choice $V_\tau \sim 15$ MeV and $V_{T_\tau} \sim 5$ MeV, we would reproduce the exact strength of the transitions to these eight levels. Thus, we consider that a justification of the choice we made for the different parameters has been provided. In Table 2 the final values of V_τ and V_{T_τ} are given. They are now nearly unique for all spins and targets.

Table 2. Strength parameters for the one-step effective interaction contributing to the (^{3}He,t) reaction.

Configuration	V_τ (MeV)	V_{T_τ} (MeV)
$d_{3/2} \rightarrow d_{3/2}$	12.5	7
$f_{7/2} \rightarrow f_{7/2}$	15	5

Footnotes and References

*Condensed from LBL-5823, to be published in Phys. Rev. C.

†Present Address: CEN Saclay, B. P. No. 2, Gif-sur-Yvette, France.

‡Present Address: Physics Department, Indiana University, Bloomington, Indiana 47401.

§Present Address: Observatoire de Paris, 92190 Meudon, France.

‖Present Address: ISN Grenoble, Grenoble, France.

1. In particular, see Argonne National Laboratory Informal Report No. PHY-1970A, January 1970, and references contained therein.

2. M. Toyama, Phys. Lett. B 38, 147 (1972).

3. G. Bertsch and R. Schaeffer, Phys. Lett. B 38, 159 (1972).

4. P. Kossanyi-Demay, P. Roussel, H. Faraggi, and R. Schaeffer, Nucl. Phys. A 148, 181 (1970).

5. G. Bruge, A. Bussiere, H. Faraggi, P. Kossanyi-Demay, J. M. Loiseaux, P. Roussel, and L. Valentin, Nucl. Phys. A 129, 417 (1969).

6. E. Rost and P. D. Kunz, Phys. Lett. B 30, 231 (1969).

7. R. Schaeffer, Nucl. Phys. A 164, 145 (1971).

8. R. Sherr, T. S. Bhatia, D. Cline, and J. J. Schwartz, Ann. of Phys. 66, 548 (1971).

9. J. R. Comfort, J. P. Schiffer, A. Richter, and M. M. Stautberg, Phys. Rev. Lett. 26, 1338 (1971).

10. J. M. Loiseaux, G. Bruge, P. Kossanyi-Demay, Ha Duc Long, A. Chaumeaux, Y. Terrien, and R. Schaeffer, Phys. Rev. C 4, 1219 (1971).

11. P. D. Kunz and E. Rost, Program CHUCK, University of Colorado, Boulder, Colorado (unpublished).

12. F. S. Goulding, D. A. Landis, J. Cerny, and R. H. Pehl, Nucl. Instr. Methods 31, 1 (1964).

13. W. R. Coker, T. Udagawa, and H. H. Wolter, Phys. Lett. B 41, 237 (1972); Phys. Rev. C 7, 1154 (1973); and Phys. Lett. B 46, 27 (1973); N. B. De Takacsy, Phys. Lett. B 42, 1 (1972); M. Toyama, Nucl. Phys. A 211, 254 (1973).

14. L. D. Rickertsen, M. J. Schneider, J. J. Kraushaar, W. R. Zimmermans, and H. Rudolph, to be published.

15. L. D. Rickertsen and P. D. Kunz, Phys. Lett. B 47, 11 (1973).

16. L. A. Charlton and P. D. Kunz, Phys. Lett. B 72, 7 (1977).

17. A. E. L. Dieperink, and P. W. M. Glaudemans, Phys. Lett. B 28, 531 (1969).

18. F. Osterfeld, T. Udagawa, and H. H. Wolter, Nucl. Phys. A 278, 1 (1977).

STUDY OF HIGH ENERGY HEAVY ION ELASTIC SCATTERING: $^{9}Be + ^{28}Si$

M.S. Zisman, J.G. Cramer,* R.M. DeVries,† D.A. Goldberg,‡ and J.W. Watson§

In recent experiments[1,2] we have investigated in a systematic fashion the elastic scattering of high energy beams of ^{6}Li, ^{12}C, and ^{16}O from a ^{28}Si target. It was found that the ^{12}C and ^{16}O projectiles exhibit behavior very different from that seen for lighter projectiles such as ^{4}He. In particular, ^{12}C and $^{16}O + ^{28}Si$ elastic scattering display diffractive, oscillatory angular distributions at high energies ($E_L \sim 200$ MeV), as opposed to the structureless fall-off associated with nuclear rainbow scattering.[3]

By using both high and low energy ^{12}C or $^{16}O + ^{28}Si$ results simultaneously, it was possible to derive in each case an energy independent six-parameter Woods-Saxon optical potential capable of fitting the ^{12}C (Ref. 1) or ^{16}O (Ref. 2) data over a large energy range. Although this was true only if a rather shallow ($V_0 \sim 10$ MeV) real potential was chosen, it is now known that a different optical model formulation--one which allows for energy dependence in the imaginary diffuseness--is capable of giving similar quality fits to the data over the same energy range.[4]

Because there appeared to be a difference between the diffractive characteristics seen for "heavy ion" projectiles such as ^{12}C or ^{16}O and the refractive behavior seen for "light ion" projectiles such as ^{4}He, the $^{6}Li + ^{28}Si$ system was also recently studied.[1] The ^{6}Li data showed significant differences from that for ^{12}C or ^{16}O. In fact, the experimental angular distribution at 135 MeV did show the effect of nuclear rainbow scattering (which is absent with the heavy ion projectiles) and furthermore, it was not found possible to obtain an energy independent six-parameter Woods-Saxon potential which fit both low and high energy data simultaneously.

Based on these observations, it is apparent that there exists a pronounced transition from light ion to heavy ion behavior which sets in between A = 6 and A = 12. For this reason, we have now embarked on a study of the $^{9}Be + ^{28}Si$ system. In terms of mapping out the transition region, this projectile is an obvious choice. Moreover, ^{9}Be allows us to explore any possible effects in the $^{6}Li + ^{28}Si$ system which are related specifically to the weak binding of ^{6}Li. It is well known that for ^{6}Li elastic scattering, potentials with a large imaginary diffuseness are required,[5] presumably due to the influence of projectile breakup. Because of the small neutron binding energy for ^{9}Be, similar results might be expected. This expectation is in fact borne out in a recent study of 50 MeV ^{9}Be elastic scattering.[6]

Data for $^{9}Be + ^{28}Si$ elastic scattering were measured in the present experiment at $E_{LAB} = 121$ and 201.6 MeV using $^{9}Be(3+)$ and the newly-developed $^{9}Be(4+)$ beams from the 88-inch cyclotron. The detector system consisted of an array of four 2.5-mm Si(Li) detectors spaced 2° apart in the lab system; energy resolution of about 300 keV allowed clean separation of the 1.78 MeV $^{28}Si(2+)$ state except at the few most forward angles ($\theta_L \sim 3°$). As in previous experiments,[1] the beam direction was monitored both by means of a split Faraday cup and by means of measuring the g.s./2+ ratio at a suitably chosen monitor angle. This technique yields beam angle uncertainties of 0.1° or less.

The measured angular distributions together with the 50 MeV data of Stahel et al.[6] are shown in Fig. 1. The curves through the data represent preliminary optical model fits based on both

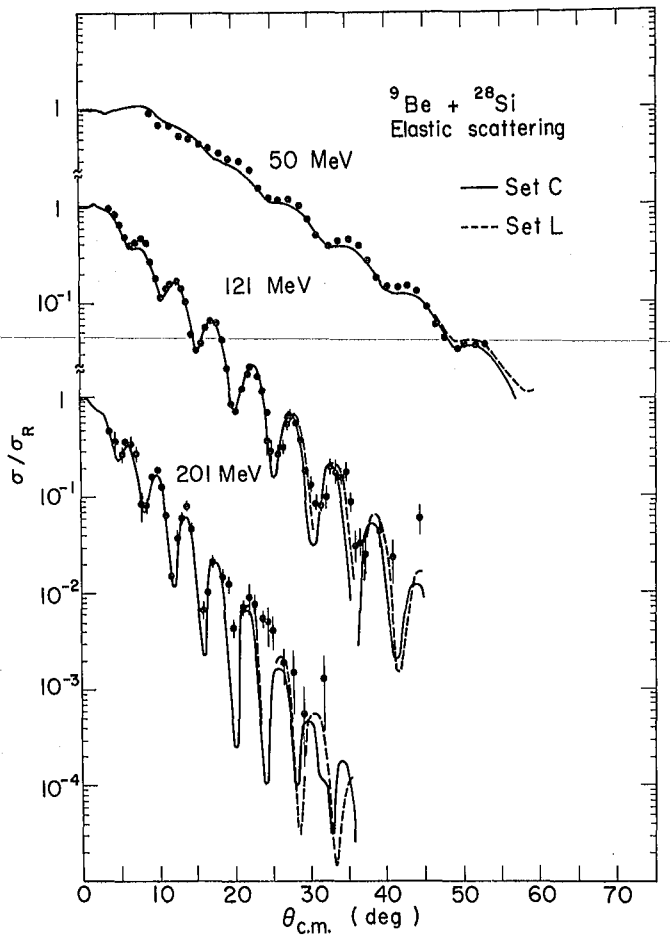

Fig. 1. Measured $^{9}Be + ^{28}Si$ elastic scattering at $E_{Lab} = 50$, 121, and 201.6 MeV. The curves are optical model fits to the data using the potentials given in Table 1. The 50-MeV data are taken from Ref. 6. (XBL 787-1334)

a Li-type potential (Set L in Table 1) and a C-type potential (Set C). It is clear that both types of potential are capable of yielding reasonable fits to the lower energy data sets, although for the highest energy the back angle points ($\theta_{c.m.} \gtrsim 23^{o}$) are not particularly well given by either potential. Attempts to fit the high energy data alone have thus far yielded no improvement on this point.

It is interesting that in this case, as opposed to the findings[1] for either ^{6}Li or ^{12}C, both a shallow (Set C) and a deep (Set L) energy independent potential give quite similar results over a very large energy range. Such an insensitivity to the real well may be a manifestation of the strong absorption due to the projectile breakup process. Hopefully, however, the inclusion of lower energy ^{9}Be + ^{28}Si elastic scattering data in our data set will ultimately allow a determination of whether ^{9}Be behaves as a light ion or a heavy ion projectile.

Table 1. Optical potentials for ^{9}Be + ^{28}Si elastic scattering.

a_I Set	V_o (MeV)	$r_R^{(a)}$ (fm)	a_R (fm)	W_o (MeV)	$r_I^{(a)}$ (fm)	a_I (fm)
L	150.0	0.727	0.877	60.85	1.015	0.791
C	12.1	1.234	0.757	51.3	1.068	0.733

(a) $R = r\,(A_1^{1/3} + A_2^{1/3})$.

Footnotes and References

*University of Washington, Seattle, Washington 98195.

†University of Rochester, Rochester, New York 14627.

‡University of Maryland, College Park, Maryland 20743.

§University of California, Davis, California 95616.

1. R. M. DeVries, D. A. Goldberg, J. W. Watson, M. S. Zisman, and J. G. Cramer, Phys. Rev. Lett. 39, 450 (1977).

2. J. G. Cramer, R. M. DeVries, D. A. Goldberg, M. S. Zisman, and C. F. Maguire, Phys. Rev. C 14, 2158 (1976).

3. D. A. Goldberg and S. M. Smith, Phys. Rev. Lett. 29, 500 (1975); D. A. Goldberg, S. M. Smith, and G. F. Burdzik, Phys. Rev. C 10, 1367 (1974).

4. G. R. Satchler, Proc. of the Symp. on Macroscopic Features of Heavy Ion Collisions, I, 33, 1976 (unpublished); G. R. Satchler, to be published.

5. H. G. Bingham, M. L. Halbert, D. C. Hensley, and E. Newman, Phys. Rev. C 11, 1913 (1975); J. E. Poling, E. Norbeck, and R. R. Carlson, Phys. Rev. C 13, 648 (1976).

6. D. P. Stahel, G. J. Wozniak, M. S. Zisman, B. D. Jeltema, and J. Cerny, Phys. Rev. C 16, 1456 (1977).

2. Macroscopic

PROTON EMISSION IN REACTIONS INDUCED BY 315-MeV ^{16}O IONS

T.J.M. Symons, P. Doll,* C.K. Gelbke,† D.L. Hendrie, J. Mahoney, G. Mantzouranis, A. Menchaca-Rocha,‡
D.K. Scott, Y.P. Viyogi,§ K. Van Bibber, and H. Wieman

In recent years, there has been a growth of interest in the study of light particle emission accompanying heavy-ion collisions. It is hoped that from these studies one may learn about both the time scale and the nature of the reaction processes. Much of our present knowledge comes from two extreme regions of bombarding energy. At low incident energies of a few MeV per nucleon, light particle emission is dominated by statistical evaporation from the compound nucleus, with small contributions from precompound emission. At the other extreme, in reactions induced by heavy ions with energies of several hundred MeV per nucleon, light particles have been observed that are characteristic of a system moving at a velocity intermediate between the target and projectile. The interpretation of these data has led to the development of the nuclear fireball model[1] in which it is assumed that the nucleons swept out in the overlapping region of target and projectile form an equilibrated system at high temperature. This model and its subsequent refinements have provided the simplest and most elegant description of the high energy data.

We report here the measurement of proton spectra in reactions induced by 315-MeV ^{16}O ions. The $^{16}O^{6+}$ beam from the LBL 88-inch cyclotron was used to bombard ^{197}Au and ^{12}C targets of 9.5 mg·cm^{-2} and 210 μg·cm^{-2} respectively. High energy protons, deuterons, and tritons were detected in a telescope consisting of 1-mm and 5-mm thick Si(Li) detectors both of 5-cm diameter and a 7.5 x 7.5 cm cylindrical NaI(Tl) detector. The detectors were mounted outside a scattering chamber and the target viewed through a Mylar window. Use of a sliding seal allowed the laboratory angle to be varied from 20° to 80°. A second telescope was mounted inside the chamber consisting of a 200-μ Si surface barrier detector, a 5-mm Si(Li) detector, and a veto detector. This telescope was used to measure the proton spectrum up to 30 MeV.

The detectors were calibrated using 45-MeV protons elastically scattered from ^{197}Au and polystyrene targets and also with protons produced in the $^{12}C(\alpha,p)^{15}N$ reaction at incident alpha energies of 65, 90, and 110 MeV. These calibration reactions produced protons between 22 and 90 MeV. In Fig. 1 we show the spectra obtained from the gold target at lab angles between 20° and 80°. The most striking feature of these spectra is the smooth dependence of the differential cross section on energy and angle, characteristic of statistical evaporation spectra from a moving system. In order to parameterize the data, we have fitted a simple Maxwellian distribution

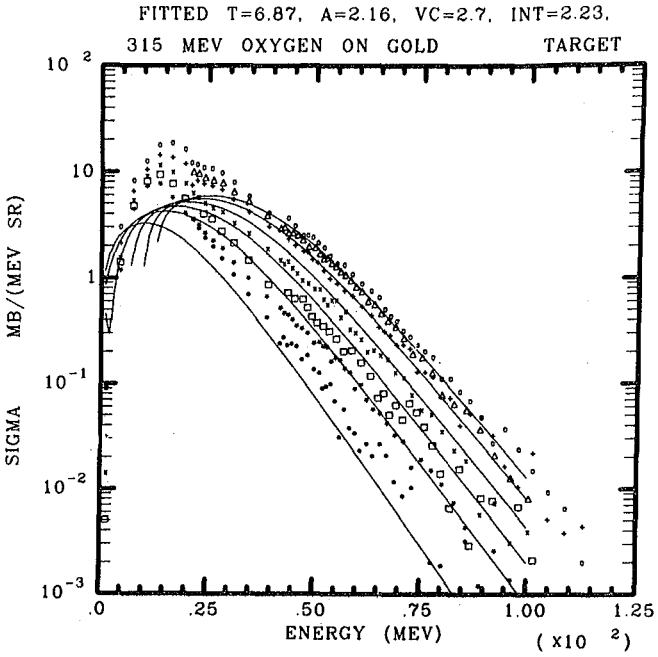

Fig. 1. Proton spectra obtained from bombardment of a 9.5 mg·cm^{-2} ^{197}Au target by a 315 MeV ^{16}O beam. (XBL 786-9166)

to the observed cross sections. In the fit, we have assumed

$$\sigma(\theta,E_L) \propto \sqrt{E_L}\,\sqrt{1 - V_C/E_C}\;\; e^{-E_C/T}$$

where θ is the laboratory angle, E_L and E_C are the proton energies in the lab and moving frames, V_C is the energy of the Coulomb barrier (taken to be 2.7 MeV), and T is the characteristic temperature of the system.

The curves shown are for a temperature of 6.9 MeV and a system moving at 0.10 c (50% of the beam velocity). Reasonable values for the ^{16}O + ^{197}Au compound nucleus are 3.3 MeV and 0.02 c, respectively, and the data are clearly incompatible with compound nuclear evaporation. Similarly, the variation of cross section with angle is too small to be explained by isotropic evaporation from the excited projectile. It should of course be noted that the low energy protons will mostly come from compound nuclear evaporation.

These results are, in fact, very reminiscent of the high-energy data which have been interpreted

with the nuclear fireball model. To investigate this further, we have performed a simple fireball calculation using the standard geometrical techniques to deduce the number of participating nucleons as a function of impact parameter.[2] Since our excitation energies are very much lower than is usual for these calculations, we have deduced the temperature from the Fermi gas distribution rather than from the classical distribution. In this model one obtains 7.6 MeV and 0.06 c for the excepted temperature and velocity, in surprisingly good agreement with the experimentally derived values.

As an alternative approach, we have also investigated the contribution to the proton cross section from precompound emission. As a first step, we follow Griffin[3] in defining the mean number of excitons in the system by plotting the log of the angle-integrated cross section vs the log of the residual excitation energy in the ^{212}At nucleus. From the shape of this graph one obtains a value of 27 for the number of excitons as shown in Fig. 2. Next, we have used the hybrid model of Blann[4] to calculate the precompound proton cross section. This cross section is very sensitive to the initial exciton number as may be seen from Fig. 3 where the calculation for 16 and 25 excitons may be compared. This 16-exciton state was made up of 8 protons and 8 neutrons (corresponding to the impinging ^{16}O nucleus) and the second calculation contained an additional 5 particles and 4 holes. It may be noted that the agreement for the energy dependence and the absolute cross section is almost prefect in the high energy region.

The rather similar results obtained by these two quite different calculations is surprising. While both models restrict the excitation energy to a small fraction of the total nuclear system, the time scales are very different, with the precompound protons being emitted at a much earlier stage of the reaction process. It also raises the interesting question as to how much of the yield observed at very much higher bombarding energies could, in fact, be explained by precompound emission rather than by the equilibrated fireball model.

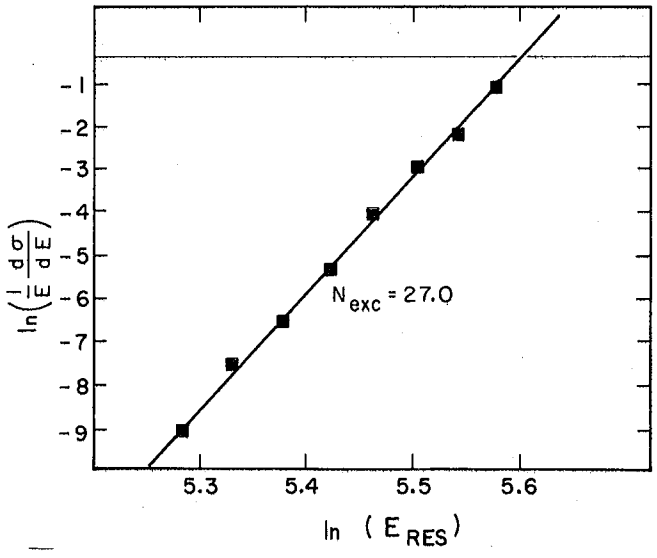

Fig. 2. Plot of logarithm of differential cross section vs logarithm of residual excitation for 315-MeV ^{16}O bombardment of ^{197}Au. (XBL 787-1413)

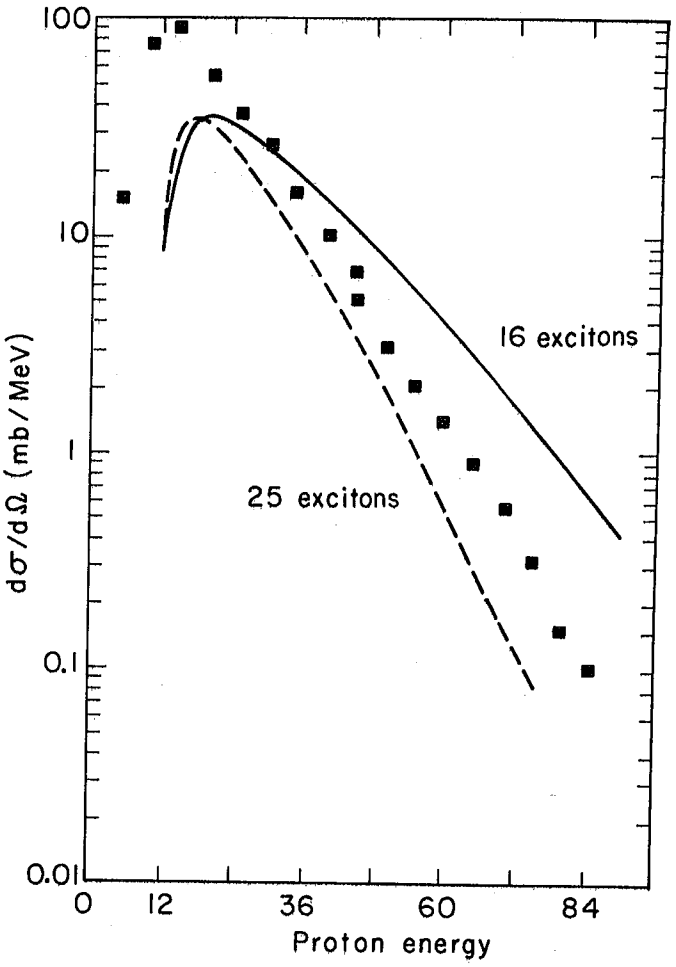

Fig. 3. Predictions of hybrid model for proton cross sections. (XBL 787-1414)

Footnotes and References

*Nato Fellow, on leave from MPI, Heidelberg, W. Germany.
†Present address: Physics Dept., Michigan State University, East Lansing, Michigan 48824.
‡On leave from Instituto de Fisica, UNAM, Mexico. Partially supported by CONACYT (PNCB 0022).
§IAEA Fellow, on Deputation from Bhabha Atomic Research Centre, Calcutta, Inda.

1. G. D. Westfall, J. Gosset, P. J. Johansen, A. M. Poskanzer, W. G. Meyer, H. H. Gutbrod, A. Sandoval and R. Stock, Phys. Rev. Lett. 37, 1202 (1976).

2. J. Gosset, H. H. Gutbrod, W. G. Meyer, A. M. Poskanzer, A. Sandoval, R. Stock and G. D. Westfall, Phys. Rev. C16, 629 (1977); J. Hüfner and J. Knoll, Nucl. Phys. A290, 460 (1977).

3. J. J. Griffin, Phys. Lett. 24B, 6 (1967).

4. M. Blann, Nucl. Phys. A235, 211 (1974).

RELATIVE THRESHOLDS FOR PRODUCTION OF IODINE ISOTOPES FROM FUSION AND TRANSFER-INDUCED FISSION REACTIONS*

M. de Saint-Simon,† R.J. Otto, and G.T. Seaborg

The reaction of ^{40}Ar ions with energies from 212 to 340 MeV impinging on a thick ^{238}U target has been studied using radiochemical methods. The formation cross sections of iodine isotopes were measured and converted to independent yields from which isotopic distributions were derived.

The iodine isotopic distributions (see Fig. 1) in the reaction ^{40}Ar + ^{238}U at different projectile energies have been shown to be composed of three reaction components corresponding to three different, although not entirely separable, processes: (a) Quasielastic transfer (QET), (b) deep inelastic transfer (DIT), (c) complete fusion (CF), followed by fission of the heavy-reaction product.

The observed unexpected stable position of the centroid of the complete fusion-induced fission distribution is found to be in agreement with calculations based on the statistical model for fission and on evaporation calculations with the "overlaid-ALICE" code. Important for this observation is the integral nature of the thick target experimental method.

Figure 1 shows that the production cross sections for iodine isotopes from QET-induced fission and CF-induced fission have a different behavior at the energies close to the Coulomb barrier, the value of the ratio of which is taken to be 200 MeV (r_o = 1.44 fm) in the laboratory system.[1,2] Figure 2 shows a plot of the ratio of the integrated cross section for the production of iodine isotopes from fission following CF to that from fission following QET. The drastic change in slope of the curve shows that the cross section for QET is a relatively predominant fraction of the total cross section near the Coulomb barrier and decreases in relative importance at higher energy.

If we assume that the overall fission mass-distribution remains symmetric and peaked near half the mass of the compound nucleus, then the trends in the iodine isotopic distributions reflect the trends in the identified reaction mechanisms and there is a higher threshold for the complete fusion than for the quasi-elastic transfer (and some of the deep-inelastic transfer) reactions.

Our objective is to estimate the relative difference between the complete fusion threshold and the interaction barrier by using the ratios shown in Fig. 2. To do this, the excitation function for the total reaction cross-section must be known and used. Due to the small number of cross-section data that we have obtained in the barrier region, we choose to take the excitation function of Sikkeland[1] as representative of the total reaction cross section. This excitation function can be relatively well estimated with the easily integrated function given in Eq. (1), using the value of r_o = 1.44 fm, as suggested by Oganesyan, to obtain B = 171 MeV (c.m.) and R = 13.85 fm.

$$\bar{\sigma}_R = \pi R^2(1 - B/E) \quad . \tag{1}$$

(Where B is the barrier energy and E is the energy of the projectile.)

$$\bar{\sigma}_R = \frac{1}{E - B}\int_B^E \sigma_R dE = \pi R^2\left(1 - \frac{B}{E - B}\ln\frac{E}{B}\right) . \tag{2}$$

An effective bombarding energy (E_{eff}) can be defined in the following way:

$$\bar{\sigma}_R = \pi R^2(1 - B/E_{eff}) \quad . \tag{3}$$

As shown in Fig. 3, a plot of $\bar{\sigma}_R$ vs $1/E_{eff}$ produces a straight line with an intercept equal to 1/B.

First approximations for the relative average complete-fusion cross section ($\bar{\sigma}_{CF}$) were obtained as the product of $\bar{\sigma}_R$ and $[(\sigma_{QET}/\sigma_{CF}) + 1]^{-1}$ and plotted against E_{eff}^{-1}. A threshold for complete fusion was obtained, but the effective bombarding energies must be recalculated, as must the cross sections for the complete fusion products since a higher barrier implies a shorter range to the barrier and a smaller number of target atoms. These corrections have been made and the final $\bar{\sigma}_{CF}$ vs E_{eff}^{-1} is plotted in Fig. 3.

Of the seven complete fusion data points that were obtained from these experiments, four $\bar{\sigma}_{CF}$ cross sections, calculated using the procedures described above and corresponding to the experimental laboratory bombarding energies of 240, 250, 270, and 290 MeV, appear to fall on a straight line, as shown in Fig. 3. The least-squares fit to these data points shown as a dot dashed line gives an intercept of 182 ± 7 MeV/(c.m.). The complete fusion cross section for the data point corresponding to the experimental bombarding energy of 340 MeV is well below the best fit line and outside the error limits for this fit. A dashed line is extended through this point to show the deviation from the solid line. Two upper limit complete-fusion cross sections were obtained at the lowest laboratory bombarding energies of 226 MeV and 212 MeV. Since 212 MeV (181 MeV c.m.) is below the first estimated complete fusion barrier, this data point does not appear in Fig. 3. Inclusion of the upper limit cross section for the 226 MeV-(lab) point, however, limits the least squares estimate (shown

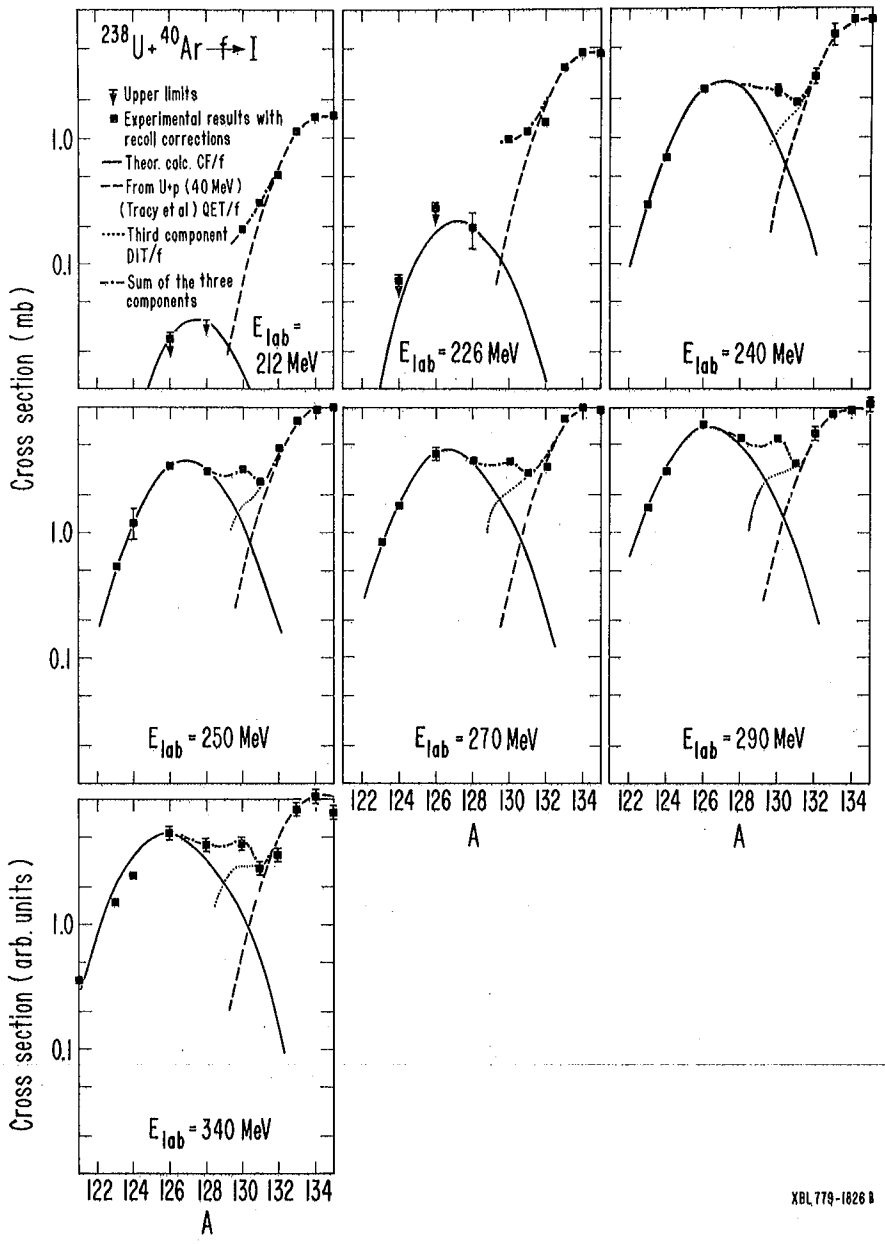

Fig. 1. Independent-yield cross sections for the production of iodine isotopes in the thick target reaction of ^{40}Ar with ^{238}U. The solid lines, dashed lines, dot-dashed lines and dotted lines are explained in the upper left frame. (XBL 779-1826B)

as a dot-dashed line) of the complete fusion threshold to 185^{+4}_{-2} MeV/(c.m.). This corresponds to a complete fusion threshold that is at least 12 MeV higher than the assumed interaction barrier of 171 MeV.

Based on elastic scattering data, Schroder and Huizenga[3] have reported a value of R = 13.6 fm for the interaction radius in the ^{40}Ar + ^{238}U reaction, which if used would give an interaction barrier of 175 MeV (c.m.). If an analysis identical to the one described above is carried out using these values, a threshold for complete fusion of 185^{+3}_{-2} MeV (c.m.) is obtained. Thus, the analysis using a barrier of 175 MeV (c.m.) indicates that the complete fusion threshold is at least 8 MeV higher than the interaction barrier. The least squares fit of the four data points corresponding to the experimental laboratory bombarding energies of 240, 250, 270, and 290 MeV give an intercept of 181 ± 8 MeV. As in the first analysis which used 171 MeV (c.m.) for the interaction barrier, the cross section, σ_{CF}, corresponding to the highest energy data point was well below (and outside the error limit of) the linear fit to the lower energy data.

We summarize these results as follows. The energy intercept obtained from a least squares fit to the complete-fusion cross sections calculated using the experimental laboratory data between 240

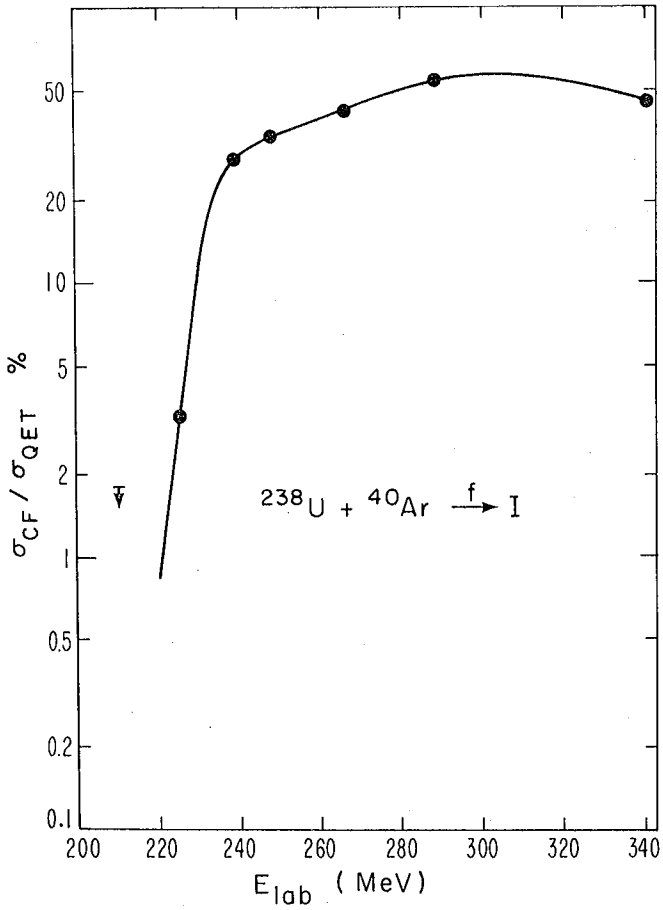

Fig. 2. The ratio (expressed as percent) of the cross section for the production of iodine isotopes by complete fusion-fission (σ_{CF}) and by quasi-elastic transfer induced fission (σ_{QET}) in the thick target reaction of ^{40}Ar with ^{238}U. The solid line is drawn to pass through the data points. (XBL 7710-6962)

and 290 MeV, is too uncertain to observe a significant difference between the extrapolated intercept value and the assumed interaction barrier. However, a linear fit of σ_{CF} vs $1/E_{eff}$ that includes the upper limit value at the near barrier experimental energy of 226 MeV (194 MeV c.m.) clearly shows that the threshold for complete fusion is at least 12 MeV (R = 13.85 fm) or 8 MeV (R = 13.6 fm) higher than the interaction barrier,

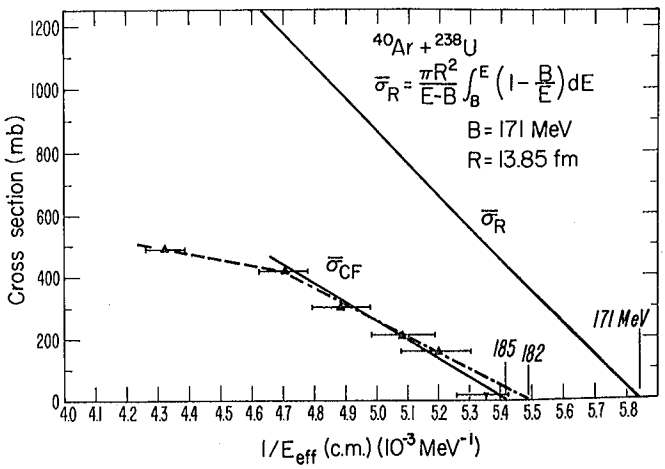

Fig. 3. A plot of $\bar{\sigma}_R$ and $\bar{\sigma}_{CF}$ vs E_{eff}^{-1} where $\bar{\sigma}_R$ is the average total reaction cross section calculated by using the parameters indicated and $\bar{\sigma}_{CF}$ is the average complete fusion cross section. See text for further explanation of the effective bombarding energy, E_{eff}, and the solid, dashed and dot-dashed lines. (XBL 786-2588)

depending on the value chosen for the interaction barrier. These values represent the smallest differences allowable within the energy uncertainty associated with the data as shown in Fig. 3. The difference between the complete fusion threshold and the interaction barrier could well be slightly larger than the values given.

Footnotes and References

*Condensed from LBL-7114; Phys. Rev. C., 18, 1651 (1978).

†Permanent Address: Laboratoire Rene Bernas, BP1, 91406 Orsay, France.

1. T. Sikkeland, Ark. Fys. 36, 539 (1967); Phys. Lett. 27B, 277 (1968).

2. Yu. Ts. Oganesyan, Yu. E. Penionzhkevich, K. A. Gavrilov, and Kim DeEn, Sov. J. Nucl. Phys. 21, 126 (1975).

3. W. U. Schroder and J. R. Huizenga, Ann. Rev. Nucl. Sci. 27, 487 (1977).

NEW EXPERIMENTAL INSIGHTS INTO THE PRODUCTION OF SUPERHEAVY ELEMENTS USING HEAVY ION REACTIONS*

R.J. Otto, D.J. Morrissey, G.T. Seaborg, and W.D. Loveland†

Attempts at the Lawrence Berkeley Laboratory to produce superheavy elements (SHE) using the reactions of ^{48}Ca with ^{248}Cm and ^{136}Xe with ^{238}U have been unsuccessful. These negative results have led us to consider the possibility that these reactions (and their associated mechanisms) do not lead to the formation of superheavy nuclei with sufficiently low excitation energies. Consequently, the number of surviving atoms of superheavy elements is well below our detection thresholds even with using relatively low estimates for prompt fission losses. A summary of some new experimental evidence, supporting the above hypothesis, is presented and possible alternative heavy-ion heavy-target combinations are suggested for SHE synthesis.

We have considered several possible reasons for negative results in the synthesis and identification of superheavy elements obtained at heavy-ion accelerator laboratories around the world. Due to the limited choice of targets above uranium, projectiles heavier than ^{40}Ar have been used. However, for projectile ions near and above the mass and charge of ^{40}Ar, quasi-elastic transfer and deep-inelastic transfer comprise a significant fraction of the total reaction cross section. The deep-inelastic transfer reaction has many characteristics that tend to obscure the observation of the complete fusion and compound nucleus-fission reactions. As a result, previous measurements of the fraction of the total reaction cross section corresponding to complete fusion can only be taken as upper limits. Furthermore, mass and energy distributions associated with binary events from heavy-ion reactions [for example, ^{40}Ar + ^{238}U (Ref. 1) or ^{40}Ar + ^{243}Am (Ref. 2)], in which complete fusion was assumed to occur, cannot be safely interpreted as corresponding to the fission of a compound nucleus.

A recently developed differential recoil range method[3] can be employed to further test this broad role of the deep-inelastic transfer process in the production of a wide range of products from bombardments with ^{40}Ar and similar ions. This method has been used to deduce the general shapes of angular distributions of products ranging from approximately one-half the mass of the compound composite system to products near the target.[4] These recoil range distributions from the reaction of 250 MeV ^{40}Ar with ^{238}U were correlated with a trend in the angular distribution of the projectile-like fragment as a function of ΔZ similar to the trend observed in the ^{40}Ar + ^{197}Au reaction.[5-9] This is a trend that has been interpreted as evidence for viewing the deep inelastic reaction mechanism as a dynamical diffusion process.[6,7,9] Complete fusion is ruled out for products with backward- or forward-peaked angular distribution since the $1/\sin\theta$-type angular distribution is expected for such a process.

These data indicated that non-complete fusion (and non-compound nuclear) processes accounted for an unexpectedly large portion of the mass distribution of the ^{48}Ca + ^{238}U reaction and, of the broad symmetric, previously labeled "fusion-fission," mass distribution of the ^{40}Ar + ^{238}U reaction.[1] Again, we can see that earlier work on the ^{40}Ar + ^{238}U system may have overestimated the cross section due to complete fusion processes. Thus we conclude that the use of ^{48}Ca as a projectile with heavy targets, considered a hopeful approach for the production of SHE's, must actually result in a much smaller production of compound nuclei than had been anticipated.

For ions heavier than argon, complete fusion-fission rapidly decreases, eliminating the possibility for production of SHE fission fragments in such reactions as krypton, xenon or uranium with uranium. In spite of the larger contribution from deep-inelastic transfer reactions, some complete fusion and compound nucleus formation is expected to occur in the ^{48}Ca + ^{248}Cm reaction. However, use of the proximity potential model[10] and the Bass model[11,12] predicts complete fusion thresholds 10 to 15 MeV higher than the interaction barrier, and the work of Saint-Simon et al.[13] using the similar reaction ^{40}Ar + ^{238}U provides experimental evidence for such an effect. As a result, the minimum attainable excitation energy for the compound nucleus ($^{296}116$) results in large prompt fission losses putting the SHE production level below the present experimental level of sensitivity.

For the ^{136}Xe + ^{238}U reaction, the probability of transferring the required number of protons and neutrons to reach the SHE region appears to be unacceptably low. This conclusion is supported by a study of the reaction of ^{136}Xe and ^{160}Gd.[14] The reaction $^{160}Gd(^{136}Xe;^{84}Kr,n's)^{212}Pb$ requires the transfer of 18 protons and 34 neutrons to ^{160}Gd from the ^{136}Xe projectile. This is the number of protons and neutrons required in a transfer from ^{136}Xe to ^{238}U to make ($^{290}110$) which is predicted to be in the "island of stability." Using a radiochemical separation procedure, an upper limit of 2×10^{-34} cm^2 was observed for production of ^{212}Pb in the reaction of 1150 MeV ^{136}Xe with a thick natural Gd target (21.9% ^{160}Gd).[14] The upper limit cross section for the reaction $^{160}Gd(^{136}Xe;^{84}Kr,n's)^{212}Pb$ is therefore 1×10^{-33} cm^2 or 1 nb. The 1 nb limit was applied to a similar or greater number of nucleons transferred from ^{136}Xe to ^{238}U by assuming that less than 10% of the Pb fragments fissioned and that the nucleon diffusion rates and the interaction times are nearly the same for the ^{136}Xe + ^{160}Gd and ^{136}Xe + ^{238}U reactions. It was pointed out that this limit is consistent with the theoretical prediction that the cross section for transfer of ~60 nucleons in the Xe + U reaction is about

1 nb.[15] Figure 1 summarizes the results of this work. The cross section for SHE production is estimated to be $\leq 4 \times 10^{-36}$ cm^2.

The possibility remains that transfer reactions using very heavy-ion projectiles such as ^{197}Au, ^{208}Pb, ^{238}U, or ^{244}Pu with ^{254}Es or ^{257}Fm targets could lead to the production of SHE nuclei at relatively low excitation energies.

Recent studies of the ^{238}U + ^{238}U reaction at Gesellschaft für Schwerionenforschung[16,17] show that, for a given average width in the charge dispersion (mass dispersion), the energy damped into internal excitation energy is less than in Xe transfer reactions.[18,15] Such an observation can be interpreted as supporting the idea that there should be significantly larger cross sections for the production of heavy transuranium elements in the reaction of U + U[16] than in the Xe + U reactions.[19] Evidence for such an effect can be seen by making a comparison of the yields of Cf and Es isotopes (ΔZ = 6 and 7, respectively) from these two reactions, where the cross sections for the production of the more neutron-excessive isotopes are 10 to 10^2 times larger from the U + U reaction.[17] Such an effect suggests the use of a very heavy target such as ^{248}Cm, ^{249}Cf, ^{252}Cf, ^{254}Es, or ^{257}Fm with a heavy-ion beam of ^{238}U (or possibly ^{197}Au, ^{208}Pb, or ^{244}Pu) as a way to produce SHE's. Figure 2 shows a number of interesting transfer reactions. The ^{165}Ho and ^{248}Cm reaction shown first could be driven by the closed shell at Z = 50. However, the diffusion process would probably favor symmetric division into two fragments near ^{208}Pb.

Based on the results with the U + U reaction[17] studies at GSI to produce ^{255}Fm, an analogous reaction of ^{238}U with ^{254}Es is written to suggest the possibility of transfer reactions to produce elements near the SHE region with reasonable

$$^{136}_{54}\text{Xe} + ^{160}_{64}\text{Gd} \rightarrow ^{212}_{82}\text{Pb} + ^{84}_{36}\text{Kr} + \text{n's}$$

$$\sigma_{DIT} \leq 1 \times 10^{-33}\ \text{cm}^2$$

Transfer to target (Δp = 18, Δn = 34)

Loss by Fission?

$$^{136}_{54}\text{Xe} + ^{238}_{92}\text{U} \rightarrow ^{290}_{180}(110) + ^{84}_{36}\text{Kr} + \text{n's}$$

$$\sigma_{SHE} \leq 1 \times 10^{-33} \left[\frac{\Gamma_n}{\Gamma_n + \Gamma_f}\right]^x \leq 1 \times 10^{-33} \times 4 \times 10^{-3}$$

$$\sigma_{SHE} \leq 4 \times 10^{-36}\ \text{cm}^2$$

Fig. 1. An upper limit cross section for the production of SHE's in the ^{136}Xe + ^{238}U reaction based on the experiments using the ^{136}Xe + ^{160}Gd reaction. Values of x = 4 and $[\Gamma_n/(\Gamma_n+\Gamma_f)]^4$ = 4×10^{-3} were used.[14] (XBL 789-11116)

$$^{165}_{67}\text{Ho} + ^{248}_{96}\text{Cm} \rightarrow ^{289}_{176}(113) + ^{124}_{50}\text{Sn}$$

$$^{165}_{67}\text{Ho} + ^{248}_{96}\text{Cm} \rightarrow ^{208}_{82}\text{Pb} + ^{205}_{81}\text{Tl}$$

$$^{238}_{92}\text{U} + ^{238}_{92}\text{U} \rightarrow ^{255}_{100}\text{Fm} + ^{221}_{84}\text{Po} \quad \sigma \approx 10^{-33}$$

Transfer (Δp = 8, Δn = 9)

$$^{254}_{99}\text{Es} + ^{238}_{92}\text{U} \rightarrow ^{271}_{164}(107) + ^{221}_{84}\text{Po}$$

Transfer (Δp = 8, Δn = 9)

$$^{257}_{100}\text{Fm} + ^{238}_{92}\text{U} \rightarrow ^{283}_{173}(110) + ^{212}_{82}\text{Pb}$$

Transfer (Δp = 10, Δn = 16)

Fig. 2. Hypothesized heavy-ion transfer reactions. Only the U+U reaction has been shown to occur experimentally.[17] No designation of emission of neutrons has been indicated. (XBL 789-11117)

cross sections. However, the formation of SHE's requires a transfer with a larger neutron-to-proton ratio, as indicated in the reaction of ^{238}U with ^{257}Fm. It is important to note that the predicted stability of the products in the SHE region for these last two reactions varies from being unstable to having detectable half-lives.[20,21] Although such reactions would have many technical difficulties associated with them, these target-projectile combinations may provide a suitable reaction pathway to the formation of SHE's not available in the reactions that have been used up to now. The success of these experiments rely on the transfer reaction mechanisms and on an extrapolation of broad Gaussian distributions of primary products (before fission) around the target nucleus extending from the millibarn region into the nanobarn region. Also, the disadvantages of the extremely small amounts of ^{254}Es and ^{255}Fm available may more than offset these advantages for their use.

Footnotes and References

*Condensed from LBL-7710 and Proc. of the Intern. Symp. on Superheavy Elements, Lubbock, Texas, March (1978).

†Permanent Address: Department of Chemistry, Oregon State University, Corvallis, OR 97331.

1. J. V. Kratz, J. O. Liljenzen, A. E. Norris, and G. T. Seaborg, Phys. Rev. C 13, 1347 (1976).

2. R. Kalpakchieva, Yu. Ts. Oganessyan, Yu. E. Penionzhkevich, and H. Sodan, Z. Physik A 283, 253 (1977).

3. R. J. Otto, M. M. Fowler, and G. T. Seaborg, Phys. Rev. C 17, 1071 (1978).

4. R. J. Otto, D. J. Morrissey, G. T. Seaborg, and W. D. Loveland, Z. Physik A 287 (1978) and Lawrence Berkeley Laboratory Report LBL-7188 (1978).

5. C. Ngo, J. Peter, B. Tamain, M. Berlanger, and F. Hanappe, Z. Physik A 283, 161 (1977).

6. L. G. Moretto, J. Galin, R. Babinet, Z. Fraenkel, R. Schmitt, R. Jared, and S. G. Thompson, Nucl. Phys. A 259, 173 (1976).

7. J. Galin, B. Gatty, D. Guerreau, M. Lefort, X. Tarrango, S. Agarwal, R. Babinet, B. Gauvin, J. Girard, and H. Nifenecker, Z. Physik A 283, 173 (1977).

8. A. G. Artukh, E. Gierlik, R. Gerstenberger, G. F. Gridnev, A. N. Mezentsev, V. L. Mikheev, T. S. Salamatina, V. V. Volkov, V. B. Zlokazov, Report, Joint Institute of Nuclear Reactions E7-10464.

9. R. Lucas, J. Poitou, H. Nifenecker, J. Peter, and B. Tamain, Z. Physik A 283, 257 (1977).

10. J. Blocki, J. Randrup, W. J. Swiatecki, and C. F. Tsang, Ann. Phys. 105, 427 (1977).

11. R. Bass, Nucl. Phys. A 231, 45 (1974).

12. R. Bass; Phys. Lett. B 47, 139 (1973).

13. M. de Saint Simon, R. J. Otto, G. T. Seaborg, Phys. Rev. C 18, 1651; and Lawrence Berkeley Laboratory Report LBL-7114 (1978).

14. R. J. Otto, A. Ghiorso, D. Lee, R. E. Leber, S. Yashita, and G. T. Seaborg, Radiochimica Acta 24(1) (1978).

15. J. R. Huizenga, Comments on Nucl. Part. Phys. 7, 17 (1976).

16. D. D. Hildenbrand, H. Freisleben, F. Puhlhofer, W. F. W. Schneider, R. Bock, D. V. Harrah, and H. J. Specht, Phys. Rev. Lett. 39, 1065 (1977).

17. J. V. Kratz, H. Ahren, W. Bruchle, G. Franz, H. Gaggeler, M. Schadel, I. Warnecke, G. Wirth, N. Tautman, M. Weis, and G. Herrmann, Report Gesellschaft für Schwerionenforschung-J-1-77 (1977); and M. Schadel et al., Phys. Rev. Lett. 41, 469 (1978).

18. U. Reus, A. M. H. Watzig, R. A. Esterlund, P. Patzelt, and I. S. Grant, Phys. Rev. Lett. 39, 171 (1977).

19. K. Wolf et al., American Physical Society Meeting, Chicago (1977), Abstract 25.7.

20. E. O. Fiset and J. R. Nix, Nucl. Phys. A 193, 647 (1972).

21. I. Reichstein and F. B. Malik, Ann. Phys. 98, 322 (1976); and F. B. Malik, private communication (1977).

LARGE CONTRIBUTION OF DEEP-INELASTIC PROCESSES TO REACTIONS OF ^{40}Ar AND ^{48}Ca WITH ^{238}U*

R.J. Otto, D.J. Morrissey, G.T. Seaborg, and W.D. Loveland†

Differential recoil range distributions have been measured for heavy-reaction products ranging from Te(Z = 52) to quasi-elastic transfer products near the charge and mass of the targets for the reactions 276-MeV ^{48}Ca + ^{238}U, 237-MeV and 250-MeV ^{40}Ar + ^{238}U, and 259-MeV ^{40}Ar + ^{197}Au.

A detailed description of the experimental recoil range distribution method has been given[1] and will only be briefly covered in this report. Thin UF_4 targets of thickness ~0.7 mg/cm^2 supported on a 3.4 mg/cm^2 aluminum backing, or a 2.4 mg/cm^2 gold foil target, were placed directly in front of a stack of 1.1 mg/cm^2 Al recoil foils and irradiated as a single package. Following the irradiation the target and Al recoil foils were separated, taped to aluminum planchets, and assayed by x-ray spectrometry. X-ray spectra were obtained for the energy region between 10 and 100 keV. We report here the results for selected representative elements from the x-ray spectra obtained for the systems studied.

To correlate the measured recoil range distributions with the center-of-mass angular distribution of a given reaction product, we have written a code[1] that calculates the recoil range distribution for any given experimental conditions and for any chosen center-of-mass angular distribution. The measured recoil range distributions for the ^{40}Ar + ^{197}Au reaction agree with range distributions calculated from the known projectile-like fragment angular distributions[2-6] for this reaction.

Figure 1 shows recoil range distributions of the product ^{237}Pu (detected via its 59.7-keV gamma ray) and a composite recoil range distribution of Te, I, Xe, and Cs species and Hf, Ta, W, Re, and Os species from the combined count rate of x-rays having energies between 27.5 keV to 31.0 keV and 55.9 keV to 62.0 keV, respectively. These results were taken from spectra obtained from the 250-MeV ^{40}Ar + ^{238}U reaction. Since ^{237}Pu is expected to be primarily a quasi-elastic transfer product, a Gaussian shaped angular distribution peaked at the classical grazing

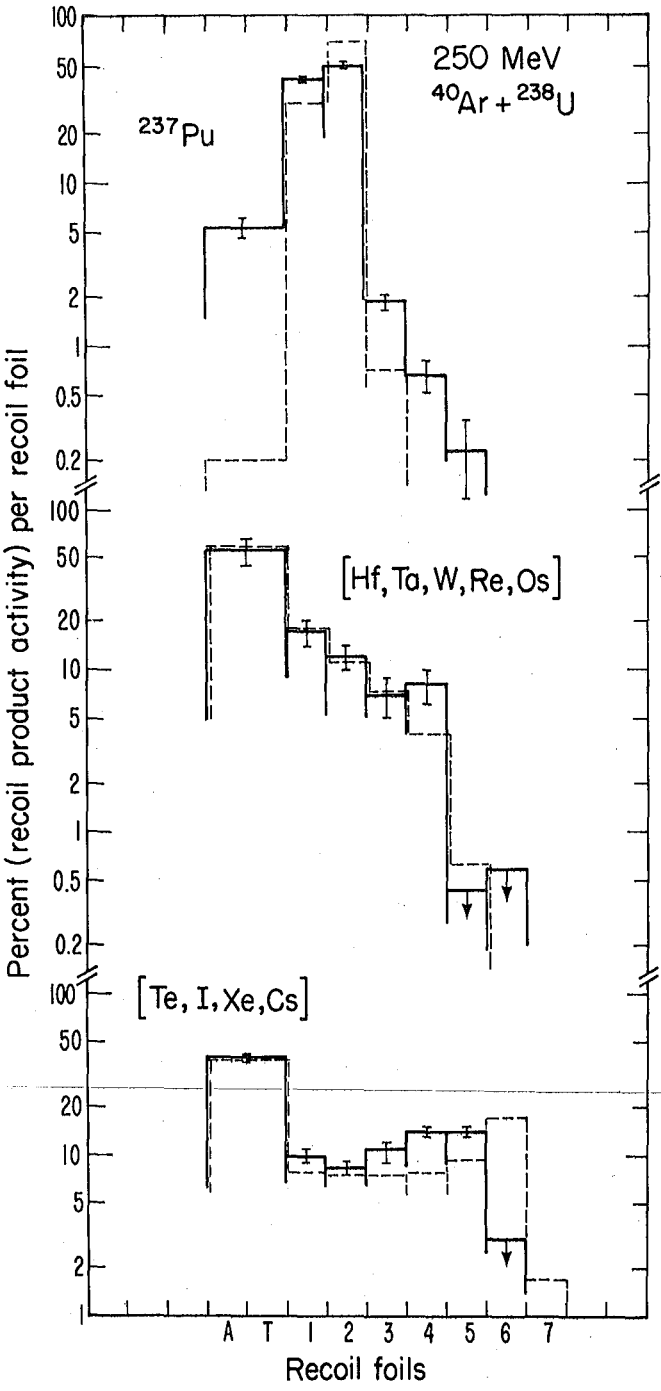

Fig. 1. Experimental (solid line) and calculated (dashed line) recoil range distributions for ^{237}Pu and the combined products of Te, I, Xe, and Cs and of Hf, Ta, W, Re, and Os from the reaction 250-MeV ^{40}Ar + ^{238}U. The bottom axis indicates the position and number of each of the forward recoil foils. (XBL 782-2383)

angle with a FWHM of 30° was used to calculate the theoretical recoil range distribution shown as a dashed line. The experimental recoil range distribution (solid line) from the combined x rays from Te, I, Xe and Cs products is compared with the calculated recoil range distribution (dotted line) for a $1/\sin\theta$ angular distribution [actually $1/\sin\theta + 0.1$)].

The calculated recoil range distributions predict somewhat longer ranges than observed; however, the relative shapes are in good agreement. The experimental recoil range distribution for products between Hf and Os (solid line) is in good agreement with the calculated recoil range distribution (dashed line) derived from an exponentially decreasing backward-peaked angular distribution.

Figure 2(a) shows the experimental recoil range distributions for the Hg(Tl) products corresponding to the x-ray peak that is a superposition of the $K\alpha_1$ x ray of Hg and the $K\alpha_2$ x ray of Tl. As shown in Fig. 2(a), these similar results come from the two reactions ^{48}Ca + ^{238}U and ^{40}Ar + ^{238}U and correspond to three different excitation energies. Calculated recoil range distributions for the Hg(Tl) products from these three reactions are shown in Fig. 2(b) and are based on three different assumptions about the heavy product angular distribution. These three functional forms are shown in Fig. 2(c). The Hg(Tl) recoil data correspond most closely to the predictions of the simple backward-peaked angular distributions (corresponding to a forward-peaked projectile-like fragment distribution). However, there is a small discrepancy at the longer ranges indicating the possibility of a small $(1/\sin\theta)$ contribution. To test such an effect we have used a background-peaked angular distribution mixed with a 10% $(1/\sin\theta)$ contribution (actually $1/\sin\theta + 0.01$). The experimental results (shown in Fig. 2(a), fall between the calculated distributions (shown in Fig. 2(b), expected for a backward-peaked plus $1/\sin\theta$-angular distribution (dotted line) and the simple backward-peaked angular distribution represented by an exponentially decreasing function (solid line).

Kalpakchieva et al.[7] have interpreted the results of correlated fragment mass distribution measurements for the ^{40}Ar + ^{243}Am reaction as possible evidence for the existence of highly mass-asymmetric fission of the compound nucleus $^{283}[113]$. Also, they have attributed the observed asymmetry ($A_H/A_L \approx 2.5$) to the preferential formation of a heavy fragment near the doubly-magic ^{208}Pb region. Such behavior has been predicted on theoretical grounds by Sandulescu and Greiner.[8]

We believe that our data indicate that non-complete fusion (and non-compound nuclear) processes account for a large portion of the mass distribution of the ^{48}Ca + ^{238}U reaction and of the broad symmetric mass distribution of the ^{40}Ar + ^{238}U reaction[9] previously attributed to "fusion-fission." It would appear to us that earlier work[9,10] on the ^{40}Ar + ^{238}U system may have overestimated the cross section due to complete fusion processes. Furthermore, since we see little difference between the compound nuclei expected to be produced in this study and the work of Kalpakchieva et al.,[7] we might expect that a careful study of the angular distribution trends as a function of Z for fragments in the Pb region would reveal backward-peaked angular distributions for the ^{40}Ar + ^{243}Am reaction. Such an observation would rule

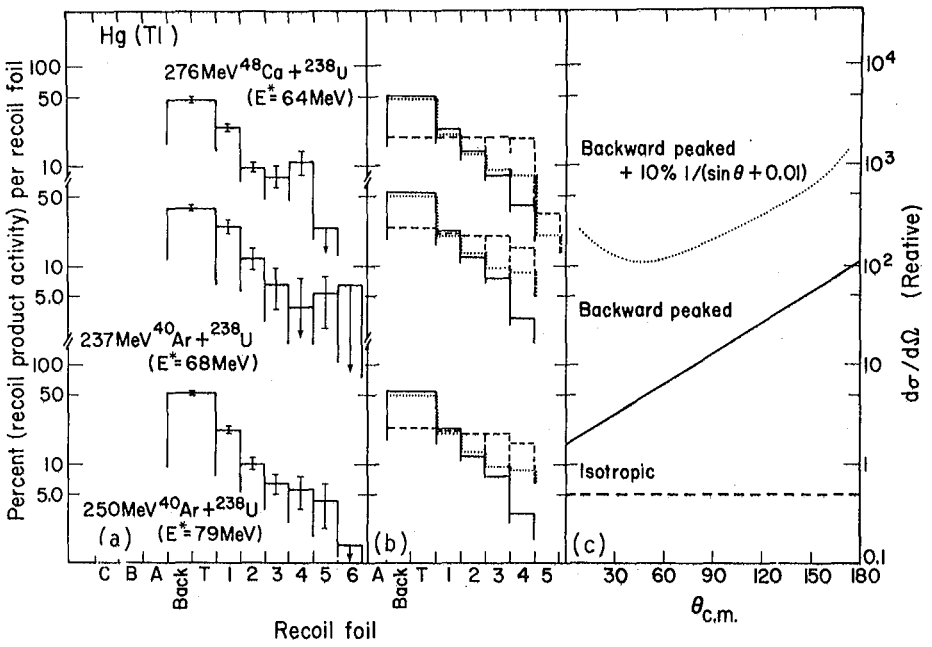

Fig. 2. (a) The experimental recoil range distributions for Hg(Tl) products from the three reactions, 276-MeV ^{48}Ca + ^{238}U and 239- and 250-MeV ^{40}Ar + ^{238}U. The excitation energies, E*, for the compound nucleus system are also given.

(b) The calculated recoil range distributions for the same reactions as shown in (a). The three calculated distributions shown in (b) for each of the Hg(Tl) distributions were calculated using the angular distributions in (c) denoted by the same type of line.

(XBL 781-89)

out a complete fusion-fission process leading to the observed mass distribution asymmetry. Perhaps the results of Kalpakchieva et al.[7] could be taken as strong evidence for shell stabilization effects in the deep-inelastic process.

Footnotes and References

*Condensed from LBL-7188, Z. Physik A 287, 97 (1978).

†Permanent address: Department of Chemistry, Oregon State University, Corvallis, OREGON 97331.

1. R. J. Otto, G. T. Seaborg, M. M. Fowler, Phys. Rev. C, 17, 1071 (1978).

2. C. Ngo, J. Peter, B. Tamain, M. Berlanger, F. Hanappe, Z. Physik A 283, 161 (1977).

3. A. G. Artukh, E. Gierlik, R. Gerstenberger, G. F. Gridnev, A. N. Mezentsev, V. L. Miheev, T. S. Salamatina, V. V. Volkov, V. B. Zlokazov, Joint Institute of Nuclear Reaction Report E7-10464.

4. J. Galin, B. Gatty, D. Guerreau, M. Lefort, X. Tarrago, S. Agarwal, R. Babinet, B. Gauvin, J. Girard, H. Nifenecker, Z. Physik A 283, 173 (1977).

5. L. G. Moretto, J. Galin, R. Babinet, Z. Fraenkel, R. Schmitt, R. Jared, S. G. Thompson, Nucl. Phys. A 259, 173 (1976).

6. R. Lucas, J. Poitou, H. Nifenecker, J. Peter, B. Tamain, Z. Physik A 283, 257 (1977).

7. R. Kalpakchieva, Yu. Ts. Oganesyan, Tu. E. Penionzhkevich, H. Sodan, Z. Physik A 283, 253 (1977).

8. A. Sandulescu, W. Greiner, J. Phys. G 3, L189 (1977).

9. J. V. Kratz, J. O. Liljenzin, A. E. Norris, G. T. Seaborg, Phys. Rev. C 13, 2347 (1976).

10. T. Sikkeland, Ark. Fys. 36, 539 (1966).

SPONTANEOUS FISSION ACTIVITIES IN THE BOMBARDMENT OF ^{248}Cm WITH OXYGEN IONS

J.M. Nitschke, L.P. Somerville, M.J. Nurmia, R.C. Eggers, and A. Ghiorso

The history of element 104 is full of controversy. The claim by the Dubna group for its discovery is based on the properties of the isotope $^{260}104$ to which they have assigned various spontaneous fission (S.F.) half-lives between 80 and 300 msec. These half-lives were obtained in bombardments of $^{22}Ne + ^{242}Pu$, $^{18}O + ^{246}Cm$, and $^{15}N + ^{249}Bk$. Attempts to find an activity with a similar half-life in Berkeley have failed repeatedly. An experiment performed with a rotating and scanning drum in 1976 showed, however, clear evidence for a 20 ± 2 msec S.F. emitter in the $^{15}N + ^{249}Bk$ and $^{16}O + ^{248}Cm$ reactions. The excitation functions were compatible with the assumption that this activity was due to compound nucleus reactions. Due to the nonspecific nature of the S.F. decay it was not possible to determine A or Z. A limit of 0.7 nb was set for the existence of the 80 msec component in the 1976 $^{15}N + ^{249}Bk$ experiment; this limit is more than one order of magnitude lower than the cross section claimed by the Dubna group for the same reaction (8 nb). However, this experiment was met with criticism in the U.S.S.R. as it had a high background level caused by the decay of ^{256}Fm [$T_{1/2}$(S.F.) = 2.63 hr].

Apart from its historical role, the isotope $^{260}104$ is of crucial importance in the understanding of the fission systematics for the heaviest elements. A simple extrapolation of the fission characteristics of the actinide isotopes would predict for $^{260}104$, a S.F. half-life in the μsec region and an even shorter value for $^{262}104$. Calculations by Randrup et al.[1] based on a semi-empirical WKB framework have, however, shown that due to the disappearance of the second fission barrier, the behavior of the fission half-lives as a function of neutron number changes drastically beyond nobelium, and the half-lives for $^{260}104$ and $^{262}104$ are predicted to be in the 10 to 30 msec region. It was therefore decided that these two isotopes should be investigated in an experiment which had a high sensitivity as well as a low background.

As was pointed out earlier, the background in most of these experiments is caused by ^{256}Md or ^{256}Fm which accumulates on the recoil catcher. A reduction of the background can be achieved by increasing the area of the catcher surface. We therefore built a detection system which has a sixty times larger area than previously used in Berkeley and a six times larger area than used in Dubna. This system consists of a giant "tape recorder" with a 2000 m stainless steel tape (12.5 μm thick and 12.5 mm wide). It is driven by a capstan which runs at constant rpm. The supply and takeup reel are driven by two variable torque motors. The linear speed of the tape is adjustable between zero and about 1.5 m/sec. The tape passes behind the target and carries the recoils to 32 mica detectors. These mica detectors start about 7 mm from the center of the target and extend over a length of 1 m to both sides. Since most of the beam intensity is lost in the stainless steel tape it is cooled through contact with a water-cooled copper block. The "tape-recorder" operates in vacuum and the target as well as the tape itself are insulated to facilitate the measurement of the beam current. During an experiment the area near the target and the first 20 cm of the tape and of the mica detectors are monitored by a television camera. By visual on-line observation it was determined that at a speed of 1 m/s the tape will support at least 4 μA of $^{16}/^{18}O^{+4}$. At the time of this writing the experiments are still in progress and the reported results are preliminary.

The parameters for the first experiment which was aimed at the production of $^{260}104$ were as follows:

1. Target: 242 μg total of ^{248}Cm (as fluoride) on 2.63 mg/cm^2 Be covered with 54 μg/cm^2 Al.
2. Effective target diameter: 6.4 mm.
3. Beam: $^{16}O^{+4}$, 92 MeV, typically 3.2 μA.
4. Total integrated beam intensity: 43.1 μA hrs.
5. Typical tape speed: 1.00 m/sec.

The beam energy of 92 MeV corresponds to the calculated peak of the excitation function for $^{260}104$. The mica detectors were scanned for fission tracks and the sums of the tracks in 10 msec bins are plotted in Fig. 1. Contrary to previous experiments, the background of ^{256}Fm is negligible. A least-squares fit with the code CLSQ gives a half-life of 19 ± 2 msec and a cross section of about 4 nb. An upper limit for a possible 80 msec component in the data shown in Fig. 1 is 0.1 nb which is in clear contradiction to the Dubna results.

It was pointed out earlier that $^{262}104$ is of particular importance to the S.F. systematics for the heaviest elements. A second experiment was therefore performed where the beam was changed from ^{16}O to ^{18}O at 93 MeV, which corresponds to the calculated peak of the excitation function for $^{262}104$; all other parameters were kept the same as in the $^{260}104$ experiment. A total of 33.5 μA hrs of $^{18}O^{+4}$ was accumulated and the fission tracks summed up in 10 msec bins are shown in Fig. 2. A single component least-squares fit to the data gives a decay of 63 ± 10 msec with a cross section of about 2.4 nb. It is too early

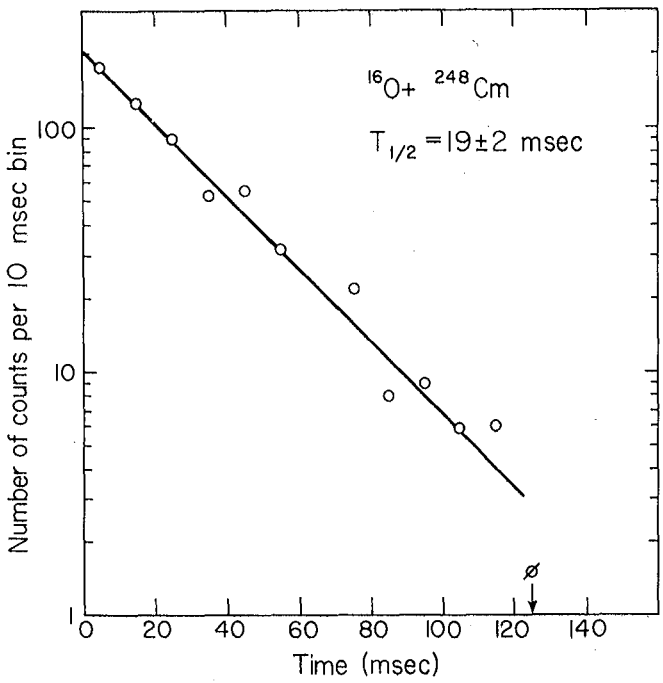

Fig. 1. Decay curve of the S.F. activity in the bombardment of ^{248}Cm with 92-MeV $^{160+4}$ ions. Integrated flux 43.1 μA hr. (XBL 788-1471)

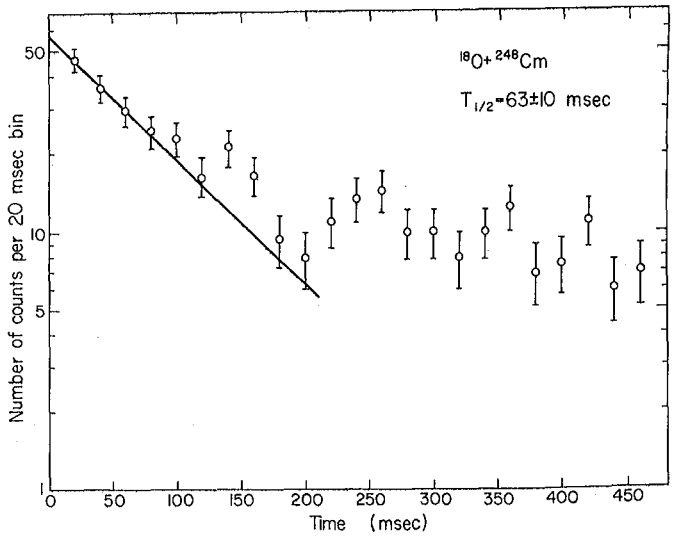

Fig. 2. Decay curve of S.F. activities in the bombardment of ^{248}Cm with 93-MeV $^{180+4}$ ions. Integrated flux 33.5 μA hr. (XBL 788-1472)

to speculate whether or not the 63 msec activity is due to the unknown isotope, ^{262}104. Only if it can be proven that the reaction mechanism is of the compound nucleus type would such a statement be justified. Should it, however, be possible to accumulate enough circumstantial evidence through excitation functions and angular distributions for the assignment of the two S.F. emitters to ^{260}104 and ^{260}104, this would lead strong support to the fission systematics as proposed by Randrup et al.[1]

Reference

1. J. Randrup et al., Phys. Rev. C 13, 229 (1976).

EVIDENCE FOR FRAGMENT DEFORMATION IN NEAR BARRIER DEEPLY INELASTIC REACTIONS OF TWO DOUBLY-MAGIC NUCLEI

R.C. Eggers, J.M. Nitschke, M.J. Nurmia, and A. Ghiorso

Although several theories have been proposed to explain deeply inelastic reactions, such reactions continue to present puzzling features. In our continuing study of the reactions of magic nuclei using the helium jet technique,[1] we have found several francium and radium isotopes as products in the reaction of ^{40}Ca on ^{208}Pb. These products are very difficult to explain as transfer products as the cross section becomes vanishingly small for such extreme multi-nucleon reactions. We have in fact seen such products before.[2] If we take the data for the francium isotopes from Fig. 1 and plot them as cross section versus mass number, we can fit a gaussian through our data points which peaks around 211.5 amu. No correction for neutron evaporation is made. The value of 211.5 amu would be predicted by assuming Z/A equilibration, as is common in deeply-inelastic reactions. Further, if we center a gaussian on mass 214 (the equilibrated Z/A value for radium) and fit it through our data for the radium isotopes as shown in Fig. 2, we can get an idea of the charge dispersion in this reaction. A gaussian constrained to be centered on the target Z and fit through the total cross section for each Z gives a charge dispersion of about 1.5 elementary charges. The reason for not seeing several other elements in this distribution is that our helium jet technique is only sensitive to a select group of nuclei. Out of this group, only ^{213}Ra is missing, and this may be due to the fact that its major alpha line at 6.62 MeV is obscured by alpha lines at 6.65 MeV due to ^{208}Fr and ^{209}Fr which are formed with higher cross section.

It seems likely that we are dealing with something similar to the deeply inelastic reaction mechanism which have been seen at much higher E/B ratios. Since a certain amount of excitation energy is required for the charge and mass diffusion to take place, we must ask where this

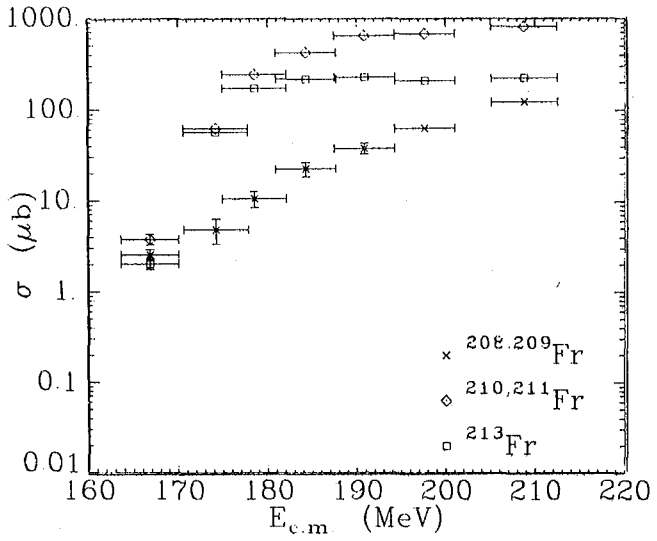

Fig. 1. Cross sections of francium isotypes as a function of different bombarding energies in the reaction ^{40}Ca on ^{208}Pb. (XBL 7810-11804)

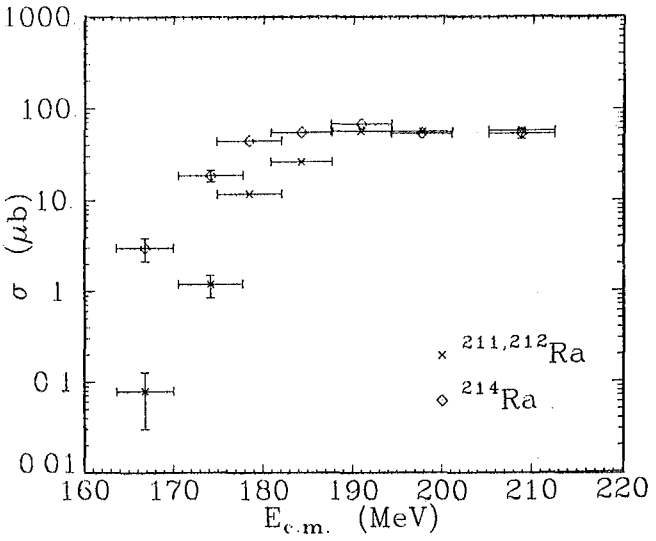

Fig. 2. Cross sections for radium isotypes as a function of different bombarding energies in the reaction ^{40}Ca on ^{208}Pb. (XBL 7810-11805)

excitation energy comes from. The excitation energy in the outgoing channels is the original center-of-mass energy plus the Q-value minus the total kinetic energy of the two fragments. An estimate of the kinetic energy may be obtained from taking the Coulomb repulsion for two spheres at a separation distance defined by some R_0 times the sum of the cube roots of the masses of the two nuclei. In order to provide at least zero excitation energy, we must assume the two fragments are highly deformed when they separate. An effective R_0 of 1.6 fm results in the minimum excitation energies quoted in Table 1. It is possible that the heavy fragment might be "caught" in a deformed state after the collision like the shape isomers known in spontaneous fission. This effect would depend on the potential energy as a function of the deformation as calculated with the Nilsson model.[3] It is important to note that the deformation "costs" little in energy (around 10 MeV) as compared to the energy gained through the effective larger separation distance of the two fragments.

The other aspects of these data which are of interest to us are the transfer products, ^{211m}Po and ^{212m}Po. We did not observe ^{211}Bi as we did in the previous experiments with ^{48}Ca and ^{40}Ar on ^{208}Pb, although this may again be due to the fact that the major alpha line of this product is in the 6.65-MeV region. We can see from Figs. 3 and 4 that our previous analysis, which gave the amount of energy shift necessary to give comparable cross section, is difficult to apply here as the shape of the excitation functions for the ^{40}Ca reactions is quite

Table 1. Minimum excitation energy for different exit channels in the $^{40}Ca + ^{208}Pb$ reaction.

Reaction and Products	Reaction Q-Value	Outgoing $E_{C.B.}$	Lowest $E_{c.m.}$	Minimum E_{ex}
$^{40}Ca + ^{208}Pb \rightarrow 36.5Si + 211.5Ra$	-44.77 MeV	120 MeV	167 MeV	3 MeV
$^{40}Ca + ^{208}Pb \rightarrow 35Si + 213Ra$	-41.33	120	167	6
$^{40}Ca + ^{208}Pb \rightarrow 34Si + 214Ra$	-36.14	120	167	11
$^{40}Ca + ^{208}Pb \rightarrow 39.5p + 208.5Fr$	-41.46	126	167	0
$^{40}Ca + ^{208}Pb \rightarrow 37.5p + 210.5Fr$	-34.58	126	167	6
$^{40}Ca + ^{208}Pb \rightarrow 35p + 213Fr$	-28.11	127	167	12

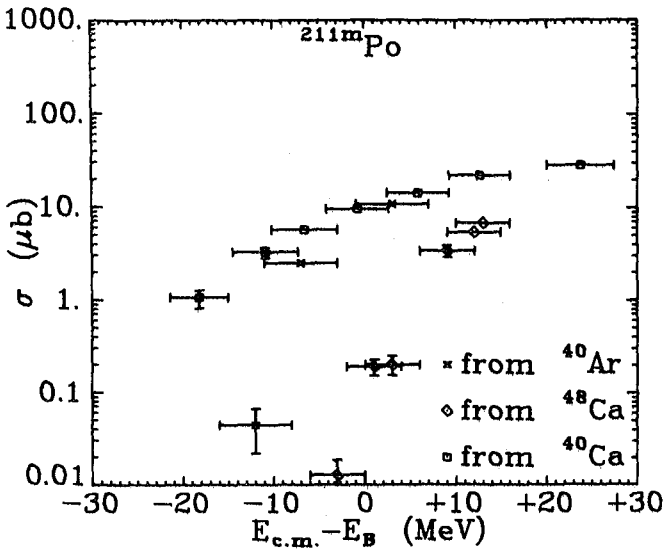

Fig. 3. Comparison of the production cross section for ^{211m}Po for different magic projectiles reacting with ^{208}Pb. (XBL 787-9753)

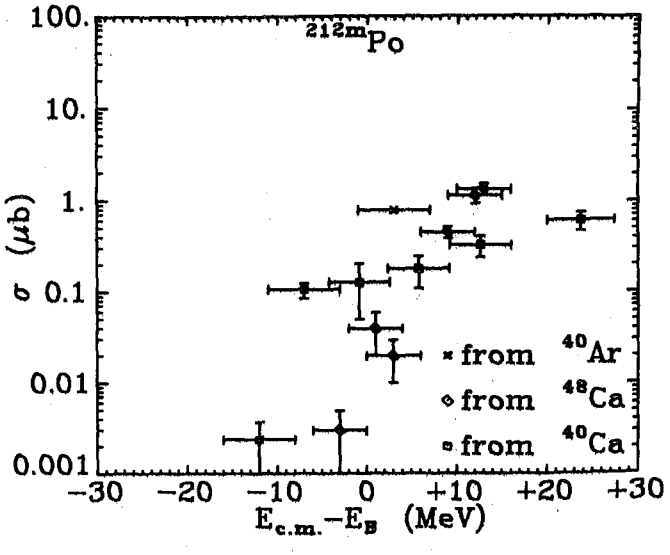

Fig. 4. Comparison of the production cross section for ^{212m}Po for different magic projectiles reacting with ^{208}Pb.

(XBL 787-9754)

different from the previous reactions. Still our data are not inconsistent with such previous analysis.

References

1. J. M. Nitschke, R. E. Leber, M. J. Nurmia and A. Ghiorso, LBL-6534 (1978).

2. R. C. Eggers, W. S. Ribbe and J. O. Rasmussen, Nucl. Phys. A 263, 500-510 (1976).

3. S. G. Nilsson, et al., Nucl. Phys., A 131, 1-66 (1969).

CHARGE AND ANGULAR DISTRIBUTIONS AS WELL AS SEQUENTIAL DECAY γ-RAY EMISSION IN HEAVY ION COLLISIONS VIEWED IN LIGHT OF THE DIFFUSION MODELS*

L.G. Moretto†

The hierarchy of the collective relaxation times in heavy-ion reactions is briefly reviewed. An improved diffusion model is introduced and applied to interpret the fragment Z and angular distributions for some typical reactions. The equilibrium in the neutron-to-proton ratio as well as the sharing of the excitation energy between fragments is studied by a coincidence method which leads to the measurement of the charge, mass, and mean number of nucleons emitted by each fragment. The final destiny of the dissipated energy is determined by measuring the atomic number of two coincident fragments, thus obtaining the missing charge as a function of bombarding energy and the Q of the reaction. The sequential fission probability of the heavy recoil is established as a function of the Z and kinetic energy of the light partner. The out-of-plane angular distribution of the fission fragments is correlated with the fissionability and interpreted in terms of various sources of angular momentum misalignment.

The γ-ray multiplicities and γ-ray angular distributions associated with deep inelastic are discussed in terms of the angular momentum transfer and in terms of the diffusion model.

Footnotes

*Abstract from LBL-6587; invited paper for the Symposium on the Macroscopic Features of Heavy Ion Collisions and the Pre-Equilibrium Process, Hakone, Japan, September 1977.

†Sloan Fellow 1974-76, extended support.

γ-RAY MULTIPLICITIES FROM A DIFFUSION MODEL INCORPORATING ONE-BODY DISSIPATION*

R. Regimbart,† A.N. Behkami,‡ G.J. Wozniak, R.P. Schmitt, J.S. Sventek, and L.G. Moretto

Recently a good deal of attention has been devoted to the experimental study of γ-ray multiplicities[1-5] in deep inelastic processes. The motivation for this study is twofold. On the one hand, one would like to clarify the mechanism of angular momentum transfer and its relation to energy transfer. There is at present an open discussion[6,7] on the relative contribution of particle transfer and phonon excitation to energy and angular momentum transfer. On the other hand, an adequate understanding of the angular momentum transfer mechanism may lead to a determination of the angular momentum fractionation[3] along the mass asymmetry coordinate and thus to a strict verification of current diffusion models.

In this paper we report a first attempt to explain the experimental data on the basis of a simple diffusion model in which the energy and angular momentum are equilibrated exclusively through particle transfer. This model has already been quite successful[8] in accurately reproducing the Z distributions and the angular distributions for individual Z values. The most recent modification of the model, to include the energy and angular momentum transfer mediated by particle exchange, has been described in detail elsewhere.[6,8] The average fragment spins $I_1(Z,E_k)$ and $I_2(Z,E_k)$ are calculated as a function of the exit channel asymmetry, Z, and kinetic energy, E_k.

The transformation from the calculated fragment spins to the γ-ray multiplicity produced by the γ-de-excitation of the two fragments is based upon the assumption that most of the fragment angular momentum is removed by stretched E2 decays. More specifically we use the following transformation:

$$M_\gamma = (1/2)[I_1(Z_1,E_k) + I_2(Z_1,E_k)] + 2\alpha \quad (1)$$

where I_1 and I_2 are the fragment spins, M_γ is the γ-ray multiplicity and α is the number of statistical γ-rays emitted by each fragment. Compound nucleus studies with heavy ion reactions indicate that α ranges from 2.5 to 4 depending upon the nucleus.

In Fig. 1 the γ-ray multiplicity, M_γ, associated with both fragments from the reactions ^{197}Au, ^{165}Ho, ^{107,109}Ag + 618-MeV ^{86}Kr, is plotted as a function of the exit channel total kinetic energy (TKE). Both the experimental and the theoretical γ-ray multiplicities have been integrated over a range of exit channel asymmetries (Z_3 = 30-39). The number of statistical γ-rays per fragment α was taken to be 3.

At the highest kinetic energies both the calculated and experimental multiplicities are low and increase rapidly with decreasing TKE.

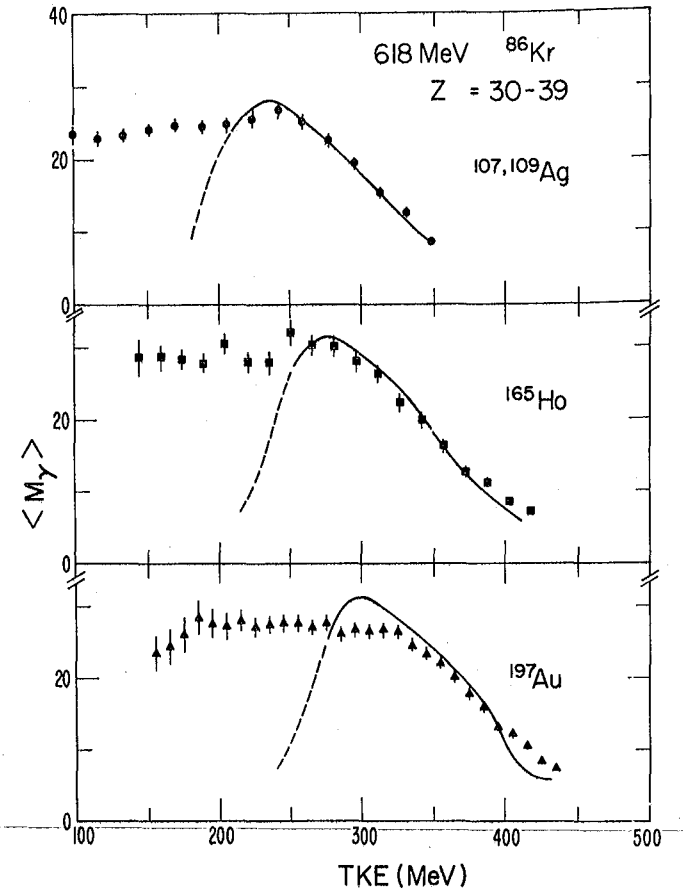

Fig. 1. M_γ vs total kinetic energy (TKE) for the reaction ^{86}Kr (618 MeV) + ^{197}Au, ^{165}Ho and ^{107,109}Ag. The experimental data (solid symbols) have been averaged over 10 Z-values near the projectile Z and the experimental TKE have been corrected for neutron evaporation. The theoretical curves (solid and dashed lines) have been calculated as described in the text. Only relative errors are shown for the data points.
(XBL 786-2553)

The agreement between theory and experiment is excellent in this region. At the lowest kinetic energies the experimental multiplicities reach a plateau and then slightly decrease again. The calculated multiplicities on the other hand reach a maximum and then decrease quite rapidly with the decreasing kinetic energy.

The early rapid increase of M_γ with decreasing kinetic energy is due to the rapid transfer of angular momentum associated with the particle transfer which occurs as the energy of relative motion is being equilibrated. The plateau in the experimental multiplicities and the maximum in

the calculated multiplicities corresponds to a regime very close to rigid rotation. The drop in the calculations (dashed curve) at low kinetic energies is due to the effect of the Coulomb energy (which in the model is taken to be that of two touching spheres) and to the fact that lower angular momenta, in the limit of rigidly rotating touching spheres, are associated with lower kinetic energies. The experimental values do not show a drop in multiplicity as large as that found in the theory because the exit channel configuration is not constrained to that of two touching spheres. Thus the deep-inelastic component is spread over an energy range extending well below the Coulomb barrier.

Examples of data and calculations of the Z dependence of M_γ in the quasi-elastic region are shown in Fig. 2. The characteristic V-shaped pattern visible in the data (open symbols) is very nicely reproduced by the calculations. Such a good agreement is consistent with the agreement observed between experiment and theory in Fig. 1 at the highest kinetic energies. From both of these figures one is tempted to conclude that particle exchange is sufficient to quantitatively explain the dependence of the angular momentum transfer upon kinetic energy loss without invoking the excitation of giant collective modes.[7]

The final aspect to be considered is the Z dependence of the γ-ray multiplicity in the deep inelastic region. Examples of data and calculations are also given in Fig. 2. (The case of $^{197}Au + ^{86}Kr$, which is marred by sequential fission[9] at large Q-values is not shown.) Again the experimental data are reproduced quite well. It must be emphasized that in this energy region the calculation predicts near rigid rotation throughout the Z range. Yet the rise of M_γ with decreasing Z, commonly considered as a fingerprint of rigid rotation,[2-4] is conspicuously absent. The reason for this behavior is to be found in the angular momentum fractionation along the mass asymmetry coordinate, as first inferred elsewhere.[3] The main cause for this angular momentum fractionation is the decrease of the interaction time with increasing ℓ.

Recently, fairly large second moments of the γ-ray multiplicities have been reported.[5] The present model can account for about 60 to 70% of the measured values. However, the statistical excitation of bending and wriggling modes in the exit channel, postulated by some of us[9] to understand both the sequential fission and the γ-ray angular distributions, generates a randomly oriented component of angular momentum (13 to 16ħ/fragment), which adequately provides the missing part of the second moments without substantially changing the first moments.

In conclusion, it appears that both the magnitude and shape of the experimental data can be adequately reproduced by our model.

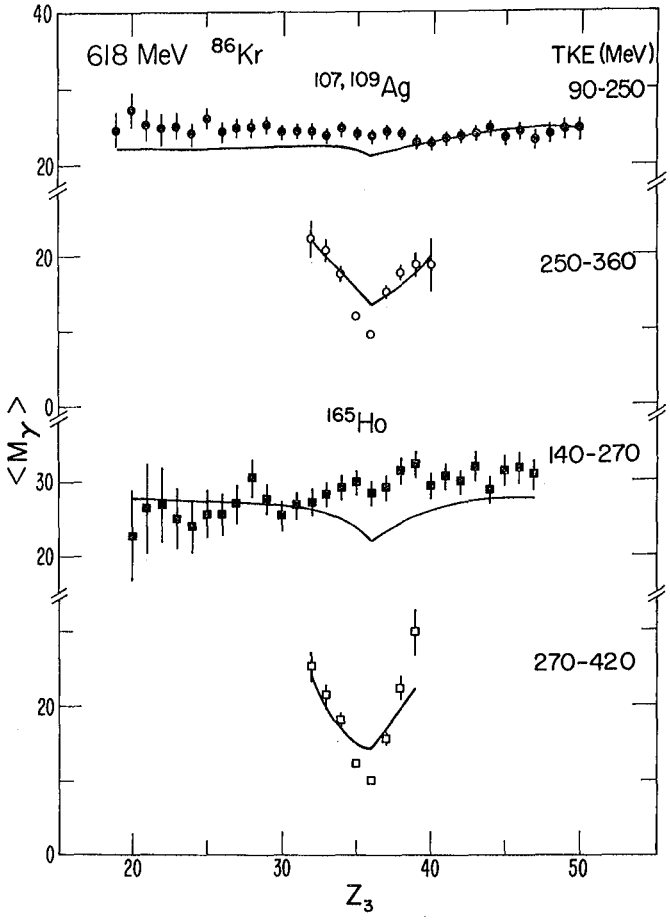

Fig. 2. M_γ vs Z_3 for the reactions ^{86}Kr (168 MeV) + ^{165}Ho and $^{107,109}Ag$. A comparison between experiment (symbols) and theory (curves) is made for both the deep-inelastic (solid symbols) and quasi-elastic (open symbols) components observed in the reactions. The cuts in TKE corresponding to these two components are given in the far right of the figure. (XBL 786-2556)

Footnotes and References

*Condensed from LBL-7751.

‡Present address: Physics Department, Pahlavi University, Shiraz, Iran.

†Present address: Laboratoire de Physique Corpusculaire, Universite de Caen, 14000 Caen, France.

1. M. Berlanger, M. A. Deleplanque, C. Gerschel, F. Hanappe, M. Leblanc, J. F. Mayault, C. Ngo, D. Paya, N. Perrin, J. Pêter, B. Tamain, and L. Valentin, J. Phys. (Paris) 37, L323 (1976).

2. P. Glässel, R. S. Simon, R. M. Diamond, R. C. Jared, I. Y. Lee, L. G. Moretto, J. O. Newton, R. Schmitt, and F. S. Stephens, Phys. Rev. Lett. 38, 331 (1977).

3. M. M. Aleonard, G. J. Wozniak, P. Glässel, M. A. Deleplanque, R. M. Diamond, L. G. Moretto, R. P. Schmitt, and F. S. Stephens, Phys. Rev. Lett. 40, 622 (1978).

4. J. B. Natowitz, M. N. Namboodiri, P. Kasiraj, R. Eggers, L. Adler, P. Gonthier, C. Cerruti and T. Alleman, Phys. Rev. Lett. 40, 751 (1978).

5. P. R. Christensen, F. Folkmann, Ole Hansen, O. Nathan, N. Trautner, F. Videbaek, S. Y. van der Werf, H. C. Britt, R. P. Chestnut, H. Freiesleben and F. Pühlhofer, Phys. Rev. Lett. 40, 1245 (1978).

6. J. S. Sventek and L. G. Moretto, Phys. Rev. Lett. 40, 697 (1978).

7. R. A. Broglia, O. Civitarese, C. H. Dasso and A. Winther, Phys. Lett. B 73, 405 (1978).

8. L. G. Moretto, J. Phys. Soc. Japan Suppl. 44, 361 (1978).

9. G. J. Wozniak, R. P. Schmitt, P. Glässel, R. C. Jared, G. Bizard, and L. G. Moretto, Phys. Rev. Lett. 40, 1436 (1978).

γ-RAY MULTIPLICITIES OBSERVED IN 476-MeV ^{56}Fe-INDUCED REACTIONS ON ^{107,109}Ag AND ^{197}Au

R. Regimbart,* G.J. Wozniak, A.N. Behkami,† R.P. Schmitt, G.J. Mathews, H. Hübel, R.M. Diamond, and L.G. Moretto

Studies of heavy-ion reactions have shown the existence of an intermediate complex consisting of two well defined fragments in contact undergoing equilibration along the various degrees of freedom.[1] To investigate the equilibration of the angular momentum degree of freedom, we have studied the transfer of extrance channel orbital momentum into intrinsic rotation of the two fragments constituting the complex. To determine the total spin of the fragments in a particular exit channel, we measured the atomic number Z_3 and the energy E_3 of the light fragment detected in a ΔE-E telescope.

The experimental setup consisted of a particle telescope (gas-ΔE, solid state E counter) and a γ-ray multiplicity filter (six 3 in. x 3 in. NaI detectors) which was placed 5 in. above the target 45° out of the reaction plane. All possible coincidences among the 6 NaI detectors and the telescope were recorded event by event. The multiplicity as a function of Z_3 and E_3 was deduced from the number of counts obtained in the different p-fold coincidences with the NaI detectors (a p-fold coincidence is a p-multiple coincidence among any combination of 6 NaI counters). The γ-detection efficiency of the NaI detectors was measured with both ^{60}Co and ^{207}Bi sources and a mean value (0.012) was taken for each detector.

The kinetic energy dependence of the γ-ray multiplicity M_γ is shown in the upper part of Fig. 1 for reaction products ($10 \leq Z_3 \leq 40$) from the reaction 476-MeV ^{56}Fe + ^{197}Au. As the lab energy of the light fragment (Z_3) decreases, M_γ increases steadily from a value of 5 in the quasi-elastic region to a maximum value of 20 in the deep-inelastic region. The steady increase of M_γ with decreasing kinetic energy is due to the rapid transfer of angular momentum associated with particle transfer, which occurs as the energy of relative motion is being equilibrated. The observed saturation of M_γ occurs in the regime of rigid rotation. The second moments illustrate a similar trend although somewhat reduced in magnitude.

To illustrate the Z-dependence of M_γ for deep-inelastic products, both the first and second moments are shown in Fig. 2 for the 476-MeV ^{56}Fe + ^{107,109}Ag reaction. Only a weak dependence on Z_3 is observed, which is very similar to the dependence observed for ^{86}Kr-induced reactions.[2]

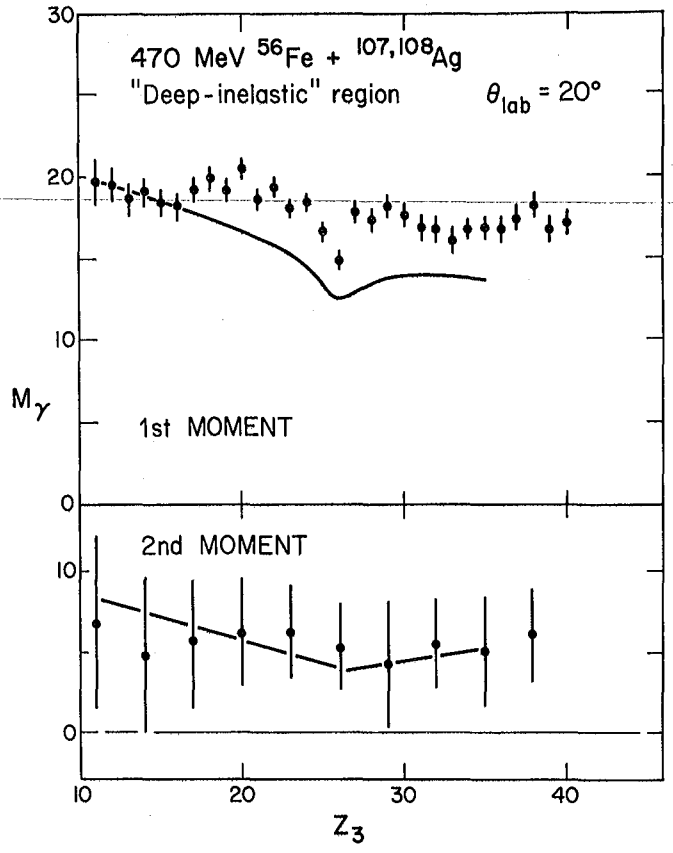

Fig. 1. M_γ vs lab energy for the reaction 476-MeV ^{56}Fe + ^{197}Au. (XBL 789-2621)

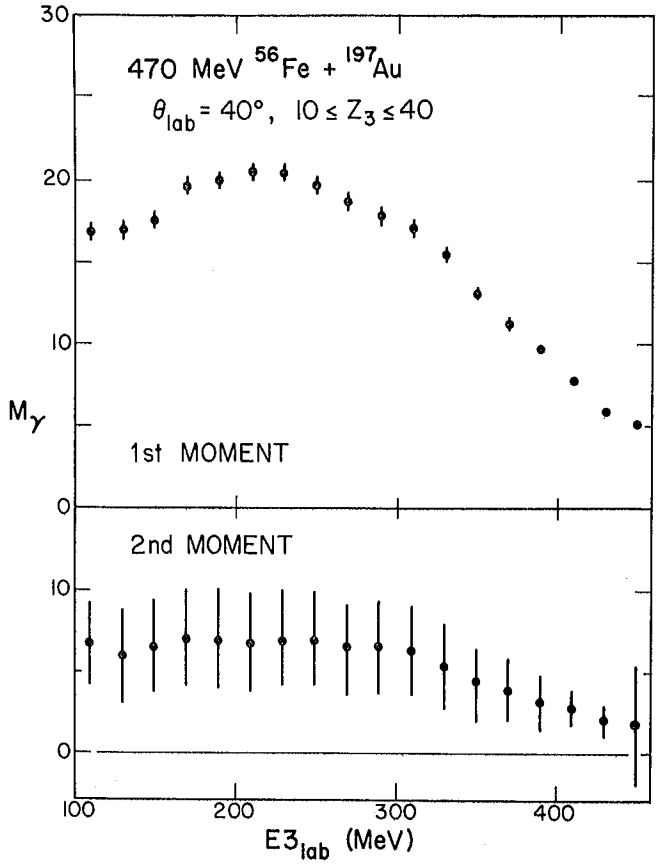

Fig. 2. First and second moments for the reaction 476-MeV ^{56}Fe + ^{107,109}Ag as a function of Z_3. A comparison between experiment (symbols) and theory (curves) is made for the deep-inelastic component observed in the reaction. (XBL 789-2620)

Model calculations (solid lines) are also shown for a simple diffusion model,[3] in which both the energy and angular momentum are equilibrated exclusively through particle transfer. One should note that both the trend and magnitude of the data are reproduced by the calculations.

In this energy region, the model calculations predict near rigid rotation throughout the Z-range, yet M_γ does not rise[4] with decreasing Z_3. The reason for this behavior is that different Z-values (asymmetries) are populated by different ℓ-windows. A similar angular momentum fractionation has been observed in ^{86}Kr-induced reactions and has been interpreted[2] as being due to the dependence on ℓ of both the interaction time and the driving potential for diffusive mass transfer.

In summary, the Fe-induced deep-inelastic reactions closely resemble ^{86}Kr-induced ones, both of which show evidence of angular momentum fractionation, in contrast to ^{40}Ar- and ^{20}Ne-induced reactions where a strong dependence of M_γ on Z_3 has been observed.

Footnotes and References

*Present address: Laboratoire de Physique Corpusculaire, Universite de Caen, 14000 Caen, France.

†Present address: Physics Department, Pahlavi University, Shiraz, Iran.

1. L. G. Moretto and R. Schmitt, J. de Phys. 37, 109 (1976).

2. M. M. Aleonard, G. J. Wozniak, P. Glässel, M. A. Deleplanque, R. M. Diamond, L. G. Moretto, R. P. Schmitt, and F. S. Stephens, Phys. Rev. Lett. 40, 622 (1978).

3. L. G. Moretto, J. Phys. Soc. Japan Suppl. 44, 361 (1978).

4. P. Glässel, R. S. Simon, R. M. Diamond, R. C. Jared, I. Y. Lee, L. G. Moretto, J. O. Newton, R. Schmitt, and F. S. Stephens, Phys. Rev. Lett. 38, 331 (1977).

KINETIC ENERGY MOMENTS AND CHARGE DISTRIBUTIONS FROM THE ^{20}Ne + ^{197}Au REACTION AT 175 AND 252 MeV

J.B. Moulton, G.J. Mathews, G.J. Wozniak, R.P. Schmitt, and L.G. Moretto

Many of the gross features which characterize heavy-ion deeply inelastic collisions are by now reasonably well understood in terms of classical dynamics and nucleon transport. Perhaps the time is ripe to examine specific features of these reactions in more detail. In this work we examine two such detailed aspects of the ^{20}Ne + ^{197}Au reaction. One feature is the behavior of the kinetic-energy distribution moments as a function of bombarding energy and product Z, the other feature is the role of secondary fission of the Au-like fragment (or compound nucleus) following the collision.

Data were obtained with 175- and 252-MeV ^{20}Ne ions from the LBL 88-inch cyclotron. Products were identified in ΔE-E ionization-counter solid state telescopes. Energy spectra were corrected for straggling in the target and gas window.

Some inferred centroids and widths as a function of Z are shown in Fig. 1 for relaxed products from the 175-MeV data. In an effort to more quantitatively understand these features model calculations have been performed and are also shown in Fig. 1. In the model the intermediate complex is treated as a canonical ensemble at thermal equilibrium whose temperature is fixed by the internal energy of the single-particle degrees of freedom. The nuclei are assumed to undergo ellipsoidal colinear deformation and to rotate rigidly. The n^{th} moment of the fragment kinetic energy is then:

$$\langle E_{KE}^{n} \rangle = \frac{\sum_{\ell_{min}}^{\ell_{max}} \left[\sigma_\ell \frac{\int E_{KE}(\rho,\ell) \exp(-V(\rho,\ell)/T)\, d\rho}{\int \exp(-V(\rho,\ell)/T)\, d\rho} \right]}{\sum_{\ell_{min}}^{\ell_{max}} \sigma_\ell} \quad (1)$$

where ρ is the deformation coordinate and V is the potential energy.

The calculated moments were corrected for neutron evaporation. Overall, the predicted centroids match the data fairly well. Some of the underestimation of the widths may be due to experimental kinematic broadening, or the neglect of proton evaporation and quantal effects in the theory.

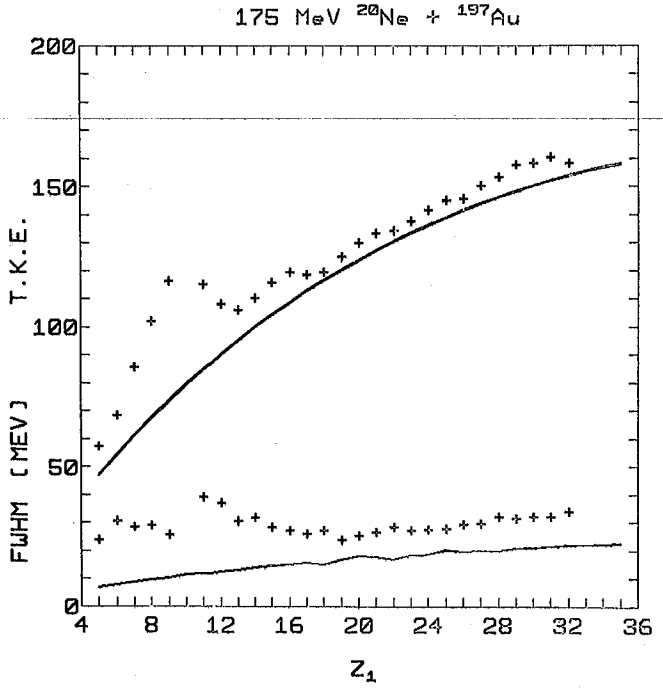

Fig. 1. Experimental two-fragment center of mass kinetic energy (upper points) and FWHM (lower points) vs the light fragment atomic number. Corrected for evaporation. Adjacent smooth curves are calculated values. 175-MeV projectile energy. (XBL 782-7425)

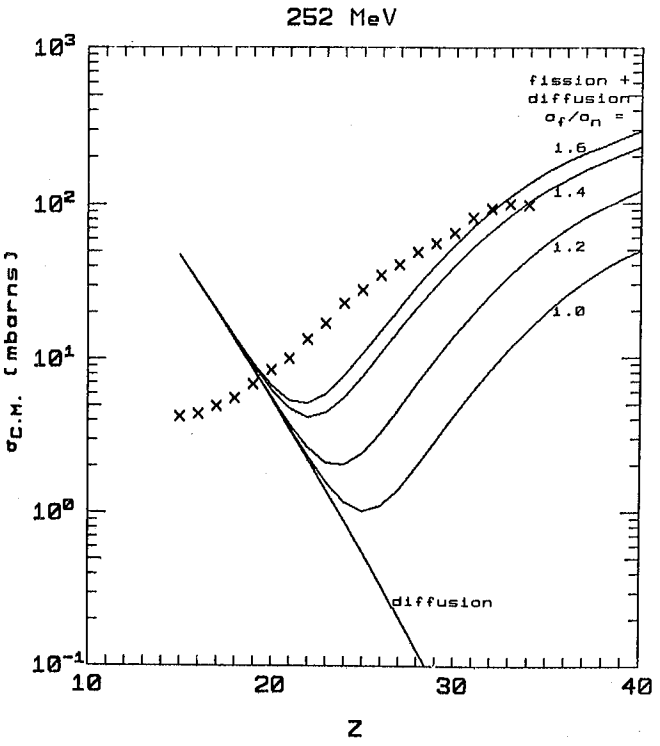

Fig. 2. Calculated diffusion and diffusion plus fission yield vs Z for 3 different values of the LDPR. The points (X's) are measured cross sections extrapolated over the full angular range. 175-MeV projectile energy. (XBL 785-8923)

The total angle-integrated charge distribution as a function of Z is shown in Fig. 2 for the 252-MeV data. It is immediately evident that the charge distribution from particle diffusion alone cannot reproduce the data. Therefore, we have supplemented the diffusion model with a calculation of secondary fission of the Au-like fragment or compound nucleus.

These results are shown as a function of the ratio of the fission to neutron level-density parameters in Fig. 2. In the model, Γ_f/Γ_n was calculated using the well known rotating liquid-drop barriers of Cohen, Plasil and Swiatecki. The gaussian charge distribution was computed according to the formulation of Nix and Swiatecki.[1]

For a_f/a_n of about 1.5, which is typical for the products of interest, the qualitative trends in the Z distribution are well reproduced.

Reference

1. J. R. Nix and W. J. Swiatecki, Nucl. Phys. 71, 1 (1965).

PROTON EMISSION IN THE REACTION ^{63}CU + 252-MeV ^{20}Ne

R.P. Schmitt, G.U. Rattazzi, G.J. Wozniak, G.J. Mathews, R. Regimbart, and L.G. Moretto

Early studies of light charged particles emitted in heavy-ion reactions displayed features that could be interpreted as mainfestations of non-equilibrium processes.[1] However, only recently has the study of such phenomena moved into the foreground of heavy-ion research.[2-4] This renewed interest has largely been motivated by a desire to uncover the details of heavy-ion reaction mechanisms, and in particular, of deep-inelastic processes. Indeed, such studies may well be instrumental in evaluating the relative importance of one-body dissipation, two-body dissipation, and the excitation of giant modes in the energy damping process. As an example, the formation of localized "hot-spots" could be expected on the basis of two-body viscosity. A possible signature of the one-body dissipation mechanism[5] involves the emission of high energy nucleons.[6] These particles would be generated through the coupling of the Fermi motion to the relative velocity of the target and projectile nuclei. If a one-body mechanism is operative and if the mean free path is long, nucleons originating from the projectile, for example, could pass through the target nucleus, collide with the potential wall and, in some cases, be transmitted as a Fermi Jet.[6] This experiment was specifically designed to investigate the possibility of such pre-equilibrium processes in the ^{63}Cu + 252-MeV ^{20}Ne reaction.

Thin, self-supporting targets of ^{63}Cu (99% enrichment) were bombarded with 252-MeV ^{20}Ne ions accelerated by the LBL 88-inch cyclotron. Light charged particles were detected in either of two particle telescopes each consisting of a 400-μm surface-barrier ΔE detector and a 1.5 in. NaI E detector. A third telescope, which consisted of an extremely uniform 11-μm ΔE detector and a 400-μm E detector, was capable of resolving Ne-like fragments with atomic numbers in the range $3 \leq Z \leq 13$. This telescope was placed directly in front of one of the light particle telescopes so that it was possible to detect coincident protons directly along the Ne-like fragment direction. During the experiment the arm supporting the heavy ion detector was placed at a fixed angle while the other counter was placed successively at different angles. Coincidences between the heavy-ion detector either of the light particle telescopes were recorded on magnetic tape as were suitably scaled-down singles events for all telescopes.

In Fig. 1(a) proton energy spectra are shown for a few representative angles. One may be impressed that the energy spectra extend up to very high energies (~60 MeV). Similar energies were observed for d's and t's. In Fig. 1(b) and (c) proton energy spectra are plotted, which are in coincidence with a heavy particle ($4 \leq Z \leq 13$). It should be noted that the proton energy spectra

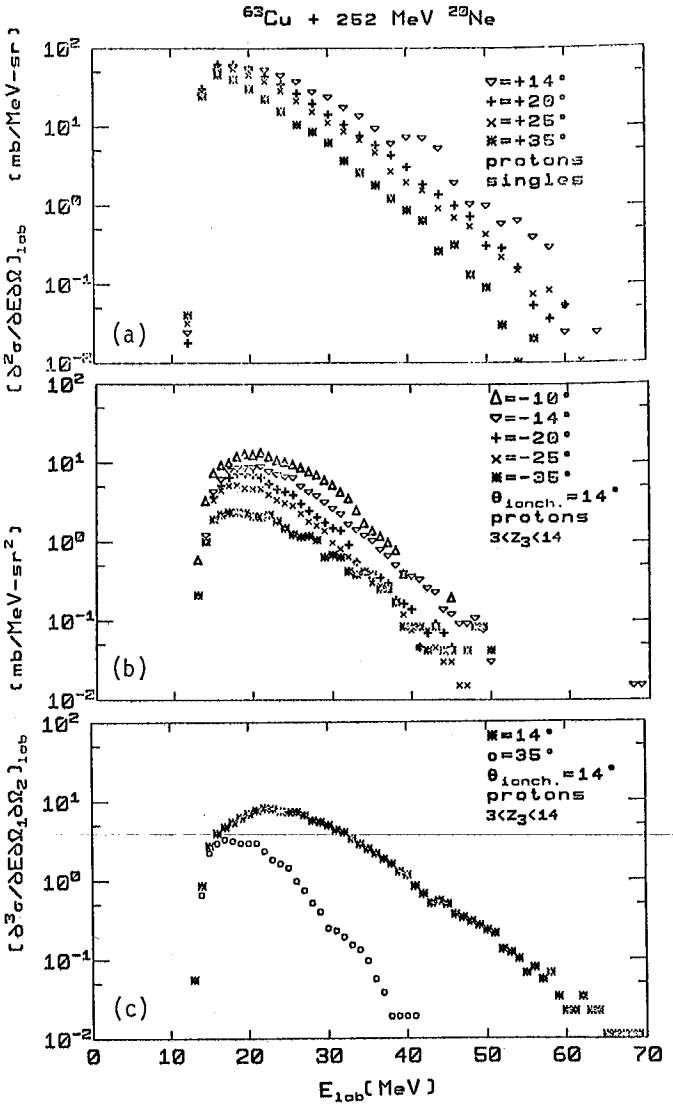

Fig. 1. (a) Protion energy spectra observed in singles mode at various lab angles.
(b) Proton energy spectra in coincidence with deep-inelastic fragments emitted at 14° on the opposite side of the beam axis.
(c) Same as (b) but for protons on the same side of the beam axis as the deep-inelastic fragments. (XBL 787-9618)

are "harder" for positive angles than for negative angles (see caption), leading to the tentative conclusion that the most energetic protons are associated with the Ne-like fragment rather than the target. This argues against Fermi jetting, which predicts that the energetic nucleons would be emitted from the target. However, the presence of orbiting could complicate this interpretation.

At this point it is clear that other mechanisms must be considered (i.e., Fermi jetting may still be present but this process alone cannot describe the pattern of proton energy spectra). The fast, light particles may be emitted by a localized excitation or hot-spot. While this possibility cannot be completely ruled out, it seems unlikely in view of the fact that the heavy ions and protons are detected at the same angle, since one would expect that the Ne-like fragments would tend to shadow the hot spot. Another possibility is that the high energy particles result from evaporation from highly excited Ne-like fragments moving at high velocities.

This latter possibility can be tested by transforming the proton energy spectra event-by-event into the moving frame of the Ne-like fragment. The results are shown in Fig. 2(a).

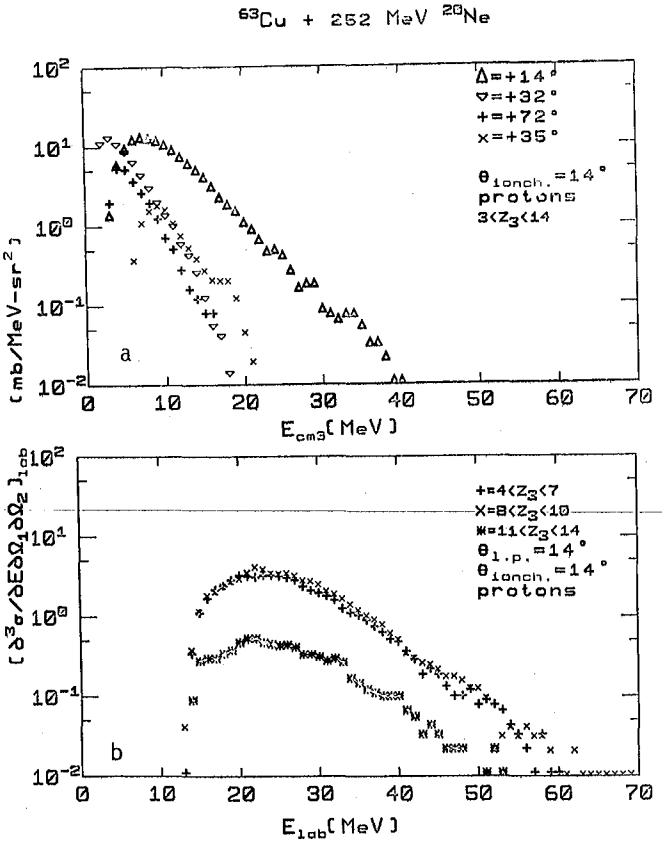

Fig. 2. (a) Proton energy spectra in the moving frame of the Ne-like deep-inelastic fragment. (b) Laboratory proton energy spectra for three different Z bins of deep-inelastic fragments. (XBL 787-9613)

For relatively large angles, the energy spectra overlap nicely as one would expect on the basis of an evaporative mechanism. However, at more forward angles, the yield is substantially greater. This may be due to the fact that the protons observed at more backward angles may be emitted from the target while those observed at 14° are emitted from the projectile. If one attributes the exponential tail of the 14° data to evaporation, one extracts a temperature of about 5 MeV, which is in rather poor agreement with simple calculations that assume that the excitation energy of the deep-inelastic products divides according to their masses. In addition, the maximum proton energy is limited by the available excitation energy in the Ne-like fragment. Consequently, at least some of the light fragments must have about 50-MeV excitation energy to account for the most energetic protons observed. In contrast, the assumption that the excitation energy is divided according to the exit channel asymmetry predicts about 36 MeV for ^{20}Ne.

Figure 2(b) shows lab proton energy spectra for three different Z bins of the Ne-like fragments. Interestingly enough, there is very little difference in the shapes of the spectra. The yield of coincident protons does depend on Z, and tends to be lowest for Z's above the projectile, where the deep inelastic cross section is small.

It is difficult to draw any definite conclusions as to the occurrence of Fermi jets or hot-spot emission in the ^{63}Cu + ^{20}Ne reaction. Although very high energy protons are observed, it is not clear that they are associated with a pre-equilibrium process since evaporation has not yet been ruled out. Even if an evaporation process is responsible, however, it still may be possible to learn some of the details of the reaction mechanism such as the sharing of excitation energy between the fragments.

References

1. H. C. Britt and A. R. Quinton, Phys. Rev. 124, 877 (1961).

2. H. Ho et al., Z. Phys. A283, 235 (1977).

3. J. W. Harris et al., Phys. Rev. Lett. 38, 1460 (1977).

4. C. K. Gelbke et al., Phys. Lett. 71B, 83 (1977).

5. J. Randrup, LBL-5847 (1976).

6. M. Robel and W. Swiatecki, this annual report.

DEEP-INELASTIC SCATTERING AND FISSION IN THE 220-MeV ^{40}Ar + ^{128}U REACTION

G. J. Mathews, L.G. Sobotka, G.J. Wozniak, R.P. Schmitt, R. Regimbart, G.U. Rattazzi, M. Lutolf, P. Bigeleisen, and L.G. Moretto

The 220-MeV ^{40}Ar + ^{238}U reaction is an interesting system in which to study the reaction mechanisms and likelihood of heavy-element formation. Recent work on a similar system,[1] 222-MeV ^{40}Ar + ^{243}Am, has indicated that the inferred mass distribution exhibits features reminiscent of the shell effects of low-energy compound-nucleus fission. In this work, we have investigated an alternative explanation of this phenomenon which should also appear in the ^{40}Ar + ^{238}U system. We propose that the peak in the mass distribution near A = 75 observed in Reference 1, may be due to a depletion of yield caused by the secondary fission of the heavy fragment ($Z \geq 82$) following a deep-inelastic collision. Also in this work we are applying these results to test diffusion model predictions of heavy-element formation.

There are several methods of testing this hypothesis. One way is to distinguish between compound-nucleus fission and deep-inelastic collisions by the possible asymmetry about 90° in the angular distribution of the latter process.[2] A more stringent test, which we also apply in this work, is to look at heavy products in coincidence with an identified fragment. If a peak in coincidence yield is produced by the increase or decrease of secondary fission of the heavy fragment, there will be a discrepancy between the singles and coincidence rate.

We did, therefore, the following experiment. The light fragment was identified in an ionization-counter solid state ΔE-E telescope. Coincidence events were detected in a solid state position-sensitive detector, which spanned an angular range of 32° in plane and 6° out of plane.

Fragment singles cross sections exhibit some interesting features. One is the absence of a peak in the singles distribution near Z=28, which would be expected for a shell effect from the complementary (Z=82) heavy fragment. The light fragments show the side-peaked angular distributions expected from deep-inelastic scattering. The fragments heavier than the projectile exhibit the transition to $1/\sin\theta_{c.m.}$ behavior consistent with fission or long lived deep-inelastic events.

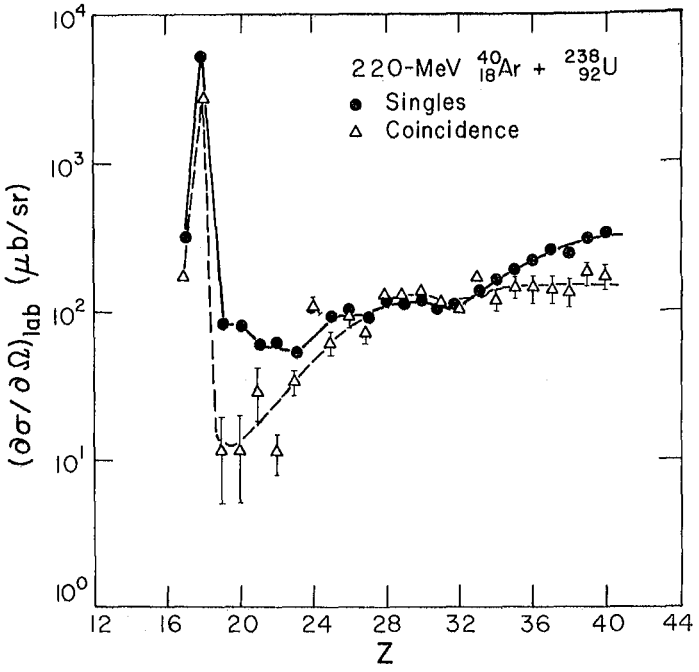

Fig. 1. Comparisons of singles coincidence charge distribution for relaxed plus quasi-elastic events. The two spectra were normalized with the elastic events. The telescope angle is 50°, the PDS angle is 70°. (XBL 789-2242)

Final conclusions can be drawn from Fig. 1 which shows a comparison of the singles and coincidence yield at one detector angle setting. The differences between the two spectra are clearly understandable in terms depletion of the binary coincidence yield due to secondary fission of the heavy fragment for Z > 82 (Z_{Light} < 28). The increase in the singles yield for Z_{Light} > 34 can be attributed to the secondary fission fragments.

References

1. R. Kalpakchieva, Yu. Ts. Ogannessian, Tu. E. Penionzhkevich, and H. Sodan, Z. Physik A283, 253 (1977).

2. R. J. Otto, D. J. Morrissey, G. T. Seaborg, and W. D. Loveland, LBL-7188 (1978).

CHARGE DIFFUSION IN THE REACTION ^{197}Au + ^{86}Kr AT 506-, 620- and 732-MeV BOMBARDING ENERGY

R.P. Schmitt, G.J. Wozniak, G. Bizard,* J.S. Sventek, and L.G. Moretto

In previous work[1] we have studied the energy spectra, charge distributions, and angular distributions of deep-inelastic fragments produced in the reaction ^{197}Au + 620 MeV ^{86}Kr. It was found that the data could be semi-quantitatively reproduced by a simple diffusion model,[2] which treats mass transfer as a diffusion process. In fact it was also possible to obtain reasonable fits to experimental data obtained with 620 MeV ^{86}Kr on a variety of targets as light as ^{nat}Ag.[3] To further test and refine the model we have studied the dependence of the ^{197}Au + ^{86}Kr system (see also Ref. 4) on bombarding energy.

A self-supporting Au foil was bombarded with 506- and 732-MeV ^{86}Kr ions produced by the SuperHILAC. Charged fragments produced in these bombardments were detected with gas-ionization, solid state ΔE,E telescopes. Energy spectra and charge distributions were measured at 12 angles.

In Figs. 1 and 2 typical Z-distributions are shown for both bombarding energies. At 506 MeV the charge distributions are all peaked near the projectile Z-value, especially for angles near the grazing angle (62° in the lab) where quasi-elastic reactions are the most intense. At more forward angles like 35° where quasi-elastic reactions are essentially absent, the charge distributions are somewhat broader and peak at Z-values above the projectile. This shift is probably the result of enhanced diffusion towards symmetry promoted by the potential energy of the intermediate complex.

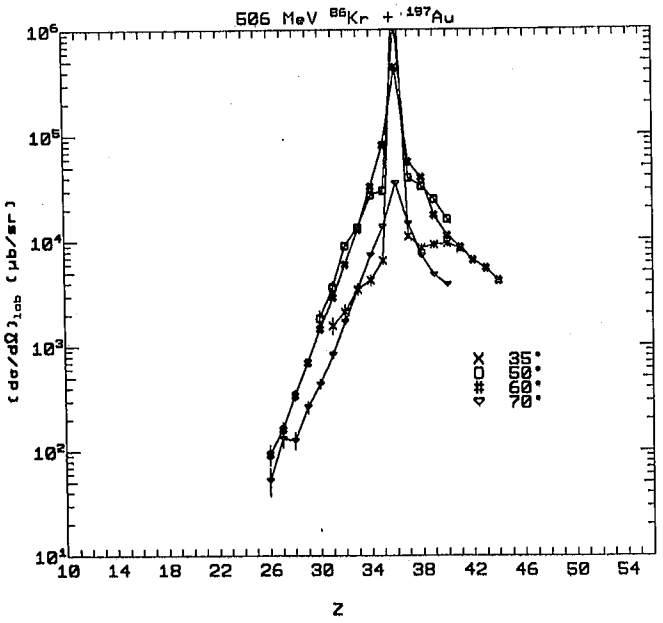

Fig. 1. Lab Z-distributions for the reaction ^{197}Au + 506-MeV ^{86}Kr. (XBL 7711-10743)

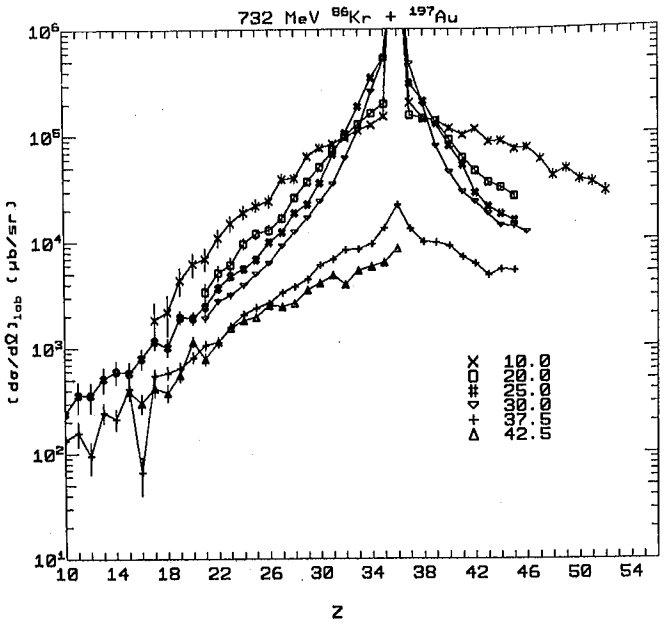

Fig. 2. Lab Z-distributions for the reaction ^{197}Au + 732-MeV ^{86}Kr. (XBL 7711-10742)

In contrast to the 506-MeV data, the charge distributions obtained at 732 MeV are quite broad (excluding those obtained at angles near the grazing); however, the yield is again concentrated in the vicinity of the projectile. The increase in the widths of the Z-distributions at 732 MeV is probably due to an increase in the temperature of the intermediate complex, which permits more extensive diffusion to occur.

Another interesting feature of the two reactions is the variation in yield with angle. At the lower bombarding energy the cross section is highest near the grazing angle; that is, the angular distributions are side-peaked. This side peaking persists throughout the Z-range of the measurements, even for atomic numbers where the contribution from quasi-elastic reactions is small. However, at 732 MeV the yield tends to fall off steadily with increasing angle, except for atomic numbers close to the projectile Z where side peaking is observed. Actually, the transition from side peaking to forward peaking occurs smoothly with Z. The overall pattern of the angular distributions for ^{197}Au + 732 MeV ^{86}Kr is similar to that observed with 620-MeV ^{86}Kr, and can be attributed to a diffusion controlled time delay in populating more extreme asymmetries.[1] By selecting Z's close to the projectile one is biased in favor of short interaction times. If the interaction time is short compared to the rotational period, the complex decays before it rotates to small angles, resulting in side-

peaked angular distributions. For longer interaction times more extensive rotation occurs so that before the complex decays it may actually rotate to and perhaps past 0°, resulting in forward-peaked angular distributions.

The fact that the angular distributions at 506 MeV are all side peaked, whereas those at 732 MeV exhibit both forward and side peaking make the reaction $^{197}Au + ^{86}Kr$ ideal (as well as challenging) for a comparison with model calculations. Recently, a more refined diffusion model has been developed, which includes energy dissipation via one-body viscosity.[5] A comparison between model calculations and the experimental data is shown in Fig. 3 for all three bombarding energies. The agreement is particularly impressive in view of the fact that the interaction times, form factors and diffusion constants have not been treated as free parameters. A more difficult test of the model is the reproduction of the experimental angular distributions as a function of Z. The results of the calculations for ^{197}Au + 506-MeV ^{86}Kr are shown in Fig. 4. Except for

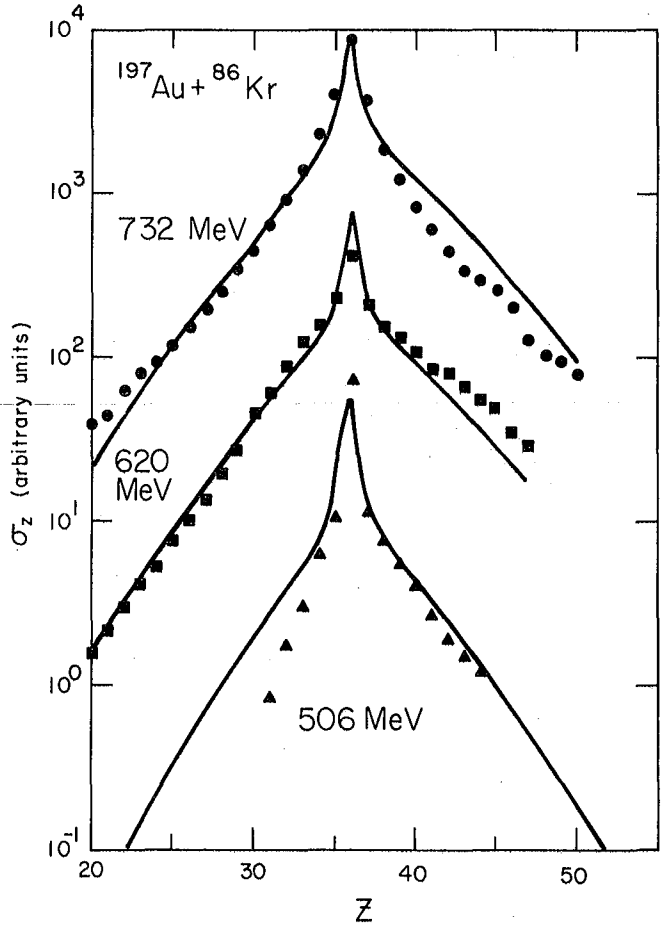

Fig. 3. Comparison between theoretical and experimental cross sections for the reaction $^{197}Au + ^{86}Kr$ at three bombarding energies.
(XBL 785-802)

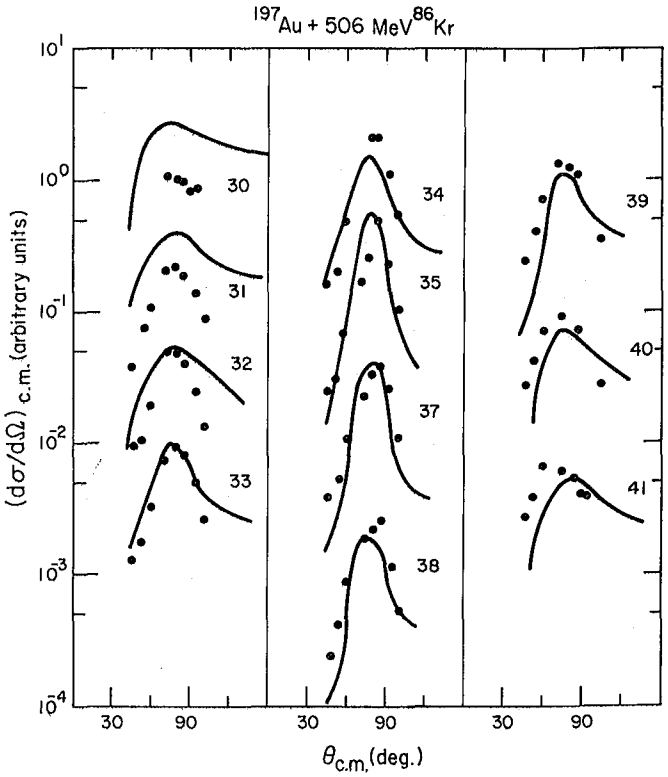

Fig. 4. Experimental and calculated angular distributions for the reaction ^{197}Au + 506-MeV ^{86}Kr.
(XBL 785-803)

the fact that the model overestimates the yield for the lowest Z's, the agreement is very good. Both the magnitudes and the shapes are reproduced. Similar agreement has been achieved for the other bombarding energies, lending credence to the diffusion model incorporating a one-body dissipation mechanism.

Footnote and References

*Present address: Laboratoiré de Physique Corpusculaire, Université de Caen, 14000 Caen, France.

1. P. Russo, R. P. Schmitt, G. J. Wozniak, R. C. Jared, P. Glässel, B. Cauvin, J. S. Sventek, and L. G. Moretto, Nucl. Phys. A 281, 509 (1977).

2. J. S. Sventek and L. G. Moretto, Phys. Lett. B 65, 326 (1976).

3. R. P. Schmitt, P. Russo, R. Babinet, R. Jared, and L. G. Moretto, Nucl. Phys. A 279, 141 (1977).

4. R. P. Schmitt, G. J. Wozniak, G. Bizard, and L. G. Moretto, elsewhere in this report.

5. J. S. Sventek and L. G. Moretto, Phys. Rev. Lett. 40, 697 (1978).

THE ENERGY DEPENDENCE OF THE REACTION $^{nat}Ag + {}^{86}Kr$

R.P. Schmitt, G.J. Wozniak, G. Bizard,* and L.G. Moretto

Although a large body of experimental data has been accumulated on the charge and angular distributions for deep-inelastic processes, comparatively little information is available on the energy dependence of these processes, particularly for heavy systems. To investigate the dependence of deep-inelastic processes on bombarding energy, we have conducted a series of experiments with 506- and 732-MeV ^{86}Kr ions on ^{nat}Ag. These results[1] complement those previously obtained at 620 MeV and should provide a basis for a detailed comparison with theory.

Thin, self-supporting ^{nat}Ag foils were bombarded with ^{86}Kr ions accelerated by the SuperHILAC. The beam energies were determined via a magnetic analysis system and should be accurate to better than 1%. Charged fragments were detected in an array of four gas-ionization ΔE, solid state E telescopes mounted in pairs on opposite sides of the scattering chamber. With this detection system, it was possible to identify atomic numbers over the range $10 \leq Z \leq 50$ at forward angles.

The energy spectra of the fragments exhibit features similar to those observed at 620 MeV incident energy: for all Z's there is a deep-inelastic or relaxed component, which peaks at energies somewhat below those expected for touching, spherical fragments; for Z's close to the projectile Z an additional quasi-elastic component is present for angles near the grazing angle. These two components are clearly separated near the grazing but tend to merge at more forward angles, implying that orbiting[2] persists over a broad range of bombarding energies for this system.

Representative lab charge distributions are shown in Figs. 1 and 2. Aside from the intense peak centered on the projectile Z, which is due to quasi-elastic reactions, the charge distributions are "fission-like" and tend to peak at symmetry ($Z \approx 41$). A most striking feature of these data is the increase in the width of the Z-distributions with bombarding energy. At 506 MeV the data for 40° span three orders of magnitude while at 732-MeV ^{86}Kr for 25°, for example, they cover little more than one decade. This dramatic variation in the width of the Z-distributions can qualitatively be understood within the framework of the diffusion model.[3,4] At the higher bombarding energies, the excitation energy is larger, allowing the intermediate complex to spread rapidly along the mass asymmetry coordinate. At the lower bombarding energy, the excitation energy is lower and diffusion is slower. Because the potential energy has a minimum at symmetry, diffusion to extreme asymmetries is inhibited. Additional effects associated with a variation in the interaction time with bombarding energy may also be present and could complicate this picture.

The angular distributions as a function of Z also depend strongly on the bombarding energy. The results for 506-MeV ^{86}Kr are given in Fig. 3. Aside from the intense side-peak observed near the grazing angle for Z's near Kr, the angular distributions tend to be peaked in the forward direction. Furthermore, the strength of the forward peaking depends on the amount of charge transferred. As charge is transferred to or from the projectile, the forward peaking becomes weaker and eventually yields to a $1/\sin\theta$ distribution. This Z-dependence of the angular distributions can be understood in terms of a diffusion model. By selecting larger mass transfers, one is effectively biasing the lifetime distribution in favor of longer interaction times, thus allowing the intermediate system to undergo more extensive rotation. The angular distributions for the 732-MeV bombarding energy are considerably more forward peaked; however, the pattern of decreasing forward peaking with increasing mass transfer is retained, providing further evidence for the above interpretation.

Using a simple model based on the master equation it is possible to semi-quantitatively reproduce the experimental data by adjusting the interaction time. Currently, attempts are being made to refine this treatment by including one-body dissipation, which would allow one to calculate the interaction time from the collision dynamics.

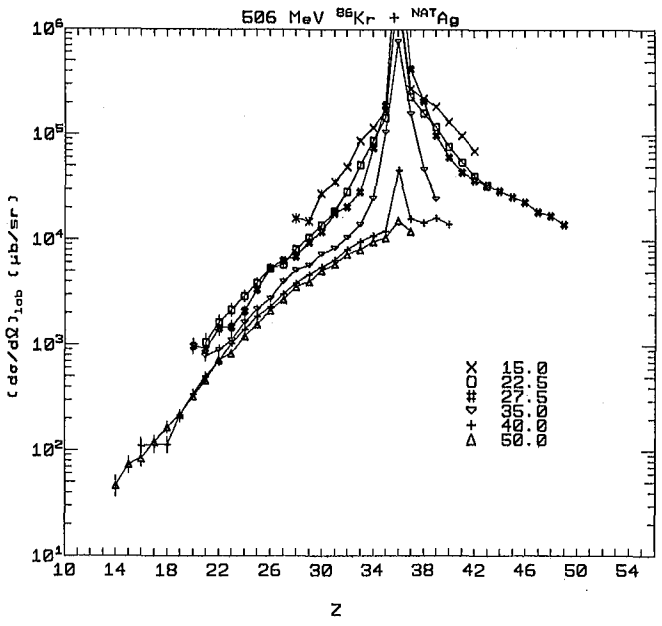

Fig. 1. Lab charge distributions for the reaction 506-MeV $^{86}Kr + {}^{nat}Ag$.

(XBL 7711-10744)

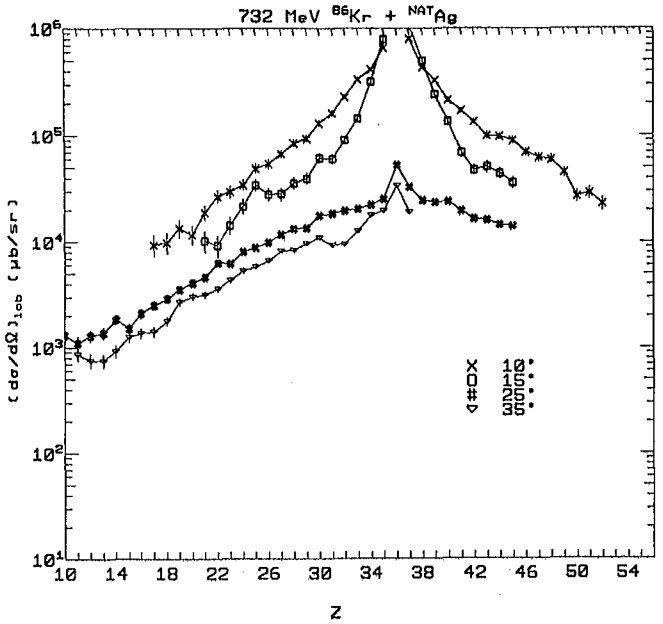

Fig. 2. Lab charge distributions for the reaction 732-MeV ^{86}Kr + ^{nat}Ag.
(XBL 711-10741)

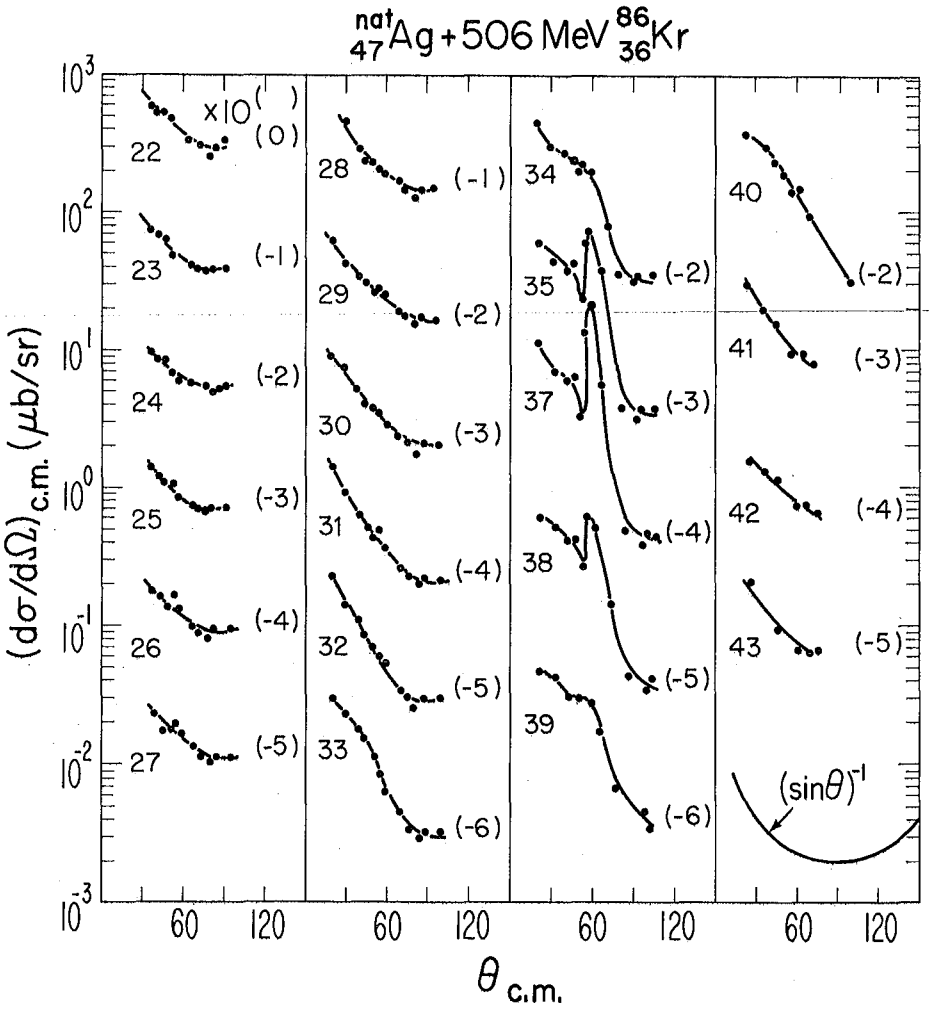

Fig. 3. Center-of-mass angular distributions for the reaction 506-MeV ^{86}Kr + ^{nat}Ag.
(XBL 781-85)

Footnote and References

*Present address: Laboratorié de Physique Corpusculaire, Universite de Caen, 14000 Caen, France.

1. R. P. Schmitt, P. Russo, R. Babinet, R. Jared, and L. G. Moretto, Nucl. Phys. A 279, 141 (1977).

2. J. Wilczyński, Phys. Lett. B 47, 484 (1973).

3. W. Nörenberg, Phys. Lett. B 53, 289 (1974).

4. J. S. Sventek and L. G. Moretto, Phys. Lett. B 65, 326 (1976).

EVIDENCE FOR ENERGY THERMALIZATION IN DEEP-INELASTIC PROCESSES: ^{63}Cu + ^{30}Ne AT 7.9, 12.6, AND 17.2 MeV/NUCLEON*

R.P. Schmitt, G. Bizard,† G.J. Wozniak, and L.G. Moretto

On the basis of single particle inclusive measurements,[1] it is evident that a large fraction of the entrance kinetic energy is dissipated in deep-inelastic collisions (DIC). However, the mechanism responsible for the damping process is not obvious, and a variety of mechanisms have been proposed.[2,3] A potentially powerful technique for exploring the details of the energy damping process involves the study of light particles emitted in association with deep-inelastic fragments.[4-6] Furthermore, such studies may yield information on the relaxation of other modes such as the degree of thermalization and the sharing of excitation energy between the primary fragments. A serious drawback in such experiments arises from the fact that the spatial correlations for light particles tend to be broad, resulting in a low coincidence efficiency. Recognizing the better spatial correlation of the heavy DIC products, we have measured the atomic numbers of the two primary decay products in coincidence. The total missing charge (ΔZ) is then easily determined as the difference between the sum of the initial atomic numbers of the system and the sum of the detected charges.

A self-supporting 560-μg/cm^2 thick ^{63}Cu foil (99% enrichment) was bombarded with ^{20}Ne ions accelerated by the Lawrence Berkeley Laboratory 88-inch cyclotron. The energies, atomic numbers and lab angles of the two heavy fragments were measured with two large-solid-angle (5° angular acceptance) particle telescopes, consisting of gas ionization ΔE detectors and solid state E detectors. At 252-MeV data were taken over the range of the angular correlation with the first telescope fixed at 42°. For the 158- and 343-MeV bombarding energies, measurements were taken only at symmetric angles, optimized for the symmetric decay channel.

For a fixed value of the atomic number detected in the first telescope (Z_1), a distribution of atomic numbers (Z_2) is observed in the second telescope in coincidence. Examples of the Z_2 distributions for $Z_1 = 16$ are shown in Fig. 1 for various cuts in the total laboratory kinetic energy of the fragments ($E_T \equiv E_1 + E_2$). The total energy has been chosen insofar as it may be more indicative of the excitation energy than

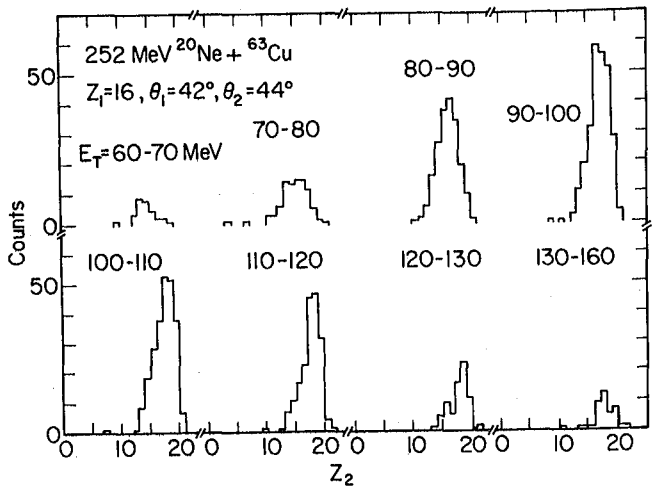

Fig. 1. Distribution in Z_2 for constant Z_1 for various cuts in the total laboratory kinetic energy of the fragments. (XBL 777-1517)

the energy of a single fragment. Although the sigmas of the Z_2 distributions are large (≈2.0), they are approximately independent of the total kinetic energy and asymmetry. The mean value of Z_2 does, however, depend on E_T: as E_T is increased the mean value of Z_2 increases.

This feature is more visible when the mean missing charge ($\Delta Z \equiv 39 - Z_1 - Z_2$) is plotted vs. E_T for various Z_1 and θ_2 (see Fig. 2a,b). Several features are immediately obvious: 1) the number of evaporated charges is large, ΔZ ranging from 4-8; 2) ΔZ decreases with increasing E_T; 3) the magnitude and shape of the ΔZ curve is essentially independent of the asymmetry of the fragments (note the clustering for different Z_1 values); 4) the above trends do not change significantly over the in-plane correlation.

The out-of-plane data (see Fig. 2c) show a pronounced angular dependence. The symmetric angle setting (θ_1 = 42°, θ_2 = 44°) is again shown for comparison. For θ_2 = 44°, ϕ_2 = 10° the mean evaporated charge ΔZ at E_T = 100 MeV is slightly

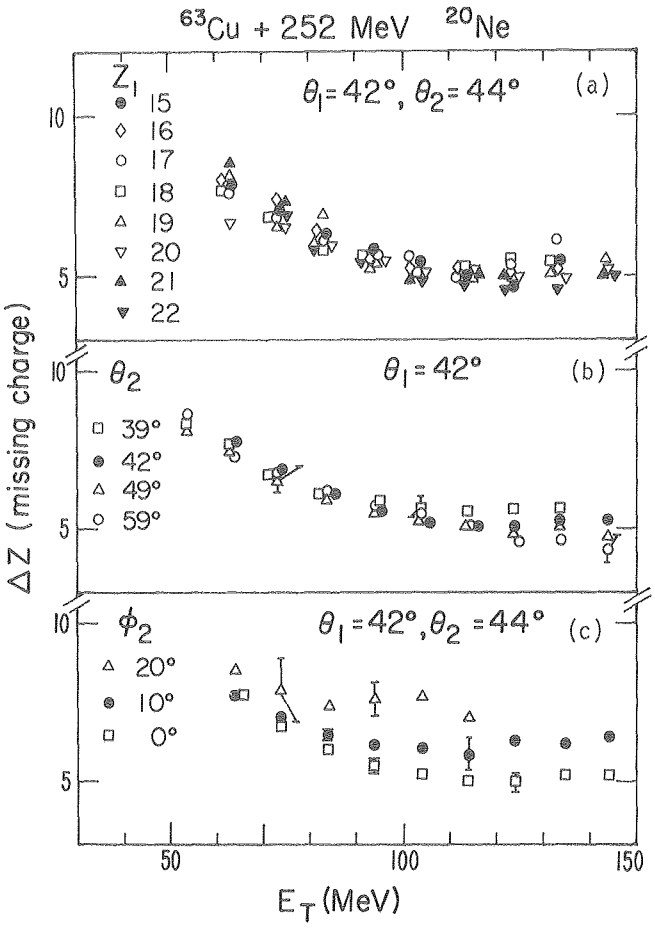

Fig. 2. (a) Mean missing charge (ΔZ) as a function of the total laboratory kinetic energy (E_T) for several exit channels. Note the false zero in the energy scale.
(b) Mean ΔZ vs E_T averaged over the exit channel asymmetry for several values of θ_2. The error bars represent the rms deviation corresponding to different asymmetries.
(c) Same as (b) except for various out-of-plane angles ϕ_2 ($\theta_2 = 44^o$). (XBL 787-2601)

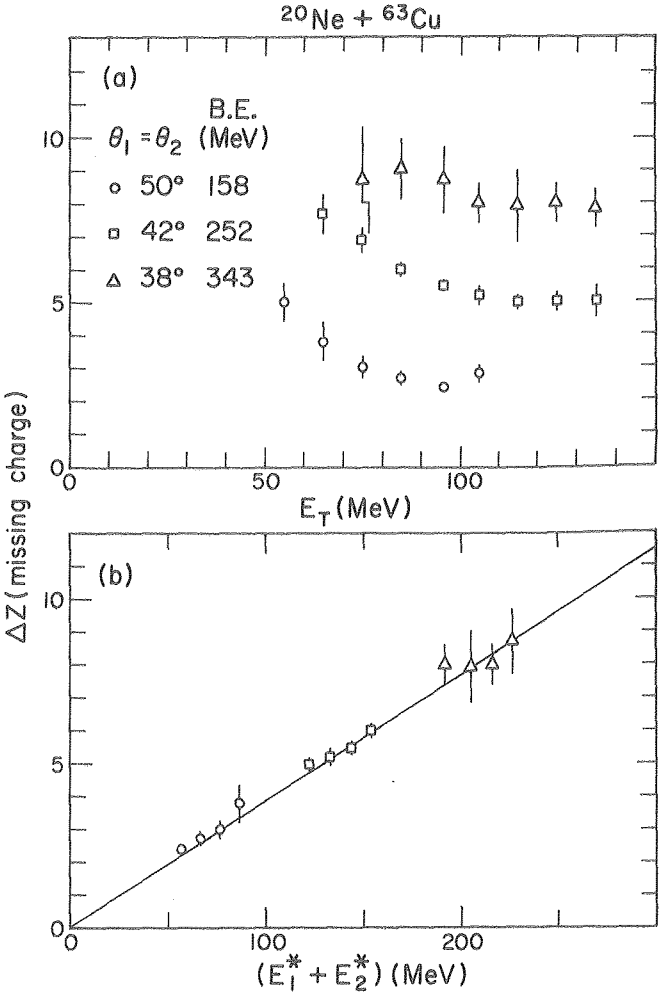

Fig. 3. (a) Mean missing charge vs. E_T for three different bombarding energies.
(b) Mean missing charge plotted as a function of the excitation energy. The line through the data points serve only to guide the eye. (XBL 783-436)

higher by about 1.0 Z-units. For $\phi_2 = 20^o$ ΔZ has increased by almost 2.5 Z-units. It seems reasonable that by looking out of the reaction plane one preferentially selects events for which more extensive particle emission has occurred, perhaps via α emission which tends to impart large recoil momentum.

In Fig. 3a the average ΔZ is plotted vs. E_T for the three bombarding energies. Again the angles have been chosen at the peak of the correlation for symmetric decay. As expected ΔZ increases with increasing bombarding energy. In Fig. 3b ΔZ has been plotted as a function of the total excitation energy deposited in the fragments. The excitation energy scale has been calculated assuming that the fragment velocities are not altered as a result of particle emission. For purposes of emphasis, only the points that are associated with relatively large cross sections have been plotted (the plotted data correspond to roughly 80% of the yield for the asymmetries considered). A smooth, almost linear increase in ΔZ with excitation energy is readily apparent implying that the excess kinetic energy is effectively thermalized over a very broad range of excitation energies. The slope of the line corresponds to about 25 MeV/charge. Since the total mass loss is about twice the evaporated charge (within experimental errors), one obtains an average energy loss per particle of ~12.5 MeV, which is consistent with estimates assuming evaporation. Of course, we have only asymmetries with $Z_1 \geq 10$. The situation may be more complicated for Z's below the projectile Z.

In conclusion, the technique of simultaneous Z identification of the major fragments is a powerful tool for studying deep-inelastic processes since one directly obtains the multiplicity of evaporated charges. It is important to note that despite the very high excitation energies most of the available phase space for the intrinsic degrees of freedom appears to be explored.

Footnotes and References

*Condensed from LBL-6571 and Phys. Rev. Lett. 41, 1152 (1978).

†Present address: Laboratoire de Physique Corpusculaire, Université de Caen, 14000 Caen, France.

1. L. G. Moretto and R. Schmitt, J. de Phys. 37, 122 (1976).

2. R. A. Broglia, C. H. Dasso, and Aa. Winter, Phys. Lett. B 61, 113 (1976).

3. J. Randrup, LBL-5847, 1976 (to be published).

4. M. Ho et al., Z. Phys. A 283, 235 (1977).

5. J. W. Harris et al., Phys. Rev. Lett. 38, 1460 (1977).

6. J. M. Miller et al., Phys. Rev. Lett. 40, 100 (1978).

EVIDENCE FOR ANGULAR MOMENTUM FRACTIONATION IN ^{86}Kr-INDUCED REACTIONS ON ^{107,109}Ag, ^{165}Ho AND ^{197}Au*

M.M. Aleonard,† G.J. Wozniak, P. Glässel,‡ M.A. Deleplanque,§ R.M. Diamond, L.G. Moretto, R.P. Schmitt, and F.S. Stephens

Heavy-ion reaction studies have shown the existence of a rotating "intermediate complex," consisting of a target-like and a projectile-like fragment, which undergoes equilibration in its various degrees of freedom.[1] These equilibration processes, like the relaxation of the relative motion, the neutron-to-proton ratio and the mass asymmetry, have been extensively investigated.[1] The angular momentum transfer from orbital to intrinsic rotation, leading to the equilibration of rotational degrees of freedom, has been investigated to a lesser degree.[2,3]

Measurements of γ-ray multiplicities M_γ have proven to be a good technique for determining the intrinsic angular momentum in compound nuceli.[4,5] This technique can be applied to deep-inelastic (DI) and quasi-elastic (QE) collisions in order to determine the angular momentum transfer as a function of mass asymmetry as determined from the light-fragment atomic number Z_3. From this dependence it is possible to obtain information on the extent to which rigid rotation has been attained.

We have studied Kr-induced reactions for targets spanning a large mass range, employing a triple coincidence method, in which the γ-rays were observed in coincidence with the light fragment and with the heavy fragment, or with one of the fission products in the case of sequential fission. Self-supporting targets (600 $\mu g/cm^2$) of ^{nat}Ag, ^{165}Ho and ^{197}Au were bombarded with a 618-MeV ^{86}Kr beam. The atomic number (Z_3) of the lighter fragment as well as its kinetic energy (E_3) was measured with a gas ΔE, solid-state E telescope, which was placed in the reaction plane at angles (θ_3) varying from 20° to 70°. In order to detect the heavy fragment from the DI reaction in coincidence, a large solid-angle, X-Y position-sensitive detector (PSD) was placed in the reaction plane on the opposite side of the beam axis.

The γ-rays were observed in a set of six 3" by 3" NaI detectors located above the target at 45° with respect to the reaction plane. The number (p-fold) of the NaI detectors in coincidence with a light fragment (Z_3) in the ΔE-E telescope was recorded event-by-event. The γ-ray multiplicities were deduced from the number of counts obtained in the different p-fold coincidences, the solid angle and efficiency of the NaI detectors.[4] Corrections for random events were made, while the contribution from neutrons was neglected (estimated to be less than ~5%).

The γ-ray multiplicities associated with the higher energy events (quasi-elastic) are shown as a function of Z_3 in Fig. 1. A characteristic V-shaped dependence is observed, indicating that the angular momentum transfer is approximately linear with mass transfer. In this feature the present results are similar to those obtained for a lighter system.[2]

The results for the multiplicities associated with the DI reactions are shown in Fig. 2 as a function of Z_3 for several lab angles (θ_3). One should notice the slight but systematic increase in multiplicity as one moves from the lighter system (Kr + Ag) to the heavier ones (Kr + Ho and Au). Also, for the lighter system M_γ is essentially constant with Z_3, while for the heavier systems an increase in M_γ is observed as Z_3 increases. Furthermore, at the backward angles one observes smaller values of M_γ than at the more forward angles (see the Au + Kr data). It is immediately obvious that the rise in M_γ with decreasing Z_3 predicted by rigid rotation and observed in the Ag + Ne system[2] is not observed here at any angle.

A possible explanation for this effect is that the complementary heavy fragment could dispose of its angular momentum by fissioning with high probability as Z_3 becomes smaller. In the case of Ag + Kr, no fission was observed

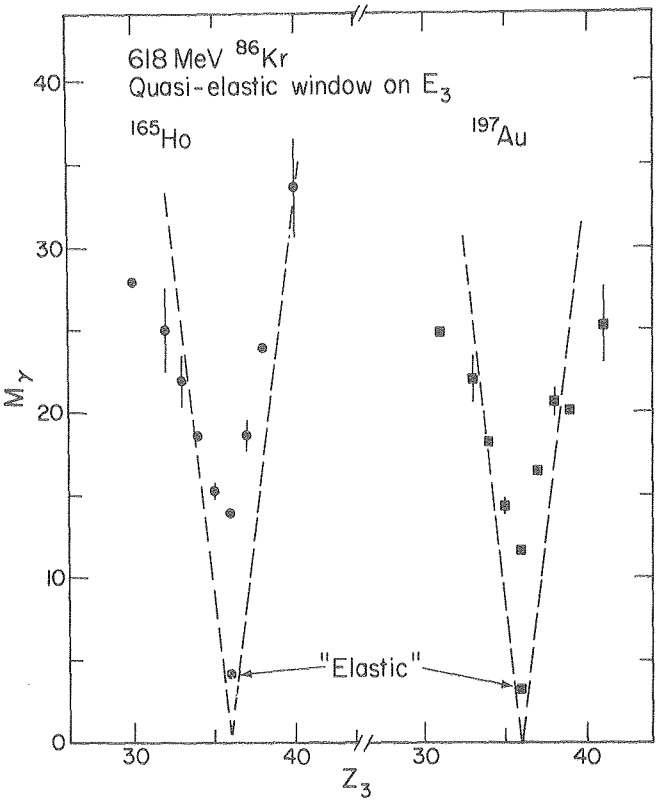

Fig. 1. M_γ for the reactions $^{86}Kr + ^{165}Ho$ and ^{197}Au; statistical error bars as shown for representative cases. The dashed lines are obtained by assuming that the fraction of the orbital angular momentum associated with the transferred mass is recovered as fragment spin.
(XBL 779-2346)

in coincidence with any fragment. For Ho + Kr some fission was observed in coincidence with the smaller Z_3's, but always in negligible amount. For Au + Kr a very large amount of fission (about 100% for $Z_3 = 30$) was observed. However, for this system the γ-ray multiplicities appear to be the same whether or not the heavy fragment undergoes fission.

In summary, the failure of M_γ to rise as Z_3 decreases is not due to sequential fission, does not seem to be due to alpha-particle emission [the out-of-plane angular widths of the heavy partner remain essentially constant (~6° FWHM) as a function of Z_3 and are completely consistent with nucleon evaporation] and, since rigid rotation is indicated by the well thermalized kinetic energies, does not appear to be due to the failure to achieve rigid rotation. We are then left with the tentative conclusion that M_γ is not rising because the low Z_3 fragments are preferentially populated by low ℓ-waves. The analysis of the Z distributions and angular distributions as a function of Z performed independently by some of us has led to the same conclusion.[1,6]

The explanation for such an effect is simple. The potential energy versus mass asymmetry depends strongly on angular momentum. In the present case, at the entrance-channel asymmetry, the potential energy slopes gently towards symmetry

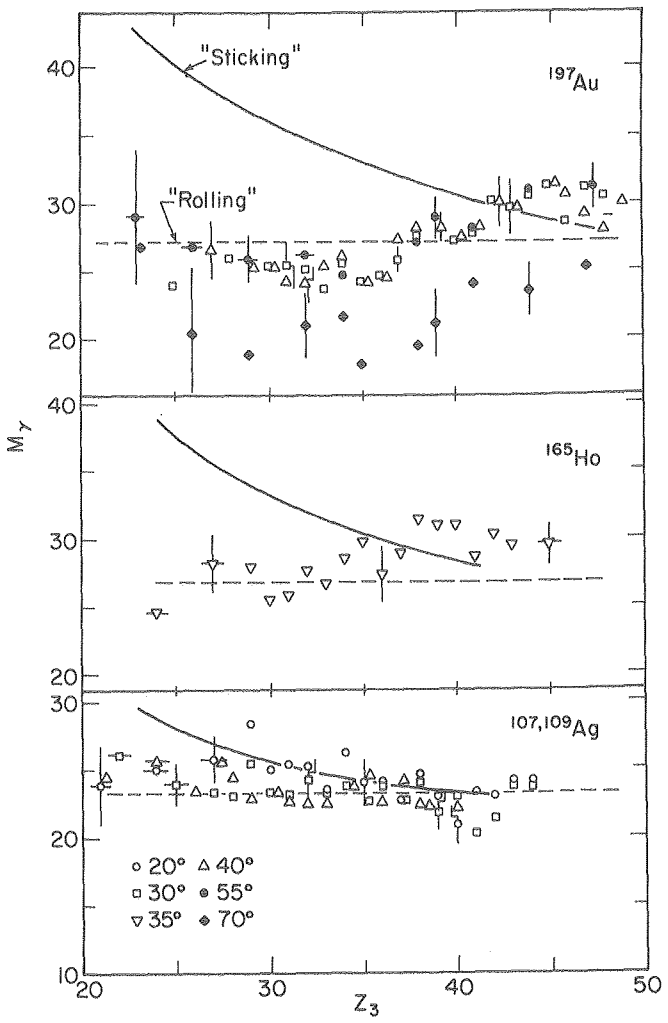

Fig. 2. M_γ vs Z_3 for the low energy components (relaxed) of the reactions $^{86}Kr + ^{197}Au$, ^{165}Ho and $^{107,109}Ag$. The solid lines correspond to the rigid-rotation limit for two touching spheres. The dashed lines correspond to the rolling limit.
(XBL 779-2345)

for small angular momentum and it becomes progressively steeper with increasing angular momentum. Therefore only the lowest ℓ-waves contribute to the population of fragments substantially lighter than the projectile. These preliminary conclusions about the fractionation of the angular-momentum distributions are of interest because of their implication for the ℓ-dependence of particle, energy, and angular momentum transfers. Further studies along the present lines will be needed to clarify these essential aspects of heavy ion reactions.

Footnotes and References

*Condensed from an article submitted to Phys. Rev. Lett. 40, 622 (1978).

†On leave from Centre d'Etudes Nucleaires de Bordeaux-Gradignan, Domaine du Haut-Vigneau, 33170 Gradignan, France.

‡Present address: Physikalisches Institut der Universität Heidelberg, Philosphenweg 12, D-69, Heidelberg, W. Germany.

§On leave from Institut de Physique Nucleaire, 91406 Orsay, France.

1. L. G. Moretto and R. Schmitt, J. Phys. C-5 37, 109 (1976) and references therein; J. R. Huizenga and W. U. Schröder, Ann. Rev. Nucl. Sci. 27 (1977) and references therein.

2. P. Glässel, R. S. Simon, R. M. Diamond, R. C. Jared, I. Y. Lee, L. G. Moretto, J. O. Newton, R. Schmitt, and F. S. Stephens, Phys. Rev. Letters 38, 331 (1977).

3. M. Berlanger, M. A. Deleplanque, C. Gerschel, F. Hanappe, M. Leblanc, J. F. Mayault, C. Ngô, D. Paya, N. Perrin, J. Péter, B. Tamain, and L. Valentin, J. Phys. L 37, 323 (1976).

4. G. B. Hagemann, R. Broda, B. Herskind, M. Ishihara, S. Ogaza and H. Ryde, Nucl. Physics A 245, 166 (1975).

5. P. O. Tjøm, F. S. Stephens, R. M. Diamond, J. de Boer and W. E. Myerhof, Phys. Rev. Lett. 33, 593 (1974).

6. L. G. Moretto, LBL-6572, presented at the Tokyo International Conference on Nuclear Structure, Sept. 1977.

EVIDENCE FOR ANGULAR MOMENTUM DEPOLARIZATION AND FOR ENHANCED SEQUENTIAL FISSION IN THE REACTION ^{197}Au (^{86}Kr, Z_3f)*

G.J. Wozniak, R.P. Schmitt, P. Glässel,† R.C. Jared, G. Bizard,‡ and L.G. Moretto

An interesting phenomenon accompanying the deep-inelastic process, namely the fission of the heavy partner, has recently been observed[1] in the reaction ^{197}Au + 979-MeV ^{136}Xe. An approach that may lead to a better understanding of this phenomenon involves studying the sequential fission process as a function of the mass and energy of the deep-inelastic fragments as well as simultaneously measuring the fission fragment angular correlation.

Our experimental apparatus consisted of a ΔE(gas), E(solid state) telescope to identify the atomic number Z_3 and energy E_3 of the light partner, and a large solid angle, X-Y position sensitive counter[2] to simultaneously detect either the heavy partner (Z_4) or one of its fission fragments. The latter detector, which has a position resolution of 1° and subtends 24° both radially and vertically, provides information on both the energy E_4 and the in- and out-of-plane angular distributions of the correlated fragments.

In Fig. 1 the fission probabilities for the heavy recoils are shown as function of the light fragment kinetic energy for representative atomic numbers. It is important to note that these fission probabilities reach astoundingly large values at the highest excitation energies, namely >80% even for recoils with an atomic number of 79. For sake of comparison the fission barrier for $\ell = 0$ is ~22 MeV in this mass region and the total fission probability at comparable excitation energies for a light-ion reaction,[3] 130-MeV ^{4}He + ^{197}Au, barely reaches 10%. The dramatically different fission probabilities indicate that the broader partial wave distribution in heavy ion reactions may allow sequential fission to select out the very highest angular momentum transfers. Thus the ℓ-distribution of the sequential fission channel may not

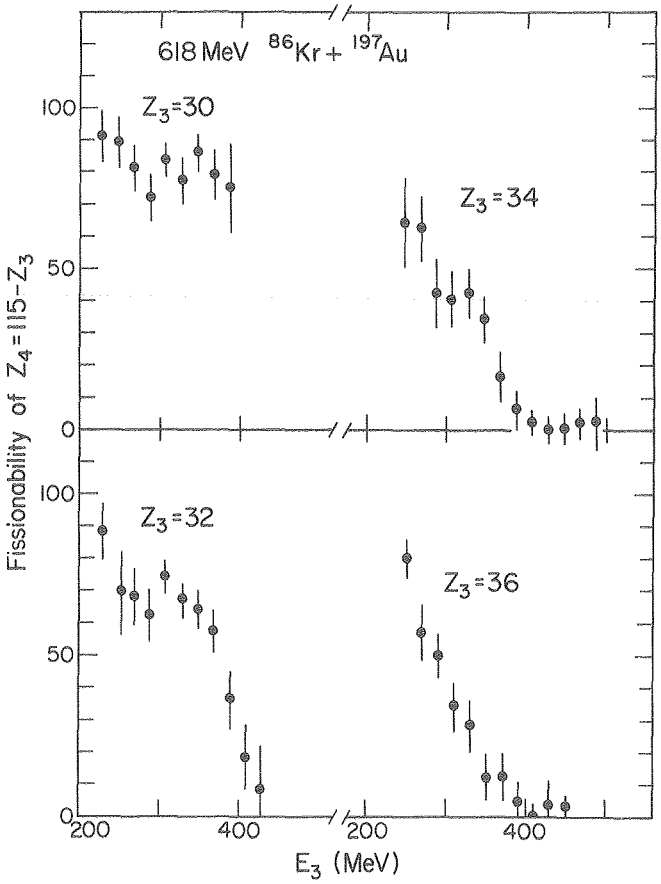

Fig. 1. Measured fission probabilities of the heavy fragment (Z_4 = 115-Z_3) as a function of the lab energy E_3 of the light fragment Z_3.
(XBL 7712-11080)

at all reflect the overall ℓ-distribution for the deep-inelastic process as a whole. This is borne out independently by the γ multiplicities,[4] which are the same whether or not the heavy recoil undergoes fission.

The out-of-plane angular distributions of the fragments from sequential fission are nearly Gaussian and peaked on the reaction plane. The FWHM of these distributions in the laboratory and in the c.m. of the recoiling heavy fragment are shown as a function of Z_3 in Fig. 2. For fission fragments originating from elements heavier than the target ($Z_3 < 36$) the c.m. width is 47°-50°, in agreement with the previously measured value,[5] which is an average over the entire Z-distribution. One should note that the out-of-plane angular distribution for a binary reaction not followed by fission (see Fig. 2) appears to be consistent with the de-excitation of both fragments mainly by neutron emission.[6]

To explain the comparable out-of-plane fission angular distribution observed in a similar reaction (610-MeV ^{86}Kr + ^{209}Bi), the authors of Ref. 5 presented calculations that assumed that the angular momentum is essentially aligned perpendicular to the reaction plane and that the fission width arises from the fission process

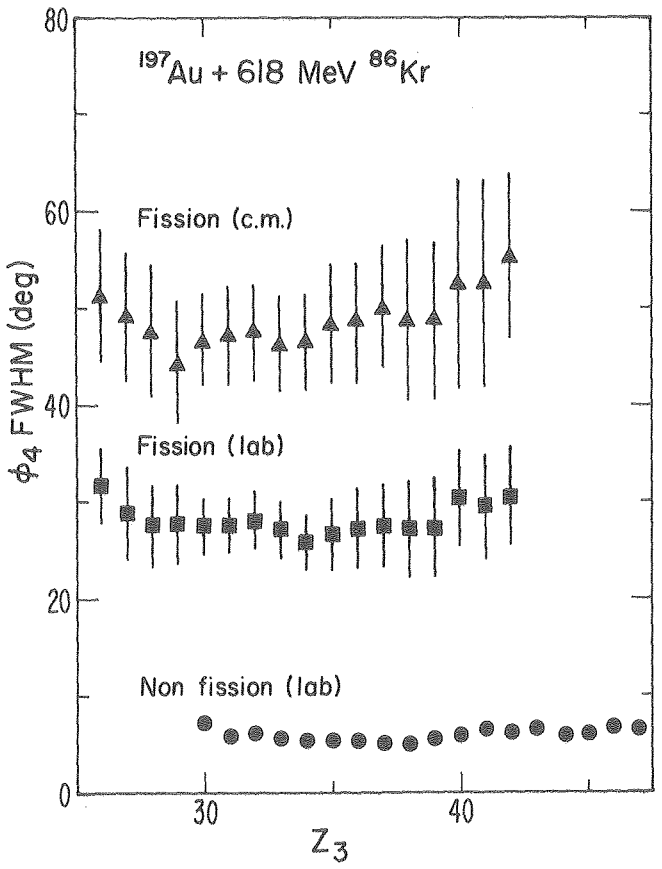

Fig. 2. Corrected FWHM of the measured out-of-plane angular correlation (ϕ_4) as a function of Z_3. (XBL 783-2453)

itself. In addition, preliminary calculations were also presented that assumed a Gaussian distribution of angular momentum perpendicular to the recoil direction ($\sigma = 27°$). The latter system is highly aligned and would create an out-of-plane angular distribution that is strongly dependent on the in-plane angle. Although both of these calculations reproduced the data presented in Ref. 5, both seemed to attribute the out-of-plane angular distribution to the fluctuation of the fission axis with respect to the plane perpendicular to the angular momentum. This conclusion could be doubtful in view of a lack of a Γ_f/Γ_T weight of the ℓ distribution and in view of recent measurements[7] of the γ-ray angular distributions. If the γ-rays emitted by an aligned system (M=J) are stretched E2 decays they should show a strong anisotropy, though attenuated by the presence of E1 decays. The expressions for the angular distributions arising from completely aligned systems are

$$\underset{E2}{W(\theta) = (5/4)(1 - \cos^4\theta)}, \quad \underset{E1}{W(\theta) = 3/4(1 + \cos^2\theta)},$$

where θ is the angle of emission with respect to the angular momentum direction.

However, the evidence[7] is that the γ-ray angular distribution is isotropic to within 5%-35%. This fact can to some extent be explained away by invoking E1 decay. However, a very unlikely 50-50 contribution from E1 and E2 is barely sufficient to explain the largest measured anisotropy of 1.35. This dilemma forces one to either abandon the assumption of stretched E2 decays, which is disastrous because it compromises all our understanding of the yrast decay, or to seek another explanation.

In ^{252}Cf ($J^\pi = 0^+$) spontaneous fission, the resulting fragments each have 7 to 8ħ of angular momentum, which is aligned perpendicular to the fission axis. This angular momentum is most likely generated by the bending oscillations of the fissioning nucleus. Recently, Berlanger et al.[7] proposed that the same effect could arise in the primary deep-inelastic process. Along the same line, but more generally, we suggest that collective modes like bending (doubly degenerate) and twisting (non-degenerate) may be thermally excited, thus generating random components in the angular momentum.

If we assume such a depolarization mechanism, simple statistical considerations lead to the following partition function (for simplicity a two equal touching sphere model is assumed):

$$Z = (4\pi)^2 \int I^2 \exp(-I^2/\mathcal{I}T)\, dT ,$$

and

$$\ln Z = a + 3/2 \ln(\mathcal{I}T) ,$$

where $\mathcal{J}$ is the moment of inertia of one fragment, T is the temperature and a is a constant. The resulting rms angular momentum per fragment is:

$$\overline{I^2} = -\frac{\partial \ln Z}{\partial[1/\mathcal{J}T]} = \frac{3}{2}\mathcal{J}T \quad .$$

For the present reaction of 618-MeV ^{86}Kr + ^{197}Ar and using r_o = 1.22 fm and T = 2-3 MeV, $(\overline{I^2})^{1/2}$ is estimated to be about 13 to 16 $\hbar$ per fragment, randomly oriented, rather than perpendicular to the recoil direction. (These results are not very sensitive to small deviations from symmetric splitting.)

By randomly coupling this angular momentum to that transferred from orbital motion (~30$\hbar$) as is inferred from γ-ray multiplicity data,[4] one obtains an rms angular momentum misalignment ϕ' of the order of 24° to 28°, more than adequate to explain by itself the sequential fission out-of-plane distribution. This misalignment comes from the deep-inelastic process itself. If this is the case, the explanation of the fission fragment out-of-plane distribution lies in a depolarization inherent to the deep-inelastic process and not in the fission mechanism. This explanation does not contradict the existence of fluctuations in the fission direction as described in Ref. 5. However, one should note that the $(\overline{I^2})^{1/2}$ generated by these bending and twisting modes may be larger than K_o and thus should be the dominant effect in producing the out-of-plane fission widths. The presence of such a depolarization substantially helps to explain the γ-ray anisotropy with a much smaller amount of E1 transitions.

Footnotes and References

*Condensed from: Phys. Rev. Lett. 40, 1436 (1978).

†Present address: Physikalisches Institut der Universität Heidelberg, Philosophenweg 12, D-69, Heidelberg, W. Germany.

‡Present address: Laboratoire de Physique Corpusculaire, Université de Caen, 1400 Caen, France.

1. P. Russo et al., Phys. Lett. B 67, 155 (1977).

2. R. C. Jared, P. Glässel, J. B. Hunter, and L. G. Moretto, LBL-6753, submitted to Nucl. Instr. & Meth.

3. See for instance L. G. Moretto, Physics and Chemistry of Fission 1973 (International Atomic Energy Agency, Vienna, 1974) 1, 329.

4. M. M. Aleonard et al., Phys. Rev. Lett. 40, 622 (1978).

5. P. Dyer et al., Phys. Rev. Lett. 39, 392 (1977).

6. B. Cauvin et al., LBL-5099, and Nucl. Phys. A 301, 511 (1978).

7. M. Berlanger et al., J. de Phys. Lett. 37, L-323 (1976).

DEUTERON, TRITON, AND ALPHA EMISSION FOR THE REACTION ^{63}Cu + 252-MeV ^{20}Ne

G.U. Rattazzi, R.P. Schmitt, G.J. Wozniak, G.J. Mathews, L. Sobotka, P. Bigeleisen, R. Regimbart, and L.G. Moretto

A characteristic feature of light charged particles emission in heavy-ion induced reactions is the very anisotropic emission of these particles. It was first pointed out by Britt and Quinton[1] that in the bombardment of Ni, Au, and Bi with ^{12}C, ^{14}N and ^{16}O, high energy alpha-particles were emitted predominantly in the forward direction, possibly due to separate contributions from direct and evaporation processes. The direct alpha-particle emission suggested that the principal direct process involved is the break-up of the incident projectile in an interaction with the target nucleus. Similar results were also reported by Galin et al.[2,3] for the reaction ^{103}Rh + ^{14}N.

We have investigated the reaction ^{20}Ne + ^{63}Cu at 252 MeV in coincidence with deuterons, tritons, and alpha particles. Thin, self supporting targets of ^{12}C, ^{63}Cu (99% enrichment), ^{nat}Ag and ^{197}Au were bombarded with 252-MeV ^{20}Ne ions accelerated by the LBL 88-inch cyclotron. Light charged particles were detected in either of two particle telescopes each consisting of 400-μm surface barrier ΔE detectors, and 1.5-in. NaI E detectors. A third telescope consisted of an extremely uniform 11.3 μm ΔE detector and a 400 μm E detector, and was capable of resolving Ne-like fragments with atomic numbers in the range $4 \leq Z \leq 13$. The Z-telescope was placed directly in front of one of the light particle telescopes so that it was possible to detect coincident light particles directly along the Ne-like fragment direction. During the experiment, the arm supporting the heavy ion telescope was placed at a fixed angle while the other light particle telescope was successively placed at different angles. Although data were taken at a number of heavy ion detector angles and a variety of targets, we shall confine our discussion to the results obtained with the ^{63}Cu target with θ_{HI} = 14° (slightly behind the grazing angle).

In Figs. 1a and 2a energy spectra are shown for deuterons in coincidence with deep-inelastic

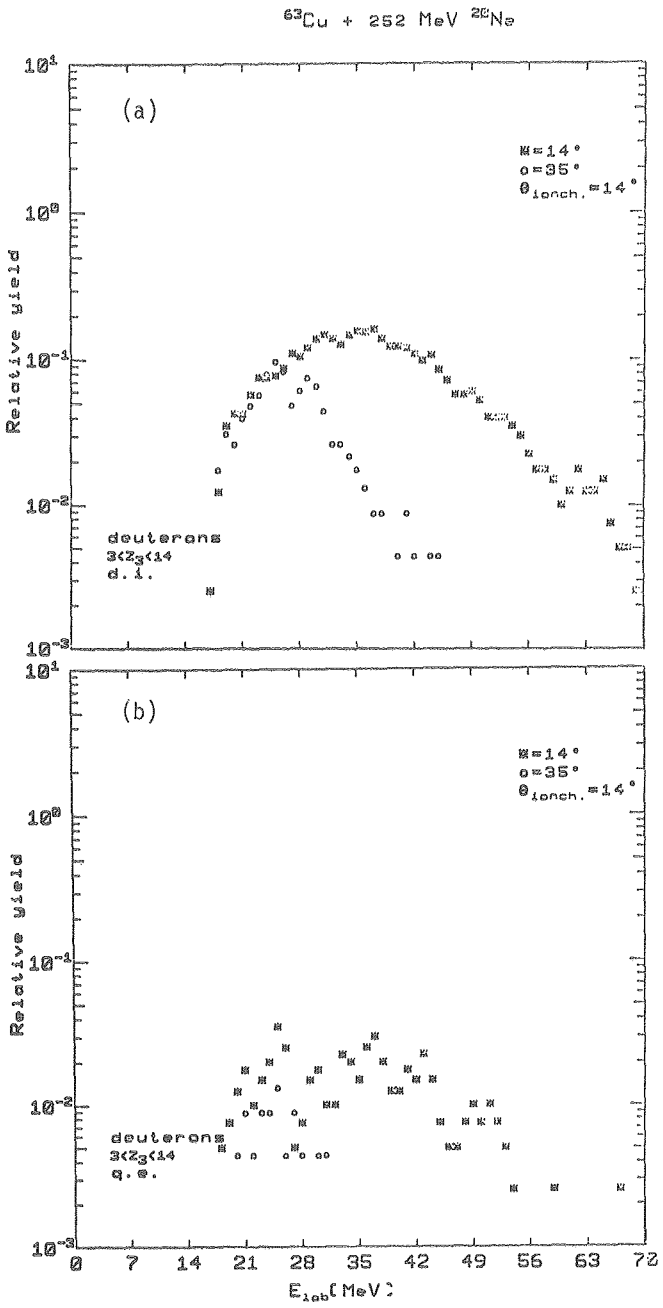

Fig. 1. (a) Energy spectra for deuterons in coincidence with the deep-inelastic component of the Ne-like fragments. The $\theta_{l.p.}$ was placed on the opposite side of the Ne-like ions detector.
(b) The same as part (a) but in coincidence with the quasi-elastic component of the Ne-like fragment. (XBL 787-9616)

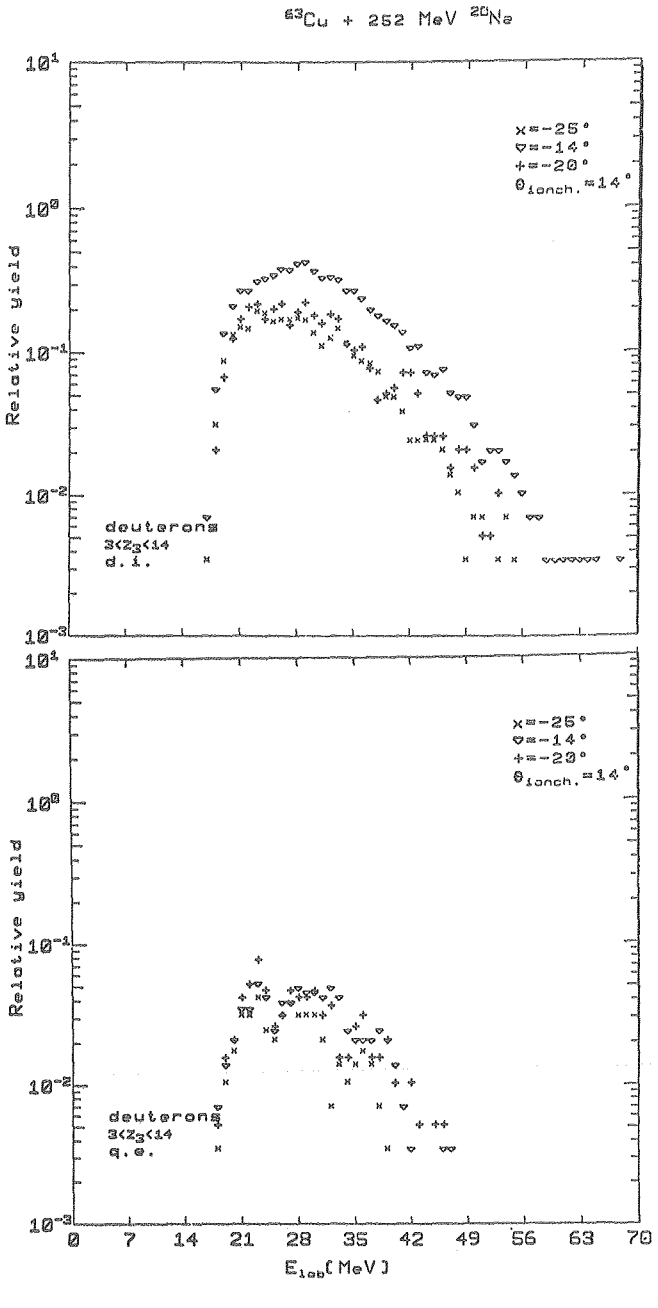

Fig. 2. The same as Fig. 1 but for positive angles (same side of $\theta_{H.I.}$). (XBL 787-9617)

fragments. In Figs. 1b and 2b the same set of angles are shown, but in coincidence with the quasi-elastic component. For both positive and negative angles, the yield of deuterons is clearly higher for the deep-inelastic component. This may simply reflect the fact that the excitation energy is higher for these fragments, resulting in more extensive light particle emission. In addition, the yield at negative angles (Ne-like fragment is emitted at positive angles) is systematically higher. This higher yield seems reasonable if one assumes that the particles emitted at negative angles are primarily associated with target emission since it should have the highest share of the excitation energy.

Gross and Wilczynski[4] suggested a piston model in which fast particles are produced by the radial component of the dissipative forces. Therefore, the fast charged particles are predicted to be emitted from the side of the target nucleus opposite the point of impact. If quasi-elastic

and deep-inelastic collisions are then associated with positive and negative deflection angles of the heavy ions, this theory leads to angular correlations that peak at negative angles $\theta_{l.p.}$ for quasi-elastic collisions and at positive angles $\theta_{l.p.}$ for deeply inelastic collisions. For the reactions studied in the present work, just the opposite pattern is observed. It is more likely that many of the light particles observed in the $^{63}Cu + ^{20}Ne$ reaction are just due to evaporation from highly excited fragments. Indeed, the assumption of evaporation seems to be consistent with many other features of the data. For example, the very high energies observed at $+14^{o}$ are not inconsistent with what one would expect if Ne-like fragments decayed through an evaporation process. On the other hand, there is evidence for pre-equilibrium processes at lower energies,[5] so it is not unreasonable to believe such a component may exist for the current system. A more detailed evaluation of the data is needed to resolve this issue.

References

1. H. C. Britt, A. R. Quinton, Phys. Rev. 124, 877 (1961).

2. J. Galin, B. Gatty, D. Guerrau, C. Rousset, U. C. Schlotthauer-Voos, X. Tarrago, Phys. Rev. C 9, 1126 (1974).

3. J. Galin, B. Gatty, D. Guerrau, C. Rousset, U. C. Schlotthauer-Voos, X. Tarrago, Phys. Rev. C 9, 1113 (1974).

4. D. H. E. Gross, J. Wilczynski, Phys. Lett. B 67, 1 (1977).

5. H. Ho, R. Albrecht, W. Dünnweber, G. Graw, S. G. Steadman, J. P. Wurm, Z. Physik A 283, 235 (1977).

Q-VALUE DEPENDENCE OF ANGULAR MOMENTUM TRANSFER IN DEEPLY INELASTIC COLLISIONS OF ^{86}Kr WITH ^{209}Bi

P. Dyer,* R.J. Puigh,* R. Vandenbosch,* T.D. Thomas,† M.S. Zisman, and L. Nunnelley‡

The reaction 610-MeV $^{86}Kr + ^{209}Bi$ is dominated by the deeply inelastic scattering process: the initial kinetic energy is strongly damped, the angular distribution is narrow and is peaked the grazing angle,[1] and the nuclear charge distribution of the light reaction products is narrow and is peaked near the charge Z=36 of the projectile. Most studies of this and similar systems have focused on the kinetic energy, and on angular and Z-distributions of the reaction products. More recently gamma ray multiplicities and angular correlations between various reaction products have been reported. To further characterize the reaction mechanism for deeply inelastic scattering, we present here the results of a measurement of the angular momentum transferred from the initial orbital angular momentum to the intrinsic spin of the heavy reaction product.

The angular momentum of a nucleus may be measured by observing the angular correlation of decay products with respect to a space-fixed axis. In this experiment we detect one of the fragments from the sequential fission of the heavy reaction product in coincidence with the projectile-like reaction product (see Fig. 1). The advantage of this technique is that the calibration of the observed anisotropies in terms of the angular momentum of the fissioning nucleus (via the K distribution) has been determined previously by measurements of fission angular correlations following compound nucleus formation, where the angular momentum input is known. We measure angular correlations with respect to the recoil axis in and out of the reaction plane. In addition to determining the magnitude of the

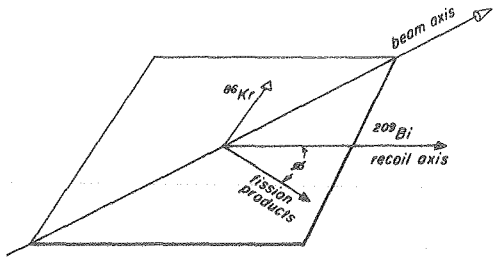

IN-PLANE CORRELATION

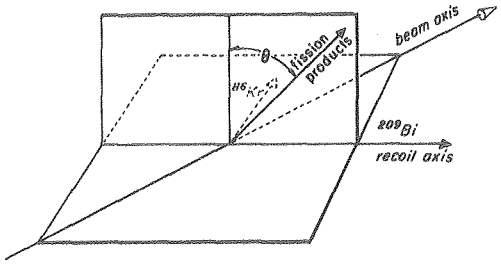

OUT-OF-PLANE CORRELATION

Fig. 1. Geometry of the experiment. The ^{86}Kr and ^{209}Bi labels designate projectile-like and target-like reaction products.

(XBL 778-9872)

angular momentum transferred, it is possible to determine the orientation of the recoil angular momentum, and thus to study further aspects of the reaction mechanism, such as non-equatorial collisions and bending modes of the reaction intermediate.

In a previous paper,[2] we presented the angular correlation obtained from fission fragments in coincidence with projectile-like reaction products of all Z's and energies. It was seen that the maximum angular momentum transferred to the heavy reaction product is large (50 to 70ħ), consistent with the limit given by sticking friction, and that this angular momentum was highly aligned perpendicular to the reaction plane. The peaking of the in-plane correlation along the recoil direction showed that the angular momentum components along the reaction plane lay primarily in the plane perpendicular to the recoil direction. In this paper we present the angular correlations for a range of energies of the projectile-like reaction product. With the energy dependence of the angular correlations and a simple model for the dependence of energy loss on impact parameter (using the dependence of the deeply inelastic cross section on energy loss and angle), we deduce the dependence of the transferred angular momentum on the initial orbital angular momentum.

In order to demonstrate the range of Q values for which this experiment is effective in determining transferred angular momentum, we show in Fig. 2 the ratio of the number of fission coincidences to that of singles projectile-like events (for all Z's) as a function of Q. It is seen that the fission probability is low for energy losses less than 75 MeV. As the number of events for this Q-value range is small, and as angular momentum fractionation effects might be important here, we consider only events for which energy losses are greater than 75 MeV.

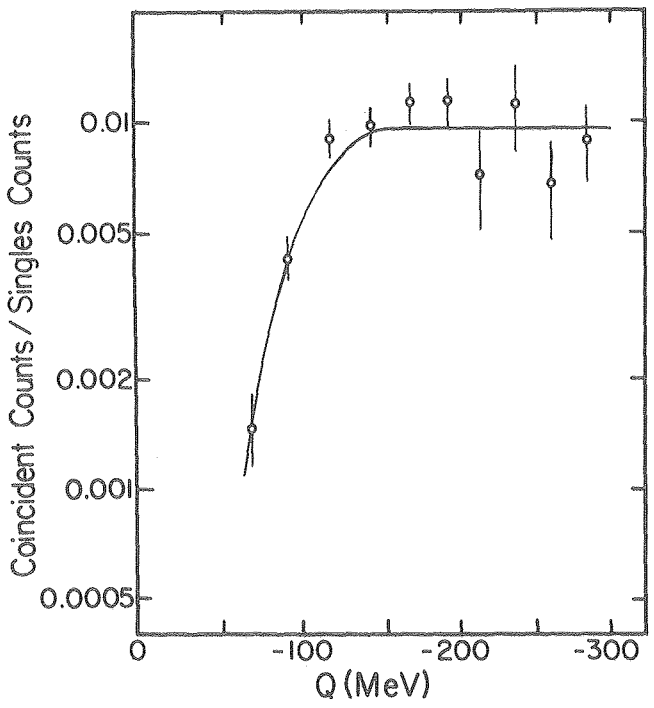

Fig. 2. Ratio of coincident events to singles events as a function of Q for the geometry in which the single detector is at -50° (lab) in the reaction plane. The solid curve is to guide the eye.

(XBL 787-1327)

The in-plane and out-of-plane angular correlations for selected Q regions (see Fig. 3) have been obtained by performing sorts with different windows (about 40 MeV wide) on the energy spectra of the light projectile-like fragments. (All Z's of the projectile-like fragment are included.) We first note that the symmetry angles of the in-plane angular distributions qualitatively track with the recoil direction. The in-plane anisotropies have been plotted relative to the Q-dependent recoil direction, which changes by 35° over the range of Q-values. Secondly, both in-plane and especially the out-of-plane anisotropies decrease with increasing energy loss. The direction of this effect is to be expected simply from the fact that the width of the K-distribution will increase with increasing excitation energy. A dependence of the angular momentum transfer on Q may either enhance or attenuate the trend expected from this effect.

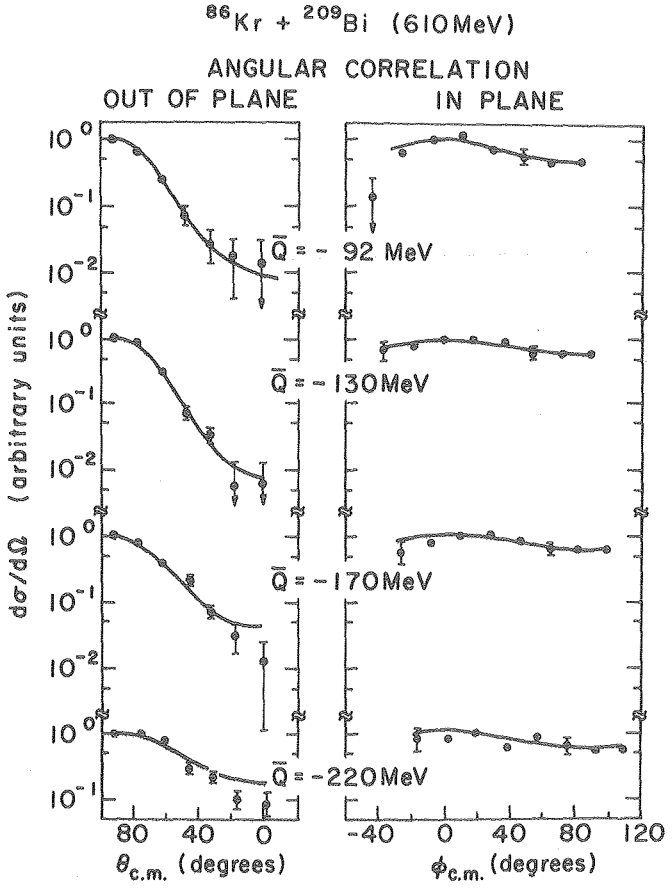

Fig. 3. In-plane and out-of-plane angular correlations for the Q-divided data. The curves are fits to the data (see text).

(XBL 787-1329)

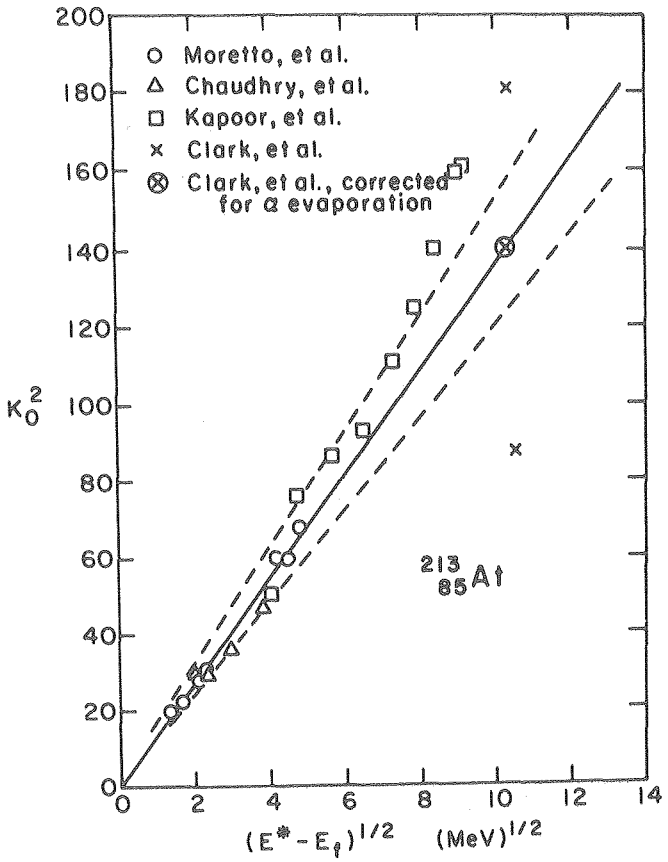

Fig. 4. Experimental K_0^2 values for the nucleus $^{213}_{85}At$ as a function of the square root of the saddlepoint excitation energy. The full curve gives the dependence of K_0^2 on excitation energy adopted in this work. (XBL 787-1328)

We have performed a quantitative analysis of these data to extract the dependence of the angular momentum transferred to the target-like fragment on Q value. For each set of data, the value of K_0^2 for the mean energy of the heavy fragment was taken from Fig. 4, which is based upon the data of Refs. 3 to 6. Since for a restricted range of energy loss, the range of J values contributing is expected to be fairly narrow, and since we can determine only the first moment of the J distribution from such data, we have assumed a single J value, denoted J_{Bi}, in this analysis. By simultaneously fitting the in-plane and out-of-plane angular correlations we determine the best-fit J_{Bi}. The standard deviation in this quantity is determined from the dependence of χ^2 on the fitting parameter. The results are given in Table 1. The J_{Bi} values decrease with increasing energy loss. If there is an inverse relation between the energy loss and the initial orbital angular momentum in the entrance channel, the results indicate a correlation between the transferred angular momentum J_{Bi} and the initial orbital angular momentum.

To relate the observed dependence of transferred angular momentum on Q to a dependence on the initial orbital angular momentum ℓ_i, we have deduced a dependence of ℓ_i on energy loss,

Table 1. The angular momentum J_{Bi} determined from fits to the Q-divided in-plane and out-of-plane angular correlations using a Gaussian distribution for the angle of the angular momentum vector with respect to the normal to the reaction plane.

$-\bar{Q}$(MeV)	$\bar{\ell}(\hbar)$	$J_{Bi}(\hbar)$
92	230	50±8
130	200	41±3
170	160	38±4
220	105	28±4

assuming an inverse monotonic relation between ℓ_i and Q. Such a dependence is expected for the higher partial waves in all theoretical models.

A plot of the J_{Bi} values versus initial orbital angular momentum is given in Fig. 5. The error bars reflect only the statistical uncertainties in determining J_{Bi} from the angular distributions. Also shown are some simple estimates of J_{Bi} for the cases of rolling and sticking spheres and for sticking spheroids where the elongation (ratio of semi-axes ~1.4) has been chosen to give a Coulomb interaction energy consistent with the most probable total kinetic energy in the deeply inelastic scattering.[1] The results are qualitatively consistent with the expectation for sticking spheroids.

The qualitative trend of J_{Bi} to increase with ℓ_i is as expected. One might in fact expect J_{Bi} to be close to the sticking limit for low ℓ_i and to be closer to the rolling limit for the more peripheral reactions where the overlap of target and projectile is small. Unfortunately

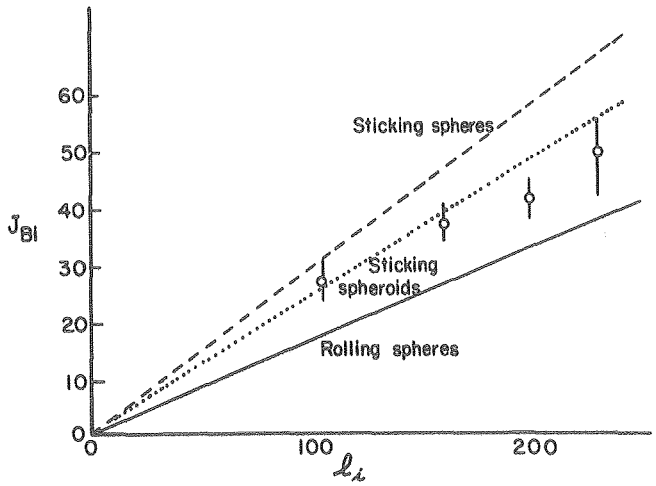

Fig. 5. Plot of angular momentum transferred to the target-like product as a function of the initial orbital angular momentum ℓ_i. The straight lines give the expectations from some simple asymptotic models.

(XBL 787-1330)

the fission barrier of ^{209}Bi is large enough that the fission probability is rather small at the low excitation energies associated with the more peripheral collisions. We observe too few events to reliably extract the angular correlations when the fission probability is low, and what events are observed may be biased due to the possibility of angular momentum fractionation.

Footnotes and References

*Permanent address: University of Washington, Seattle, Washington 98195.

†Permanent address: Oregon State University, Corvallis, Oregon 97331

‡Permanent address: Chemeketa Community College, Salem, Oregon 97309

1. K. L. Wolf, J. P Unik, J. R. Huizenga, J. Birkelund, H. Freiesleben, and V. E. Viola, Phys. Rev. Lett. 33, 1105 (1974).

2. P. Dyer, R. J. Puigh, R. Vandenbosch, T. D. Thomas, and M. S. Zisman, Phys. Rev. Lett. 39, 392 (1977).

3. R. Chaudhry, R. Vandenbosch, and J. R. Huizenga, Phys. Rev.126, 220 (1962).

4. L. G. Moretto, R. C. Gatti, and S. G. Thompson, LBL-1666 (unpublished).

5. S. S. Kapoor, H. Baba, and S. G. Thompson, Phys. Rev. 144, 965 (1966).

6. R. G. Clark, W. G. Meyer, M. M. Minor, C. T. Roche, and V. E. Viola, Z. Physik 274, 131 (1975).

SEQUENTIAL FISSION IN DEEPLY INELASTIC COLLISIONS BETWEEN HEAVY IONS: COINCIDENCE STUDIES OF HEAVY FRAGMENTS IN REACTIONS OF 730-MeV ^{86}Kr WITH Au*

M. Rajagopalan,† L. Kowalski,‡ D. Logan,§ M. Kaplan,§ J.M. Alexander,† M.S. Zisman and J.M. Miller||

In reactions of energetic Kr ions with heavy target nuclei, there is a high probability for very inelastic collisions in which the primary reaction products differ very little in mass from the incident projectile and target, respectively, but there is a large kinetic energy loss into internal degrees of freedom. For the system ^{86}Kr + ^{197}Au at an initial ^{86}Kr energy of 730 MeV, the energy damping, or -Q, exhibits a broad distribution from zero (for elastic reactions) to more than 350 MeV.[1] A part of this energy must be taken up as excitation energy of the two separating fragments, and hence it is generally recognized that heavy nuclei like Au could receive enough energy and angular momentum to undergo fission. Thus one must expect a certain amount of sequential fission to occur after a heavy nucleus is excited in a hard reactive collision. It is also possible that some other multibody divisions might occur prior to fragment separation and equilibration (instantaneous fission).[2] Both of these processes are distinctly different from fusion-fission in which two (fission) fragments are formed by scission of a compound nucleus.

In a recent paper[3] we have reported some aspects of alpha and proton emission in the reaction 724-MeV ^{86}Kr + ^{197}Au. Here we present, for the same reaction system, our results from "heavy-heavy" coincidence experiments which were initiated to determine the relative frequency of two-body vs. multibody events, and to measure the probability of sequential fission as a function of Q.

A schematic diagram of the experimental configuration is shown in Fig. 1. The beam of

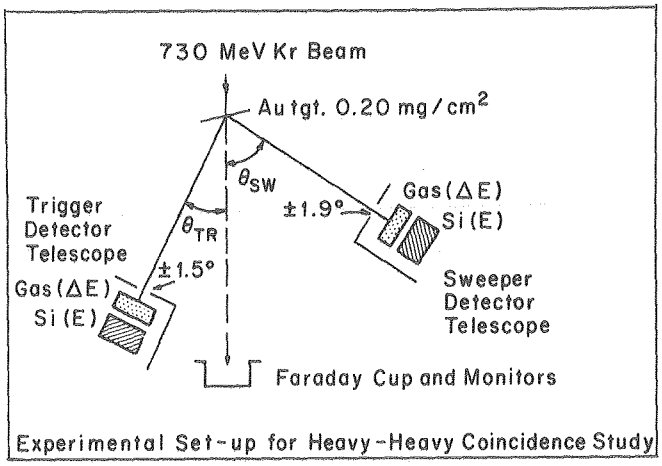

Fig. 1. Experimental arrangement for measuring coincidences between two heavy fragments. The trigger telescope was at fixed angles of 30°, 35.7°, or 41.4°, while the sweep telescope was moved over the range 30°-70°. (XBL 787-1331)

730-MeV ^{86}Kr ions was provided by the SuperHILAC accelerator of the Lawrence Berkeley Laboratory. Two gas telescopes, each consisting of a ΔE gas ionization chamber and an E surface barrier detector, were used to detect the heavy fragments and provide Z identification and energy measurement. The "trigger" detector telescope was placed at a series of fixed angles θ_{tr} (30°, 35.7°, and 41.4°) and the "sweep" detector telescope was moved through the angular range θ_{sw} = 30°-70° to measure the angular correlations of heavy fragments both in the reaction plane and out

of the plane. Coincidence and non-coincidence events were collected at the same time. The individual signals from each detector, as well as the output from a time-to-amplitude converter (TAC), were recorded event-by-event on magnetic tape. In the present series of experiments, a very thin Au target (0.20 mg/cm^2) was used to minimize energy degradation of the heavy Au-like fragments. Both the target and the gas ionization chamber were thin enough to record the Au elastic peak (~40 MeV) in the sweep telescope when the trigger telescope was placed at 20° during calibration runs with ^{86}Kr elastic scattering.

The mass identifications of the heavy-fragment coincidence events were performed in two ways. The first method depends on Z identification of the individual fragments based on their ΔE and E measurements in the gas telescopes. The derived masses, labeled A_Z, are close to the valley of β-stability and were obtained by an iterative method. The second method of identification was based on strict binary kinematic relationships, which lead to the result:

$$\frac{A_{tr}}{A_{sw}} = \frac{E_{sw}}{E_{tr}} \times \frac{\sin^2\theta_{sw}}{\sin^2\theta_{tr}} \quad , \qquad (1)$$

where the subscripts tr and sw refer to the trigger and sweep telescopes, respectively, and A and E are the mass numbers and kinetic energies of the primary fragments. By assuming that $A_{tr} + A_{sw} = 283$ (the total mass), the values of A_{tr} and A_{sw} could be calculated event-by-event for all the observed coincidence events. The masses deduced from this kinematic analysis, after correction for the evaporation of light particles, are labeled A_k.

With these procedures all events from a given set of angles θ_{sw} and θ_{tr} could be organized into a mass-mass matrix (A_Z vs A_k) for the trigger telescope as illustrated schematically in Fig. 2a. In each experimental run (one set of telescope angles), the events that are located close to the 45° line in the mass-mass matrix are binary, while those that lie away from this line are nonbinary. Despite occasional ambiguities and relatively poor statistics (maximum of 350 coincidences per run), we found that four kinds of events (see Fig. 2a) could be clearly identified in this way. First are those (I) where Kr-like fragments were detected in the trigger telescope. Second are those (II) that may be due to fusion-fission or symmetric quasi-fission events. Third are those (III) in which Au-like fragments reach the trigger detector. And fourth are those (IV) for which the values of A_Z and A_k differed significantly. We ascribe the events from the last group to multibody reactions, which we take to be largely sequential fission. The discrepancy between A_Z and A_k is a consequence of applying binary kinematics to nonbinary reactions, and the existence of two distinct groups of type IV events is consistent with expectations for a sequential fission process. Angular correlations of coincidence events were obtained for the different groups at each fixed angle of the

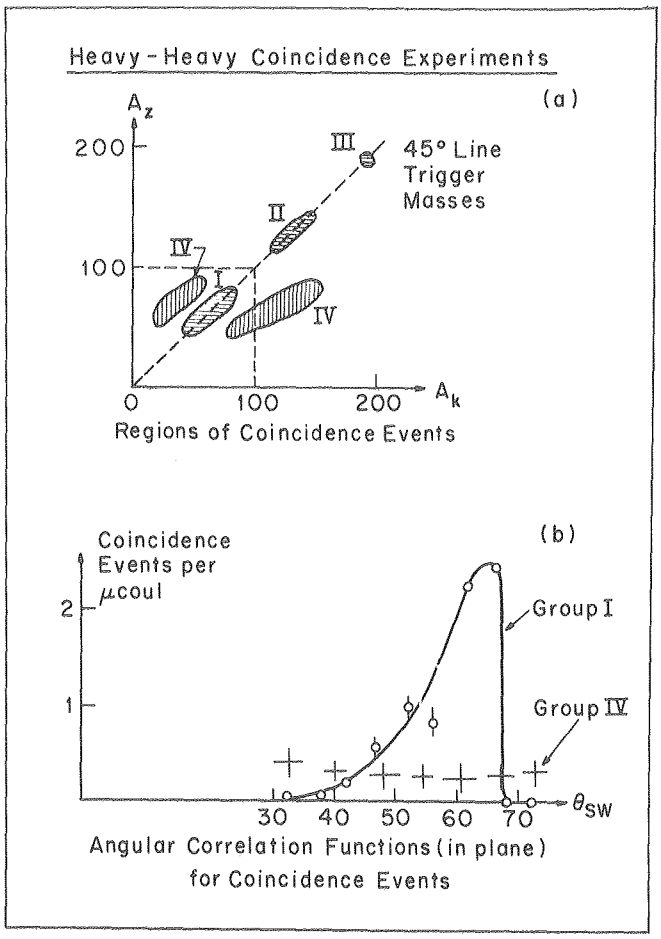

Fig. 2. (a) Schematic representation of the mass-mass matrix (for the trigger telescope) used to clarify events. For clarity regions I and IV are shown as separate. Actually a subtraction was made for type IV events in the region for type I.

(b) In-plane angular correlation for types I and IV events for $\theta_{tr} = 35.7°$.

(XBL 787-1332)

trigger telescope. Typical examples of such correlations for groups I and IV (at a trigger angle of 35.7°) are presented in Fig. 2b. The very different behavior for group I and group IV events is evident. The angular correlation functions for the nonbinary events (IV) are quite flat both in and out of the reaction plane (sweeping limits from 30° to 70° in the plane and up to 10° out of plane). This is in sharp contrast to the relatively well-defined maximum at the kinematic angle for the group I binary events.

We have attempted to extract from our data an excitation function for the sequential fission events; that is, the dependence of sequential fission probability on the inelastic energy transfer (-Q or E^*) in the collision. This excitation function can then be compared to observed fission fractions in compound-nucleus reactions to gain insight into the spin-division in the reaction.[4] Our procedure for doing this

can be illustrated by reference to Fig. 3. This figure shows our experimental data for the three trigger telescope angles θ_{tr} = 30°, 35.7°, and 41.4°. The upper parts of Fig. 3 give the energy loss spectra for (singles) events seen in the trigger detector telescope, with the abcissa labeled as -Q. The lower parts of Fig. 3 give the angular correlation curves for the heavy (coincident) fragments at each trigger telescope angle. (The abscissa scales in the lower parts of the figure correspond with the scales in the upper parts of the figure, so that values of θ_{sw} match the average Q's calculated for that angle.) The solid curves, through the solid points, are the expected angular correlations predicted from binary kinematics and the singles data. The dashed curves, through the open points, are the measured angular correlations for real binary events observed in the coincidence experiments (group I events in Fig. 2a). For the 30° data, the two curves have been normalized at their maxima to give the coincidence efficiency via the elastic scattering that dominates at this trigger angle. This same normalization was used for the calculated curves at 35.7° and 41.4°.

The differences between the calculated and observed angular correlation curves provide a measure of the nonbinary events, and indicate that the fission probability (more generally the multibody breakup probability) increases with the excitation energy of the heavy partner. (The larger discrepancy in coincident events at θ_{tr} = 41.4° compared to θ_{tr} = 35.7° is a reflection of the differences in relative intensities of quasi-elastic and deeply inelastic components at these angles.)

If we assume that the multibody-breakup reactions occur in two distinct sequential steps, then we can relate these measurements to compound-nucleus studies. A comparison of these data with the excitation function for the fission fraction of ^{194}Hg compound nuclei, directly measured[4] in the reaction $^{12}C + ^{182}W \rightarrow ^{194}Hg^*$, suggests that the heavy reaction products in deeply inelastc collisions of $^{86}Kr + ^{197}Au$ are about as fissionable as the compound nuclei from the $^{12}C + ^{182}W$ system at corresponding excitation energies. From the similarity of fissionability (and Z value) for these products, we infer that the Au-like products of deeply inelastic collisions emerge from the primary collision with intrinsic spins comparable to the corresponding ^{194}Hg compound nuclei.[4]

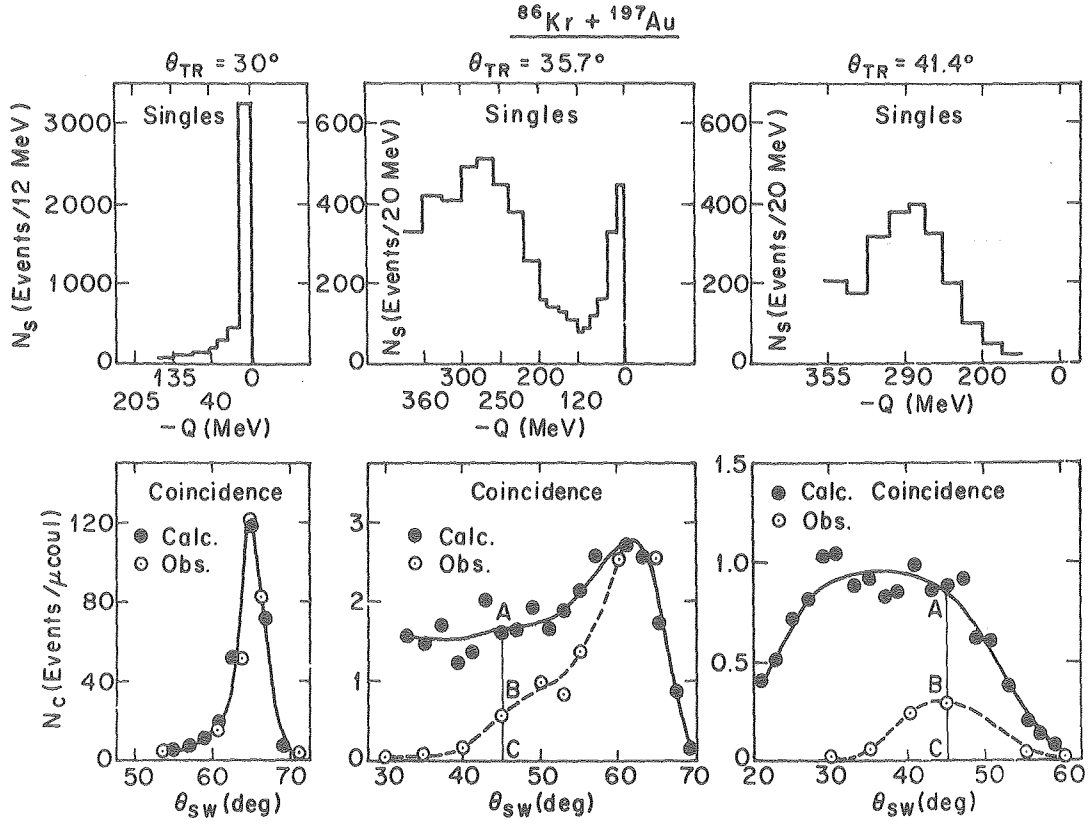

Fig. 3. (Top) Energy loss spectra observed in the trigger detector telescope in the singles mode at three angles. (Bottom) Calculated and observed angular correlations for heavy fragment coincidence events of type I. The fraction of missing coincidences at each sweep angle is the ratio (AB/AC). The Q scales in the upper parts of the figure correspond with the θ_{sw} scales in the lower parts of the figure. (XBL 787-1333)

Footnotes and References

*Condensed from a paper submitted to Phys. Rev. C.

†Permanent address: Department of Chemistry, State University of New York at Stony Brook, Stony Brook, New York 11794.

‡Permanent address: Montclair State College, Upper Montclair, New Jersey 07043.

§Permanent address: Department of Chemistry, Carnegie-Mellon University, Pittsburgh, Pennsylvania 15213.

‖Deceased. Formerly at Department of Chemistry, Columbia University, New York, New York 10027.

1. G. L. Catchen, J. M. Miller, D. Logan, D. Benson, N. H. Lu, M. Rajagopalan, J. M. Alexander, T. W. Debiak, M. Kaplan, and M. S. Zisman, to be published.

2. H. H. Deubler and K. Dietrich, Phys. Lett. B 62, 369 (1976); H. H. Deubler, K. Lekkas, P. Sperr, and K. Dietrich, Z. Physik A 284, 237 (1978).

3. J. M. Miller, G. L. Catchen, D. Logan, M. Rajagopalan, J. M. Alexander, M. Kaplan, and M. S. Zisman, Phys. Rev. Lett. 40, 100 (1978).

4. J. M. Miller, D. Logan, G. L. Catchen, M. Rajagopalan, J. M. Alexander, M. Kaplan, J. W. Ball, M. S. Zisman, and L. Kowalski, Phys. Rev. Lett. 40, 1074 (1978).

C. RELATIVISTIC HEAVY IONS

1. Projectile and Target Fragmentation

STUDY OF ARGON-INDUCED REACTIONS AT 213 MeV/NUCLEON

Y.P. Viyogi,* T.J.M. Symons, F. Bieser, H. Crawford, P. Doll,† D.E. Greiner, C.K. Gelbke,‡ H.H. Heckman, D.L. Hendrie, P.J. Lindstrom, J. Mahoney, C. McParland, D.K. Scott, K. Van Bibber, G.D. Westfall, and H. Wieman

At low incident energies ($\leq$10 MeV/nucleon) the study of the ^{40}Ar + ^{232}Th system has led to spectacular advances in our knowledge of deeply-inelastic scattering and the existence of exotic neutron rich nuclei.[1] At these energies the reaction mechanism is dominated by the diffusion of nuclear matter between the nuclei,[2] resulting in the emission of fragments from the equilibrated dinuclear system. At higher energies ($\sim$ GeV/nucleon), the reaction is dominated by target and projectile fragmentation,[3] the fragments in this case being emitted by the sudden abrasion or shearing of a piece of nuclear matter from the projectile.[4] Studies[5] with ^{16}O beams at various energies reveal that the nuclear temperature derived from momentum spectra and isotope-production cross sections have similar values. This parameter can also be derived[6] using the ground state abrasion model without invoking the concept of temperature. This degeneracy of different models, which are conceptually very different, is an intriguing problem. It might be expected that the use of heavier projectiles, such as ^{40}Ar, could give more insight into the reaction mechanisms. With these aims in mind, we have begun studies of ^{40}Ar induced reactions over a wide energy range from MeV/nucleon to GeV/nucleon.

Here we report on first results at 213 MeV/nucleon. The experiment used the ^{40}Ar beam of $\sim 10^8$ particles/sec from the Bevalac to bombard thorium and carbon targets of thickness ~150 mg/cm^2 and 400 mg/cm^2, respectively. The reaction products were detected in a telescope of nine 5-mm solid state counters, capable of stopping fragments ranging from argon to oxygen. Identification of isotopes was achieved with the help of the techniques described in Ref. 7. Several identifications and χ^2-consistency tests were used to eliminate bad events arising from reactions in counters and statistical fluctuations in energy loss. The technique permits separation of all isotopes of elements up to argon. We have measured energy spectra and production cross section of isotopes for elements with Z=8 to Z=16.

The widths of the energy spectra of the emitted fragments may be used to extract the "temperature" of the emitting system, if it is assumed that the system was in thermal equilibrium.[8] Such a procedure has been adopted[5,9] in analyzing the momentum spectra of fragments emitted in ^{16}O-induced reactions at 20 MeV/nucleon and 2.1 GeV/nucleon. The value of the temperature comes close to 8 MeV, the so-called "boiling point of nuclear matter".[6] Alternatively if the reaction is viewed as a fast process, the width of the momentum distribution samples the Fermi momentum of the projectile. The width is parametrized by $\sigma_0 = P_F\sqrt{5}$, where P_F is the Fermi momentum. Then the two prescriptions are related[8,9] by $\sigma_0^2 = mT\ A-1/A$ where m is the nucleon mass, A is the projectile mass number and T is the temperature. The value of σ_0 for T $\approx$ 8 MeV is 86 MeV/c. Figure 1(a) shows the results of applying the method to the energy spectrum of ^{34}S and ^{16}O in the argon induced reaction, using σ_0 = 83.7 MeV/c and 71.0 MeV/c, and Fig. 1(b) shows the values of σ_0 for various fragments. They lie around a mean value of 90 MeV/c, similar to that for the ^{16}O induced reactions. (The final values may be approximately 10% lower since the contribution to the energy width due to the thick targets has not yet been taken into account.)

An alternative approach to obtain the "temperature" has been the use of Q-value systematics for production cross sections of a series of isotopes.[5] At low energies the systematics using the ground state Q-value Q_{gg} works extremely well.[10] The production cross sections are proportional to $\exp(Q_{gg}/T)$, where T is the temperature of the dinuclear system in thermal equilibrium. At very high energies (2.1 GeV/nucleon) it has been shown[11] that similar systematics can be used to obtain the "temperature" of the emitting system. The production cross sections in this case are proportional to $\exp(Q_F/T)$ where Q_F is the fragmentation Q-value for the most dominant channel. Instead of using the single most dominant channel, one can also sum[5] over many channels. Then the systematics should lead to a constant, $C(N,Z) = \sigma(\exp)/\Sigma\ \exp(Q_F/T)$ independent of N,Z. It has been shown in Ref. 5 than C(N,Z) is fairly constant over a wide range of fragment masses in ^{16}O induced reactions at 20 MeV/nucleon and 2.1 GeV/nucleon. Also, the values of "temperature" obtained in all these analyses of ^{16}O induced reactions agree with those obtained from the momentum spectra.

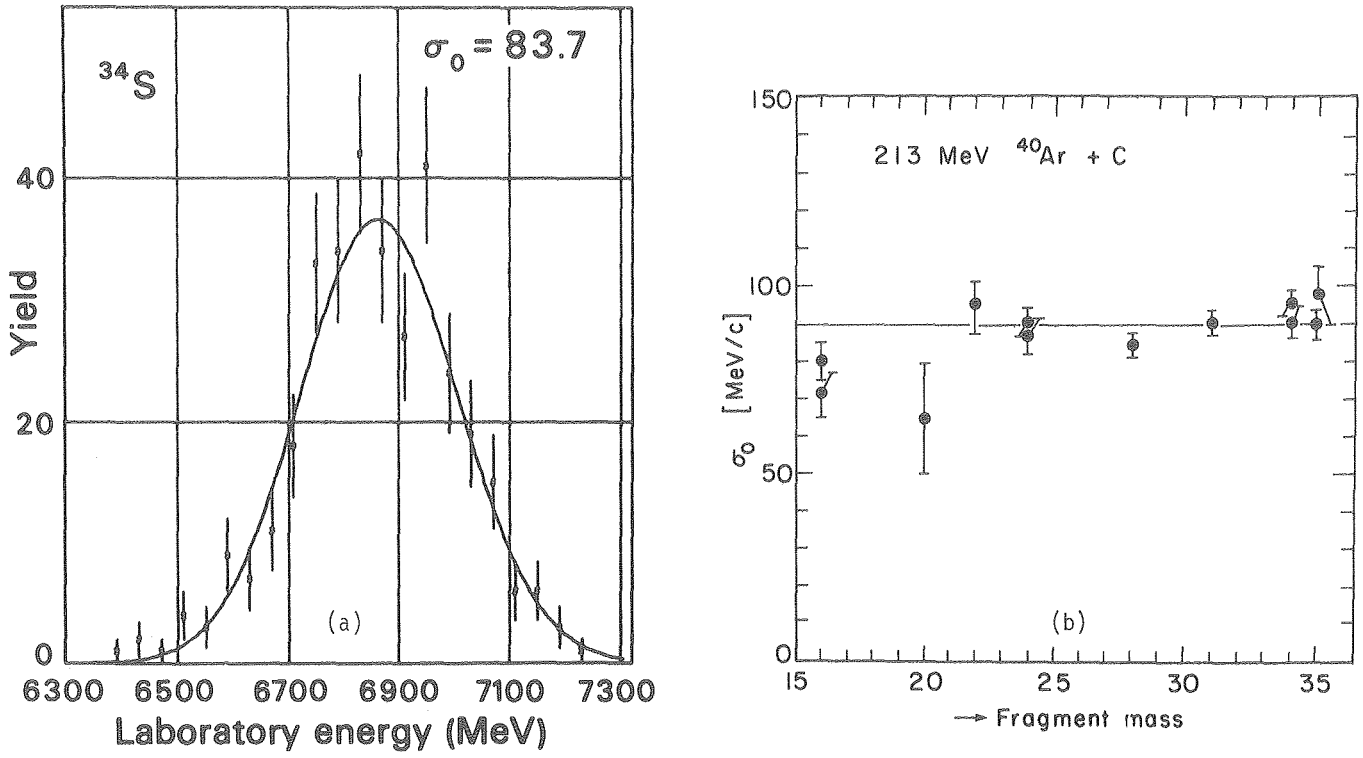

Fig. 1. (a) Energy spectrum of ^{34}S, with fitted Gaussian (continuous curve). The experimental data are shown with statistical errors.
(b) σ_0 obtained from energy spectra of various fragments with masses ranging from 16 to 35.
[(a) XBL 786-1052 (b) XBL 787-1410]

In Fig. 2 we have plotted the ratio C(N,Z) as a function of fragment mass for nuclei close to the projectile mass. All the energetically open fragmentation channels were taken into account and the parameter T was varied to give the best fit to experimental cross sections. The value of T obtained in this analysis is (12 ± 2) MeV which is substantially higher than the value of approximately 8 MeV obtained for the ^{16}O induced reactions. It is also higher than the value of T inferred from the energy spectra in Fig. 1. The results imply that the fast process is likely to be the correct description, and the degeneracy of the fast and slow processes for ^{16}O induced reactions is indeed removed by using the argon beam.

If we adopt the fast process as the correct description, then the data should be described by the abrasion-ablation model. The widths of the isotope distributions are of considerable interest in this model, on account of attempts to explain them by introducing correlations into the nuclear ground state.[12,13] The widths of the primary abrasion distribution are narrower with correlations included. Figure 3 shows the distribution of magnesium isotopes along with the predictions of abrasion-ablation model[14] ignoring correlations. The predictions of the model appear to agree well with the experimental width. The figure also shows data from the ^{40}Ar + ^{48}Ca reaction at 6 MeV/nucleon[15] and for the p + ^{238}U reaction at 800 MeV.[16] It is seen that all the distributions look almost similar and hence very careful measurements are required

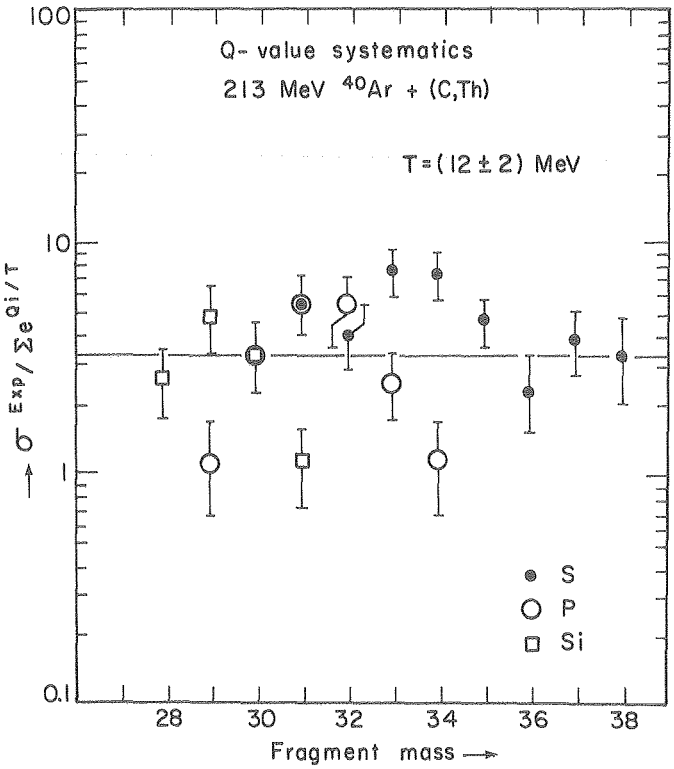

Fig. 2. The ratio $C(N,Z)=\sigma/\Sigma\exp(Q_F/T)$ as a function of fragment mass number. The derived value of T is (12±2) MeV.

(XBL 787-1411)

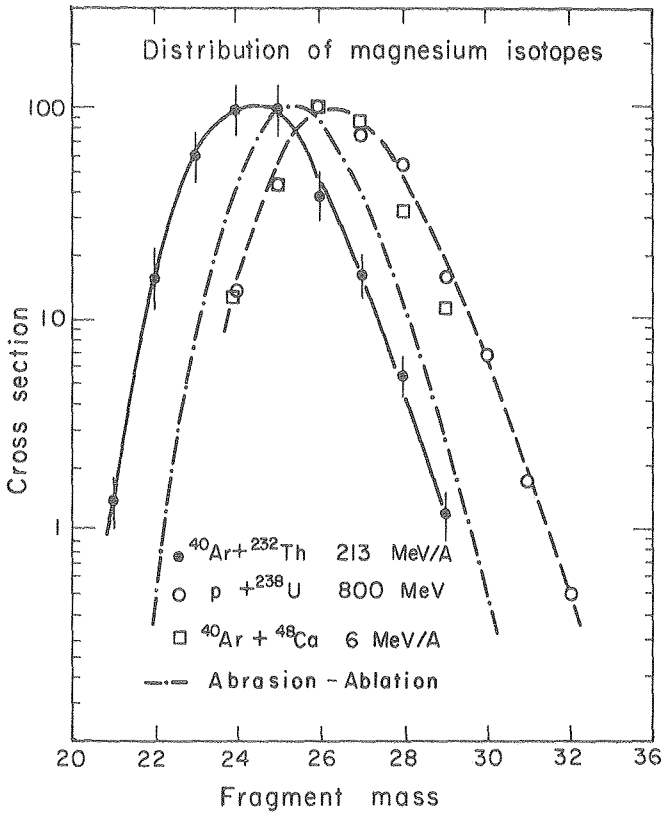

Fig. 3. Production cross section of Mg isotopes in various experimental studies along with the abrasion-ablation model predictions.
(XBL 787-1412)

to extract information about the primary distribution of the fragments. It is clear, however, that the position of the peak of the distribution shifts toward the $(\bar{N}/Z)$ value of the projectile at higher energies and this behavior could provide a powerful method for producing nuclei far from stability using neutron rich beams such as ^{48}Ca.

Footnotes and References

*IAEA Fellow, on deputation from Bhabha Atomic Research Center, Calcutta, India.

†NATO Fellow, on leave from Max Planck Institut, Heidelberg, Germany.

‡Present address: Physics Dept., Michigan State University, East Lansing, MI 48824.

1. A. G. Artkukh, G. F. Gridnev, V. L. Mikheev, V. V. Volkov, and J. Wilczynski, Nucl. Phys. A 215, 91 (1973).

2. W. U. Schröder and J. R. Huizenga, Ann. Rev. Nucl. Sci. 27, 465 (1977).

3. A. S. Goldhaber and H. H. Heckman, LBL-6570, to be published in Ann. Rev. Nucl. Sci.

4. J. Hüfner, C. Sanders, and G. Wolschin, Phys. Lett. B 73, 289 (1978).

5. C. K. Gelbke, C. Olmer, M. Buenerd, D. L. Hendrie, J. Mahoney, M. C. Mermaz, and D. K. Scott, Phys. Rev. 42, 311 (1978).

6. D. K. Scott, M. Bini, P. Doll, C. K. Gelbke, D. L. Hendrie, J. L. Laville, J. Mahoney, A. Menchaca-Rocha, M. C. Mermaz, C. Olmer, T. J. M. Symons, Y. P. Viyogi, K. Van Bibber, H. Wieman, and P. J. Siemens, LBL-7729.

7. Y. P. Viyogi, T. J. M. Symons, F. Bieser, H. C. Crawford, P. Doll, D. E. Greiner, C. K. Gelbke, H. H. Heckman, D. L. Hendrie, D. Jones, P. J. Lindstrom, J. Mahoney, C. McParland, D. K. Scott, K. Van Bibber, G. D. Westfall and H. Wieman, "Isotope Identification in a Multi-Element Detector Telescope," in this Annual Report.

8. A. S. Goldhaber, Phys. Lett. B 53, 306 (1974).

9. C. K. Gelbke, D. K. Scott, M. Bini, D. L. Hendrie, J. L. Laville, J. Mahoney, M. C. Mermaz, and C. Olmer, Phys. Lett. B 70, 415 (1977).

10. V. V. Volkov, Sov. J. of Nucl. Phys. 6, 420 (1976).

11. V. K. Lukyanov and A. I. Titov, Phys. Lett. B 57, 10 (1975).

12. J. P. Bondorf, G. Fai, and O. B. Nielson, NBI Preprint 78-6.

13. D. J. Morrissey, W. R. Marsh, R. J. Otto, W. Loveland, and G. T. Seaborg, LBL-6579.

14. R. Oliveira, private communication.

15. J. Barrette, P. Braun-Munzinger, C. K. Gelbke, H. L. Harney, H. E. Wegner, B. Zeidman, K. D. Hildenbrand, and U. Lynen, to be published in Nucl. Phys. A (1978).

16. G. W. Butler, D. G. Perry, L. P. Remsberg, A. M. Poskanzer, J. B. Natowitz, and F. Plasil, Phys. Rev. Lett. 38, 1380 (1977).

STUDY OF PROJECTILE FRAGMENTATION OF ^{12}C, ^{16}O BEAMS AT 90 MeV/NUCLEON

K. Van Bibber, D.L. Hendrie, B.G. Harvey, D.K. Scott, H.H. Wieman, L.S. Schroeder, J.V. Geaga, S.A. Chessin, and J.Y. Grossiord

In an attempt to understand the energy dependence of peripheral heavy-ion reactions, we have undertaken a study of the fragmentation of ^{12}C, ^{16}O projectiles at 90 MeV/nucleon using several targets (Be, Al, Cu, Ag, Au, and Th). Beams of intensities 10^6-10^8 particles/spill from the Bevalac were delivered to our target area in Line 30-1; fragments of $Z \geq 3$ were detected in a multi-element silicon-germanium telescope, which provided good isotope identification and energy measurement. Absolute cross sections were determined by measuring the beam flux in an ion chamber downstream calibrated prior to each run. The beam size and position were monitored continuously downstream from the target with a Morgado wire chamber; periodic upstream monitoring was performed likewise. The targets were typically 100-500 mg/cm^2 in areal density. A helium bag was positioned between the target and the detector and beam dump in order to reduce the "target-out" contribution to the spectra due from interactions of the beam with the air.

A typical spectrum is shown in Fig. 1. The mean energy corresponds essentially to the velocity of the beam, and the spectra are approximately Gaussian in shape with a noticeable low energy tail. Angular distributions were measured between 2^o and 8^o and show a more rapid fall-off for the heavier isotopes than for the lighter isotopes (see Fig. 2). Model calculations have been compared to the data, assuming an isotropic, Gaussian momentum distribution for the fragment in the projectile frame.[1] Furthermore, the integrated yields for each isotope were extracted by extrapolating the angular distributions to zero degrees. (For the isotopes with the most steeply falling angular distributions, approximately half of the cross section appears between our smallest angle measured and 0^o.)

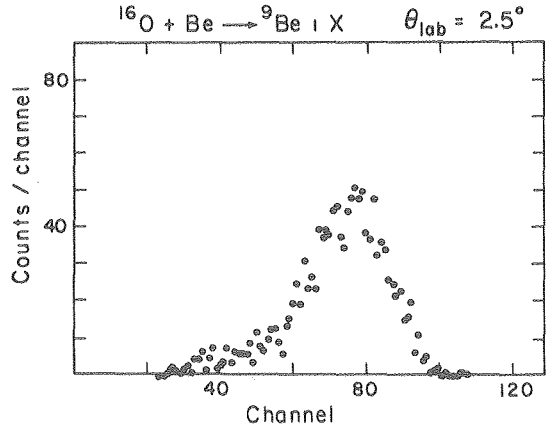

Fig. 1. Spectrum of ^9Be, observed in the bombardment of the Be target by ^{16}O at 90 MeV/A.
(XBL 787-1339)

In comparison with experiments at 20 MeV/nucleon, 200 MeV/nucleon and 2.1 GeV/nucleon,[2-4] we find the following interesting features in our data:

1) Possibly a large increase in the fraction of the total reaction cross section occupied by heavy fragments ($Z \geq 3$) in the vicinity of 100 MeV/nucleon, not evident at either 20 or 200 MeV/nucleon;

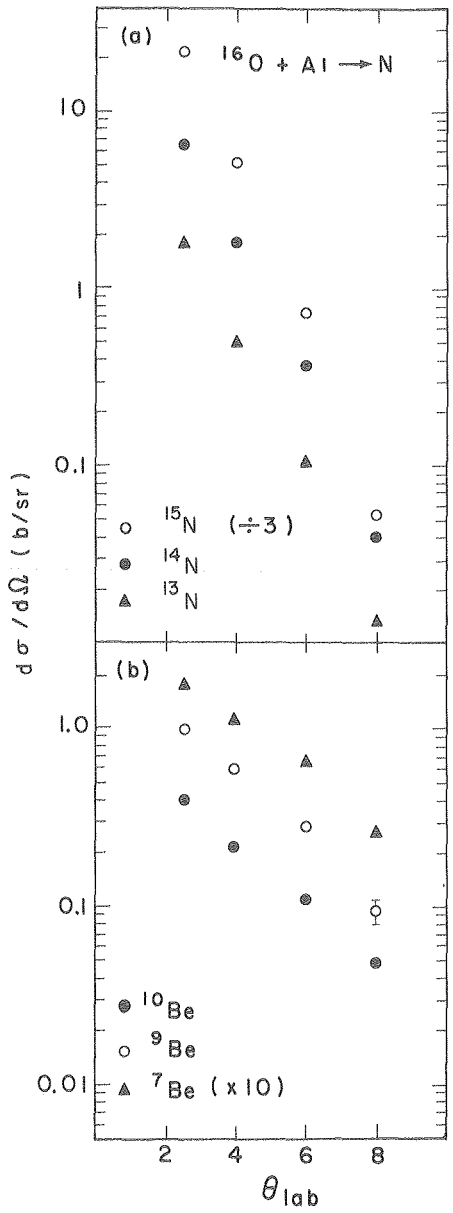

Fig. 2. Angular distributions for ^{16}O + Al→ a) nitrogen isotopes, b) beryllium isotopes. (Lab angle in degrees.)
(XBL 787-1340)

2) Sharp disagreement with the systematics of momentum widths with fragment mass observed at the other energies (see Fig. 3).[4]

The widths in the projectile frame are independent of fragment mass, having an average value of ~240 MeV/c, and are independent of target. Furthermore, although the widths shown in Fig. 3 were derived from the energy spectra at θ_{lab} = 2.5° (corresponding approximately to the width of the momentum distribution in the longitudinal component), the perpendicular components extracted from the angular distributions are the same within errors. These results imply an isotropic breakup of the projectile. No theoretical suggestion to date can account for either phenomenon, and an excitation function will be performed shortly to confirm these results, as well as to map out a more detailed energy dependence.

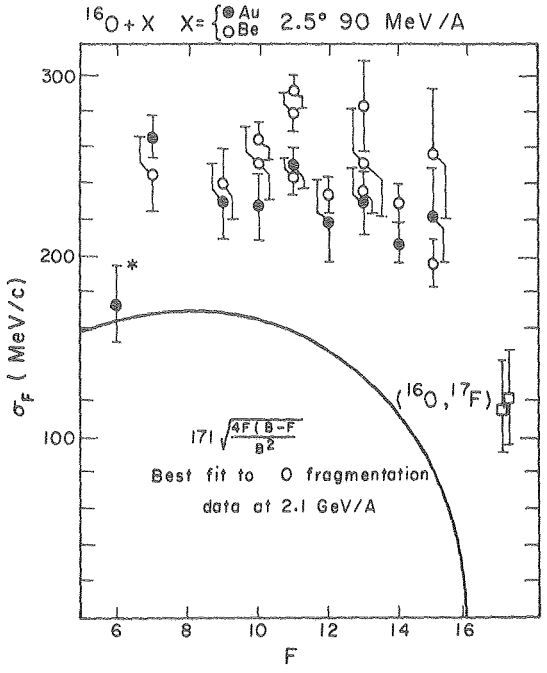

Fig. 3. Widths of fragment momentum spectra in the projectile frame, as a function of fragment mass. The ^{6}Li point is anomalously low due to part of the spectrum punching through the detector stack.

(XBL 787-1341)

It is also noteworthy that significant cross sections exist for the proton pickup reaction (^{16}O,^{17}F) with all targets (~4 mb for Au). The angular distributions decrease exponentially with angle with the exception of that for the gold target, which shows a grazing "shoulder" in the vicinity of θ_{lab} = 4°. The Q-value for this reaction is very nearly that for pickup of a free proton (≈ -100 MeV). For the carbon bombardments, the (^{12}C,^{13}C) reaction is observed, but no significant cross section is found for any nitrogen isotopes.

References

1. A. S. Goldhaber, Phys. Lett. B 53, 306 (1974).

2. M. Buenerd, C. K. Gelbke, B. G. Harvey, D. L. Hendrie, J. Mahoney, A. Menchaca-Rocha, C. Olmer, and D. K. Scott, Phys. Rev. Lett. 37, 1191 (1976).

3. R. Kullberg, K. Kristiansson, B. Lindkvist, and I. Otterlund, Nucl. Phys. A 280, 491 (1977); Y. P. Viyogi, T. J. M. Symons, F. Bieser, H. Crawford, P. Doll, D. E. Greiner, C. K. Gelbke, H. H. Heckman, D. L. Hendrie, P. Jones, P. J. Lindstrom, J. Mahoney, C. McParland, D. K. Scott, K. Van Bibber, G. D. Westfall, and H. Wieman, in preceeding article of this Annual Report.

4. P. J. Lindstrom, D. E. Greiner, H. H. Heckman, Bruce Cork, and F. S. Bieser, LBL-3650 (unpublished); D. E. Greiner, P. J. Lindstrom, H. H. Heckman, Bruce Cork, and F. S. Bieser, Phys. Rev. Lett. 35, 152 (1975).

FRAGMENTATION OF ^{4}He, ^{12}C, ^{14}N, AND ^{16}O NUCLEI IN NUCLEAR EMULSION AT 2.1 GeV/NUCLEON*

H.H. Heckman, D.E. Greiner, P.J. Lindstrom, and H. Shwe†

In this comparative study on the interactions of relativistic nuclei in nuclear research emulsion we have measured the mean-free-path lengths of ^{4}He, ^{12}C, ^{14}N, and ^{16}O nuclei at 2.1 GeV/nucleon, and have examined the topological features of the projectile fragmentation of ^{12}C, ^{14}N, and ^{16}O nuclei, with specific attention to the angular distributions of the Z = 1 and 2 fragments and the prong and charge-multiplicity distributions.

The emulsion stacks used in this experiment were fabricated from Ilford G.5 pellicles, 600 μm thick, and exposed to the beams parallel to the emulsion's planes. The scanning technique for each beam was to select an incident ion 1 to 2 mm from the entrance edge and scan along the track until the ion interacted or left the pellicle. The beginning and terminal points of each track segment were recorded by three-coordinate digitized

Table 1. Interaction mean-free-path lengths (cm) in Ilford emulsion calculated by using parameters K and b_0 that best fit experimental data.

		Beam			
	Fitted Parameter	^{4}He	^{12}C	^{14}N	^{16}O
Experiment		12.8±0.7	13.8±0.5	13.7±0.6	13.0±0.5
Karol (Ref. 1)	K = 0.52±0.06	22.5	14.1	13.2	12.4

microscopes with 1-μm readout accuracy. Recorded for each event were the number and, for relativistic secondaries, the charges of the secondary fragments. The interactions were qualitatively classified as to type, depending upon their visual characteristics:

Type 1 Projectile fragmentation only. No visible target fragmentation. Also denoted as $n_h = 0$ events, where n_h is the number of nonrelativistic particles emitted from the interaction.

Type 2 Projectile fragmentation with target breakup, $n_h \geq 1$.

Type 3 Catastrophic destruction of projectile and target nuclei. No forward-cone fragments from the projectile are evident.

Type 4 Target fragmentation only. No detectable change in charge of projectiles, i.e., the inverse of Type 1.

We have selected events of Type 1 for special examination in that they represent the "cleanest" examples of projectile fragmentation. These events were intensively examined for all secondary fragments. Because the velocities of nuclear fragments of the beam projectile are near the velocity of the beam, $\beta = 0.95$, the grain densities of the secondary tracks are related to Z^2 of the fragment. Charge estimates for ionizing tracks $Z \leq 3$ were thus greatly simplified, requiring only rudimentary grain-density measurements.

The path length followed for each beam was sufficient to obtain at least 10^3 interactions. Table 1 gives the interaction mean-free-path lengths that result after correcting for undetected neutron or proton stripping. To fit these lengths we employed the analytic expression for the reaction cross section given by the "soft spheres model" of Karol.[1] This model utilizes the experimentally measured density distribution parameters (i.e., the half central density radius and the 90%-10% surface skin thickness parameter) and energy-dependent nucleon-nucleon cross sections. Taking the average nucleon-nucleon cross section $\bar{\sigma}$ to be given by $K\bar{\sigma}$ (2.1), where $\bar{\sigma}$(2.1) is the experimental nucleon-nucleon cross section and K is an adjustable parameter, a best fit was obtained when $K = 0.52 \pm 0.06$. The corresponding path lengths are given in Table 1. From the value of K, we conclude that the mean-free-path measurements in emulsion do not constitute a measure of the total reaction cross section (one which corresponds to $K \approx 1$), but determine a cross section that involves greater inelasticity and increased energy transfer more properly identified with nucleus transmutation reactions.

About 12% of the interactions of ^{12}C, ^{14}N, and ^{16}O beam particles with emulsion nuclei lead to "pure" projectile fragmentation, characterized by no detectable target fragmentation, i.e., $n_h = 0$. We have selected these interactions for specific study of the projected angular distribution for charge Z = 1 and 2 secondary fragments and of the topological features of the fragmentation of ^{12}C, ^{14}N, and ^{16}O nuclei, presented in terms of the prong-number and charge-multiplicity distribution.

The projected angular distributions for both Z = 1 and Z = 2 fragments emitted from $n_h = 0$ type events in emulsion are in agreement with the single-particle inclusive spectra.[2] Thus when we compare the momentum distributions of fragments measured in single-particle inclusive experiments with the momentum distributions of fragments produced in interactions selected on the basis of knowledge of the state of the target, we find no difference between them.

To demonstrate some of the topological features of the fragmentation process for the $n_h = 0$ type interactions, we plot in Fig. 1 the charged-prong number (n), and in Fig. 2 the charge-multiplicity (Z*) distributions of the secondary fragments as a function of Z_{max}, the charge of the principal fragment, i.e., highest Z produced in the fragmentation of ^{12}C, ^{14}N, and ^{16}O projectiles. The quantity

$$Z^* = \sum_{i=1}^{n} |Z_i|$$

is the sum of the (absolute) charges of the n secondary particles. Before discussing some of the details presented in Figs. 1 and 2, we wish to point out that in no case, out of 1000 observed interactions for each of the ^{12}C, ^{14}N, and ^{16}O beam projectiles, did we observe a fragmentation event that yielded two or more secondaries with Z > 2, irrespective of the amount of target

excitation. Thus two-product fragmentation events such as $^{14}N \rightarrow {}^{7}Be + {}^{7}Li$ were not observed. The cross section for their production is therefore $\lesssim 10^{-3}$ of the total reaction cross section.

Notable features of the data presented in Figs. 1 and 2 are the following:

1) For $Z_{max} = 1$ events (where all fragments are singly charged, hence, include only the hydrogen isotopes and mesons of both charges) the number of prongs (Fig. 1) is in all cases equal to, or greater than, the atomic number of the projectile.

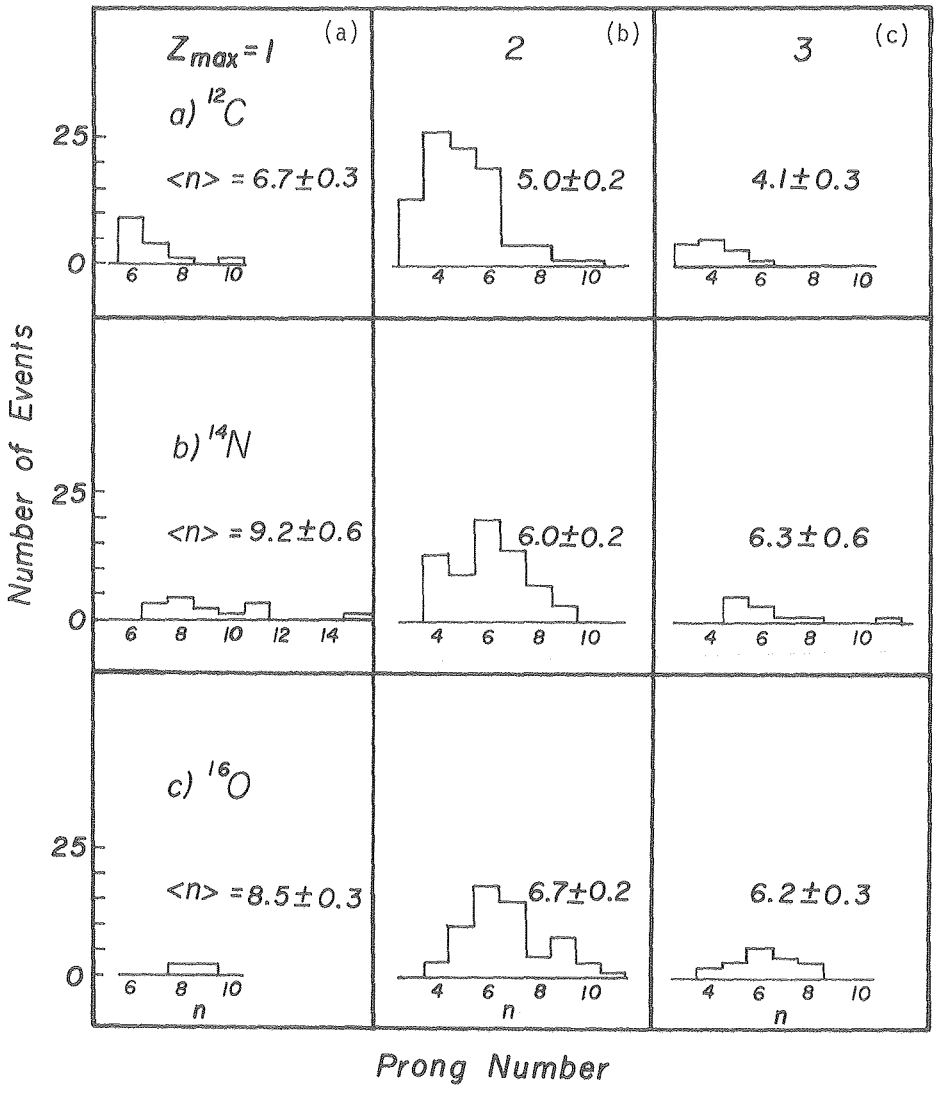

Fig. 1. Histograms of the prong-number distributions for the fragmentation of a) ^{12}C; b) ^{14}N; and c) ^{16}O nuclei in nuclear emulsion, $n_h = 0$ type interactions. Data are ordered as to the maximum charge, Z_{max}, emitted in the fragmentation for $1 \leq Z_{max} \leq 3$ only. The mean prong number $\langle n \rangle$ is indicated for each distribution. (XBL 776-9316)

2) The fragmentation of ^{14}N nuclei shows differences when compared with the ^{12}C and ^{16}O data: These are the high probability for complete fragmentation of ^{14}N into Z = 1 particles (11 ± 4% vs 7 ± 2% and 2 ± 2% for ^{12}C and ^{16}O, respectively) and the high multiplicity of these events, 9.2 ± 0.6. The $\langle Z^* \rangle$ for ^{14}N is 8.5 ± 0.1 for the $1 \leq Z_{max} \leq 3$ events, giving a charge excess of 1.5 ± 0.1--about twice that observed for ^{12}C and ^{16}O.

Footnotes and References

*Condensed from Phys. Rev. C 17, 1735 (1978).
†Present address: East Stroudsburg State College, East Stroudsburg, PA.

1. P. J. Karol, Phys. Rev. C 11, 1203 (1975).

2. D. E. Greiner, P. J. Lindstrom, H. H. Heckman, B. Cork, and F. S. Bieser, Phys. Rev. Lett. 35, 152 (1975).

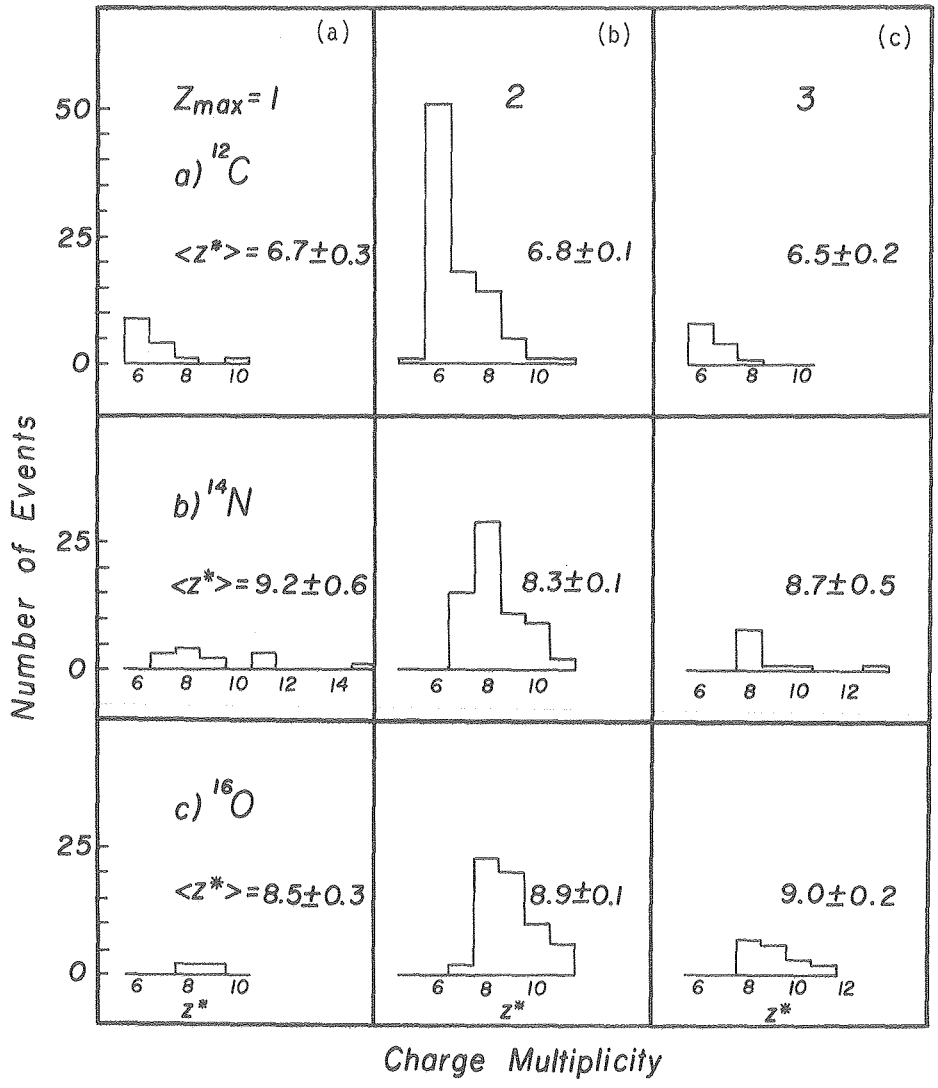

Fig. 2. Histograms of the charge multiplicity distributions for the fragmentation of a) ^{12}C; b) ^{14}N; and c) ^{16}O. The quantity

$$Z^* = \sum_{i=1}^{n} |Z_i|$$

where $|Z_i|$ is the absolute charge of the nth prong. The histograms are based on the same events used for Fig. 1, and are also ordered as to Z_{max}. The mean-charge multiplicity is indicated for each distribution.

(XBL 776-9317)

PERIPHERAL COLLISIONS OF 2 GeV/NUCLEON Fe NUCLEI IN NUCLEAR EMULSION. I. LIGHT PROJECTILE FRAGMENTS

E.M. Friedlander, H.J. Crawford,* R.W. Gimpel, D.E. Greiner, H.H. Heckman, and P.J. Lindstrom

Observations on 374 collisions of 1.88 GeV/nucleon Fe nuclei in Ilford G-5 nuclear track emulsion, in which at least one projectile fragment of $Z \geq 3$ was emitted within a 6° cone, have revealed several unexpected features of projectile breakup.

1. We observe the onset of copious multiple fragmentation. Table 1 shows the probabilities for observing $\geq n_F$ projectile fragments with $Z \geq 3$ for our Fe events compared to results from a similar argon exposure. The double fragments increase threefold and triple fragments occur for the first time in sizable numbers with the Fe beam. Figure 1 shows a microprojection drawing of such a "triple-fragment" event. The fragments are most likely N, C, and Li and are accompanied by 5 α-particles in the fragmentation region.

Table 1. Probabilities for emission of $\geq n_F$ fragments with $Z \geq 3$.

Beam \ n_F	1	2	3
Fe	(73 ± 3)%	(13 ± 2)%	(1.1±0.4)%
A	(59 ± 3)%	(3.5 ± 1.3)%	--

The remarkable feature of this event is that although the primary charge (26) is practically completely bound in the fast nuclear fragments, 7 relativistic $Z = 1$ tracks (most likely pions) are emitted in a wide cone. The small number of target-related tracks (3 black and 1 grey) indicates either a light (CNO) target nucleus or a very peripheral collision with a heavy (Ag,Br) emulsion constituent.

2. The relatively high α-particle multiplicities allow for the first time a study of the α multiplicity distribution.

Figure 2 shows a plot of the quantity

$$y \equiv \ell n[k!P(k)] \quad , \tag{1}$$

where P(k) is the probability for emitting k α-particles vs k. On such a plot a Poisson distribution will appear as a straight line

$$y = -m + k \ \ell n \ m \quad , \tag{2}$$

where m is the mean of the Poisson distribution. The straight line on Fig. 2(a) shows the Poisson distribution for the experimental value $m = 2.07 \pm 0.07$, which gives an excellent fit. This observation has direct implications for

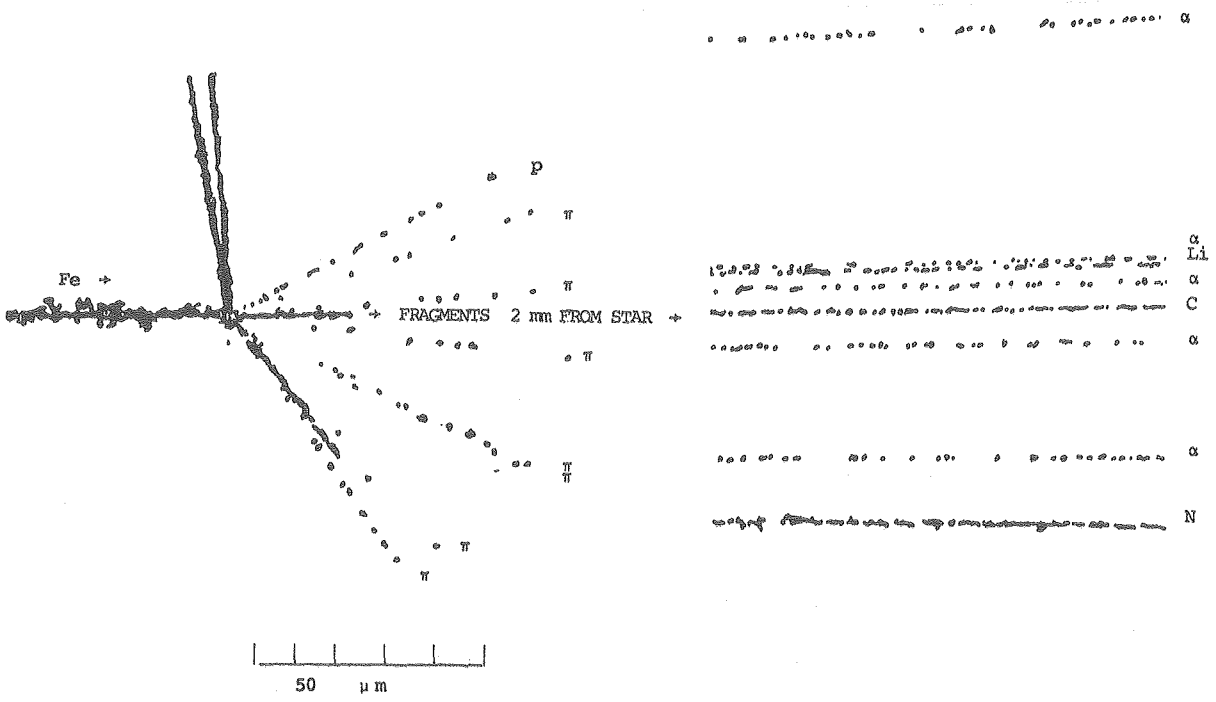

Fig. 1. Microprojection drawing of a typical three-fragment event. The fragments are most likely C, N, and Li.
(XBL 787-9760)

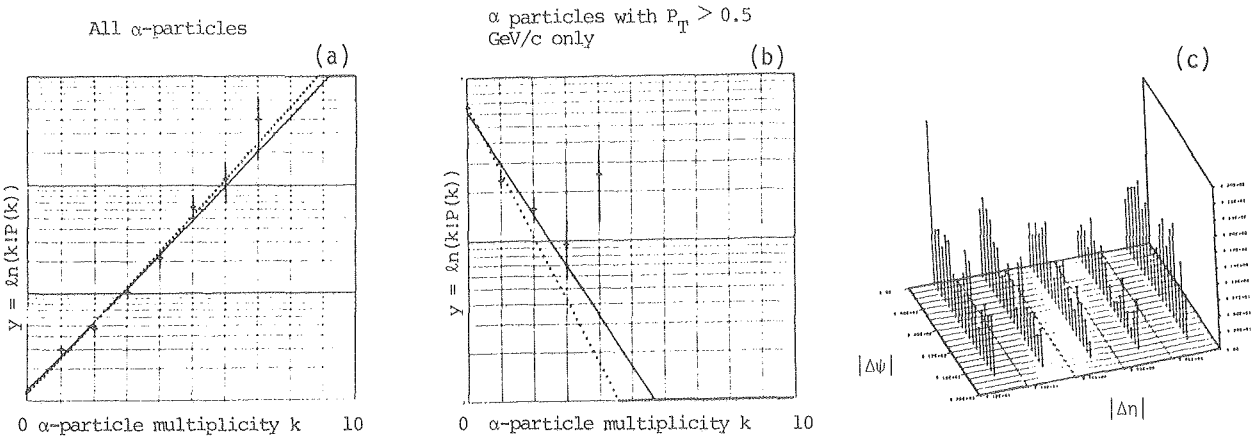

Fig. 2. (a) Linearized Poisson plot for the multiplicity distribution of all alphas. (b) Same as 2(a) for alphas with $p_T > 0.5$ GeV. (c) Bi-variate distribution of differences in azimuth and pseudorapidity for α-pairs.
(XBL 787-9761)

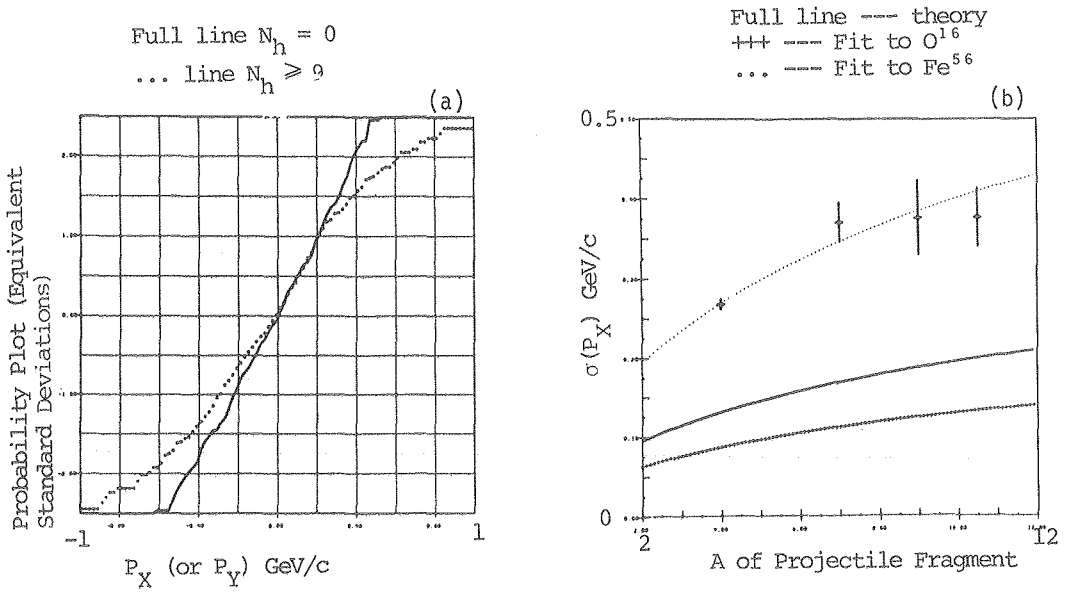

Fig. 3. (a) Probability plot of the p_X projection distribution of α-transverse momenta: Full line $N_h = 0$; dotted line $N_h \geq 1$. (b) Dispersion of the p_X-distribution for α, Li, Be and B plotted against fragment mass. The curves are: bottom = fit to ^{16}O data, full line = theory; dotted line = fit to Fe data (this experiment).
(XBL 787-9762)

the mechanism of projectile fragmentation since it implies uncorrelated emission and little clustering for the bulk of the alphas. However, as can be seen in Fig. 2(b), for α-particles with a relatively large transverse momentum (>0.5 GeV/c) significant departures from a Poisson distribution are observed. It can be shown that the deviation is in a direction opposite to that expected from a binomial distribution (which is significantly excluded by the data of Fig. 2(a), too).

3. Our data show a significant enhancement of α-particle pairs with very small relative momenta. Figure 2(c) shows the bivariate frequency distribution of differences $|\Delta\psi|$ (in azimuth) and $|\Delta\eta|$ (in pseudorapidity) of all combinations of two-alpha particles from our events. The narrow spike at $|\Delta\psi| < 10^o$, $|\Delta\eta| < 0.25$ has a probability $<10^{-3}$ to occur as a statistical fluctuation. Comparison of the transverse momentum distribution of these α-pairs with that of stable Be-fragments observed in the same sample of events shows that at most ~1/3 of these pairs can be accounted for in terms of the decay of the ground state of Be^8. Since Be^8 decay is known to be dominated by its first excited state (which would lead to much broader angular distributions), some of the α-α correlation must be of a different

origin. A tentative interpretation in terms of "identical boson-boson" interference effects suggests the need for a significant increase in statistics of narrow α-pairs.

4. The transverse momentum distributions which should reflect best the "thermal" motion in the projectile system, are in flagrant discrepancy with theoretical predictions. The distributions show a marked target dependence, both in shape and parameter values. Figure 3(a) shows a probability plot of transverse momentum P_x-projections which should be Gaussian for a Boltzmann gas. This is indeed the case for events with $N_h = 0$, i.e., without any slow target fragments (full line). However, events with $N_h \geq 9$ [collisions with heavy (Ag,Br) targets] show a marked departure from a Gaussian. If one tries to assign "temperatures" to these curves we obtain ~12 MeV for $N_h = 0$ and ~25 M V for $N_h \geq 9$. If the latter is decomposed into two Gaussians they correspond to temperatures of ~15 MeV and ~30 MeV.

Figure 3(b) shows the r.m.s. deviation σ of the P_x distributions for different projectile fragments. The full curve is the theoretical prediction of Lepore and Ridell.[1] Crosses represent the fit to a parabolic fragment mass dependence obtained with O^{16} projectiles by Greiner et al.[2] The dotted line is the best fit of a parabolic expression

$$\sigma^2 = \sigma_0^2 \cdot 4F(B-F)/B^2 \quad , \qquad (3)$$

where B and F are the beam and fragment masses, respectively, to our data. The fit is obviously good; however, the constant σ_0^2 is ~1 order of magnitude higher than the value observed with oxygen projectiles and a factor ~2 off from the theoretical prediction.[1] If one tries to assign σ_0^2 a "thermal" meaning according to Goldhaber,[3] we obtain again a temperature in the range 25-30 MeV.

5. The charges of all projectile fragments up to boron have been determined by measurement of gap-length distributions (heavier fragments, measured photometrically, will be dealt with in a subsequent publication). We have been able to make a complete analysis of 57 events involving only fragments of $Z \leq 5$. Figure 4 shows the target dependence of various fragmentation parameters, in terms of the number N_h of target fragments ($N_h = 0$, $N_h = 1 \ldots 8$, $N_h \geq 9$).

It is obvious that events with $N_h = 0$ are a class qualitatively apart from the rest of the events. More of the primary charge is bound in He and (Li, Be, B) fragments. The mean number n_s of relativistic prongs is low and the charge excess ($26 - \Sigma Z_{i\geq 2} - n_s$), which is most likely interpreted as charged pions, is nil. The transverse momentum distributions of both He and Li fragments are narrower than in the bulk of the events.

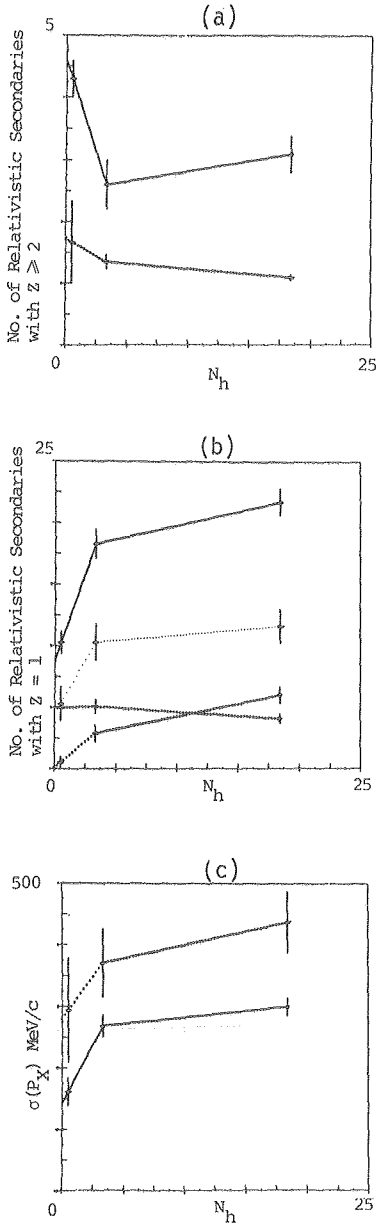

Fig. 4. N_h-dependence of: (a) mean multiplicity of alphas-(upper line), Li-(lower line); (b) mean multiplicity of relativistic Z = 1 secondaries from top to bottom: all Z = 1, protons outside 6° cone, protons inside 6° cone, charged pions; (c) dispersion of p_x-distribution: alphas (upper line), Li (lower line). (XBL 787-9763)

Between $N_h = 1 \ldots 8$ and $N_h \geq 9$ (essentially light and heavy targets) there is surprisingly little change in most parameters in spite of weak but consistent trends. The only exception is the strong increase in the pion multiplicity. If this fact is associated with the weak change in the number of projectile protons, it is very hard to explain in any "independent nucleon" scattering model and is highly suggestive of collective effects.

Footnote and References

*Space Sciences Laboratory, University of California, Berkeley, CA 94720.

1. J. V. Lepore and R. J. Riddell, Jr., LBL-3086 (1974).

2. D. E. Greiner, P. J. Lindstrom, and H. H. Heckman, Bull. Am. Phys. Soc. 17, 488 (1972); also H. H. Heckman, Relativistic Heavy Ion Seminar, Internal LBL Report, unpublished (1973).

3. A. S. Goldhaber, Phys. Lett. B53, 306 (1974).

FRAGMENTATION OF RELATIVISTIC ^{56}Fe*

G.D. Westfall, Lance W. Wilson, P.J. Lindstrom, H.J. Crawford, D.E. Greiner, and H.H. Heckman

With the recent acceleration of iron to relativistic energies at the Bevalac, the direct measurement of the astrophysically interesting fragmentation of iron is now possible. Employing a simple transmission detector system, elemental production cross sections for elements from Z = 13 to Z = 25 were measured for a variety of targets ranging from H to U using a 1.88 GeV/nucleon ^{56}Fe beam. In addition, the charge-changing ($\sigma_{\Delta Z \geq 1}$) and mass-changing ($\sigma_{\Delta A \geq 1}$) cross sections were extracted. The mass-changing cross sections can be applied directly to calculations of cosmic ray propagation. The elemental production cross sections, though not directly applicable, can be used to improve the phenomenology used in cosmic ray calculations.

The apparatus consisted of a beam definition, a thick target, and an effective charge identification module. Each module was composed of lithium-drifted silicon detectors. The detectors were 3 mm thick and had 1500 mm^2 active area (44 mm diameter). The beam definition module contained two detectors and the effective charge module contained four detectors. The targets used were typically half a mean free path in thickness. Cross sections for a hydrogen target were obtained by a subtraction of C from CH_2 targets.

Charge definition in both the beam defining and fragment measuring modules was accomplished by a multiple ΔE measurement. An average charge, $\bar{Z}$, and a consistency check, χ^2, were formed for each event. However, since each interaction could produce many minimum ionizing charged particles, the effective charge module will measure an effective charge,

$$Z^* = \sum_{n=1}^{N} \left(Z_i^2\right)^{1/2}$$

where Z_i is the charge of the ith particle out of a total of N particles. If one of the particles has a charge much greater than the others, its charge will dominate the sum of squares producing a leading charge effect. Different leading charges were easily separated and the production of a given element from ^{56}Fe was equated with the observation of the corresponding leading charge.

The elemental production cross sections, $\sigma(Z)$, for elements with Z = 13 to 25 produced from a relativistic ^{56}Fe beam are given in Table 1 and Fig. 1 for the 10 different targets. Corrections were made for target-out background, zero detector thickness extrapolation, and multiple interactions in the thick targets. The cross sections represent an average over the energy loss in the thick targets, which was typically 0.15 GeV/nucleon.

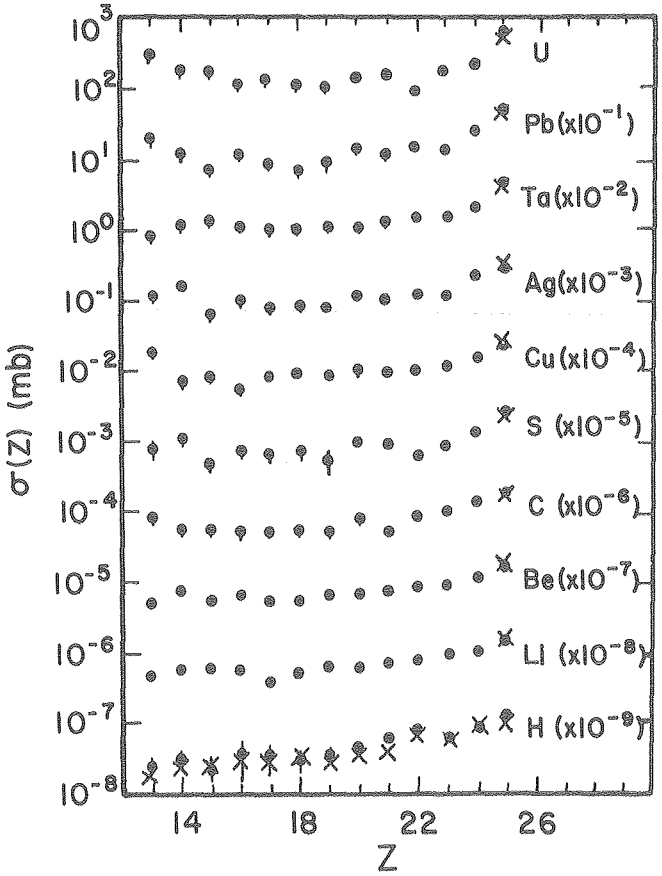

Fig. 1. Elemental production cross sections, $\sigma(Z)$, for ^{56}Fe at 1.88 GeV/nucleon. The x's for the H target represent the results of the semi-empirical model of Silberberg and Tsao. The x's for the $\sigma(Z = 25)$ data for all targets refer to a calculation of the Coulomb-enhanced removal of one proton. (XBL 787-9610)

Table 1. Elemental production cross sections for 1.88 GeV/nucleon ^{56}Fe beams in mb.

Target Z	H	Li	Be	C	S	Cu	Ag	Ta	Pb	U
13	25±10	50±5	50±7	83±11	78±18	179±27	112±19	81±14	191± 37	307±79
14	31±9	57±5	75±8	57±10	106±14	72±11	158±20	115±20	119± 22	169±28
15	22±10	57±6	57±8	59±10	50±8	88±15	64±13	133±20	78± 16	176±34
16	37±24	56±6	63±8	54±10	74±12	56±11	96±13	109±17	116± 19	116±22
17	36±17	38±4	54±7	53±7	66±14	86±13	79±14	101±18	90± 19	133±22
18	31±9	55±6	54±7	55±9	74±13	95±15	84±14	100±18	73± 15	113±19
19	36±9	56±5	65±7	52±7	55±21	88±14	79±11	111±20	90± 19	105±15
20	47±11	64±6	68±7	78±11	97±14	98±14	118±14	107±17	144± 22	143±19
21	62±11	67±6	77±8	54±9	91±13	100±15	104±13	129±18	111± 17	153±21
22	82±13	75±6	83±9	87±11	64±10	101±14	124±16	152±19	148±22	95±16
23	60±11	88±7	88±9	100±11	86±12	121±15	117±15	150±19	142±25	181±27
24	80±13	98±7	111±9	124±13	128±16	149±16	218±21	206±22	242±15	208±22
25	127±24	141±18	156±21	181±27	250±22	219±20	280±23	457±34	509±40	646±43

The distribution of elemental production cross sections for each target is generally nearly flat. No odd-even Z effects are visible. Exceptions to the general trend of flatness occur in the form of enhancement near Z = 13 and near Z = 25 for the heavier targets. The turn-up near Z = 25 represents the Coulomb-enhanced removal of one proton from the projectile. The turn-up around Z = 13 can be attributed to the breakdown of the leading charge effect. This breakdown could be due to the enhanced breakup of the projectile into many smaller charged particles by the heavier targets.

The measured elemental production cross sections for the fragmentation of 1.88 GeV/nucleon ^{56}Fe on a H target can be compared to the semi-empirical model of Silberberg and Tsao.[1] The semi-empirical model slightly overestimates the elemental production cross sections but is still statistically consistent with the present experiment.

Another comparison is made in Fig. 1 between the $\sigma(Z = 25)$ for all targets and a semi-empirical model. This model describes the enhanced one-proton removal from the projectile by absorption of a virtual photon via the giant dipole resonance. This process seems to account for the enhanced $\sigma(Z = 25)$ for the heaviest targets.

The charge-changing cross section, $\sigma_{\Delta Z \geq 1}$ is defined to be the cross section for the removal of at least one charge from the projectile. The measured charge-changing cross sections for a relativistic ^{56}Fe beam on 10 different targets are given in Table 2. The charge-changing cross sections contain the same energy averaging and experimental corrections as the elemental cross sections.

Another quantity related to $\sigma_{\Delta Z \geq 1}$ is the mass-changing cross section, $\sigma_{\Delta A \geq 1}$, which is defined as the charge section for removing at least one nucleon. This cross section can be found from $\sigma_{\Delta Z \geq 1}$ by adding in the contribution from neutron loss that could not be measured in this experiment. These values are presented in Table 2. The stated errors include errors in the added neutron loss contribution as well as those from the charge-changing cross sections.

Table 2. Charge-changing cross sections, $\sigma_{\Delta Z \geq 1}$, and mass-changing cross sections, $\sigma_{\Delta A \geq 1}$, for 1.88 GeV/nucleon ^{56}Fe.

Target	$\sigma_{\Delta Z \geq 1}$ (b)	$\sigma_{\Delta A \geq 1}$ (b)
H	0.68±0.04	0.75±0.05
Li	1.34±0.03	1.43±0.04
Be	1.57±0.03	1.67±0.05
C	1.56±0.05	1.66±0.06
S	2.07±0.08	2.22±0.09
Cu	2.71±0.07	2.94±0.10
Ag	3.34±0.08	3.71±0.14
Ta	4.34±0.08	4.97±0.20
Pb	4.33±0.15	5.10±0.27
U	5.02±0.11	5.92±0.29

Footnotes and References

*Condensed from LBL-7162, submitted to Phys. Rev. C.

1. R. Silberberg and C. H. Tsao, Astrophys. J. 25, Suppl. 220, 315 (1975), and Proceedings of the 14th Int. Cosmic Ray Conference, München 7, 2315 (1975).

WHAT GOVERNS THE PRODUCTION OF HEAVY TARGET RESIDUES IN RELATIVISTIC HEAVY-ION REACTIONS?*

D.J. Morrissey, W. Loveland,† and G.T. Seaborg

It is common when discussing RHI reactions to describe experiments in terms of the projectile velocity (i.e., 2.1 GeV/amu, etc.) or to compare the results of relativistic heavy-ion reactions with results from reactions induced by protons of equivalent velocity. Preliminary measurements by Kaufman et al.,[1] however, suggested that the recoil properties of some of the product nuclei from the reaction of 25 GeV ^{12}C with Au resembled more the recoil properties of the same products produced in reactions with 28 GeV protons rather than 3 GeV protons. Piqued by this suggestion, we bombarded Ta with 8.0 GeV (i.e., 400 MeV/amu) ^{20}Ne ions in hopes that the known dramatic differences between the reaction of Ta with ~400 MeV protons[2] and GeV energy protons[3] would manifest themselves in the target residue mass and charge distributions (see Fig. 1).

A Ta foil (of thickness 164.6 Mg/cm^2 surrounded by 5.4 mg/cm^2 mylar catcher foils) was irradiated for 247 min in a beam of 8.0 GeV ^{20}Ne ions of intensity ~1.64×10^{10} particles/min at the Lawrence Berkeley Laboratory Bevalac. Gamma-ray spectrometric measurements of the radioactivity induced in the target and catcher foils began 14 hr after bombardment and continued for about 5 weeks. Approximately 60 radionuclides were identified in this study on the basis of their γ-ray energy, half-life, and radiation abundances.

Independent and cumulative radionuclide yields were calculated from the radioactivity measurements on the irradiated foils. Using the procedures described elsewhere,[4] independent yield formation cross sections were calculated for all radionuclides, Gaussian charge dispersions [of the form $P(Z,A) = (2\pi\sigma^2)^{-1/2}\exp(-(Z-Z_p)^2/2\sigma^2)$] were fitted to the data, and the charge dispersions were integrated to give the isobaric yields. Figure 1 shows the product mass distribution for the reaction of 8.0 GeV ^{20}Ne with Ta and the corresponding distributions for the reaction of 340 MeV and 5.7 GeV protons with Ta. Comparison of the data in Fig. 1 shows the dramatic agreement between the mass distributions of 8.0 GeV ^{20}Ne and 5.7 GeV protons and striking disagreement between 8.0 GeV ^{20}Ne reaction mass distribution and the distribution resulting from the interaction of equivalent velocity protons with the same target. A similar result is obtained when one compares the Z_p functions from these reactions. The total integrated cross section for species with A > 40 is 2.5 barns. Using the Bradt-Peters geometrical form for the reaction cross section,[5]

$$\sigma_R = \pi r_o^2\left(A_1^{1/3} + A_2^{1/3} - b\right)$$, and the parameters

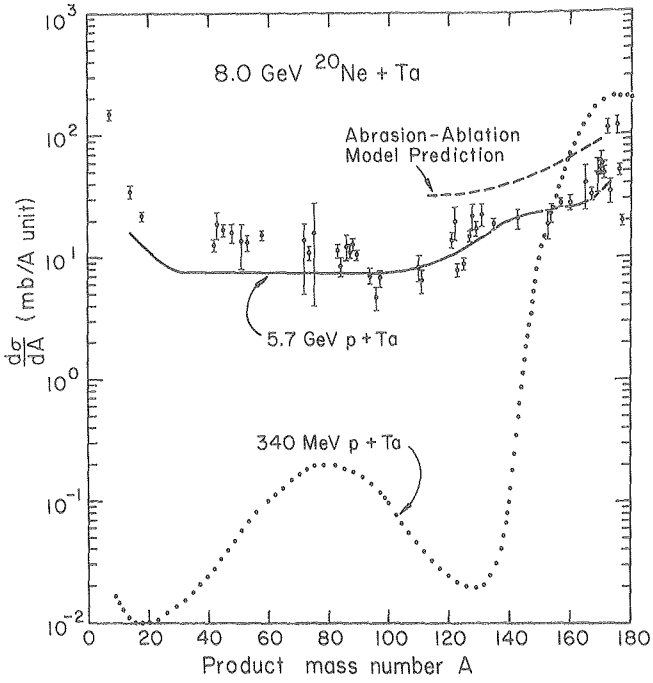

Fig. 1. Product mass distribution from the reaction of 8.0 GeV ^{20}Ne with Ta. Dotted curve is the data of Nervik and Seaborg,[2] solid curve is the data of Grover,[3] while the dashed line is the prediction of the abrasion-ablation model.
(XBL 786-1171)

obtained by Heckman et al.[6] for $A_1 = 20$, $r_o = 1.37$ fm and $b = 0.51$, one obtains a reaction cross section of 3.64 barns. Thus, our results set an upper limit on the extent of central projectile-target collisions in which no survivors (with mass number A > 40) occur at <30% of the total reaction cross section.

Also shown by the dashed curve in Fig. 1 is the prediction of the abrasion-ablation model for the product mass distribution for this reaction.[7,8] In this picture of RHI collisions both the target and projectile nuclei are assumed to be hard spheres and the projectile nucleus is assumed to follow a straight line trajectory. Primary residues or target spectators are those fragments that remain after the overlap region between the two sharp spheres is removed from the target nucleus by the interaction (abrasion). These primary residues are assumed to have an excitation energy due to the increased surface area of the distorted fragments,[7] and are de-excited through a statistical evaporative cascade with fission

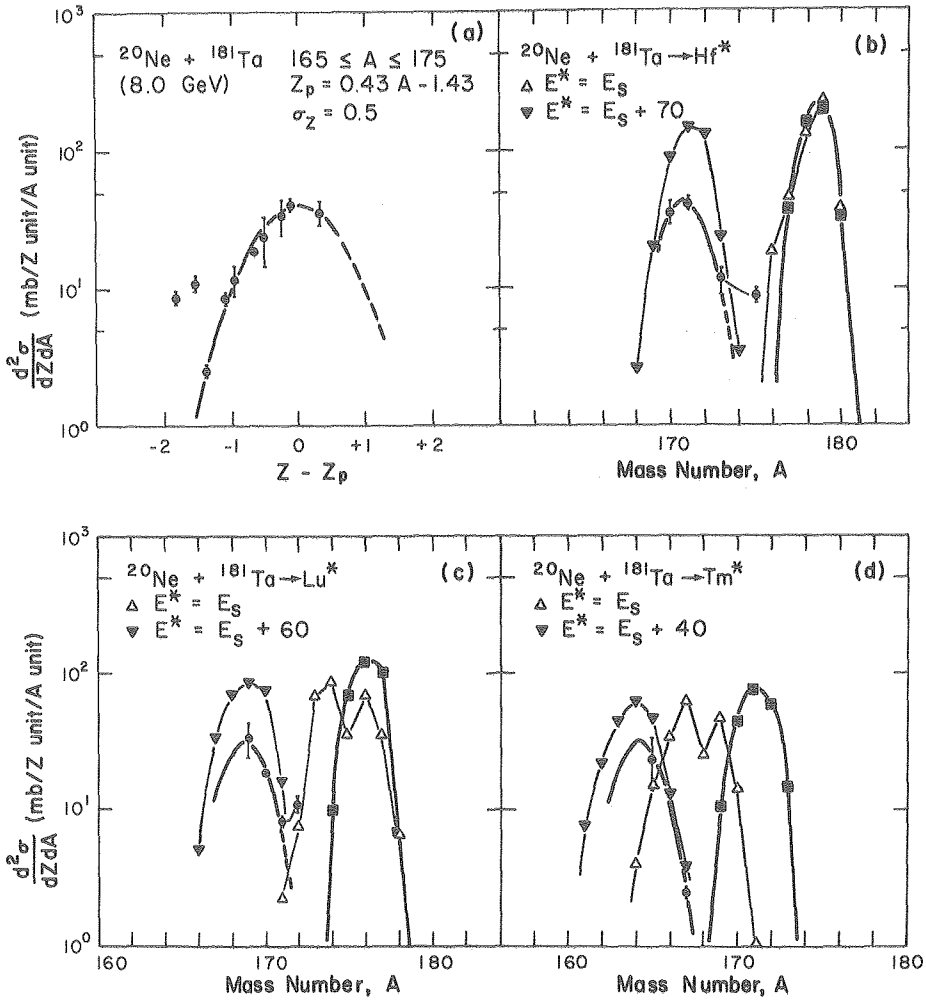

Fig. 2. (a) Charge dispersion curve for the near target residues from the reaction of ^{20}Ne with ^{181}Ta. (b) Comparison of the measured data for Hf isotopes, solid points, with the abrasion-ablation calculations (see text). (c) and (d) are same as (b) but for Lu and Tm fragments, respectively.

(XBL 786-1172)

competition[8] (ablation). Figure 1 shows that the shape of the target residue distribution is correctly predicted by this model (indicating that the shape of this distribution is largely governed by geometrical factors), but the magnitude of the cross section is over-estimated by a factor of two. This difference may represent a breakdown of the strict participant-spectator assumption of the abrasion model of RHI reactions at 400 MeV/nucleon.

Using the primary residue charge dispersion prescription of Morrissey et al.[8] with the abrasion-ablation model of the interaction, information can be obtained on the excitation energy deposited in the spectator target fragment by the interaction. In Fig. 2(a) we show the charge dispersion curve for those fragments with mass number A between 165 and 175. (We note that the two most neutron-excessive products, ^{175}Hf and ^{172}Lu shown in Fig. 2(a), do not seem to be a part of the Gaussian distribution that characterizes the remainder of the products. These neutron excessive products may be due to contributions from secondary reactions in the target.) These fragments with $165 \leq A \leq 175$ are isotopes of Hf, Lu and Tm, and these data have been replotted as mass dispersions in Figs. 2(b), 2(c) and 2(d). Also shown in these latter figures are the calculated values of the primary product production cross sections using the prescription of Morrissey et al.[8] (solid squares) as well as the predicted secondary product distribution assuming the primary product excitation energy is simply that of excess surface energy, E_S, of the residue (solid triangles). The size of E_S varies with the number of nucleons removed and has average values of ~5 MeV, ~15 MeV and ~35 MeV for Hf, Lu, and Tm fragments, respectively. The calculated secondary product yields assuming this excitation energy do not resemble the experimental data; however, if one assumes the total excitation energy of these primary fragments is ~75 MeV independent of product mass, then, as shown in Figs. 2(b), 2(c), and 2(d), the calculations reproduce both the centroid and the widths of the product distributions. As before, though, the cross sections are overestimated by a factor of ~2-3.

What governs the production of heavy target residues in relativistic heavy-ion reactions? The total energy of the incoming projectile rather than its velocity appears to determine the yields

of the target residue nuclei. It should be noted, however, that the excitation energies of the near target residues are relatively low when compared to the excitation energies predicted as the result of the interaction of either equivalent velocity or equivalent total energy protons. The general success of the simple abrasion-ablation model, along with the failure of the Monte-Carlo intranuclear cascade model (which assumes each projectile and target nucleon interact as single particles) in describing the residue mass distributions, argues that the relativistic heavy ion interacts as a single entity with the target nucleus.[8] As our data show, it appears that some of the target residue nuclei are produced in interactions involving significant overlap of the central densities of projectile and target [$b \sim 0.55(R_p + R_t)$]. These "hard" collisions would appear to offer exciting opportunities to study new aspects of nuclear reaction dynamics.

Footnotes and References

*Condensed from LBL-7718, accepted for publication in Z. Phys. A.

†Permanent address: Dept. of Chemistry, Oregon State University, Corvallis, OR 97331.

1. S. Kaufman, E. D. Steinberg, and B. D. Wilkins, Phys. Rev. Lett. 41, 1359 (1978).

2. W. E. Nervik and G. T. Seaborg, Phys. Rev. 97, 1092 (1955).

3. J. R. Grover, Phys. Rev. 126, 1540 (1957).

4. I. Binder, LBL-6526 (1977); W. Loveland, D. J. Morrissey, R. J. Otto, and G. T. Seaborg, LBL-6527 (1977).

5. H. C. Bradt and B. Peters, Phys. Rev. 77, 54 (1950).

6. H. H. Heckman, D. E. Greiner, P. J. Lindstrom, and H. Shwe, Phys. Rev. C 17, 1735 (1978).

7. J. D. Bowman, W. J. Swiatecki, and C. F. Tsang, LBL-2908 (1973).

8. D. J. Morrissey, W. R. Marsh, R. J. Otto, W. Loveland, and G. T. Seaborg, Phys. Rev. C 18, 1267 (1978). (accepted for publication); LBL-6529 (1977); and see also D. J. Morrissey et al., "Calculation of Target Residue Mass and Charge Distributions in Relativistic Heavy-Ion Reactions," in this Annual Report.

NON-SCALING BEHAVIOR OF PION PRODUCTION AT 180° IN p-NUCLEUS COLLISIONS BELOW 5 GeV*

S. Chessin, J. Geaga, J.Y. Grossiord,† J. Harris, D. Hendrie, L. Schroeder, R. Truehaft, and K. Van Bibber

In a comprehensive study of particle production at 180° by relativistic nuclear beams at the Berkeley Bevalac, we have measured the single particle inclusive spectra of $\pi^{\pm}$, p, d, t's produced by beams of p, α, C, Ar striking various nuclear targets. High energy particle production at backward angles is particularly interesting since most processes are either strictly forbidden or at least severely constrained by kinematics [e.g., $pp \rightarrow \pi(180^0) + x$, $p^{\pi}_{max} \lesssim$ 250-300 MeV/c in the lab system], thus enhancing the possibility that cooperative phenomena play a major role in such particle production.

We discuss only one of the features observed in these studies; namely, the lack of scaling of pions produced at 180° by proton beams. The following reaction was studied:

$p + A \rightarrow (\pi^{\pm})180^0 + x$ (A = C,Al,Cu,Sn,Pb),

with proton beams of 0.8, 1.05, 2.1, 3.5, and 4.9 GeV. It has been observed that forward pion production[1] scales for proton beams of bombarding energies as low as ~1 GeV. By scaling, we mean that the invariant cross section,

$$E/p^2 \frac{d^2\sigma}{d\Omega dp} ,$$

depends only on the scaling parameter $x' = (p/p_{max})_{cm}$ and is independent of energy. Using a hard scattering model, Schmidt and Blankenbecler[2] were able to obtain an impressive fit to the forward pion production data (projectile fragmentation region). Using this same model they then predict that pion production in the backward direction (target fragmentation region) would behave as: $(1 - x')^{6A-5}$, where A = atomic number of the target employed. Figure 1 shows our preliminary data for backward π^-'s produced by 1.05, 2.1, and 4.9 GeV protons. A clear energy dependence is observed in these data, so that the concept of scaling does not hold for pion production at backward angles. We do note, however, that the backward pion cross section does follow a behavior of the form $(1 - x')^n$. The solid line through the data point in Fig. 1 represents such a fit with n = 23 for the 1.05 GeV data, n = 30 for the 2.1 GeV data, and n = 65 for the 4.9 GeV results. The model of Ref. 2 for a Cu target predicts $n \approx 373$ (independent of bombarding energy). We should point out that their model was meant to apply near the kinematic limit in these reactions (i.e., $x' \approx 1$) and that these data only go up to $x' \lesssim 0.45$ at best.

In conclusion, although pion production in the forward direction is observed to scale,

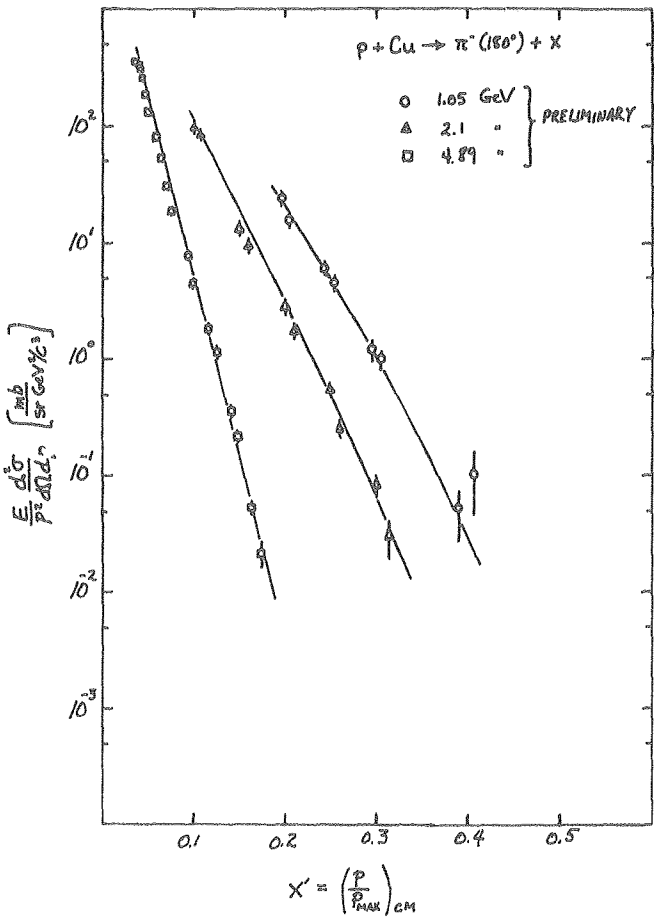

backward pion production does not show such a feature. The hard scattering model of Schmidt and Blankenbecler[2] with its quark-like counting rules, which was successful when applied to the forward data, fails when applied to backward (180°) pion production. Indeed, the interesting question arises as to why it worked so well on the forward production data? It is possible that the apparent scaling of the data is simply fortuitous. Perhaps one can distinguish more easily the flowers from the weeds with particle production at backward angles?

Footnotes and References

*Condensed from Bull. Am. Phys. Soc. 23, 48 (1978).

†Present address: Institut de Physique Nucleaire de Lyon, Lyon, France.

1. J. Papp, J. Jaros, L. Schroeder, J. Staples, H. Steiner, and J. Wiss, Phys. Rev. Lett. 34, 601 (1975).

2. I. A. Schmidt and R. Blankenbecler, Phys. Rev. D 15, 3321 (1977).

Fig. 1. Lorentz invariant cross section vs x' for π^- production at 180° by 1.05, 2.1, and 4.9 GeV protons on Cu target. (XBL 786-9450)

2. Central Collisions

SINGLE PARTICLE INCLUSIVE MEASUREMENTS OF RELATIVISTIC HEAVY-ION COLLISIONS

H.H. Gutbrod, J. Gosset,* J.-C. Jourdain,† C.H. King, G. King, Ch. Lukner,‡ W.G. Meyer, Nguyen Van Sen,§ A.M. Poskanzer, A. Sandoval, R. Stock, G.D. Westfall, and K.L. Wolf

Despite the complexity of relativistic heavy-ion reactions with their characteristically high multiplicity of reaction products, precise single particle inclusive measurements yield information on the average multiplicity and on the details of energy and momentum dissipation in the reaction observed. Furthermore, if the particles detected are clusters, there is information on the correlation of nucleons and their formation process. Because all theories of relativistic heavy-ion reactions presently give predictions of cross sections within a factor of 2-4, accurate data are needed for comparison. For more detailed studies, the single particle inclusive data of reactions with small impact parameter are highly desired; this selection can be obtained by measuring associated charged particle multiplicities.

With these two goals in mind, a large set of data was taken using projectiles from proton to ^{40}Ar on targets from ^{27}Al to ^{238}U at bombarding energies from 250 MeV/nucleon to 2.1 GeV/nucleon. The systems studied are presented in Table 1. Reaction products were detected in a multicounter telescope[1] inside of a newly built scattering chamber (Fig. 1). The particles π^+, p, d, t have been identified as to mass, charge, energy, and reaction angle. Simultaneously, for each event detected, the associated multiplicity

Table 1. The target, projectile, and energy combinations for which data were taken.

	Energy	Targets				
Proj.	(GeV/nucleon)	Al	Ca	Ag	Au	U
p	1.05					X
^{4}He	0.4	X				X
	1.05					X
^{20}Ne	0.25					X
	0.40	X		X	X	X
	1.05					X
	2.1					X
^{40}Ar	0.4		X			X
	1.05		X			X

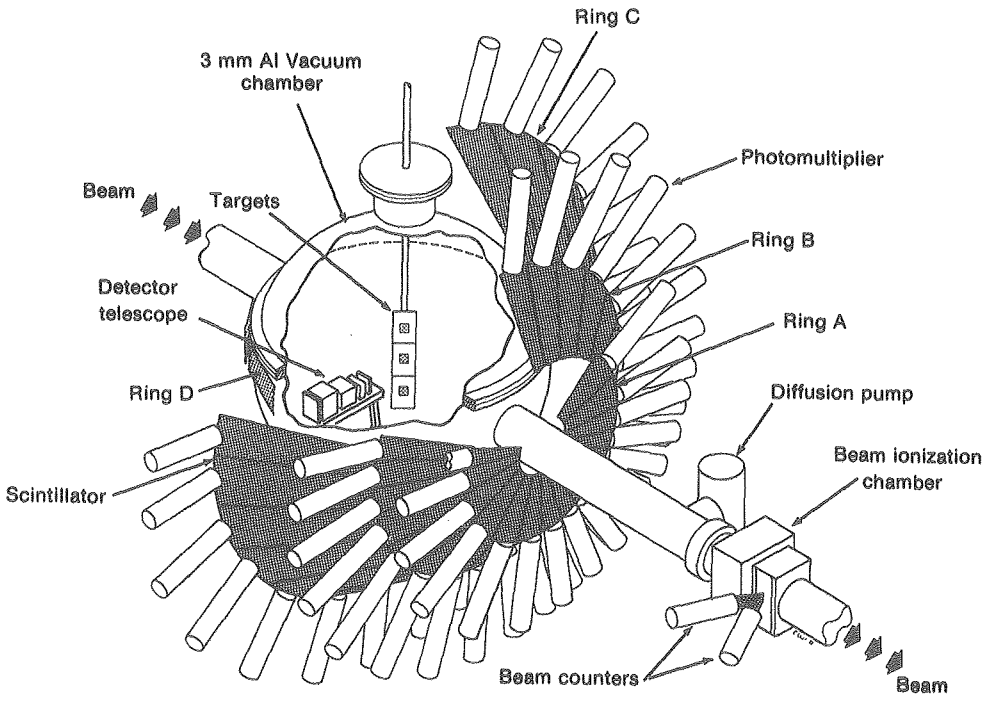

Fig. 1. The scattering chamber is shown containing the Si-Ge telescope and surrounded by the 80 plastic scintillators. (XBL 782-7229C)

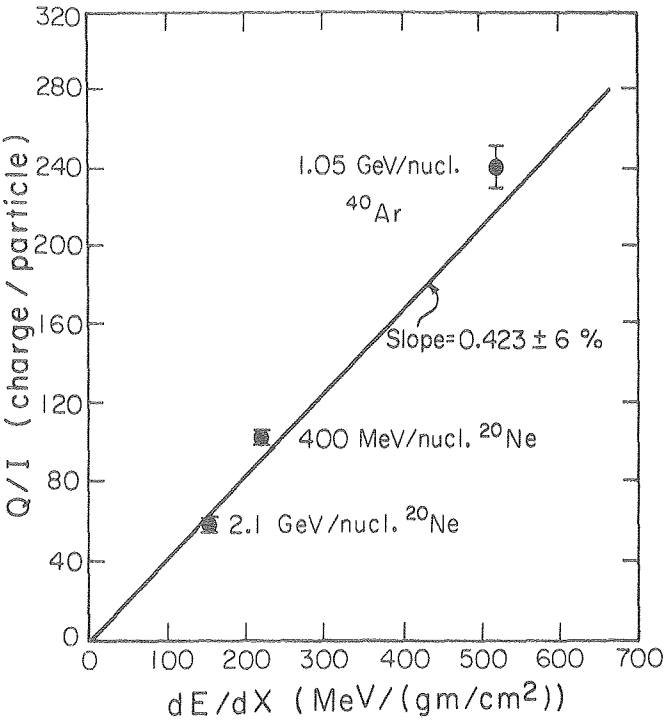

Fig. 2. The response of the beam ionization chamber per incident particle as a function of the theoretical dE/dx. The slope of the best fit line is 81% of that calculated from the physical characteristics of the ionization chamber.
(XBL 787-1350)

and multiplicity pattern in ϕ and θ was measured in 80 scintillators coupled to photomultipliers (see Fig. 1).

A special effort was made to improve the absolute normalization of the data to resolve some questions raised in connection with the old data.[2] For that purpose, the beam line was modified to insure a clearer beam, which resulted in a dramatic improvement of the background conditions at forward angles. The beam ionization chamber downstream of the target (see Fig. 1) has been calibrated by a beam scintillator system[3] consisting of a) a 1/4" x 5" x 5" scintillator and b) a 1/4" x 5" x 5" sampling scintillator (plastic containing scintillation fibers) with an effective area of 2.7% of the full scintillator. Thus, it was possible to calibrate the ionization chamber with various particle beams and define its calibration curve (Fig. 2). During the data-taking runs, the linearity of the beam ionization chamber was checked with a ΔE-E solid state counter telescope, and no change in the response of the ion chamber and its electronic system was observed, even for high intensity ^{40}Ar beams. The solid angle of the telescope was defined by measuring the distance of the first detector from the target and by measuring its active area optically and by α-particle measurements from a calibrated ^{241}Am source.

The proton double differential cross sections are shown in Fig. 3 for ^{20}Ne on U at 400 MeV/nucleon. The absolute cross sections are given with 20% uncertainty. The spectra have been corrected for reaction losses[4] and for losses due to scattering out of the detector (calculated

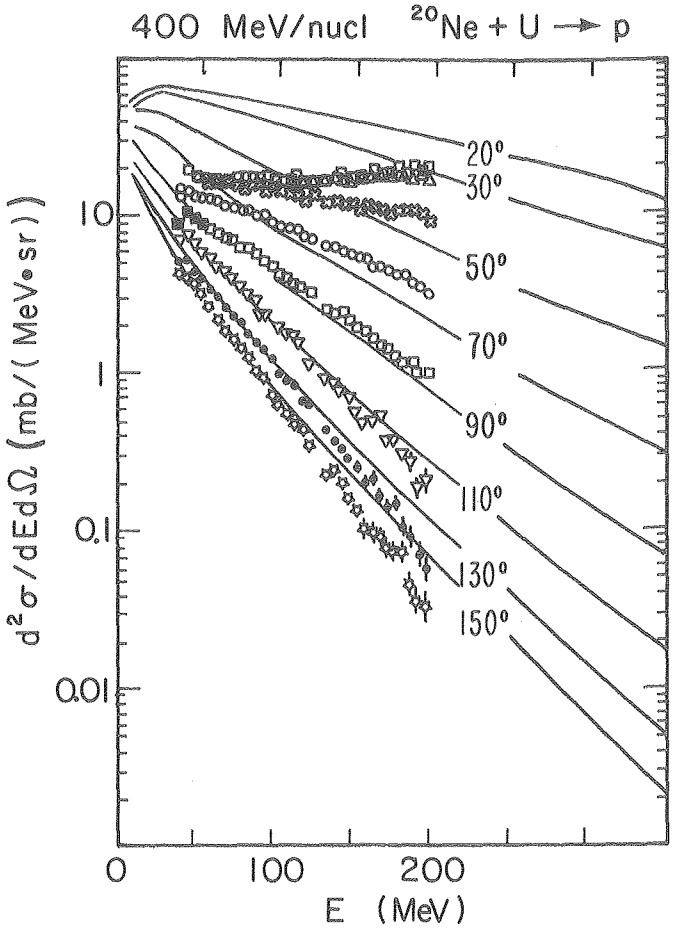

Fig. 3. Proton energy spectra in the laboratory at several angles with respect to the beam. The solid curves are the firestreak calculation.[6]
(XBL 787-1326)

with the code ANGLE).[5] The largest correction for protons at 200 MeV amounted to 25%. For the deuteron and triton spectra, the reaction losses were calculated for low energies (E_d < 30 MeV, E_t < 50 MeV) according to

$$R = \pi R^2 \left(1 - \frac{Z_1 Z_2}{E R}\right)$$

with

$$R = 1.43\ (A_1^{1/3} + A_2^{1/3}).$$

Above that energy, a constant value for σ_R was taken.

Comparisons with the firestreak model[6] show that the forward angle data are not described by the model, whereas at backward angles there is qualitative agreement. Good agreement is found when the data are compared with hydrodynamical calculations.[7] A more thorough test will be made when data selected on high multiplicity are compared with calculations of only small impact parameter collisions.

Footnotes and References

*Present address: DPN/ME, CEN Saclay, 91190 Gif-sur-Yvette, France.

†Present address: Institut de Physique Nucleaire, 91406 Orsay, France.

‡Present address: GSI, Darmstadt, W. Germany.

§Permanent address: Institut des Sciences Nucleaires, Grenoble, France.

1. Nuclear Science Annual Report, Lawrence Berkeley Laboratory Report LBL-6575 (1977), p. 147.

2. J. Gosset, H. H. Gutbrod, W. G. Meyer, A. M. Poskanzer, A. Sandoval, R. Stock, and G. D. Westfall, Phys. Rev. C 16, 629 (1977).

3. W. Holly, G. Schnurmacher, and A. Zingher, private communication.

4. D. F. Measday and C. Richard Serre, Nucl. Instrum. Meth. 76, 45 (1969).

5. K. G. R. Doss, private communication.

6. J. Gosset, J. Kapusta, and G. D. Westfall, Phys. Rev. C 18, 844 (1978).

7. A. A. Amsden, A. S. Goldhaber, F. H. Harlow, and J. R. Nix, Phys. Rev. C 17, 2080 (1978).

PION PRODUCTION IN RELATIVISTIC HEAVY-ION COLLISIONS

K.L. Wolf, J. Gosset,* H.H. Gutbrod, J.-C. Jourdain,† C.H. King, G. King, Ch. Lukner,‡ W.G. Meyer, Nguyen Van Sen, A.M. Poskanzer, A. Sandoval, R. Stock, and G.D. Westfall

With the equipment described,[1] low energy positive pion spectra with their associated charged particle multiplicities have also been measured. Stopped π^+ mesons were separated from π^- with a pion-positron delayed coincidence requirement for the decay sequence

$$\pi^+ \xrightarrow{25\ \text{nsec}} \mu^+ + \nu$$

and

$$\mu^+ \xrightarrow{2.2\ \text{sec}} e^+ + \nu + \nu$$

taking place in the germanium crystals. Decay curves characteristic of the muon's 2.2μ sec muon lifetime were observed in time spectra collected during data acquisition. The π^+ energy spectra were corrected for chance coincidences, multiple scattering losses, reaction losses, escape of positrons from detector surfaces, target thickness and energy of the μ^+ decay. Losses due to decay in flight are small and, according to calculations, are largely compensated by in-scattering of muons.

Examples of π^+ spectra obtained in this study are shown in Fig. 1(a) and (b) for ^{20}Ne on ^{238}U at projectile energies of 250 MeV/nucleon and 2.1 GeV/nucleon, respectively. It can be seen that laboratory angular distributions are nearly isotropic at 250 MeV/nucleon and are somewhat forward peaked at 2.1 GeV/nucleon, over the pion energy range measured here. The solid lines are the results of the nuclear firestreak calculation.[2] Good agreement is obtained for the magnitude of the cross sections, which vary a factor of ≈50 between the two bombarding energies. At 2.1 GeV/nucleon, the rather flat spectra are reproduced by the calculation over the limited pion energy range measured. However, at 250 MeV/nucleon the spectra are more sharply peaked than predicted, possibly indicating the need for a more microscopic calculation, like the independent particle (nucleon-nucleon) model of Bertsch[3] or the similar calculation of Jakobsson et al.,[4] which includes the readsorption of pions. The effects of nucleon-nucleon collisions in pion production should be more easily observed for a light target in which the effect of pion absorption and multiple scattering is minimized. In fact, pion inclusive spectra for the ^{20}Ne + ^{27}Al reaction at 400 MeV/nucleon are very similar in the regions of target and projectile rapidities to the pion data of Cochrane et al.[5] for the 730 MeV proton-induced reactions on hydrogen and carbon. The rapidity plot in Fig. 2 for the ^{20}Ne + ^{27}Al reaction shows cross section contours at low $P_\perp$ around the target and projectile rapidities, corresponding to these spectator sources. Figure 3 shows the result of gating the spectra on high associated multiplicity involving more central collisions, which enhances the intermediate rapidity region.

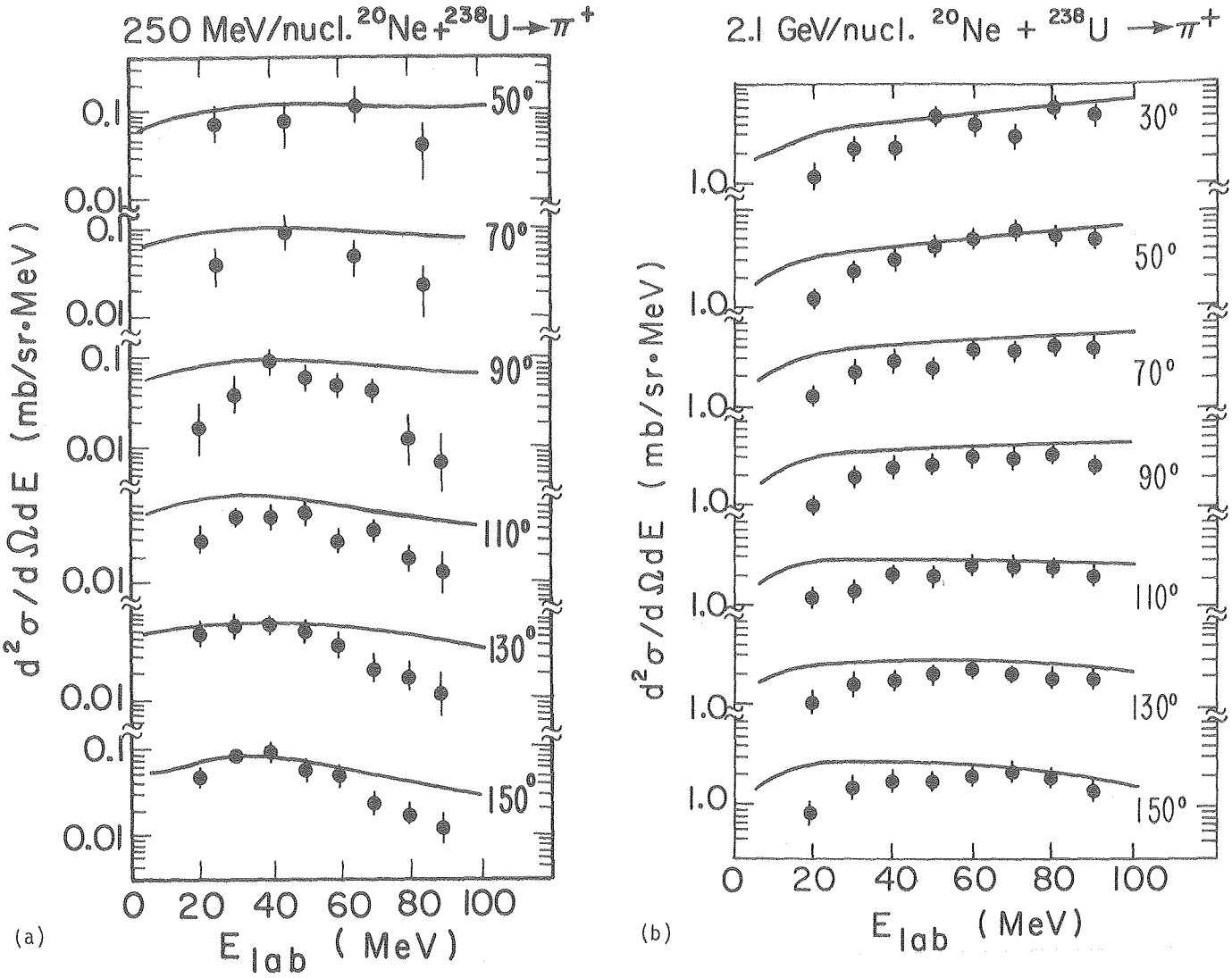

Fig. 1(a,b). Pion double differential cross sections in the laboratory frame. Solid curves are results of a firestreak calculation[2] with no renormalization. [(a) XBL 787-1317; (b) XBL 787-1318]

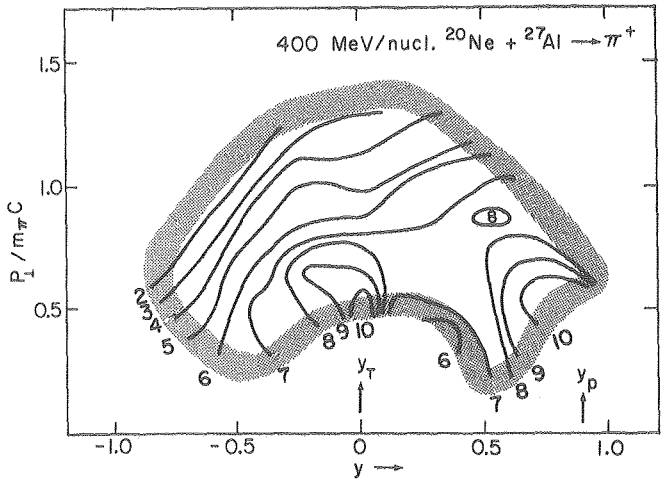

Fig. 2. Contours of Lorentz invariant cross section (E/p^2) $(d^2\sigma/d\Omega dp)$ [mb/(sr x MeV^2)] x 10^4 for pions as a function of transverse momentum and rapidity, y. (XBL 787-1336)

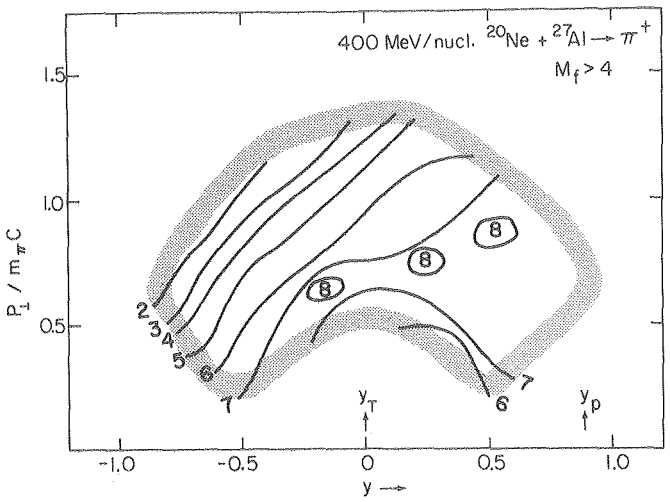

Fig. 3. The same as Fig. 2, but gated on the upper half of the associated charged particle multiplicity observed in 50 paddles. Cross sections are multiplied by a factor of two for comparison. (XBL 787-1337)

Footnotes and References

*Present address: DPN/ME, CEN Saclay, 91190 Gif-sur-Yvette, France.

†Present address: Institut de Physique Nucleaire, 91406 Orsay, France.

‡Present address: GSI, Darmstadt, W. Germany.

§Permanent address: Institut des Sciences Nucleaires, Grenoble, France.

1. H. H. Gutbrod, J. Gosset, J.-C. Jourdain, C. H. King, G. King, Ch. Lukner, W. G. Meyer, Ngugen Van Sen, A. M. Poskanzer, A. Sandoval, R. Stock, G. D. Westfall, and K. L. Wolf, this Annual Report.

2. J. Gosset, J. I. Kapusta, and G. D. Westfall, Phys. Rev. C 18, 844 (1978).

3. G. F. Bertsch, Phys. Rev. C 15, 713 (1977).

4. B. Jakobsson, J. P. Bondorf and G. Fai, preprint (1978).

5. D. R. F. Cochrane et al., Phys. Rev. D 6, 3085 (1972).

CHARGED-PARTICLE MULTIPLICITIES OF RELATIVISTIC HEAVY-ION COLLISIONS

C.H. King, J. Gosset,* H.H. Gutbrod, J. -C. Jourdain,† G. King, Ch. Lukner,‡ W.G. Meyer, Nguyen Van Sen, A.M. Poskanzer, A. Sandoval, R. Stock, G.D. Westfall, and K.L. Wolf

Perhaps the most basic piece of information to be obtained from the study of relativistic heavy-ion collisions is the average multiplicity of fragments produced. We have been determining $\langle M \rangle$ as part of the analysis of data taken with the apparatus described.[1,2] This consists of a solid state telescope, which triggers a tag-counter array of 80 plastic scintillators in 4 azimuthal rings. The telescope was designed to measure double-differential, single-particle inclusive cross sections, but it can also be used as a counter for the passage of all charged particles above a lower energy threshold. Analyzing the data in this latter mode, the average multiplicity of charged particles can be determined in a straightforward way, since $\langle M \rangle = \sigma/\sigma_r$, where σ is the integral single-particle inclusive cross section and σ_r is the total reaction cross section. Average multiplicities determined in this manner, with a lower energy threshold of approximately 30 MeV/nucleon and integrated between laboratory angles 10^o and 180^o, are shown in Fig. 1 for the case of Ne + U at three energies.

Assuming clean-cuts between sharp spheres,[3,4] as in the nuclear fireball model,[5,6] the average number of protons participating in a heavy-ion reaction is

$$N_p = \frac{Z_{targ.}^{2/3} A_{proj.} + Z_{proj.} A_{targ.}^{2/3}}{\left(A_{proj.}^{1/3} + A_{targ.}^{1/3}\right)} .$$

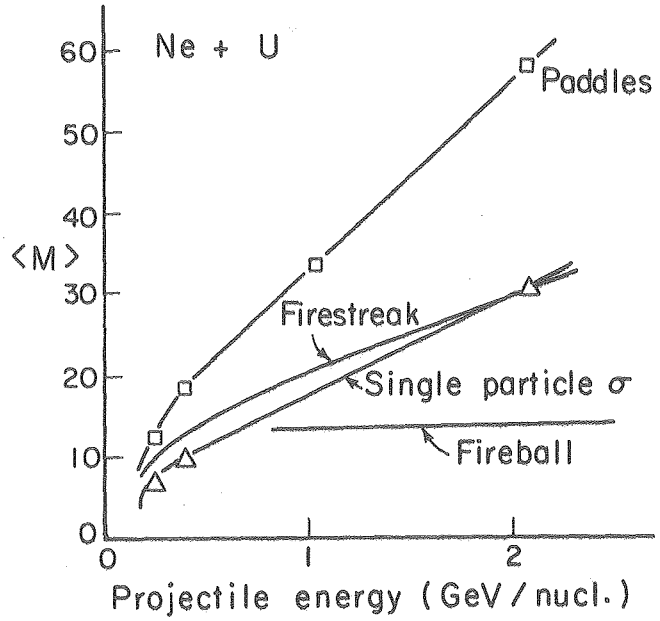

Fig. 1. Average charged particle multiplicities ⟨M⟩ for the Ne + U system as a function of the Ne projectile energy. Those determined from the single particle inclusive cross sections are indicated by triangles and compared with those determined from firestreak calculations as described in the text. The line labeled "firestreak" indicates the value of N_p, the number of proton participants for this projectile and target combination. The squares indicate the average multiplicities determined from the tag-counter array associated with a trigger particle at $\theta_{lab} = 90^o$. (XBL 787-1321)

As can be seen in Fig. 1, the measured multiplicities lie below N_p at 0.25 and 0.4 GeV/nucleon but rise at 2.1 GeV/nucleon to a value of about twice N_p. Our angular limits of integration and low energy threshold restrict the number of particles we observe, and this, as well as the formation of composites among the participants, can cause the observed multiplicity to fall below N_p. On the other hand, pion production and contributions from spectator protons will increase the charged particle multiplicity. Recently[7] calculations using the nuclear firestreak model[8] have been performed which, by assuming the equilibrium of nuclear reactions in the interaction region,[9] determine composite particle and pion cross sections as well as the proton cross section. In addition, some contribution from spectators is obtained by using diffuse surfaces on the projectile and target. The multiplicities determined from such calculations corresponding to our experimental energy threshold and angular range are shown in Fig. 1 and reproduce the trend of the measurements quite well.

Another measurement of multiplicity can be obtained from the plastic-scintillator array, which is sensitive to all charged particles with $E \gtrsim 25$ MeV/nucleon. However, it should be noted that this multiplicity may be different from that determined using the single-particle inclusive cross section, since it is the multiplicity associated with the telescope trigger. The average multiplicity was determined by adapting the standard techniques developed for γ-ray multiplicity measurements,[10] correcting for missing solid angle, coincidence summing, and accidental and deadtime probabilities, assuming uniform azimuthal distributions and no correlations in particle emission.

Average multiplicities ⟨M⟩ associated with all particles in the telescope at $\theta_{Lab} = 90^o$ are presented for various target-projectile combinations at four projectile energies in Fig. 2. The multiplicities are plotted vs the quantity N_p defined above. For the most part,

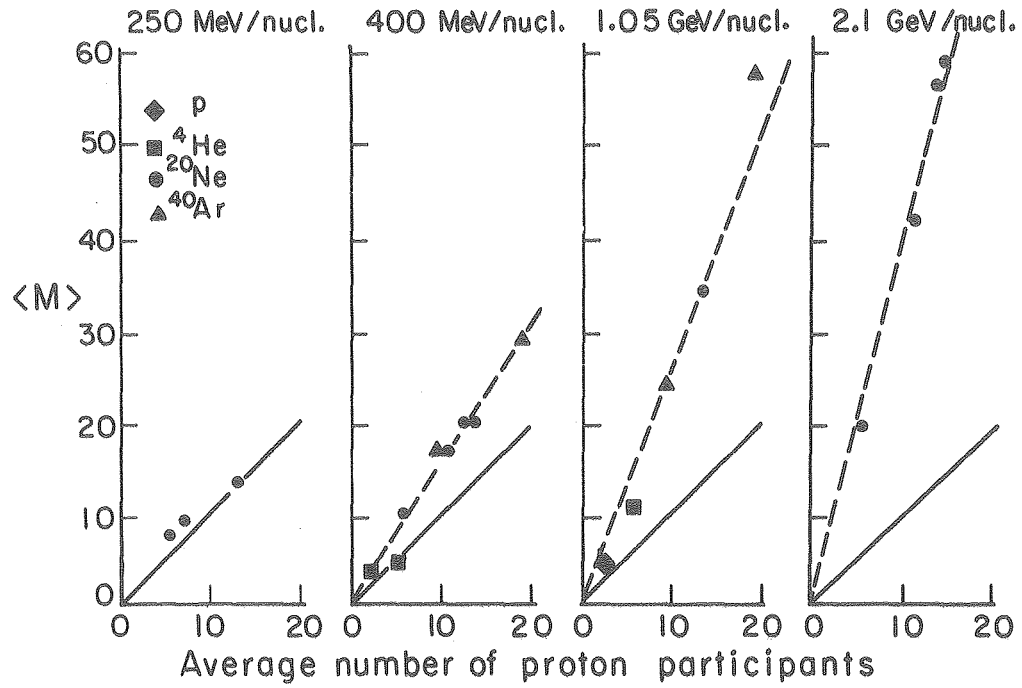

Fig. 2. The average multiplicity obtained from the tag-counter array plotted vs N_p, the average number of proton participants calculated from the fireball geometry. These are multiplicities associated with a proton in the telescope at 90° to the beam. Data from many different target-projectile combinations are shown at four bombarding energies. The dashed lines are to guide the eye through the data. The solid lines are drawn at 45° to represent the results expected from the fireball geometry. (XBL 787-1322)

the observed associated multiplicites fall along a straight line at all four projectile energies. However, the multiplicities determined from the tag-counter array are approximately a factor of two larger than those determined from the single-particle inclusive cross section as shown in Fig. 1 for the case of Ne + U. This presumably indicates that a trigger particle at $\theta_{Lab} = 90°$ strongly biases the observed event in favor of larger multiplicites and hence, presumably, more central collisions.

Footnotes and References

*Present address: DPN/ME, CEN Saclay, 91190 Gif-sur-Yvette, France.

†Present address: Institut de Physique Nucleaire, 91406 Orsay, France.

‡Present address: GSI, Darmstadt, W. Germany.

§Permanent address: Institut des Sciences Nucleaires, Grenoble, France.

1. J. Gosset et al., Lawrence Berkeley Laboratory Report, LBL-6575, p. 147.

2. H. H. Gutbrod, J.-C. Jourdain, C. H. King, G. King, Ch. Lukner, W. G. Meyer, Ngugen Van Sen, A. M. Poskanzer, A. Sandoval, R. Stock, G. D. Westfall, and K. L. Wolf, this Annual Report.

3. J. D. Bowman, W. J. Swiatecki, and C. F. Tsang, LBL-2908 (1973), unpublished.

4. J. Hüfner and J. Knoll, unpublished (1977).

5. G. D. Westfall et al., Phys. Rev. Lett. 37, 1202 (1976).

6. J. Gosset et al., Phys. Rev. C 16, 629 (1977).

7. J. Gosset, J. I. Kapusta, and G. D. Westfall, Phys. Rev. C 18, 844 (1978).

8. W. D. Myers, Nucl. Phys. A 296, 177 (1978).

9. A. J. Mekjian, Phys. Rev. Lett. 38, 640 (1977); Phys. Rev. C 17, 1051 (1978).

10. G. B. Hagemann et al., Nucl. Phys. A 245, 166 (1975).

SIGNATURES OF CENTRAL AND PERIPHERAL RELATIVISTIC HEAVY-ION INTERACTIONS

H.H. Gutbrod, W.G. Meyer, Ch. Lukner,* and A. Sandoval

The results of a recent experiment utilizing relativistic heavy ions from the Bevalac imply that low energy (1 to 5 MeV/nucleon) light particles ($4 \leq Z \leq 12$) arising from interactions of Ne projectiles with heavy targets (Ag, Au, U) are produced predominantly in central relativistic heavy-ion collisions and that fission fragments from targets such as U are only produced in peripheral interactions.

The experiment utilized a ΔE-E telescope consisting of a large volume methane gas ionization chamber ΔE detector and silicon surface barrier E detectors. In addition, an array of five silicon detectors was employed to measure the energy and correlation angle of coincident light and heavy fragments. In order to obtain a measure of the multiplicity of charged particles (above an energy of 25 MeV/nucleon) associated with observing a particle in the telescope, an array of 80 plastic scintillators coupled to photomultiplier tubes was used. The scintillators were arranged in three azimuthal rings as shown in Fig. 1.

It has widely been accepted in the field of relativistic heavy-ion physics that central and peripheral collisions can be distinguished by the charged particle multiplicity resulting from such collisions. Central collisions are violent and produce a large multiplicity of fast charged particles, which are emitted over all of 4π, and peripheral collisions are gentle and produce a very small multiplicity of fast charged particles, which are strongly forward focused.

Figure 2 shows three distinctively different associated charged particle multiplicity distributions. The distribution associated with a fission fragment at 90^0 in the laboratory shows a prominence of zero multiplicity events, whereas that associated with detecting a π^+, p, d, or t at the same laboratory angle shows a reasonable number of zero as well as high multiplicity events. In contrast to this, the distribution associated with observing an oxygen fragment at 90^0 displays a marked absence of zero multiplicity events with the highest mean multiplicity. Based on these observations, one can conclude that observing a low energy target fragment ($4 \leq Z \leq 12$) at 90^0 in the laboratory is on the average a signature of a central relativistic heavy-ion collision with heavy targets such as Au and U.

Preliminary analysis of the energy spectra and angular distributions of the detected fragments shows that oxygen fragments are being emitted from a system that is moving at a velocity ($\beta_{\parallel}$) approximately ten times faster than that of the fissioning nucleus. This observation supports the earlier assumption that more momentum is transferred from the projectile to the target

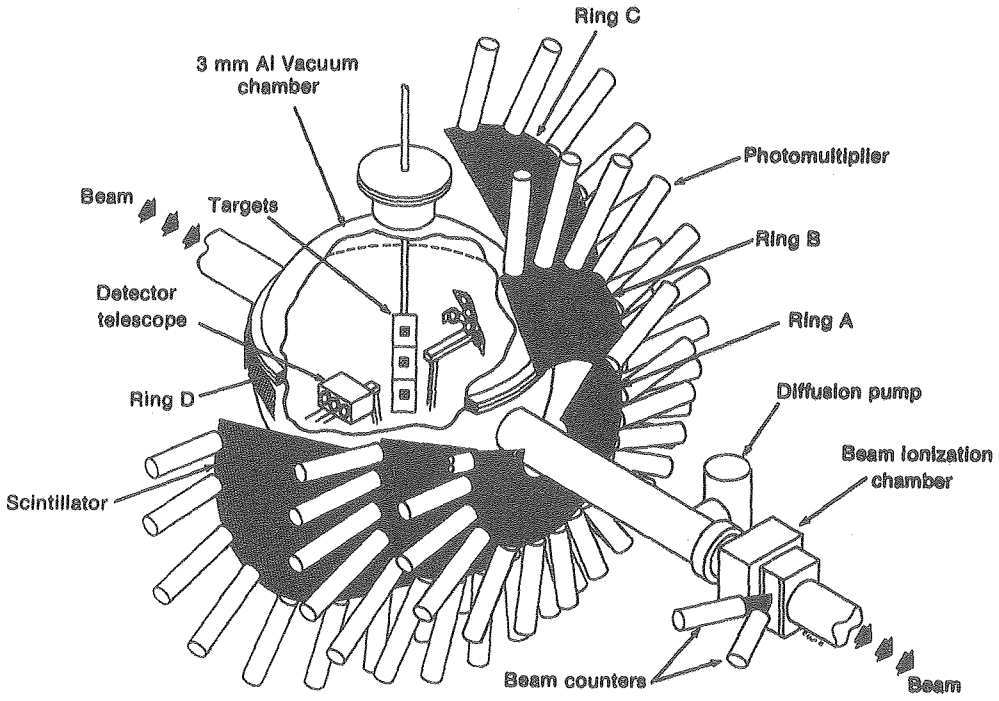

Fig. 1. The experimental arrangement.
(XBL 782-7229D)

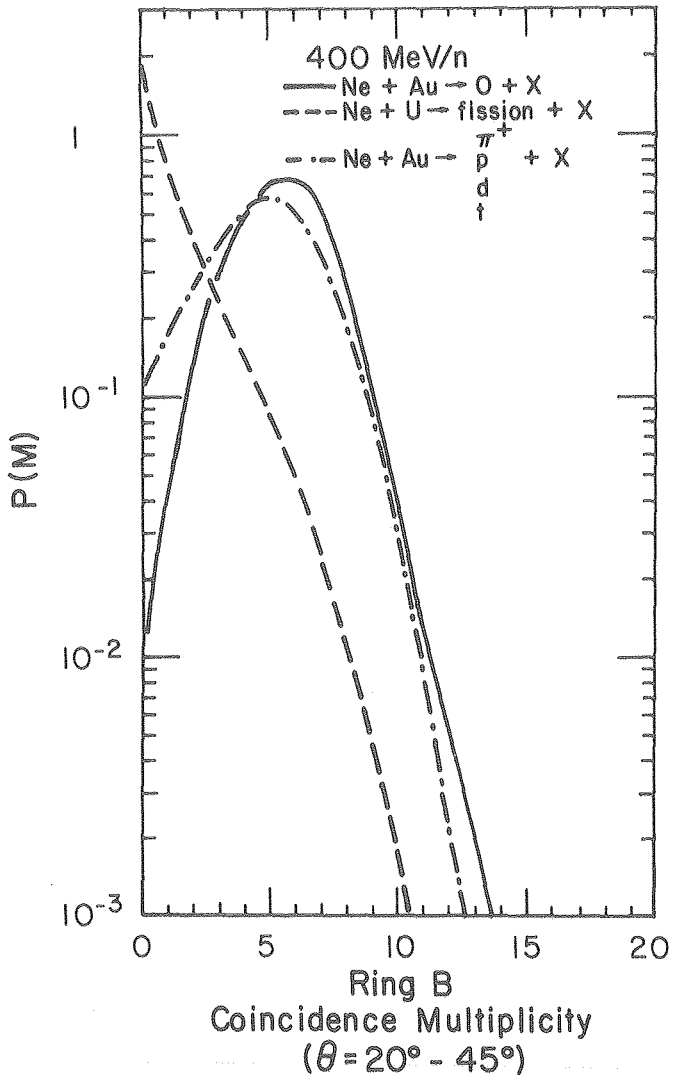

nucleus in central than in peripheral interactions. A quantitative determination of the velocities of the moving systems emitting the observed fragments will yield information concerning the mechanism of momentum transfer between the projectile and target.

The observed kinetic energy spectra of the fission products can be explained in terms of Coulomb-repulsion between the two fission fragments. However, the measured energy spectra for non-fission events cannot be explained in such a simple manner. For light targets such as Ag, the sum of the Z of the detected light fragment ($Z \leq 13$) and the number of charged particles detected in the multiplicity array almost equals the sum of the Z of the projectile and the target. Therefore, for light particles from a Ag target, there is no evidence for a complementary heavy fragment, thus ruling out the simple explanation of a very asymmetric fission-like process.

In-plane correlated emission is observed between slow heavy fragments ($Z = 26$) and fast charged particles detected in the multiplicity array. This correlation may be evidence for a collective interaction of target and projectile nucleons or it may be a result of multiple nucleon-nucleon scattering. It is hoped that further analysis of the data will answer this question.

Footnote

*Present address: Gesellschaft für Schwerionen-forschung Institut, Darmstadt, W. Germany.

Fig. 2. Multiplicity distributions associated with various fragments.

(XBL 787-1261)

STREAMER CHAMBER STUDIES OF CENTRAL COLLISIONS

A. Sandoval,* R. Stock,† J.V. Geaga, J.Y. Grossiord, and L. S. Schroeder

The large amount of single particle inclusive cross sections from relativistic heavy-ion interactions that have been measured in the last year has shown the need for more exclusive measurements to differentiate between models that have been put forward to describe them, and to get a signature from the early compressed stage in a central interaction.

The streamer chamber, with its 4π solid angle and 100% charged particle efficiency, is perfectly suited for doing such multiparticle correlations.

We have done a streamer chamber run for equal projectile and target mass by using Ar on KCl at 1.8 GeV/nucleon. About 4,000 pictures of interactions in the inelastic trigger mode were taken to define the bias of the main experiment, which consisted of about 15,000 pictures of central collisions (see Fig. 1). This central collision trigger was done by requiring a signal corresponding to at most two protons in the downstream scintillator. The events have been scanned for negative tracks; electrons and π^- and positive tracks; fast (minimum ionizing) and slow tracks. Multiplicity distributions for the central trigger are shown in Fig. 2. The mean π^- multiplicity was found to be 5.9, while the mean total charged particle multiplicity is 42.

For each interaction, the total charged particle multiplicity can be written as:

$$M_{tot} = Z_p + Z_t + 2\,M_\pi - \sum_i (Z_i - 1) M_{cluster_i} - Z_{n.o.} ,$$

the last two terms being the charge bound in clusters and the non-observed particles due to their low energy. From this we find that for the central trigger in the average we have 6 charges not accounted for, if we assume that all the observed tracks are single charged fragments.

The events are being measured and will be analyzed for π^- pair correlations.

Footnotes

*University of Marburg, Germany.

†Gesellschaft für Schwerionenforschung Institut.

MASS-INDEPENDENT CORRELATION OF FRAGMENT VELOCITY AND SOURCE VELOCITY IN NUCLEUS-NUCLEUS AND PROTON-NUCLEUS COLLISIONS*

P.B. Price and J. Stevenson

Thermal models[1-4] have been used to account for the fragment spectra seen in relativistic nucleus-nucleus and proton-nucleus reactions. In the "target fragmentation" regime, where fragments have $\beta \lesssim 0.3$, their angular and energy distributions bear some resemblance to Maxwellians viewed in a "recoiling source" frame, but several parameters are required to fit the spectra for a single fragment type,[4] and the relative yields of different fragment types have not been explained. Nevertheless, the term "evaporation" continues to be used in discussions of target fragmentation. We point out some important common features of energy spectra of light and heavy fragments from nucleus-nucleus and proton-nucleus reactions, and we indicate the difficulties these features pose for thermal models.

We have converted data from Refs. 4-8 into graphs consisting of contours of constant invariant cross section in momentum space. Figure 1 shows several examples. The labels on the contours give the log of σ_{inv} in $\mu b/sr(MeV)^2/c$.

The most remarkable feature of the graphs is the extremely isotropic emission of all fragments, in the appropriate moving frame, for the reactions at multi-GeV/nucleon energies. The best fits to the contours of constant σ_{inv} for the reactions 5.5 GeV p + U → X + anything and 2.1 GeV/nucleon Ne + U → X + anything are circles with centers on the positive $P_{||}$ axis. The centers of the circles move to increasing values of $P_{||}$ as the radii of the circles increase. For the 400 MeV/nucleon Ne + U fragment data the contours are approximately circular at angles larger than $\sim 60^0$, but there is an additional contribution to σ_{inv} at angles near the forward direction, as can be seen in Fig. 1(c). When we fit the data at large angles to circles, we find that their centers move along the positive $P_{||}$ axis to values that increase with their radii.

Figure 2 shows the correlations between β_S and β_r that we find from graphical analyses of four sets of single-particle inclusive reactions. For each reaction β_S is strongly correlated with β_r and there is no systematic shift of the correlation line with fragment mass. We interpret the correlations in Fig. 2 as follows. Collisions at various impact parameters produce excited, recoiling sources with a wide distribution of recoil velocities and masses. For each fragment the invariant cross section has its own dependence on β_S and β_r, not shown in Fig. 2. In the target fragmentation regime, a collision leading to a source with a given β_S results in isotropic emission of fragments with the same β_r. Figure 2 is a result of averaging over a large number of collisions at various impact parameters. The mechanism of fragment emission, in the regime $\beta_S \lesssim 0.2$, $0.1 \lesssim \beta_r \lesssim 0.4$, involves a characteristic radial velocity instead of a characteristic kinetic energy and is thus not primarily thermal in nature. (In thermal emission, particles should have the same distribution of kinetic energies, not of kinetic energy per nucleon or of momentum per nucleon.)

We have used the same graphical method to analyze the mass dependence of the correlation, β_S vs β_r, calculated from several models of nucleus-nucleus collisions. Neither the various forms of the fireball model[1] nor the firestreak model[2,3] can account both for the strong correlation of β_S with β_r, independent of fragment mass, and for the isotropic contours.

We conclude that target fragmentation appears to be a nonthermal process characterized by isotropic emission of fragments at radial velocities independent of fragment mass. One mechanism by which fragments of different mass might be ejected isotropically with the same radial velocity distribution would be through the hydrodynamic radial expansion of a compressed recoiling target.[8,9] It would be interesting to use a number of detectors at different angles to look for such nonthermal emission.

Footnotes and References

*Condensed from Phys. Lett. B 78, 197 (1978).

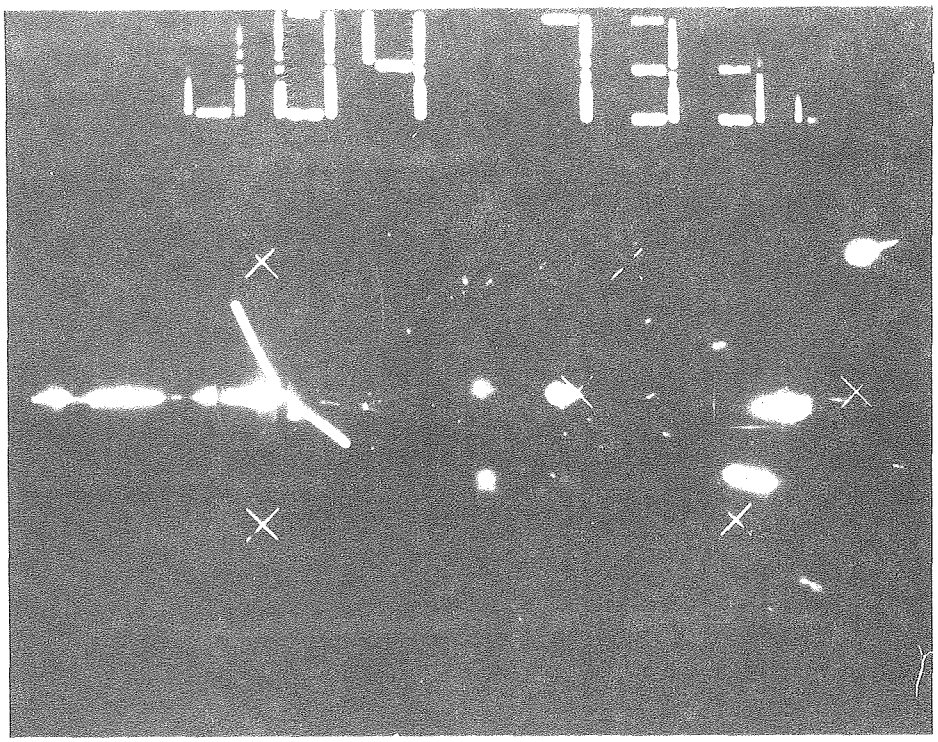

Fig. 1. Central collision of a 1.8 GeV/nucleon Ar in a KCl target. Negative tracks are bent up.
(CBB 785-5172)

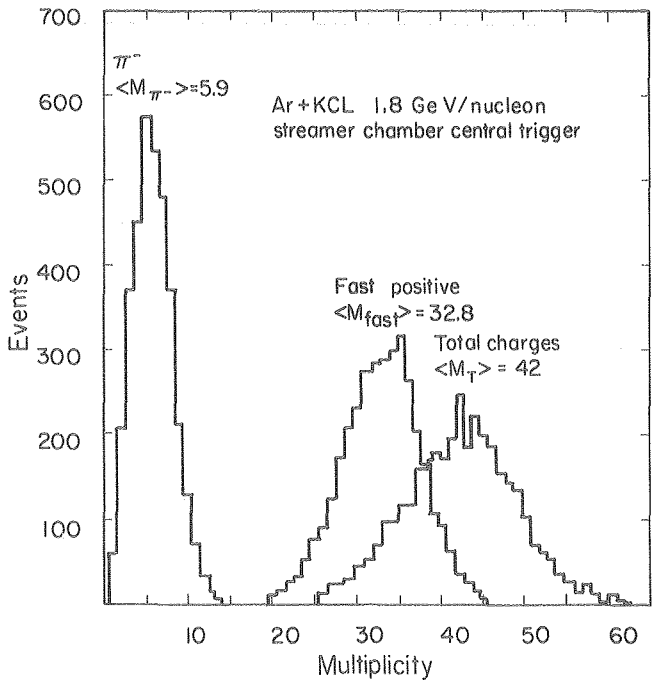

Fig. 2. Multiplicity distributions for the central collision trigger.
(XBL 788-1452)

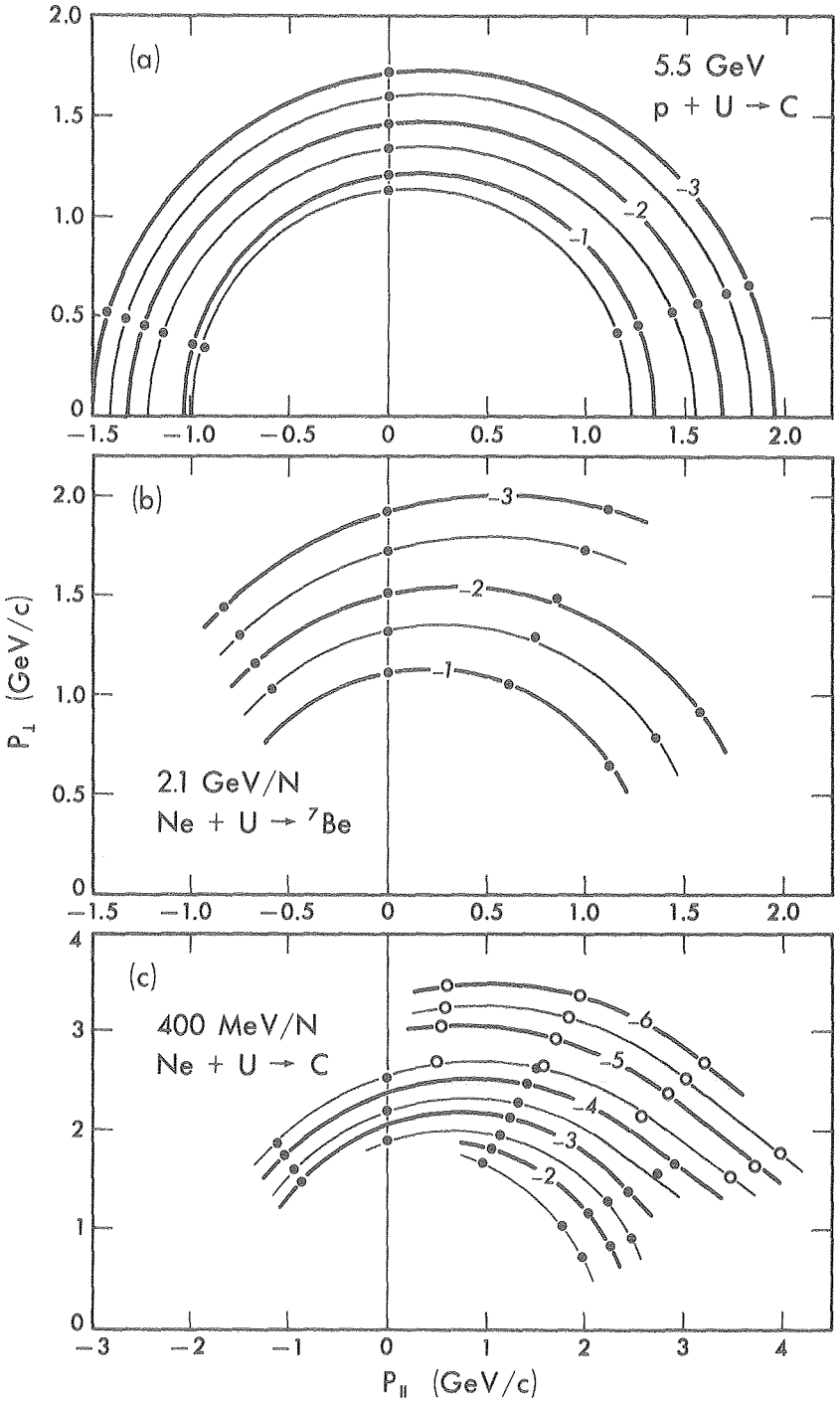

Fig. 1. Curves are arcs of circles except in (c) at angles less than 60^{0} and large momenta. Open circles in (c) are from data in Ref. 6; points in (a), (b), and (c) are from data in Refs. 4, 7, and 7, respectively.

(XBL 787-1276)

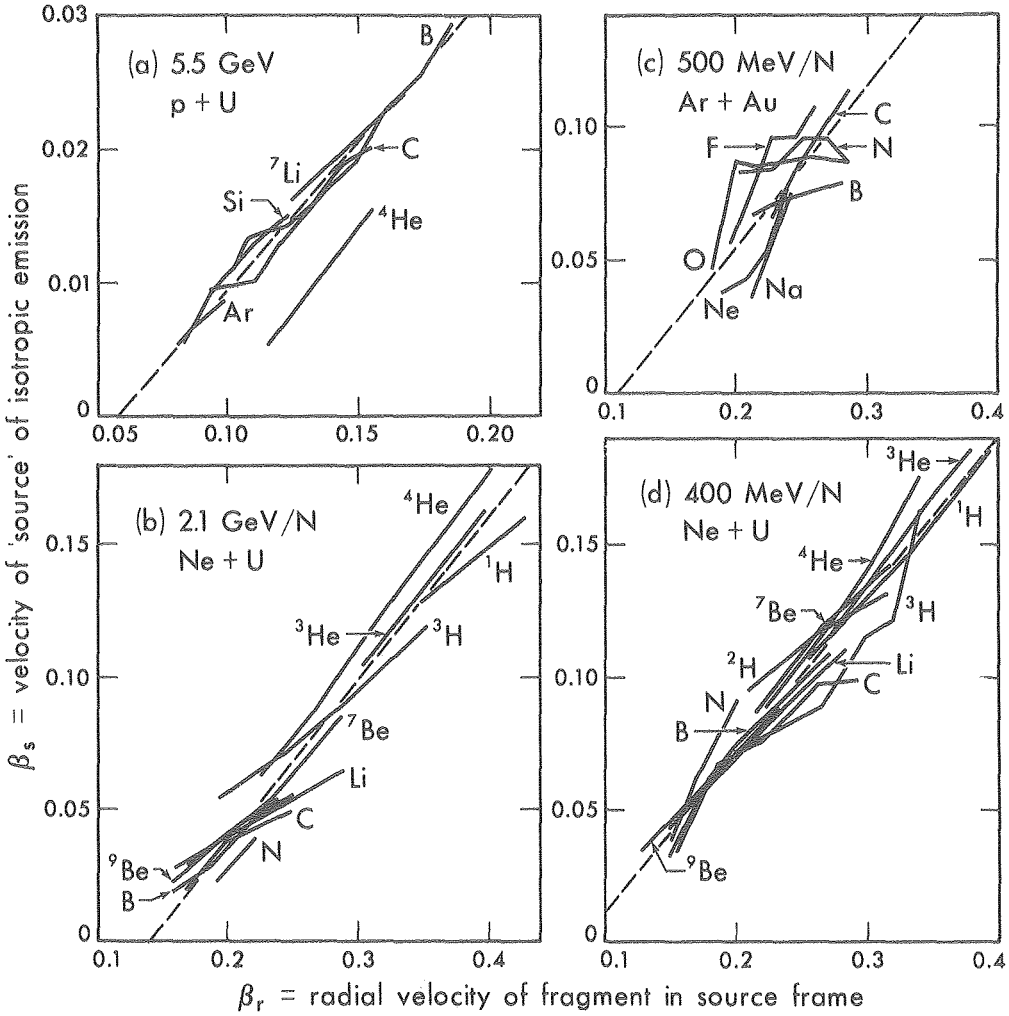

Fig. 2. Mass-independent correlations of β_s with β_r for various fragments and reactions. The dashed lines are least-squares lines.

(XBL 787-1277)

1. G. D. Westfall, J. Gosset, P. J. Johansen, A. M. Poskanzer, W. G. Meyer, H. H. Gutbrod, A. Sandoval, and R. Stock, Phys. Rev. Lett. 37, 1202 (1976).

2. W. D. Myers, LBL-6569 (1977).

3. J. Gosset, J. I. Kapusta, and G. D. Westfall, submitted to Phys. Rev. C.

4. A. M. Poskanzer, G. W. Butler, and E. K. Hyde, Phys. Rev. C 3, 883 (1971).

5. H. H. Gutbrod, A. Sandoval, P. J. Johansen, A. M. Poskanzer, J. Gosset, W. G. Meyer, G. D. Westfall, and R. Stock, Phys. Rev. Lett. 37, 667 (1976).

6. J. Stevenson, P. B. Price, and K. Frankel, Phys. Rev. Lett. 38, 1125 (1977).

7. J. Gosset, H. H. Gutbrod, W. G. Meyer, A. M. Poskanzer, A. Sandoval, R. Stock, and G. D. Westfall, Phys. Rev. C 16, 629 (1977).

8. J. D. Stevenson, Ph. D. thesis, University of California, Berkeley, November 1977.

9. J. P. Bondorf, S. I. A. Garpman, and J. Zimànyí, Nucl. Phys. A 296, 320 (1978).

DETECTION OF MASSIVE UNSTABLE PARTICLES IN INCLUSIVE TRANSVERSE MOMENTUM SPECTRA*

E. M. Friedlander

For the last two decades, the distribution of the transverse momentum component p_T of secondaries from high energy hadronic collisions (abbreviated hereafter as p_T-spectra) has provided valuable information about the mechanism of multiple particle production, especially after the discovery of a specific "large-p_T behavior" at the CERN ISR.

In the innumerable investigations of this subject, p_T-spectra have always been treated as essentially smooth curves and all model predictions tested against experiment[1,2] have been equally smooth. Actually, one wonders why p_T-spectra should have been thought of as smooth in the first place. Indeed we know that a large fraction of the pions or kaons observed in the final state arise from the decay of short-lived intermediate states, many of which have two-body decay channels with non-negligible partial widths.

The aim of this work is to draw attention to the fact that in measurements at 90° CMS, especially of the kind carried out at the CERN ISR,[3,4] decay products from short-lived massive objects (abbreviated hereafter as SMO) will produce structures in the p_T-spectra which can be used to detect the parent particle. Indeed some evidence of such effects is already at hand.

If the SMO is created at rest it is obvious that its decay will produce tertiaries (say, pions) with a δ-type p_T-spectrum, say, $\delta(p_T - p_C)\, dp_T$. At first sight it might seem that the angular and momentum distribution of the parent SMO will wash out this sharp line. This, however, is not so. Indeed, all particle production spectra are steeply falling. Furthermore, decay kinematics allow observation of tertiaries at 90° CMS only for a very restricted range of (low) rapidities of the SMO. As a result, it can be shown that the spectrum of tertiaries at 90° is always peaked at a momentum close to p_C. If the SMO mass M* is relatively low (as is, e.g., the case of ρ or ϕ mesons) the peak in the 90° pion or kaon spectrum will be located in a region where it is drowned in the continuum. However, for really massive particles like, the G-meson or the charmed D-meson, the decay momentum p_C is so high that, even with an unfavorable phase-space and/or branching ratio to two-body decay, the D-decay can become competitive to the point when it is able to distort the slope of the (steeply falling) continuum.

Figure 1(a) shows the 90° p_T-spectrum of pions from $D \to \kappa + \pi$ decay obtained by Monte Carlo. D-mesons were produced in a $\sqrt{s}$ = 53 GeV p-p collision with a flat rapidity distribution and a "reasonable" transverse momentum distribution. It is obvious that a sharp peak in the pion spectrum is present close to p_C. A change to

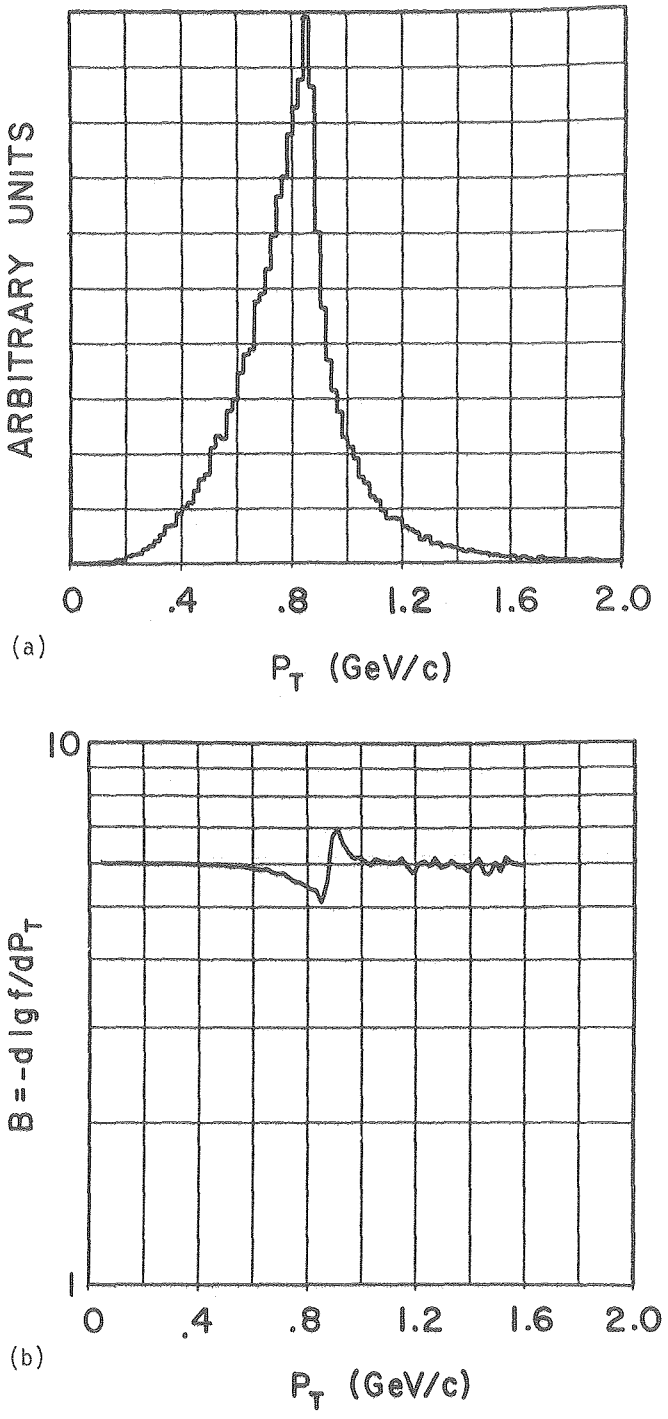

Fig. 1. (a) Pion spectrum at 90° CMS expected from $D \to \kappa + \pi$ decays (arbitrary units).
(b) Logarithm slope of a pion spectrum resulting from superposition of 0.002% $D \to \kappa + \pi$ [Fig. 1(a)] and of a pion continuum falling like $\exp(-6p_p)$.
[(a) XBL 787-9646 (b) XBL 787-9647]

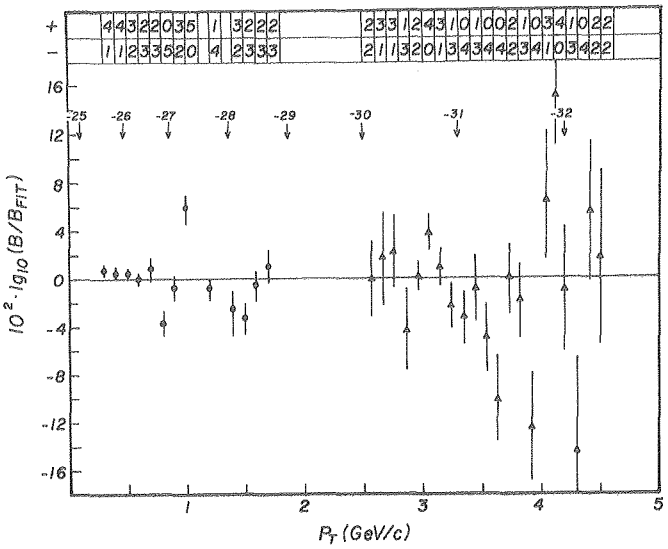

Fig. 2. Deviations from an exponential fit of the logarithmic slopes of pion spectra measured at the CERN ISR; circles = $\pi^{\pm}$, weighted mean from runs at $\sqrt{s}$ = 23, 31, 45, 53, and 63 GeV; triangles = π^0, weighted mean of runs 23, 31, 45, and 53 GeV; numbers on top of each experimental point show how often positive (+) and negative (-) deviations occurred in the different runs.
(XBL 787-9648)

isotropic D-production in the pp CMS only enhances the sharpness of the peak.

Figure 1(b) shows the distortion produced by this decay spectrum when it is superimposed on an exponential pion background 5000 times richer in particles.

Obviously, the heavier the hypothetical SMO, the better a chance it stands to pierce the background.

As to existing experimental evidence, Fig. 2 shows a summary of pion spectra observed at the ISR for $\sqrt{s}$ going from 21 to 63 GeV. The logarithmic slope

$$B \equiv \frac{d}{dp_T} \ell n \left(E \frac{-d^3\sigma}{dp^3} \right)_{y=0} \qquad (1)$$

is plotted against p_T. The measurements cover the range 0.2-5 GeV, over which the continuum intensity (indicated by decimal logarithms of the differential cross section above the arrows) drops by 7 orders of magnitude. The points are weighted averages from a) 5 $\sqrt{s}$-values below 2 GeV (charged pions);[3] b) 4 $\sqrt{s}$-values (neutral pions) above 2 GeV.[4] A significant "wiggle" is seen in the charged pion spectrum at the value predicted for the decay of the D-meson (~0.85 GeV/c). The numbers on top of Fig. 2 show the frequency of positive and negative deviations from an exponential fit in the independent runs with different values of $\sqrt{s}$. The obvious non-random behavior of these numbers at the "wiggle" is independent proof for statistical significance of the latter.

The absence of a similar "wiggle" in the proton spectra (χ^2/n = 14/10) measured with the same experimental setup proves that B is not distorted by errors in the momentum calibration.

The π^0-spectrum shows evidence for at least two "wiggles" which, if taken at face value and assigned to two-body decays of new, hypothetical SMOs would place these in the mass range of M* ≈ 7-9 GeV.

This raises the urgent need for a new generation of high accuracy p_T-experiments.

Footnotes and References

*Condensed from a paper to be submitted to Phys. Rev. Lett.

1. Recent review of large p_T phenomena where the data are compared only with constituent model predictions can be found in S. D. Ellis and R. Stroynowski, Rev. Mod. Phys. 49, 753 (1977).

2. E. M. Friedlander and R. M. Weiner, LBL-7724.

3. B. Alper et al., Nucl. Phys. B 100, 237 (1975).

4. F. Busser et al., Phys. Lett. B 46, 471 (1973).

STATISTICAL INFERENCE FROM INCLUSIVE SPECTRA IN MULTIHADRON PRODUCTION: A CAVEAT*

E.M. Friedlander

In 1969 Feynman[1] suggested that some of the difficulties involved in the analysis of final states induced by very high energy beams and involving multiple emission of particles might be circumvented by focusing attention on one secondary only and ignoring the multitude of final states associated with it. The hope that such "inclusive" processes, symbolized by

$$a + b \to c + \text{"anything"} \quad , \tag{1}$$

where "anything" might indeed imply anything from 1 to, say, 100 secondaries, might yield pertinent information on fundamental physical facts has since motivated innumerable experiments of this kind.

The aim of the present paper is to draw attention to the fact that, in principle, at least, this hope has been vain, to the extent that statistical inference based on counts of "c"-particles is impossible without the very knowledge about the "anything" term in Eq. (1) which one tries to ignore in an inclusive measurement. Whether the incertitude induced by this ignorance in the conclusions drawn from an inclusive measurement matters or not from a practical viewpoint depends essentially on both the physics of "anything" and the experimental arrangement, and must be decided on a case-to-case basis.

At the root of the trouble lies the fact that basic counting statistics, investigated and established a few decades ago in the study of radioactive (e.g., α, or β) decays involving the emission of single particles have been mechanically transplanted into the analysis of processes leading to multiple particle emission where their use is no longer automatically justified.

In any "spectral" measurement we pick out some numerical characteristic θ of the particle (e.g., its angle of emission, momentum, etc.) and try to estimate the elementary probability p for θ to fall within a given range of values.

If a single particle is emitted in each event and the number m of events occurring in any given time interval is distributed according to the Poisson law

$$W(m/M) = \exp(-M)\, M^m/m! \quad , \tag{1}$$

the probability h(k) of detecting exactly k events in the same interval is

$$h(k) = \exp(-Mp)(Mp)^k/k! \quad , \tag{2}$$

i.e., in this case the number k of counts recorded in a given spectral interval described by p is also Poisson distributed about a mean

$$K \equiv \langle k \rangle = Mp \quad . \tag{3}$$

Hence the relative standard deviation ε_k of k is

$$\varepsilon_k^2 = 1/K \quad . \tag{4}$$

If, however, n particulates are emitted in each event and

$$r \equiv nm \tag{5}$$

is the (random) number of particles produced in any given time interval, h(k) is again formally given by an equation similar to (2),

$$h(k) = \sum_{r=k}^{\infty} W_1(r|M,n)\, B_1(k|r,p) \quad , \tag{6}$$

but now W_1 is no longer a Poisson distribution even if W is, and B_1 may or may not be binomial (see below).

It is obvious that, strictly speaking, statistical inference about p, say, obtaining a confidence interval with a given probability level, requires explicit knowledge of h(k). Even in the simplest cases h(k) cannot be obtained in closed form (except, of course, for n = 1!).

Figure 1 shows the result of numerical evaluation of h(k) for p = 0.1. The curves are for successive (constant) multiplicities n of 1 (the Poisson case), 2, 4, 8, and 16. M was adjusted so as to keep the mean of k constant at K = 30. With increasing n the curves get considerably broader than the Poisson distribution with the same mean.

Further complications (often essential) arise from the facts that

(a) n is itself a random variable distributed more or less widely about some mean value N; its probability law P(n) called the multiplicity distribution (or the set of normalized topological cross sections) cannot be derived from "first" statistical principles but belongs to the physics of the particle-producing process.

(b) The emitted particles are not independent (if only because of conservation laws) and B_1 is never a truly binomial distribution.

(c) p may not be a constant but may, and often does, depend on the value of n.

Consider again a time interval t in which a (random) number m of events have been produced in the target. Denote by x_i (i = 1,2,. . .,m) the number of counts recorded by a given detector from the ith event. Then (with $X \equiv \langle x \rangle$),

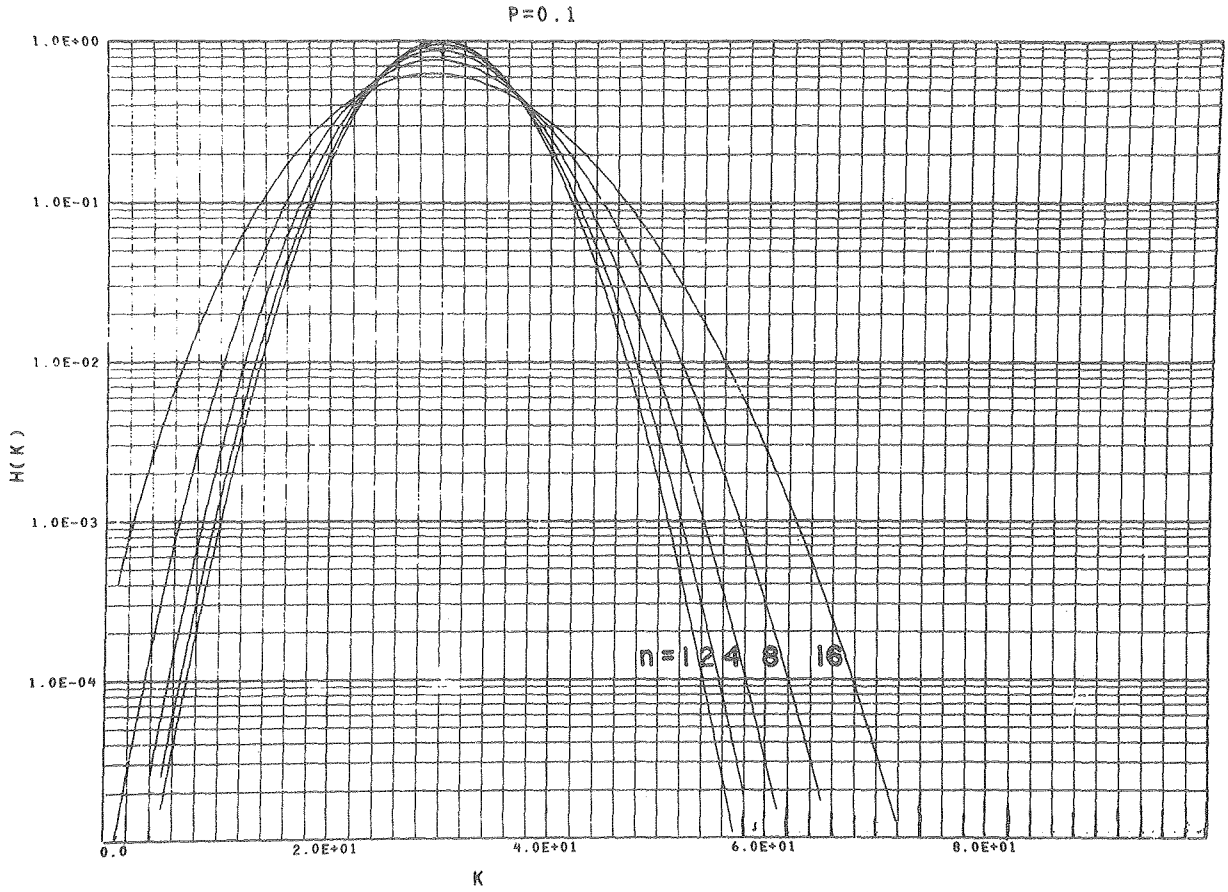

Fig. 1. h(k) for fixed n-values at p = 0.1.
(XBL 786-9386)

$$k = \sum_{i=1}^{m} x_i \quad , \quad K = MX \quad , \qquad (7)$$

and it can be shown that

$$\varepsilon_k^2 = (1/K) \times (1 + \varepsilon_x^2) \quad . \qquad (8)$$

Comparing Eqs. (4) and (8) we see that in order to reach the same accuracy ε_k as in the case of a Poisson distribution (n = 1) with the same mean (K) we have to increase the measuring time by a factor

$$\tau \equiv K\varepsilon_k^2 = X(1 + \varepsilon_x^2) \quad . \qquad (9)$$

X and τ are the criteria by which we can judge the relative merits or shortcomings of different experimental situations. In particular, we shall call biased any situation leading to X not being simply proportional to p.

Table 1 answers the questions: 1) is the estimate biased?; 2) are the errors larger than the Poisson errors?

A look at Table 1 shows that, in principle at least, the situation is hopeless. No experimental device is both unbiased and "Poisson." Indeed, we seem to be faced with a typical case of Murphy's law since a single counter (case b) which presents no difficulty in collecting almost unlimited statistics is "Poisson" anyway, while a bubble chamber (case a) where both picture taking and scanning are a slow and painstaking process have errors much in excess of the Poisson one and need considerably improved statistics in order to reach a given accuracy.

An interesting case is that of measurement of an angular asymmetry. If the two complementary space regions have contained k_1 and k_2 particles, respectively, the usual symmetry coefficient α is

$$\alpha = (k_1 - k_2)/(k_1 + k_2) \quad . \qquad (10)$$

If $\alpha^2 \ll 1$, i.e., when one checks an apparently symmetrical distribution for the presence of a slight asymmetry

$$\tau_\alpha \cong (NC_2 + 1)/2 \quad . \qquad (11)$$

For example, for pp collisions at 200 GeV, N = 7.65, C_2 = 1.258, and τ_α = 5.31; in other words, more than five times more events are necessary in order to show that a significant asymmetry is present than would have been necessary, e.g., in the case of μ-e decay!

As to the bias of estimates from single counter measurements, let us assume that an energy spectrum is measured, which is expected to behave exponentially with a mean value corresponding to some "temperature" T. Then the apparent temperature T' derived by taking the observed counts at face value is related to the true temperature (e.g., in the case of nuclear collisions of relativistic heavy ions) by

Table 1. Are "unpleasant" effects present in X/τ ?

	Multiplicity Distribution			
	n = const.		P(n)	
Method of detection	n = 1	n ≠ 1	$\partial p/\partial n = 0$	$\partial p/\partial n \neq 0$
Visual	no/no	no/yes	no/yes	yes/yes
Single counter (ν=1)	no/no	yes/no	yes/no	yes/no
Hodoscope counter (ν>1)	no/no	yes/yes	yes/yes	yes/yes

$$T' \cong T(1 + 53p) \quad . \qquad (12)$$

For p as low as 1% it is seen that T' is in error by ~50%. It is obvious that such biases may play an important part in comparing inclusive spectra with theoretical expectations.

Which of the (admittedly extreme) situations discussed above represents the lesser evil depends on the kind of conclusions one would like to draw from the experiment and becomes to a large extent a matter of taste. In the author's opinion the safest bet is still visual recording which is unbiased and where selected fixed topologies make the $\partial p/\partial n \neq 0$ mess easy to avoid.

Footnote and Reference

*Condensed from a paper submitted to Hadronics, LBL-7733.

1. R. P. Feynman, Phys. Rev. Lett. 23, 1415 (1969).

EVIDENCE ON THE TIME SCALE FOR PION EMISSION IN RELATIVISTIC HEAVY-ION COLLISIONS

J.O. Rasmussen and J. Sullivan

An important question for many processes associated with relativistic heavy-ion collisions is the time scale for emission of energetic particles from the collision zone. Will the spectator pieces move free of the hot matter before significant particle emission, or will the spectators be bathed in particles from the explosion? In the latter case the spectators will receive higher excitation energy and will modify the primary distributions of particles from the "fireball."

We believe the π^+ inclusive spectra for 800 MeV/nucleon neon bombardments[1] support a fast time scale of π^+ emission because there appears a (3,3) resonance shadowing effect in the plots of invariant cross sections in the rapidity vs $p_\perp$ plane. The (3,3) resonance in the pion-nucleon system shows up not only in the pion-nucleon scattering but also in various pion nucleus reactions.

Sternheim and Silbar[2] have reproduced Cochran's pion production data[3] from 730 MeV protons on nuclei by a simple model calculation. The double-differential cross sections in the model come from the fundamental nucleon-nucleon distribution modified by absorptive passage of protons and pions in the nuclear medium. An empirical linearly energy-dependent mean free path for pions is assumed and constants fitted. (See the recent re-examination of the problem by R. Landau.)[4] The pion interaction cross section in the nuclear medium is a rising function below the (3,3) resonance due to the predominantly p-wave nature of the interaction dominated by the $\Delta(1232)$.

Low energy π^+ production differential cross sections with a 800 MeV/nucleon ^{20}Ne beam show an unusual structure. For Pb targets there seems to be a dip in the cross section around 90^o in the lab system. For the nearly equal mass NaF target the contour plot of the Lorentz-invariant cross section for π^+ shows a forward-backward peak around 100 MeV (c.m.). This feature is quite similar to the $p + P = \pi^+ + X$ data of

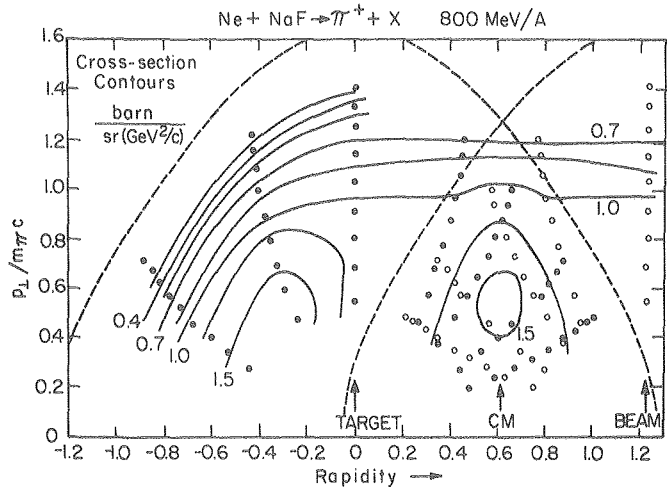

Fig. 1. Contour plot of Lorentz-invariant cross sections for π^+ production by 800 MeV/nucleon ^{20}Ne on NaF. The horizontal scale is rapidity y in the laboratory frame, and the vertical is perpendicular momentum $p_\perp/m_\pi c$. Projectile and center-of-mass rapidities are indicated. The dashed lines represent the 230 MeV/c resonance absorption loci in target and projectile spectator matter. (XBL 788-5510)

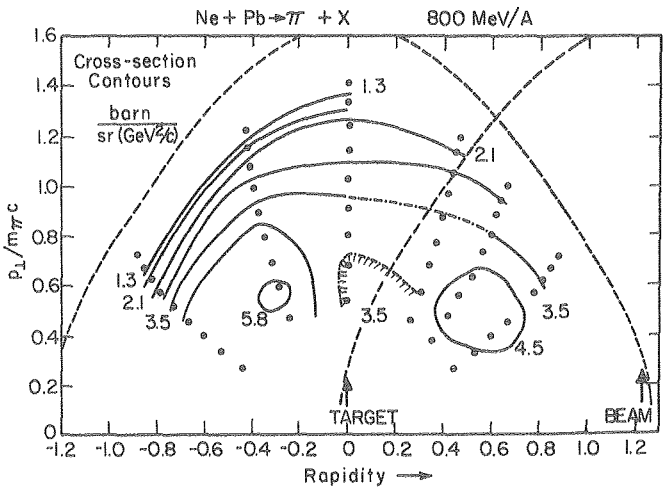

Fig. 2. Same as Fig. 1 except for Pb target (XBL 788-5511)

Cochran et al.[3] at 730 MeV bombarding energy. Thus, for this system most of the pions have not suffered collisions to lose the memory of their energy and angle at formation. What bears on the time-scale problem is the apparent suppression of pions with speeds near the (3,3) resonance in the projectile and target frames.

Figures 1 and 2 are rapidity vs $p_\perp$ contour plots of inclusive π^+ spectra for NaF and Pb targets, respectively. The dashed lines are the loci of the (3,3) resonance centered in the target and projectile frames. The correspondence of these loci with the valleys is evident, although the valley lies at ~230 MeV/c rather than the 280 MeV/c of the free-space resonance. This shift is close to that noted in pion-nucleus total cross sections by Cooper.[5]

Thus, the evidence is that pion emission occurs on a fast time scale with substantial shadowing effects by spectator matter. Future theoretical work needs to take these spectator effects into account.

References

1. K. Nakai, V. Chiba, I. Tanihata, S. Nagamiya, H. R. Bowman, J. G. Ioannou, and J. O. Rasmussen, Proc. Int. Conf. Nucl. Struct. (contributed paper) Tokyo, 1977.

2. M. M. Sternheim and R. R. Silbar, Phys. Rev. D 6, 3117 (1972); Phys. Rev. C 8, 492 (1973).

3. D. R. F. Cochran, P. N. Dean, P. A. M. Gram, E. A. Knapp, E. R. Martin, D. E. Nagle, R. B. Perkins, W. J. Shlaer, H. A. Thiessen, and E. D. Theriot, Phys. Rev. D 6, 3085 (1972).

4. R. H. Landau, Phys. Rev. C. 17, 2144 (1978).

5. M. D. Cooper, Am. Inst. Phys. Conf. Proc. 33 (Meson-Nuclear Physics, Carnegie-Mellon, 1976), p. 237.

PION PRODUCTION NEAR THRESHOLD IN HEAVY-ION COLLISIONS*

G.M. Crawley,† W. Benenson,† G. Bertsch,† E. Kashy,† J.A. Nolen,† J.O. Rasmussen, M. Koike,‡ H. Bowman, M. Sasao, J. Ioannou, M.C. Lemaire,§ J. Sullivan, and L.F. Oliveira‖

The production of pions in heavy-ion collisions in the energy range 100-400 MeV poses interesting problems for theorists and experimentalists alike. The interest in this energy range stems from the possibility of having a strong interpenetration of the two nuclei (with a density increase of a factor of 2) without masking possible collective effects associated with high nuclear densities. Another interesting aspect is that the threshold for significant pion production in free nucleon-nucleon collisions (~280 MeV/A) is encompassed by this energy region. According to current theoretical ideas on pion-nucleon interactions, nuclear matter is not far from a phase transition involving the pion field (pion condensation).[1] Models for the behavior of the pion in nuclear matter show peculiarities such as a near-zero or negative effective mass for the pion.[2] Under such conditions, pions can be produced in the interactions of nucleons with the potential field,[3] in addition to production in the collision of nucleons with each other. The rate of pion production is thus increased by the potential field mechanism.

On the experimental side, the emulsion studies on the pion production cross section at energies near threshold is conflicting. In one case a very high pion multiplicity per collision is reported;[4] but more recent experiments[5,6] determined a much lower upper limit for pion production. The aim of the present experiment is to answer the basic question of whether enhanced or inhibited pion production is taking place below the threshold. An independent-particle Fermi motion mechanism[7] will provide the basis of comparison. According to this model, the near-threshold pion production is due to a combination of the Fermi momentum distributions of the two nuclei. Since this model does not take any collective effects into account, discrepancies by orders of magnitude could provide an indication of such effects.

Our research group is engaged in a series of experiments using a different approach. Pions are detected using plastic scintillator telescopes in a 180° magnetic spectrometer set up specifically for these measurements. In Fig. 1 the detection system set up is given. The three arrays of scintillators were located along with the corresponding lead collimators in such a way as to measure pions (emitted near 0° with respect to the beam direction) and energies between 30 and 90 MeV. Measurements were made with 250 MeV/nucleon and 400 MeV/nucleon argon beams from the Berkeley Bevalac facility. Targets used were KCl and Pb. Thus far the KCl data have been partially analyzed. The preliminary results are given in Table 1.

The data indicated that ratios of the yields of pions at ~0° for 400 and 250 MeV/nucleon is about 2:1 for the 54.6 MeV pions and about 4:1

Table 1. Relative cross section of pion production for argon on KCl.

	Emitted π^+ energy	
Projectile energy	54.6 MeV	87.0 MeV
250 MeV/nucleon	0.18±0.07	0.28±0.04
400 MeV/nucleon	0.38±0.14	1.00±0.14

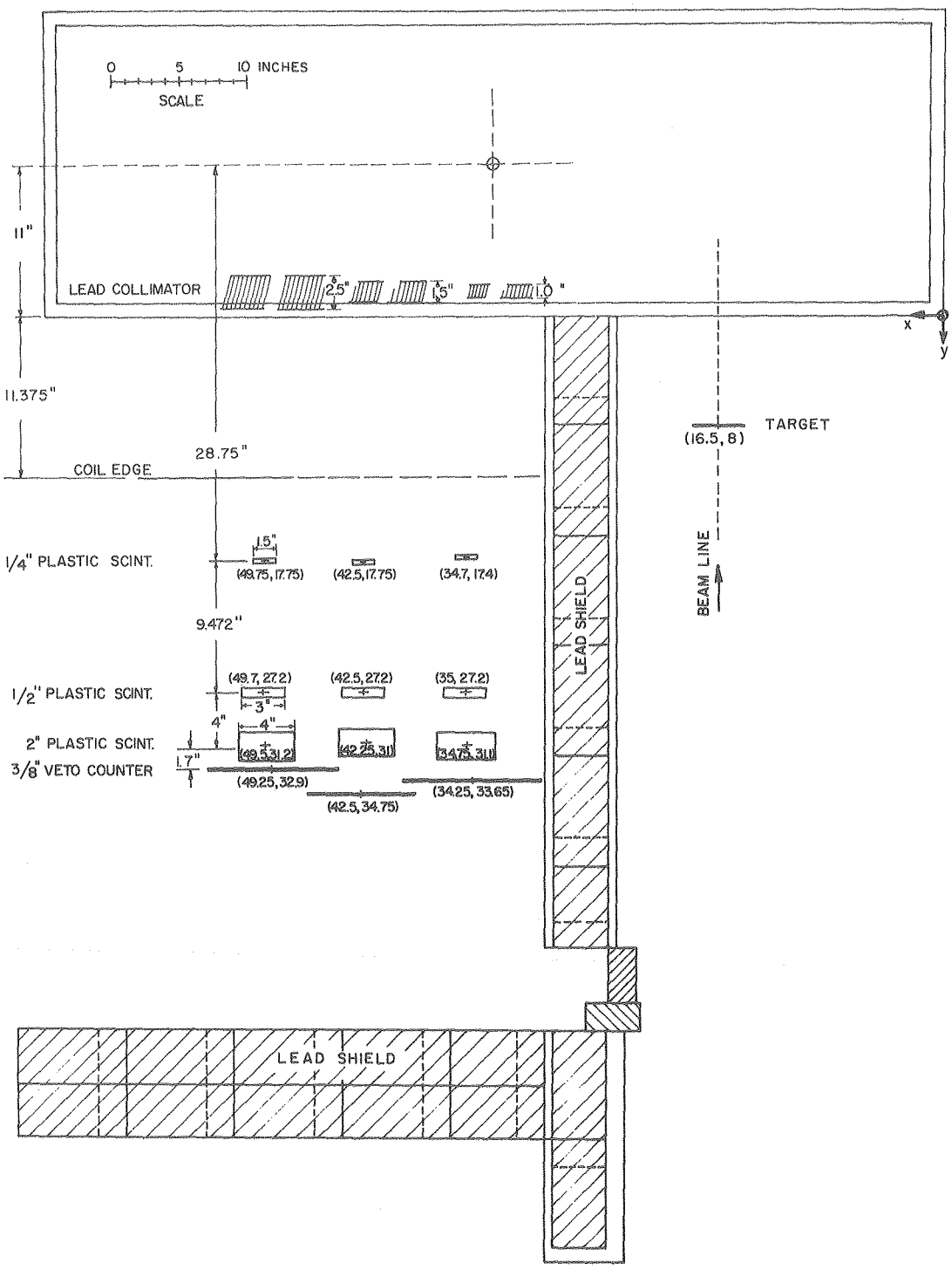

Fig. 1. Experimental set up for the measurement of threshold pion production using a magnetic spectrometer. (XBL 788-5544)

for the 87 MeV pions. These ratios appear to be consistent with theoretical predictions[7] as well as the lower limits established in the emulsion experiments.[5,6] Further measurements with our experimental set up are scheduled for the near future.

Footnotes and References

*Work also supported by the National Science Foundation under Grant No. Phy 78-01684.

†Permanent address: Cyclotron Laboratory, Michigan State University, East Lansing, MI 48824.

‡Permanent address: Institute for Nuclear Studies, Univ. of Tokyo, Midori Cho, Tanashi Shi, Japan.

§On leave from C.E.N., Saclay, France.

‖Supported by CNEN-Brazil.

1. A. B. Migdal, JETP (Sov. Phys.) 34, 1184 (1972); Phys. Rev. Lett. 31, 257 (1973); Phys. Lett. B 45, 448 (1973); Nucl. Phys. A 210, 421 (1973).

2. G. Bertsch and M. Johnson, Phys. Rev. D 12, 2230 (1975).

3. R. Sawyer, Nucl. Phys. A 271, 235 (1976).

4. P. J. NcNulty, G. E. Farrell, R. C. Filz, W. Schimmerling, and K. G. Vosburgh, Phys. Rev. Lett. 38, 1519 (1977).

5. P. J. Lindstrom, H. J. Crawford, D. E. Greiner, R. Hagstrom, and H. H. Heckman, Phys. Rev. Lett. 40, 93 (1978).

6. R. Kullberg, A. Oskarsson, and I. Otterlund, Phys. Rev. Lett. 40, 289 (1978).

7. G. Bertsch, Phys. Rev. C 15, 713 (1977).

D. TABLE OF ISOTOPES PROJECT, ATOMIC PHYSICS, AND MAGNETIC MONOPOLES

TABLE OF ISOTOPES PROJECT

E. Browne, J.M.H. Chong, J.M. Dairiki, D.P. Kreitz, C.M. Lederer, T. Prussin, M.E. Schwartz, M.A. Sharp, and V.S. Shirley

The publication of the seventh edition of the Table of Isotopes[1] in 1978 concluded a seven-year project involving a total effort of more than 50 man-years. Over 30,000 journal articles, reports, conference proceedings, private communications, and theses were used as source material for the present edition. In terms of both reference citations and data, the seventh edition is a factor of 4 times as large as the sixth; the complexity of the level schemes has increased even more--by almost an order of magnitude. The literature cutoff varies from about January 1977, for the lightest mass chains, to December 1977, for the heaviest.

The Table of Isotopes contains an extensive introduction which explains the scope, nomenclature, and evaluation policies used in the table. The authors' criteria for data selection are based on a determination to present the best measurements--clearly indicating conflicting results and avoiding redundancy.

The layout of the data in a single table (as opposed to the double-table format of the sixth edition) is described in Fig. 1, reproduced from the Introduction of the Table of Isotopes. Data categories included in the tabulated listings are more fully delineated in the Contents (Fig. 2). Several significant changes have been introduced in the present edition. Reported uncertainties are included for all quantities in tabular data listings. Smaller italic numbers following any value represent the uncertainty in the last place(s). A new reference-code format "journal volume page(year)" permits direct look-up of an article without the need to look up the code. A brief (12-page) list of the reference codes replaces a full bibliography, which otherwise would have increased the seventh edition by about 300 pages.

Figure 3 illustrates how a mass chain compilation is presented in the Table of Isotopes; a portion of the data for mass number A = 202 is shown. Sophisticated computer facilities and extensive programming (described in previous annual reports)[2,3] have made it possible to present the data in a variety of type sizes, styles, and intensities. The pages are thumb-tabbed by mass number for rapid data access.

Appendices include material of general interest to users of the Table of Isotopes (see

Fig. 1. Description of data layout in the Table of Isotopes, from the Introduction. (XBL 786-9447)

II. General Features of the *Table of Isotopes*

II.A. *Layout:* An Isotope Index, ordered by atomic number (Z) and subordered by mass number (A), precedes the main table. It contains all stable nuclei, radioisotopes, and isomers that appear in the *Table of Isotopes*. (R-rated isotopes - those identified only in nuclear reactions - do not appear in the Isotope Index.) In addition to the isotope designation, the index includes the natural abundance, half-life, class (certainty of identification), and the number of the page on which the tabular data entry is found in the main table.

The main table is ordered by mass number and subordered by atomic number. For each mass number there is an abbreviated mass-chain decay scheme, showing the adopted half-lives, spin-parity assignments, and decay energies (Q-values) for the isobars, and the decay relationships between them. Noted near this scheme are the initials of the compiler(s) and, following a semicolon, those of the reviewer.

Following the mass-chain decay scheme, tabulated data and detailed nuclear level schemes are given for individual isotopes. Tabulated data entries are included for each ground state or isomer with half-life $\gtrsim$1 s. A few shorter-lived isomeric species are also included - e.g., fission isomers and a few "historic" isomers, such as ^{24m}Na. The data include natural abundance, mass excess, nuclear spin, thermal neutron cross sections, all categories of data on radioactive decay, and excited-state half-lives. Data categories are shown to the left in **bold serif** type. The data are printed in sans-serif (plain) type. Each entry under a given data category concludes with the reference code or codes in braces {}. Longer data entries (radiation data in particular) begin on a new line, indented to the left of any continuation lines.

Detailed level schemes are given for each isotope (A,Z) for which there is information beyond that shown on the mass-chain decay scheme. The schemes are separated into a "decay-level" scheme, showing levels and transitions observed in the decay of all parent isotopes and isomeric states, and a "reaction" scheme, summarizing the information derived from nuclear reaction studies. Absence of a decay-level scheme, a reaction scheme, or both, means that excited levels have not been observed or that the scheme is not well established.

Decay-level schemes include all levels established in radioactive decay studies. Reaction schemes include most levels observed in nuclear reactions; when it is necessary to omit levels because of space limitations, the number of omitted levels, the energy cutoff above which they occur, and (usually) the reactions which populate them are noted in a comment. Not included are most neutron-capture resonances and other unbound states (e.g., giant resonances); these states are generally outside the scope of the present compilation, with a few exceptions in the light-element region. Some references to unbound levels other than neutron resonances are included under "other reactions" or "others".

Contents

Fig. 2. Table of Contents from the seventh edition of the Table of Isotopes. (XBL 786-9448)

Contents, Fig. 2). Three of the appendices deserve further comment. Appendix II contains tables of convenient standards for calibration of γ-ray conversion-electron, and α-particle measurements. The γ-ray standard tables, prepared with the assistance of R. A. Meyer, are the first such tables to present γ-ray energies based on the new "gold standard,"[4] the 411.80441±15 keV transition in ^{198}Au decay.

Appendix IV has been added to include information on half-thicknesses for γ-ray absorption and on the range and stopping power for absorption of electrons and various nuclei (protons through ^{136}Xe) in different stopping media.

Appendix VII is an updated version of the Table of Nuclear Moments[5] published in 1975. This table will continue to be updated (production is computerized), and future editions will appear at 2- or 3-year intervals.

It is expected that the seventh edition of the Table of Isotopes will be the last in the series started in 1940. The project will continue to serve the basic and applied nuclear science community by participation in the new U. S. and international program for nuclear data compilation.

References

1. C. M. Lederer and V. S. Shirley, eds.; E. Browne, J. M. Dairiki, and R. E. Doebler, principal authors; A. A. Shihab-Eldin, L. J. Jardine, J. K. Tuli, and A. B. Buyrn, authors; Table of Isotopes, Seventh Edition, John Wiley and Sons, Inc., New York (1978).

2. E. Browne, J. M. Dairiki, R. E. Doebler, J. M. Hollander, L. J. Jardine, C. M. Lederer, A. A. Shihab-Eldin, V. S. Shirley, and M. Whalley, LBL-2366 (1974), p. 3.

Fig. 3a, b. A portion of the data for mass number A = 202 taken from the Table of Isotopes. Included is the mass-chain decay scheme which begins each A-chain compilation, Tabulated data listings for several of the A = 202 isotopes, and "decay-level" schemes, "reaction" schemes, and their references for ^{202}Hg and ^{202}Tl. Note the stackplotting of all γ-ray transitions which proceed to the same final level in the ^{202}Hg reaction scheme. [(a) XBL 786-9445; (b) XBL 786-9446]

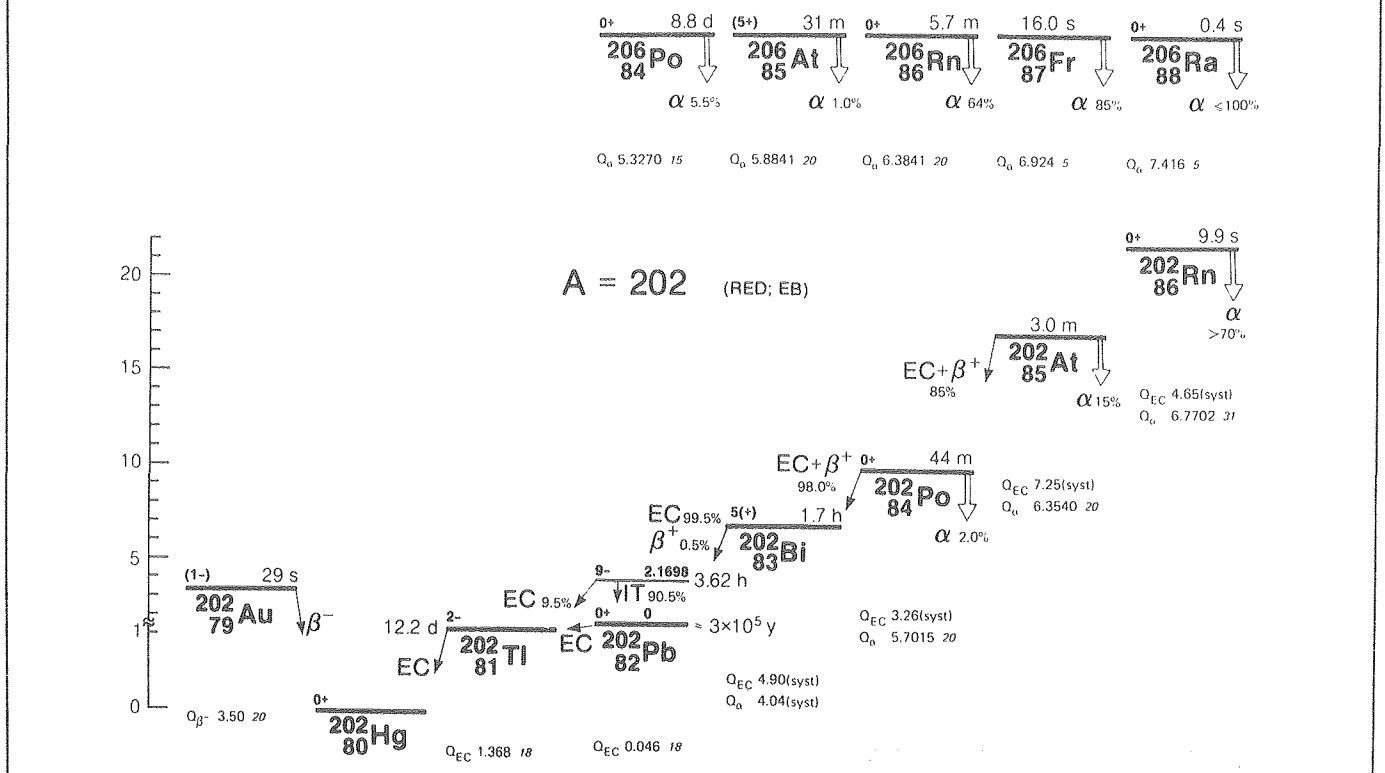

$^{202}_{79}$Au

Δ: −23.86 20 {ANDT 19 175(77)}
%: β^- {PR 164 1545(67)}
$t_{1/2}$: 29 3 s {NP A184 157(72), SFen 42 267(72)}; 30 3 s {PR 164 1545(67)}; 27 2 s {JINC 34 1087(72)}; **others:** {PPSL 65A 945(52)}
Class: A; **Ident:** chem {PPSL 65A 945(52)}; cross bomb, genet energy levels {PR 164 1545(67), NP A184 157(72)}
Prod: ^{202}Hg(n,p) {PR 164 1545(67), PPSL 65A 945(52), NP A184 157(72)}; ^{205}Tl(n,α) {PR 164 1545(67), NP A184 157(72)}
β^-: (see also ^{204}Au)
3.5 2 (≈90%) *scint* {PR 164 1545(67)}
2.7 3 *obs* {JINC 34 1087(72)}
γ: (**norm:** $\gamma_{0.440}$ (γ ≈10%), from level scheme) $\gamma_{0.440}$ ($\dagger_\gamma$100), **0.5203** 4 ($\dagger_\gamma$11 3), **0.9086** 4 ($\dagger_\gamma$18 3), $\gamma_{0.960}$ ($\dagger_\gamma$<4), **1.1254** 4 ($\dagger_\gamma$25 5), **1.2037** 4 ($\dagger_\gamma$21 5), **1.3065** 5 ($\dagger_\gamma$23 5) *Ge(Li), Ge(Li)-scint γγ coinc, Ge(Li)-scint γβ coinc* {NP A184 157(72)}
others: {JINC 34 1087(72), PR 164 1545(67)}

$^{202}_{80}$Hg

%: 29.8 (^{198}Hg/^{202}Hg ratios vary from 0.336 to 0.341) {BNL-NCS-50605(77)}
Δ: −27.356 6 {ANDT 19 175(77)}
I: 0 0 {ZP 72 423(31), PRSL 130A 558(31)}
σ_0: 5.0 4 {PC77 Holden}
$t_{1/2}$(0.440): 264 ps *Coulomb excit* {NP A147 161(70)}, 245 ps *nucl res fluor* {PR 98 200(55)}; **others:** {CR 242 1284(56), Phca 22 1129(56), PR 103 1801(56)}

$^{202}_{80}$Hg levels – References

Decay: NP A184 157(72), NP 75 81(66), IDO-17222(67), IIso 26 403(75)
^{201}Hg(n,γ): PR C11 546(75); **others:** NP A243 413(75), NP A135 241(69), PR 164 1548(67), NIM 36 29(65), IzF 27 1377(63), NP 21 66(60), NP 13 525(59)
Coul. ex.: NP A147 61(70); **others:** CR 242 1284(56), Phca 22 1129(56), PR 103 1801(56)
^{202}Hg(d,d'): PR C5 1678(72)
Other reactions:
^{202}Hg(n,n'): ZP 183 323(65)
^{202}Hg(n,n'γ): NP 80 198(66)
^{202}Hg(γ,γ'): NP A218 95(74)

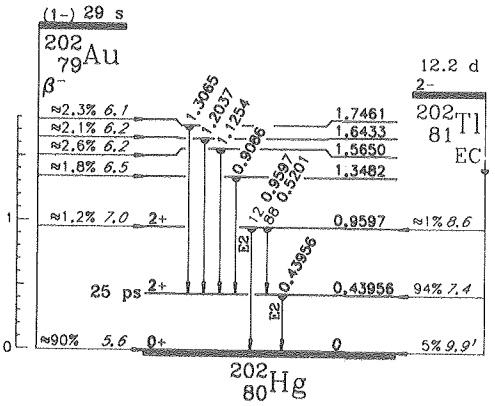

(a)

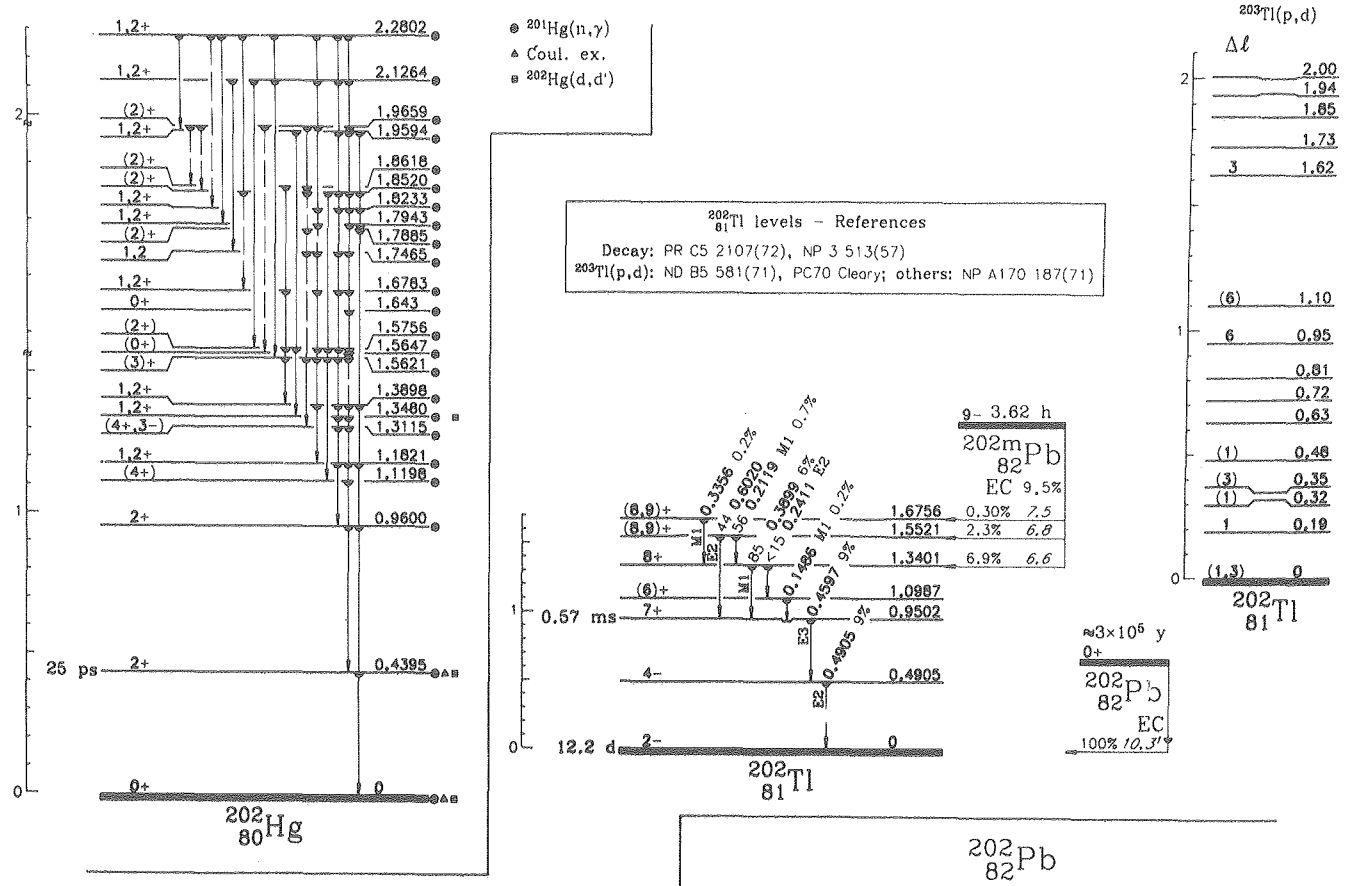

$^{202}_{81}Tl$

Δ: −25.988 *18* {ANDT 19 175(77)}
I: 2 *AB* {BAPS 3 319(58)}
%: EC {PCam 36 490(40), ZP 119 602(42)}; no β^+ {PR 79 1014(50)}
$t_{1/2}$: 12.23 *2* d {IIso 26 403(75)}; 12.4 *1* d {NP 75 81(66)}; 12.0 *1* d {Phca 23 1056(57)}; 12.50 *25* d {JINC 35 2139(73)}; **others:** {PR 86 565(52), PR 79 1014(50), PR 60 619(41)}
Class: A; **Ident:** chem, excit {PCam 36 490(40), PR 60 619(41)}
Prod: ^{202}Hg(d,2n) {PCam 36 490(40)}; ^{201}Hg(d,n) {Phca 25 326(59)}; ^{203}Tl(d,t) {Phca 25 326(59)}
γ: **0.43956** *1*, **0.52013** *7 Ge(Li)* {IIso 26 403(75)}
0.43942, **0.52033**, **0.95974** *Ge(Li)* {IDO−17222(67)}
(norm: $\gamma_{0.440}$ (γ 91 *1*%), from level scheme, RED) $\gamma_{0.440}$ ($\dagger_\gamma$100), $\gamma_{0.520}$ ($\dagger_\gamma$1.03), $\gamma_{0.960}$ ($\dagger_\gamma$0.133) *scint, scint−scint γγ coinc* {NP 75 81(66)}
0.43914 (K/L_{1+2}/L_3 3.3/1/0.29) *mag conv* {PR 92 918(53)}
Hg LX ($\dagger_\gamma$1.866), Hg KX ($\dagger_\gamma$100 *2*), $\gamma_{0.440}$ ($\dagger_\gamma$100 *3*, e_K/γ ≈0.034, K/L 2.7) *mag conv, scint, ion ch* {Phca 23 1056(57), Phca 22 208(56)}
$\gamma_{0.440}$ ($\dagger_\gamma$100, $\dagger_K$ 100), $\gamma_{0.960}$ ($\dagger_\gamma$0.0745, $\dagger_K$ 0.0133 *13*) *mag conv, scint* {NP 62 337(65)}
$\gamma_{0.440}$ ($\dagger_\gamma$100), $\gamma_{0.520}$ ($\dagger_\gamma$≈0.1), $\gamma_{0.960}$ ($\dagger_\gamma$0.103) *scint, scint−scint γγ coinc* {ArkF 17 337(60)}
$\gamma_{0.440}$ ($\dagger_\gamma$100), $\gamma_{0.520}$ ($\dagger_\gamma$0.4106), $\gamma_{0.960}$ ($\dagger_\gamma$0.0536) *scint, scint−scint γγ coinc* {Phca 25 326(59)}
others: {NP A184 157(72), NuoC s10v14 509(59)}
γγ(θ): {PL 26B 374(68)}
$t_{1/2}$(0.950): 570 *10* μs {CEA−R−2900(66)}, 565 *10* μs *delay coinc* {NP 61 129(65)}, 585 *25* μs *delay coinc* {PR 112 1958(58)}, 600 *20* μs {NP A241 135(75)}, 608 *22* μs {NP A102 534(67), OesS 175p2 163(66)}, 536 *15* μs *delay coinc* {JINC 35 2139(73)}; **others:** {ZETF 45 1344(63), ArkF 12 237(57), PR 101 1067(56)}
EC(0): EC(L)/EC(K) 0.220 $^{+20}_{-15}$ {NP 75 81(66)}
EC(0.440): EC(L)/EC(K) 0.196 *2* {NP 75 81(66)}; **others:** {NuoC s10v14 509(59), Phca 25 333(59), Phca 23 1056(57), PPSL 69A 70(56), PR 96 548(54), PR 79 1014(50)}
EC(0.960): EC(L)/EC(K) 0.305 *20* {NP 75 81(66)}; **others:** {ArkF 17 337(60)}

$^{202}_{82}Pb$

Δ: −25.942 *11* {ANDT 19 175(77)}
%: EC {PR 96 548(54)}
$t_{1/2}$: ≈3×10^5 y *yield* {PR 96 548(54)}; **others:** {PR 78 191(50), PR 72 766(47)}
Class: A; **Ident:** chem, genet, mass spect {PR 96 548(54)}
Prod: ^{203}Tl(d,3n) {PR 96 548(54)}
$t_{1/2}$(levels): **1.383:** 1.972 ns *delay coinc* {ZP A280 371(77)}, 2.00 *15* ns *delay coinc* {ArkF 14 439(59)}
2.208: 424 ns *delay coinc* {NP A229 230(74)}

$^{202m}_{82}Pb$

Δ: −23.772 *11* {ANDT 19 175(77)}
%: IT 90.5%, EC 9.5% {PR C5 2107(72)}
$t_{1/2}$: 3.62 *3* h {ArkF 12 237(57)}; **others:** {Phca 20 521(54), PR 93 1433(54)}
Class: A; **Ident:** chem, excit {Phca 20 521(54), PR 93 1433(54)}; chem, mass spect {NP 3 513(57)}
Prod: ^{203}Tl(d,3n) {Phca 20 521(54), PR 93 1433(54)}; ^{203}Tl(p,2n) {PR C5 2107(72)}
γ with EC: (intensities relative to $\dagger_\gamma$100 for $\gamma_{0.787}$ (with IT)) **0.14855** *15* ($\dagger_\gamma$0.45 *15*, e_K/γ 2.9, K/L 6.1 *12*), **0.21192** *7* ($\dagger_\gamma$1.53, e_{L1}/γ 0.14), **0.24111** ($\dagger_K$0.202, K/L_{1+2}/L_3 183/10/4.05), **0.33555** *10* ($\dagger_\gamma$0.45 *10*, e_K/γ 0.23, K/L ≈5), **0.38994** *7* ($\dagger_\gamma$12.4 *10*, e_K/γ 0.18, K/L 6.3), **0.45972** *7* ($\dagger_\gamma$17.3 *10*, e_L/γ 0.041, K/L_{1+2}/L_3 182/10/2.02), **0.49047** *7* ($\dagger_\gamma$18.4 *10*, e_L/γ 0.0073, K/L_{1+2}/L_3 3911/10/1.23), **0.60195** *8* ($\dagger_\gamma$1.21, e_K/γ 0.016) *Ge(Li), mag conv, Ge(Li)−Ge(Li) γγ coinc* {PR C5 2107(72), NP 3 513(57), Phil s7v46 61(55), Phil s7v46 65(55), RED}
γ with IT: (**norm:** $\gamma_{0.422}$ (γ 86 *1*%), from level scheme, RED) **0.12475** *9* ($\dagger_\gamma$1.13), **0.1293** *1* ($\dagger_\gamma$0.083, e_L/γ ≈700, K/L_1/L_2/L_3 <0.02/≈0/1.9/1.0), **0.2403** *1* ($\dagger_\gamma$($\gamma_{0.240}$+$\gamma_{0.241}$(with EC)) 2.23, $\dagger_K$0.312, K/L 5.06), **0.41732** ($\dagger_\gamma$0.82), **0.422126** ($\dagger_\gamma$172 *9*, e_K/γ assumed 0.030, K/L_{1+2}/L_3 314/10/1.83), **0.54763** ($\dagger_\gamma$0.25 *8*, e_K/γ 0.35, K/L_{1+2}/L_3 9^{+1}_{-4}/10/1.74), **0.657496** ($\dagger_\gamma$65 *3*, e_K/γ 0.0053, K/L 5.57), **0.786996** ($\dagger_\gamma$100, e_K/γ 0.079, K/L_{1+2}/L_3 131/10/≈1), **0.95452** ($\dagger_\gamma$2.04), **0.960705** ($\dagger_\gamma$184 *15*, e_K/γ 0.0056, K/L_{1+2}/L_3 548/10/≈0.7) *Ge(Li), mag conv, Ge(Li)−Ge(Li) γγ coinc, mag−mag ee coinc* {PR C5 2107(72), NP 3 513(57), RED}
$\gamma_{0.422}$ (e_K/γ 0.0322), $\gamma_{0.787}$ (e_K/γ 0.0884) *semicond−scint eγ coinc* {NP 56 689(64)}
(intensity relative to $\dagger_\gamma$100 for $\gamma_{0.787}$) **1.38285** ($\dagger_\gamma$6.4 *1*×10^{-4}, K/L 3.47) *Ge(Li), Si(Li) conv* {PR C12 338(75), RED}
γ: others: {ArkF 11 105(56), Phca 20 521(54), PR 93 1433(54)}

(b)

3. E. Browne, J. M. Dairiki, R. E. Doebler, L. J. Jardine, C. M. Lederer, E. Leon, M. Rinneberg, A. A. Shihab-Eldin, V. S. Shirley, and M. Whalley, LBL-4000 (1975), p. 3.

4. E. G. Kessler, Jr., R. D. Deslattes, A. Henins, and W. C. Sauder, Phys. Rev. Lett. 40, 171 (1978).

5. V. S. Shirley and C. M. Lederer, Table of Nuclear Moments, Proceedings of the Conference on Hyperfine Interactions Studied in Nuclear Reactions and Decay, Invited Papers with Table of Nuclear Moments, E. Karlsson and R. Wäppling, eds. (Almqvist and Wiksell Intern., Stockholm, 1975).

ENERGY LOSS OF RELATIVISTIC HEAVILY IONIZING PARTICLES*

S.P. Ahlen

An accurate theory of the energy loss mechanisms of relativistic heavily ionizing particles (such as heavy nuclei, antinuclei and magnetic monopoles) has important applications in a wide variety of fields. These range from the detection and identification of heavy particles in the primary cosmic radiation to ground based accelerator work for which detailed knowledge of heavy ion stopping power and dose distribution is required.

Recent experimental[1-3] and theoretical[4-6] work involving fast ($E > 1$ MeV/amu) heavy ions ($Z \geq 1$) has indicated that deviations from the standard first order stopping power theory of Bethe[7] are due to three effects:

(1) the Bloch effect[4,8] which results in reduced stopping power ($-Z^4$ correction term) due to the finite lateral extent of the close collision electron beam;

(2) the Lindhard effect[4] which results in enhanced stopping power for positive ions ($+Z_1^3$ correction term) due to polarization of atomic electron distributions in close and distant collisions;

(3) the Mott effect[5] which results in enhanced stopping power for positive ions (up to Z_1^7 terms) due to the deviation of the exact Mott cross section from the First Born Approximation of this cross section.

For fast projectiles ($E > 50$ MeV/amu), the Bloch and Mott corrections dominate. They are small for singly charged particles (<1%), moderate for fast iron nuclei (~3% enhancement of stopping power), and large for uranium nuclei (~17%). The demonstration of the validity of the Bloch correction[1] is quite interesting insofar as it relates to a direct measurement of a scattering process which is neither describable by classical physics nor by simple plane wave quantum mechanical scattering. This is made possible by atomic binding which presents the heavy-ion projectile in its rest frame with a localized electron beam unattainable with particle accelerators. Another interesting result implied by the results of Ref. 1 is that the close collisions cannot legitimately be considered from the point of view of free electron scattering by the projectile. This conclusion follows from the fact that the Lindhard correction, verified in Ref. 1, consists of both close and distant collision polarization corrections.

The stopping power of magnetic monopoles can be calculated along lines similar to those for electric charges.[9] Corrections analogous to the Bloch and Mott corrections can be applied to the resulting expression. Polarization corrections are absent, however, due to the lack of a longitudinal interaction between monopoles and atomic electrons. This fact complicates the process of the slowing of monopoles in conductors since resistive losses, rather than dielectric screening, limit the distant collision energy loss. General symmetry considerations demonstrate that the monopole stopping power depends only on the magnitude of its charge, in contrast to the case for electric charges.

Footnote and References

*Condensed from an article submitted to Rev. Mod. Phys.

1. H. H. Andersen, J. F. Bak, H. Knudsen, and B. R. Nielsen, Phys. Rev. A 16, 1929 (1977).

2. S. Datz, J. Gomez del Campo, P. F. Dittner, P. P. Miller, and J. A. Biggerstaff, Phys. Rev. Lett. 38, 1145 (1977).

3. G. Tarlé and M. Solarz, Phys. Rev. Lett. 41, 483 (1978).

4. J. Lindhard, Nucl. Instrum. and Meth. 132, 1 (1976).

5. S. P. Ahlen, Phys. Rev. Lett. 39, 1398 (1977).

6. S. P. Ahlen, Phys. Rev. A 17, 1236 (1978).

7. H. Bethe, Ann. Phys. (Leipzig) 5, 325 (1930).

8. F. Bloch, Ann. Phys. (Leipzig) 16, 285 (1933).

9. S. P. Ahlen, Phys. Rev. D 17, 229 (1978).

FURTHER MEASUREMENTS AND REASSESSMENT OF THE MAGNETIC-MONOPOLE CANDIDATE*

P.B. Price, E.K. Shirk,† W.Z. Osborne,‡ and L.S. Pinsky‡

Within the stack, consisting of 35 Lexan detectors and of 3 nuclear emulsions, in which the unusual event was found,[1] we have measured tracks of ~200 cosmic ray nuclei with $26 \leq Z \leq 83$, which provide an internal calibration of the response of the detectors. Our measurements in Lexan and in emulsion together show that the unusual particle produced a knockon electron energy distribution incompatible with any known nucleus. The track etch rate and its gradient in Lexan give the quantity $|Z|/\beta$ and, if the particle was a nucleus, a lower limit on its velocity. We found $|Z|/\beta \approx 114$ at each of 66 positions in the Lexan stack extending over a range of ~1.4 g/cm^2. The best fit to the Lexan data alone would be for a hypothetical superheavy element with $Z \approx 108$ to 114 and β such that $Z/\beta \approx 114$. A known nucleus with $90 \leq Z \leq 96$ would also give an acceptable fit to the Lexan data if it fragmented once in the stack with a loss of about two units of charge, keeping $Z/\beta \approx 114$. A nucleus with $Z < 90$ could maintain $Z/\beta \approx 114$ only by a properly spaced set of fragmentations. A nucleus with β as low as 0.6 could fit the Lexan data only if it fragmented at least 8 times in succession, with a probability ~10^{-17}. In the 200 μm G-5 emulsion, visual measurements of the track "cores" produced by relatively low-energy electrons (≤10 keV) are consistent with the Lexan result that the unusual particle had $|Z|/\beta \approx 114$. However, measurements of the density of silver grains at radial distances greater than ~10 μm show that the particle produced far fewer high-energy (≳50 keV) knockon electrons in each of the three emulsions than would a known nucleus with $Z/\beta = 114$. If it were a known, long-lived nucleus with $Z \leq 96$, and therefore having $0.84 \geq \beta > 0.6$ in order to fit the Lexan data, its signals in the three emulsions imply a very low Z/β of only ~85 instead of 114. The abnormally small production rate of long-range electrons observed in all three emulsions and illustrated in Fig. 1 is the essential evidence that we have found a unique particle. A monopole does not provide an acceptable fit to all of the data. A slow particle ($\beta \approx 0.4$) could fit all of the observations, provided its mass were so great (>10^3 amu) that it did not slow appreciably in the 1.4 g/cm^2 stack. A fast ($0.7 \lesssim \beta \lesssim 0.9$) antinucleus with $Z/\beta \approx -114$, because of its low Mott cross section for production of high-energy knockon electrons, could fit the data, especially if it fragmented once with loss of one or two units of charge. An ultra-relativistic

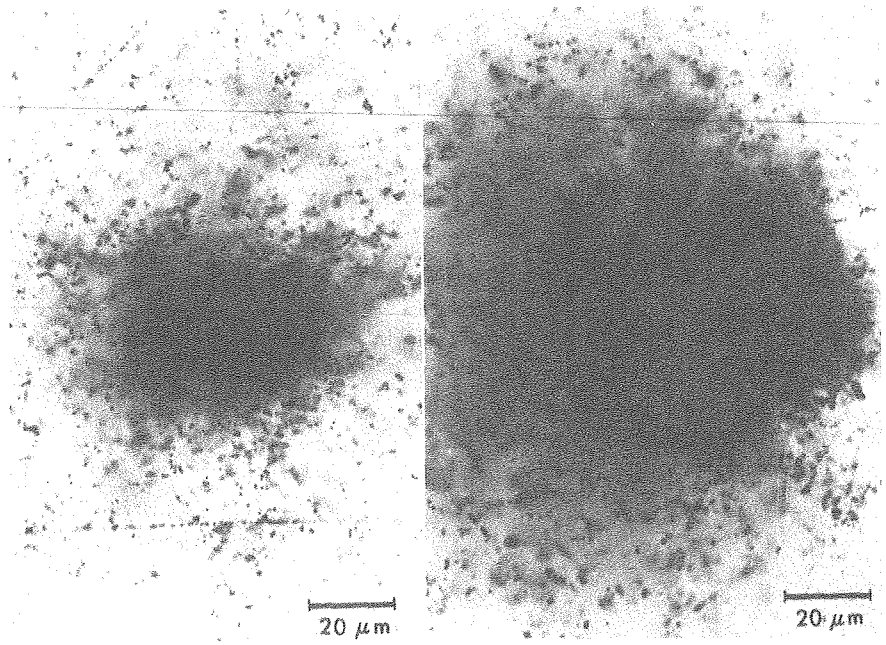

Fig. 1. Photomicrographs in G-5 emulsion (a) the track of the unusual particle, with $Z/\beta = 114$ and zenith angle $\theta = 10^0$; and (b) the track of a nucleus with $Z = 75$, $\beta = 112$, and $\theta = 14^0$. For both tracks the regions in focus is about one-third of the way below the top surface of the emulsion. From energy deposition theory, both tracks should contain about the same number of silver gains if the unusual particle were a normal nucleus. Clearly the unusual particle produced far too few energitic knockon electrons. (XBB 783-3218)

($\beta \gtrsim 0.99$) superheavy element with $Z \approx +110$ to $+114$ can also account for the data and is not in conflict with any negative searches. Our knowledge of the Z- and β-dependence of the response of Lexan appears sufficient to preclude values of $|Z/\beta|$ less than ~110. An explanation of the weak distant energy deposition in terms of fluctuations by a normal nucleus or locally insensitive emulsion regions appears to be unlikely. Freak occurrences such as a 10^{20} eV jet or an upward moving nucleus do not fit the data. Having achieved only an incomplete characterization of a single example of what appears to be a new particle, we emphasize the obvious--that further examples of such particles must be found before its identity can be established.

Footnotes and References

*Abstract of paper that appeared in Phys. Rev. D 18, 1382 (1978).

†Dept. of Physics, University of California, Berkeley, CA 94720.
‡Dept. of Physics, University of Houston, Houston TX 70004.

1. P. B. Price, E. K. Shirk, W. Z. Osborne, and L. S. Pinsky, Phys. Rev. Lett. 35, 487 (1975).

II. THEORY OF NUCLEAR COLLISIONS

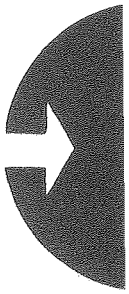

A. MICROSCOPIC

TIME DEPENDENCE OF INTERACTION PICTURE TRANSITION AMPLITUDES TO TO ALL ORDERS OF PERTURBATION THEORY*

S.K. Kauffmann

Given an initially prepared state $|\psi(t_o)\rangle$ at time t_o, a complete orthonormal measurement basis set $\{|p\rangle\}$, and a dynamical Hamiltonian H that governs the subsequent time evolution of the state vector $|\psi(t)\rangle$, a central task of quantum theory is to describe the time dependence of the measurement transition probabilities[1]

$$P_{\psi(t_o)\to p}(t) \equiv \left|\langle p|\psi(t)\rangle\right|^2 \quad . \tag{1}$$

The measurement basis set $\{|p\rangle\}$ will be assumed to have among its complete set of commuting (diagonal) observables, an energy, which is described by the measurement Hamiltonian K

$$K|p\rangle = E_p|p\rangle \quad . \tag{2}$$

It is most convenient to work in the measurement picture

$$|\psi_I(t)\rangle \equiv e^{iK(t-t_o)/\hbar}|\psi(t)\rangle \quad , \tag{3}$$

which is usually called the interaction or Dirac picture.

We note that the initial condition

$$|\psi_I(t_o)\rangle = |\psi(t_o)\rangle \tag{4}$$

and the measurement transition probabilities

$$P_{\psi(t_o)\to p}(t) = \left|\langle p|\psi_I(t)\rangle\right|^2 \tag{5}$$

are not affected in form by our change to the measurement picture. However, the Schroedinger equation for $|\psi_I(t)\rangle$ is

$$i\hbar\frac{\partial|\psi_I(t)\rangle}{\partial t} = V_I(t)|\psi_I(t)\rangle \quad , \tag{6}$$

where

$$V_I(t) = e^{iK(t-t_o)/\hbar}(H-K)e^{-iK(t-t_o)/\hbar} \quad . \tag{7}$$

It is convenient to denote $(H-K)$ as V, called the interaction Hamiltonian. We may write the Schroedinger equation (6) in integral form, incorporating its initial condition

$$|\psi_I(t)\rangle = |\psi(t_o)\rangle + \left(-\frac{i}{\hbar}\right)\int_{t_o}^{t} dt'\, V_I(t')|\psi_I(t')\rangle \quad . \tag{8}$$

By iterating Eq. (8) we generate the time-dependent perturbation series

$$\langle p|\psi_I(t)\rangle = \langle p|\psi(t_o)\rangle + \sum_{n=1}^{\infty}\langle p|\psi_I^{(n)}(t)\rangle \quad , \tag{9}$$

where

$$\langle p|\psi_I^{(n)}(t)\rangle = \left(-\frac{i}{\hbar}\right)^n\int_{t_o}^{t}dt_1\int_{t_o}^{t_1}dt_2\cdots\int_{t_o}^{t_{n-1}}dt_n \langle p|V_I(t_1)V_I(t_2)\cdots V_I(t_n)|\psi(t_o)\rangle \tag{10a}$$

$$= \left(-\frac{i}{\hbar}\right)^n\sum_{p_1}\cdots\sum_{p_n}V_{pp_1}V_{p_1p_2}\cdots V_{p_{n-1}p_n}\langle p_n|\psi(t_o)\rangle \times \int_{t_o}^{t}dt_1\cdots\int_{t_o}^{t_{n-1}}dt_n \exp\left\{\frac{i}{\hbar}\left[(E_p-E_{p_1})(t_1-t_o) + (E_{p_1}-E_{p_2})(t_2-t_o) + \cdots + (E_{p_{n-1}}-E_{p_n})(t_n-t_o)\right]\right\} \tag{10b}$$

$$= \left(-\frac{i}{\hbar}\right)^n\sum_{p_1}\cdots\sum_{p_n}V_{pp_1}\cdots V_{p_{n-1}p_n}\langle p_n|\psi(t_o)\rangle \times \int_0^{(t-t_o)}d\tau_1\int_0^{\tau_1}d\tau_2\cdots\int_0^{\tau_{n-1}}d\tau_n\, e^{-\frac{i}{\hbar}(E_{p_1}-E_p)(\tau_1-\tau_2)}\cdots \times e^{-\frac{i}{\hbar}(E_{p_{n-1}}-E_p)(\tau_{n-1}-\tau_n)}e^{-\frac{i}{\hbar}(E_{p_n}-E_p)\tau_n} \quad . \tag{10c}$$

For the physically relevant $t \geq t_o$, the multiple convolution integrals in (10c) may be easily

Laplace-transformed, and Eq. (10) then is rewritten in terms of the inverse Laplace transform

$$\langle p|\psi_I^{(n)}(t)\rangle = \sum_{p_1}\cdots\sum_{p_n} V_{pp_1}\cdots V_{p_{n-1}p_n}\langle p_n|\psi(t_0)\rangle \times \frac{1}{2\pi i}\int_{c-i\infty}^{c+i\infty} ds\ \frac{e^{(t-t_0)s}}{s}\left(\frac{1}{(E_p-E_{p_1})+i\hbar s}\right)\cdots \times \left(\frac{1}{(E_p-E_{p_n})+i\hbar s}\right) \tag{11}$$

where $c>0$.

The only singularities of the integrand in Eq. (11) are poles along the imaginary axis. Since $(t-t_0)\geq 0$, we may readily close the integration contour with a semicircle extending into the left half s-plane and evaluate the integral as the sum of residues at the poles

$$\langle p|\psi_I^{(n)}(t)\rangle = \sum_{p_1}\cdots\sum_{p_n} V_{pp_1}\cdots V_{p_{n-1}p_n}\langle p_n|\psi(t_0)\rangle \times \left\{\left(\sum_{j=1}^{n}\frac{e^{-\frac{i}{\hbar}(E_{p_j}-E_p)(t-t_0)}}{(E_{p_j}-E_p)\prod\limits_{\substack{i=1\\ i\neq j}}^{n}(E_{p_j}-E_{p_i})}\right)+\frac{1}{\prod\limits_{i=1}^{n}(E_p-E_{p_i})}\right\} \tag{12a}$$

$$=\sum_{p_1}\cdots\sum_{p_n} V_{pp_1}\cdots V_{p_{n-1}p_n}\langle p_n|\psi(t_0)\rangle \times \sum_{j=1}^{n}\frac{\left(e^{-\frac{i}{\hbar}(E_{p_j}-E_p)(t-t_0)}-1\right)}{(E_{p_j}-E_p)\prod\limits_{\substack{i=1\\ i\neq j}}^{n}(E_{p_j}-E_{p_i})}\ . \tag{12b}$$

For many purposes the full time dependence given in Eq. (12) is not very useful, rather the limiting (asymptotic) time dependence of the n^{th} order measurement amplitude,

$$\langle p|\psi_I^{(n)}(+\infty)\rangle \equiv \lim_{(t-t_0)\to+\infty}\langle p|\psi_I^{(n)}(t)\rangle \tag{13}$$

is desired. This is most easily calculated in the inverse Laplace form given in Eq. (11). Denoting $\tau\equiv(t-t_0)$, we change integration variable to $z=\tau s$, and may readily calculate the limit as $\tau\to+\infty$, with $a\equiv\tau c>0$ kept finite

$$\frac{1}{2\pi i}\int_{c-i\infty}^{c+i\infty} ds\ \frac{e^{\tau s}}{s}\left(\frac{1}{(E_p-E_{p_1})+i\hbar s}\right)\cdots\left(\frac{1}{(E_p-E_{p_n})+i\hbar s}\right)$$

$$=\frac{1}{2\pi i}\int_{a-i\infty}^{a+i\infty} dz\ \frac{e^{z}}{z}\left(\frac{1}{(E_p-E_{p_1})+i\hbar(z/\tau)}\right)\cdots\times$$

$$\left(\frac{1}{(E_p-E_{p_n})+i\hbar(z/\tau)}\right)$$

$$\xrightarrow[\tau\to+\infty,\ a>0]{}\left(\frac{1}{2\pi i}\int_{a-i\infty}^{a+i\infty} dz\ \frac{e^{z}}{z}\right)\cdots\times \tag{14a}$$

$$\left\{\lim_{\varepsilon\to 0+}\left[\left(\frac{1}{(E_p-E_{p_1})+i\varepsilon}\right)\cdots\times\left(\frac{1}{(E_p-E_{p_n})+i\varepsilon}\right)\right]\right\} \tag{14b}$$

$$=\lim_{\varepsilon\to 0+}\left[\left(\frac{1}{(E_p-E_{p_1})+i\varepsilon}\right)\cdots\left(\frac{1}{(E_p-E_{p_n})+i\varepsilon}\right)\right]. \tag{14c}$$

From Eq. (11) and Eq. (14), we have the simple result that

$$\langle p|\psi_I^{(n)}(+\infty)\rangle = \langle p|\left(V\left(\frac{1}{(E_p-K+i\varepsilon)}\right)\right)^n|\psi(t_0)\rangle\ . \tag{15}$$

Let us note that the limiting process leading to Eq. (15) is wrong if $|\psi(t_0)\rangle$ is itself precisely a member of $\{|p\rangle\}$, the situtión which is obtained in the usual formal scattering theory. We consider here only initial states which are <u>superpositions</u> of measurement basis members.

Given the form of the n^{th} order asymptotic measurement amplitudes from Eq. (15), it is

convenient to formally define the "incoming wave asymptotic bra" as follows:

$$\langle p^-| \equiv \sum_{n=0}^{\infty} \langle p| \left(V \left(\frac{1}{E_p - K + i\varepsilon} \right) \right)^n \qquad (16a)$$

$$= \langle p| + \langle p| V \left(\frac{1}{E_p - H + i\varepsilon} \right) . \qquad (16b)$$

It has the property

$$\langle p|\psi_I(+\infty)\rangle = \langle p^-|\psi(t_o)\rangle \quad , \qquad (17)$$

and satisfies the equation

$$\langle p^-| = \langle p| + \langle p^-| V \left(\frac{1}{E_p - K + i\varepsilon} \right) . \qquad (18)$$

Further, given an operator O diagonal in the measurement basis $\{|p\rangle\}$,

$$O|p\rangle = O_p|p\rangle \quad , \qquad (19)$$

we readily obtain a convenient expression for its asymptotic expectation value

$$\langle \psi(t)|O|\psi(t)\rangle = \sum_p \left| \langle p|\psi(t)\rangle \right|^2 O_p \qquad (20a)$$

$$\xrightarrow[(t-t_o)\to+\infty]{} \sum_p \left| \langle p^-|\psi(t_o)\rangle \right|^2 O_p . \qquad (20b)$$

Our results bear a considerable resemblance to formal scattering theory,[2] especially the useful Lippmann-Schwinger form of Eq. (18).

The primary difference is that an incoming wave asymptotic bra rather than an outgoing wave asymptotic ket is involved. Also, our large time results break down in case $|\psi(t_o)\rangle$ is actually a member of the measurement basis set $\{|p\rangle\}$, which is precisely the assumption of formal scattering theory. What we have done is complementary to formal scattering theory, and is tailored to initial states which are unavoidable superpositions of the measured final states (e.g., nuclei which break up as the result of a collision). Shorter time transient behavior may, whether or not $|\psi(t_o)\rangle$ is is a member of $\{|p\rangle\}$, be studied using Eq. (12) and Eq. (9).

Footnote and References

*Condensed from LBL-7140.

1. R.P.Feynman and A.R.Hibbs, Quantum Mechanics and Path Integrals (McGraw-Hill, New York, 1965), p.164.

2. M.L.Goldberger and K.M.Watson, Collision Theory (Wiley, New York, 1964), Chap. 5.

QUANTUM CHROMODYNAMICS AT HIGH TEMPERATURE*

J.I. Kapusta

In the last few years there has been a surge of interest in relativistic many-body systems. This has largely been due to progress in elementary particle physics, in which gauge theories of the strong, electromagnetic and weak interactions have come to prominence. From renormalization group arguments and experiment it is known that the electromagnetic and weak interactions have a coupling constant that is small except for energies approaching those of cosmological magnitude. Furthermore, the standard gauge theory of the strong interactions, quantum chromodynamics, has a coupling constant which is large at low energy but becomes small at energies of the order of several proton masses. (For a review, see Ref. 1.) As opposed to standard strong interaction field theories, where the fields are associated with ordinary hadrons and consequently large coupling constants, it is reasonable to expect that a perturbative expansion of thermodynamic quantities converges at high densities and temperatures. At present perturbation theory is the only "reliable" calculational tool in relativistic quantum field theories. In this paper we calculate the thermodynamic potential of quantum chromodynamics at finite temperature for an arbitrary number of fermions with arbitrary masses and chemical potentials. The calculation is explicit in orders two and three, and an outline is given of the fourth order. A calculation in fourth order for finite temperature and finite masses will involve considerably more work than at zero temperature and zero mass.[2]

Let us consider the predictions of quantum chromodynamics. The coupling constant α_c is the renormalization group running coupling constant depending on the temperature T and chemical potentials μ. The quark masses m_u, m_d, and m_s also depend on T and μ. Assuming zero net baryon number, charge and strangeness, we obtain the curves shown in Fig. 1. There are a number of interesting points about this graph. Due to asymptotic freedom the expansion seems to be converging very well at high temperature. In fact, keeping just the first three terms seems to be enough above about $T \approx 500$ MeV.

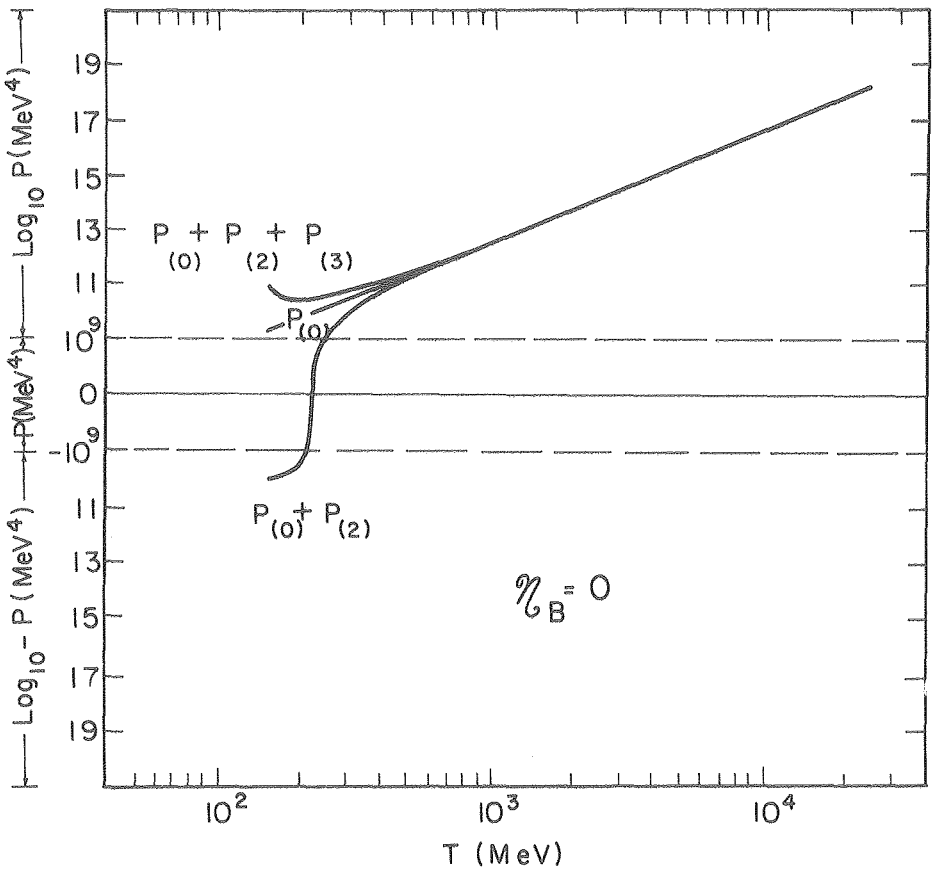

Fig. 1. The pressure plotted as a function of temperature at zero baryon number density. $P_{(n)}$ denotes the contribution in order g^n. Note the convergence of the expansion at high temperature. (XBL 788-1592)

When $\mu = 0$, the subtraction point $M \approx 4T$. Thus the expansion converges rapidly when $\alpha_c \lesssim 0.1$, corresponding to $g^2/4\pi \lesssim 0.4$. However, when T is reduced to 230 MeV, then $P_{(3)} = -P_{(2)} = P_{(0)}$ and so the first three terms cannot be expected to yield a good approximation to the true answer. This corresponds to $\alpha_c \gtrsim 0.3$, or $g^2/4\pi \gtrsim 1.2$. One might expect that by keeping more terms in the expansion of $P = -\Omega$ and by solving the renormalization group equation to higher order in α_c, the temperature above which a perturbative expansion is valid could be pushed down. Certainly there is no obvious way of deciding upon the radius of convergence of the expansion within our calculational framework. At lower temperatures one must worry about the mechanism of confinement, which is a long range nonperturbative phenomenon. Also our choice of subtraction point will no longer be valid if the quarks and gluons are clustering into hadrons. The best we can do is to say that the strong coupling of quarks and gluons probably results in their confinement to hadrons at temperatures of order $T \approx 200 \pm 100$ MeV. The question of a phase transition cannot be properly addressed.

Footnote and References

*Condensed from LBL-7745.

1. H.D.Politzer, Phys. Rev. C14, 129 (1974).

2. B.A.Freedman and L.D.McLerran, Phys. Rev. D 16, 1130, 1147, 1169 (1977).

AMPLITUDE FOR TRANSITIONS BETWEEN MOLECULAR (TWO-CENTER) CHANNELS*

K. Pruess

For some time there has been considerable interest in describing quasi-elastic reactions induced by heavy ions in terms of a "molecular" picture, utilizing two-center states to describe internal motion.[1-5] Work along these lines has been inspired, in part, by the intuitive appeal of two-center single particle states, and in part by a failure of conventional reaction theories, based upon "atomic" channels, to account for experimental data.[3,5]

An obstacle to the molecular approach has been the fact that no satisfactory method was known for computing cross sections for transitions between two-center states.[5-7] We derive an exact formula as well as a practically useful DWBA-type approximation.

The amplitude for a rearrangement reaction from some initial channel i into a final channel f' can be written

$$T_{f'i} = \langle \Phi_{f'} | V' | \Psi_i^{(+)} \rangle \quad , \qquad (1)$$

where $\Psi_i^{(+)}$ is an eigenstate of the full many-body Hamiltonian H, with ingoing waves only in the entrance channel.[8] $\Phi_{f'}$ is an eigenstate of $H_0' = h_\beta + T_\beta$, with h_β the internal motion Hamiltonian and T_β the kinetic energy operator appropriate for the exit channel. $V' = H - H_0'$ is the interaction causing the transition. Equation (1) is not in general useful because $\Psi_i^{(+)}$ is not known. Two-potential theory enables us to rewrite Eq. (1) in terms of distorted waves which can be easily calculated.[8] To this end auxiliary Hamiltonians are introduced:

$$H_1' = H_0' + V_0' \qquad (2)$$

and likewise for the entrance channel (unprimed quantities). V_0 and V_0' are chosen as optical potentials, depending upon relative distance only, which describe elastic scattering. Equation (1) becomes[8]

$$T_{f'i} = \langle \phi_\beta \chi_\beta^{(-)} \Big| V_1' \frac{i\varepsilon}{E + i\varepsilon - H} \Big| \phi_\alpha \chi_\alpha^{(+)} \rangle . \qquad (3)$$

Here $\phi_{\alpha,\beta}$ are the internal motions in entrance and exit channels, respectively, which are eigenstates of the free separated nuclei.

The distorted waves in Eq. (3) are eigenstates of $T_\alpha + V_0$ (entrance channel) and $T_\beta + V_0'$ (exit channel), respectively. The interaction causing the rearrangement is $V_1' = H - H_1'$.

The formal development leading to Eq. (3) holds for any choice of the auxiliary Hamiltonians H_1, H_1', provided that $V_0|\Phi_i\rangle$ and $V_0'|\Phi_{f'}\rangle$ be state vectors with finite norm. We generalize Eq. (3) to the case where the internal motion is represented by two-center states, which parametrically depend upon the relative distance between the nuclei. We define a two-center Hamiltonian appropriate for the entrance channel as

$$h_\alpha^{\underset{\sim}{r}_\alpha} = t_{xb} + v_{xb} + v_{xA}(\underset{\sim}{r}_{xb} + \underset{\sim}{r}_\alpha) + V_{Ab}(r_\alpha), \qquad (4)$$

where t_{xb} and v_{xb} are kinetic and potential energy, respectively, of x with respect to b, v_{xA} is the potential between x and A, and V_{Ab} is the core-core potential. The two-center states and energies depend parametrically upon the relative motion vector $\underset{\sim}{r}_\alpha = \underset{\sim}{r}_{aA}$:[2,4]

$$h_\alpha^{\underset{\sim}{r}_\alpha} \phi_{\alpha j\Omega}^{\underset{\sim}{r}_\alpha}(\underset{\sim}{r}_{xb}) = \varepsilon_{\alpha j\Omega}(r_\alpha)\, \phi_{\alpha j\Omega}^{\underset{\sim}{r}_\alpha}(\underset{\sim}{r}_{xb}) \quad . \qquad (5)$$

We restrict ourselves to spherically symmetric potentials v_{xb} and v_{xA}, in which case the projection Ω of angular momentum j on the internal symmetry axis is a good quantum number. Following the treatment of Ref. 1, we define internal motion states

$$|\phi_{\alpha jm}^{\underset{\sim}{r}_\alpha}) = \sum_\Omega D_{m\Omega}^j(\hat{r}_\alpha) |\phi_{\alpha j\Omega}^{\underset{\sim}{r}_\alpha}) \qquad (6)$$

which asymptotically have good m rather than good Ω.

In order to express the transition amplitude Eq. (1) in terms of molecular states as given by Eq. (6), we must introduce an auxiliary Hamiltonian which does not couple different molecular channels.

$$H_1 = \sum_{\alpha jm} P_{\alpha jm}^{\underset{\sim}{r}_\alpha} (h_\alpha^{\underset{\sim}{r}_\alpha} + T_\alpha) P_{\alpha jm}^{\underset{\sim}{r}_\alpha} \quad , \qquad (7)$$

where

$$P_{\alpha jm}^{\underset{\sim}{r}_\alpha} = |\phi_{\alpha jm}^{\underset{\sim}{r}_\alpha}) (\phi_{\alpha jm}^{\underset{\sim}{r}_\alpha}| \qquad (8)$$

projects onto a single molecular channel. The sum in Eq. (7) extends over a number of channels in partition (a,A). H_1 does not cause transitions between molecular channels so that

$$(E - H_1) |\phi_{\alpha jm}^{\underset{\sim}{r}_\alpha} \chi_\alpha^{(+)}\rangle = 0 \qquad (9)$$

has one-channel solutions and defines distorted waves $\chi_\alpha^{(+)}$ which describe elastic scattering for

molecular channels. The auxiliary Hamiltonian Eq. (7) differs from the free motion Hamiltonian by

$$V_o = H_1 - H_o = \sum_{\alpha jm} \left[P^{\vec{r}_\alpha}_{\alpha jm} (h^{\vec{r}_\alpha}_\alpha + T_\alpha) P^{\vec{r}_\alpha}_{\alpha jm} \right] - h_\alpha - T_\alpha \ . \quad (10)$$

The state vector $V_o|\Phi_i\rangle$ has finite norm, as the difference

$$\phi^{\vec{r}_\alpha}_{\alpha jm} - \phi_{\alpha jm} \underset{r_\alpha \to \infty}{\sim} 0 \ . \quad (11)$$

In fact, the difference in Eq. (11) vanishes exponentially for large r_α.[4] Similar definitions and considerations apply for the exit channel. Because of the finite norms of $V_o|\Phi_i\rangle$ and $V_o'|\Phi_{f'}\rangle$ the formal development of the "two-potential method" can be carried over unchanged from Ref. 8. Instead of Eq. (3) we obtain

$$T_{f'i} = \langle \phi^{\vec{r}_\beta}_{\beta j'm'} \chi^{(-)}_\beta | V_1' \frac{i\varepsilon}{E + i\varepsilon - H} | \phi^{\vec{r}_\alpha}_{\alpha jm} \chi^{(+)}_\alpha \rangle \ , \quad (12)$$

with

$$V_1' = H - H_1' = H - \sum_{\beta j'm'} P^{\vec{r}_\beta}_{\beta j'm'} (h^{\vec{r}_\beta}_\beta + T_\beta) P^{\vec{r}_\beta}_{\beta j'm'} \ . \quad (13)$$

Equation (12) gives an exact expression for the transition amplitude between molecular states. Approximations can be obtained by expanding $i\varepsilon/(E + i\varepsilon - H)$ in powers of $V_1' = H - H_1'$. The lowest order approximation, which is analogous to the usual DWBA, amounts to just dropping the inverse operator, i.e.,

$$T^{(1)}_{f'i} = \langle \phi^{\vec{r}_\beta}_{\beta j'm'} \chi^{(-)}_\beta | V_1' | \phi^{\vec{r}_\alpha}_{\alpha jm} \chi^{(+)}_\alpha \rangle$$

$$\approx \langle \phi^{\vec{r}_\beta}_{\beta j'm'} \chi^{(-)}_\beta | T_\beta | \phi^{\vec{r}_\alpha}_{\alpha jm} \chi^{(+)}_\alpha \rangle \ . \quad (14)$$

To obtain the last line we have dropped terms involving the difference $h^{\vec{r}_{Ab}}_\beta - h^{\vec{r}_\beta}_\beta$. This represents a no-recoil approximation. Equation (14) gives the amplitude for one-step transitions between molecular channels, the transition operator being the kinetic energy of relative motion. This equation appears to be well suited for computing heavy-ion induced one-nucleon transfer reactions at low relative motion energies.

Footnote and References

*Condensed from an article submitted to Nucl. Phys. A and LBL-7747.

1. J.Y.Park, W.Scheid, and W.Greiner, Phys. Rev. C 6, 1565 (1972).

2. K.Pruess, Nucl. Phys. A 278, 124 (1977).

3. G.Delic, K.Pruess, L.A.Charlton, and N.K.Glendenning, Phys. Lett. B 69, 20 (1977).

4. K.Pruess and P.Lichtner, Nucl. Phys. A 291, 475 (1977).

5. L.A.Charlton, G.Delic, N.K.Glendenning, and K.Pruess, J. Phys. Soc. Japan 44 (1978), suppl. p.272.

6. D.R.Bates, in D.R.Bates (ed.), Atomic and Molecular Processes (Academic Press, New York and London, 1962).

7. R.McCarroll, in P.G.Burke and B.L.Moisewitsch (eds.), Atomic Processes and Applications (North Holland, Amsterdam, New York, Oxford, 1976).

8. L.S.Rodberg and R.M.Thaler, Introduction to the Quantum Theory of Scattering (Academic Press, New York and London, 1967).

TWO-STEP TRANSITIONS THROUGH THE CONTINUUM

L.A. Charlton,* G. Delic,† N.K. Glendenning, and K. Pruess

Polarization of single particle states in nucleus-nucleus collisions, i.e., "molecular" distortion caused by the force field of an approaching nucleus, can be represented with the two-center shell model (see preceding report).[1] An alternative description in terms of the more customary asymptotic states (one-center shell model) is also possible. In the asymptotic picture, rearrangement reactions involving polarized single particle states can be viewed as indirect processes via a large number of excited intermediate states, each of which contributes weakly and coherently.[2] It appears plausible that the strongest coherence can be expected for those intermediate states which involve the least possible number of transitions. In fact, each transition will make the states more complex and will therefore increase the likelihood of random phase cancellations. We are investigating the two-step part of the multi-step amplitude as the most likely candidate for significant effects.

For a one-neutron transfer reaction from an initial partition $\alpha = (a,A)$ to a final partition $\beta = (b,B)$ $(a = b + x,\ B = A + x)$, the two-step amplitude is

$$T_{\alpha\to\Sigma\beta'\to\beta} = \sum_{\beta'} \langle \chi_\beta^{(-)} | (\phi_\beta | v_{xb} | \phi_{\beta'})\ G_\beta^{(+)}\ (\phi_{\beta'} | v_{xA} | \phi_\alpha) | \chi_\alpha^{(+)} \rangle \qquad (1)$$

with the Green's operator

$$G_{\beta'}^{(+)} = (E + i\eta - \varepsilon_{\beta'} - H_1')^{-1} . \qquad (2)$$

(The notation is defined in the preceding report.)

Equation (1) involves a sum over discrete and an integral over continuum intermediate states $\phi_{\beta'}$ with energy $\varepsilon_{\beta'}$. β' represents the quantum numbers $(n'\ell'j'm')$ for bound states, and $(\varepsilon'\ell'j'm')$ for continuum states, respectively.

In principle, the summation and integration in Eq. (1) has to be extended over all angular momenta $\ell' = 0, 1, 2, \ldots$; $j' = \ell' \pm \frac{1}{2}$; $-j' \leq m' \leq j'$; $0 \leq \varepsilon' < \infty$ (plus bound states). Practically, only a finite number of ℓ'-states can be taken into account. Also, the energy range has to be limited. Moreover, a discrete set of ε'-values must be used.

As a step towards computing the full amplitude Eq. (1), we have investigated the range of $\ell'\varepsilon'$ which will give the most significant contributions. For the reaction $^{40}Ca(^{16}O,^{15}O)^{41}Ca$ we have evaluated bound states ϕ_α, ϕ_β, intermediate continuum states $\phi_{\beta'}$, inelastic form factors $(\phi_\beta | v_{xb} | \phi_{\beta'})$, and distorted waves χ_α, χ_β. We arrive at the following conclusions.

The two-step transfer is strongly localized in space (see Fig. 1). The ranges of relative and intrinsic coordinates $\underset{\sim}{r}_\alpha$, $\underset{\sim}{r}_{xb}$ (entrance channel) or $\underset{\sim}{r}_\beta$, $\underset{\sim}{r}_{xA}$ (exit channel) are restricted

a) by strong absorption: the distorted waves χ become negligible inside a strong absorption radius, which is somewhat larger than the sum of nuclear radii;

b) by the fast decaying tails of the transition potentials $v_{xA}(r_{xA})$ and $v_{xb}(r_{xb})$; and

c) by the somewhat more slowly decaying tails of the bound states $\phi_\alpha(r_{xb})$ and $\phi_\beta(r_{xA})$.

Therefore, two-step transitions are restricted to a range $R_{gr} \pm \Delta R$ of relative motion coordinates $|\underset{\sim}{r}_\alpha|$ and $|\underset{\sim}{r}_\beta|$ near the grazing distance R_{gr}, inside of which absorption sets in, and outside of which the participating bound states become negligibly small. In our example, $R_{gr} \approx 10$ fm and $\Delta R \approx 1 - 2$ fm. For transfer from $\phi_\alpha \to \phi_{\beta'}$ to be possible the particle x has to be within the range of v_{xA} (left circle in Fig. 1), i.e., the tail of the initial state ϕ_α must penetrate into v_{xA}. Because the tail decays exponentially, contributions to transfer will preferably come from that part of v_{xA} which is closest to b (horizontally shaded region in Fig. 1), corresponding to $r_{xA} \approx 4 - 6$ fm. For inelastic de-excitation $\phi_{\beta'} \to \phi_\beta$ the particle x must be within the range of v_{xb}, i.e., the tail of the final state ϕ_β must penetrate into v_{xb}. Because of the decaying tail of ϕ_β, inelastic de-excitation will preferably occur in the region which is shaded vertically in Fig. 1, typically corresponding to $r_{xA} \approx 6 - 9$ fm.

The spatial localization places severe restrictions on energy ε' and angular momentum ℓ' of continuum intermediate states. For significant two-step transitions, $\phi_{\beta'}$ must have a large amplitude inside both shaded regions. For transfer it is the internal part of $\phi_{\beta'}$ (inside the potential v_{xA}) which contributes. Thus we require that $\phi_{\beta'}$ be large in the internal region. This is obviously the case near a resonance, which

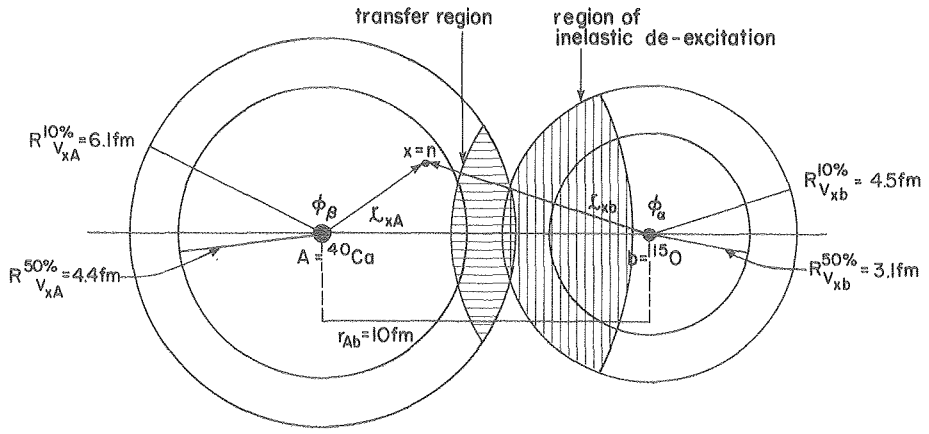

Fig. 1. Spatial localization of two-step transfer. A grazing situation is depicted, with the cores A and b a distance r_{Ab} = 10 fm apart. The "range" of the potentials for transfer (V_{xA}) and inelastic de-excitation (V_{xb}), respectively, is indicated with circles on which the potentials have diminished to 50% and 10%, respectively, of their central depth. The transfer region is bounded to the left, and the inelastic region to the right, by the decay of the bound states ϕ_α and ϕ_β, respectively. The boundary lines correspond to the radial parts of the bound states decreasing by one order of magnitude over the shaded regions.(XBL 787-1245)

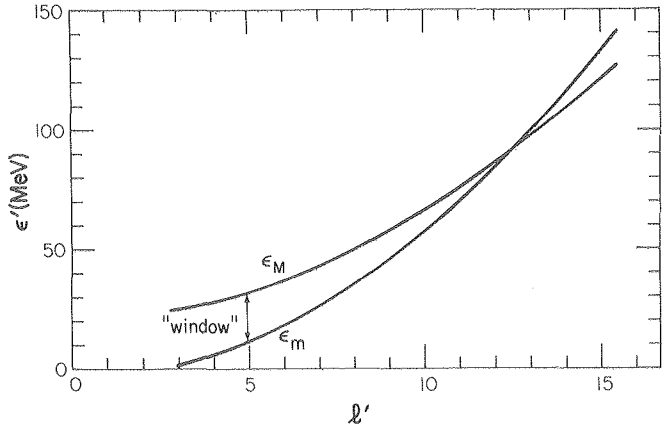

Fig. 2. Energy window for two-step transfer $^{40}Ca + ^{16}O \rightarrow ^{41}Ca^* + ^{15}O \rightarrow ^{41}Ca + ^{15}O$. For $\varepsilon' < \varepsilon_m$ transfer is inhibited by the centrifugal barrier. For $\varepsilon' > \varepsilon_M$ inelastic de-excitation is weak due to rapid oscillations and phase cancellations. The window vanishes for $\ell' \gtrsim 13$. The curves are approximate, with $\varepsilon_m(\ell')$ estimated from phase shifts of continuum states $\phi_{\beta'}$, and $\varepsilon_M(\ell')$ estimated from inelastic form factors. (XBL 787-1246)

therefore enhances transfer. For large angular momenta (estimated at $\ell' \gtrsim 13$ in our example) transfer and inelastic de-excitation become negligible due to angular and radial oscillations and cancellations. For each angular momentum ℓ' there is an energy $\varepsilon_m(\ell')$, increasing with ℓ', below which $\phi_{\beta'}$ does not penetrate into the transfer region, due to the centrifugal barrier. There is also an energy $\varepsilon_M(\ell')$, increasing with ℓ' more slowly than $\varepsilon_m(\ell')$, above which inelastic de-excitation becomes negligible due to fast oscillations of $\phi_{\beta'}$ and resulting phase cancellations. Thus, two-step transitions are restricted to a finite range of intermediate angular momenta and, for each angular momentum ℓ', to a finite energy "window" $\varepsilon_m(\ell') \leq \varepsilon' \leq \varepsilon_M(\ell')$ (see Fig. 2).

From our calculations of inelastic form factors we predict the strongest two-step transitions for relatively small intermediate angular momenta ($\ell' < 7$) and for small intermediate energies ($\varepsilon' < 20$ MeV). A strong resonant contribution is expected from the $\ell' = 2$ continuum at $\varepsilon' \approx (2 \pm 1)$ MeV. We estimate that two-step transitions through continuum states of $^{40}Ca + n$ will be much stronger than those via bound states of ^{41}Ca. For example, the $\ell' = 3$ continuum will yield about two orders of magnitude more cross section than two-step transitions through the $1f_{5/2}$ bound state of ^{41}Ca.

Footnotes and References

*Now at Oak Ridge National Laboratory, Oak Ridge, Tennessee.

†Now at Technische Hochschule Darmstadt, Darmstadt, W.Germany.

1. G.Delic, K.Pruess, L.A.Charlton, and N.K.Glendenning, Phys. Lett. B 69, 20 (1977).

2. L.A.Charlton, G.Delic, N.K.Glendenning, and K.Pruess, J. Phys. Soc. Japan 44 (1978), suppl. p.272.

B. MACROSCOPIC

CLASSICAL-LIMIT DESCRIPTION OF ROTATION-VIBRATIONAL BAND EXCITATION IN DEFORMED EVEN-EVEN NUCLEI*

R. Donangelo,† L.F. Oliveira,‡ J.O. Rasmusen and M.W. Guidry§

Classical-limit S-matrix theory (CLSM) for rotational excitation of deformed nuclei by heavy-ion projectiles[1-5] may be extended to investigate other processes in heavy-ion scattering having classical analogs. In this paper we extend the CLSM to the case where both rotational and vibrational modes of the target nucleus are excited by the heavy-ion projectile. We concentrate specifically on the rotational signature of the vibrational bands in deformed even-even nuclei.

Let us consider, as in Ref. 3, an even-even target nucleus with an axially symmetric shape, and a projectile nucleus, incident with zero impact parameter on the target nucleus. We assume the projectile to be spherical and disregard any projectile excitation during the collision process.

The classical Hamiltonian for this system may be written as

$$H(r,\chi,p_r,p_\chi) = \frac{p_r^2}{2m} + \frac{p_\chi^2}{2}\left(\frac{1}{\mathcal{J}} + \frac{1}{mr^2}\right) + \frac{Z_p Z_T e^2}{r} + \frac{Z_p Q_0^{(2)} e^2 P_2(\cos\chi)}{2r^3} + V_{\ell>2}^{Coul}(r,\chi) \qquad (1)$$

where $V_{\ell>2}^{Coul}(r,\chi)$ represents multipole-monopole Coulomb interactions of higher order than quadrupole.

The angle χ is defined by the symmetry axis of the target and the line joining the centers of target and projectile; r is the distance between these centers, p_χ and p_r are the quantities canonically conjugate to χ and r, defining the rotational angular momentum of the target and the relative linear momentum between target and projectile, respectively. The term $V_{\ell>2}^{Coul}(r,\chi)$ is given explicitly by

$$V_{\ell>2}^{Coul}(r,\chi) = \sum_{\ell>2} \frac{Z_p Q_0^{(\ell)} e^2 P_\ell(\cos\chi)}{2r^{\ell+1}} \qquad (2)$$

where

$$Q_0^{(\ell)}e \equiv 2\int r^\ell P_\ell(\cos\theta)\,\rho(r,\theta)d^3r \qquad (2a)$$

and $\rho(r,\theta)$ is the nuclear charge density. For an illustration of the coordinate system and definition of the remaining parameters, see Ref. 5. The classical limit of the quantum-mechanical S-matrix is given in section 2.2 of Ref. 5 as

$$S_{0\to I}^{J=0} = \tfrac{1}{2}\sqrt{2I+1}\int_0^\pi P_I(\cos\bar{\chi})\sqrt{\sin\chi_0 \sin\bar{\chi}\,\frac{d\bar{\chi}}{d\chi_0}}\; e^{i\phi'}\, d\chi_0 \qquad (3)$$

where ϕ' is given by

$$\phi' = -\frac{1}{\hbar}\int [r(t)dp_r(t) + \chi(t)dp_\chi(t)] + \frac{1}{\hbar}\int_{\tilde{r}_T}^{r} \tilde{p}_r d\tilde{r} + \sigma_0(n_0) + \sigma_I(n_I) \qquad (4)$$

The quantities appearing in Eqs. (3) and (4) are those used in Ref. 5. This expression may be integrated numerically, or evaluated by saddle-point methods, to yield a highly accurate approximation to the quantum-mechanical S-matrix. However, we may simplify evaluation of this expression in the limit that the higher-order multipole terms of $V_{\ell>2}^{Coul}(r,\chi)$ are small compared to the quadrupole term in Eq. (1). In that case, the S-matrix elements [Eq. (3)] may be calculated by considering $V_{\ell>2}^{Coul}(r,\chi)$ as a perturbation on the phase ϕ', neglecting its effect on the classical orbit itself. The contribution to the phase of $V_{\ell>2}^{Coul}(r,\chi)$ in this limit is given by

$$\Delta\phi'_V = \phi'_{V\neq 0} - \phi'_{V=0} = \frac{1}{\hbar}\int_{-\infty}^{\infty} V\big(r(t),\chi(t)\big)\,dt \qquad (5)$$

where $r(t)$, $\chi(t)$ in Eq. (5) are evaluated with the unperturbed Hamiltonian, i.e., setting $V_{\ell>2}^{Coul} = 0$ in Eq. (1).

For a single term of $V_{\ell>2}(r,\chi)$ in Eq. (2), we have

$$\Delta\phi'_{V_\ell} = \frac{1}{\hbar}\int_{-\infty}^{\infty} \frac{Z_p Q_0^{(\ell)} e^2 P_\ell\big(\cos\chi(t)\big)}{2r(t)^{\ell+1}}\,dt \quad . \qquad (6)$$

Since $\ell > 2$ and $\chi(t)$ varies slowly for excitation of a heavy target, most of the contribution to the integral in Eq. (6) is around the point of closest approach (CA) of the trajectory. Therefore, we

replace $\chi(t)$ in Eq. (6) by its value at this point χ_{CA}; $\Delta\phi'_{V_\ell}$ is now given by

$$\Delta\phi'_{V_\ell} \approx \frac{1}{2\hbar} Z_p Q_0^{(\ell)} e^2 P_\ell(\cos\chi_{CA}) \int_{-\infty}^{\infty} \frac{dt}{r(t)^{\ell+1}} \quad . \quad (6a)$$

Replacing ϕ' in Eq. (3) by

$$\phi'_{V\neq 0} = \phi'_{V=0} + \sum_{\ell>2} \phi'_{V_\ell} \qquad (7)$$

$$i \sum_{\ell>2} \phi'_{V_\ell}$$

and expanding e in terms of Legendre polynomials, the S-matrix element can be written as:

$$S^{J=0}_{0\to I} = \tfrac{1}{2}\sqrt{2I+1} \int_0^\pi P_I(\cos\bar{\chi}) \sqrt{\sin\chi_0 \sin\bar{\chi} \frac{d\bar{\chi}}{d\chi_0}}$$

$$\times\ e^{i\phi'_{V=0}} \left\{ 1 + \sum_{\ell>2} C_\ell P_\ell(\cos\chi_{CA}) \right\} d\chi_0 \quad . \quad (8)$$

In this form the contribution from each multipole deformation ($\ell > 2$) appears explicitly as a form factor $P_\ell(\cos\chi_{CA})$ multiplied by a strength coefficient C_ℓ.

We reiterate that in this approximation all quantities appearing in Eq. (8) are evaluated considering the Hamiltonian [Eq. (1)] with $V^{Coul}_{\ell>2}(r,\chi)$ set equal to zero.

In the previous derivation of Eq. (8) we considered the target to have a permanent deformation, but the same formalism can be used for the case of nuclear shape vibrations.

To fix ideas let us assume we have a deformed target nucleus with just a quadrupole deformation, and we are interested in studying a particular harmonic multipole vibration of order 2^ℓ. From the previous section it is straightforward to add other permanent deformations or vibrations.

The Hamiltonian for this system is now

$$H(r,\chi,q,p_r,p_\chi,n) = \frac{p_r^2}{2m} + \frac{p_\chi^2}{2}\left(\frac{1}{\mathcal{I}} + \frac{1}{mr^2}\right) + \hbar\omega_\ell(n+\tfrac{1}{2})$$

$$+ \frac{Z_p Z_T e^2}{r} + \frac{Z_p Q_0^{(2)} e^2 P_2(\cos\chi)}{2r^3} + V^{Coul}_{\ell>2}(r,\chi,q,n) \qquad (9)$$

where

$$V^{Coul}_{\ell>2}(r,\chi,q,n) = \frac{Z_p Q_0^{(\ell)}(q,n)\, e^2 P_\ell(\cos\chi)}{2r^{\ell+1}} \quad . \quad (10)$$

In Eqs. (12,13), q is the phase of the vibration, and n, the classical analog of the vibrational quantum number, is canonically conjugated to q.

Using a similar formalism as before, we obtain

$$S^{J=0}_{0,0\to I,n} = \frac{\sqrt{2I+1}}{2} \int_0^\pi d\chi_0\, P_I(\cos\bar{\chi})$$

$$\times \sqrt{\sin\chi_0 \sin\bar{\chi} \frac{\partial\bar{\chi}}{\partial\chi_0}}\ e^{i\phi_{V=0}}$$

$$\times \frac{1}{2\pi} \int_0^{2\pi} dq_0 \sqrt{\frac{\partial\bar{q}}{\partial\bar{q}_0}}\ e^{i(\phi'_{V_\ell} + \bar{q}n)}. \qquad (11)$$

By expanding $\exp(i\phi'_{V_\ell})$ as before [Eqs. (9,10)] we find that

$$S^{J=0}_{0,0\to I,n} = \frac{\sqrt{2I+1}}{2} \int_0^\pi d\chi_0 P_I(\cos\bar{\chi})$$

$$\sqrt{\sin\chi_0 \sin\bar{\chi} \frac{\partial\bar{\chi}}{\partial\chi_0}}\ F_n\ e^{i\phi'_{V=0}} \left(1 + C_\ell P_\ell(\cos\chi_{CA})\right) \qquad (12)$$

where

$$F_n \equiv \frac{1}{2\pi} \int_0^{2\pi} d\bar{q} \sqrt{\frac{\partial\bar{q}}{\partial\bar{q}_0}}\ e^{i\bar{q}n} \quad . \quad (13)$$

We again see the perturbation appearing as a form factor multiplying the integrand of the unperturbed CLSM expression [Eq. (3)]. The form factor has the same functional form as in the case of small permanent deformations, which is to be expected if these are considered as vibrations with a very large period compared to the collision time.

Footnotes and References

*Condensed from LBL-7720, to be published by Nucl. Phys. A.

†Present address: Instituto de Física, Universidade Federal do Rio de Janeiro, Rio de Janeiro, Brazil.

‡Supported by CNEN-Brazil.

§Present address: Department of Physics and Astronomy, University of Tennessee, Knoxville, Tennessee 37830.

1. S.Levit, U.Smilansky, and D.Pelte, Phys. Lett. B 53, 39 (1974).

2. H.Massmann and J.O.Rasmussen, Nucl. Phys. A 243, 155 (1975).

3. R.Donangelo, M.W.Guidry, J.P.Boisson, and J.O.Rasmussen, Phys. Lett. B 64, 377 (1976).

4. M.W.Guidry, H.Massmann, R.Donangelo, and J.O.Rasmussen, Nucl. Phys. A 274, 183 (1976).

5. M.W.Guidry, R.Donangelo, J.P.Boisson, and J.O.Rasmussen, Nucl. Phys. A 295, 482 (1978); and R.Donangelo, LBL-5825, Ph.D. Thesis (1977) unpublished.

THE INCORPORATION OF SHELL EFFECTS INTO A DIFFUSION MODEL

A.N. Behkami* and L.G. Moretto

It is interesting to determine the importance of shell effects in deep-inelastic reactions. To evaluate the effect of shell features on the magnitude of the cross section and the angular distributions, we have incorporated all the relevant features of the shell model into a diffusive model of mass transfer for heavy ion reactions. Several authors[1-3] have discussed in detail the analytical formulation of the Strutinski-like potential energy normalization and a general formalism for the level density calculation on the basis of an arbitrary set of single particle levels including pairing. In the present work we shall only discuss the calculations made for the $^{86}Kr + ^{197}Au$ reaction. To calculate the distribution of products from a deep-inelastic reaction, we a) compute the single-particle energies and spins, b) compute the potential energy of the interacting system by means of a Strutinsky procedure, and c) evaluate the level densities.

The potential energy for the interacting system with the inclusion of shell corrections is given by

$$V(N,Z,E) = E_{LD} + E_W \qquad (1)$$

where E_{LD} is the potential energy calculated with the liquid drop model and E_W is the shell correction. The shell correction consists of three terms:

$$E_W = E_{SM} - E_{STR} - E_{pair} \qquad (2)$$

where E_{SM} is the shell model energy, E_{STR} is the smoothed-out shell model energy obtained with a

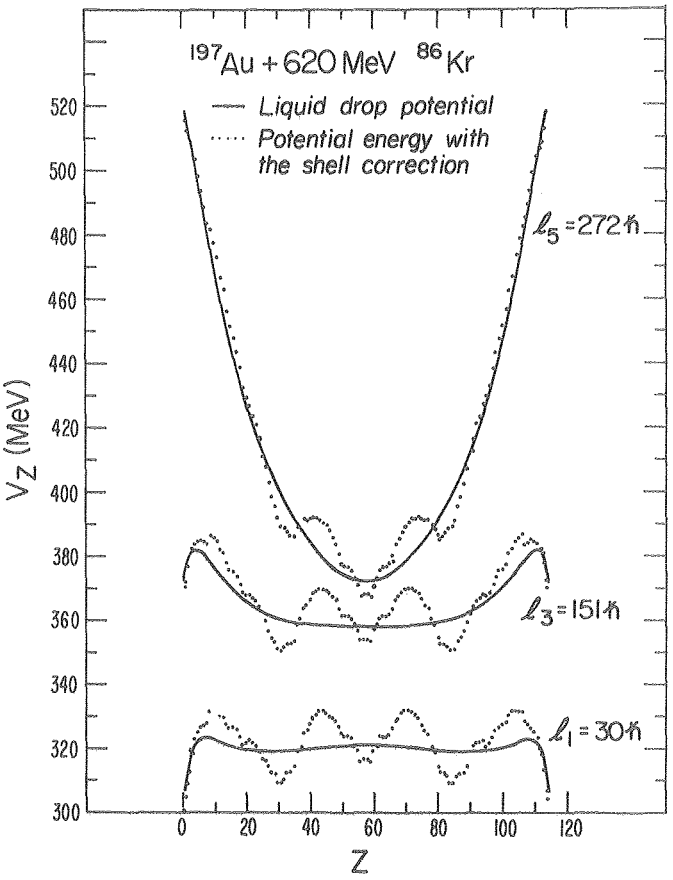

Fig. 1. Calculated potential energy for the reaction 620 MeV $^{86}Kr + ^{197}Au$ without (solid line) and with (dashed line) shell corrections.
(XBL 787-2607)

modified Strutinski procedure, and E_{pair} is the average pairing energy. In our calculations we have used the liquid drop parameters of Myers and Swiatecki.[4] A comparison of the potential energy of the interacting system with and without shell corrections for the reaction 620 MeV $^{86}Kr + ^{197}Au$ is shown in Fig. 1. With the inclusion of shell corrections, pockets appear in the potential energy surface for fragments with Z near magic numbers.

We have calculated the nuclear level densities utilizing the shell model with the incorporation of pairing effects as has been discussed elsewhere.[5,6] Utilizing the potential energy (with shell corrections) shown in Fig. 1 and the calculated nuclear level densities for all possible asymmetries, we have calculated the product Z-distribution from the reaction 620 MeV $^{86}Kr + ^{197}Au$. The preliminary results show that the peak position of the calculated Z-distribution is shifted closer to the projectile Z, in better agreement with experiment than earlier calculations, which neglected shell effects.

Footnotes and References

*Present address: Physics Department, Pahlavi University, Shiraz, Iran.

1. V.M.Strutinsky, Nucl. Phys. A 95, 420 (1967).

2. L.G.Moretto and R.Stella, Phys. Lett. B 32, 558 (1970).

3. L.G.Moretto, Nucl. Phys. A 182, 641 (1972).

4. W.D.Myers and W.J.Swiatecki, Nucl. Phys. A 81, 1 (1966).

5. L.G.Moretto, Nucl. Phys. A 216, 1 (1973).

6. A.N.Behkami and J.R.Huizenga, Nucl. Phys. A 217, 78 (1973).

THEORETICAL CORRELATION BETWEEN ENERGY DISSIPATION, ANGULAR MOMENTUM TRANSFER, AND CHARGE DIFFUSION IN DEEP-INELASTIC REACTIONS

J.S. Sventek and L.G. Moretto

A central problem in the analysis of deep inelastic reactions is the determination of mass, charge, and angular distributions for individual angular momentum bins.[1-3] In principle, distributions can be derived by plotting the cross section $\partial^2\sigma/\partial Z\partial[TKE]$ in the charge vs total kinetic energy (Z - TKE) plane and drawing lines on this map corresponding to constant entrance channel angular momenta (ℓ). The resulting distributions as a function of ℓ-bin can then shed light on quantities such as the Fokker-Planck coefficients for describing the time-dependence of the charge-asymmetry degree of freedom.[1] Two different empirical prescriptions for drawing the lines of constant ℓ have been suggested. The first prescription[1,3] calls for the lines to be drawn at constant TKE, parallel to the Z-axis. This prescription has been widely used, perhaps because of its simplicity. In the second infrequently used prescription,[2] the lines of constant ℓ are drawn parallel to the Coulomb energy of two touching fragments. It is important to determine the correct constant angular momentum contour lines in order to assess the possible systematic errors introduced by the empirical prescriptions. For instance, analyses of the kind mentioned above, employing the first prescription, have been used to determine diffusion coefficients and to evaluate the energy loss per exchanged particle in some heavy ion reactions.[1,3] In particular, the results of the latter estimate seem to indicate an energy loss per exchanged particle much larger than that expected from a one-body dissipation mechanism.[4]

In the limit of infinite radial friction (the relevance of which is discussed in a later section of this letter), there are two limiting patterns these lines should display, corresponding to the two extreme regimes associated with the rotational degrees of freedom of the intermediate complex. In the first limiting case the reaction occurs with no transfer of angular momentum from orbital motion to intrinsic spin. In this case, the angular momentum of relative motion as a function of Z, $\ell_{rel}(Z,\ell)$, is a constant independent of Z and equal to ℓ. The total kinetic energy can be calculated as

$$TKE(Z,\ell) = V_{Coul}(Z) + \frac{\hbar^2[\ell_{rel}(Z,\ell)]^2}{2\mu_Z d_Z^2} \qquad (1)$$

where μ_Z and d_Z are the reduced mass and the distance between centers for the charge-asymmetry

specified by Z. The curves in Fig. 1a show examples for this case, assuming the shape of the complex to be two touching spheres.

In the second limiting case the complex is rotating as a rigid body at the time of scission, regardless of the impact parameter (ℓ-wave). In this case, the relative angular momentum is Z-dependent, and given by

$$\ell_{rel}(Z,\ell) = \frac{\mu_Z d_Z^2}{\mu_Z d_Z^2 + I(Z) + I(Z_T - Z)} \cdot \ell \qquad (2)$$

where I(Z) is the moment of inertia of a fragment with charge Z about its own axis and Z_T is the total charge in the composite system. The curves in Fig. 1b show examples of this behavior for the same ℓ-waves as for the previous case.

If angular momentum transfer (from orbital to intrinsic spin) is mediated by nucleon exchange between the reaction partners, the amount of ℓ-transfer must be a function of the number of nucleon exchanges, which is directly related to the interaction time. Qualitatively, one would expect the correct curve for near grazing ℓ-waves to look like the dotted curve in Fig. 1c.

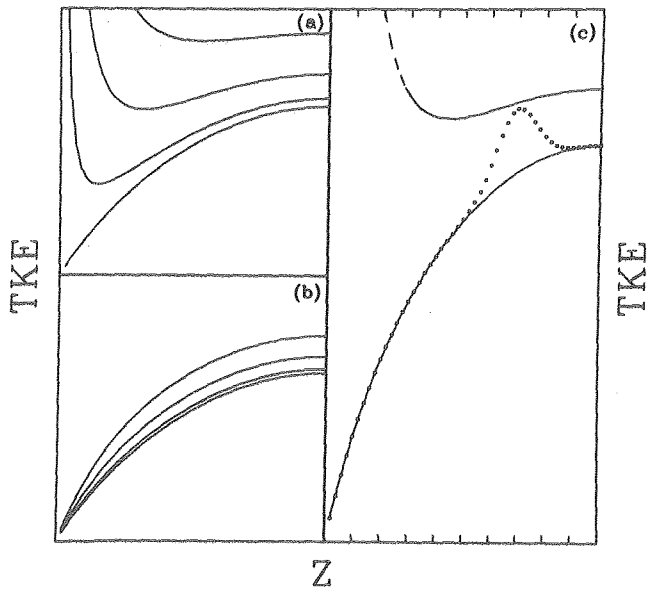

Fig. 1. (a) Lines of constant total angular momentum (ℓ) in the Z - TKE plane if no transfer to spin occurs.
(b) Same quantities if complex rotates rigidly at scission.
(c) Qualitative expectations for correct lines of constant ℓ. (XBL 7711-10426)

Consistent with the experiment, it is assumed that the radial kinetic energy is dissipated immediately at the interaction radius. The analysis is restricted to a system of two spheres separated by an ℓ-dependent distance, d(ℓ), dynamically determined as described further on in the text. We need to calculate how the orbital angular momentum (ℓ_{rel}) is transferred into the spins of the nuclei (ℓ_1,ℓ_2) and the function dependence of ℓ_1 and ℓ_2 on the asymmetry of the complex (Z). This calculation may be performed in two steps.

(1) The complex, initially at symmetry Z_p, is assumed to live a time t and to decay with asymmetry Z. The average rate of change of the charge of nucleus 1 is $\dot{Z}_1 = (Z - Z_p)/t$. Since the charge-to-mass ratio has been shown experimentally to equilibrate on a much faster time scale than the charge-asymmetry mode, one may write

$$\dot{A}_1 = (Z - Z_p)\,\alpha/t \qquad (3)$$

where A_1 is the mass of nucleus 1 and α is the A/Z ratio for the composite system. The average rate of nucleon transfer from one nucleus to the other is given by $n_o\sigma$, where n_o is the bulk flux of nuclear matter, and σ is the effective window between the nuclei.[5] By forcing the system to arrive at asymmetry Z, at time t, we impose an asymmetry on the right (r_{12}) and left (r_{21}) nucleon transfer rates, which can be written as

$$\begin{aligned} r_{12} &= n_o\sigma - \tfrac{1}{2}\dot{A}_1 \quad , \\ r_{21} &= n_o\sigma + \tfrac{1}{2}\dot{A}_1 \quad . \end{aligned} \qquad (4)$$

Knowing these transfer rates, we can write the following system of coupled differential equations for the spins and the orbital angular momenta:

$$\begin{aligned} \dot{\ell}_1 &= d_1\,[r_{12}d_1(\dot{\theta} - \dot{\theta}_1) + r_{21}d_2(\dot{\theta} - \dot{\theta}_2)]/\hbar \quad , \\ \dot{\ell}_2 &= d_2\,[r_{12}d_1(\dot{\theta} - \dot{\theta}_1) + r_{21}d_2(\dot{\theta} - \dot{\theta}_2)]/\hbar \quad , \\ \dot{\ell}_{rel} &= -(\dot{\ell}_1 + \dot{\ell}_2) \quad , \end{aligned} \qquad (5)$$

where d_1 and d_2 are the distances of the nuclear centers from the window, and $\dot{\theta}$, $\dot{\theta}_1$, $\dot{\theta}_2$ are the rotational frequencies for the orbital motion, spin 1 and spin 2, respectively. By integrating the Eqs. (5) and (3), subject to the proper initial conditions, we arrive at values for $\ell_1(Z,\ell,t)$ and $\ell_2(Z,\ell,t)$.

(2) The functions $\ell_1(Z,\ell)$, $\ell_2(Z,\ell)$ are obtained by integrating out the time dependence. The average lifetime of the complex for a given ℓ-wave is approximated as the time necessary for the dynamical system with no mass transfer to return to the strong absorption radius under the influence of Coulomb plus Proximity potentials and subject to Proximity friction.[5]

The quantity $d(\ell)$ (mentioned earlier) is the average value of the distance between centers along the trajectory using the Proximity Flux function $\Psi(r)$ [5] for the probability weight function.

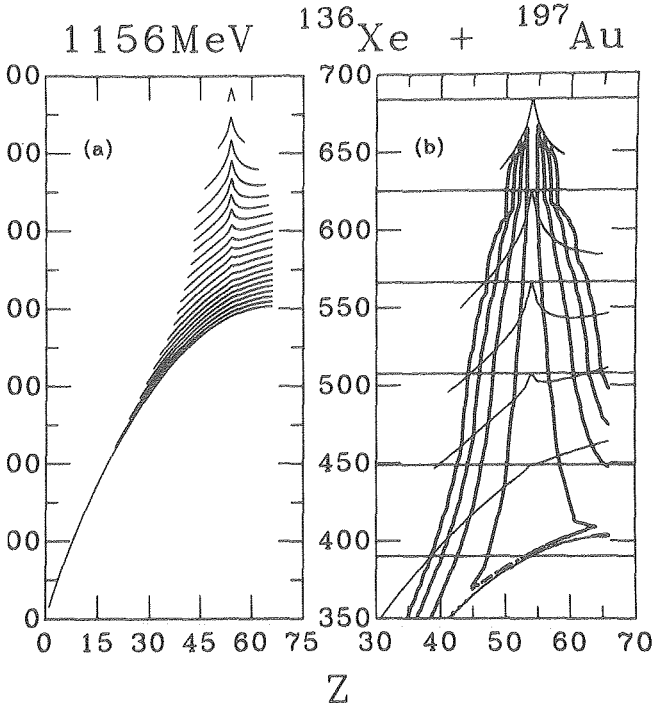

Fig. 2. (a) Lines of constant ℓ calculated for 1156 MeV ^{136}Xe + ^{197}Au using the present model.
(b) Contours of constant $\partial^2\sigma/\partial Z\partial$[TKE] for the same reaction with parallel cuts and calculated cuts drawn in.
(XBL 7711-10427)

It is also necessary to weight the $\ell_i(Z,\ell,t)$ by the probability for forming the system Z at time t. This function, $\phi(Z,t)$, can be obtained by solving a Master Equation or an associated Fokker-Planck equation.

Figure 2a shows the predictions of the model for the system 1156 MeV ^{136}Xe + ^{197}Au. Each pair of adjacent lines brackets 5% of the reaction cross section. Figure 2b shows the upper portion of Fig. 2a, with contours of constant cross section (as calculated by the Fokker-Planck equation) drawn in. The horizontal lines divide the data into ten bins, 30 MeV wide (only every other line

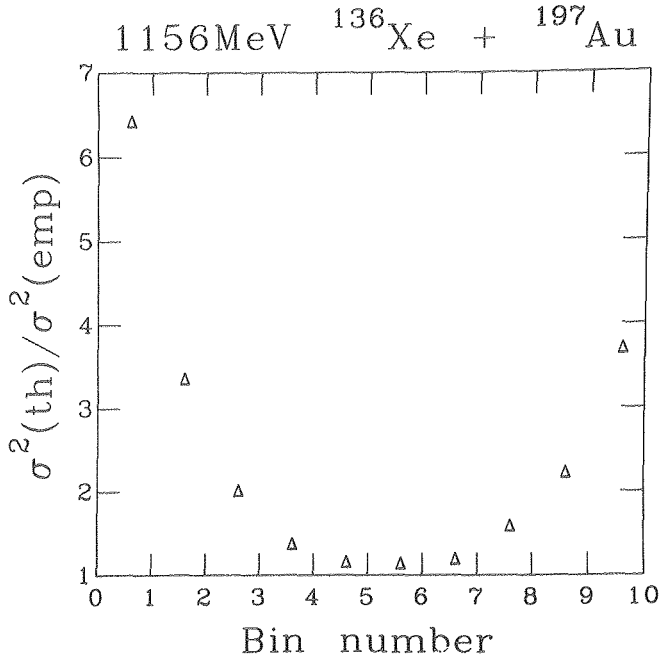

Fig. 3. Ratio of σ_Z^2 from calculated lines and empirical lines vs bin number. The bin number may be related to TKE loss by the following relation: TKE loss = 30·(bin number - ½)MeV.
(XBL 7711-10428)

is shown for ease of viewing). The lines of constant ℓ calculated by the model are chosen to coincide with the parallel lines at the Z of the projectile. Figure 3 is a plot of the ratio of the variance predicted by the present model and the variance derived from the parallel cuts. Note the large difference for the first few bins. It is exactly in this energy region that the previously mentioned discrepancy between experiment and theory was found. If the empirical variances are in error by as much as is indicated by the present work (see Fig. 3), then the discrepancy between experiment and theory disappears.

Footnotes and References

*Condensed from LBL-6596; published in Phys. Rev. Letters 40, 697 (1978).

1. J.R.Huizenga and W.U.Schröder, preprint UR-NSRL-144 (1977), to appear in Ann. Rev. of Nucl. Sci. 27.

2. L.G.Moretto and R.Schmitt, J. de Phys. 11, C5-109 (1976).

3. R.Vandenbosch, M.P.Webb, T.D.Thomas, and M.S.Zisman, Nucl. Phys. A 269, 210 (1976).

4. J.Blocki, Y.Boneh, J.R.Nix, J.Randrup, M.Robel, A.J.Sierk, and W.J.Swiatecki, preprint LBL-6536 (1976).

5. J.Randrup, preprint LBL-5847 (1976).

CHARGE, ENERGY, AND ANGULAR MOMENTUM TRANSFER IN THE SYMMETRIC $^{93}_{41}Nb + ^{93}_{41}Nb$ REACTION

G.J. Mathews, P. Bigeleisen, G.J. Wozniak, R.P. Schmitt, R. Regimbart, G. Rattazzi, L. Sobotka, A. Behkami, L.G. Moretto, J.S. Sventek, R.M. Diamond, H. Hübel, and F. Stephens

I. Introduction

Reaction products from a symmetric system are of interest for two reasons. On the one hand a symmetric system affords a more sensitive test of diffusion-model calculations, as will be explained in section II. On the other hand a symmetric system is perhaps the only system for which the possible role of giant resonances in the initial stages of energy dissipation can be isolated. This will be discussed in section III.

II. Comparison with Diffusion-Model Calculations

To see how a symmetric system provides a more sensitive test of the diffusion model, it is worthwhile to examine the effective potential energy of the system as a function of asymmetry and angular momentum. This potential energy is shown in Fig. 1 for two overlapping spheres. The point to note is that the derivative of the potential with Z is zero at the injection point and does not change much over a large range of Z and ℓ. These qualitative remarks should remain true even if the system deviates significantly from a configuration of two overlapping spheres. The effect of this feature of the reaction can be seen by recourse to the Fokker-Planck approximation in the notation of Ref. 1 which gives for the time evolution of the population of channel Z,

$$\dot{\phi}(Z,t) = -\frac{\partial}{\partial Z}\left[\mu_1\phi(Z,t)\right] + \tfrac{1}{2}\frac{\partial^2}{\partial Z^2}\left[\mu_2\phi(Z,t)\right] .$$

where

$$\mu_1 \cong -\kappa f \left(\frac{\partial V}{\partial Z}\right)/T$$

$$\mu_2 \cong 2\kappa f \quad .$$

When the derivative of the potential is zero, only the spreading velocity μ_2 remains, which is independent of the potential. Hence, to first order in a symmetric system we are sampling only the form factor, κf, which is the effective particle transfer rate.[2]

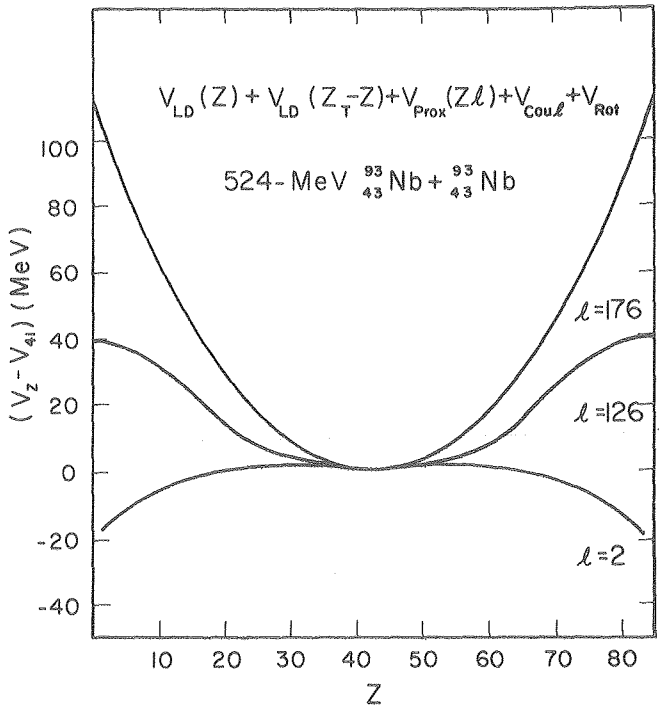

Fig. 1. Effective potential energies for the 524-MeV $^{93}_{41}Nb + ^{93}_{41}Nb$ reaction.

(XBL 787-1265)

In Fig. 2 we show the experimental total angle-integrated charge distribution obtained with ionization – counter solid-state telescopes. Also shown for comparison are results from the most recent diffusion-model calculations[3] obtained in the one-body framework with no free parameters. Although the overall agreement is quite good there does appear to be a systematic underestimation of the cross sections for the lighter Z's. The agreement at higher Z's is not necessarily significant since those data may be subject to systematic errors due to difficulty in identifying Z-lines and the fact that angular distributions included few

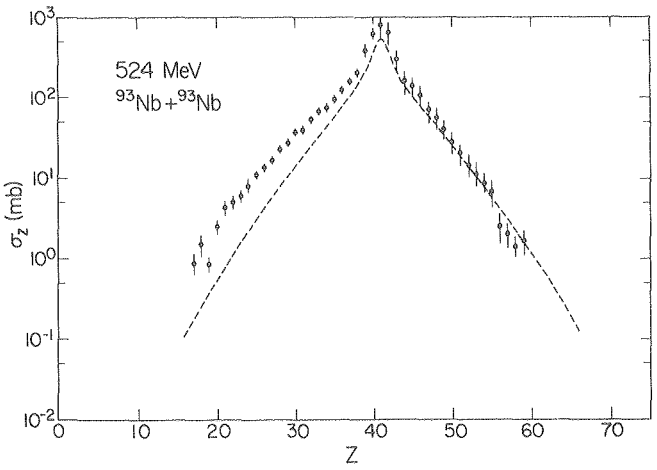

Fig. 2. Charge distribution for the 524-MeV $^{93}_{41}Nb + ^{93}_{41}Nb$ reaction.

(XBL 784-663)

points. An effort has been made to reconcile the theory with the data by the inclusion of secondary particle evaporation. The result, however, is that for the average excitation energies (~20-30 MeV) computed in the diffusion-model framework, the light Z's are displaced by only about one charge unit, an insufficient amount to produce agreement. The tentative conclusion is therefore that we are observing a deficiency of the diffusion model form factors derived from the one-body arguments. Except for this normalization problem, the agreement in the angular distribution (not shown) is reasonable.

III. Possible Role of Giant Resonances

Recently, a good deal of excitement has been generated over the possibility of observing resonances in symmetric light-ion reactions at angles far forward of the grazing angle. Should the interpretations of the phenomena as giant resonances be correct, this observation could provide much insight into the energy dissipation mechanism in heavy-ion collisions. Although a clear identification of the resonance structure in the energy spectrum requires charge and mass isolation, we see some evidence for structure in the Z = 41 spectrum shown in Fig. 3. The bump in the spectrum near 480 MeV lab energy would correspond to about 20 MeV excitation of the system, consistent with giant mode excitation.

Perhaps the most distinctive feature of the giant resonances is their associated low angular momentum. Therefore we have also obtained γ-ray multiplicities as a function of energy for this reaction. Unfortunately, however, the statistics

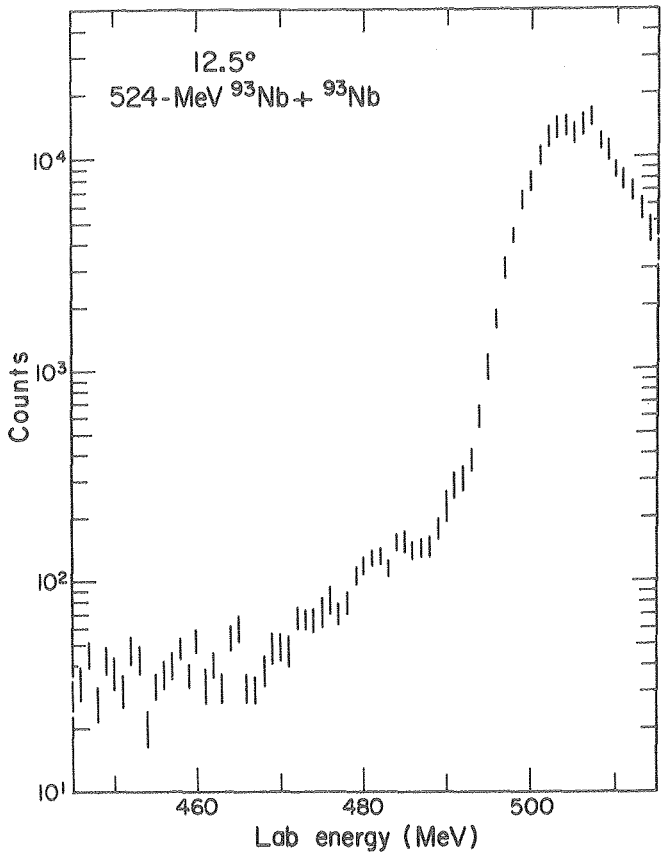

Fig. 3. Energy spectrum for Z = 41 fragments from the 524-MeV $^{93}_{41}Nb + ^{93}_{41}Nb$ reaction.

(XBL 784-710)

at present are too poor to indicate a correlation between the structure in the energy spectrum and the associated multiplicity. We have also employed a large-solid-angle position-sensitive detector in this experiment to kinematically isolate the ^{93}Nb binary reactions and to provide crude mass identification. Convincing results, however, are pending the accumulation of better statistics.

References

1. L.G.Moretto and R.Schmitt, J. de Phys. 11, C5-109 (1976).

2. L.G.Moretto, in Proceedings of the Tokyo International Conference on Nuclear Structure (Tokyo, Japan, 1977).

3. J.S.Sventek, elsewhere in this report.

4. N.Frascaria, C.Stéphan, P.Colombani, J.P. Garron, J.C.Jacmart, M.Riou, and L.Tassan-Got, Phys. Rev. Lett. 39, 918 (1977).

THE LIGHT ELEMENT ABUNDANCES, GALACTIC EVOLUTION, AND THE UNIVERSAL BARYON DENSITY

G.J. Mathews and V.E. Viola, Jr.

The present mean universal mean baryon density, ρ_b, is of particular interest because in Friedmann cosmologies with no cosmological constant, it is this quantity together with the Hubble constant, H_o, which determines the spatial curvature of the universe, i.e., whether it is open or closed. The available indicators of ρ_b have been reviewed in detail by Gott et al.[1] They concluded that the most stringent upper limit to ρ_b (and, in particular, the only datum that seems to preclude the possibility of a closed universe) comes from the present deuterium abundance.

In this paper we propose an alternative method to evaluate the range of permissible values of ρ_b. The method considers the abundance of both D and ^{7}Li. By utilizing the abundance ratio of ^{7}Li to D, we show here that the difficulty associated with the astration process can be essentially cancelled from the problem. Further, this method is slightly more sensitive to ρ_b than the method which uses the D abundance alone.

The method we propose is quite straightforward. To begin with, the present mass fraction of D and ^{7}Li, (X_D^P and $X_{^7Li}^P$) in the interstellar medium can be written as the sum of galactic (X^G) and big-bang (X^{BB}) contributions,

$$X_D^P = F_D X_D^{BB} + X_D^G \qquad (1)$$

$$X_{^7Li}^P = F_{^7Li} X_{^7Li}^{BB} + X_{^7Li}^G \ . \qquad (2)$$

The quantities F_L ($L = D, ^7Li$) are the fraction of the primordial material of each species that has survived astration. These quantities depend on the details of galactic evolution and are not known. Nevertheless, we demonstrate here that these quantities are both nonzero and nearly identical, and therefore can be cancelled from the problem of finding the limits to ρ_b.

If the ratio of the abundance of the primordial material, L, in a star of mass m at the end of its main sequence lifetime to the interstellar abundance of L at time t is small, then the quantities F_L take the analytical form

$$F_L(t) = e^{-S(t)}\left[1 + \int R(t)\, e^{S(t)}\right]dt \ , \qquad (3)$$

$$S(t) = \int\left[\int E(t,m)dm + R(t)\right] dt \ . \qquad (4)$$

E(t,m) is the fractional rate of increase of the interstellar medium by ejection of material from stars which have evolved from the main sequence. R(t) is the fractional rate of increase of the interstellar medium by infall. No L-dependent terms appear on the right-hand side. Therefore,

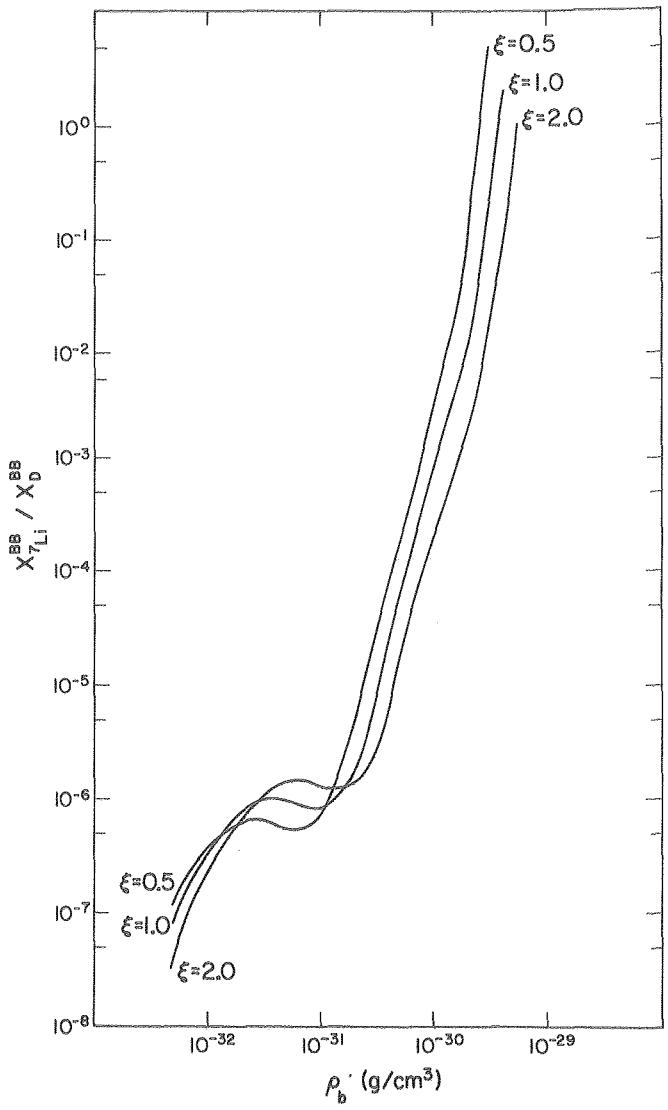

Fig. 1. The ratio of ^{7}Li to D mass fractions as a function of the present baryon density for a present background temperature of 2.8°K. The curve labeled $\xi = 1.0$ corresponds to the standard big bang.[2] The curves labeled $\xi = 0.5, 2.0$ correspond to a scaling of the free expansion trajectory consistent with the range of the observed ^{4}He abundance.

(XBL 784-662)

$F_{^7Li}(t) = F_D(t)$. Further, this equality will continue to be true even if the relative destruction rates of ^{7}Li and D in stellar interiors differ by orders of magnitude as long as they are both small compared to unity. Finally, it is worthwhile to note that the quantity S(t) is finite over the lifetime of the galaxy. Therefore the present value of F_L is nonzero. This means that we can take the ratio of Eqs. (1) and (2) and make use of the equality of the surviving fractions of primordial material to write,

$$\frac{(1-G_{^7Li})X^P_{^7Li}}{X^P_D} < \frac{X^{BB}_{^7Li}}{X^{BB}_D} < \frac{X^P_{^7Li}}{X^P_D(1-G_D)} \quad , \qquad (7)$$

which is true in principle even if only a few atoms of primordial ^{7}Li and D have survived galactic evolution! The quantities $G_{^7Li}$ and G_D correspond to the fraction of ^{7}Li or D which is of non-big-bang origin. Although these quantities are not well known, the dependence of $(X^{BB}_{^7Li}/X^{BB}_D)$ on the baryon density is rather steep. Therefore, conclusions can be reached about ρ_b even over a broad range of possible values for $G_{^7Li}$ and G_D.

The sensitivity of the ratio $X^{BB}_{^7Li}/X^{BB}_D$ to ρ_b can be seen in Fig. 1 where we plot the results obtained from the big-bang nucleosynthesis code of Wagoner.[2] In the region of interest (near $10^{-31} \leq \rho_b \leq 10^{-30}$) the ratio varies as $\rho_b^{3.6}$. This is to be compared with the X_D value alone which varies as ρ_b^{-2} in the same region.

In Table 1 the range of inferred values are given for ρ_b and Ω (the ratio of the present density to that required to close the universe). These results are very close to the results obtained by Gott et al. using X_D alone, which showed that $\rho_b = 4(3)\times10^{-31}$ g/cm^3 for $\xi = 1$, $G_D = 0$, and $F_D = 0.5$, yet the present results are less model-dependent since the parameter F_D has been eliminated.

Table 1. Calculated values of $X^{BB}_{^7Li}/X^{BB}_D$, ρ_b, and Ω.

Best guess	$X^{BB}_{^7Li}/X^{BB}_D$	ρ_b (gm/cm^3)	Ω $H_o = 50$
$\xi = 1$, $G_D = 0.0$, $G_{^7Li} = 0.15$	2.1×10^{-4}	$7.1(1.0)\times10^{-31}$	0.15(2)
$G_D = 0.90$, $G_{^7Li} = 0$	2.5×10^{-3}	1.4×10^{-30}	0.30
$G_{^7Li} = 0.90$, $G_D = 0$	2.5×10^{-5}	4.0×10^{-31}	0.09
$\xi = 0.5$	2.1×10^{-4}	5.5×10^{-31}	0.12
$\xi = 2.0$	2.1×10^{-4}	1.0×10^{-30}	0.21

References

1. R.J.Gott, J.E.Gunn, D.N.Schramm, and B.M. Tinsley, Ap. J. 194, 543 (1974).

2. R.V.Wagoner, Ap. J. 179, 343 (1973).

A DYNAMICAL MONTE-CARLO DESCRIPTION OF NUCLEON TRANSPORT IN HEAVY-ION COLLISIONS

G.J. Mathews, J.S. Sventek, and L.G. Moretto

The diffusion model, which describes the heavy-ion interaction in terms of non-equilibrium statistical nucleon transport, has enjoyed rather convincing success for a large number of target, projectile, and energy combinations.[1,2] Nevertheless, one uncomfortable feature of this model has been the reliance on time-averaged estimates of the dynamical features of the system, e.g., the potential energy, the diffusion window, etc. A further limitation of the diffusion model to date stems from its sheer size. A proper treatment requires a diagonalization of at least an $n_z \times n_z$ matrix ($n_z = z_{tgt} + z_{proj}$) for each ℓ-wave, where n_z can become large, $\gtrsim 100$, for even moderately heavy systems.

In this work we describe a model of transport in heavy-ion collisions which circumvents both of these difficulties associated with conventional diffusion-model descriptions. The scenario we propose, with the expectation that this is a more accurate description of the way in which Nature proceeds, is the following: the classical equations of motion for two spherical nuclei interacting under the Coulomb and proximity forces are solved and coupled with the time-dependent probability of nucleon transfer. A random number decides when a transfer occurs. Following a transfer the dynamical quantities are then adjusted for the dissipation and geometrical changes introduced by the transfer and the solution of the classical equations of motion continued.

The code has the distinct advantage of being small enough to allow calculations for even the heaviest systems to be performed on a small computer. Although many events must be calculated, the computations are quite rapid so that the calculation is not cost-prohibitive.

Since by now it is widely recognized that charge and mass transfer are highly correlated, we simplify the discussion here to consider only charge-unit transfer. However, the generalization to independent neutron and proton degrees of freedom should be obvious.

The rate equation for the time evolution of a channel, Z, is

$$\dot{P}_Z(t) = -[\Lambda_+(Z,t) + \Lambda_-(Z,t)]\, P_Z(t) \quad , \quad (1)$$

where P_Z is the probability that the system is in channel Z at time t. The $\Lambda_\pm(Z,t)$ are the transition probabilities for the system to find itself in the $Z \pm 1$ configuration. Similarly, from the relative rates for forming the $Z \pm 1$ system,

$$\dot{P}_{Z\pm1}(t) = \Lambda_\pm(t)\, P_Z(t) \quad , \quad (2)$$

we obtain the probability that the system has translated in one direction or the other

$$P_{Z\pm1}(t+dt) = P_{Z\pm1}(t) + \frac{\Lambda_\pm(t)}{\Lambda_+(t) + \Lambda_-(t)} \times \left(P_Z(t) - P_Z(t+dt)\right) \quad . \quad (3)$$

To compute the time evolution of the system then, we begin with the initial conditions; $P_Z(t_0) = 1$, $P_{Z\pm1}(t_0) = 0$. Equations (1) and (2) are then solved along with the equations of motion until a transfer occurs, at which point the variables and form factors as well as the initial conditions are reset at the new asymmetry.

If the system transfers a charge unit (or nucleon) from one nucleus to the other in the one-body picture, that charge unit carries its corresponding collective linear and angular momentum. In the framework of this model we readjust the coordinates of the system in the following way:

We assume a constant overlap during the interaction, so that the new radius R' is

$$R' = R + C_{Z_1\pm1} + C_{Z_2\mp1} - C_{Z_1} - C_{Z_2} \quad , \quad (4)$$

where R is the radius before the interaction, and C_Z is the central nuclear radius.[3]

The transfer carries with it the linear momentum associated with its collective motion:

$$\vec{p} = \frac{m}{M}\vec{P} \quad , \quad (5)$$

where $\vec{P}$ is the center-of-mass momentum prior to the transfer, M is the mass of the fragment in which the particle initially resided, and m = A/Z is the effective mass of the transferred charge unit, so that

$$\vec{P}' = \vec{P} - \vec{p} \quad . \quad (6)$$

For the angular momentum transfer we assume rigid body inertias for the nuclei. The transferred angular momentum for a transfer from fragment 1 to 2 is,[4]

$$\ell_{Z_1+1} = -md_{Z_1}^2\dot{\theta}_{Z_1} \quad (7)$$

$$\ell_{Z_1-1} = md_{Z_1}d_{Z_2}(\theta - \dot{\theta}_{Z_2}) + md_{Z_2}\dot{\theta}_{Z_2} \quad (8)$$

where d_Z is the distance from the nuclear center to the window between the two fragments.

Past calculations[5] have estimated the average interaction time of the two ions by the lifetime of the entrance-channel trajectory of the two interpenetrating ions. The beauty and simplicity of the Monte Carlo treatment is that this quantity is automatically derived from the calculation for all asymmetries.

In Fig. 1 we show some calculated lifetimes and variances. The most striking feature of the lifetimes is the tendency to saturate at lower ℓ-waves. This same phenomenon would be observed in a trajectory with no diffusion or dissipation.

Also worth mentioning is the variance in the lifetimes. The first thing to note is that there is, in general, no strictly linear relation between τ and σ^2. The second point to note is that the variances are quite small, $\sigma^2 \sim 0.05\,\tau$, indicating a very narrow spread of lifetimes. Values of as large as $1.5\,\tau$ have been employed in past calculations.[1] It should be kept in mind, however, that not all thermal fluctuations are included in these calculations.

Charge distributions for 620-MeV ^{86}Kr + ^{197}Au are shown in Fig. 2 and compared with the experi-

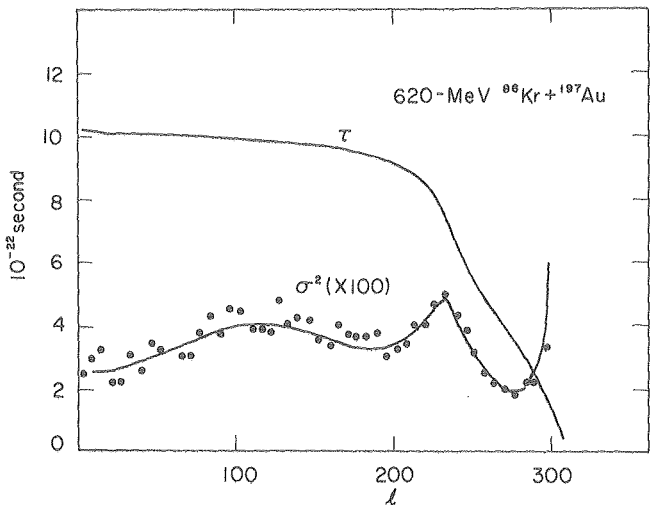

Fig. 1. Calculated average lifetimes and variances. (XBL 787-1253)

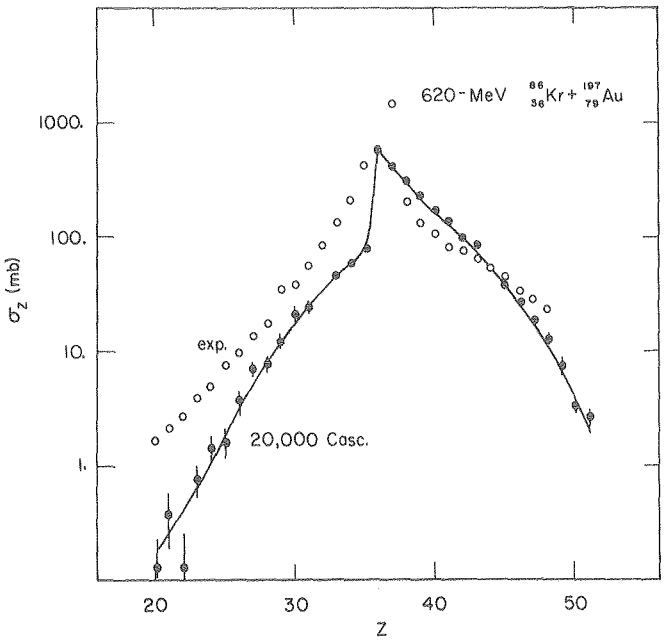

Fig. 2. Calculated and experimental total charge distribution for 620-MeV $^{86}_{36}Kr + ^{197}_{79}Au$.
(XBL 787-1255)

mental data. The first point to make note of is that the overall trend in the data is well reproduced. Nevertheless, there does seem to emerge a discrepancy for Z's far removed from the projectile. This feature is even more apparent in lighter ion calculations.

In the calculated gamma-ray multiplicities (not shown) there is a similar effect of insufficient angular momentum transfer, symptomatic in the one-body picture of insufficient diffusion.

The key to the deficiency of the model is in the angular distributions. Although the side peak in the angular distributions is reproduced, this side peak persists for Z's well away from the projectile. This is evidence that the lifetimes for the system calculated for the trajectory of two spherical nuclei undergoing particle exchange are simply too short.

Perhaps the way out of this problem is to introduce an aspect of the scenario which has not been considered explicitly in previous treatments, namely, that the intermediate complex is expected to undergo neck formation. This neck may be expected to increase the lifetime and diffusion window in the exit channel. Efforts are currently under way to incorporate this feature schematically into the calculations.

Other proposed refinements of the code include consideration of proton and neutron degrees of freedom separately. In this way the charge equilibration process can be studied. Also the interfacing of the code to a second Monte Carlo code, which computes particle evaporation and secondary fission, is under way.

References

1. L.G.Moretto and R.Schmitt, J. de Phys. 11, C5-109 (1976).

2. L.G.Moretto, Proceedings of the Tokyo International Conference on Nuclear Structure (Tokyo, Japan, 1977).

3. W.D.Myers, Nucl. Phys. A 204, 465 (1973).

4. J.S.Sventek and L.G.Moretto, Phys. Rev. Lett. 40, 697 (1978).

5. J.S.Sventek and L.G.Moretto, elsewhere in this report.

ASYMMETRY-DEPENDENT ANGULAR MOMENTUM DISTRIBUTIONS RESULTING FROM A DIFFUSIVE MASS TRANSFER MECHANISM*

J.S. Sventek

Average gamma-ray multiplicities $\langle M_\gamma \rangle$ in coincidence with deep-inelastic products have been measured for a variety of systems,[1-4] with the most recent measurements[5,6] providing the second and third moments of the multiplicity distributions. A general feature of the data is that for those systems in which essentially all ℓ-waves lead to deep-inelastic products, the multiplicities display very little dependence upon asymmetry.[1,5,6] This behavior seems to be due to the preferential population of asymmetries far removed from the entrance channel asymmetry by smaller ℓ-waves than those that populate asymmetries near the entrance channel. The second moments of the M_γ distributions are systematically larger than those expected from a triangular $2\ell+1$ distribution.[5,6] (The ratio of the standard deviation of the M_γ distribution and the mean value, $\rho \equiv \sigma/\langle M_\gamma \rangle$, has been measured experimentally to be $\rho \approx 0.5$, independent of asymmetry, while a $2\ell+1$ distribution predicts $\rho = \sqrt{2}/4 \approx 0.35$. This discrepancy is not particularly surprising since a $2\ell+1$ distribution does not predict the correct multiplicities for the systems for which the second moments have been measured.

The purpose of this report is to show that systems exhibiting the features described above can be described by rigid rotation accompanied by diffusive mass transfer. An analytic model is used to explore the general dependence of the angular momentum distributions upon mass-asymmetry.

In order to simplify the calculations, it is assumed that the time dependence of the mass asymmetry mode can be described by a solution to a Fokker-Planck differential equation with no drift, i.e., a purely diffusive degree of freedom.[7,8] Such a solution takes the form

$$P(Z,t) = \frac{1}{[4\pi\mu_2 t]^{\frac{1}{2}}} \exp\left[-\frac{(Z-Z_p)^2}{2\mu_2 t}\right] \quad (1)$$

where P is the probability of producing a complex with asymmetry Z after an interaction time t, Z_p is the entrance channel asymmetry, and μ_2 is the spread coefficient for the mass asymmetry mode. The cross section due to a collision with impact parameter b can be expressed as

$$\frac{\partial^2\sigma}{\partial Z \partial b}(Z,b) = 2\pi b\, P(Z,\tau(b)) \quad (2)$$

where $\tau(b)$ is the interaction time for the trajectory with impact parameter b. It has been well established experimentally[9,10] that the interaction times $\tau(b)$ must be a decreasing function of b. The simplest form such a function may take (and the form used) is

$$\tau(b) = \tau_o\left(1 - \frac{b}{b_{max}}\right) . \quad (3)$$

Substituting Eq. (3) into (2), defining $\beta_Z \equiv (Z-Z_p)^2/2\mu_2\tau_o$, and changing variables to $\eta = b/b_{max}$, one arrives at

$$\Phi(\beta,\eta) = \frac{\eta}{[1-\eta]^{\frac{1}{2}}} e^{-\beta/(1-\eta)} , \quad (4)$$

where multiplicative factors independent of β and η are ignored. The function $\Phi(\beta,\eta)$ is the distribution function for the cross section as a function of asymmetry β and angular momentum η; for fixed β, it represents the angular momentum distribution function for that asymmetry. It is the moments of this distribution function, and their dependence upon asymmetry, which is of interest and may be compared with experiment.

Given the angular momentum limits η_1,η_2 $(0 \leq \eta_1 < \eta_2 \leq 1$; η_1 may account for compound nucleus cross section and η_2 may delimit the quasi-elastic cross section) and the asymmetry β, one may write the moments of the angular momentum distribution as

$$\mu_m = \int_{\eta_1}^{\eta_2} \eta^m \Phi(\beta,\eta)\, d\eta . \quad (5)$$

By making the change of variable $x = (1-\eta)^{-1}$ and defining $u_i \equiv (1-\eta_i)^{-1}$ for $i = 1,2$, one arrives at

$$u_m = \sum_{i=0}^{m+1} (-1)^i \frac{(m+1)!}{(m+1-i)!\,i!} \xi_i(u_1,u_2,\beta) , \quad (6a)$$

where

$$\xi_i(u_1,u_2,\beta) = \int_{u_1}^{u_2} x^{-(i+3/2)} e^{-\beta x}\, dx . \quad (6b)$$

The integrals ξ_i are determined from a recurrence relation.

In order to compare with experiment, it is necessary to evaluate algebraic combinations of the normalized moments

$$\upsilon_i = \mu_i/\mu_o .$$

The most frequently quoted parameters describing a distribution are listed in Table 1.

Consider a system in which essentially all impact parameters contribute to the deep-inelastic process, implying $\eta_1 \approx 0$ and $\eta_2 \approx 1$. In order to account for events in which the kinetic energy is incompletely damped, it is assumed that $\eta_1 = 0$ and $\eta_2 = 0.9$, thus allowing 20% of the cross section for incompletely damped (QE) events. Plotted in Fig. 1 are $\langle\eta\rangle$, σ, γ, and ρ as a function of asymmetry. Three very striking features emerge:

1. Angular momentum fractionation ($\langle\eta\rangle$ decreases as a function of β)[1] is a natural occurrence for systems with this type of angular momentum window.

2. The ratio ρ exceeds the $2\ell+1$ value for nearly all asymmetries.

3. The skewness γ changes sign as a function of asymmetry. This fact is easily understood since the distribution for $\beta \approx 0$ is nearly a $2\ell+1$ distribution, with an associated $\gamma < 0$. As β increases, the highest ℓ-waves play a lesser role in populating the larger asymmetry (due to the short lifetimes), with the result that the angular momentum distributions become more symmetric and eventually display a positive skewness.

Table 1. The most frequently quoted parameters describing an angular momentum distribution.

Name	Order	Expression
mean	1	$\langle\eta\rangle = \upsilon_1$
variance	2	$\sigma^2 = \upsilon_2 - \upsilon_1^2$
skewness	3	$\gamma = \dfrac{(\upsilon_3 - 3\upsilon_1\upsilon_2 + 2\upsilon_1^3)}{2\sigma^3}$

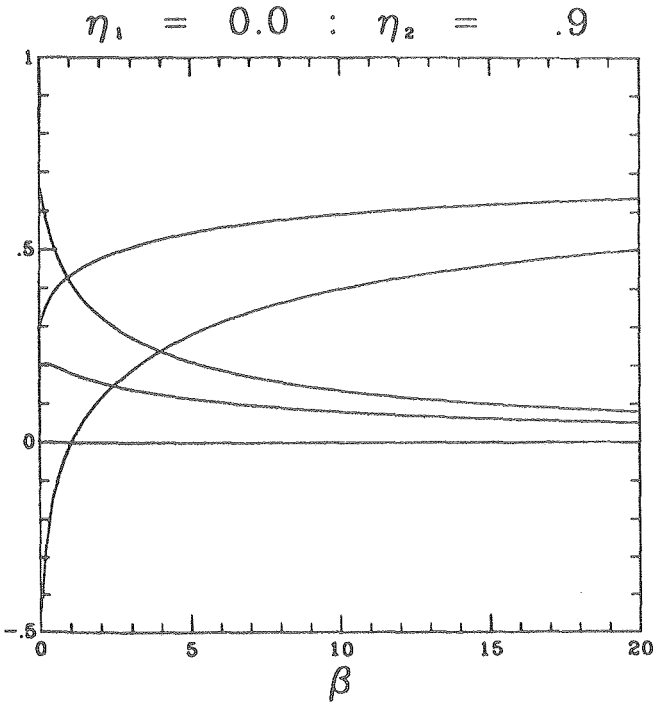

Fig. 1. Plots of $\langle\eta\rangle$, σ, γ, ρ as a function of for $\eta_1 = 0$, $\eta_2 = 0.9$. (XBL 785-8899)

In order to compare with experiment it is necessary to correlate β with Z. From previous work in fitting data from 620-MeV $^{86}Kr + ^{197}Au$, the following parameters were used:

$$\mu_2 = 1 \text{ (charge unit)}^2 / 10^{-22} \text{ sec} ,$$

$$\tau_o = 2.5 \times 10^{-21} \text{ sec} .$$

The curve of asterisks in Fig. 1 is a plot of the multiplicities assuming rigid rotation and E2 multipolarity of the resulting gamma rays. As can be seen, the multiplicities are approximately constant as a function of Z, in agreement with the data. The large values of ρ measured for similar systems has also been shown to be predicted. The data on the skewness is harder to compare, as in Ref. 5 the skewness is given as a function of energy loss integrated over asymmetry. Preliminary data at LBL[6] indicates that the skewness for most asymmetries for a similar system are positive for the deep-inelastic products.

Footnote and References

*Condensed from LBL-7716.

1. M.M.Aleonard, G.J.Wozniak, P.Glässel, M.A. Deleplanque, R.M.Diamond, L.G.Moretto, R.P.Schmitt, and F.S.Stephens, Phys. Rev. Lett. 40, 622 (1978).

2. P.Glässel, R.S.Simon, R.M.Diamond, R.O.Jared, I.Y.Lee, L.G.Moretto, J.O.Newton, R.Schmitt, and F.S.Stephens, Phys. Rev. Lett. 38, 331 (1977).

3. M.Berlanger, M.A.Deleplanque, C.Gerschel, F.Hanappe, M.Leblanc, J.F.Mayault, C.Ngo, D.Paya, N.Perrin, J.Peter, B.Tamain, and L.Valentin, J. Phys. 37, L323 (1976).

4. J.B.Natowitz, M.N.Namboodiri, P.Kasiraj, R.Eggers, L.Adler, P.Gonthier, C.Cerruti, and T.Alleman, Phys. Rev. Lett. D 4, 751 (1978).

5. P.R.Christensen, F.Folkmann, O.Hansen, O.Nathan, N.Trautner, F.Videbaek, S.Y.van der Werf, H.C.Britt, R.P.Chestnut, H.Freiesleben, and F.Puhlhofer, preprint (March 1978).

6. G.J.Wozniak, R.P.Schmitt, L.G.Moretto, R.M. Diamond, and F.S.Stephens, in preparation.

7. W.Norenberg, Phys. Lett. B 52, 289 (1974).

8. L.G.Moretto and R.Schmitt, J. Phys. 11, C5-109 (1976).

9. L.G.Moretto, B.Cauvin, P.Glässel, R.Jared, P.Russo, J.Sventek, and G.Wozniak, Phys. Rev. Lett. 36, 1069 (1976).

10. W.U.Schroder, J.R.Birkelund, J.R.Huizenga, K.L.Wolf, and V.E.Viola, Phys. Rev. C 16, 623 (1977).

11. J.S.Sventek and L.G.Moretto, Phys. Lett. B 65, 326 (1976).

TOWARD A UNIFIED DIFFUSION MODEL

J.S. Sventek

The success of the Diffusion Model in predicting the observables in deep-inelastic collisions[1-3] has lent credence to a master equation description of the motion of nuclear systems along the mass-asymmetry degree of freedom. This report describes enhancements to the model which permit all quantities to be determined from first principles. Reference 1 may be consulted for a complete description of the model prior to the changes described here.

Previous investigations[2,3] have shown that the assumption of two touching spheres for the shape of the intermediate complex in deep-inelastic collisions is too simplistic; in fact, for some of the heavier systems,[3] the data seem to indicate that the complex shape is better described by two overlapping spheres. In order to determine these overlaps, and also to calculate the interaction times, classical dynamics under the influence of the proximity potential[4] and proximity friction[5] is used. For each partial wave, the average overlap along the trajectory and the interaction time are calculated for a nuclear system with no mass transfer. These quantities are then used in the sections described below.

The driving potential for the mass-asymmetry master equation is calculated assuming the nuclear overlap remains constant as a function of asymmetry for a given partial wave, and has the value calculated above. Previous versions of the model assumed that the overlap was zero (touching spheres) for all partial waves and for all asymmetries. The transition matrix element formerly had the following form:

$$\Lambda = \kappa f \exp\left(-\frac{\Delta V}{2T}\right) \qquad (1)$$

where κ was a parameter with units of charge flux, f was the areal form factor, ΔV was the difference in the driving potential between the initial and final states, and T was the nuclear temperature. They now have the following form:

$$\Lambda = n_0\left[2\pi \frac{R_1 R_2}{R_1 + R_2} b\right] \Psi(s) \exp\left(-\frac{\Delta V}{\mathcal{T}}\right) \qquad (2)$$

where n_0 is the one-sided flux of charges [and has the same value as κ in Eq. (1)], the quantity in brackets is equivalent to f in Eq. (1), $\Psi(s)$ is a unitless function describing the modification of the flux for compact or extended shapes, and $\mathcal{T}$ is the average energy of a nucleon above the potential barrier between the two nuclear potential wells. In the limit of two touching spheres $\Psi \approx 1$ and $\mathcal{T} \approx 2T$, thereby resulting in Eq. (1).

Reference 2 introduced the concept of the probability distribution for the lifetime of the complex, denoted $\Pi(t)$, which was a gaussian centered about the interaction time. A Brownian motion analysis of the motion along the radial coordinate for nuclear systems indicates that the variance and centroid of the time distribution are related by

$$\sigma^2 = \tfrac{1}{4}\tau \quad . \qquad (3)$$

Comparisons of some experimental data and the results calculated using the modified theory may be found elsewhere in this report.[6] As can be seen, the agreement is quite good. Further comparisons are being carried out to check the behavior of the theory when:

a) The same target is bombarded by several different projectiles with approximately the same energy/nucleon;

b) Several different targets are bombarded by the same projectile with the same energy;

c) The same target is bombarded by the same projectile at several different energies;

d) A symmetric target-projectile system interacts at several different energies.

References

1. L.G.Moretto and J.S.Sventek, Phys. Lett. B 58, 26 (1975).

2. J.S.Sventek and L.G.Moretto, Phys. Lett. B 65, 326 (1976).

3. P.Russo, R.P.Schmitt, G.J.Wozniak, R.C.Jared, P.Glässel, B.Cauvin, J.S.Sventek, and L.G.Moretto, Nucl. Phys. A 281, 509 (1977).

4. J.Blocki, J.Randrup, W.J.Swiatecki, and C.F.Tsang, Ann. Phys. 105, 427 (1977).

5. J.Randrup, Nordita preprint (January 1978).

6. See Fig. 3 in "Charge Diffusion in the Reaction ^{197}Au + ^{86}Kr at 506, 620 and 732 MeV Bombarding Energy."

EXCHANGE INTERPRETATION OF ANOMALOUS BACK ANGLE HEAVY ION ELASTIC SCATTERING*

M.S. Zisman

In the past few years a number of groups have been engaged in making careful studies of heavy ion elastic scattering.[1-4] For example, data for the ^{16}O + ^{28}Si system have presently been obtained over the (laboratory) energy range of 33 - 215 MeV. While the results of a "global" optical model search yielded[1] a strongly absorbing, energy independent potential (E18, see Table 1) which fit the data rather well at both high and low energies, the intermediate energies, roughly

TABLE 1. Optical model and bound state parameters.

Set	V (MeV)	r_R [a] (fm)	a_R (fm)	W (MeV)	r_I [a] (fm)	a_I (fm)
			$^{16}O + ^{28}Si$			
E18 [b]	10.0	1.35	0.618	23.4	1.23	0.552
016C	10.0	1.36	0.57	3.6	1.38	0.38
Bound state [c]	--	1.25	0.75	--	--	--

[a] $R = r \times (A_p^{1/3} + A_t^{1/3})$.

[b] Ref. 1.

[c] Depth adjusted to match separation energy.

$40 \leq E_{lab} \leq 60$ MeV, gave evidence for oscillations which were not reproduced by the optical model in any systematic fashion. In particular, it was found that any optical potential which produced suitable back angle oscillations at these intermediate energies invariably predicted that these oscillations would grow more pronounced at higher energies, at variance with the experimental data.

Very recently, additional information on this problem was provided by Braun-Munzinger et al.,[5] who extended the $^{16}O + ^{28}Si$ data at $E_{lab} = 55$ MeV back to 180° by bombarding Al_2O_3 targets with a ^{28}Si beam and measuring the recoil ^{16}O ions at forward angles. These data showed a highly structured angular distribution at c.m. angles beyond about 60°. In fact, the angles beyond about 140° were described rather well by an angular distribution of the form $|P_{26}(\cos\theta)|^2$. Analysis of the data showed[5] that the entire angular distribution can be fit by adding a Regge pole or shape resonance term directly to the "background" S-matrix as calculated with an optical potential such as E18.

As another approach to explaining the highly structured angular distribution obtained for back angle elastic scattering of $^{16}O + ^{28}Si$ at $E_{lab} = 55$ MeV, we note that this sort of behavior is rather similar to the sort of effects one sees in the scattering of comparable mass heavy ions at intermediate energies.[6-8] In many such cases the data have been successfully fit by considering an exchange mechanism (generally called "elastic transfer"). Although the size of the transferred "cluster" in the $^{16}O + ^{28}Si$ system is much larger than those generally considered by this mechanism, it seemed worthwhile (albeit somewhat implausible) to see what effects might be predicted by this model in the present case.

The kinematics of the elastic transfer process are illustrated in Fig. 1. On the left-hand side, we have incoming particle A scattering from a composite particle B = A' + x, where A' is the "core" and x is a nucleon or nucleon cluster, through a scattering angle θ. On the right-hand side, we consider the transfer reaction A + (A'+ x) → A' + (A+x) at angle π-θ, where x is transferred from A' to A. Clearly, if cores A and A' are

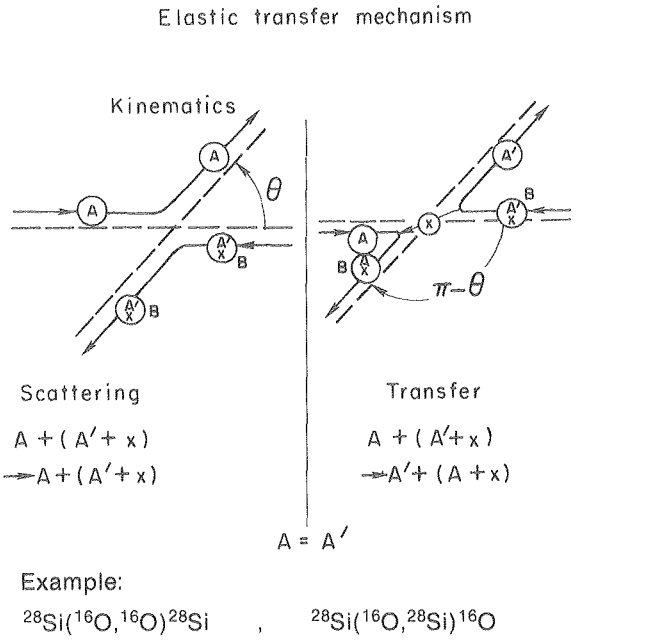

Fig. 1. Kinematics of an elastic transfer reaction. The transfer reaction at π-θ is indistinguishable from the elastic scattering at angle θ.
(XBL 761-2003A)

identical, both of these processes lead to the appearance of a particle A at θ and B at π-θ and are therefore indistinguishable. Quantum mechanically, such a process is one term in a fully antisymmetrized DWBA calculation. Normally such exchange terms are small and are ignored, but in certain cases where the exchange of the cores is equivalent to a simple transfer reaction, the exchange amplitude can be comparable to the direct term.[9]

In practice, calculations of this mechanism have been carried out by a variety of techniques ranging from the LCNO approximation[10] to no-recoil DWBA calculations[7] and, finally, to full finite-range DWBA calculations.[6,8] In the $^{16}O + ^{28}Si$ system, we are considering transfer of a relatively large cluster, ^{12}C. For this reason it is obvious that only a full-finite range approach is appropriate. Therefore all calculations described here were carried out with the code LOLA.[11] Briefly, one adds coherently the elastic scattering amplitude at θ (as obtained from an optical model calculation) to the transfer amplitude at angle π-θ (from the DWBA calculation) which is weighted by the appropriate spectroscopic factor, S. Note that in the case of elastic transfer the symmetry of the reaction means that only a single spectroscopic factor is required to describe the process. To be consistent with other authors,[6,12] included in the cross section expression is an additional phase between the two amplitudes. This is often done in such calculations because other mechanisms (e.g., channel coupling effects), can in principle cause a phase shift in the interference pattern at different energies. However, for the calculations discussed here the phase $\alpha = 0$, expected for transfer of a spin-zero cluster between two 0^+ cores, will be used. Although no theoretical calculation of the spectroscopic factor for ^{28}Si →

$^{16}O + ^{12}C$ is available, one can at least hope that the value resulting from elastic transfer calculations will be energy independent. Because of deficiencies with our choice of a simple cluster wave function, as opposed to a more realistic microscopic calculation, and our lack of knowledge about the parameters of the Woods-Saxon well used to generate the bound state, it is in any case not obvious that one should expect to find that the "theoretical" value of S is the one that will reproduce the measured data.[13]

Figure 2a shows the data of Braun-Munzinger et al.[5] along with (separate) optical model and DWBA calculations for the elastic scattering and the $^{28}Si(^{16}O,^{28}Si)$ reaction, respectively. (The spectroscopic factor used in the figure and in all of the $^{16}O + ^{28}Si$ calculations discussed here is S = 0.3.) Optical parameter sets and bound state parameters are listed in Table 1. We see from Fig. 2a that the back angle data are given quite well by the DWBA calculation. Furthermore, it is clear that in this case the interference between the two processes will be most pronounced in the angular region near 90°. The result of coherently adding the two processes is shown in Fig. 2b. As expected, the forward and backward angular reactions remain more or less unchanged, while the angular region

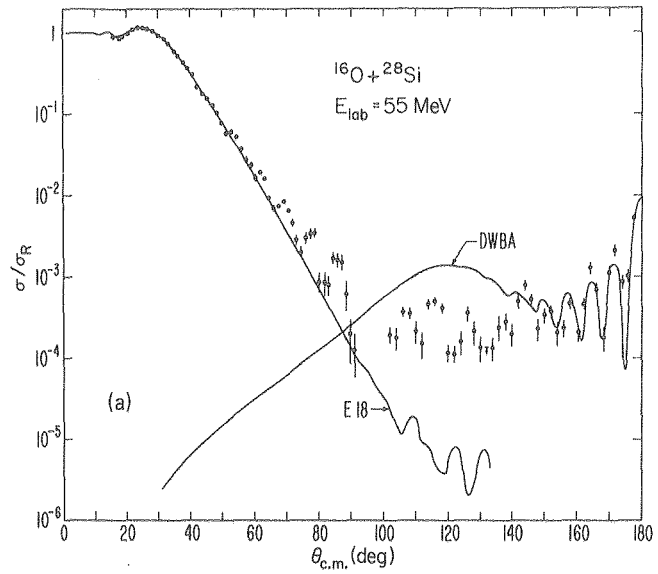

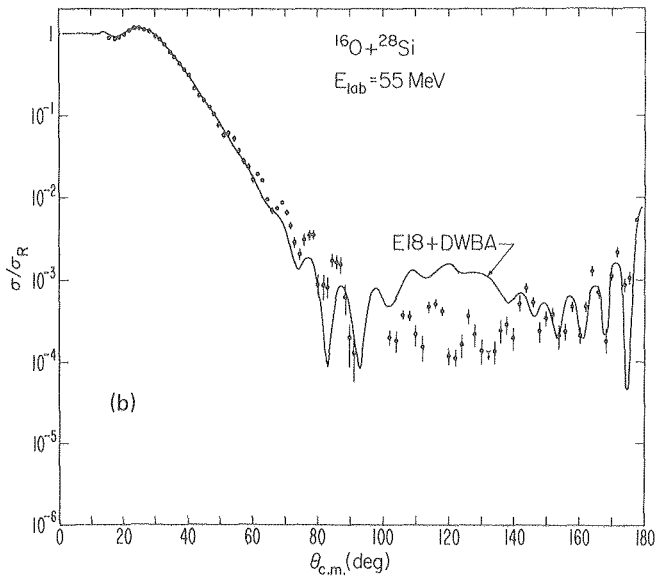

Fig. 2. (a) Optical model and DWBA calculations for $^{16}O + ^{28}Si$ at E_{lab} = 55 MeV, compared with data of Ref. 5. The DWBA calculations (S = 0.3) have been reflected about $\theta_{c.m.}$ = 90°. Optical model and bound state parameters are given in Table 1.
(b) Coherent addition of the cross sections shown in (a).

[(a) XBL 7710-2081 (b)) XBL 7710-2087]

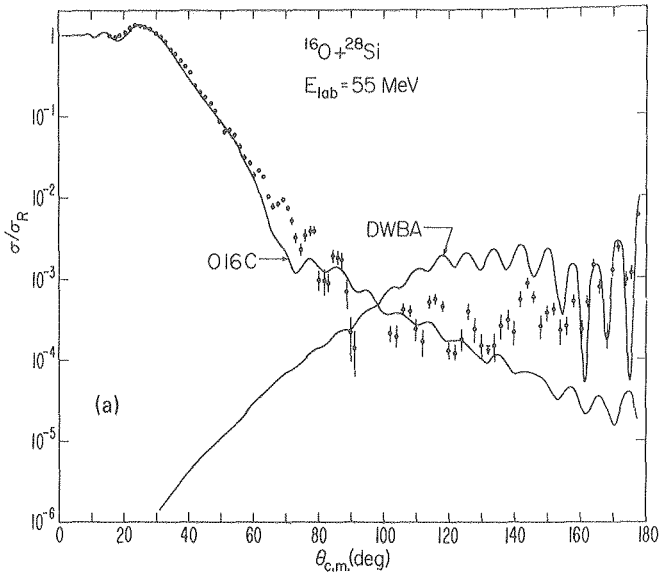

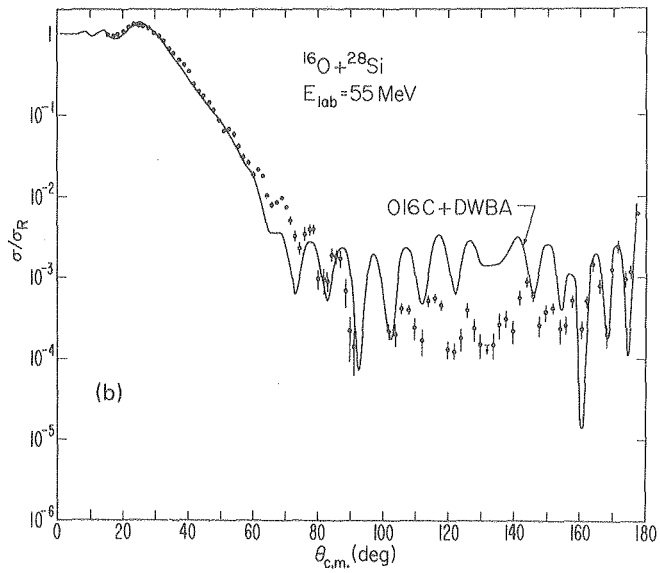

Fig. 3. (a) Optical model and DWBA calculations for $^{16}O + ^{28}Si$ at E_{lab} = 55 MeV, using optical potential O16C. The DWBA calculations (S = 0.3) have been reflected about $\theta_{c.m.}$ = 90°. Optical model and bound state parameters are given in Table 1.
(b) Coherent addition of the cross sections shown in (a).

[(a) XBL 7710-2084 (b) XBL 7710-2088]

between about 60°-100° shows strong interference effects, in agreement with the experimental data.

The remaining discrepancy with the experimental data is that in the angular region near 120° there is not predicted to be as much structure as was observed. In order to improve this aspect, in Fig. 3a a different optical potential set was tried which (probably because of reflection from the imaginary well) gives more elastic cross section at back angles. It is possible that this technique is mocking up some other effect, such as coupled channels[13]; the choice of this optical potential (set 016C in Table 1) is justified by the fact that in this formalism, it is necessary to have some reasonable amplitude to "interfere" with. As can be seen, this change doesn't have a major effect on the DWBA part of the calculation. The results of the coherent addition are shown in Fig. 3b. Now we find that the phase of the data is well reproduced over the whole angular range, although the magnitude in the 100°-150° region is still too large. This deficiency, which is common also to the calculations[5] employing Regge poles, may be solved by a judicious choice of optical parameters. Alternatively, it could be related to some sort of channel coupling effect.

Assuming this model is appropriate, we next ask what it predicts at higher and lower energies. Figure 4a shows the elastic transfer predictions for $^{16}O + ^{28}Si$ at 38 MeV compared with data from Ref. 2. We find, as expected, that the interference pattern gets weaker at middle angles and moves toward larger angles. The predicted oscillations near 90° are compatible with the existing data. Finally, in Fig. 4b we compare our model to existing $^{16}O + ^{28}Si$ data at 81 MeV. Again we find at least qualitative agreement, that is, the interference region is just beginning at about the place where the (structureless) data stop.

In summary, we see that elastic transfer calculations for $^{16}O + ^{28}Si$ appear capable of explaining the available data, at least qualitatively, with respect to the existence and phase of the back angle oscillations. However, some modification of the usual strongly absorbing optical potential E18 is required to raise the back angle elastic cross sections to a level that allows strong interference over a large angular range. Although more experimental data are clearly needed, it appears from the present results that an exchange mechanism may play a role in the anomalous back angle elastic scattering seen in the $^{16}O + ^{28}Si$ system.

Footnote and Reference

*Condensed from LBL-7102.

1. J.G.Cramer, R.M.DeVries, D.A.Goldberg, M.S. Zisman, and C.F.Maguire, Phys. Rev. C 14, 2158 (1976).

2. D.S.Gale and J.S.Eck, Phys. Rev. C 7, 1950 (1973).

3. R.M.DeVries, D.A.Goldberg, J.Watson, M.S.Zisman, and J.G.Cramer, Phys. Rev. Lett. 39, 450 (1977).

4. R.M.DeVries, D.S.Shapira, N.Anantaraman, R.Cherry, M.R.Clover, and H.E.Gove, to be published.

5. P.Braun-Munzinger, G.M.Berkowitz, T.M.Cormier, C.M.Jachcinski, J.W.Harris, J.Barrette, and M.J. LeVine, Phys. Rev. Lett. 38, 944 (1977).

6. W.N.Reisdorf, P.H.Lau, and R.Vandenbosch, Nucl. Phys. A 235, 490 (1975).

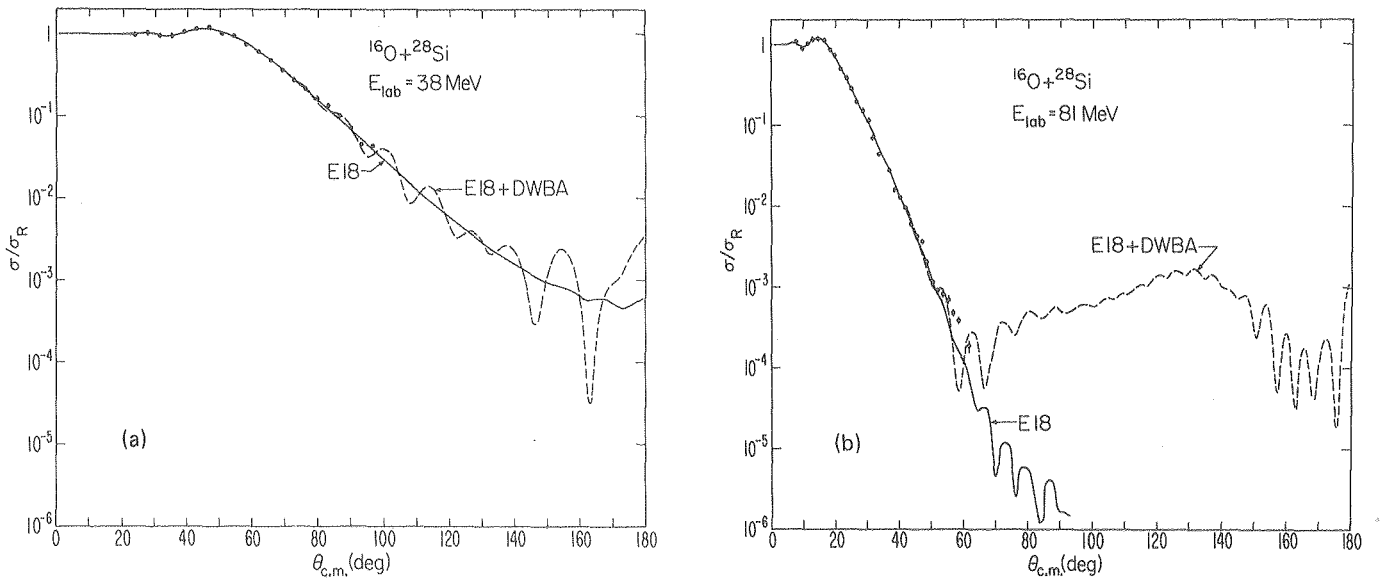

Fig. 4. (a) Optical model and elastic transfer calculations for $^{16}O + ^{28}Si$ at E_{lab} = 38 MeV, compared with the data of Ref. 2.
(b) Optical model and elastic transfer calculations for $^{16}O + ^{28}Si$ at E_{lab} = 81 MeV, compared with the data of Ref. 1.

[(a) XBL 7710-2086 (b) XBL 7710-2089]

THE GIANT E1 MODE AND ITS ENERGY BROADENING FROM THE CHARGE DISTRIBUTIONS IN HEAVY-ION REACTIONS

L.G. Moretto, J. Sventek, and G. Mantzouranis

The giant E1 mode is best known through its photoexcitation which is manifested in a peak at an energy $E = 78\ A^{-1/3}$ MeV with a width of typically 4-6 MeV. The same degree of freedom is involved in the charge distribution at fixed mass asymmetry in binary heavy-ion reactions (and in fission). The equilibration of the E1 mode in heavy-ion reactions, or the equilibration of the neutron-to-proton ratio of the two fragments, occurs quite fast, faster in fact than the mass asymmetry degree of freedom, possibly due to exchange effects which allow for charge transfer without mass transfer. Accordingly, the most probable charges can be obtained by minimizing the potential energy of the two fragments in contact with respect to the charge of one of the fragments at constant fragment mass. This well documented feature of heavy-ion reactions only provides information about the potential energy term of the collective E1 Hamiltonian. In principle one could obtain information for the whole Hamiltonian by a measurement of the charge distribution at fixed mass. Since in the great majority of cases the E1 phonon energy is expected to be much larger than the temperature, the E1 mode is expected to be in its ground state. As an example, let us consider the reaction Ni + Ar at 280 MeV bombarding energy whose mass and charge distribution has been studied in detail.[1] From the maximum linear dimension of the intermediate complex one obtains the relevant E1 phonon energy:

$$\hbar\omega = 94/d = 8 - 10 \text{ MeV} ,$$

where d is the semimajor axis of the intermediate complex. From the internal excitation energy of the complex one obtains

$$T = \sqrt{E_x/a} = 2 \text{ MeV} .$$

Since $\hbar\omega/T \simeq 4\text{-}5 \gg 1$, the collective E1 mode should be mainly in its ground state. Therefore the Z distribution at fixed mass asymmetry should be given by the modulus square of the ground state wave function and the second moment of the distribution is expected to be

$$\sigma_z^2 = \frac{\hbar\omega}{2c} \simeq 0.6 - 0.8 \text{ (charge units)}^2 ,$$

where c is the stiffness constant associated with the E1 mode, or

$$V_{(E1)} = \tfrac{1}{2} c (z - z_0)^2 .$$

The analysis of the experimental charge and mass distribution shows that mass and charge are strongly correlated as expected, with a correlation coefficient r = 0.97. However, the intriguing result for the second moment of the Z distribution at constant A is

$$\sigma_z^2 = 0.3 \text{ (charge units)}^2 ,$$

substantially smaller than expected. The disagreement is all more the evident since the experimental σ_z^2 should be (and has not been) corrected for particle evaporation, which may decrease its value[1]. Even more surprising is the fact that the experimental value of σ_z^2 is well reproduced if one assumes just a classical statistical distribution in Z, namely

$$\sigma_z^2 = T/c \simeq 0.3 \text{ (charge units)}^2 .$$

The outstanding problem is then to understand why the distribution in Z is classical rather than quantal, as expected.

The explanation may reside in the damping of the collective E1 mode. In photoexcitation, the giant resonance is mainly a 1p,1h state and presumably owes its width to the coupling into the 2p,2h states. In the present case, at relatively high excitation energy (60 MeV), the collective mode is an (np,nh) state which may couple into (n+1p, n+1h), or (np,nh), or again, ((n-1)p, (n-1)h) states.[2,3]

The resulting damping is energy-dependent and due mainly to the increasing density of the doorway states with increasing energy. It is interesting to see the consequence of this coupling to the Z distribution. Following Bohr and Mottelson[4] with a simple generalization, we can describe the coupling of the collective state $|a\rangle$ to the doorway states $|\alpha\rangle$. The exact state $|i\rangle$ is given by

$$|i\rangle = |a\rangle + \frac{P}{E_i - H_0 - V} V|a\rangle ,$$

with $P = \sum_\alpha |\alpha\rangle\langle\alpha|$, H_0 is the unperturbed Hamiltonian and V is the perturbation.

The relevant charge distribution is given by

$$p_i(z) = \int dx |\psi_i(z,x)|^2 ,$$

where $\psi_i(z,x) = \langle z,x|i\rangle$ and x denotes all other variables that must be projected out. In order to compare theory with experiment we have to consider the average of the distribution over an energy interval around E_i. We can write

$$p_i(z)_{ave} = \int dx \left[|\{\psi_i(z,x)\}_{ave}|^2 + \{|\psi_i^{f\ell}(z,x)|^2\}_{ave} \right]$$

with $\psi_i^{f\ell} = \psi_i - \{\psi_i\}_{ave}$ the "fluctuating" wave function. The fluctuating part can be shown to be responsible for the broadening of the distribution. It leads to a statistical distribution for Z. We want to show that the first term can lead to a narrowing of the distribution. For this purpose we have to consider the averaged Green function $\{1/E_i - H_0 - V\}_{ave}$. This average has been considered extensively in the literature.[4] For large systems and high excitation energies only the average diagonal matrix elements of the resolvent have to be considered and it can be shown that

$$\left\{ \langle \alpha \left| \frac{1}{E_i - H_0 - V} \right| \alpha \rangle \right\}_{ave} = \frac{1}{E_i - E_\alpha - i\Gamma} \quad ,$$

where Γ is the imaginary part of the "equivalent optical potential" describing the dissipation of the state $|a\rangle$ into the states $|\alpha\rangle$. The amplitude of the state $|a\rangle$ contained in the average eigenstate $|i\rangle$ is given by

$$c_a(i) = \left(1 + \sum \frac{V_{\alpha a}^2}{(E_i - E - i\Gamma)^2} \right)^{-\frac{1}{2}} \quad ,$$

In summary, and omitting for simplicity the bracket of the average,

$$|i\rangle = c_a(i)\ |a\rangle + \sum_\alpha c_\alpha(i)\ |\alpha\rangle \quad .$$

The next step is to establish that the sum over α in the above equation is a coherent one and thus the corresponding term describes a wave packet, i.e., it leads to a narrowing of the distribution. One can prove that if $V_{a\alpha}$ is random, the vectors $|\alpha\rangle$ contain phases which destroy the random property of $V_{a\alpha}$. Having established this point from first principles, we are entitled to use as first guess a simple-as-possible model. The average wave function associated with the charge asymmetry coordinate can be written as

$$\phi_i(z) = c_a(i)\ \psi_a(z) + \frac{1}{D} \int_0^\infty dE_\alpha\ c_\alpha(i)\ \psi_\alpha(z) \quad , \quad (1)$$

where D is the level spacing of the available doorway states and $\psi_a(z)$ is the ground state wave function of the E1 mode: $\psi_a(z) = \sqrt{2\pi\hbar\omega/c}\ \exp[-cz^2/2\hbar\omega]$ Qualitatively one sees already that, as the coupling increases, the integral in Eq. (1) becomes progressively dominant and the more $|\alpha\rangle$ states that are called into play by the strength of the coupling, the narrower $\phi_i(z)$ becomes. As a qualitative first

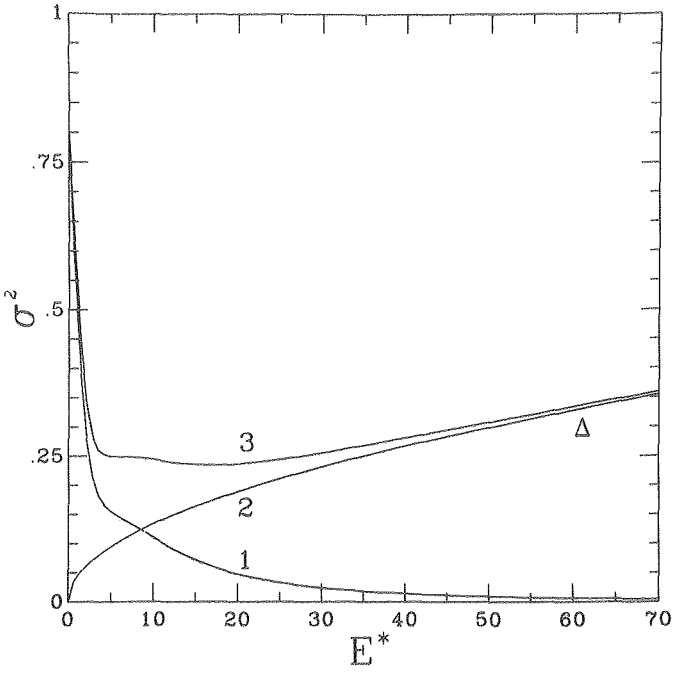

Fig. 1. Curve 1 shows the energy dependence of the quantal and curve 2 the energy dependence of the classical statistical width. Curve 3 represents the sum of both widths and the point indicates the experimental value. (XBL 785-8897)

guess on the $\psi_\alpha(z)$ we can use the plane wave expression

$$\psi_a(z) = \sqrt{2\pi\hbar\omega/c}\ \exp\left(iz\sqrt{c/2\hbar\omega}\sqrt{E_\alpha/D_1} \right) ,$$

where the plane waves are normalized to unity in a z box of volume corresponding to that of the harmonic oscillator.

The integral in Eq. (1) can be evaluated by integration in the complex plane and gives as a result:

$$2\pi\ \exp\left(-iz\sqrt{c/2\hbar\omega}\ \sqrt{1/D_1}\ \sqrt{E_1 - i\Gamma} \right) .$$

The second moment of the z distribution, σ_z^2, can then be obtained from the z distributions given by the modulus square of Eq. (1). The calculated second moment of the distribution σ_z^2 vs. excitation energy is given in Fig. 1. The narrowing of the distribution with increasing energy is quite evident. Since this calculation does not include thermal fluctuations, they are introduced in the simplest way,

$$\sigma_z^2 = \sigma_{z,Q}^2 + \sigma_{z,T}^2 \quad ,$$

where the labels Q and T stand for quantal and thermal.

The possibility of experimentally observing the minimum of σ_z^2 and its rapid rise with decreasing energy is of extreme interest because it would provide us with information on the damping of a giant resonance in a hot nucleus. This is particularly true in view of the extremely difficult alternatives, like gamma decay from highly excited nuclei, etc. The only experimental result shown in the figure is a heavy ion example. Similar data are available in fission.

Footnote and References

*Condensed from LBL-7732.

1. B.Gatty, D.Guerreau, M.Lefort, J.Pouthas, X.Tarrago, J.Galin, B.Cauvin, J.Girard, and H.Nifenecker, Z. Physik A 273, 65 (1975).

2. F.C.Williams,Jr., Phys. Lett. B 31, 184 (1970).

3. C.Bloch, Nucl. Phys. 4, 503 (1957).

4. A.Bohr and B.R.Mottelson, Nuclear Structure, Vol. II (W. H. Benjamin, Inc., Reading, Mass., 1975).

A RELATION BETWEEN NUCLEAR DYNAMICS AND THE RENORMALIZATION GROUP*

G. Mantzouranis

In a recent paper[1] a method has been proposed for describing some aspects of nuclear motion. The purpose of the present work is to reconsider the physical foundation of this method. Our goal is to cast the problem of nuclear dynamics in a form suitable for treatment with the methods of the renormalization group.

The basic idea on which the work in Ref. 1 is based might be expressed generally by the following statements. The nucleus is a large but finite system; the range of its force is small in comparison to its nuclear volume. Thus, we may expect that many nuclear properties should be insensitive to the "details" of the nuclear two-body potential.

This expectation is likely to be fulfilled in the energy spacing between subsequent single particle or collective (rotational and vibrational) states, the shape parameters and the energy-averaged cross sections. This is confirmed by the success of macroscopic models for the collective motion (rotation of a rigid body or oscillating fluid). These models disregard the details of the quantum system at short distances. On the other hand, the evaporation model might serve as an example of a theory which operates with the optical model potential and the single particle level densities, i.e., with quantities which are insufficient for the specification of the two-body potential in its details.

The basic concept of the present work will be the introduction of a minimal length Λ^{-1}, or, equivalently, a cutoff wave number Λ. The minimal length should be larger than the range of the two-body force but smaller than the dimensions of the system. The non-trivial hypothesis of our method is that we assume some observables to have expectation values. The renormalization group theory $(RG)^2$ appears as a possible tool in order to justify our method a priori. Recent investigations show that the expectation values of one-body operators are fixed points of the RG, i.e., they are independent of the details of the force.

Footnotes and References

*Condensed from LBL-6598; to be published in Phys. Rev. C.

1. G.Mantzouranis and H.C.Pauli, Preprint MPIH-1977-V16, submitted to Phys. Rev. C.

2. Shang-keng Ma, Rev. Mod. Phys. 45, 589 (1973).

C. RELATIVISTIC

ABRASION-ABLATION CALCULATIONS OF LARGE FRAGMENT YIELDS FROM RELATIVISTIC HEAVY-ION REACTIONS*

L.F. Oliveira,† R. Donagelo,‡ and J.O. Rasmussen

In this work we attempt to interpret results of target or projectile fragmentation experiments with high energy heavy ions.[1,2] We calculate cross sections for production of heavy fragments considered to be produced in peripheral collisions. We stress that the calculations described apply equally well for both target and projectile fragmentation processes. Which process one chooses to study is merely a choice of reference frame.

The abrasion-ablation model introduced by Bowman, Swiatecki and Tsang[3] describes the reaction as a two-stage process. In the fast stage (abrasion) the nucleons within the overlap zone interact with each other and are sheared away from either the projectile or the target. The projectile fragment follows its trajectory with practically the same velocity as before, while the target fragment slowly recoils. Both fragments are excited as a result of the abrasion, and they later dissipate this excitation energy by undergoing particle evaporation (ablation).

To calculate the abrasion part of the reaction we can use the geometrical picture of either the clean-cut fireball model or the firestreak model; we restrict outselves to the former. From this part of the calculation we obtain the excitation energies and the cross sections for formation of the so-called primary residues.

Before starting the evaporation stage (ablation) we must specify the proton-neutron composition of the abraded nucleons. We assume that each nucleon target nucleon has a Z_T/A_T probability of being a proton.

With the primary fragment Z, N and E distributions determined by the abrasion stage, we start statistical particle evaporation from each primary residue with the OVERLAID ALICE code[4] to obtain the partial yields of the final (observed) fragments. Finally, we sum the partial yields of each final fragment over all primary residues, and obtain the final yields, which are to be compared with the experimental values.

In Fig. 1 we compare the results of our calculations (solid line) with the experimental data of Westfall et al.[2]. They have studied the fragmentation of ^{56}Fe at 1.8 GeV/ nucleon by several targets at the Bevalac. Our calculated results for both cases presented (C and Cu targets) are higher than the experimental values, especially for the near projectile elements

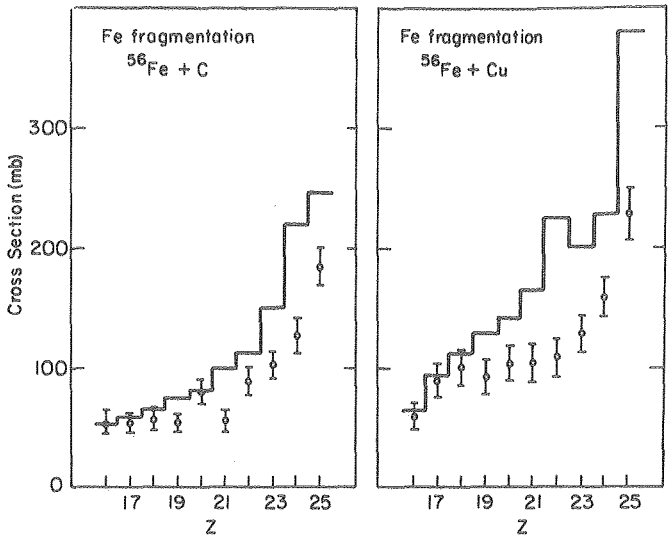

Fig. 1. Comparison between results of our calculations (pure abrasion-ablation) and experimental data of Ref. 2. Dots with error bars correspond to experimental data and bars are theoretical results. Dotted lines on histograms indicate experimental error bars. (XBL 788-5509)

(Z = 25 and 24). We think we understand this feature: in the abrasion-ablation model as used here, the cross sections for the elements close to the projectile (or target, in case of a target fragmentation study) are really dominated by the abrasion stage. The abrasion cross sections for the elements one or two nucleons removed from the projectile (target) are quite high, but the excitation energies calculated with the extra surface energy term alone are not enough to induce appreciable particle evaporation from these nuclei. An examination of Fig. 3 (which will be explained later) also leads to the same conclusion: it is necessary to introduce a mechanism for energy deposition other than the extra surface energy. Hüfner et al.[5] encountered a similar situation in their calculations and proposed a final state interaction mechanism for energy deposition. We followed their idea and introduced a similar process in our calculations.

Since the nucleon-nucleon elastic scattering cross section at high energies is largely forward peaked, it is good approximation to assume (at such energies) that the incident projectile nucleon follows a straight-line trajectory (without changing

its initial direction) while a struck target nucleon moves in the plane perpendicular to the projectile direction. Based on the above approximation, we further assume that 50% of the struck target nucleons are directed toward the target spectator piece, depositing in it part of the recoil energy.

In Ref. 6 the differential elastic scattering nucleon-nucleon cross section is presented as a function of t--the square of the four-momentum transfer to the target nucleon. From this angular distribution, we evaluated the average four-momentum transfer t by

$$\langle t \rangle = \frac{\int_0^\infty t \frac{d\sigma}{dt} dt}{\int_0^\infty \frac{d\sigma}{dt} dt} \quad , \tag{1}$$

which is related to the average kinetic energy of the recoiling target nucleon by

$$\langle t \rangle = 2m_N \langle E_{recoil} \rangle \quad . \tag{2}$$

From the energy dependence of $d\sigma/dt$ and Eqs. (1) and (2) we obtain the average recoil energy $\langle E_{recoil} \rangle$ as a function of the lab energy/nucleon of the projectile.

As the recoiling nucleon advances through the spectator piece, it loses energy in further N-N collisions. We calculate the deposited energy by assuming the recoiling nucleon energy to be given by[7]

$$\frac{dE}{dx} = -\frac{\alpha}{\lambda} E \quad , \tag{3}$$

where λ is the nucleon mean free path, and α is the fraction of energy lost in each collision. In the calculation presented here, we take $\alpha = 0.25$ (see Ref. 7) and

$$\lambda = \frac{1}{\rho \sigma_{NN}} \quad , \tag{4}$$

where $\rho = 0.17$ Fm^{-3} is the nuclear matter density and σ_{NN} is the N-N cross section, assumed to be $\approx 300/E$ Fm^2 (a fair approximation for $E < 150$ MeV).

Finally, the average deposited energy E_{FSI} is calculated by averaging over all possible orientations on the half plane of the spectator piece, i.e.,

$$\langle E_{FSI} \rangle = \frac{1}{\pi} \int_0^\pi E_{dep}(\theta) d\theta . \tag{5}$$

Table 1 presents the values we obtained for the three cases we study in this work.

As stated before, we assume that each struck nucleon has a 50% chance of passing through the spectator, depositing E_{FSI} of excitation on the average. Therefore, each primary residue with mass number $A_T' = A_T - a$ can have from 0 to a final state interaction according to a binomial distribution given by:

Table 1. Average energy deposited by a nucleon undergoing FSI.

Spectator	Lab Energy (MeV/nucleon)	$\langle E_{FSI} \rangle$ (MeV)
^{40}Ca	400	35.3
^{56}Fe	1800	38.8
Cu	2000	41.5

$$\text{Prob}(m_{FSI}) = \left(\frac{a}{m_{FSI}} \right) \frac{}{2^a} \quad . \tag{6}$$

where a is the number of abraded nucleons.

The total excitation energy of a primary fragment (A_T'), which has undergone m_{FSI} final state interactions, is given by

$$E^* = E_{surf}(a) + m_{FSI} \cdot \langle E_{FSI} \rangle \quad . \tag{7}$$

$E_{surf}(a)$ is the extra surface energy term, which is a function only of the number of nucleons removed.

In Fig. 2 we show a comparison between the results of our calculations with FSI and the same experimental data of Fig. 1. The agreement is generally better than before, except for $Z = 25$ which now presents the opposite situation, i.e., the calculated value is less than the experimental result. We interpret this discrepancy at $Z = 25$ as an indication of the effects of other peripheral processes not included in our calculations, such as Coulomb dissociation via the giant El resonance of the projectile[8] or a dissociation of the projectile in the nuclear field of the target.[9]

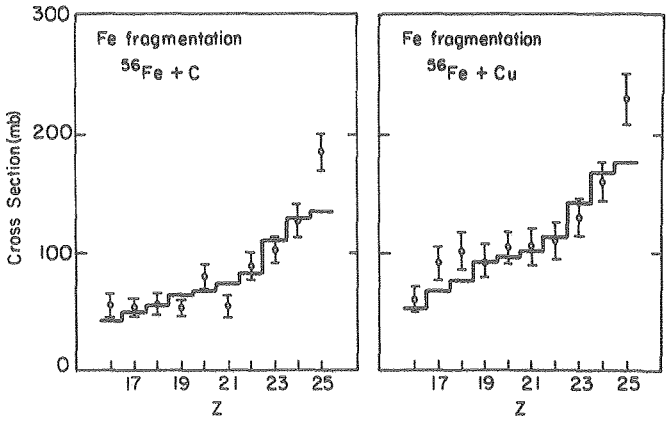

Fig. 2. Same as Fig. 2 but with FSI included in the theory. (XBL 788-5508)

A comparison between the results of our calculation and the experimental results of the TOSABE Group[1] is shown in Fig. 3. They utilized in-beam gamma-ray techniques to study the fragmentation of ^{40}Ca following interaction with high energy alpha and carbon projectiles. Most nearly measuring nuclide yields are the intensities of the $2^+ \rightarrow 0^+$ transitions in doubly-even products. Also a few radioactive isotopes (shown on the left side of the figure) were identified by measuring the off-beam spectra between the one-second beam spills. The histograms represent the experimental data, and the full and dashed lines are, respectively, the results of our calculations with and without FSI. Again the inclusion of FSI substantially improves the results, expecially for those isotopes with masses close to the target mass.

The abrasion-ablation model with the clean-cut fireball abrasion and the OVERLAID ALICE evaporation code has proven to be very useful in studying peripheral reactions between high energy heavy ions. However, the yields obtained with the pure abrasion-ablation model for the elements with masses very close to the target mass are too high as compared to experimental data. The reason for this lack of agreement is believed to be the low values of the excitation energy after removal of one or two nucleons from the target as calculated, assuming only an extra surface energy contribution. This led us to include a final state interaction (FSI) mechanism in the calculations. Then the agreement between the theoretical and experimental results, although not perfect, improved substantially in most cases. It is important to point out that there are no free parameters in the calculations presented in this work.

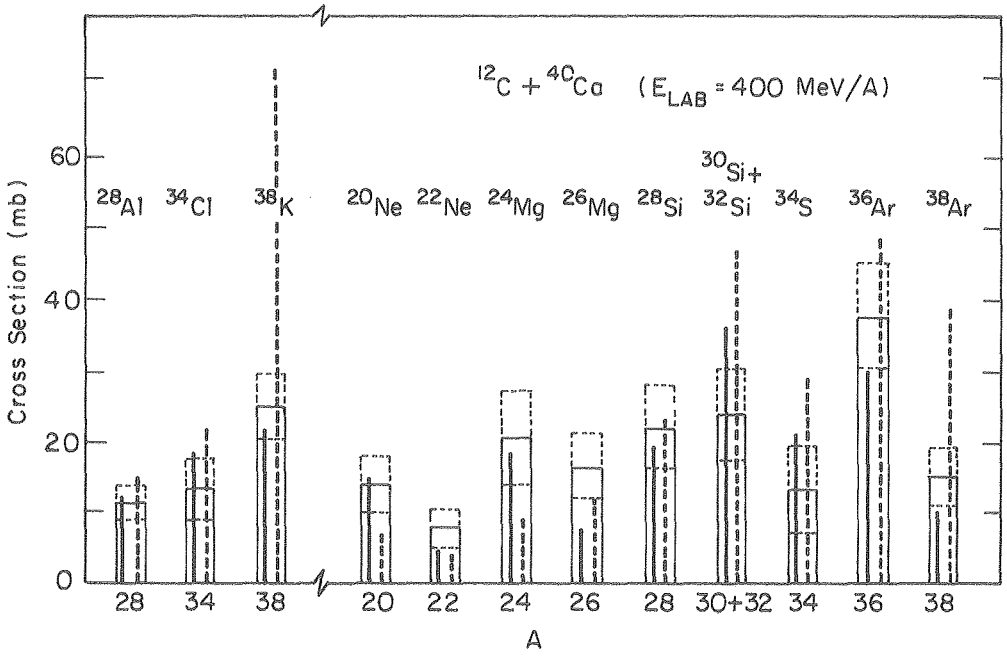

Fig. 3. Comparison between theoretical results and experimental data of Ref. 1. Histograms correspond to experimental data, and full and traced bars are results of our calculations with and without FSI, respectively. Dotted lines on histograms indicate experimental error bars. (XBL 784-4923)

Footnotes and References

*Condensed from LBL-7731.
†Supported by CNEN-Brazil.
‡Present address: Instituto de Fisica, Universidade Federal do Rio de Janeiro, Ilha do Fundao, Rio de Janeiro, Brazil.

1. T. Shibata, H. Ejiri, J. Chiba, S. Nagamiya, K. Nakai, R. Anholt, H.Bowman, J. G. Ioannou, E. A. Rauscher, and J. O. Rasmussen, Lawrence Berkeley Laboratory Report, LBL-7189 (1978), to be published in Nucl. Phys. A.

2. G. D. Westfall, P. J. Lindstrom, D. E. Greiner, H. J. Crawford, Lance W. Wilson, and H. H. Heckman, Bull. Am. Phys. Soc. 23, 27 (1978), and private communication.

3. J. D. Bowman, W. J. Swiatecki, and C. F. Tsang, Lawrence Berkeley Laboratory Report, LBL-2908 (1973), unpublished.

4. M. Blann, OVERLAID ALICE, USAEC report COO-3494-29, unpublished.

5. J. Hüfner, K. Schäfer, and B. Schürmann, Phys. Rev. C 12, 1888 (1975).

6. O. Benary, L. R. Price, and G. Alexander, NN and ND Interactions (Above 0.5 GeV/c)--A Compilation, Lawrence Livermore Laboratory Report, UCRL-20000 (1970).

7. J. Hüfner, C. Sander, and G. Wolschin, Phys. Lett. B 73, 289 (1978).

8. X. Artru and G. B. Yodh, Phys. Lett. B 40, 43 (1972).

9. J. Rasmussen, R. Donangelo, and L. Oliveira, Proceedings of the IPCR Symp. on Macroscopic Features of Heavy-Ion Collisions and Pre-Equilibrium Process, Hakone, Japan (1977), p. 440.

CALCULATIONS WITH THE NUCLEAR FIRESTREAK MODEL*

J. Gosset,† J.I. Kapusta, and G.D. Westfall

Recently a large amount of experimental data concerning relativistic heavy-ion reactions has become available.[1-4] The data considered here consist of single particle inclusive spectra of pions, nucleons, and light nuclei up to ^{4}He. These spectra were measured for a variety of target-projectile-incident energy combinations over a wide range of observed energies and angles. It is hoped that in relativistic heavy-ion collisions, new phenomena can be studied such as density isomers or pion condensates. However, the calculation of observable quantities resulting from these exotic phenomena are not yet possible. A calculation incorporating known phenomena would be useful in predicting what one would expect to observe in these reactions if nothing unusual were taking place.

The nuclear firestreak model describes relativistic heavy-ion collisions by assuming that the interaction between the nuclei is localized to the overlapping volume. In this volume the interaction proceeds via colinear streaks of nuclear matter[5] from the target and projectile that undergo completely inelastic collisions. This nuclear matter is treated as a thermodynamic system in chemical equilibrium[6] which allows the calculation of the relative concentrations of pions, nucleons, and light nuclei and their distribution functions. The model incorporates one variable parameter, the freeze-out density, ρ_c, which is uniquely determined to be 0.12±0.02 hadrons/fm^3.

To treat the nuclear density distributions with diffuse surfaces incorporated in the model, one can subdivide the projectile and target into infinitesimal streaks parallel to the relative motion of the colliding nuclei.[5] Each of these streaks is characterized completely by the relative amount η of material coming from the projectile. Here $\eta = N_P/(N_P + N_A)$, where N_P and N_A are the numbers of contributing nucleons from the projectile and target. Considered in the chemical equilibrium are pions, Δ's, nucleons, and light nuclei up to A = 5 including their excited states. The stable particle spectra thus consist of a sum of two components, a thermal one and a resonance two-body decay one, resulting from all the possible

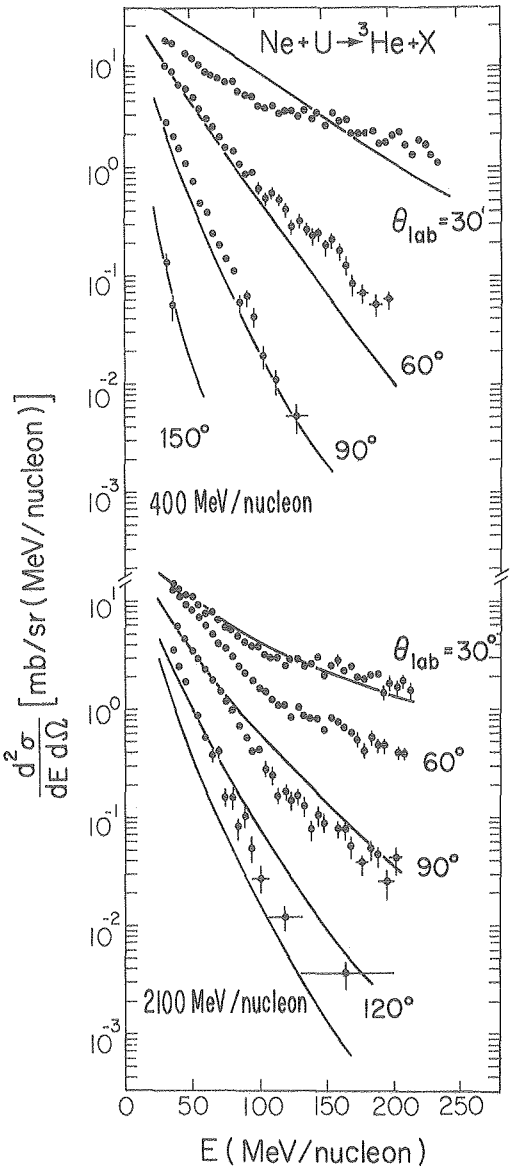

Fig. 1. Spectra of ^{3}He in the lab from the bombardment of U by Ne at 400 and 2100 MeV/nucleon. The model predictions have been multiplied by 2. Data is from Ref. 1. (XBL 781-64)

two-body decays of resonances which are themselves emitted with a thermal spectrum.

In comparing the model to the existing data one finds good agreement except for some conflicting normalizations. The largest discrepancy occurs for the high energy pions which are overestimated by about a factor of five. Two typical comparisons between existing data and the model are given. The comparison for protons observed from Ne on Pb at 800 MeV/nucleon is shown in Fig. 1.[3] The model gives a good representation of the observed data.

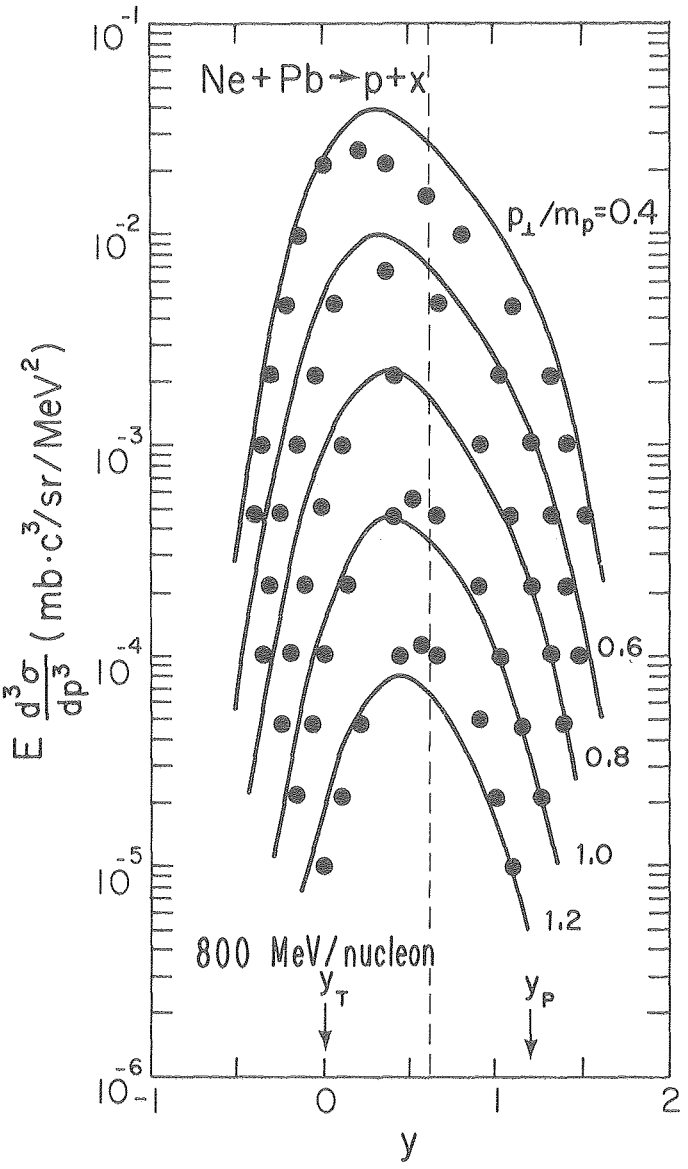

Fig. 2. Invariant cross section vs rapidity at fixed transverse momentum for protons from the bombardment of Pb by Ne at 800 MeV/nucleon. The dashed line represents the nucleon-nucleon center-of-mass frame. Error bars (not shown) range from 20% for the large cross sections to 100% for the small cross sections. Data is from Ref. 3. (XBL 7711-11412)

Figure 2 shows ^{3}He spectra from 400 and 2100 MeV/nucleon Ne on U.[1] The theory has been multiplied by a factor of two. Agreement is good everywhere for the 400 MeV/nucleon data except at 30°. The predicted angular distribution for the 2100 MeV/nucleon data seems to be less forward peaked than the observed spectra.

In conclusion, the exact quantum field theory treatment of relativistic heavy-ion reactions is probably not a realistic goal. However, the relatively good success of the nuclear firestreak model may help point the way toward more comprehensive models or theories of these reactions.

Footnotes and References

*Condensed from Phys. Rev. C 18, 844 (1978) and LBL-7139.

†Permanent address: DPN/ME, Centre d'Etudes Nucleáires de Saclay, 91190 Gif-sur-Yvette, France.

1. J. Gosset, H. H. Gutbrod, W. G. Meyer, A. M. Poskanzer, A. Sandoval, R. Stock, and G. D. Westfall, Phys. Rev. C 16, 629 (1977).

2. V. Perez-Mendez, A. L. Sagle, E. T. B. Whipple, F. Zarbakhash, G. Igo, M. M. Gazzaly, J. B. Carroll, J. V. Geaga, J. B. McClelland, M. A. Nasser, H. Spinka, and R. Talaga, Lawrence Berkeley Laboratory Report, LBL-7278.

3. S. Nagamiya, I. Tanihata, S. Schnetzer, L. Anderson, W. Brückner, O. Chamberlain, G. Shapiro, and H. Steiner, Lawrence Berkeley Laboratory Report, LBL-6770.

4. K. Nakai, J. Chiba, I. Tanihata, S. Nagamiya, H. Bowman, J. Ioannou, and J. O. Rasmussen, Proc. of the Intern. Conf. on Nuclear Structure, Tokyo, Vol. 3 (1977); also, private communication.

5. W. D. Myers, Nucl. Phys. A 296, 177 (1978).

6. A. J. Mekjian, Phys. Rev. Lett. 38, 640 (1977); J. Bond, P. J. Johansen, S. E. Koonin, and S. Garpman, Phys. Lett. B 71, 43 (1977); J. I. Kapusta, Phys. Rev. C 16, 1493 (1977).

THE STATISTICS OF THE FIREBALL MODEL*

G. Mantzouranis

Recently the fireball model has been proposed in order to calculate the inclusive spectra of light particles emitted in heavy-ion collisions at relativistic energies.[1] Methods which are similar in spirit have been applied for the study of the hadronic spectrum at very high energies.[2] Our goal is to derive the fireball model using more microscopic procedures and to connect it with the standard compound nucleus model for light-projectile-induced reactions at low energies. This way the success of the fireball in explaining data will become less mystifying.

Our program starts with a formal expansion for the scattering matrix in terms of unknown parameters. Our next observation that the cross sections extracted from actual experiments are averaged over a relatively broad energy interval (I) due to limited experimental resolution. Therefore, these cross sections (i.e., the bilinear expressions of the S-matrix) can only contain those parts of the nuclear dynamics which have a characteristic energy scale larger than I. This loss of information of the nuclear details enable us to derive expressions for the averaged quantities which depend only on limited features of the parameters involved in the exact S-matrix. In this work we adopt the point of view of the phenomenological S-matrix theory so far as averaged quantities are concerned. Indeed, it is only for these quantities that the original space of parameters can be cast into a simple and informative form. We have shown that the particular form of the fireball corresponds to the normal distribution of the parameters in the original S-matrix and thus, the fireball has the same roots as the conventional statistical spectroscopy.[3,4] Strong collective effects, like the exotic ones, should appear as violations of the normal distribution.

Footnote and References

*Condensed from LBL-7712.

1. J. Gosset, H. H. Gutbrod, W. G. Meyer, A. M. Poskanzer, A. Sandoval, R. Stock, and W. G. Westfall, Phys. Rev. C 16, 629 (1977).

2. N. K. Glendenning and Y. J. Karant, Phys. Rev. Lett. 40, 374 (1978).

3. J. P. Draayer, J. B. French, S. S. M. Wong, Ann. of Physics 106, 472 (1977).

4. P. A. Moldauer, Phys. Rev. B 135, 642 (1964).

^{12}C ON ^{12}C AT 800 MeV/NUCLEON: ONE FIREBALL OR TWO?

S. Das Gupta

Preliminary data[1] of ^{12}C on ^{12}C at 800 MeV/nucleon showed very significant asymmetry in the proton invariant cross section as measured in the c.m. For the same energy, the value of $Ed^2\sigma/p^2dpd\Omega$ is 5 to 6 times higher at 30^o over that at 90^o. The one-fireball model will clearly fail to explain this asymmetry. A two-fireball model, which goes over to the one-fireball model for heavier ions, explains the data of ^{12}C on ^{12}C and also of ^{20}Ne on NaF.[2] Let "a" refer to the piece of the projectile and "b" to the piece of the target that forms the fireball. Then, in the c.m. of the fireball

$$p_a^f = (1 - y)\, p_a^i \quad ,$$

$$p_b^f = (1 - y)\, p_b^i \quad .$$

Here the superscript i and f refer to before and after the collision. In the one-fireball model, y = 1; in the two-fireball model we take it to be

$$y = 1 \quad \text{if} \quad n_{ab} > n \quad ,$$

$$y = n_{ab}/n \quad \text{if} \quad n_{ab} \leq n \quad .$$

Here n_{ab} is the number of nucleons involved in the collision; the physical idea is that if the number of nucleons involved is not large enough, then each piece is slowed down but not completely stopped. With the value of $n \approx 24$ the model fits all the known preliminary data at 800 MeV/nucleon incident energy and predicts that, for Ar on Ar, the proton asymmetry will be considerably reduced.

References

1. S. Nagamiya et al., Nuclear Sciences Annual Report, Lawrence Berkeley Laboratory Report, LBL-6575 (1977), p. 150.

2. S. Nagamiya et al., Proc. Intern. Conf. on Nuclear Structure, Tokyo, 1977, published as Suppl. to J. Phys. Soc. Japan 44, 378 (1978).

"SMALL," "LARGE," AND "VERY LARGE" TRANSVERSE MOMENTA IN A UNIFIED HYDRODYNAMICAL DESCRIPTION*

E.M. Friedlander and R.M. Weiner†

Strong interaction physics can hardly be understood without an adequate explanation for the specific features of the transverse momentum distribution $f(p_T)$ of secondaries produced in high-energy hadronic collisions.

Two apparently related effects, viz., the behavior of transverse momentum spectra at "large" p_T in p-p collisions and the "enhancement" of such spectra in p-nucleus collisions, are shown to follow in a natural way from a hydrodynamical model in which the space-time evolution of the system is taken into account.

Up to $p_T \approx 5$ GeV/c a single value (close to $u^2 \approx 1/7$) for the velocity of sound in hadronic matter gives a consistent description of all experimental facts. Recent observations at very large p_T (5-15 GeV/c) require a jump to $u^2 \sim 1/4$, suggesting the possibility of a phase transition of the second kind.

The hydrodynamical model (h.m.) of Landau contains as an essential ingredient Pomeranchuk's observation[1] that in hadron-hadron collisions the system is initially at such a high pressure that the mean free path of the created particles is much smaller than the dimensions of the system; thus no emission of particles can take place before the system has expanded and hence cooled down to a "decay" temperature $T_c \sim m_\pi$. This explains why the bulk of the particles has limited transverse momenta ($\langle p_T \rangle \sim 0.3$ GeV/c).

It is clear, however, that emission at $T > T_c$ cannot be absolutely forbidden and this must lead to leakage of particles from the excited system before expansion has ended.

We are interested in the probability of particle emission at different temperatures T, hence at different times t. We shall use the one-dimensional solution of the Khalatnikov equation for the relativistic hydrodynamical potential χ in order to derive T(t) and thus to describe the evolution of the system.

The expression which follows is valid both for p-p and p-nucleus collisions. In the latter case, the incident proton is assumed to collide with a nuclear tunnel of length l which, in turn, depends on the impact parameter b.

T(t) is given implicitly by

$$t(T)_{y=0} = \frac{\ell+d}{4uw}\left\{\int_0^\tau e^{-wt}\, I_0\,[(w-1)t]\, dt + e^{w\tau}\, I_0\,(w-1)\tau] + \frac{\ell-d}{2u^2 w}\,(1 - e^{-\tau})\right\}, \tag{1}$$

where d is the proton diameter, I_0 is the modified Bessel function

$$w \equiv \frac{1+u^2}{2u^2}\ , \quad \tau \equiv \ell n(T/T_0)\ , \tag{2}$$

u is the velocity of sound and T_0 is the initial temperature given (in units of m_π) by

$$T_0 = \left(\frac{\varepsilon_0}{\lambda}\right)^{\frac{1}{2w}}\ ; \tag{3}$$

ε_0 is the energy density.

The invariant cross section $f(p_T)$ reads

$$f(p_T)_{y=0} \sim \frac{1}{p_T}\int_0^{t_c} dt \int_{m_\pi}^{\infty} dm \int_0^R b^2 db\ F\ (t)\ \phi_{BE}(p_T, T(t), m) \tag{4}$$

where

$$\phi_{BE}(p_T,T,m) \equiv \frac{p_T^2}{e^{\frac{\sqrt{p_T^2+m^2}}{T}} - 1} \tag{5}$$

is the Bose-Einstein distribution and t_c is the "moment of decay" defined by

$$T(t_c) = T_c\ ; \tag{6}$$

R is the target radius, and m the mass of the secondary. F(t) is the decay probability per time interval, i.e., a function which describes the time evolution of the leakage process. The simplest assumption about F, used hereafter, is that F is a constant; this implies equal emission probabilities in equal time intervals.

We have applied the results of the model discussed above to the analysis of p-p collisions at the CERN ISR[2-4] and p-nucleus collisions at FNAL.[5] Besides normalization the only quantity to be fitted is u. The results of the fits for the p_T-range 0-5 GeV/c are shown in Figs. 1 and 2. Figure 3 shows a complete picture of the pion p_T-spectrum at $\sqrt{s}$ = 53 GeV (ISR) from 0 to 15 GeV/c with the newest data[2] included.

Our results can be summarized as follows:

1) From $p_T \sim 0.1$ up to $p_T \sim 5$ GeV/c the data for both p-p and p-A collisions (in the

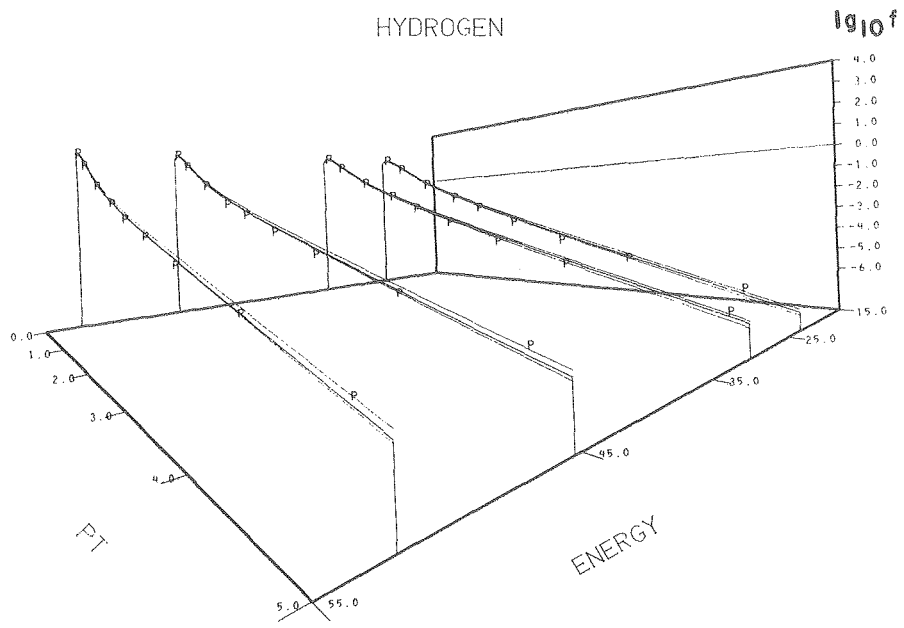

Fig. 1 Three-dimensional plot of $\log_{10}[f(p_T)]$ for pp(ISR) collisions at four energies. Here and in the other figures the invariant cross section is in $mb/(GeV/c)^3$; characters related to the target (B = Be, T = Ti) identify experimental points; their size is not related to the value of experimental errors. Thin curves delimit the 0.5% confidence interval on u^2.

XBL 785-8925)

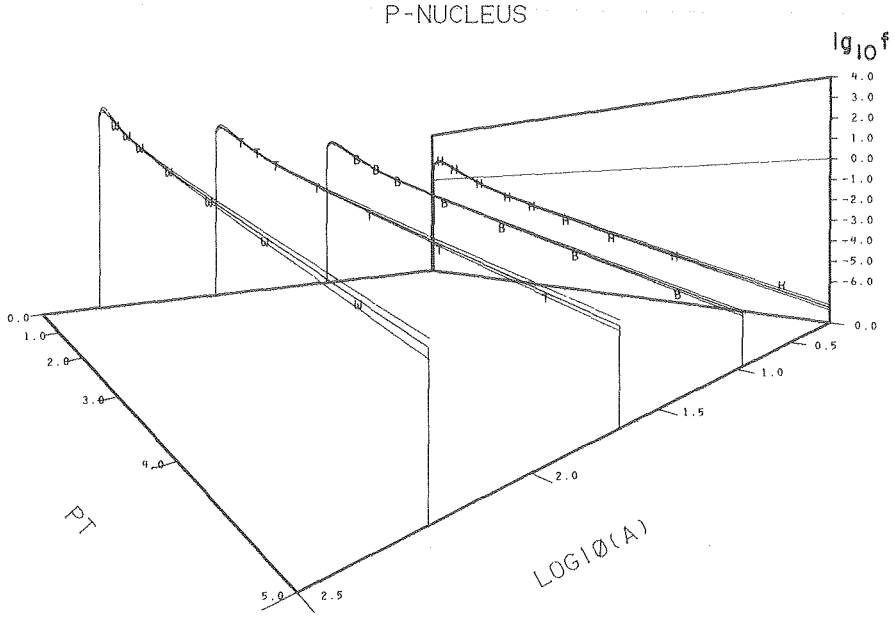

Fig. 2. Same as Fig. 1 for a constant energy ($\sqrt{s}$= 23 GeV) and four different target nuclei (target scale is $\log_{10}$ A)

(XBL 785-8927)

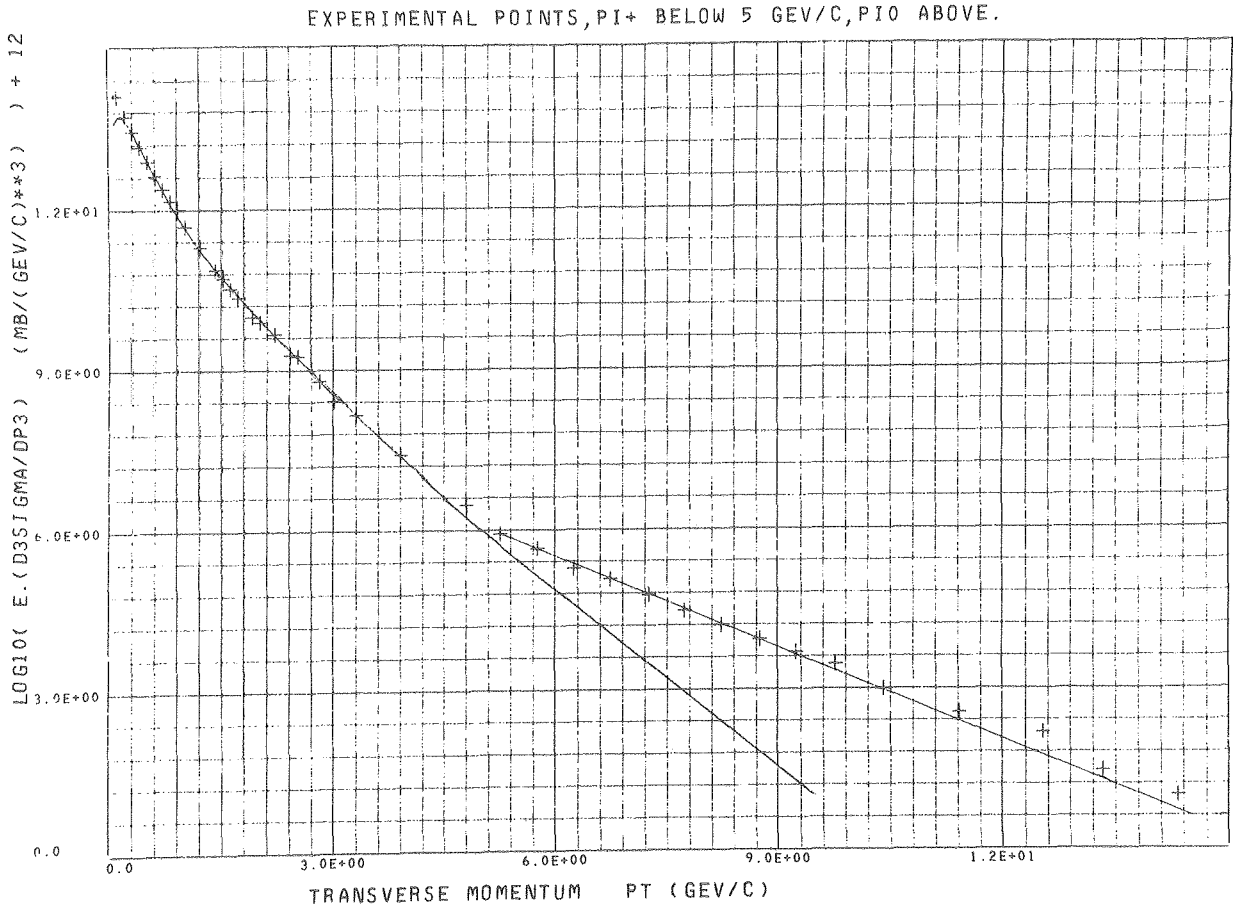

Fig. 3 $f(p_T)$ in pp (ISR) collisions at 54 GeV covering the whole range of p_T (0-15 GeV/c). The points beyond 5 GeV (π^0 from the most recent experiment)[2] are independently fitted by an exponential.

(XBL 785-8926)

energy range covered by FNAL and ISR experiments) can be well fitted by our model with a value of u in the narrow range ($1/\sqrt{6.4}$ - $1/\sqrt{6.8}$; this range is compatible with values obtained for u from the h.m. when analyzing rapidity distributions in p-p and p-nucleus collisions.[6,7]

2) The fits are rather sensitive to small (~5%) variations in u^2 (see Table 1).

3) While in most other models, "new physics" are invoked to explain the departure from a simple exponential in p_T beyond ~1 GeV/c, in the hydrodynamical approach the "large p_T" region (1-5 GeV/c) appears as a smooth and natural continuation of the "low p_T" region.

4) Beyond, say, 4-5 GeV/c our Eq. (7) turns for all practical purposes into an exponential

$$f(p_T) \sim e^{-\frac{p_T}{T_0}} \qquad (7)$$

As can be seen from Fig. 3, in the "very large p_T" region (5-15 GeV/c) the (most recent) data deviate strongly from this asymptotic form. However, they are remarkably well fitted by an exponential ($\chi^2 \sim 4$ with 11 degrees of freedom) with a higher initial temperature T_0(~5 m_π instead of ~2 m_π). Such a high T_0 can be understood in our model if u jumps from a value of ~$1/\sqrt{7}$ to ~$1/\sqrt{4}$.

It is gratifying to observe that the h.m. with only one free parameter, viz., u (which, however, is already pinned down to within a few percent of our fitted value by independent experimental facts) gives such a consistent description of the p_T spectra over nine orders of magnitude in cross sections.

Footnotes and References

*Condensed from a paper submitted to Phys. Rev. Lett.

†Present address: Los Alamos Scientific Laboratory, Los Alamos, New Mexico; permanent address: Dept. of Physics, University of Marburg, Marburg, Germany.

1. I. Ya. Pomeranchuk, Dokl. Akad, Nauk SSSR 78, 884 (1951).

2. B. Alper et al., Nucl. Phys. B 100, 237 (1975).

3. F. Busser et al., Phys. Lett. B 46, 471 (1973).

4. A. G. Clark et al., CERN preprint (1978).

5. J. W. Cronin et al., Phys. Rev. D 11, 3105 (1975).

6. B. Anderson et al., Nucl. Phys. B 112, 413 (1976).

7. N. Masuda and R. M. Weiner, submitted to Phys. Rev. D.

Table 1. Fitted values of $1/u^2$ and figures of merit FOM = $(\chi^2-N)/\sqrt{2N}$ where N is the number of degrees of freedom. FOM should be asymptotically normal (0,1).

Target	$\sqrt{s}$	$(1/u^2)$fitted	FOM
H(ISR)	23	6.80	5.8
H(ISR)	31	6.68	7.5
H(ISR)	45	6.68	4.7
H(ISR)	53	6.61	2.2
Be	23	6.90	22.4
Ti	23	6.68	9.4
W	18	6.80	6.1
W	23	6.48	3.5
W	27	6.44	4.4

MULTIPLICITY DISTRIBUTIONS OF CREATED BOSONS: THE COMBINANTS TOOL *

S.K. Kauffmann and M. Gyulassy

Collisions or other excitation processes often create bosons in systems where none were present initially. We call P(n), the probability that n bosons were produced by the process, the created boson multiplicity distribution. The domain of P(n) is the non-negative integers (n = 0,1,2,...), and it seems reasonable to postulate, bearing in mind any reasonable quantum description of boson creation,[1] that there is a non-zero probability to produce no bosons at all, i.e.,

$$P(0) > 0. \tag{1}$$

We have, in addition, the usual probability distribution conditions

$$P(n) \geq 0 \quad , \quad n = 1,2,... \tag{2}$$

and

$$\sum_{n=0}^{\infty} P(n) = 1. \tag{3}$$

A very useful tool for studying P(n) is the generating function

$$F(\lambda) \equiv \sum_{n=0}^{\infty} \lambda^n p(n) \quad , \tag{4}$$

which may be re-expressed as

$$F(\lambda) = \exp\left[\sum_{k=1}^{\infty} C(k)(\lambda^k - 1)\right] \quad , \tag{5}$$

where

$$C(1) = \left(\frac{P(1)}{P(0)}\right) \quad , \tag{6a}$$

$$C(2) = \left(\frac{P(2)}{P(0)}\right) - \frac{1}{2}\left(\frac{P(1)}{P(0)}\right)^2 \quad , \tag{6b}$$

$$C(3) = \left(\frac{P(3)}{P(0)}\right) - \left(\frac{P(1)}{P(0)}\right)\left(\frac{P(2)}{P(0)}\right) + \frac{1}{3}\left(\frac{P(1)}{P(0)}\right)^3 \quad , \tag{6c}$$

etc., or generally

$$C(k) = -\sum_{n_1=0}^{k} \cdots \sum_{n_p=0}^{\left[\frac{k}{p}\right]} \cdots \sum_{n_k=0}^{1} (-1+\sum_{r=1}^{k} n_r)! \left\{\prod_{q=1}^{k} \frac{1}{n_q!}\left(-\frac{P(q)}{P(0)}\right)^{n_q}\right\} \delta(k, \sum_{r=1}^{k} r n_r) \quad , \tag{7}$$

These combinants C(k) are, like cumulants,[2] additive for sums of independent boson multiplicity random variables. They have a more immediate kinship to experimental data than moments or cumulants, however, for each combinant is a finite combination of unnormalized probabilities.

The cumulants may be neatly expressed in terms of the combinants

$$\kappa_j = \sum_{k=1}^{\infty} k^j C(k) \quad , \quad j = 1,2,\ldots \quad , \quad (8)$$

as may be the factorial cumulants

$$\chi_j = \sum_{k=j}^{\infty} \frac{k!}{(k-j)!} C(k) \quad , \quad j=1,2,\ldots \quad . \quad (9)$$

The created boson multiplicity distribution may be re-expressed directly in terms of its combinants as the very general convoluted multiple Poisson distribution[3]

$$P(n) = \sum_{n_1=0}^{\infty} \sum_{n_2=0}^{\infty} \cdots \left\{ \prod_{k=1}^{\infty} \frac{(C(k))^{n_k} e^{-C(k)}}{n_k!} \right\} \delta\left(n , \sum_{r=1}^{\infty} r n_r \right) \quad . \quad (10)$$

The "black body" multiplicity distribution of mass ν spinless neutral bosons within a box of volume V at temperature T is a convoluted multiple Poisson with

$$C(k) = \frac{1}{k} \left(\frac{V \mu 3 c 3}{2\pi^2 \hbar^3} \right) \left(\frac{k_B T}{k \mu c^2} \right) K_2 \left(\frac{k \mu c^2}{K_B T} \right) \quad , \quad k=1,2\ldots \quad , \quad (11)$$

where k_B is the Boltzmann constant and K_2 is the modified Bessel function.[3] In thermodynamic models of nuclear collisions, $C(k) \ll C(1)$ for all $k \geq 2$, allowing the distribution to be adequately approximated by an ordinary Poisson.[3,4]

Combinants are useful as well in solving master rate equations for created boson multiplicity distributions in certain non-equilibrium models.[3,5] Assume that $\gamma_K^+(t)$ is the time-dependent rate for the instantaneous emission of a group of k bosons (e.g., from the decay of a k-boson resonance), while $\gamma^-(t)$ is the time-dependent rate for instantaneous single boson absorption. We derive

$$\frac{dP(n,t)}{dt} = \gamma^-(t) \left((n+1)P(n+1,t) - nP(n,t) \right) + \sum_{k=1}^{\infty} \gamma_k^+(t) \left(P(n-k,t) - P(n,t) \right) \quad , \quad (12)$$

where $P(n,t=0) = \delta_{no}$.

In terms of $F(\lambda,t)$, the time-dependent generating function, Eq. (12) becomes

$$\frac{\partial F(\lambda,t)}{\partial t} = (1-\lambda)\, \gamma^-(t)\, \frac{\partial F(\lambda,t)}{\partial \lambda} + \sum_{k=1}^{\infty} \gamma_k^+(t) (\lambda^k - 1)\, F(\lambda,t) \quad . \quad (13)$$

Now we make a convoluted multiple Poisson ansatz

$$F(\lambda,t) = \exp\left[\sum_{k=1}^{\infty} C(k,t)(\lambda^k - 1) \right] \quad , \quad (14)$$

where $C(k,t=0) = 0$, $k=1,2,\ldots$. This results in the coupled system of equations

$$\frac{dC(k,t)}{dt} = \gamma_k^+(t) - \gamma^-(t) \left[kC(k,t) - (k+1)C(k+1,t) \right] \quad \text{for } k=1,2,\ldots \quad . \quad (15)$$

Provided that $\gamma_k^+(t)$ and $\gamma^-(t)$ approach appropriate limits at large times, we may solve for the combinants at large times

$$C(k,t=+\infty) = \frac{1}{k} \sum_{q=k}^{\infty} \left(\frac{\gamma_q^+(+\infty)}{\gamma^-(+\infty)} \right) \quad . \quad (16)$$

We have discussed some models of created boson multiplicity distributions with the aim of illustrating the natural applicability and power of combinants in a variety of theoretical approaches. This, together with the natural relation of combinants to the finite set of multiplicity frequencies which make up experimental data, should make combinant analysis a standard tool for both theoretical and experimental study of most created boson multiplicity distributions.

Footnote and References

*Condensed from LBL-7700, and J. of Phys. A 11, 1715 (1978).

1. J. D. Bjorken, and S. D. Drell, Relativistic Quantum Fields (New York: McGraw-Hill, 1965), p. 202.

2. R. S. Burington and D. C. May, Handbook of Probability and Statistics (Sandusky: Handbook Publishers, 1953), Chapters 7 and 9.

3. M. Gyulassy, and S. K. Kauffmann, Phys. Rev. Lett. 40, 298 (1978).

4. R. Hagedorn, Cargese Lectures in Physics, Vol. 6, E. Schatzman, ed. (New York: Gordon and Breach, 1973), p. 713.

5. R. Malfliet and Y. Karant, Nuclear Science Annual Report, Lawrence Berkeley Laboatory Report, LBL-5075 (1975), p. 270.

DYNAMICAL THEORY OF PION MULITIPLICITY DISTRIBUTIONS IN NUCLEAR COLLISION

M. Gyulassy and S.K. Kauffmann

In the first part[1] of our studies on pion multiplicity distribution in heavy-ion collisions, we obtained a very good agreement with data using a thermodynamic fireball model for pion production. In the second part of our studies we ask the question of whether the assumption of chemical and thermal equilibrium was really necessary. To this end we formulated a dynamical theory of multiplicities.[2] Our conclusion is that the assumption of equilibration is not necessary and that a very large class of dynamical models leads to the same good agreement with data. This result shows that impact parameter averaged multiplicity distributions are not sensitive to the dynamics. Therefore, only carefully selected near central collisions events should be investigated in the future. In that case, deviations from a simple Poisson form could serve as truly significant signals for unusual coherent Pion production and absorption mechanisms.

Our dynamical theory is specified by a set of average rates, $\gamma_k^{\pm}(t)$, for producing and absorbing correlated groups of k pions. For example, $\gamma_1^{\pm}(t)$ could specify the average rates for $NN \rightleftharpoons NN\pi$, while $\gamma_k^{\pm}(t)$ for $k \geq 2$ could describe multipion resonance production and absorption (such a resonance would have to include k π's in its possible decay products to be included in $\gamma_k^{\pm}(t)$ for the data studied here). We expect that all rates must be strongly time dependent since the nucleon space and momentum distribution $f(\vec{x},\vec{p},t)$ varies rapidly during heavy-ion collisions.

The probability of producing a correlated group of k pions between times t and t + dt is then $\gamma_k^+(t)\,dt$. Also, the probability of coherently absorbing a group of k pions between t and t + dt, when there were n pions at t, is $C(n,k)\,\gamma_k^-(t)\,dt$, where $C(n,k) = n!/((n-k)!k!)$. The master equation for P(n,t) may then be obtained[2] by expressing P(n,t + dt) in terms of $P(n\pm k,t)$ and the above probabilities

$$\frac{dP(n,t)}{dt} = \sum_{k=1}^{\infty} \gamma_k^+(t)\,[P(n-k,t) - P(n,t)] \qquad (1)$$

$$+ \sum_{k=1}^{\infty} \gamma_k^-(t)\,[C(n+k,k)\,P(n+k,t) - C(n,k)\,P(n,t)]$$

where $P(n,t) \equiv 0$ for $n < 0$ is understood. Note that in this formulation, we ignore statistical correlations due to Bose statistics and consider only dynamic correlations due to coherent production and absorption mechanisms.

The time-dependent generating function then satisfies

$$\frac{\partial F}{\partial t}(\lambda,t) = \sum_{k=1}^{\infty} (\lambda^k - 1) \left[\gamma_k^+(t)\,F(\lambda,t) - \gamma_k^-(t)\,\frac{1}{k!}\,\frac{\partial^k F}{\partial \lambda^k}\right] \qquad (2)$$

The boundary conditions $F(1,t) = 1$ and $F(\lambda,0) = 1$ stem from the normalization of P(n,t) and the initial condition $P(n,0) = \delta_{n0}$.

If multipion absorption can be neglected, i.e., $\gamma_k^- = 0$ for $k \geq 2$, then the solution of Eq. (2) is

$$F(\lambda,t) = \exp\left\{\sum_{k=1}^{\infty} N(k,t)(\lambda^k - 1)\right\}, \qquad (3)$$

where N(k,t) are the time dependent combinants[3] of the convoluted multiple Poisson generated by $F(\lambda t)$. These N(k,t) satisfy

$$\frac{dN(k,t)}{dt} = \gamma_k^+(t) + \gamma_1^-(t)\,(k+1)\{N(k+1,t) - kN(k,t)\}. \qquad (4)$$

Note that N(k,t) converges to a unique equilibrium solution as $t \to \infty$. However, $N(k,\infty)$ for $k > 1$ arise here from dynamic correlations rather than from the statistical correlations leading to Eq. (3).

Our main result can be stated as follows: when correlations between pions can be neglected, i.e., $N(1,t) \gg N(k \geq 2,t)$ at the observation time $t = t_{obs}$ (for example, when $\gamma_k^{\pm}(t) = 0$ for $k \geq 2$), then $P(n,t_{obs})$ is a simple Poisson with mean $N(1,t_{obs})$ (at a fixed impact parameter). This means that a very large class of dynamical models exists that gives identical results to

the fireball model. In particular, equilibrium need not be reached! The only requirements on those models is that $N(1,t_{obs}) \gg N(k \geq 2,t_{obs})$ and that the average pion multiplicity $\langle n \rangle \approx N(1,t_{obs})$ is correctly given.

References

1. S. K. Kauffmann and M. Gyulassy, Nuclear Science Annual Report, Lawrence Berkeley Laboratory Report, LBL-6575, (1976-77) p. 200.

2. M. Gyulassy and S. K. Kauffmann, Phys. Rev. Lett. 40, 298 (1978).

3. S. K. Kauffmann and M. Gyulassy, J. Phys. A 11, 1715 (1978).

INTERACTION OF A POPULATION INVERSION WITH QUANTIZED SINGLE MODE RADIATION IN A CLOSED BOX

S.K. Kauffmann

It has been speculated that high energy, heavy-ion collisions may give rise to pion excitation population inversions in the form of a significant ratio of delta resonances to nucleons in the overlap region.[1] The following model calculation is most appropriate for considering the quantum optics of a closed, resonance-tuned box containing the population inversion--a situation one can hardly expect a nuclear collision to reproduce. Still, since the model is soluble, it can give a first feeling for this type of physics, and serve as one reference point in the search for collective pion phenomena in high energy, heavy-ion collisions.

The model consists of N two-level systems ("atoms"), each with exitation energy $\hbar\omega$, and a single (tuned) mode of frequency ω of a quantized boson field which interacts linearly with the "atoms." The model Hamiltonian is[2]

$$\mathcal{H} = \hbar\omega\left[a^+a + \sum_{i=1}^{N} \sigma_+^i\sigma_-^i + \alpha \sum_{i=1}^{N} (a^+\sigma_-^i + a\sigma_+^i)\right] \qquad (1)$$

where a^+ creates a boson of the tuned mode, while σ_+^i is the Pauli ladder operator which takes ith "atom" to its excited level. The total number of excitations n, i.e., bosons plus excited "atoms," is a conserved quantum number. The quantum number n is an eigenvalue of

$$n_{exc} = a^+a + \sum_{i=1}^{N} \sigma_+^i\sigma_-^i \qquad (2)$$

which commutes with $\mathcal{H}$.

In the very simple case that N = 1, with that isolated atom initially excited and no bosons present (simplest case of a total population inversion), the mean number of bosons (which cannot exceed one) which appear at subsequent time t is $\sin^2[(\alpha\omega)(t-t_0)]$. Such periodic solutions are typical of this Hamiltonian, for there is no mechanism for the single mode bosons to escape the box and "turn off the interaction." Note that the coupling strength α may be physically defined via the frequency of the spontaneous transition of an isolated atom. Here we are interested in the case of large N, which we shall see produces periodic solutions whose frequencies are of the order $(N^{1/2}\alpha\omega)$, and which can depart strongly from the sinusoidal.

To diagonalize $\mathcal{H}$ in the general case, it is convenient to introduce the "atomic" excitation quasi-"spin" operators

$$S_\pm \equiv \sum_{i=1}^{N} \sigma_\pm^i \qquad (3a)$$

and

$$S_0 \equiv \left(\sum_{i=1}^{N} \sigma_+^i\sigma_-^i\right) - \frac{N}{2} \quad , \qquad (3b)$$

which have the formal commutation relations of angular momentum, though they have nothing to do with physical angular momentum. S_0 clearly is just the number of "atomic" excitations minus N/2. We may rewrite

$$\mathcal{H} = \hbar\omega[a^+a + S_0 + \frac{N}{2} + \alpha(a^+S_- + aS_+)] \qquad (4)$$

and note that $\mathcal{H}$ also commutes with total "spin" operator

$$S^2 \equiv S_0^2 + \frac{1}{2}(S_-S_+ + S_+S_-) \qquad (5)$$

whose eigenvalues are $s(s+1)$ where s may take on the values $(N/2)$, $(N/2) - 1, \ldots, [(N \bmod 2)/2]$. The integer quantum number $q \equiv ((N/2) - s)$ is sometimes more convenient. When the total number n of excitations is specified, $q \leq n$, and on this (n,q) subspace, the Hamiltonian reduces to a d-dimensional matrix, where $d = \min(n, N-q) - q + 1$. Unfortunately, we are interested in large N with virtually total initial population inversion, so that $n \approx N$, initial $S_0 \approx N/2$ implying $s \approx N/2$, which makes $q \ll N$ and thus $d \approx N$. Exact diagonalization of these large matrices seems intractable.

The presence of such large quantum numbers suggests that a "classical" solution should be adequate. The Hamiltonian, with its two-level "atoms," has no direct classical analogue, but we readily construct one by deriving the Heisenberg equations of motion and then interpreting them as c-number equations.[2]

The following two Heisenberg equations follow from the commutation relations plus use of the constants of motion

$$\dot{S}_0 = i\alpha\omega \ (a^+ S_- - a S_+) \tag{6a}$$

$$\ddot{S}_0 = 2(\alpha\omega)^2 [3S_0^2 + ((N-1) - 2n) S_0 - s(s+1)] \ . \tag{6b}$$

Equation (6b) may be reduced to first order form through further use of the commutation relations

$$(\dot{S}_0)^2 = 4(\alpha\omega)^2 [S_0^3 + (\tfrac{1}{2}(N-1) - n) S_0^2 - (s^2 + s - \tfrac{1}{2}) S_0 + R]$$

where R is a time independent operator to be chosen so that the equation is explicitly verified at $t = t_0$.

We note, from Eq. (6a), that the expectation value of $\dot{S}_0$ vanishes for any state having a definite number of bosons or atomic excitations. We intend to use such states as initial states. Thus, in the interpretation of Eq. (7) as a c-number equation, R is to be chosen as the time-independent constant which causes the right side of the equation to vanish at $t = t_0$. The value of S_0 at $t = t_0$ is taken to be the initial number of "atomic" excitations minus (N/2), as per Eq. (3b). Such initial conditions provide the c-number form of Eq. (7) with unique solutions, namely elliptic functions, which are, of course, periodic.

In particular, if no bosons and n excited "atoms" ($n \leq N$) are present initially, and we specify the quantum number q [which must satisfy $q \leq \min(n, N-n)$], we obtain for $N_B(n, q; t) \equiv (n - (N/2) - S_0)$, the number of bosons at time t,

$$N_B(n,q;t) = (n-q)\,cn^2\left(K\left(\frac{n-q}{N-2q+1}\right) - (N-2q+1)^{1/2}(\alpha\omega)(t-t_0)\right) \tag{8}$$

where cn is a Jacobian elliptic function analogous to the cosine and $K((n-q)/(N-2q+1))$ is the corresponding complete elliptic integral of the first kind[3] [as the argument $m = ((n-q)/(N-2q+1))$ approaches zero, $cn \to \cos$ and $K \to (\pi/2)$].

If we do not choose to specify the value of q, we must take a weighted average of $N_B(n, q; t)$ over the allowed values of q, the weights being equal to the number of states having the given q value divided by the total number of states having n "atomic" excitations. The latter is just the binomial coefficient ${}_N C_n$, while the former is the degeneracy of angular momentum $s = ((N/2) - q)$ that results from the addition of N spin-1/2's, which may be calculated to be $({}_N C_q - {}_N C_{q-1})$. Thus, we must calculate

$$N_B(n;t) = \sum_{q=0}^{\min(n,N-n)} N_B(n,q;t)\, P_n(q) \ , \tag{9a}$$

where

$$P_n(q) = \left(\binom{N}{q} - \binom{N}{q-1}\right) \Big/ \binom{N}{n} \tag{9b}$$

such that

$$\sum_{q=0}^{\min(n,N-n)} P_n(q) = 1 \ . \tag{9c}$$

When more than half the population is initially inverted, i.e., $n \gtrsim ((N/2) + \sqrt{N})$, we note that $P_n(q)$ is very strongly peaked near $q=(N-n)$, and calculate, approximately,

$$\langle q \rangle = \sum_{q=0}^{N-n} q P_n(q) \approx (N-n)\left(\frac{2n-N}{2n-N+1}\right) \tag{10}$$

to obtain

$$N_B(n;t) \approx \left((2n-N) + \left(\frac{N-n}{2n-N}\right)\right) \times cn^2\left(K(m) - \left((2n-N) + 2\left(\frac{N-n}{2n-N}\right)\right)^{1/2} \times (\alpha\omega)(t-t_0)\right) \tag{11a}$$

where

$$m \approx 1 - \left(n/((2n-N)^2 + 2(N-n))\right) . \qquad (11b)$$

The function $N_B(n;t)$ has the half-period

$$(\Delta t) \approx K(m)/\left[\left((2n-N) + 2\left(\frac{N-n}{2n-N}\right)\right)^{1/2} (\alpha\omega)\right] \qquad (12)$$

which corresponds to a frequency of order $(N^{1/2}\alpha\omega)$. Such a rapid frequency suggests that the time-weighted behavior of the fraction of bosons discharged, $F_B(t) \equiv (N_B(n;t)/n)$, be studied. The time-weighted probability density for $F_B(t)$ to have the value f_B is

$$p(f_B) = \left(\frac{1}{\Delta t}\right)\int_0^{\Delta t} \delta(f_B - F_B(t))\, dt = \left(\frac{1}{\Delta t}\right)\frac{d}{df_B}\left(F_B^{-1}(f_B)\right) \qquad (13a)$$

where

$$0 \leq f_B \leq \left(\frac{1}{n}\right)\left((2n-N) + \frac{(N-n)}{(2n-N)}\right) . \qquad (13b)$$

Since the derivatives of inverse elliptic functions are elementary functions, $p(f_B)$ is readily calculated. Here we only display the asymptotic result in the interesting limit of total initial population inversion

$$p(f_B) \sim [\log(16N)\, f_B(1 - f_B)^{1/2}]^{-1} \quad \text{as} \quad n \to N \to \infty \qquad (14)$$

where

$$0 \leq f_B \leq 1.$$

The distribution becomes very asymmetric, with most of the probability concentrated near $f_B = 0$, i.e., favoring zero fractional boson discharge and a maintenance of the full population inversion in the time-averaged sense. Indeed, in this limit, the time averaged mean fractional boson discharge is

$$\bar{f}_B \sim (2/\log(16N)) \qquad (15)$$

which, for $N = 10^{23}$, is about 4% rather than the 50% one might have guessed. The time averaged persistence of such almost total initial population inversions is a consequence of the strong departure of the elliptic function of Eq. (11a) from the sinusoidal in this instance. Phase space considered alone would have given $\bar{f}_B = 50\%$.

The cases of less than full initial population inversion have also been examined in detail using the methods presented here. As the initial percentage population inversion is decreased, the elliptic oscillations behave more sinusoidally, and the sharply peaked probability factor $P_n(q)$ tends to dominate the results. The upshot is, however, an even more negligible fractional boson discharge, with $\bar{f}_B$ of order $N^{-1/2}$ when the initial population inversion is near 50%, and $\bar{f}_B$ of order N^{-1} as the initial population inversion falls below 50%.

The somewhat surprising results of this model, then, are the very rapid oscillations combined with the time averaged stability of an initial population inversion against free interchange of its excitations with the resonantly tuned mode of the closed box.

I wish to thank M. Gyulassy for stimulating consideration of this problem, Y. Karant for discussing his small excitation number result, and S. Garpman for discussion of a "pion laser" conjecture in heavy-ion collisions.

References

1. M. Gyulassy, Preprint of Invited Talk for the Symposium on Relativistic Heavy-Ion Collisions at G.S.I., Darmstadt, Germany, LBL-7704.

2. H. Haken and H. Sauermann, Z. Physik 173, 261 (1963).

3. M. Abramowitz and I. A. Stegun, Handbook of Mathematical Functions (National Bureau of Standards, Washington, 1965), Chapters 16-17.

HIGH ENERGY NUCLEAR COLLISIONS IN THE RESONANCE DOMINATED REGION

N.K. Glendenning and Y. Karant

It is experimentally known that for each new hadronic flavor threshold, a rich resonance spectrum ensues for the next few GeV mass interval. It has been conjectured that the hardonic mass spectrum continues indefinitely and in the statistical bootstrap model, this manifests itself

in an exponentially growing spectrum.[1] Assuming that it is possible to form equilibrated hot hadronic matter of nuclear dimensions (a nuclear fireball) in a nucleus-nucleus collision, we model the rate of disassembly of such a fireball.[2]

The problem is this: Given different model mass spectra (different worlds), which certainly give a different composition of the nuclear fireball, how do these differences manifest themselves at the detectors asymptotically far from the interaction? Equivalently, only the hadronically stable particles can reach the detectors, and we are interested in predicting their signal at the detectors.

The question cannot be answered in a physically satisfactory manner within purely equilibrium gas thermodynamics. The difficulty is that the detectors are located at infinite volume, and the nuclear fireball has no walls; so if it were to expand to any large volume without emitting particles in the process, it would reach such a low energy density that all worlds look essentially the same.

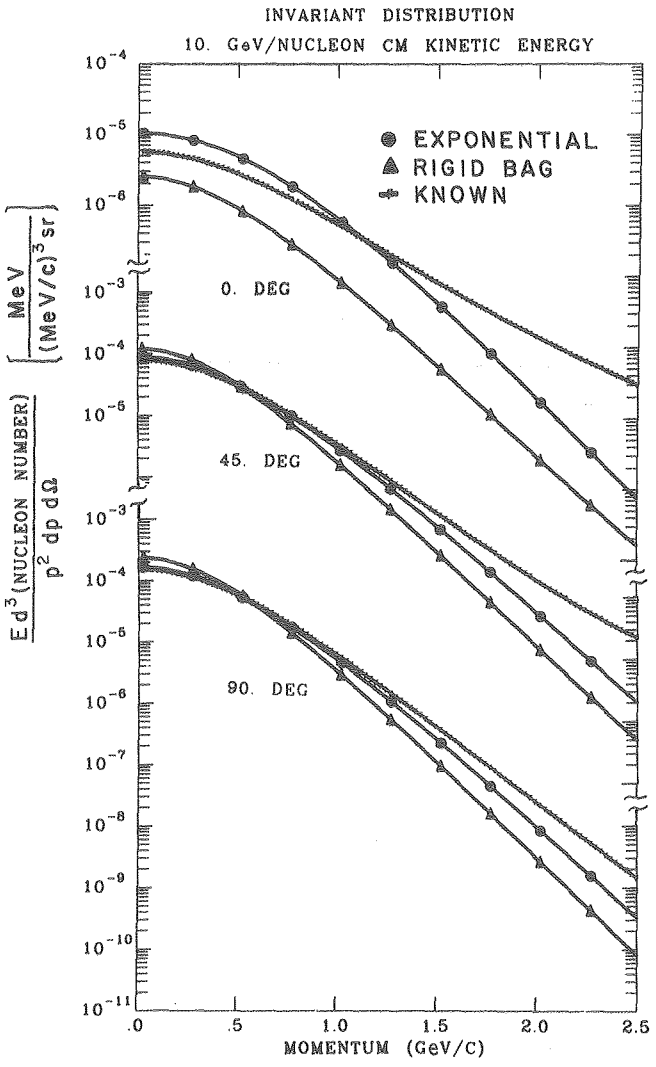

Fig. 1. Lorentz invariant double differential nucleon distribution for a symmetric A = 50 collision at 10 GeV/nucleon. (XBL 786-9150)

Instead, one must realize that there are three processes occurring simultaneously: expansion, radiation of stable particles, and decay of hydronic resonances. Assuming that it is possible to form initially an equilibrated nuclear fireball, the lighter, faster particles will travel further from its surface than the more ponderous resonances, resulting in a general expansion. In fact, stable particles moving faster than the general expansion speed and within a mean free path of the surface will escape to the detectors. Meanwhile, the increase in available phase space due to the volume expansion will permit resonance decay, which we assume can be described by thermodynamics.

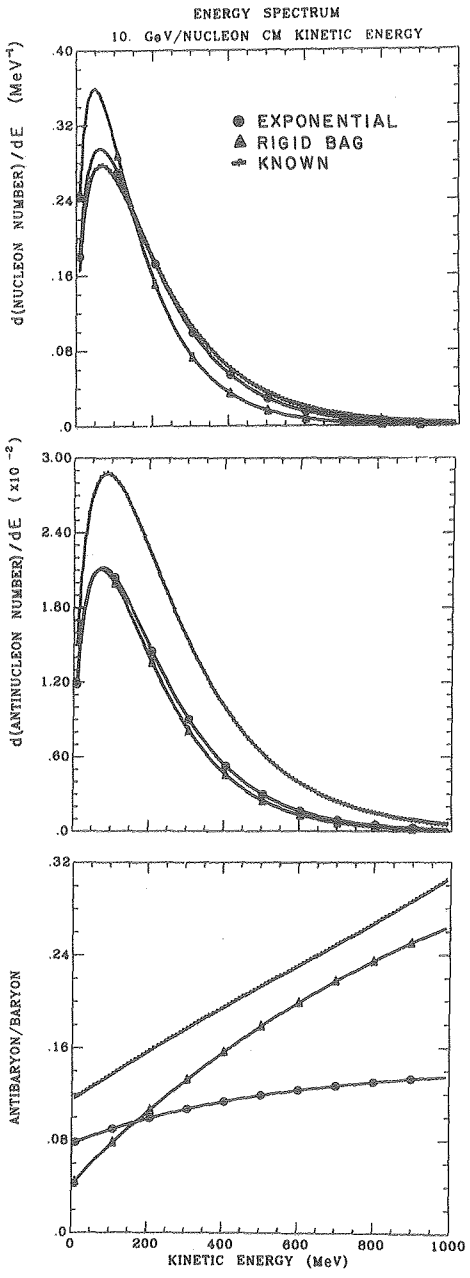

Fig. 2. Particle energy spectra for the same collision as in Fig. 1. (XBL 786-9147)

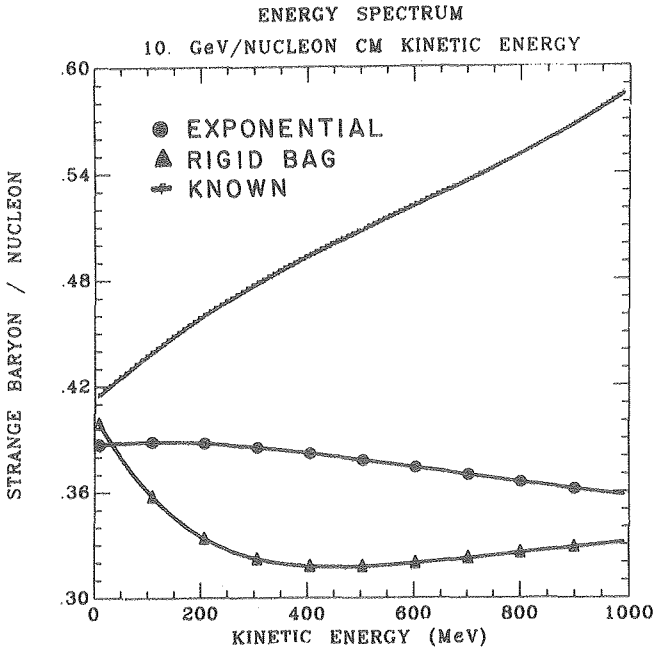

Fig. 3. The energy spectrum ratio of strange baryons to nucleons for the collision of Fig. 1. (XBL 786-9145)

We incorporate these three features in a model in which we have included flavors: up, down, and strange. By isospin averaging (assuming Z = N in the initial system), we have three constraints: total energy (E), baryon number (B) and strangeness (S). We insure that the sum of radiation plus remainder in the fireball is conserved. We have normalized the strange continua by simple quark counting arguments, and we have assumed that at any stage, the fireball of volume is an ellipsoid characterized by two parameters: $R_{\parallel}$, $R_{\perp}$. Then, at any stage, the invariant distribution of species is:

$$\frac{Ed^3N}{d^3P} = \frac{gVE}{(2\pi)^2 \exp\left(\frac{E-\mu}{T}\right) \pm 1} \frac{3}{4\pi(R_{\perp}^2 + 2R_{\parallel}^2)}$$

$$(R_{\parallel}^2 \sin^2\theta + R_{\perp}^2 \cos^2\theta)$$

where g = degeneracy, μ = chemical potential, T = temperature, V = emitting volume.

We display a typical result in Fig. 1, in this case the invariant nucleon distribution at three center-of-mass angles as viewed in a colliding beam system. Exponential refers to a Hagedorn-type mass spectrum, rigid bag a power law(m^5 for baryons, m^2 for mesons), and known is only the experimentally discovered resonances. One can see that despite the evolution of the fireball through many temperatures and shapes, the final observables look much like straight lines over much of the momentum region. However, the normalizations and slopes change with angle.

In Fig. 2 we plot the energy spectrum, integrated over all angles, of the nucleons, antinucleons, and their ratio. Note that only for the exponential spectrum is this ratio essentially flat.

Finally, in Fig. 3, we plot the ratio of strange baryons ($\Lambda\Sigma\Xi\Omega$) to the nucleons, indicating that in all cases, substantial hypernucleus formation is possible.

References

1. R. Hagedorn, Cargese Lectures in Physics, Vol. 6, G. Schatzman, ed. (Gordon and Breach, New York, 1973).

2. N. K. Glendenning and Y. Karant, Phys. Rev. Lett. 40, 374 (1976).

THERMODYNAMIC BEHAVIOR OF NON-STRANGE BARYONIC MATTER

S.A. Garpman,* N.K. Glendenning, and Y. Karant

Experiments during the last few years have shown that high energy inelastic heavy-ion collisions may deposit significant amounts of "heat" into nuclei. To explore the data within the realm of local equilibrium thermodynamics, it is essential to know the equation of state for highly excited baryonic matter. To be a realistic description, the equation of state must reflect nuclear matter properties like binding and short-range repulsion. An interesting analytical model of this kind has been suggested by Walecka.[1,2] In that model two boson fields (a scalar and vector meson) were coupled to the nucleon field. By solving a linearized Dirac equation for the nucleon field, it was possible to get explicit expressions for the thermodynamical variables at finite temperatures. In Refs. 1-4 only the nucleon was considered as a possible baryonic state. However, with rising temperatures (≥50 MeV) the baryon resonances, i.e., N* and Δ, will populate significantly as has been seen in relativistic Fermi gas calculations.[5,6] We examine the effect of including explicit interactions between hadrons, in the mean field approximation, on the dependence of ultra-high energy nuclear collisions on the asymptotic hadron spectrum. By doing so, we also hope to learn about the possible existence of metastable nuclei[7]

Table 1. Scalar density ρ_S[fm^{-3}] resonances included.

T(MeV) \ Compression[a]	1/2	1	2	3	4
125	0.735	0.735	0.735	0.735	0.735
125	0.431	0.428	0.410	-	-
125	0.0706	0.137	0.262	-	-
100	0.0718	0.139	0.249	0.324	0.372
50	0.0770	0.148	0.257	0.316	0.354

[a]Defined as baryon density/normal nuclear matter density.

Table 2. Nucleon chemical potential $\mu/m_N c^2$ (dimensionless) resonances included.

T(MeV) \ Compression[a]	1/2	1	2	3	4
125	0.00204	0.00407	0.00814	0.0122	0.0163
125	0.0126	0.0258	0.0594	-	-
125	0.384	0.345	0.212	-	-
100	0.539	0.478	0.346	0.270	0.237
50	0.752	0.638	0.477	0.423	0.398

[a]Defined as baryon density/normal nuclear matter density.

Table 3. Pressure P [MeV/fm^3] resonances included.

T(MeV) \ Compression[a]	1/2	1	2	3	4
125	143.	162.	237.	361.	536.
125	-91.3	-71.3	10.8	-	-
125	11.1	24.5	66.0	-	-
100	8.73	19.6	62.2	156.	309.
50	3.73	8.61	45.4	148.	306.

[a]Defined as baryon density/normal nuclear matter density.

and about eventually occurring supercritical field phenomena.

We include all 18 discrete resonances in the equation of state. With the baryon density ρ_B and the temperature T as known quantities one has to solve two transcendental equations for the unknown parameters: the baryon scalar density and chemical potential. In Tables 1 and 2 the calculated scalar densities and nucleon chemical potentials are displayed. Note that for a temperature of 125 MeV, there exist three branches at low baryon density. As the scalar density increases the effective masses of the resonances decrease and at some point the effective masses of the lower vacuum mass resonances will pass zero. When the effective mass of the nucleon passes zero, the $\Delta(1232)$ resonance state will be mostly populated. Due to its high statistical weight, it forms a metastable state[7] which has a signature of a negative pressure, as can be seen in Table 3.

In Figs. 1-3 we compare the equation of state at T = 100 MeV for three different models: i) Walecka's model, ii) Walecka's model with resonances included and finally, iii) relativistic Fermi gas in chemical equilibrium.

As can be seen, the energy density curves for the three cases are not very different. Nonetheless, the pressure curves are entirely different due to the strong short-range repulsion in Walecka's model. However, as can be seen, the inclusion of resonances softens the equation of state considerably. On course, the pressure of the relativistic Fermi gas is much smaller than for the other two models. It is interesting to note that the entropy curve for case ii) will show an increase when thresholds for populations in higher lying resonances are passed. The relativistic Fermi gas will have an entropy curve similar to case ii) but with slightly higher entropy for moderate baryon densities.

We also examine the effect of including both discrete resonances and an exponentially growing continuum. We include 9 discrete resonances below 1680 MeV and from there on a continuum. The mass degeneracy factor we assume to be a Hagedorn spectrum.[5,8]

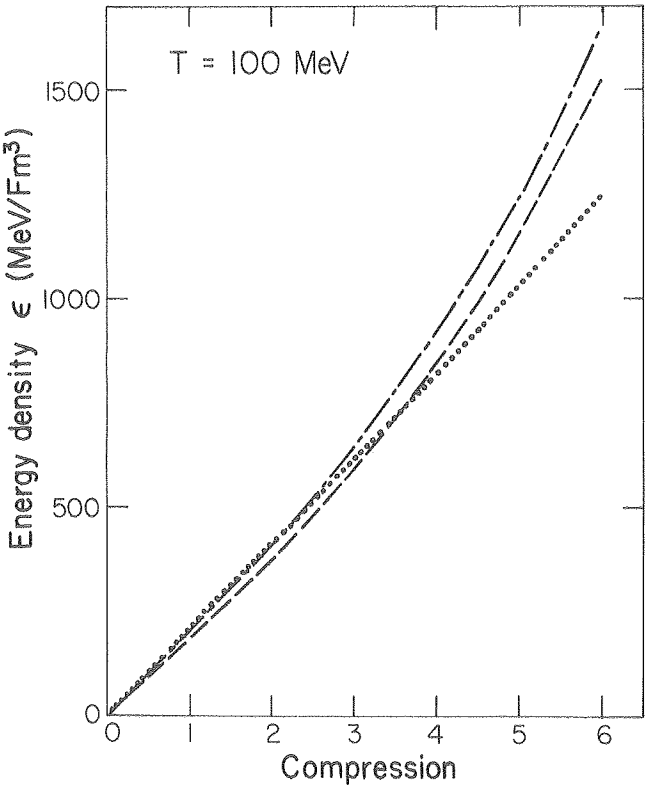

Fig. 1. The energy density vs the compression, defined as baryon density/normal nuclear matter density where we choose 0.17 [fm^{-3}] for normal nuclear matter density, for a fixed temperature of 100 MeV. Three different models are displayed: i) Walecka's model (dashed line), ii) Walecka's model with 18 discrete resonances included (dot dashed line), and iii) free relativistic Fermi gas of 18 discrete resonances (dotted line).
(XBL 787-1242)

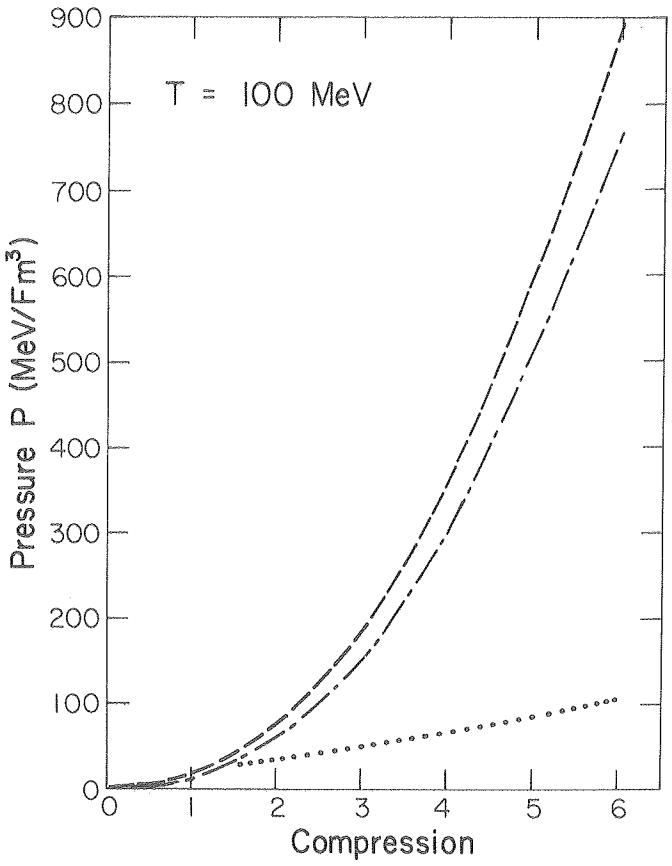

Fig. 2. The pressure vs the compression for a fixed temperature of 100 MeV. Three different models are displayed: i) Walecka's model (dashed line), ii) Walecka's model with resonances included (dot dashed line), and iii) free relativistic Fermi gas of the resonances (dotted line).
(XBL 787-1243)

$$h(s) \approx \frac{m_N^{\,e^{s(m_N c^2/T_o)}}}{3m_\pi s^3 (m_N c^2/T_o)^3} \quad s > 12\, n_\pi/m_N \qquad (1)$$

The limiting temperature $T_o = 0.958\, m_\pi c^2$ is chosen as in Ref. 5; m_N and m_π are the vacuum masses of the nucleon and pion, respectively. The normalization is made in a symmetric five pion mass interval centered at 1400 MeV, so as to agree with the observed non-strange baryons. Counting the spin-isospin degeneracy factors we have totally 88 states available in this interval. At lower temperature ($T \leq 100$ MeV), in the baryon density interval considered, the continuum will not contribute much. However, as the temperature approaches the limiting temperature, the continuum will strongly influence the thermodynamical behavior, at least at finite baryon densities. In Table 4 we show the two lower branches at a fixed temperature of 125 MeV. As can be seen by inspecting Tables 1 and 4, these two branches are only slightly modified by the presence of

Table 4. Thermodynamical properties when a continuum is included T = 125 MeV.

Compression	ρ_S[fm^{-3}]		$\mu/m_N c^2$ (dimensionless)		ε[MeV/fm^3]		ρ[MeV/cm^3]		S/B (dimensionless)	
1/2	0.0724	0.315	0.354	0.0269	139.	663.	10.8	-54.4	10.3	55.9
1	0.142	0.306	0.304	0.0589	287.	659.	22.9	-32.2	9.98	26.8

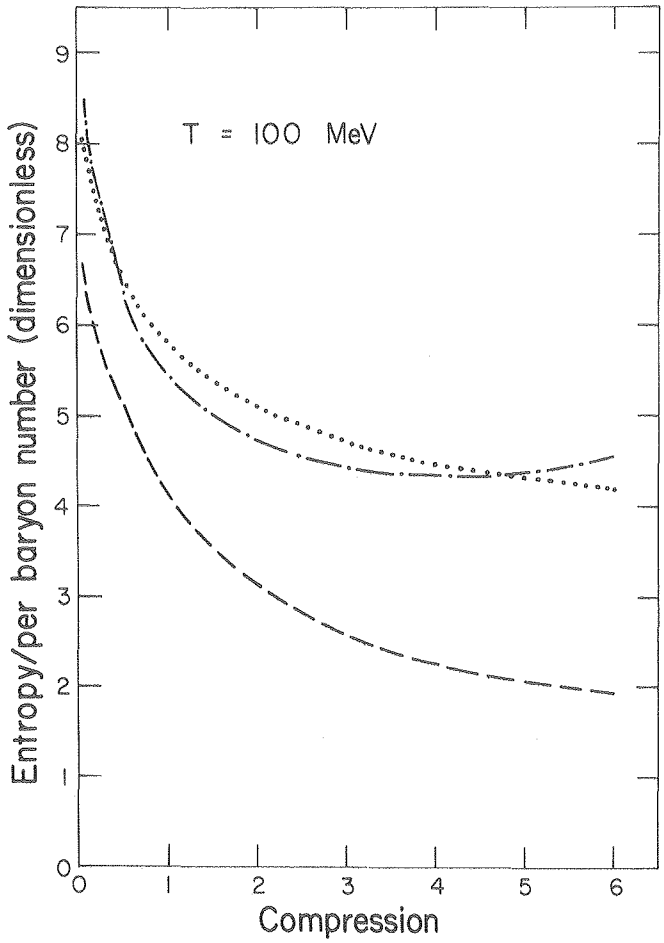

Fig. 3. The entropy per baryon vs the compression for a fixed temperature of 100 MeV. Three different models are displayed: i) Walecka's model (dashed line), ii) Walecka's model with resonances included (dot dashed line) and finally iii) free relativistic Fermi gas of the resonances dotted line). (XBL 787-1241)

the continuum. The third branch, however, is very sensitive to the continuum (where most of the population lies) due to the exponential increase of the Hagedorn spectrum with mass. It is of particular interest to note that the metastable "Δ(1232) state" survives the inclusion of a continuum of resonances.

Footnote and References

*On leave from Rensselaer Polytechnic Institute, Troy, New York 12181, USA.

1. J. D. Walecka, Phys. Lett. B 59, 109 (1975).

2. J. D. Walecka, Ann. Phys. 83, 491 (1974).

3. S. A. Chin and J. D. Walecka, Phys. Lett. B 52, 24 (1974).

4. R. A. Freedman, Phys. Lett. B 71, 369 (1977).

5. N. K. Glendenning and Y. Karant, Bull. Am. Phys. Soc. 22 (1977) and Phys. Rev. Lett. 40, 374 (1978); N. K. Glendenning, Invited paper Hirschegg, Austria, January 16, 1978, (LBL-7165).

6. J. I. Kapusta, LBL-6504, submitted to Phys. Rev. C.

7. G. F. Chapline, M. H. Johnson, E. Teller, and M. S. Weiss, Phys. Rev. D 8, 4303 (1973).

8. R. Hagedorn in Cargèse Lectures in Physics, Vol. 6, E. Schatzman, ed. (Gordon Breach, NY, 1973).

INCLUSIVE PION PRODUCTION IN RELATIVISTIC PROTON COLLISIONS WITH NUCLEI: A REEXAMINATION

R.H. Landau

The production of pions in relativistic heavy-ion collisions is currently being measured in part with the hope that pions may signal the formation of abnormal nuclear matter. These experiments,[1,2] which provide inclusive pion spectra for both forward and backward hemispheres,

reveal unexplained trends which may provide clues to the reaction mechanism or to some interesting new physics. Unfortunately, there do not exist equally complete data on the inclusive π production by protons on nuclei--except at one energy.[3] In this work we reexamine these proton-nucleus π production data of Cochran et al.[3] in an effort to provide a comparison and foundation for understanding π production in heavy-ion collisions.

To determine the separate $X_R (= k_\pi^{cm}/(k_\pi^{cm})_{max})$ and $k_\perp$ ($= k \sin\theta$) dependence of these data, we have examined them with a two-dimensional bicubic spline interpolation routine. In this way we have examined the cross section E/k^2, $d^2\sigma/d\Omega dk$ vs. θ_{cm}(pC) for the pC $\rightarrow \pi^-$ X reactions at several c.m. pion energies. The π^+ cross sections for production for C are almost identical in shape but a factor ~5 times larger. Viewed in the c.m. systems, very similar results (isotropy at low energies, forward peaking at high energies) are obtained for heavier nuclei. The similarity in shape for inclusive π production from such

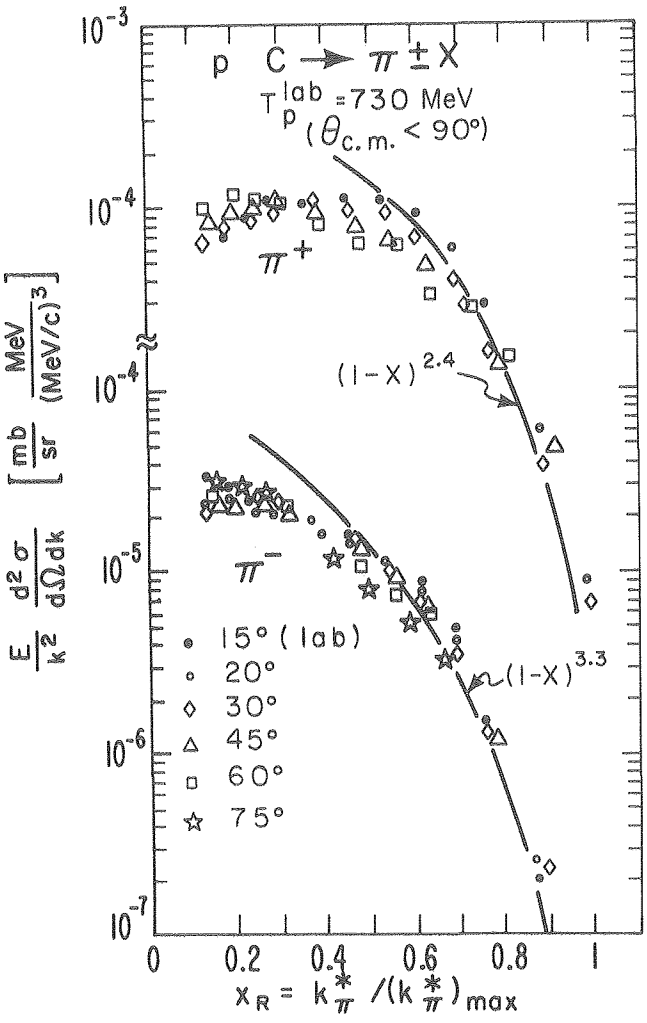

Fig. 1. Invariant cross section for $\pi^\pm$ production by protons from carbon vs. the scaling variable x_R, for emission angles less than 90°. The points are those of Ref. 5 with the exponential $k_\perp$ variation of Eq. (2) removed.

(XBL 781-2353)

different size nuclei indicates the absence of "diffractive" (but not necessarily multiple scattering) effects which would give additional structure for Pb. In fact, these angular dependences are so uniform in most cases that they can all be fit fairly well with a function of the form $\exp[-r_2 k_\perp^2]$ with $r_2 \approx 20(\text{GeV/c})^{-2}$. Again we see little effect in r_2 or r_3 due to nuclear size (the r_2 dependence reflects a nuclear fireball of ~110 MeV temperature).

Following a suggestion by Nagamiya et al.[1] we have tried to obtain a clue to the reaction mechanism by examining the cross sections in the proton-target nucleon c.m. (assuming "frozen" nucleons, for example and comparing these to the elementary proton-proton π production cross sections. We have found that the actual pp data show only moderate angular dependence with a maximum asymmetry of ~2 at $T_\pi \approx 100$ MeV reflecting the P_{33} resonance. The p-nucleus data, on the other hand, are similar to the pp data for $\theta < 90^\circ$, but develop a strong backward peak at $T_\pi \approx 100$ MeV, when viewed in this pp reference frame. This is just a reflection of the large cross section for low energy pions at backward angles present in the p-A c.m. which get transformed to high energies when viewed in the pp c.m. Physically, then, it appears that the forward angle data can be simply represented as some type of convoluted pN $\rightarrow \pi$X cross sections,[2] but that there is some different mechanism which produces high energy backward pions. A possibility would be proton scattering from a cluster, i.e., coherently from several nucleons.

Since scaling seems to work at energies of 1 GeV and above,[4] it is natural to query if the 730 MeV E/k^2, $d^2\sigma/d\Omega dk$ also fall on a universal curve when plotted vs. x_R. We have found that for $x_R \gtrsim 0.4$, the 730 MeV forward angle ($\theta_\pi < 90^\circ$) data fall quite close to the 1-5 GeV data, with the 1 GeV and 730 MeV data within ~20% of each other. Furthermore, the x_R dependence of these data can be parameterized as $(1-x_R)^H$, with different values of H for scattering into the forward and backward hemispheres (~3 and 13). The data points of Ref. 3 with the $k_\perp$ dependence removed are shown in Fig. 1 for pions with $\theta_{cm} < 90^\circ$, and in Fig. 2B for pions with $\theta_{cm} > 90^\circ$. The solid curves in Fig. 1 represent our average fit which, including the $k_\perp$ dependence, is of the form:

$$\frac{E}{k^2}\frac{d2\sigma}{d\Omega dk} = E(s)(1-x_R)^H \exp[-r_n k_\perp^n] \qquad (1)$$

Schmidt and Blankenbecler[5] (B) have taken the relativistic hard collision model that describes elementary particle reactions in terms of partons and extended it to describe the relativistic collisions of nuclei. In the high energy limit, this theory predicts cross sections of the form (1) with power H = 3 for forward angles (beam fragments) and H = $6A_T$-5 (=1243) for backward angles (target fragments).

It is somewhat of a puzzle that the forward-angle data scale has a power-law behavior in general agreement with Schmidt and Blankenbecler,

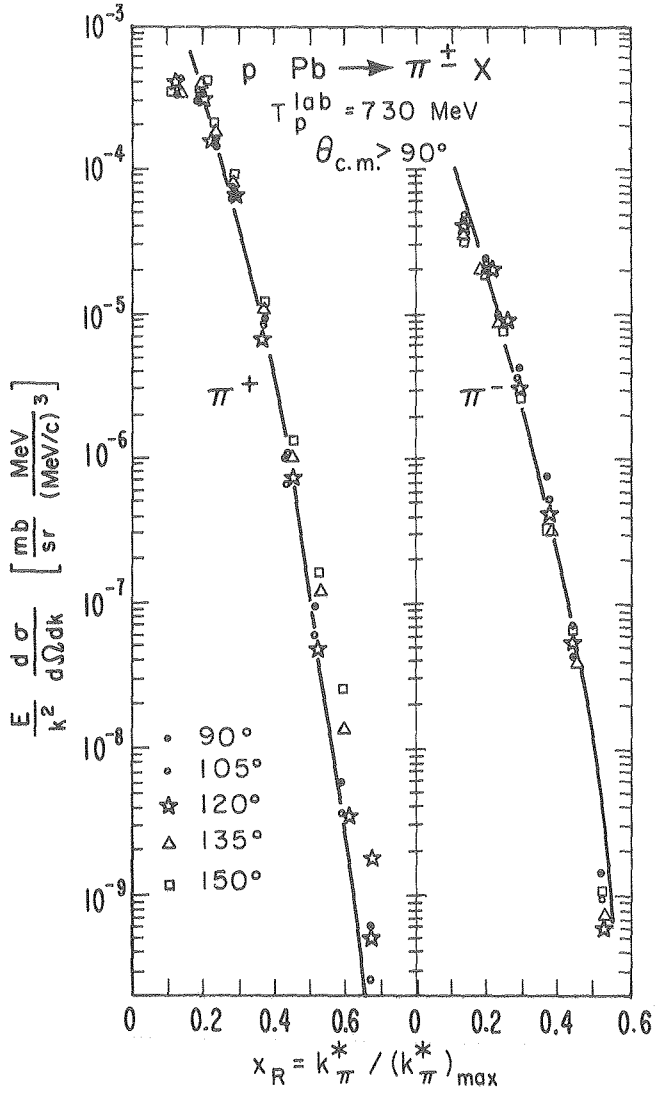

Fig. 2. Same as Fig. 1, except now for backward pins, $\theta_{cm} > 90^{o}$ and a Pb target. The curves here represent Fermi averaged, Lorentz-transformed $pp \rightarrow \pi X$ cross sections.

(XBL 781-2366)

but that the back-angle data--which "scale" even better--do so with a power so different from the theory's prediction. If we assume that the theory is valid for this low an energy, the small power, ~13, indicates that the large momentum transferred to the nucleus is being absorbed by only one or a few nucleons and not equally distributed amongst "A" nucleons (as Schmidt and Blankenbecler assume). In fact, since H = 6A-5 (for the most consistent model of the NN force) these data suggest that back-angle pions are produced from clusters with A ≈ 1-3.

Stimulated by this intriguing possibility, Gyulassy and Landau[6] have carried this non-coherent production idea somewhat further and find that the shape of these spectra are consistent with production from a few nucleon clusters, or even from a single nucleon with Fermi motion. The solid curves in Fig. 2 are in fact Fermi-averaged, Lorentz-transformed $pp \rightarrow \pi X$ cross sections. We find that the production of pions from both C and Pb, while showing different power-law behavior (12 vs. 15), can still be simply related to the same elementary production process. The details of this calculations, plus a more complete examination of inclusive π production by protons and heavy ions at various energies, are found in Ref. 6.

Footnotes and References

*Condensed from LBL-7169, Phys. Rev. C17, 2144 (1978).

†On leave from Oregon State University, Corvallis, Oregon 97331.

1. S. Nagamiya, I. Tanihata, S. Schnetzer, L. Anderson, W. Brückner, O. Chamberlain, G. Shapiro, and H. Steiner, Lawrence Berkeley Laboratory, Report LBL-6770, presented at VIIth Int. Conf. on High-Energy Physics and Nucl. Structure, Zürich, 1977.

2. K. Nakai, J. Chiba, I. Tanihata, S. Nagamiya, H. Bowman, J. Ioannou, and J. O. Rasmussen, VIIth Int. Conf. on High-Energy Physics and Nucl. Structure, Zürich, 1977.

3. D. R. F. Cochran, P. N. Dean, P. A. M. Gram, E. A. Knap, E. R. Martin, D. E. Nagel, R. B. Perkins, W. J. Shlaer, H. A. Thiessen, and E. D. Theriot, Phys. Rev. D 6, 3085 (1972).

4. J. Papp, J. Jaros, L. Schroeder, J. Staples, H. Steiner, A. Wagner, and J. Wiss, Phys. Rev. Lett. 34, 601 (1975); J. Papp, Ph.D. thesis, Lawrence Berkeley Laboratory, Report LBL-3633, unpublished (1975).

5. I. A. Schmidt and R. Blankenbecler, Phys. Rev. D 15, 3321 (1977).

6. R. H. Landau and M. Gyulassy, Lawrence Berkeley Laboratory, Reports LBL-7748 and LBL-7719.

INCLUSIVE PION PRODUCTION IN RELATIVISTIC NUCLEAR COLLISIONS*

R.H. Landau† and M. Gyulassy

The study of high-energy pion production in relativistic nuclear collisions promises to provide insight into the production mechanism and into fundamental aspects of nuclear structure. The discovery[1] of scaling in inclusive pion production and the success of the elegant hard

scattering model[2] in accounting for the data encourage one to believe that the reaction mechanism may be both simple and universal. Furthermore, pions produced with momenta larger than those possible in elementary nucleon-nucleon collisions (at the same energy per nucleon) can arise only as a result of nuclear binding effects, i.e., the coherent interaction of many nucleons or large internal Fermi momenta. The hope is, therefore, that by studying the highest energy single-particle fragments the high momentum tail of nuclear wave functions and/or many-body correlations in nuclei can be studied.

One of the most intriguing aspects of the momentum dependence of $R(B + A \to \pi + X) \equiv Ed\sigma/d^3p$ is the apparent scaling (independence of beam energy) in the projectile fragmentation region ($\theta_L^\pi \approx 0^o$) when plotted as a function of the (radial) scaling variable $x_{BA} = k_\pi^*/k_\pi^*(\max)$.[1] Such scaling in the projectile[1] fragmentation region has been explained in the context of the nuclear hard scattering parton model of Ref. 2. However, Chessin et al.[3] and Landau[4] have recently discovered that in the target fragmentation region ($\theta_L^\pi \approx 180^o$) there is a strong energy dependence of the shapes of R (hence a lack of scaling) and that the slopes are much smaller in magnitude than predicted in Ref. 2.

We have considered a general hard scattering (cluster) model in which

$$R(B+A(c) \to \pi^-(180^o)+X) = N \int_{-\infty}^{\infty} dp_z \rho_c(p_z) R(B+c \to \pi^-(180^o)+X) p. \quad (1)$$

Here "c" is a cluster of c nucleons in A, and $R(Bc \to \pi X)$ is the on-shell π production rate in beam-cluster collisions. The phase space factor p in Eq. (1) includes the ratio of relative flux factors and constrains the domain of integration so that only kinematically allowed pions are produced. For high incident energies ($\gtrsim$ 1 GeV/nucleon), p is taken to be

$$p = \theta(1 - x_{Bc})\theta(1 - x_{BA}) \quad , \quad (2)$$

so that the absolute kinematic bound on the pion momenta $k_\pi^*(\max)$ is enforced in both the Bc and BA center-of-mass systems. For pion production in the projectile fragmentation region ($\theta_L \approx 0^o$), A and B are simply interchanged in Eqs. (1) and (2) and the cluster c then refers to a group of nucleons in beam B.

To parameterize the beam-cluster rate in Eq. (1), we follow the invariant counting rules of Ref. 2,

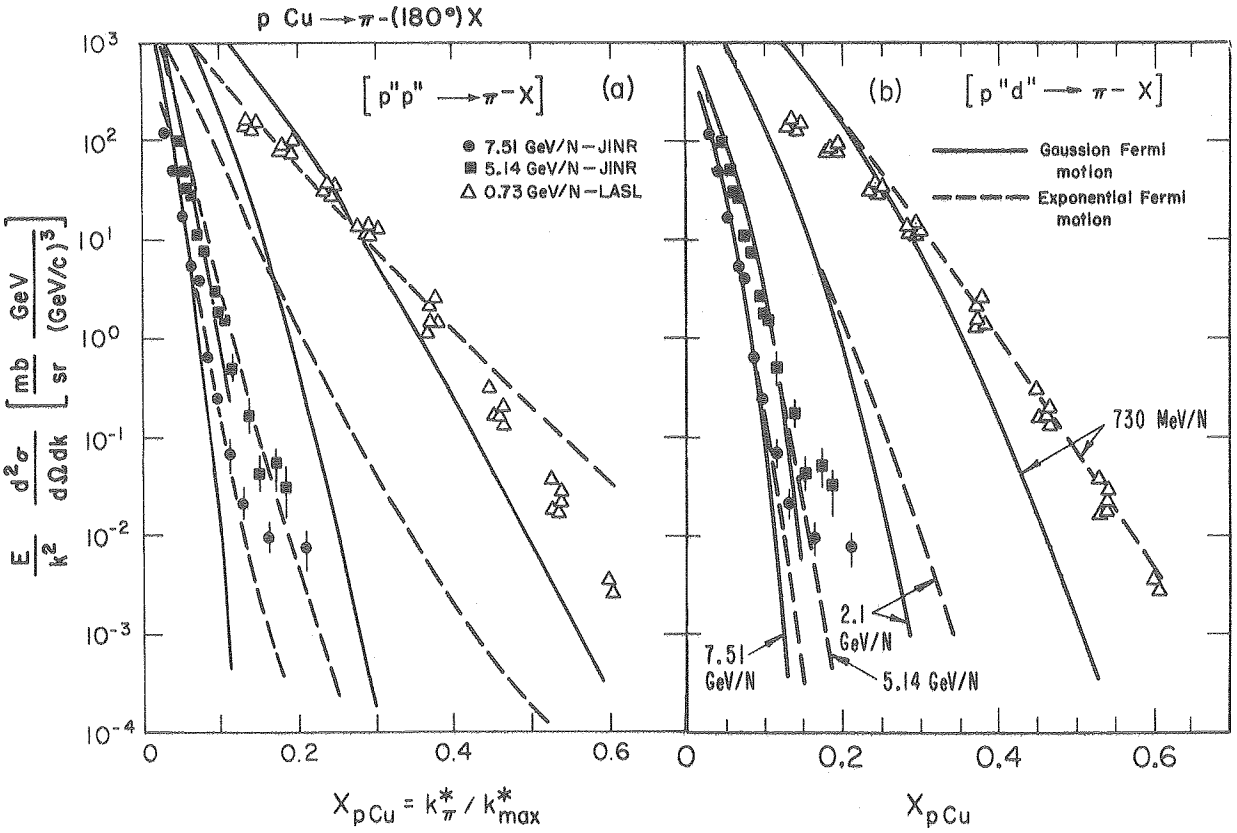

Fig. 1. The invariant cross section for $p + Cu \to \pi^-(180^o)+X$ calculated with π production from one nucleon (a) or from a two-nucleon cluster (b). The solid curves were calculated with a Gaussian Fermi momentum distribution, the dashed curves with an exponential.

(XBL 786-1169)

$$R(B+c \to \pi^-(180^o)+X) \propto (1-x_{Bc})^{S_{Bc}},$$

$$S_{Bc} = 6c-3-2\delta_{B,1} \ . \qquad (3)$$

For back-angle pions, S_{Bc} is known experimentally only for one- and two-nucleon clusters (c = 1,2) and is correctly given by Eq. (3).

Equation (1) modifies the model of Ref. 2 by allowing only a smaller cluster of c < A nucleons to scatter coherently, and in this way is similar in spirit to various cluster models. By restricting to small clusters, it is clear from Eq. (3) that the slope S_{Bc} will be much smaller than S_{BA}. Furthermore, an explicit energy dependence of the shape of R is introduced as a result of the kinematic constraint in Eq. (2).

For the cluster momentum distribution $\rho_c(p_z)$, we consider two possible forms. The first is the Gaussian suggested by fragmentation experiments, $\rho_c(p_z) \propto \exp(-p_z^2/2\sigma_z^2)$, with $\sigma_z \approx 130$ MeV/c independent of c. The second form is the exponential suggested in inclusive proton experiments, $\rho_c(p_z) \propto \exp(-|p_z|/p_o)$, with $p_o \approx 100$ MeV/c. Both forms differ from the standard cluster models which assume ρ_c becomes broader with increasing c. We regard the c dependence of ρ_c as an open question.

In Fig. 1 we examine the reaction p + Cu → π^- (180°) + X. In Fig. 1(a) are the results of Eq. (1) for single-nucleon clusters (c = 1), and in Fig. 1(b) for "deuteron" clusters (c = 2). Both the magnitude and the energy dependence of the shapes of R are well reproduced with c = 1 or 2. The exponential form for ρ(p), however, leads to better agreement than the Gaussian form. We note that the preliminary data[3] at 2 GeV/nucleon also have a shape very similar to the predicted dashed curve in Fig. 1.

Other data in the target fragmentation region that we have examined are those on p + d → π^-(180°) + X at 730 MeV and 7.5 GeV and preliminary data[3] on α + Cu → π^-(180°) + X at 1 and 2 GeV/Nucleon. The shapes of these spectra are also consistent with either c = 1 or 2 in Eq. (1). An interesting feature of the pd data is the apparent scaling between 0.73 and 7.5 GeV; i.e. the parton model[2] appears to work for such a light target. We have, however, traced the cause of this scaling to simple kinematic effects. In particular, the energy dependence of the Lorentz transformation involved in Eq. (1) for light targets is much weaker than for the heavy target considered in Fig. 1.

A crucial second test of Eq. (1) is in the projectile fragmentation region. In Fig. 2 we compare data on d + C → π^-(2.5°) + X and α + C → π^-(2.5°) + X at 1 and 2 GeV/nucleon with predictions of Eq. (1) (with A ↔ B). Again the one- and two-nucleon cluster models reproduce the shapes with the same $\rho(p_z)$ as used in the

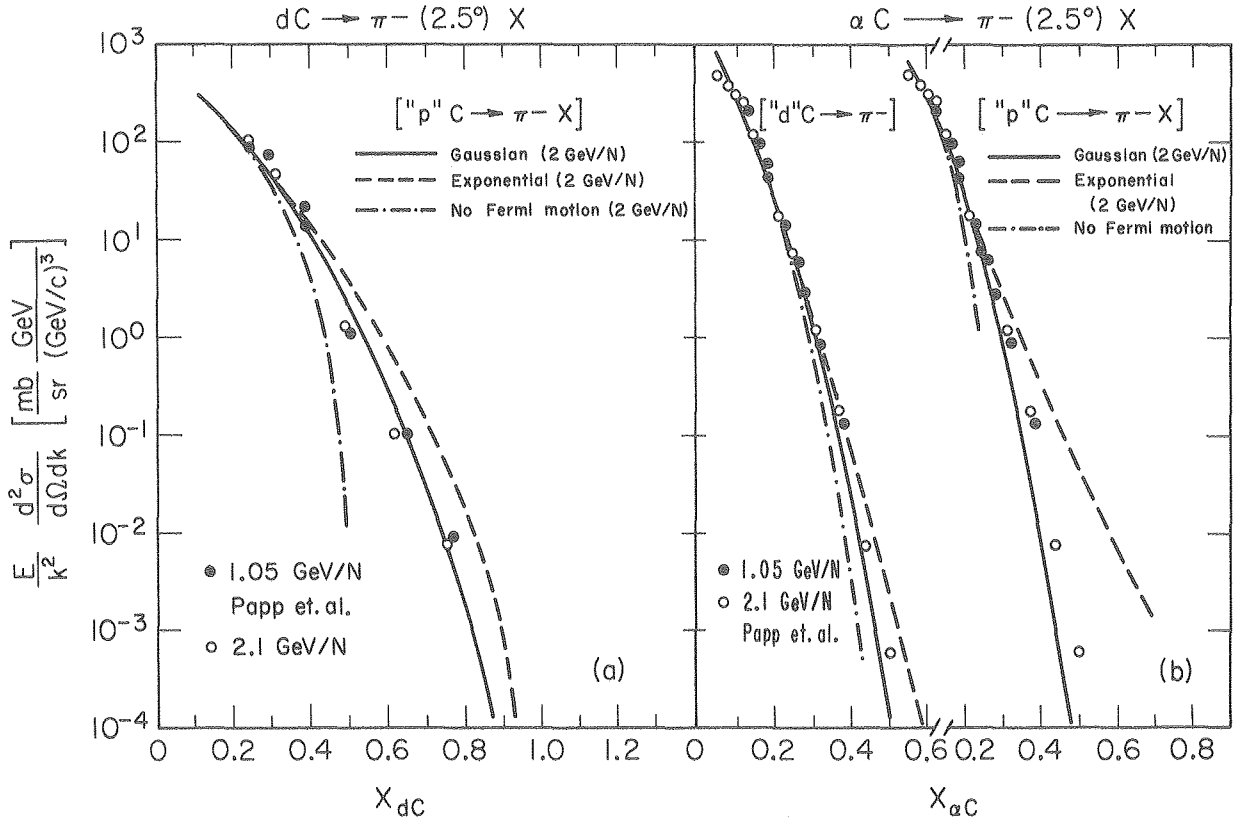

Fig. 2. The invariant cross section for forward pion production for d and α beams incident on carbon. As in Fig. 1, a one- and two-nucleon cluster model is examined for each of two internal momentum distribution functions. For this beam fragmentation, the "clusters" are within the projectile nucleus. (XBL 784-8256)

target fragmentation region. Here, however, the clusters are in the beam nuclei. The relative insensitivity of the calculated curves to the pseudo-Fermi motion distribution $\rho(p_z)$ is in contrast to the much greater sensitivity in the target fragmentation region, Fig. 1. In addition, the apparent scaling feature of these data also follows from Eq. (1) simply as a result of the weak energy dependence of the relevant Lorentz transformations in the projectile fragmentation region.

We conclude from this study that hard scattering models are valuable phenomenological tools--phenomenological since off-shell effects as well as initial and final state interactions are contained in the pseudo-Fermi distribution function.[6] In particular we have learned that much of the differences between pion production data in nuclear collisions can be attributed to simple kinematic effects. "Scaling" in the projectile fragmentation is a specific example of such kinematic effects. Second, we have found that single nucleon-nucleon or light cluster-cluster collisions are sufficient to explain the data if a universal exponential distribution is used. Thus, only a small degree of coherent interactions seems to be needed to explain the data. Third, we found that in Eq. (1) the energy dependence of the elementary nucleon-cluster rates were necessary in order to account for the data. Finally, we found that the data were sensitive to Fermi motion, but that no unambiguous relation could be established between $\rho(k)$ in Eq. (1) and the true Fermi motion. In summary, we have found that a universal exponential tail explains the shape of all available data on pion production in the projectile and target fragmentation regions.

We are currently studying proton-inclusive data within the same framework.

Footnotes and References

*Condensed from LBL-7746 and LBL-7719, submitted to Phys. Rev. C and Phys. Rev. Lett., respectively.

†On leave from Oregon State University, Corvallis, Oregon 97331.

1. J. Papp, J. Jaros, L. Schroeder, J. Staples, H. Steiner, A. Wagner, and J. Wiss, Phys. Rev. Lett. 34, 601 (1975); J. Papp, LBL-3633, Ph.D. thesis, unpublished (1975).

2. I. A. Schmidt and R. Blankenbecler, Phys. Rev. D 15, 3321 (1977).

3. S. Chessin, J. Geaga, J. E. Grossiord, D. Hendrie, L. Schroeder, B. Trenhart, K. Van Bibber and C. Wuest, Bull. Am. Phys. Soc. 23, 48 (1978).

4. R. H. Landau, Phys. Rev. C 17, 2144 (1978).

5. D. E. Greiner, P. J. Lindstrom, H. H. Heckman, B. Cork, and F. S. Bieser, Phys. Rev. Lett. 35, 152 (1975).

6. R. D. Amado and R. M. Woloshyn, Phys. Lett. B 69, 400 (1977); C. F. Perdrisat, S. Frankel and W. Frati, Univ. of Pennsylvania, preprint UPR052 (March 10, 1978).

AN ENERGY-DEPENDENT PHASE SHIFT ANALYSIS OF PION-NUCLEON SCATTERING BELOW 400 MeV†

G. Rowe,* M. Salomon,* and R.H. Landau‡

Elastic scattering experiments provide information on the on-shell scattering amplitude which in turn can be related to the phase shift in each eigenchannel such that the unitarity of the scattering amplitude is insured. These phase shifts are employed in numerous pion-nucleon and pion-nucleus interaction calculations. Unfortunately, the emphasis in recent years of extending and intensifying our knowledge of these phase shifts at higher and higher energies has proceeded without accurate determination of the low energy phases. Indeed, the task of accurately measuring the low energy phases in all the partial waves is presently being assumed by the meson factories.

In this work we fit an analytic function of energy to the most recent S, P, and larger D wave πN phase shifts determined by various groups for different energies below 400 MeV with the aim of providing a smooth "best" fit to all modern πN phases.

Table 1. The resonance parameters used in phase shift fats.

Channel	χ	ω_o (MeV)	q_o (MeV/c)	Γ_o (MeV)
S_{11}	0.44	1550	477	105
S_{31}	0.31	1655	550	170
P_{11}	0.61	1435	393	230
P_{13}	0.23	1815	656	255
P_{31}	0.22	1850	678	200
P_{33}	0.99	1233	228	116
D_{13}	0.54	1525	459	125
D_{15}	0.43	1670	560	155

Table 2. πN phase shift parameter.

Channel	b $[10^{-2}m_\pi^{-}(2\ell+1)]$	c $[10^{-3}m_\pi^{-}(2\ell+3)]$	d $[10^{-4}m_\pi^{-}(2\ell+5)]$	N	χ^2/N-3	Scattering Length $[m_\pi^{-}(2\ell+1)]$
S_{11}	16.8 ± 0.75	-35.4 ± 5.4	27 ± 11	38	4.7	0.185 ± 0.008
S_{31}	-11.2 ± 0.20	-30.7 ± 1.1	21 ± 2	54	1.1	-0.098 ± 0.003
P_{11}	-5.71 ± 0.54	25.4 ± 2.1	-29 ± 3	35	1.8	-0.047 ± 0.004
P_{13}	-1.31 ± 0.08	1.22 ± 0.32	-0.4 ± 0.3	40	1.2	-0.013 ± 0.002
P_{31}	-2.91 ± 0.08	3.45 ± 0.27	-1.5 ± 0.2	53	0.6	-0.029 ± 0.002
P_{33}	11.4 ± 0.30	-15.4 ± 2.1	7.2 ± 2.1	49	1.8	0.205 ± 0.050
D_{13}	0.109 ± 0.012	-0.031 ± 0.062	0.003 ± 0.065	54	0.4	0.0013 ± 0.0005
D_{15}	0.112 ± 0.007	-0.270 ± 0.030	0.19 ± 0.02	57	0.7	0.0012 ± 0.0005

The pure nuclear phase shifts in each eigenchannel are fit with an analytic function which incorporates the threshold behavior expected for a finite range interaction plus a term which represents the nearest πN resonance:

$$Y_\ell(q) \quad \frac{\tan\delta_\ell}{q^{2\ell+1}} = b + cq^2 + dq^4 + \frac{x\Gamma_0\omega_0 q_0^{-(2\ell+1)}}{\omega_0^2 - \omega^2} \quad ,$$

where q is the πN c.m. momentum and ω is the πN c.m. energy. The resonant parameters, x, Γ_0, q_0, ω_0, were fixed at the values given in the Particle Properties Table 1 and are reproduced in Table 1.

The values of the parameters b, c, and d were determined for each πN eigenchannel by fitting the "data points", $\tan\delta_\ell/q^{2\ell+1}$, or scattering lengths with the function in Eq. (1). A linear least-squares method was used with each datum point having its published error, or an assigned error. In addition, an error of 2% was assumed for all values of momentum q to account for the energy uncertainty.

The fitted parameters b, c, and d are given in Table 2 along with the number of data points, the chi square, and the deduced scattering length. Although we find the fits are reasonable in all channels, there is considerable deviation of the data from the best fit. This is a prime reason for the need of such a fit. All χ^2 values indicate reasonable fits with the exception of S_{11} where there seem to be large systematic errors or an underestimate of statistical errors.

In Table 2 are also listed the deduced values of the scattering lengths for each eigenchannel. Our analysis also produces a slightly negative isoscalar scattering length $(a_1 + 2a_3 = (-0.011\pm0.008)m_\pi^{-1}$ comparable with the values listed in Ref. 2.

In general, our analysis matches continuously to the higher energy analysis of Almehed and Lovelace[3] but provides a smoother and more valid extrapolation to lower energies. For T_π < 100 MeV our results differ significantly from the CERN theory analysis, particularly in the S wave isoscalar amplitude. These differences have already been shown to be significant for low energy pion-nucleus scattering and would change most of the potential and field theory models for the low energy πN interaction.

Footnotes and References

†To be published in Phys. Rev. C.

*University of British Columbia, Vancouver, Canada V6T 1W5.

‡On leave from Oregon State University, Corvallis, Oregon 97331.

1. Particle Data Group, Rev. of Mod. Phys. 48, 1 (1976).

2. M. M. Nagels et al., Nucl. Phys. B 109, 44 (1976).

3. S. Almehed and C. Lovelace, Nucl. Phys. B 40, 157 (1972).

THE CONTRIBUTION OF QUASI-ELASTIC SCATTERING TO PION-NUCLEUS TOTAL CROSS SECTIONS*

A.W. Thomas† and R.H. Landau‡

One of the encouraging aspects of studying pion-nucleus interactions at intermediate energy is the progress made in understanding experiments from first principle theories. Recent elastic data in the region of 50 MeV and below, where the weakness of the elementary πN amplitudes leads one to expect theory to work very well, have however proven difficult to fit. This has stimulated a proliferation of theoretical papers, which produce varying degrees of agreement with the data. It seems likely that with minor parameter adjustment many of these calculations could fit the elastic data. Clearly it is valuable to find as many independent checks on validity of the theory as possible.

In this work we attempt to clarify the reaction content of several common optical model calculations. While it is possible that the constraint we suggest may eliminate some off-shell models, it seems more likely that our ideas should serve to constrain the first-order part of each model. In particular, we argue that many standard optical models have inherent in them a gross overestimate of the quasi-elastic part of the total cross section (which leads us to seriously question the meaning of such optical model fits to total cross-section data). We suggest that this is a significant defect, which should be avoided in future work.

All pion-nucleus optical potentials derive from the same multiple-scattering series. The main differences arise from the form assumed for the off-shell behavior of the elementary πN t-matrix, and the approximations necessary to obtain numerical results. We use (a semi-factorized form)[1] of the first-order optical potential, based on a separable model of the πN interaction, and including three-body corrections

$$U_{(1)}(\underline{k}',\underline{k}) \sim (A-1) \sum_a \int d\underline{p}\ \psi_a^*(\underline{p}-\underline{q})\ t_{\pi N}(E_{3\text{-body}} = K^+_{inc} - E_B - (\underline{p}+\underline{k})^2/2m)\ \psi_{a(p)} \quad . \tag{1}$$

Many other calculations use a "two-body" interaction energy, sometimes with angle ($\underline{q}$) dependence:

$$E_{2\text{-body}} = E_\pi(\underline{k}) + E_N(\underline{p}-\underline{q}/2) \quad . \tag{2}$$

The theoretical foundation of potential (1) is rather well understood. For example, Tandy et al.[2] have been able to prove on the basis of unitarity arguments (within a pion-nucleon-core model) that the only absorptive process contained in the first-order potential is quasi-elastic scattering. (Intuitively this is obvious since Eq. (1) involves only the elastic πN amplitude and nuclear ground state wavefunction.)

Let us make the important observation that using $E_{3\text{-body}}$ in Eq. (1) means that regardless of the magnitude of the nucleon Fermi momentum, if there is not sufficient pion energy for nucleon knock-out (i.e., $K_{inc} < E_B$), the πN t-matrix must be evaluated for energy below threshold. Thus the t-matrix and optical potential are real. In this case there is no absorption in $U^{(1)}$.

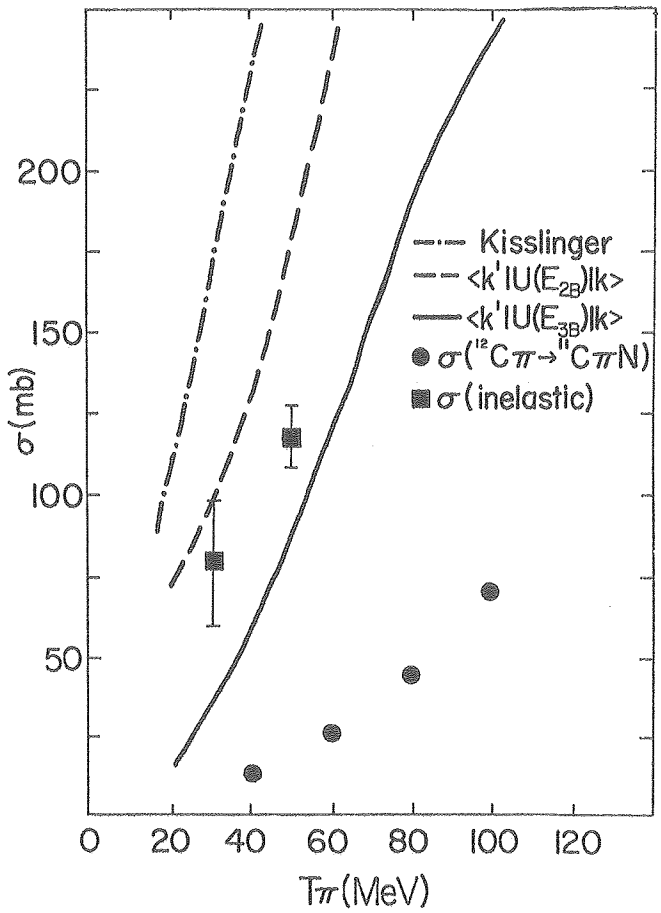

Fig. 1. Comparison of the total cross section for the (π,πN) reaction for a Kisslinger potential (dot-dashed curve), a p-space, separable-πN, optical potential with two-body energy (dashed curve) and a p-space, separable πN, optical potential with the three-body energy (solid curve). The dots represent an estimate of the lower limit of "data" and the boxes are an upper limit σ (inel) . (XBL 7810-11697)

Clearly in or near the region where t is evaluated below threshold in $U^{(1)}$ ($T_\pi \lesssim 50$ MeV), the three-body model guarantees elastic unitarity, whereas more conventional potential models (e.g., using $E_{2\text{-body}}$) do not. Thus we question the interpretation of fits to low energy cross sections given by these models, since the absorption contained in them may be in serious error.

The main shortcoming in the data available to test these ideas is the absence of total $(\pi,\pi N)$ cross-section measurements at these low energies. Thus, as data representing the lower limit to $\sigma(\pi, \pi N)$ we take the sum of the experimental cross section for a π^+ and π^- to interact with ^{12}C and leave ^{11}C in a particle stable state.[3] Since as the energy increases there are more single nucleon channels open than just these two, these data represent a lower limit which we expect to be fairly close to the full $\sigma(\pi,\pi N)$ at the lowest energies ($T_\pi \lesssim 50$ MeV). As data representing a (rather high) upper limit to $\sigma(\pi,\pi N)$, we take the total inelastic cross section as deduced from low energy π^+ ^{12}C elastic data.

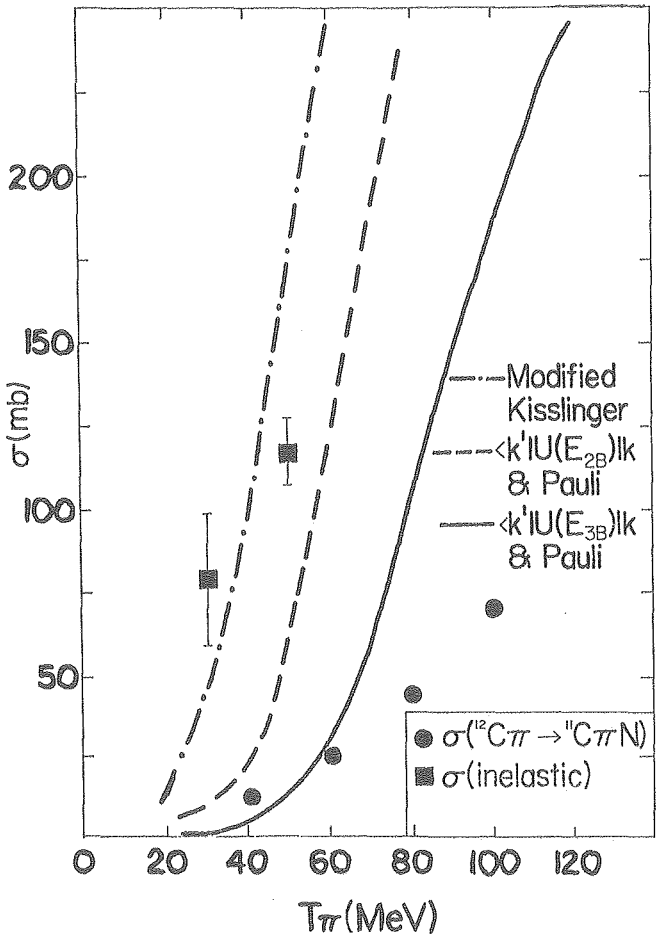

Fig. 2. Same as Fig. 1, except now with various types of "Pauli effect" modifications.
(XBL 7810-11696)

In Fig. 1 we compare the $\sigma(\pi,\pi N)$ implicit in several "simple" optical potentials to the lower- and upper-limit data. We see that the standard Kisslinger and separable πN potentials with $E_{2\text{-body}}$ are 1-2 orders of magnitude greater than the lower limit and exceed the rather high upper limit! This is clearly an important qualitative failure of these theories. Introduction of the elastic unitarity constraint by using $E_{3\text{-body}}$ reduces the cross section by a factor of 2-5, thus providing considerable improvement, yet still yielding a cross section which appears too large at lower energy where we expect the lower limit to be met.

In Fig. 2 we examine the influence of the Pauli exclusion principle on these cross sections.[1] Although these are only an approximate treatment of one of the mechanisms for the reduction of the outgoing nucleon wave, the effect on $\sigma(\pi,\pi N)$ is qualitatively correct. In fact, considering the level of accuracy expected of this calculation and that at higher energies the calculated cross section should move closer to the upper limit, the use of $E_{3\text{-body}}$ plus Pauli principle effectively eliminates the discrepancy of an order of magnitude in the 40-60 MeV region.

Footnotes and References

*To be published in Phys. Lett.

†TRIUMF, University of British Columbia, Vancouver, Canada.

‡On leave from Oregon State University, Corvallis, Oregon 97331.

1. R. H. Landau and A. W. Thomas, Nucl. Phys. A (accepted for publication).

2. P. C. Tandy, E. F. Redish, and D. Bolle, Phys. Rev. C 16 1924 (1977).

3. B. J. Dropesky, G. W. Butler, C. J. Orth, R. A. Williams, G. Friedlander, M. A. Yates, S. B. Kaufman, Phys. Rev. Lett. 34, 821 (1975).

COMPARISON OF MODELS OF HIGH ENERGY NUCLEAR COLLISIONS

M. Gyulassy

In an attempt to keep track of the large number of theoretical models that have been proposed for nuclear collisions, a review report[1] and seminar[2] have been written up. These reports will be extended into a Physics Reports article next year.

The reports[1,2] contain an overview of the expectations, hopes, and goals of nuclear collisions research as well as the obstacles in the way deducing the equation of state of nuclear matter. The models that are discussed in detail are the following: fireball, firestreak, 1 and 2 fluid hydrodynamics, row on row cascade, intranuclear cascade codes, and classical equation of motion models. In Ref. 1 the results on the homework problem: Ne + U → p + $\bar{X}$ are emphasized. In Ref. 2 models for light composites and pion production are also considered. The need to focus experimentally on near central ($b \approx 0$) collisions is emphasized.

References

1. M. Gyulassy, Lawrence Berkeley Laboratory, Report LBL-6594, Proceedings of the Int. Symp. on Nuclear Collisions and their Microscopic Description, Bled, Yugoslavia, Sept. 1977, in Fizika 9 (1977) Supplement 4, p. 623.

2. M. Gyulassy, in Proceedings of the Special Bevalac Research Meetings, November 1-3, 1977, Lawrence Berkeley Laboratory, Report LBL-7141, p. 74.

PION CONDENSATION WITH CONSTRAINTS OF PCAC AND NUCLEAR MATTER

D. Vautherin and M. Gyulassy

We have completed calculations on the existence of pion condensation in dense nuclear matter using a theory that is constrained to reproduce 1) normal nuclear saturation properties ($E/A = -16$ MeV at $\rho = \rho_0$ as well as 2) the cherished properties of strong interactions summarized by partially conserved axial currents (PCAC).

Our objective was to see if predictions of pion condensations would survive when both the above physical constraints are imposed on the theory. Our conclusion is that this pionic phase transition is indeed compatible with those constraints. This result gives us added confidence that pion condensation could eventually be observed in high energy nuclear collisions.[1]

The calculation employs an effective relativistic Lagrangian [2,3] (the σ model) supplemented by chiral symmetry breaking terms $L^1_{SB} = c_1\sigma$ and $L^2_{SB} = c_2\pi^2$. The equation of state of nuclear matter is first calculated in the mean field approximation assuming no pion condensation, i.e., $\langle\vec{\pi}\rangle = 0$. Then, to investigate whether the system is unstable with respect to pion condensation we calculate the response of the system to an external pion field

$$\langle\pi_0(x)\rangle = a\cos(\vec{q}\cdot\vec{x}), \langle\pi_\pm\rangle = 0 . \quad (1)$$

Given Eq. (1) the change in the meson field energy (per nucleon),

$$\frac{\Delta E_M}{A} = \frac{1}{A}\int d^3x \,\frac{1}{2}\left\{(\nabla\pi_0)^2 + m_\pi{}^2\pi_0^2\right\} =$$

$$\frac{3\pi^2}{8p_F^3}\,a^2\,(q^2 + m_\pi{}^2) , \quad (2)$$

where p_F is the Fermi momentum. The change in the fermion energy is then evaluated in second order as[3]

$$\frac{\Delta E_F}{A} = -3\,\frac{g_s{}^2a^2}{3\,2\,m^*}\left\{x^2 + x\,(1-\frac{x^2}{4})\,\ln\left|\frac{2+x}{4-x}\right|\right\}, \quad (3)$$

where $x = q/p_F$, $g_S = 10$, and m^* is the effective nuclear mass determined self-consistently in the mean field approximation.[2,3]

From Eqs. (2) and (3) it is clear that for sufficiently low nuclear densities $\Delta E_M + \Delta E_F > 0$, and hence the system is stable. However, beyond some critical density ρ_C, determined by $\Delta E_M + \Delta E_F = 0$, nuclear matter will be unstable with respect to neutral pion condensation.

With the parameters g_S and m^* determined by the constraints of nuclear saturation and PCAC, we find that the critical density is

$$\rho_C = 0.44\,\rho_0$$

for a condensate momentum $q = 1.4\ f_m^{-1}$. The further inclusion of $\pi N\Delta$ as well as NN and $N\Delta$ interactions is then expected to increase ρ_o beyond ρ_o, as in many other calculations.[4] The important point is that with the Lagrangian that we have constructed,[2] contrained by nuclear saturation as well as PCAC, the phenomenon of neutral pion condensation is still expected to occur for nuclear densities $\gtrsim \rho_o$.

References

1. M. Gyulassy and W. Greiner, Ann. Phys. 109, 485 (1977).

2. D. Vautherin and M. Gyulassy, Nuclear Science Annual Report 1976-1977, LBL-6575, p. 205.

3. D. Vautherin and M. Gyulassy, Nuclear Matter, PCAC, and Pion Condensation, LBL-7197, April 1978, submitted to Phys. Rev. C.

4. G. E. Brown and W. Weise, Physics Reports C27, 1 (1976).

CURRENT PION PROCESSES IN NUCLEAR COLLISIONS

M. Gyulassy

One of the primary reasons for studying high energy nuclear collisions is the hope that under the extreme conditions ($\rho \gtrsim 2$, $E^* \sim 100$ MeV/nucleon) generated in such collisions, new phenomena will be observed associated with the coherent interactions of a large number of nucleons. Of particular interest is the possibility that pionic instabilities[1,2] could occur under such conditions. The problem has been to find experimental observables that would be sensitive to such phenomena.

The main direct effect of pionic instabilities is expected[1,2] to be an enhancement of the effective elastic and inelastic nucleon-nucleon cross sections during the nuclear collision. However, the enhancement has been estimated to be only a factor of 2-4 so that no drastic effects are likely.

This moderate enhancement should lead to more rapid thermalization. However, once thermal equilibrium is reached, the memory of the interesting dynamical path is lost. Therefore the bulk of the single nucleon inclusive spectrum would not show any effects of such instabilities.

Even the pion multiplicity distributions would not be sensitive to such instabilities.[3] This is because the reduction of the thermalization time compensates for increase of the π production rate (see Ref.3).

However, one observable, the $\pi^-\pi^-$ double inclusive cross section, could eventually provide a sensitive tool to measure the degree of coherence of the pion field from nuclear collisions.[3] To demonstrate this consider a simple model for π production where the pion source is treated as a classical (c-number) current, $J(\tilde{x},t)$. The S-matrix in the pion sector can then be explicitly solved for,[3] and hence all inclusive pion probabilities can be calculated:

$$P_m(k_1 \ldots k_m) = \left| j(k_1)^2 \right| \ldots \left| j(k_m)^2 \right| , \qquad (1)$$

where $j(k)$ is essentially the on-shell space-time Fourier transform of the source current.

The striking feature of Eq. (1) is that the m-pion correlation function

$$C_m(k_1 \ldots k_m) \equiv \frac{P_m(k_1 \ldots k_m)}{P_1(k_1) \ldots P_1(k_m)} - 1 \qquad (2)$$

vanishes identically for all m. This is in sharp contrast to what is expected from the GGLP effect,[4] due to Bose statistics

$$C_2(\tilde{k},\tilde{k}+\tilde{q}) = \left| \rho(\tilde{q}, \sqrt{k^2 + m_\pi^2} - \sqrt{(\tilde{k}+\tilde{q})^2 + m_\pi^2} \right|^2 , \qquad (3)$$

where $\rho(\tilde{q},q_o)$ is the space time Fourier transform of the space distribution of pion sources $\rho(\tilde{x},t)$.

The difference between Eq. (3) and the result obtained with Eq. (1) lies in the coherence of the pion field. The pion field leading to Eq. (1) is in fact described by a coherent state as is a laser field in optics. On the other hand, Eq. (3) follows only for completely chaotic fields as produced for example by a random current

$$J(k) = \sum_{i=1}^{N} e^{i\phi_i} j_i(k) , \qquad (4)$$

where ϕ_i are random phases.

Experimentally, then, by measuring $C_2(\vec{k},\vec{k})$, the $\tilde{q} = 0$ point, the observation of $C_2(\vec{k},\vec{k}) < 1$ would imply that there is at least partial coherence in the pion field. A completely coherent field would be signalled by $C_2(\vec{k},\vec{k}) = 0$.

Further work on the effect of isospin conservation and final state interaction is in progress.[5]

References

1. M. Gyulassy and W. Greiner, Ann. Phys. 109, 485 (1977).

2. M. Gyulassy, Proceedings of the Topical Conference on Heavy-Ion Collisions, Fall Creek Falls State Park, June 13, 1977, LBL-6525, p. 457.

3. M. Gyulassy, Coherent Pion Processes in Nuclear Collisions, LBL-7704, April 1978.

4. G. Goldhaber et al., Phys. Rev. 120, 300 (1960).

5. L. Wilson, M. Gyulassy, S. K. Kauffmann and Y. Karant, in preparation.

A CLASSICAL MANY BODY CALCULATION OF RELATIVISTIC NUCLEAR COLLISIONS*

J.D. Stevenson

Proton emission in relativistic ^{20}Ne + U collisions has been attributed by Westfall et al.[1] to evaporation from a nuclear "fireball" with temperature $\tau \approx 50$ MeV and recoil velocity $\beta = V/c \approx 0.25$. Light composite nucleus formation has been explained in terms of a final state interaction among nucleons[2] or alternatively as thermal emission[3,4] from a fireball. The idea that thermal equilibrium can be achieved within collision times of $\approx 10^{-22}$ sec is difficult to believe. Microscopic descriptions[5,6] have generally only been able to reproduce the gross features of the proton spectra, often differing at points by a factor of 10. A detailed microscopic model of heavy-ion collisions would be valuable in providing a baseline of what is to be expected in the absence of any exotic phenomena. I will describe a classical many body calculation of heavy-ion collisions I have developed that may fill this role.

The central assumption of this calculation is that relativistic nucleus-nucleus collisions may be treated as a succession of free two-body nucleon-nucleon collisions. The calculation proceeds as follows. At the beginning of each collision all nucleons are assigned randomly chosen positions in the projectile and target nuclei, which are assumed to be spherical with diffuse surfaces. Similarly the momentum, in the target or projectile frame, of each nucleon is chosen out of a Fermi distribution with $P_{fermi} = 265$ MeV/c. Nucleons are assumed to follow straight-line trajectories and to interact at the point of closest approach if their separation d satisfies $\pi d^2 \leq \sigma(E_{cm})$ where σ is the appropriate experimental nucleon-nucleon total cross section, which depends on the center-of-mass energy E_{cm} of the pair. If this condition is satisfied the scattering angle is randomly chosen from experimental elastic scattering angular distributions, tabulated by Chen.[7] Finally, both nucleons must have momenta satisfying the exclusion principle, $P > P_{fermi}$ in the lab frame, or the collision is forbidden. Scattering is assumed to take place in a potential well of depth $V_0 = 45$ MeV.

One difficulty with this calculation is that there is no way to account simply for formation of light composite particles, which account for much of the emitted matter.[2] If these particles are formed by final state interactions, then the observed proton spectrum will be modified from its pre-final state interaction or "primordial" form.[6] The primordial proton spectrum is given by

$$\left(\frac{d^2\sigma}{d\Omega dE}\right)_{primordial} = \sum_{\substack{all \\ isotopes}} Z \frac{d^2\sigma(Z,A)}{d\Omega dE} \quad , (1)$$

where E is the energy per nucleon and the sum is over all isotopes. In practice only hydrogen and helium isotopes contribute significantly. Figures 1 and 2 compare the model proton spectrum with the experimental primordial spectrum from Eq. (1) for 250 and 400 MeV/nucleon ^{20}Ne + U and 400 MeV/nucleon ^4He + U.[1,2] In all cases the calculations reproduce the shape of the primordial proton spectrum with RMS fractional errors of about 25%. Note that the data have all been lowered a factor of three in Figs. 1 and 2 from the originally published values. Recently the authors of Ref. 1 have made new measurements[8] which show that their spectra for ^{20}Ne + U → p + x at 250 and 400 MeV/nucleon should be lowered by a factor of 2 to 2.5. Although they have not yet checked all their hydrogen and helium isotope data, or data for ^4He + U collisions, these will probably be lowered by similar factors. This essentially eliminates any discrepancy between this calculation and the data.

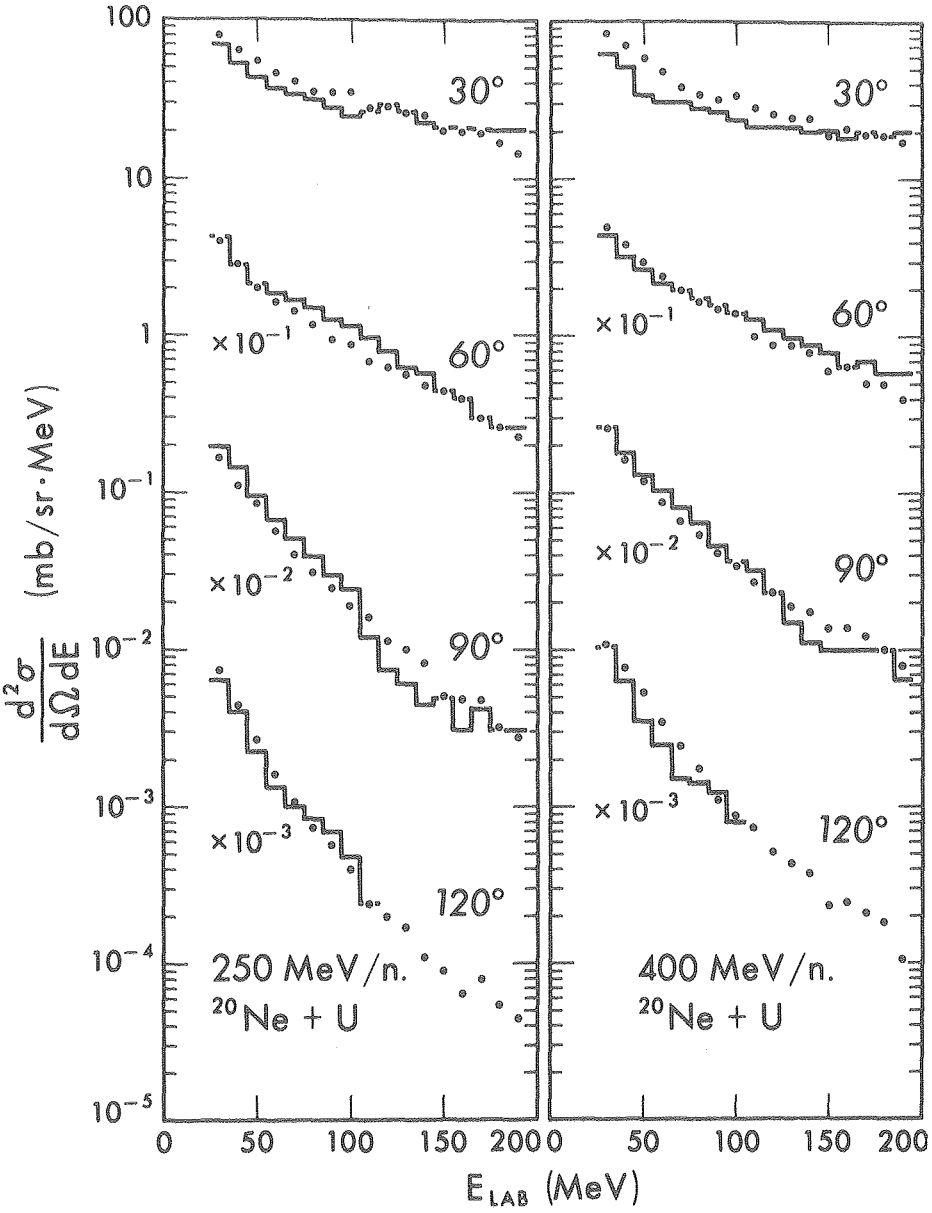

Fig. 1. Single particle inclusive cross section for production of protons in ^{20}Ne + U collisions. The solid line is based on the calculations presented in this article. See text regarding the normalization of the data.

(XBL 787-1262)

It is of some interest to know if the onset of pion production radically alters the nucleus-nucleus collision process. Figure 3 compares the calculation with data[9] for 800 MeV/nucleon ^{20}Ne + NaF → p + x. The calculation yields relatively good agreement over a wide dynamic range despite the fact that it does not include pion production. The calculation does, however, systematically overestimate the data at high momenta.

This calculation is in excellent agreement with a single particle inclusive proton data from relativistic heavy-ion collisions at beam energies of 250 MeV/nucleon and 400 MeV/nucleon. Although this calculation does not include pion production, it accounts reasonably well for the production of protons in nucleus-nucleus collisions at beam energies of 800 MeV/nucleon. This calculation shows that the radical assumption that a hot nuclear fireball[10] is formed in nucleus-nucleus collisions is not necessary to explain existing experimental results.

Footnote and References

*Condensed from an article submitted to Phys. Rev. Lett.

1. G. D. Westfall, J. Gosset, P. J. Johansen, A. M. Poskanzer, W. G. Meyer, H. H. Gutbrod,

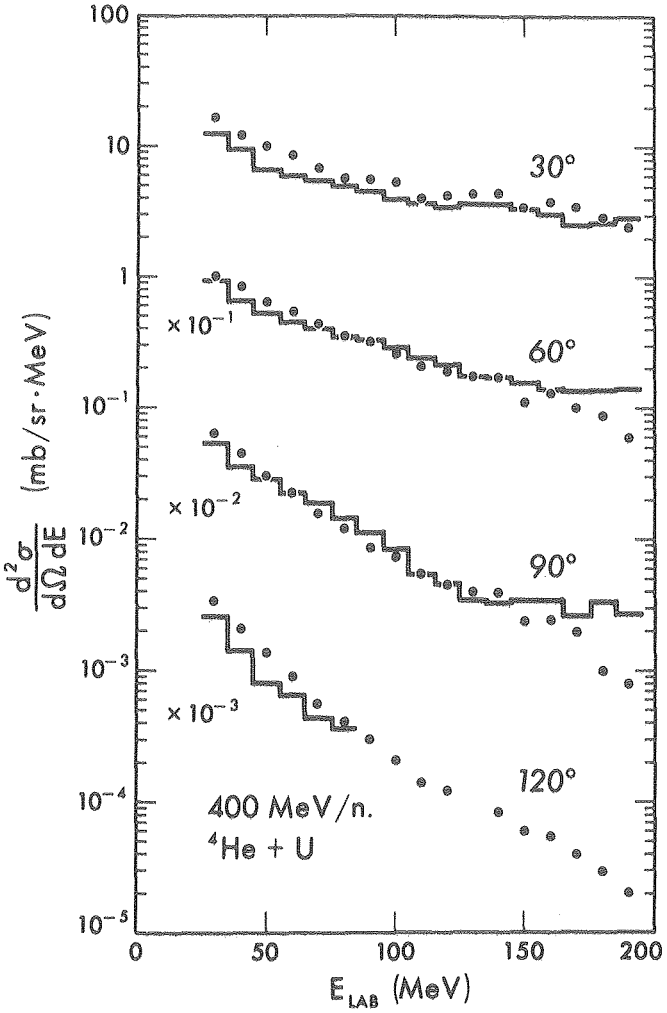

Fig. 2. Single particle inclusive cross section for production of protons in 400 MeV/nucleon ^{4}He + U collisions. The solid line is based on calculations presented in the article. See text regarding the normalization of the data.

(XBL 787-1263)

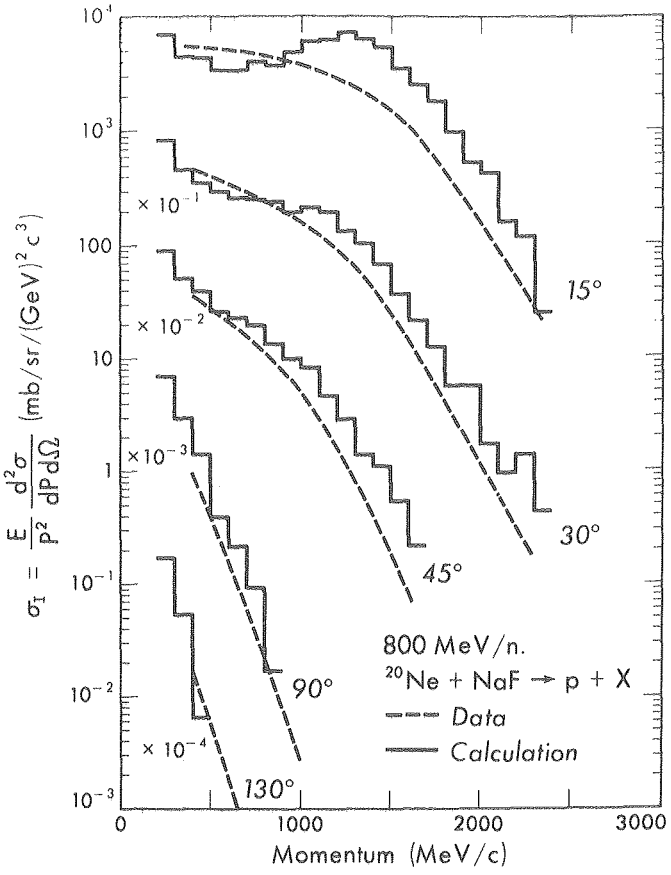

Fig. 3. Single particle inclusive cross section for production of protons in 800 MeV/nucleon ^{20}N + NaF collisions.

(XBL 787-1264)

A. Sandoval, and R. Stock, Phys. Rev. Lett. 37, 1202 (1976).

2. H. H. Gutbrod, A. Sandoval, P. J. Johansen, A. M. Poskanzer, J. Gosset, W. G. Meyer, G. D. Westfall, and R. Stock, Phys. Rev. Lett. 37, 667 (1976).

3. A. Mekjian, Phys. Rev. Lett. 38, 640 (1977).

4. J. Stevenson, P. B. Price, and K. Frankel, Phys. Rev. Lett. 38, 1125 (1977).

5. A. A. Amsden, J. N. Ginocchio, F. H. Harlow, J. R. Nix, M. Danos, E. C. Halbert, and R. K. Smith, Phys. Rev. Lett. 38, 1055 (1977).

6. J. R. Nix, Los Alamos preprint 77-2952 (1977).

7. K. Chen, Z. Fraenkel, G. Friedlander, J. R. Grover, and J. M. Miller, Phys. Rev. 166, 949 (1968).

8. A. M. Poskanzer, private communication.

9. S. Nagamiya, I. Tanihata, S. Schnetzer, L. Anderson, W. Brückner, O. Chamberlain, G. Shapiro, and H. Steiner, LBL-6770.

10. J. Gosset, J. I. Kapusta, and G. D. Westfall, LBL-7139.

CALCULATION OF TARGET RESIDUE MASS AND CHARGE DISTRIBUTIONS IN RELATIVISTIC HEAVY-ION REACTIONS*

D.J. Morrissey, W.R. Marsh, R.J. Otto, W. Loveland,† and G.T. Seaborg

The abrasion-ablation model of Bowman et al.[1] has been used to calculate the mass distribution of the target-like residues produced in relativistic heavy-ion reactions. In this model, the target and projectile nuclei are assumed to be sharp spheres that make "clean cuts" through one another during the relativistic heavy-ion reaction. The number of nucleons removed from the target nucleus, and therefore the corresponding size of the target residue left behind, is calculated as a function of impact parameter by calculating the intersecting volume of the target and projectile nuclei, and each impact parameter is weighted by its geometrical probability. The neutron/proton ratio of the removed nucleons is assumed to be the same as that of the target nucleus.

Each target residue is assumed to have an excitation energy given by multiplying the nuclear surface energy coefficient (~0.9-0.95 MeV/fm^2) by the "excess" surface area of the residue. This "excess area" is the surface area of the residue immediately after the collision (typically the residue has a "bite" taken out of it) less the surface area of a sphere of equivalent volume.[1] A standard statistical de-excitation calculation involving multiple particle emission with provision for neutron-fission-charged particle emission competition is then carried out to construct the secondary product residue mass distribution from the primary distribution and the excitation energy of each primary species.

The number of nucleons removed a from a spherical target nucleus of mass number A_1 and radius R_1 struck at impact parameter b by a spherical nucleus of mass number A_2 and radius R_2 has been approximated as[2]

$$a(\nu,\beta) = A_1 F(\nu,\beta) \quad , \tag{1}$$

where F is a function of the dimensionless parameter ν, specifying the relative sizes of the two nuclei and the dimensionless parameter β, specifying the impact parameter,

$$\nu = \frac{R_1}{R_1 + R_2} \quad , \tag{2}$$

$$\beta = \frac{b}{R_1 + R_2} \quad ,$$

Swiatecki[2] (also see Gosset et al.[3]) has given the formulas for the function $F(\nu,\beta)$.

The same geometry problem of calculating the intersecting volume of target and projectile nuclei can be solved by numerical integration techniques, and has been done by Westfall.[3] In this solution the lens-shaped volume that is the region of overlap of the two sharp spheres at a given impact parameter is reduced to the sum of the overlap areas of a series of two-dimensional disks. We term the formulation of Swiatecki[2,3] and that of Westfall[3] as the analytic and numerical formulations, respectively.

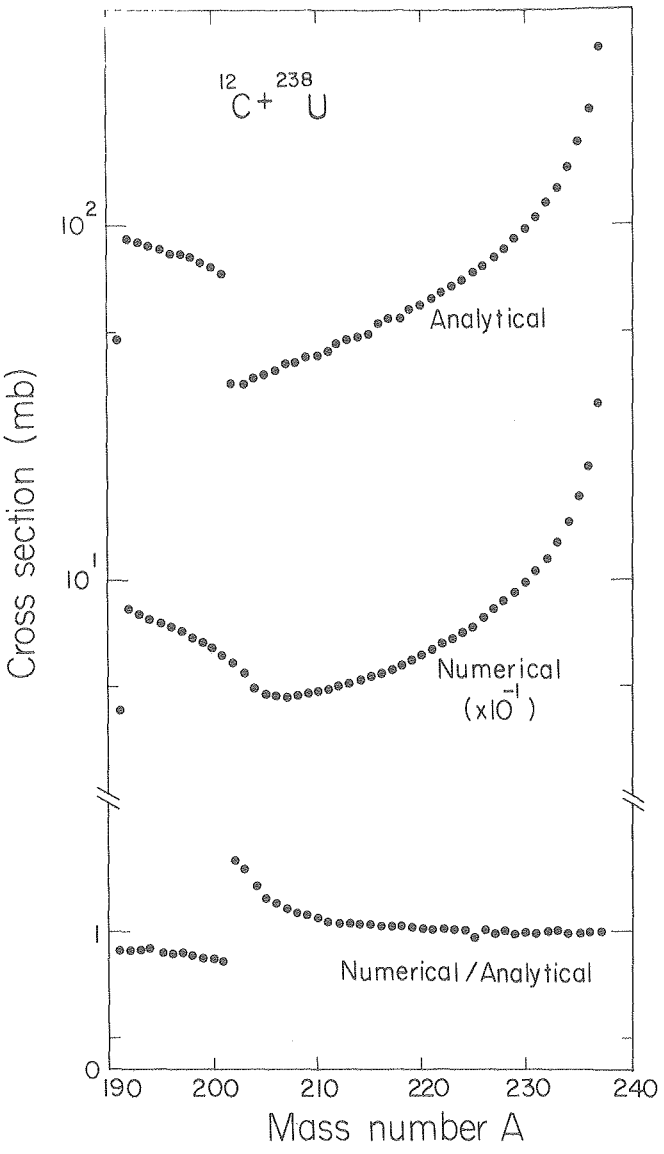

Fig. 1. Calculated cross sections as a function of target residue mass number A for the ^{12}C + ^{238}U system. For a discussion of the analytical and numerical formulations, see text.

(XBL 7710-2122)

Once we have calculated the number of nucleons removed a at any given impact parameter b, we can calculate the primary residue production cross section simply as

$$\sigma(A_1\text{-}a) = \pi\left\{[b(a - 0.5)]^2 - [b(a + 0.5)]^2\right\}, \quad (3)$$

taking advantage of knowing the inverse function b(a). We have chosen not to write an explicit function for b(a) but rather to evaluate Eq. (1) for 500 evenly spaced values of β and do linear interpolations between evaluations.

We have developed a computer program to calculate the primary residue production cross sections using the LBL CDC-7600 computer. Figure 1 shows the primary residue cross section as a function of residue mass number for the $^{12}C + ^{238}U$ system. For comparison purposes we show the results from the analytic and numerical calculations of $a(\nu,\beta)$, as well as the ratio of the numerical to the analytic results. This ratio shows two features of the relation between the two methods of calculations: 1) they agree quite well in the region of grazing collisions; 2) there is a sharp discontinuity in the analytical formulation as the outer surface of the projectile crosses the sharp edge of the target nucleus and the projectile is completely eclipsed by the target. This leads to a significant error in the analytic formulation in this region. The analytic formulation does have the advantage of requiring less computer time (1.074 CPU sec vs. 13.841 CPU sec for the $^{12}C + ^{197}Au$ case) and is useful for treating the most peripheral collisions or looking at gross features of the distributions. We have used the more accurate numerical formulation in all calculations.

The de-excitation of the primary residues was calculated using a modified version of the computer code OVERLAID ALICE,[4] which traced the course of the neutron-fission-charged particle emission competition. The angular momentum of the primary residues was assumed to be 10 $\hbar$ or less.[5]

Up to now we have not said anything about the dispersion of the number of neutrons and protons in the primary or secondary residues (other than the previously outlined calculations, which do give the average (Z,A) of each primary or secondary species). We have investigated two prescriptions for calculating the charge dispersions of the primary residues. The first of these, due to Rasmussen et al.[6] suggests that the probability of forming a target residue with a given Z and A can be expressed in terms of the total cross section for that mass number A, by the hypergeometric expression:

$$\sigma(Z,A) = \frac{\binom{Z_1}{z}\binom{N_1}{n}}{\binom{A_1}{a}}\,\sigma(A) \quad , \quad (4)$$

where the primary residue mass number $A = A_1 - a$, Z_1, N_1 and A_1 refer to the number of protons, neutrons, and nucleons originally in the target, and z, n, and a refer to the number of protons, neutrons, and nucleons removed from the target in the interaction. This expression, of course, simply calculates the dispersion in the number of neutrons and protons removed from the target as equivalent to the relative number of ways of distributing neutrons and protons in an assembly of a nucleons.

As an alternative model for the charge dispersions based upon different physical considerations, we have developed the idea that in a "clean-cut" sudden interaction such as postulated in the abrasion-ablation model, the fluctuations in the number of swept-out target protons can arise from zero point vibrations of the giant dipole resonance (GDR) of the target nucleus. The GDR has been described as an out-of-phase vibration of the neutrons against the protons. Myers et al. have recently treated the GDR in terms of the droplet model of the nucleus.[7] In this treatment they derived a harmonic oscillator (HO) potential to describe the motion of the neutrons against the protons.

The distribution in displacements of the neutrons relative to the protons can be obtained from the displacement expectation values using the wavefunction for the lowest state of a harmonic oscillator. Such displacements follow a Gaussian distribution with width parameter σ_{disp}, given by

$$\sigma_{disp} = \frac{d_{ctp}}{\sqrt{2}} = \frac{2.619}{A^{1/2}}\left(\frac{u^2}{(1+u)^3}\right)^{1/4} \quad , \quad (5)$$

where d_{ctp} is the classical turning point of the vibration. We say that the dispersion in the number of target protons removed in the "instantaneous clean-cut" of the RHI interaction is given by

$$\sigma_Z = \sigma_{disp}\left(\frac{da}{db}\right)\frac{Z_1}{A_1} \quad , \quad (6)$$

where (da/db) is the rate of change of the number of nucleons removed with impact parameter. We use this σ_Z parameter in a Gaussian charge dispersion expression of the form

$$\sigma(Z,A) = \left[\frac{1}{(2\pi\sigma_Z^2)^{1/2}}\exp\left\{\frac{-[Z-a(Z_1/A_1)]^2}{2\sigma_Z^2}\right\}\right]\sigma(A) \quad (7)$$

to calculate the cross section for producing a primary residue species (Z,A) where $A = A_1 - a$. The excitation energy of each isobar is calculated as described above, and the OVERLAID ALICE calculations are done to predict the secondary product charge dispersions.

In Fig. 2 we compare the predictions of the hypergeometric model and the giant dipole resonance model for yields of Au isotopes formed in the 25.2 GeV ^{12}C + Pb reaction with experi-

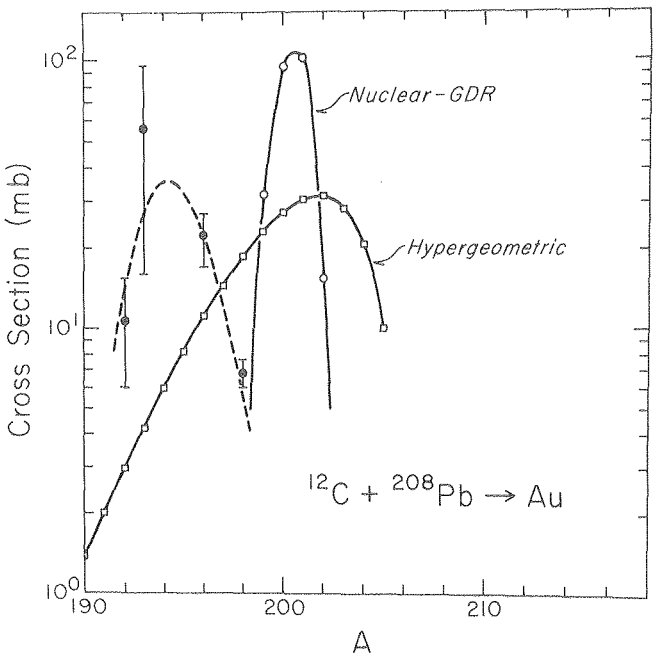

Fig. 2. A comparison of the primary product distributions calculated using the GDR and hypergeometric models of the Au isotopes formed in the reaction of ^{12}C with ^{208}Pb. Also shown are the experimental data of Ref. 5.

(XBL 784-8242)

mental data.[5] The calculated distributions represent primary product distributions, before the de-excitation process, but one can already see that the hypergeometric model predicts unusually large widths to the isotopic distributions, in clear variance with the experimental data. Since the hypergeometric model allows for unphysical possibilities such as removing all a nucleons as neutrons alone or protons alone, this prescription gives an upper limit to the primary neutron-proton dispersion. For small numbers of nucleons removed from the target (such as studied by Rasmussen et al.[6] in the interaction of ^{4}He and ^{12}C projectiles with ^{40}Ca targets), this model appears to work satisfactorily but appears to give only upper limits for the width of the charge dispersions when larger amounts of mass are removed from the target. Because of this feature, secondary product charge dispersions were not calculated for the hypergeometric model.

Figures 3 and 4 show the calculated secondary product charge distributions using the GDR model for the Sc nuclides formed from the reaction of 25.2 GeV ^{12}C with Cu and the Au nuclides formed from the reaction of 25.2 GeV ^{12}C with Pb, respectively. These secondary product distributions are compared with the experimenta data of Cumming et al.[8] and Loveland et al.,[5] respectively. The Sc distributions are amazingly well fit by the GDR model (which has no free parameters in it). The Au distributions are not described as well by the GDR model (although still described creditably) due to two features: (a) the appearance of a sawtooth in the calculated

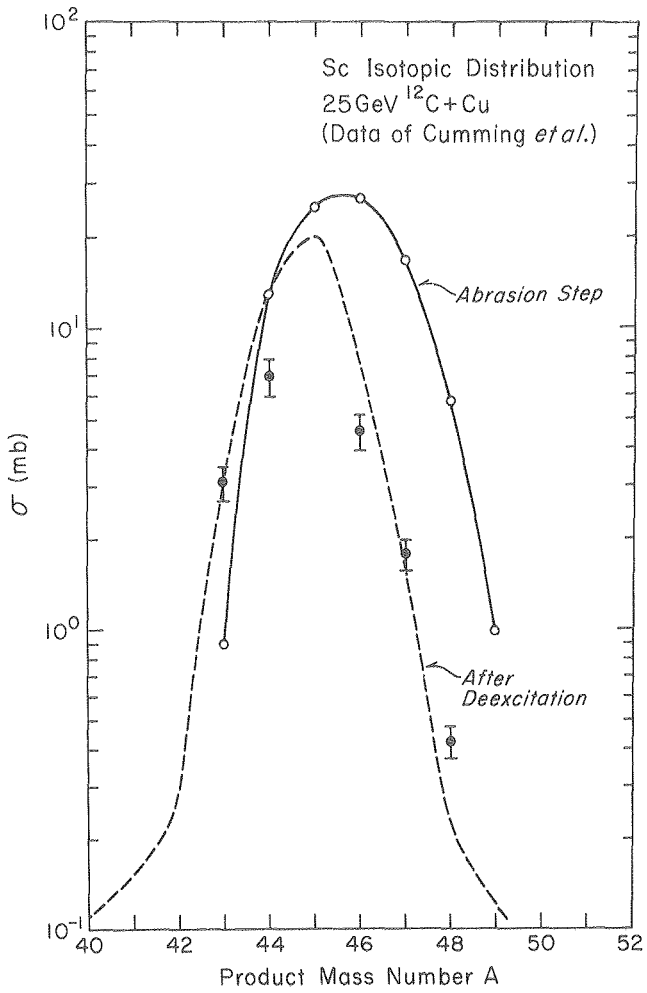

Fig. 3. Calculated Sc secondary product distribution (solid line) for the reaction of ^{12}C with Cu using the GDR model. Experimental data are those of Cumming et al.[8] Dashed line is the calculated primary product distribution from the GDR model.

(XBL 783-7909)

secondary product distribution (due to odd-even effects in the neutron evaporation process) not seen in the experimental data; and (b) some apparent underestimation of the excitation energy of the target-like products leading to a calculated mean n/p ratio of the secondary residues greater than that seen experimentally.

What have we learned from these calculations? It would appear that the gross features of the heavy secondary residue mass and charge distributions from RHI interactions are well described by the simple ideas of the parameter-free abrasion-ablation and GDR models of the mass and charge distributions, respectively, in which the RHI-nucleus interaction is a "quick, clean-cut" of the entire projectile acting as a single particle through the target, leading to smaller excitation energies. It will be interesting to direct further measurements of the heavy target residue mass and charge dispersions towards exploring the linear and angular momentum of the residues and to explore the energy dependence of these interactions.

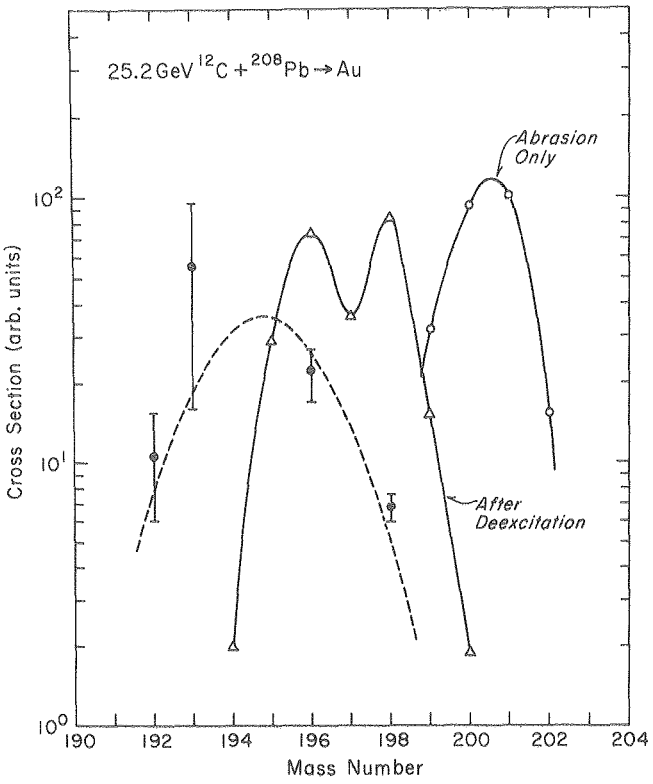

Fig. 4. Same as Fig. 3 except the products are Au isotopes, the reaction is ^{12}C + Pb, and the experimental data are those of Loveland et al.[5]
(XBL 783-7908)

Footnotes and References

*Condensed from LBL-6579, to be published in Phys. Rev. C 18, 1267 (1978).

†Permanent address: Department of Chemistry, Oregon State University, Corvallis, OR 97331.

1. J. D. Bowman, W. J. Swiatecki, and C. F. Tsang, LBL-2908, 1973, unpublished.

2. W. J. Swiatecki, private communication, 1977.

3. J. Gosset, H. H. Gutbrod, W. G. Meyer, A. M. Poskanzer, A. Sandoval, R. Stock and G. D. Westfall, Phys. Rev. C 16, 629 (1977); G. D. Westfall, private communication, 1977.

4. F. Plasil and M. Blann, Phys. Rev. C 11, 508 (1975); also see M. Blann, USERDA Report No. COO-3494-29, Rochester, N.Y. (1976).

5. W. Loveland, R. J. Otto, D. J. Morrissey, and G. T. Seaborg, Phys. Lett. B 69, 284 (1977).

6. J. O. Rasmussen, R. Donangelo, and L. Oliveira, LBL-6580, 1977, and Proceedings of the IPCR Symposium on Macroscopic Features of Heavy-Ion Collisions and Pre-equilibrium Process, Hakone, Japan (1977) p. 440.

7. W. D. Meyers, W. J. Swiatecki, T. Kodama, L. J. El-Jaick, and E. R. Hilf, Phys. Rev. C 15, 2032 (1977).

8. J. B. Cumming, R. W. Stoenner, and P. E. Haustein, Phys. Rev. C 14, 1554 (1976).

III. APPARATUS

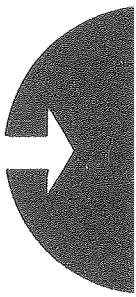

A. ACCELERATOR OPERATIONS AND DEVELOPMENT

88-INCH CYCLOTRON OPERATION, DEVELOPMENT, AND STUDIES

J. Bowen, L. Glasgow, R.A. Gough, D.L. Hendrie, and R. Lam

In the period from July 1977 through June 1978, the cyclotron was scheduled for 20 eight-hour shifts per week for experiments in nuclear science, isotope production and beam development. There were a total of five weeks of scheduled shutdown during this period for machine improvements and general maintenance. Allocation of accelerator time is shown in Table 1. The unscheduled down time of 2.1% represents only those failures in machine components resulting in significant loss of time to the experimental program. The current list of available beams and intensities is shown in Table 2, with the energy range available for each ion. Figure 1 shows the operating distribution of these beams in the last nine years. New beams developed in the past year include $^{3}He^{+1}$, $^{9}Be^{4+}$, $^{12}C^{6+}$, $^{14}N^{7+}$, $^{16}O^{2+}$, $^{16}O^{8+}$, $^{20}Ne^{3+}$, $^{20}Ne^{8+}$, $^{35}Cl^{7+}$, $^{35}Cl^{8+}$ and $^{40}Ar^{9+}$. In addition several other machine solutions have been implemented for the radioisotope dating program to accelerate low intensities ($< 10^{2}$ part/sec) of $^{13,14}C$, ^{10}Be, ^{36}Cl, ^{129}I and other ions.

A new grid matching transformer for the final power amplifier tube has been built and installed. The transformer was wound with simple RG58 50Ω coaxial cables replacing the specially constructed twisted pair cables. Other miscellaneous electrical improvements include additional safety interlock circuits on the RF tank, power

Table 1. 88-inch cyclotron operating time distribution (7/77-6/78)

	Hours	%
Operating		
Experimental program		79.3
Beam development		5.5
Sub total	7064	84.8%
Maintenance		
Routine		4.4
Scheduled shutdown		8.6
Unscheduled shutdown		2.1
Sub total	1280	15.1%
Total	8344 hrs.	

88-INCH CYCLOTRON PARTICLE DISTRIBUTION HISTORY

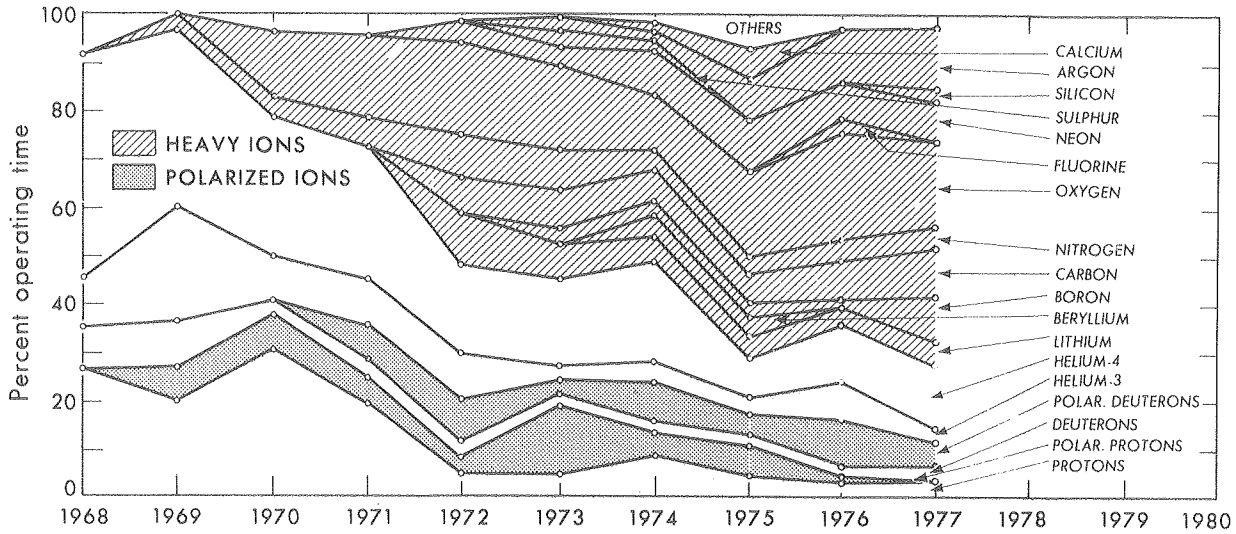

Fig. 1. The 88-inch cyclotron particle distribution history. (XBL 772-402A)

Table 2. 88-inch cyclotron available beam list, July 1978

Ion	Energy[a] (MeV)	External Beam (epA)[b]
p	0.2-55	100-20
p(polarized)	6-55	0.3
d	0.5-65	100-20
d(polarized)	10-65	0.3
$^{3}He^{1+}$	2-47	>20
$^{3}He^{2+}$	4-140	100-10
$^{4}He^{2+}$	3-130	100-10
$^{4}He^{2+}$	130-140	~0.5
$^{6}Li^{1+}$	2-23	10
$^{6}Li^{2+}$	23-93	5
$^{6}Li^{3+}$	93-195	0.5
$^{7}Li^{2+}$	20-80	5
$^{9}Be^{2+}$	15-62	5
$^{9}Be^{3+}$	62-140	2
$^{9}Be^{4+}$	140-249	0.05
$^{10}B^{2+}$	14-56	10
$^{10}B^{3+}$	56-126	50
$^{10}B^{4+}$	126-224	0.3
$^{11}B^{2+}$	12-51	10
$^{11}B^{3+}$	51-115	50
$^{11}B^{4+}$	115-204	0.3
$^{12}C^{2+}$	12-47	>20
$^{12}C^{3+}$	47-105	30
$^{12}C^{4+}$	105-187	5
$^{12}C^{5+}$	187-292	0.05
$^{12}C^{6+}$	292-384	10^{4} part/sec
$^{14}N^{2+}$	10-40	20
$^{14}N^{3+}$	40-90	15
$^{14}N^{4+}$	90-160	15
$^{14}N^{5+}$	160-250	2
$^{14}N^{6+}$	250-360	10^{6} part/sec.
$^{14}N^{7+}$	360-448	10^{2} part/sec.
$^{15}N^{4+}$	84-150	15
$^{16}O^{2+}$	9-35	>5
$^{16}O^{3+}$	35-79	20
$^{16}O^{4+}$	79-140	20
$^{16}O^{5+}$	140-219	2
$^{16}O^{6+}$	219-315	0.3
$^{16}O^{7+}$	315-429	~50 epA
$^{16}O^{8+}$	429-512	0.2 part/sec.
$^{18}O^{4+}$	70-124	>10
$^{19}F^{3+}$	30-66	5
$^{19}F^{4+}$	66-118	10
$^{19}F^{5+}$	118-184	2
$^{20}Ne^{3+}$	28-63	>10
$^{20}Ne^{4+}$	63-112	10
$^{20}Ne^{5+}$	112-175	5
$^{20}Ne^{6+}$	175-252	1
$^{20}Ne^{7+}$	252-343	0.01
$^{20}Ne^{8+}$	343-448	~50 epA
$^{22}Ne^{5+}$	102-159	5
$^{24}Mg^{4+}$	50-93	2
$^{24}Mg^{5+}$	93-146	0.2
$^{25}Mg^{4+}$	50-90	2
$^{26}Mg^{4+}$	48-86	2
$^{28}Si^{5+}$	80-125	1
$^{28}Si^{6+}$	125-180	0.2
$^{28}Si^{7+}$	180-245	0.05
$^{32}S^{6+}$	100-158	2
$^{32}S^{7+}$	158-214	0.2
$^{35}Cl^{7+}$	144-196	0.5
$^{35}Cl^{8+}$	196-256	0.14
$^{37}Cl^{7+}$	136-185	0.08
$^{40}Ar^{2+}$	3.5-14	0.4
$^{40}Ar^{6+}$	87-126	4
$^{40}Ar^{7+}$	126-172	2
$^{40}Ar^{8+}$	172-224	0.5
$^{40}Ar^{9+}$	224-280	10^{5} part/sec.
$^{40}Ar^{10+}$	280-350	10^{3} part/sec.
$^{40}Ca^{6+}$	87-126	1
$^{40}Ca^{7+}$	126-172	0.2
$^{56}Fe^{10+}$	180-250	1 part/sec.
$^{84}Kr^{2+}$	1.6-6.6	0.001[c]
$^{84}Kr^{12+}$	200-240	1 part/sec.
$^{197}Au^{13+}$	102-120	2 part/sec.
$^{197}Au^{14+}$	120-140	0.1 part/sec.

(a) Energy range for heavy ions indicates nominal maximum energy for the particular charge state down to the energy which can be reached from the next lower charge state. Beams can also be run with lower charge than shown at energies below 1 MeV/nucleon.

(b) Electrical microamperes except as noted.

(c) 15th harmonic.

amplifier and modulator, additional capacity to improve ripple filtering on the 4 kW and 150 W power supplies, and doubling the current capacity of the rectifier bridge on the pulsed arc ion source power supply. Safety and reliability factors on this supply have also been improved by changes in the mounting and cooling of the current limiting resistors.

The frequency lowering calculations have now been verified on the 1/4 scale model of the RF system. While it is possible to reduce the lower limit of frequency to ~4.5 MHz, power savings which would accrue from additional low frequency operation would be more than offset by the increased RF drive power which would be required at the higher frequencies.

Another study has been undertaken to determine the maximum current which can safely be delivered through the coils of the main magnet. Mechanical considerations have set an upper limit of 3300 A corresponding to an increased $K_{bending}$ value for the cyclotron of 160 MeV, 15% higher than the present value of 140 MeV. Plans are in progress to boost the current output of the power supply from its present upper limit of 2800 A. A test beam of $^{12}C^{4+}$ ions was accelerated to 193.4 MeV (K = 145 MeV) as part of this study.

Development of a simple μsec beam pulsing system has begun using a vertical electrostatic deflection plate which is mounted in the center region. Initial tests showed that ~1.5 kV pulses will suppress external beam intensities by better than 1/1000 without causing undue center region heating from the deflected beam. A high voltage pulsed power supply from the HILAC has been modified to increase its repetition rate to ~200 kHz.

Design and fabrication of a second dee tank cryopumping system is nearing completion. Some of the necessary dee tank modifications have been made and the compressor and refrigeration units have been ordered.

Design changes have been made to numerous cyclotron components to improve their reliability, ease of fabrication and maintenance. These include changes in ion source related parts such as the anodes, cathode holders and base insulators and the addition of an improved, direct-substitute gas valve panel assembly and a fourth ion source shaft. The Inconel center region inserts have been replaced with molybdenum units of simpler design. The deflector high voltage electrode mounting pins have been simplified to permit quicker replacement of electrodes and insulators. This should significantly reduce radiation exposure to maintenance personnel.

Modifications to a commercial sandblaster have been substantially completed to satisfy Environmental Health and Safety requirements which must be met before using the unit for cleaning of slightly radioactive ion source parts.

A liquid nitrogen trap has been incorporated into the vacuum system roughing line to provide a means of removing water from the vacuum tanks and lines in the event that a water line breaks and leaks into the system.

Tests of the filament-heated Penning Ion Gauge (PIG) source were completed, producing as much as 30μ A of 90 MeV $^{14}N^{3+}$. Control of arc parameters and source output was possible by tuning the bombarder power supply to vary the auxiliary heating supplied the cathodes.

Considerable effort has been spent developing heavy ion beams in the 20-35 MeV/nucleon region. Many of these beams have been produced (so far) at intensities $<10^9$ particles/sec and the use of a Si(Li) particle detector located in Cave 5B has been a necessary tool in this work. Fully stripped beams of ^{12}C, ^{14}N and ^{16}O have been produced at 32 MeV/nucleon with intensities of $>10^4$, 10^2 and $\sim10^{-1}$ particles/sec, respectively. To extend the energies of these fully stripped heavy ions beyond 32 MeV/nucleon, a 140 MeV alpha solution has been developed to serve as a model beam. The intensity of the alpha beam was deflector limited to ~0.4 μA. Continuing studies are planned to optimize the deflector solution and to determine the vertical focusing limit of the cyclotron for these beams.

Sensitive beam monitoring equipment is being developed to facilitate the transport of these weak beams to the target areas. Several CRT phosphors (similar to the dial marking phosphors used routinely by the HILAC) can be used with picoamp level beams. Scintillator/photomultiplier systems are also under development, capable of counting individual beam particles and providing crude energy measurements.

A PET computer with 8 K RAM and an interface to the silent 700 printer has been acquired. It is presently used as a stand-alone computer programmed to calculate magnetic rigidities, cyclotron frequencies and optics parameters for any requested particle. It also calculates beam energy, given cyclotron RF or M41 NMR frequency. Masses of all stable ions through Ar^{40} are stored in core. Ways to store machine settings on the PET for any particle and energy are being explored.

POLARIZED ION SOURCE IMPROVEMENTS AT THE 88-INCH CYCLOTRON

P. von Rossen and H.E. Conzett

In order to improve both the precision and the data-collection efficiency for experiments with polarized beams, an automatic and rapid spin-flip control system has been developed and installed at the 88-inch cyclotron. The control system switches the polarized-source RF transitions, and it simultaneously directs the data to appropriate memory locations of the data acquisition system, as shown in Fig. 1.

The existing power supplies for the RF transition units have been modified to be controllable with external signal pulses. Rise and fall times of about 10 μs have been achieved for the RF power output of the modified units. To provide full flexibility for any experimental requirement, the spin-flip control unit can be programmed to give different weighting factors for each of the three polarization states (+,0,-) and, also, to select the right combination of RF transitions for proton vector-polarization and deuteron tensor-polarization, respectively. With the installation of a third RF transition, the system will be expanded to provide automatic selection of the deuteron vector-polarization states as well. Different sequences for switching between various polarization states can be selected.

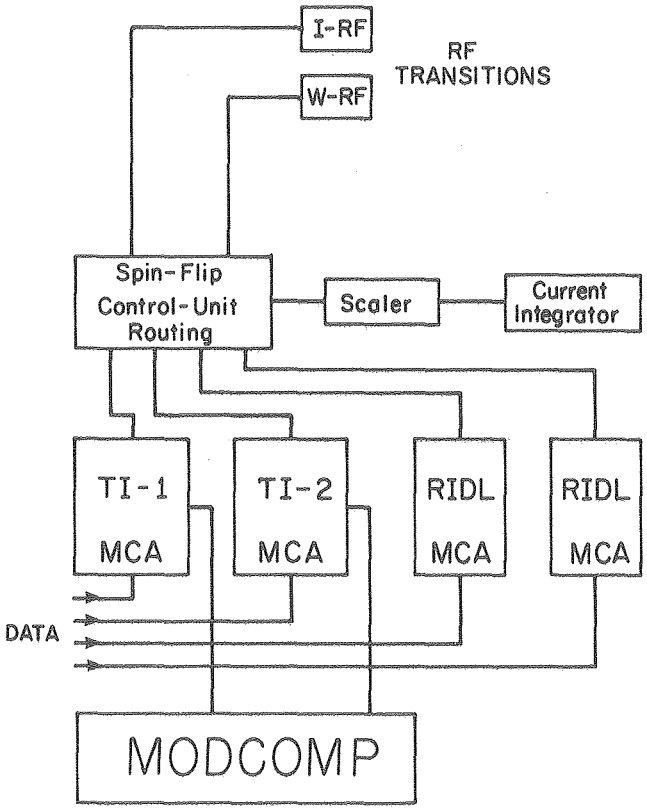

Fig. 1. Schematic diagram of the automatic spin-flip and data-acquisition control system. (XBL 788-2625)

The control unit can be triggered by any of several parameters, such as clock time, accumulated monitor counts, or integrated beam charge. The latter was shown to be best suited for most of our experiments. The switching rate can be chosen over a wide range by using any of the decade outputs of the scaler (cf., Fig. 1). A switching interval of about 1 second has given excellent results in standard scattering experiments. Since the flight time of the projectile between the RF transitions and the experimental target ranges up to hundreds of microseconds, the output routing pulses, which direct the data to appropriate storage locations, can be delayed up to 500 μs.

In order to provide the rapid spin-flip capability for polarized protons, it was necessary to install a new 1480 MHz RF transition unit (ANAC, Inc. Model 2940) along with an existing 7.5 MHz transition. With this arrangement, the spin-state selection is made in the neutral atomic beam, so that there are essentially no changes in beam size, position, or intensity correlated with the spin flipping. This permits substantially more precision to be achieved in experiments, and it is an experimental condition that is absolutely essential for our experiment to test for parity-violation in $\vec{p}$-p scattering at 50 MeV. Since the new RF cavity was not designed for operation in vacuum, there were some initial problems with multipactoring in the cavity. These difficulties were met by coating the cavity surface with a thin sprayed teflon layer. Initial test measurements with the new transition resulted in a polarization of 0.74. We expect this to be improved somewhat by slight modifications in the magnetic field shape and by experience in the tuning procedure.

RADIOISOTOPE DATING WITH THE 88-INCH CYCLOTRON*

R.A. Muller, E.J. Stephenson,† and T.S. Mast

Since July 1976, we have been studying and developing the potential of the 88-inch cyclotron for radioisotope detection and dating.[1-4] This cyclotron is much larger and more powerful than required for dating, but its flexibility and ability to tune rapidly to accelerate almost any isotope has enabled us to study several different applications. We now have demonstrated the sensitivity of using the cyclotron for the detection at natural concentrations of tritium, beryllium-10, carbon-14, and chlorine-36.

The key feature that allows direct detection of low-level radionuclides is the high energy of the emerging beam, which allows particle-identification techniques to be used on an atom-by-atom basis. Without such particle identification, direct counting is impossible because unstripped background ions with the same charge-to-mass ratio always appear in the beam. For carbon-14 the main background is nitrogen-14. In order to apply the particle identification techniques the nitrogen beam intensity must be reduced to the level which will not damage or cause pile-up in the silicon detectors. When tandem accelerators are used for radiocarbon dating[5] this reduction occurs in the negative ion source. For the cyclotron we have developed a technique that achieves the required reduction after acceleration. We have built and used for this purpose a simple gas cell which completely stops the nitrogen beam while allowing the carbon-14 atoms to pass.

The separation technique makes use of the fact that the range of carbon-14 atoms is approximately 30% longer than that of nitrogen-14. Uniformity of the stopping material is essential to ensure the minimum range-straggling for the nitrogen ions. The best material we have found to meet this requirement is gas, separated from the cyclotron vacuum by a thin window. We found that 1/3μ of gold foil will support 1 atm of pressure difference if supported by a grid with gaps no larger than 1/3 mm (Fig. 1). Gold and platinum are convenient window materials because their high atomic number Z inhibit nuclear charge-exchange interactions which can generate spurious carbon-14 atoms. For the same reason, xenon was chosen for the gas.

With the xenon gas cell we were able to eliminate completely 10 nA of ^{14}N ions. A plot of the nitrogen penetration as a function of xenon pressure is shown in Fig. 2, measured using a single particle detector. The curve shows discrimination to a level of 10^{-9}; in several hours of coincident detection using both ΔE and total E detection, not a single nitrogen event perturbed the xenon cell, implying a discrimination factor for the coincident system better than 10^{-14}.

For the range separation performed in the original tritium experiment[1] a single piece of aluminum foil was used. Because of the low level of background ^3He and its much shorter range than ^3H, non-uniformities in the foil were not critical. For beryllium-10 a solid foil is probably acceptable; for our measurements the xenon cell was used. For chlorine-36 the high uniformity of the xenon cell is essential. The "thickness" of the cell in milligrams per cm^2 can be adjusted remotely by changing the pressure of the xenon gas. The range-separation technique should prove to be valuable for those using tandems as well as cyclotrons.

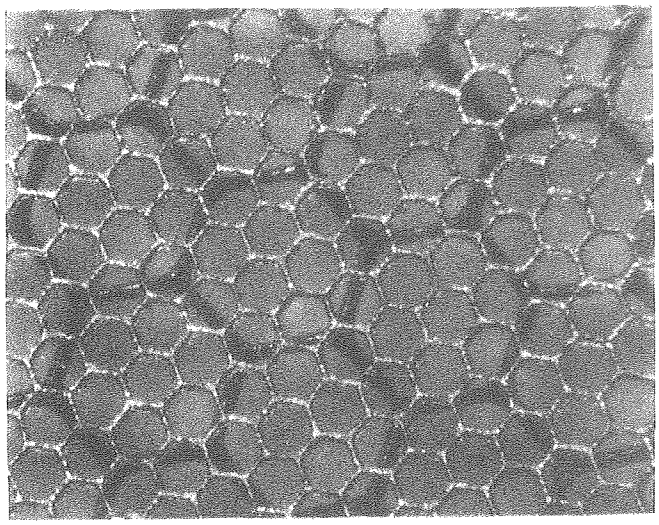

Fig. 1. The thin foil separating the xenon in the range cell from the vacuum of the cyclotron is supported on a tungsten grid, with hexagonal openings 0.33 mm in diameter. This grid is only 25μ thick, and is supported in turn by a heavier 100μ -thick tungsten grid with hexagonal openings 0.1 mm in diameter. The entire structure gives a clear aperture of 65%, over which 0.3 μ-thick gold foil can support a 1-atm pressure difference. (XBL 781-163)

Except for the case of carbon-14, the levels of background radioisotopes in real time from nuclear charge exchange reactions may, however, prove to be the ultimate limit to the cyclotron approach. For carbon-14 our sensitivity at present is limited by a high level of carbon-14 within the graphite-lined tank of the 88-inch cyclotron produced from years of scraping deuteron beams. The level of this carbon, which finds its way into the ion source during a run, has varied from 1/3 to several times the level of carbon-14 in the sample being measured. We have made dates in spite of this background by rapidly switching sample gases to allow the comparison of the unknown with a blank and a reference standard. The results of a blind measurement[2,3]

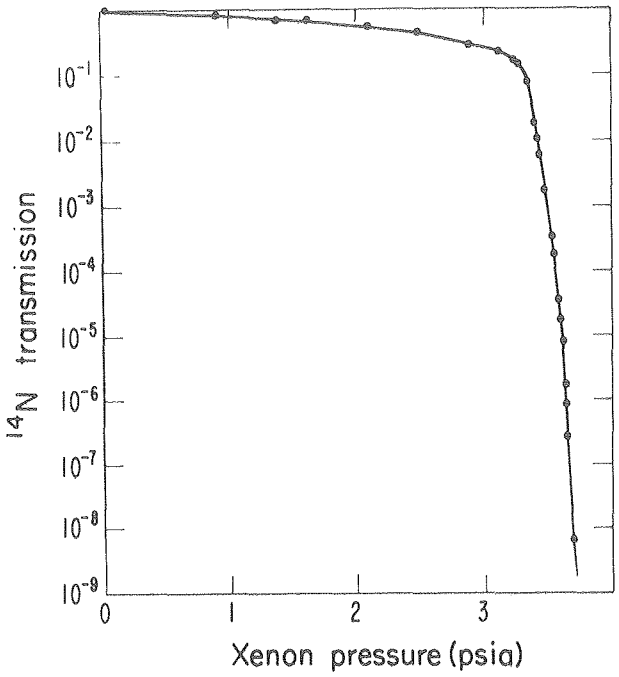

Fig. 2. Nitrogen-14 transmission through the xenon cell as a function of xenon pressure. The nitrogen-14 was detected with a single ionization chamber with a threshold energy loss of 0.8 MeV. When coincident detectors were used, the discrimination against nitrogen was found to be better than 10^{14}.

(XBL 783-2411)

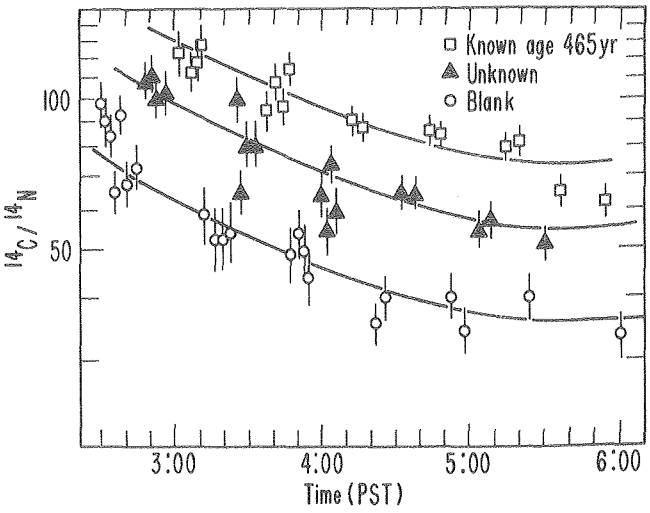

Fig. 3. The $^{14}C/^{14}N$ ratio as a function of time, for a blind sample.[2,3] The carbon-14 was measured with an ionization chamber, silicon-detector telescope. The nitrogen-14 was measured by integrating the current from slits which collimate the beam soon after it emerges from the cyclotron and well before it enters the xenon gas cell. Three samples were alternated: one of known age 465 years; a sample known to contain no carbon-14; and the unknown. The fit corresponds to an age of 5900 years, where the "standard" radiocarbon half-life of 5570 years has been assumed.

(XBL 7712-11088)

of a sample are shown in Fig. 3. In this run the measured age (in radiocarbon years) was 5900 ± 800, with the large error dominated by the statistics of the background subtraction. The Rochester tandem group has a similar background; their ability to measure dates as old as forty thousand years is a reflection of the fact that their background is about a factor of ten lower than ours.

In the carbon-14 measurements the carbon was conveniently introduced to the ion source in the form of CO_2 gas. The efficiency for acceleration of the $^{14}C^{3+}$ ions could be varied between 10^{-5} and 3×10^{-4}; in a typical run it was 3×10^{-5}.

We have made nearly a dozen successful "nonblind" tests, and the successful "blind" test shown in the figure. More recently, however, we made a blind measurement in which our answer differed greatly from the answer achieved by decay-dating: we misestimated the age of an 8,000-year old sample dated by Rainer Berger to be 18,000 years old. This was the only collagen sample we have measured, and we suspect that impurities in the CO_2 affected the performance of the ion source, changing the level of background appropriate to subtract. The best hope for the elimination of such systematic errors lies in the elimination of the background. The easiest way to achieve this will be to use an external ion source which can pre-accelerate the ions to tens of keV before they enter the contaminated tank of the cyclotron. The design and construction of such a source is now under way, and we expect it to be operational later this year.

In our ^{10}Be measurements no comparable background has been detected. We have measured $^{10}Be/^{9}Be$ ratios in beryllium metal at the 10^{-9} level, comparable to that expected in sea floor sediments. We observed 800 ^{10}Be per second in our detectors, and the background was less than one count in five minutes. Our sensitivity for ^{10}Be is better than 10^{-14}, justifying all the optimism expressed in Ref. 1. A comparable sensitivity was achieved when BeO was substituted for beryllium metal in our Penning Ion Gauge (PIG) sputter source, but we have not yet achieved an accurate date with BeO.

Accurate ^{10}Be dating will require rapid cycling between samples of known and unknown concentrations. Since the samples are presently introduced in the back insert of the PIG source they cannot now be readiy changed in the internal ion source. The new external ion source will allow this rapid cycling.

For ^{36}Cl our demonstrated sensitivity is 10^{-12} for the ratio $^{36}Cl/Cl$. This sensitivity is sufficiently good to make ^{36}Cl an attractive

tool for measuring the age of water in potential nuclear waste storage sites, useful in determining the geologic isolation of the deep site from the surface.

After only one and a half years of development, the accelerator approach has already proven its potential for several radioisotopes. Except for the case of carbon-14, there have been no unanticipated backgrounds, and we are optimistic that the full predicted[1] sensitivity of the accelerator approach will soon be utilized.

Footnotes and References

*Condensed from LBL-7585, and Proceedings, Rochester Conference on Radiocarbon Dating with Accelerators (April 1978).

†Present address: Argonne National Laboratory, Argonne, Illinois 60439.

1. R. A. Muller, LBL-5510 (Sept. 1976); Science 196, 489 (1977).

2. R. A. Muller, E. J. Stephenson, T. S. Mast, Radioisotope Dating with an Accelerator: A Blind Measurement, Lawrence Berkeley Laboratory Report, LBL-7249 (December 1977), submitted to Science.

3. E. J. Stephenson, T. S. Mast, and R. A. Muller, Radiocarbon Dating with a Cyclotron, LBL-7579 (April 1978), to be submitted to Nucl. Inst. Meth.

4. R. A. Muller, E. J. Stephenson, and T. S. Mast, Papers presented at the Conference on Radiocarbon Dating with Accelerators, LBL-7585.

5. D. E. Nelson, R. G. Korteling, W. R. Scott, Science 198, 509 (1977); C. L. Bennett et al. Science 198, 509 (1977); C. L. Bennet et al., preprint, Radiocarbon Dating Using Electrostatic Accelerators: Dating of Milligram Samples, to be published.

B. NUCLEAR INSTRUMENTATION

ISEE-C HKH HIGH ENERGY COSMIC RAYS

D.E. Greiner, F.S. Bieser, and H.H. Heckman

The goal of this experiment is to understand the origin of the flux of high energy cosmic rays. The contribution this experiment will make is a comprehensive measurement of the isotopic abundances (^{1}H to ^{64}Ni) of the cosmic ray flux near earth. To demonstrate the relevance of such an isotopic measurement, we will trace, in a highly qualitative fashion, the flux from the source to the observation point near earth.

SOURCE: If the abundances and energy spectra of all isotopes produced in the source were known, then we could try various source models to see if we could identify a unique source or set of sources. There are nucleosynthesis models[1] that predict the source isotopic abundances having relatively few parameters. Thus a knowledge of as many of the isotopic fluxes as possible from the source can be used to pick between source models. In this respect the Fe group elements are particularly sensitive indicators.[2]

We consider the source flux to be conceptually represented by a matrix $S_{A,Z}(E,t)$, whose elements are labeled by A and Z, each element containing the energy and time dependence of its labeled isotope. Actually, the time dependence here is assumed to be quite small as we observe the integral of the flux over many sources and times. We will now follow this flux toward earth and see in a qualitative fashion how it is modified by the processes that take place.

ACCELERATION: The cosmic rays must be accelerated to relativistic energies. This acceleration can take place during creation or after an appreciable delay.[3] Whatever process is responsible for the acceleration, we know the E dependence of the $S_{A,Z}$ will change. There are other effects that change the magnitude of the $S_{A,Z}$ even to the extent of removal of certain isotopes. As an example, consider the isotopes produced in the source that decay solely via electron capture. They are stable once they are stripped and at high velocity; however, they will decay during a delay between formation and acceleration. Such isotopes are called "source clocks" and are sensitive to the density of material near the source and in the interstellar region, e.g., ^{56}Ni (6.1 D), ^{55}Fe (7.6 Y), ^{53}Mn (2 MY), ^{44}Ti (47 Y). The point is, that after acceleration, the relative abundances have changed. Knowledge of the cross sections of electron capture and loss, time of delay, and the electron density along the path are needed to determine the changes in relative abundance. If we represent the acceleration phase by a symbolic operator, A, which does the proper mixing and energy changes to our source flux, then the new composition after acceleration is $AS_{A,Z}(E,t)$.

PROPAGATION: Once up to relativistic velocities, the cosmic rays spend on the average as long as 16 million years[4] moving through the interstellar medium. During this flight the flux is altered by fragmentation. This is a major alteration to the relative abundances. In order to predict the effect of the propagation phase, one uses a model of propagation that will typically contain parameters such as the average time of travel and the density of the interstellar medium. The most important ingredients of the model are the relative fragmentation cross sections. In general terms, the propagation can be represented by an operator P that uses the model and cross sections to predict how the cosmic rays break up and thus enhance lower A fluxes. Long-lived isotopes such as ^{10}Be (1.6 MY), ^{26}Al (0.88 MY), ^{36}Cl (0.31 MY) are called "secondary clocks." Their production and loss in the propagation process make their abundance quite sensitive to the time of travel. We are now approaching the solar system and have a flux $PAS_{A,Z}$.

MODULATION: As the cosmic rays approach the solar system we expect their rigidities to be altered by interaction with the solar fields and wind. Indeed, the flux does vary in time and is correlated to the solar cycle. However, the spatial extent of this variation is still unknown. Hopefully, missions traveling to large distances from the sun (MJS) or high solar latitudes (OOE) will provide conclusive results regarding solar modulations of cosmic rays.

The mixing of isotopes may be low in the modulation process if we integrate over the entire energy spectrum of each isotope. The uncertainty comes from the fact that some, perhaps appreciable, amount of flux fails to penetrate the solar system to the observation point. Representing the modulation by the operator M, we now have the observable flux:

$$F_{A,Z} = M\ P\ A\ S_{A,Z} \quad .$$

What we see is what we get after a major alteration of the source flux. The goal is to measure $F_{A,Z}$ and solve for $S_{A,Z} = A^{-1}P^{-1}M^{-1}F_{A,Z}$. To invert this equation reliably, a detailed knowledge of $F_{A,Z}$ is essential. Given a choice of models and measured $F_{A,Z}$, one must determine the most consistent set of models and parameters in order to arrive at $S_{A,Z}$.

The more measured parameters one has to over-determine the problem, the better the chances are of finding an unambiguous solution.[5] A comprehensive measurement of the cosmic ray isotope abundances over a wide range of elements is a

major contribution to the attempt to understand the origins of the cosmic rays.

The instrument built to perform these measurements is described in LBL-7163. This method of multiple energy loss identification has been successfully applied at the Bevalac in an exotic isotope search equipment performed by a collaboration of the Heckman/Greiner and Hendrie/Scott groups.

References

1. W. D. Arnett and D. D. Clayton, Nature 227, 780 (1970).

2. K. K. Hainebach, E. B. Norman, and D. N. Schramm, Ap. J 203, 245 (1976).

3. A. Soutoul, M. Casse, and E. Juliusson, Proc. 14th Int. Cosmic Ray Conference (Munich, Germany) 1, 343 (1975).

4. M. Garcia-Mũnoz, G. M. Mason and J. A. Simpson, Proc. 15th Int. Cosmic Ray Conference (Plovdiv, Bulgaria) 1, 307 (1977).

5. M. Garcia-Mũnoz, G. M. Mason, and J. A. Simpson, Proc. 15th Int. Cosmic Ray Conference (Plovdiv, Bulgaria) 1, 301 (1977).

THIN WINDOW Si(Li) DETECTORS FOR THE ISEE-C TELESCOPE*

J.T. Walton, H.A. Sommer, D.E. Greiner, and F.S. Bieser

An experiment on the NASA ISEE-C Heliocentric satellite is designed to determine the isotopic composition of cosmic rays. A multi-detector telescope of lithium-drifted silicon [Si(Li)] detectors is to be used for this purpose. To provide the necessary identification, the telescope must contain ten detectors[1,2] of large area (1500 mm^2), 5-mm thick with thickness variations of less than ±0.2% (±10 μm). Furthermore, to minimize the dead-layer effects between the detectors in the telescope, the Li-diffused contact must be less than 15 μm. Finally, the detectors are required to have less than 10 μA leakage and less than 300 keV noise at an RC shaping time constant of 5 μS.

The detectors were examined for noise, leakage current, and thickness uniformity. A final examination, before selection for the flight instrument, involved the use of a high energy Ar beam to determine detector uniformity. Figure 1 shows the experimental arrangement used for this tests.

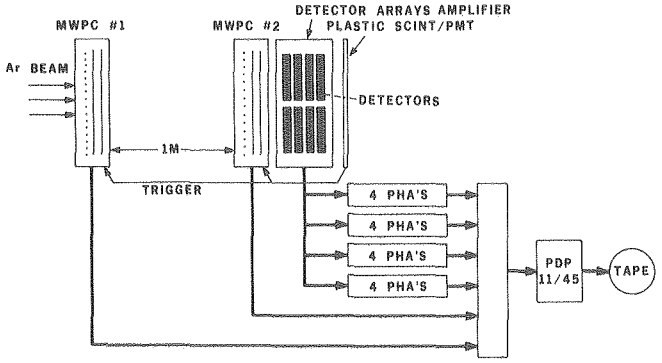

Fig. 1. Experimental arrangement at the Bevatron used to measure detector uniformity. The three-layer Multi-Wire Proportional Chamber (MWPC) defines the beam location to within 1 mm.
(XBL 7710-10096)

A broad ^{40}Ar Bevalac beam (482 MeV/Amu) at the Lawrence Berkeley Laboratory Bevatron was directed through the two, three-plane multi-wire chambers to the detector stack. The multi-wire chambers define the beam trajectories to within 1 mm through the stack. Only ^{40}Ar ions which passed completely through the silicon detectors and were detected in the plastic scintillator were recorded. The detector stack consisted of 4 planes, each containing a square array of 4 detectors, thereby allowing 16 detectors to be tested simultaneously.

Data obtained from the experiment was analyzed for each detector in terms of 90 equal area segments. The average signal amplitude from each segment and the average signal for the entire detector was calculated. The percentage deviation of each segment signal average from the entire detector average was calculated. The number of segments and their percentage deviation from the total detector average energy signal is shown for two detectors in Fig. 2.

The number of events in each segment was used to determine the accuracy of the average energy determination of the segment. Many of the segments had insufficient counts for the averages to be determined at the level of precision required. For all the detectors measured, there were segments whose accuracy was so poor due to insufficient counts that the results in those segments had to be discarded. Unfortunately, the Bevalac beam intensity was very low during these measurements and the availability of accelerator time has not permitted repetition of the experiment. Consequently in assessing the Bevalac data, the accuracy of the measurements was a big factor in selecting detectors for the flight telescope. In Fig. 2 a normal distribution curve whose variance is equal to the calculated variance (i.e., accuracy) in the experimental data is plotted as curve 1, while a second normal

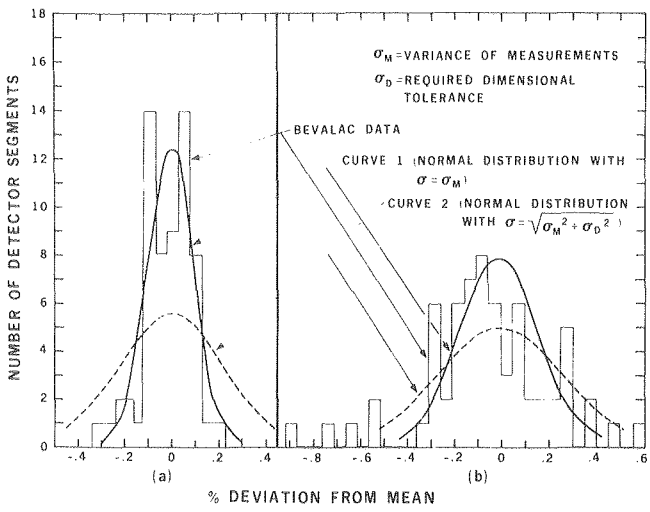

Fig. 2. Bevalac uniformity measurement results. The ordinate gives the number of detector segments within a band of 0.05% with the percentage deviation from the mean average energy given on the abscissa. Detectors that meet the specifications are typified by (a) while those that exceed the specifications are typified by (b). Normal distribution function fits to the data are given by curves 1 and 2. (XBL 7710-10170)

distribution curve 2 indicates the expected results if the accuracy of the measurements is folded in with the allowed dimensional variation of ±0.2% (±10 μm).

Figure 2a presents data where the measurements were considered sufficiently good for the detector to be selected as a flight detector since it is clear that the Bevalac histogram falls well within the calculated expectations. For this detector, the thickness spread must be smaller than the ±0.2% requirement.

Figure 2b presents similar data on a detector not selected as a flight detector since the Bevalac histogram falls outside the calculated expectations.

This work has demonstrated the feasibility of fabricating large area Si(Li) detectors meeting stringent requirements on the thickness uniformity and on the Li-diffused contact thickness.

Finally, the Bevalac data would indicate that no good evidence exists to suggest that signal amplitude variations are caused by any factor other than thickness variations. Where the Bevalac measurement has shown thickness variations substantially greater than the expected inaccuracy of the measurement, these variations have been confirmed by the optical measurements.

The assistance of E. E. Haller in interpreting the Bevalac data is gratefully acknowledged.

Footnote and References

*Condensed from LBL-6434.

1. D. E. Greiner, Nucl. Inst. and Methods 103, 291-308 (1972).

2. D. E. Greiner, Proc. 15th International Cosmic Ray Conference (Plovdiv, Bulgaria, 1977).

ISOTOPE IDENTIFICATION IN A MULTI-ELEMENT DETECTOR TELESCOPE

Y.P. Viyogi,* T.J.M. Symons, F. Bieser, H.J. Crawford, P. Doll,† D.E. Greiner, C.K. Gelbke,‡ H.H. Heckman, D.L. Hendrie, D. Jones, P.J. Lindstrom, J. Mahoney, C. McParland, D.K. Scott, K. Van Bibber, G.D. Westfall, and H. Wieman

The identification of isotopes by the conventional ΔE-E technique has frequently been used in experiments at lower energies.[1] Here one employs a thin ΔE detector and a thick E detector which stops the particles of interest. Various algorithms[1] are used to produce particle identification signals (PI) both in analog instruments and in computer programs. The most frequently used algorithm is:[2]

$$PI = (E+\Delta E)^n - E^n \propto TM^{n-1} Z^2 \quad , \qquad (1)$$

where T is the thickness of the ΔE-detector, and M,Z are the mass and charge of the particle. The exponent n has to be suitably chosen so that PI is independent of the total energy. A typical value of n for lower mass particles (up to ^{16}O of a few hundred MeV) is 1.73.

At much higher energies of the order of a few GeV, the use of a two- or three-detector telescope becomes impractical. The maximum thickness of Si detectors, permitted by the present state-of-the-art, is limited to about 5 mm, whereas the ranges of particles such as ^{16}O at 200 MeV/nucleon is about 40 mm. In experiments at these high energies, all types of fragmentation products are encountered. In experiments designed particularly to study the highly neutron-rich exotic nuclei and of the detailed reaction mechanisms, the identification of isotopes up to argon becomes essential. A technique of isotope identification, where many detectors are used in the telescope, has been described in Ref. 3. The method gives excellent mass resolution but is computationally expensive.

Here we describe a method of isotope identification in a multi-element detector telescope

that employs the conventional technique of Eq. (1) and uses the information from all the detectors up to the stopping detector. The method leads to a χ^2-distribution function, and by selecting events from the central region of the χ^2-distribution, it is possible to reject events due to reactions in the detector stack or due to statistical fluctuation in energy loss. This procedure greatly improves the peak-to-valley ratio for the different isotopes. The method is sufficiently simple to use in on-line programs.

Consider a stack of detectors, each of thickness T_i, and assume that a particle of mass M, charge Z, and total energy E_{tot} stops in detector s of the stack. Different combinations of these s detectors can be used as ΔE and E detectors and a PI signal can be calculated from Eq. (1). For simplicity we restrict ourselves to only one detector as ΔE, labelled i, and all others in the stack from i+1 to s are combined as the E detector. The corresponding PI is

$$(PI)_i = \frac{(E_i + \Delta E_i)^n - E_i^n}{T_i} = K M^{n-1} Z^2 \quad \ldots \quad (2)$$

where K is a constant. For a particle stopping in the detectors, we can calculate a total of (s-1) PI signals. The weighted mean of the (s-1) PI signals is

$$\overline{PI} = \frac{\sum (PI)_i / \varepsilon_i^2}{\sum 1/\varepsilon_i^2} \quad , \quad (3)$$

where ε_i denotes the errors in estimating PI signals using Eq. (1). To first order, the error can be approximated to the errors in measuring the energy signals in different detectors. An estimate of ε_i comes from differentiating Eq. (2) with respect to E and ΔE, giving,

$$\varepsilon_i^2 = \left(\frac{\partial PI}{\partial E}\right)^2 \delta E^2 + \left(\frac{\partial PI}{\partial \Delta E}\right)^2 \delta \Delta E^2 \quad . \quad (4)$$

We assume that all the energy measurments in various detectors are uncorrelated, so that the errors can be combined quadratically.

A χ^2-function is defined as

$$\chi^2 = \sum_{i=1}^{s-1} \frac{(\overline{PI} - (PI)_i)^2}{\varepsilon_i^2} \quad \ldots \quad (5)$$

This method has been used in the analysis of data from ^{40}Ar-induced reactions at 213 MeV/nucleon performed at the Bevalac. The detector telescope consisted of nine elements, each of 5-mm thickness, sufficient to stop isotopes of all elements from argon to oxygen. Good mass resolution can be obtained using a single exponent of 1.78 for particles of Z=8 to Z=16.

Figure 1 shows a 2-D plot of $\overline{PI}$ versus total energy for n = 1.78. We have used a slightly modified PI function, $(PI)^{1/n-1}$, which is proportional to $MZ^{2/(n-1)}$. Figure 2 shows the mass spectra for Z=8, including and excluding the tails of the χ^2-distribution, to show the effect of the χ^2 gate on reducing the background and improving the mass resolution. For example, ^{15}O appears only as a shoulder in Fig. 2a superimposed on the tail of the more abundant ^{16}O group, whereas in Fig. 2b, all isotopes are clearly separated.

To identify individual isotopes, we use the fact that a plot of $MZ^{2/(n-1)}$ (or equivalently, $M^{n-1} Z^2$) versus the observed channel number in PI should be linear through the origin. This method works well for lower Z elements and a mass resolution as good as 0.1 to 0.2 mass units is easily achieved. For the higher Z elements, the resolution deteriorates until for Z = 16, it is close to 0.5.

A major limitation of the method is the failure to distinguish between very neutron-rich and very neutron-deficient isotopes of adjacent Z-values. This degeneracy is easily removed by using rigidity measurements in a magnetic spectrometer. This technique is presently being developed.

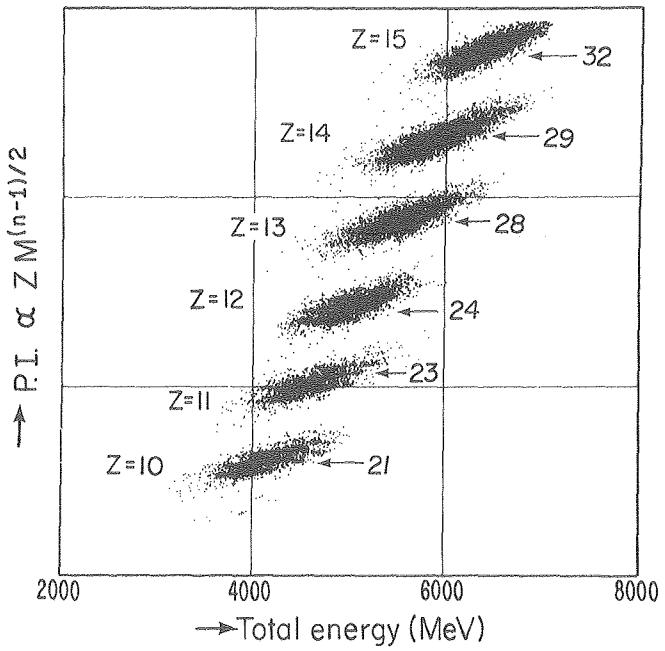

Fig. 1. Two-dimensional plot of PI vs. total energy, using n = 1.78, for particles produced by ^{40}Ar + ^{12}C at 213 MeV/nucleon.
(XBL 786-2548)

Footnotes and References

*IAEA Fellow, on deputation from Bhabha Atomic Research Centre, Calcutta, India.

†Nato Fellow, on leave from MPI, Heidelberg, West Germany.

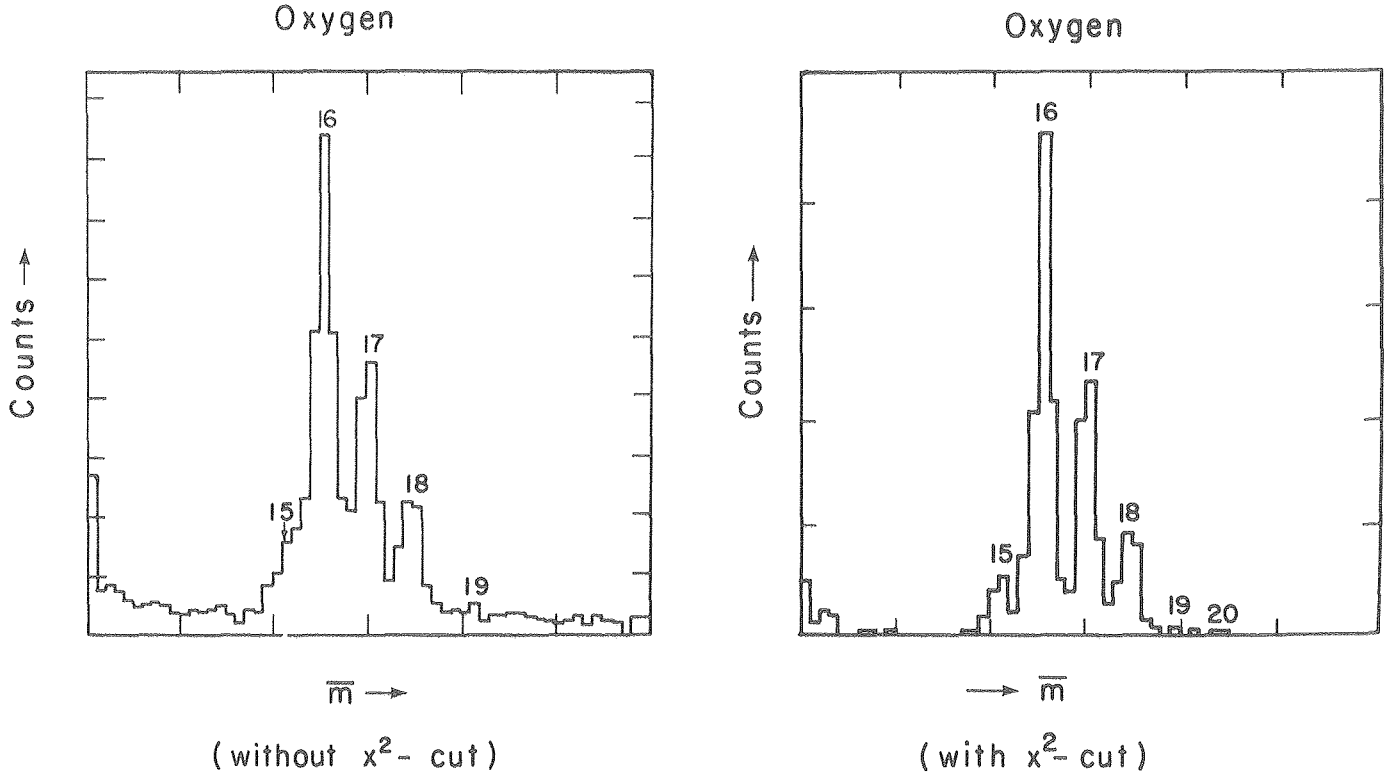

Fig. 2. Mass spectrum of oxygen isotopes stopping in detector 8, (top) without, and (bottom) with x^2-gates. [(a) XBL 787-1415; (b) XBL 787-1416]

‡Present address: Physics Department, Michigan State University, East Lansing, Michigan 48824.

1. J. B. A. England, Techniques in Nuclear Structure Physics (John Wiley and Sons, 1974), Vol. II, p. 463.

2. F. S. Goulding, B. G. Harvey, Ann. Rev. Nucl. Sci. 25, 167 (1975).

3. D. E. Greiner, Nucl. Instr. and Methods 103, 291 (1972).

STREAMER CHAMBERS—THEIR USE FOR NUCLEAR SCIENCE EXPERIMENTS*

L.S. Schroeder

A variety of visual detectors have been developed studying the interactions of elementary particles (π, K, p,...) and nuclei with matter. Included among these are cloud chambers, flash tubes, bubble chambers, spark chambers and streamer chambers. Streamer chambers made their appearance on the detector scene in the early 1960's[1,2] and were developed for eventual use in experiments. This development was primarily geared to studies of elementary particle interactions. As such, streamer chambers were often used to complement and extend the large amount of work that had been done on exclusive final states using bubble chambers. Streamer chambers offer several advantages, including: large solid-angle ($\sim 4\pi$), ability to be selectively triggered (usually by fast electronic detectors such as scintillators surrounding the chamber), and high multi-track efficiency and good angular and momentum information.

Figure 1a shows a schematic of a charged particle passing through a streamer chamber. Scintillation counters S1 and S2 record the passage of the particle through the gas volume (often a Ne/He mixture at atmospheric pressure, 90% Ne, 10% He). During this passage through the chamber gas, the incident charged particle creates ion pairs along its trajectory. These pairs in turn start to diffuse and eventually recombine if nothing further is done. However, if a fast coincidence between S1 and S2 is formed, it can be used as an event trigger to generate a high voltage pulse which is placed on the electrodes surrounding the chamber volume. Usually a Marx generator and a Blumlein are used to generate and shape this pulse. The high voltage pulse (typically in the range of 500-700 kV) creates a strong electric field in the chamber which causes the ion pairs to accelerate and to multiply in the chamber gas. By restricting the pulse to a short duration (10-20 ns), the final breakdown in the gas and the creation of a spark from one electrode to the other is suppressed. Only the early stage of the spark development occurs, i.e., the development of streamers. Typically, in the streamer chamber mode of operation, the electric field is about 20-25 kV/cm. Now if the chamber volume is transparent, then a camera which photographs the light from the streamers generated will see their development from two to several millimeters (depending on operation) along the electric field lines when the camera view is normal to the electric field. If transparent electrodes, such as wire grids are used, the camera can view the light from the streamers end-on. In this case the streamers then appear as a series of bright dots (Fig. 1b), much the same as one sees when looking at bubble chamber photographs. Finally, if the streamer chamber volume is placed in a magnetic field of suitable strength, the curvature of charged particles

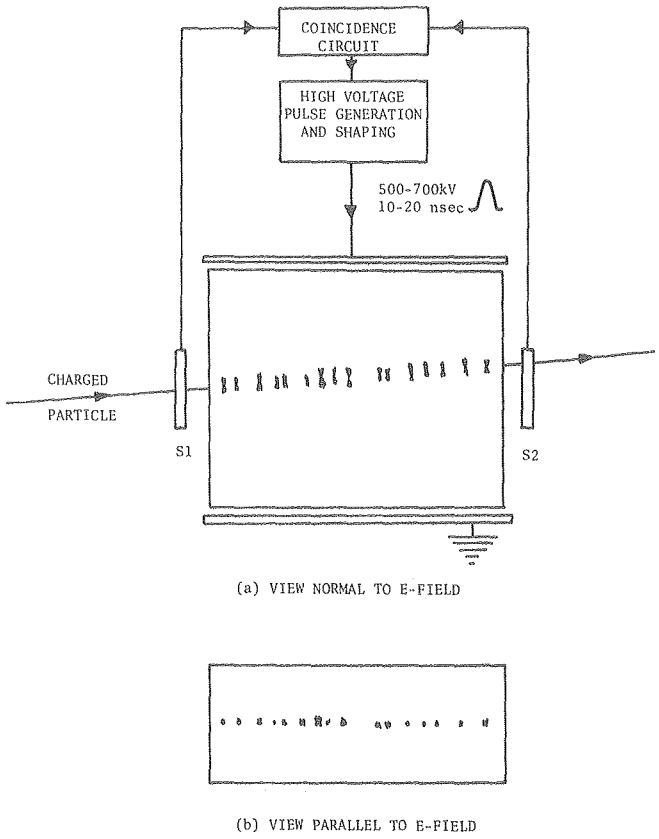

Fig. 1. (a) Schematic diagram showing passage of a charged particle through the streamer chamber gas volume. Streamers develop to several millimeters along the applied E-field; (b) if the streamers are viewed end-on (i.e., in direction parallel to E-field), they appear as a series of bright dots. (XBL 783-7506)

in this magnetic field can be measured. The scanning and measuring of this film is then handled in a manner similar to the treatment of bubble chamber film.

Although considerable use has been made of streamer chambers for high energy particle physics studies, their use in nuclear science work has been quite limited. Some of the areas of study have included: a) study of coherent nuclear scattering processes, b) conventional nuclear physics (e.g., search for double ß-decay), c) study of hadron-nucleus elastic and inelastic scattering, d) high-energy heavy-ion interaction experiments.

The LBL streamer chamber has been used to study nucleus-nucleus interactions using projectiles up to ^{40}Ar with energies up to $\sim$2 GeV/nucleon.

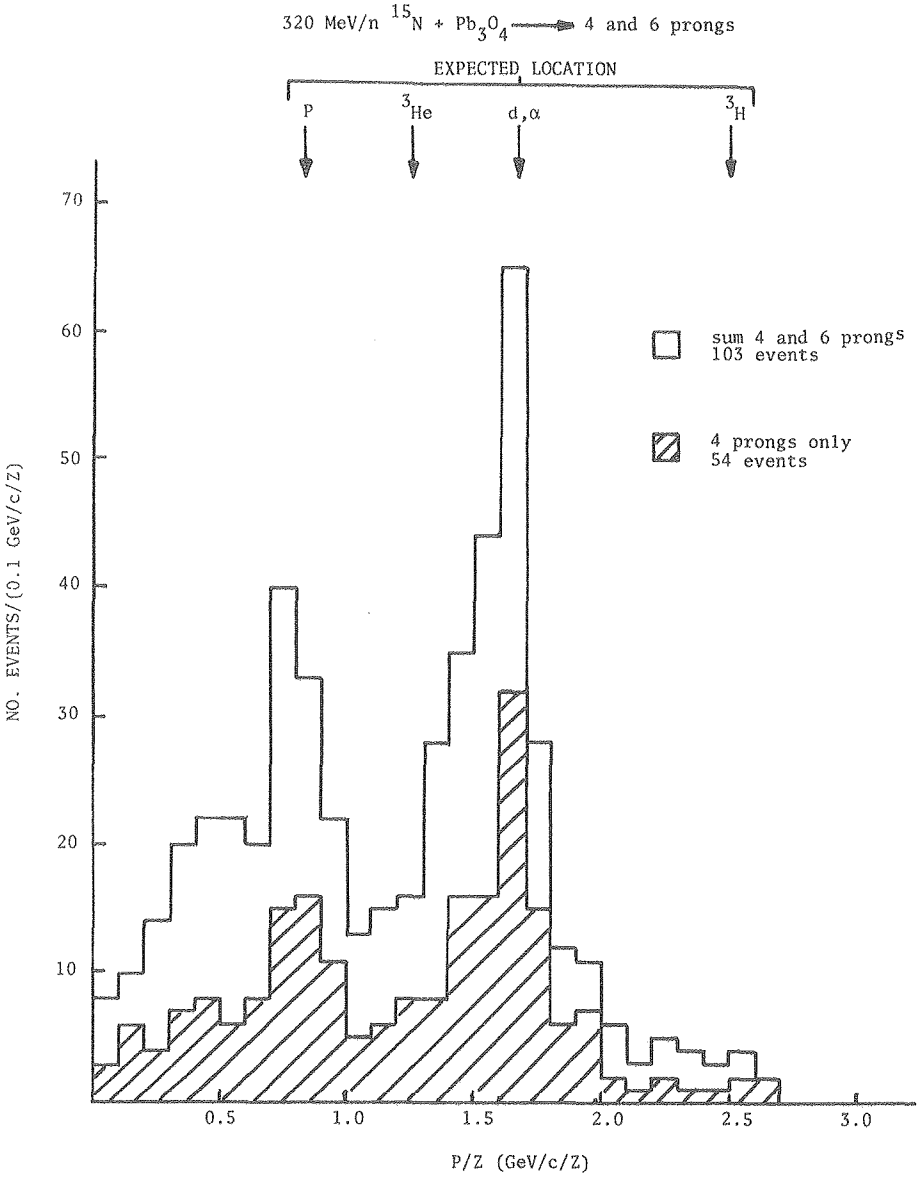

Fig. 2. Rigidity (p/z) distribution for fragments arising from 4 and 6 prong events. (XBL 783-7505)

The primary thrust of this program has been to study central collisions (as many as 125 charged tracks in a single event have been observed in these studies). Early results on negative pion multiplicities have been reported.[3] Multiplicity distributions are easily obtained by simply scanning and counting the tracks in each interaction. If in addition the tracks are measured, one can obtain rigidity (p/Z) distributions like the one shown in Fig. 2. The two prominent peaks observed can be identified as protons (near 0.83 GeV/c/z) and deuterons or alphas (near 1.66 GeV/c/z). The arrows in Fig. 2 indicate the "expected location" of these particles if they were fragmented from the incident projectile without any change in energy (i.e., come out with the momentum/nucleon of the projectile). This effect is observed in all light-projectile fragmentation studies.[4]

Streamer chambers have not as yet found wide application for nuclear science studies. In one sense, they appear to be ideal tools for studying hadron-nucleus and nucleus-nucleus collisions, since they allow the interaction to be studied in an exclusive sense (meant here to mean that all charged products of the reaction are observed). However, certain drawbacks appear. Among these are the fact that particle identification is difficult when using streamer chambers, unless external counters (e.g., scintillators, solid state detectors, etc.) are used to aid in the identification. The extremely large multiplicities observed in heavy-ion collisions point out the difficulty that confronts the experimenter. Even if you are able to measure a large sample of such tracks in a single interaction, what do you do with all the information? How do you use it to unravel the complex interaction that has occurred? These are strong challenges to the experimentalist. Imagine the collision of a uranium beam of a few GeV/nucleon with a uranium target. For a central collision with high associated pion multiplicity, one might

have between two and three hundred charged tracks emerging from the interaction!

However, this tone is perhaps too pessimistic. For the investigation of hadron-nucleus interactions, streamer chambers have an interesting potential, since they allow us to go beyond the single-particle inclusive measurements which have largely dominated the field. Even for high-energy nucleus-nucleus experiments, the streamer chamber will be a useful survey tool for beams at least up to Fe and perhaps beyond. One can study some of the cluster aspects of light nuclei by using the projectile fragmentation process to provide a small amount of energy to unbind the projectile. In such processes only a few particles ($\leq$10) appear in the final state and are perfectly amenable to conventional film processing techniques. There still remain many good experiments to be done with streamer chambers over the next few years. The potential applications at cyclotron energies are particularly intriguing.

Footnote and References

*Condensed from LBL-7707, which will be published in a special edition of Nucl. Instrum. and Methods entitled "Detectors in Nuclear Science".

1. G. E. Chikovani, V. N. Roinishvili and V. A. Mikhailov, Nucl. Instr. and Methods 29, 261 (1964).

2. B. A. Dolgoschein, B. U. Rodionov, and B. I. Luchkov, Nucl. Instr. and Methods 29, 270 (1964).

3. S. Y. Fung, W. Gorn, G. P. Kiernan, F. F. Liu, J. J. Lu, Y. T. Oh, J. Ozawa, R. T. Poe, L. Schroeder, and H. Steiner, Phys. Rev. Letters 30, 292 (1978).

4. H. H. Heckman, D. E. Greiner, P. J. Lindstrom, and F. S. Bieser, Phys. Rev. Letters 28, 926 (1972).

DESIGN AND CONSTRUCTION OF A STREAMER CHAMBER FOR THE 88-INCH CYCLOTRON

K. Van Bibber, D.L. Hendrie, D.K. Scott, B.G. Harvey, W. Pang, M. Avery, H. Wieman, and R. Lam

A prototype streamer chamber of active volume (15 cm x 9.5 cm x 5 cm) has been constructed for use at the 88-inch cyclotron. The device is a single gap chamber, with both the anode and cathode consisting of nickel mesh of 97% optical transparency. The body is fabricated of Lucite (see Fig. 1). The rather stringent pulsed high-voltage requirements for successful operation of such a chamber (pulses of the order of 10-20 kV/cm and of duration $\approx$10 ns) are provided by a three-stage Marx generator and pulse-forming network,[1] also fabricated on site.

The JUPITER C-magnet has been modified and lowered into Cave 5 of the 88-inch cyclotron. The gap of the magnet was widened to 7" to accommodate the chamber, which will lie flat on the lower pole tip, and a mirror mounted at

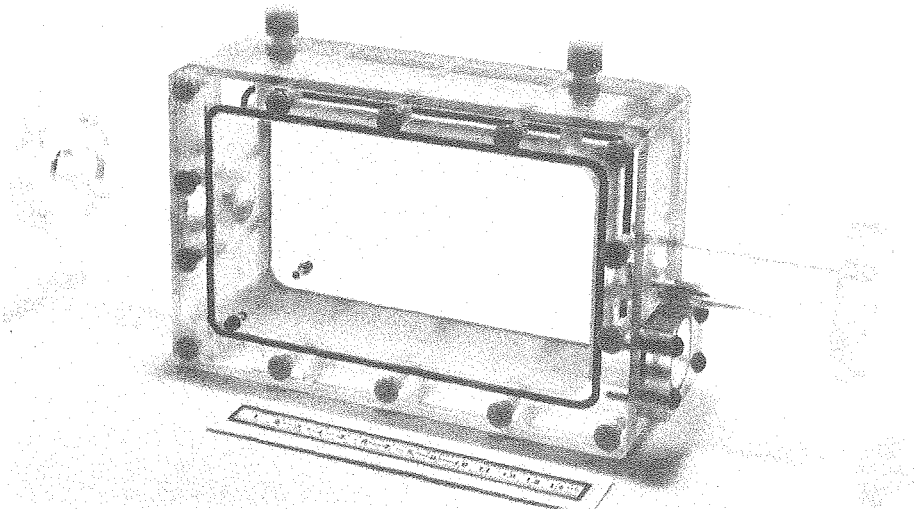

Fig. 1. Streamer chamber for the 88-inch cyclotron. Beam traverses chamber left to right; port at lower right (blanked off in photo) allows the forward angle trigger.

(XBB 782-1905)

an angle of 45° permitting the camera to record the events perpendicular to the curvature of the tracks.

Events will be recorded on 35-mm film by a single Flight Research camera. The trigger initially will consist of a scintillator-phototube counter behind a forward angle port to look selectively at quasi-elastic and fragmentation events. Ultimately the chamber will be run in a "hybrid" mode, where each event will be triggered by a signal from a standard ΔE-E silicon telescope outside of the chamber, permitting isotope identification of the fragment; for each frame exposed, a corresponding event would be written onto computer tape. Although internal targets are contemplated, first tests will be made simply with the Ne-He (90%-10%) volume gas as a target. Estimated rates are >10,000 events/day.

Tests of the chamber with a ^{106}Ru β^- source have been performed and streamers of good quality photographed (see Fig. 2).

The possibilities of the chamber are exciting. Much beam development at the cyclotron has been devoted to extracting fully stripped beams of the lighter heavy ions with energies of 35 MeV/nucleon. Although possibly too weak for normal solid-state counter work (for example, 10^4/sec of $^{12}C^{6+}$), the beam intensities are ideal for the streamer chamber which cannot be operated above 10^5-10^6 pps. Furthermore, such a 4π visual technique will provide a powerful insight into reaction mechanisms at beam intensities above the Fermi energy and the speed of sound in nuclear matter.

References

1. Our pulsed-shaping network is essentially that of P. Rice-Evans and I. Hassairi, Nucl. Instr. & Methods 106, 345 (1973).

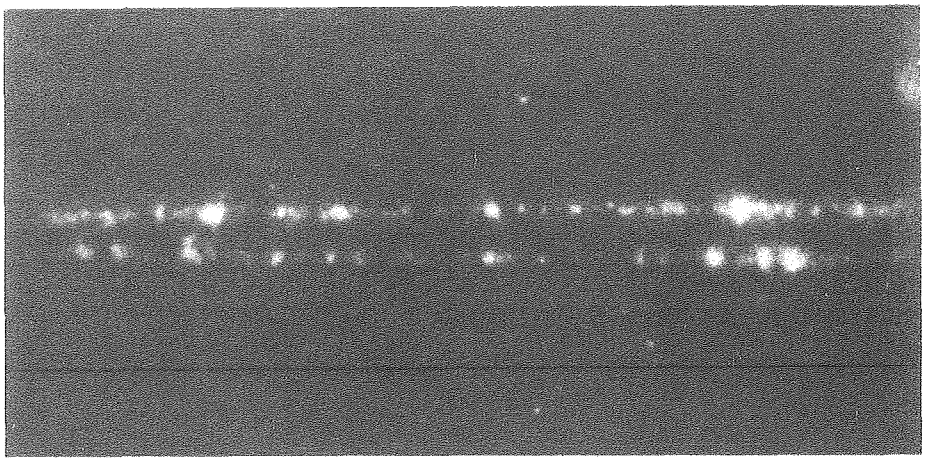

Fig. 2. Streamers of source β^- particles traveling along beam axis. Distance between the two tracks ≈0.75 cm.

(XBB 784-4162)

RESPONSE OF SCINTILLATORS TO RELATIVISTIC HEAVY IONS*

S.P. Ahlen and M.H. Salamon

In addition to being of great interest to experimentalists from a wide range of disciplines for purely practical reasons, the investigation of the response of scintillators to radiation is of considerable interest insofar as it relates to solid state and polymer physics. For these reasons we have undertaken an extensive survey of the response of a large number of liquid, organic and inorganic scintillators to fast heavy particles with Z = 1, 10, 18 and 26. This is a continuation of research initiated with the calibration of a cosmic ray telescope.[1]

In a period of six days, in the last week of April, 1978, we successfully exposed our samples to 600 MeV/amu ^{20}Ne, ^{40}Ar and ^{56}Fe, each run lasting for 16 hours. The samples included pure polyvinyltoluene (PVT), various concentrations of p-terphenyl in PVT, pure liquid p-xylene, various concentrations of PPO in p-xylene and

the commercial samples NE110, Pilot B, Pilot Y, Pilot F, Pilot 425, UVT acrylic and Tl doped NaI. The UVT acrylic and Pilot 425 are Cerenkov radiators, their scintillation level being quite low. The energies of the beams were varied with the use of an automated lead absorber with a solid state detector serving to discriminate against charge changing nuclear interactions. Temporal drifts were corrected for with the use of an ^{241}Am doped NaI crystal calibration light pulser.

Preliminary analysis of the data has revealed the following results:

a) Although many aspects of the scintillation light emitted by the commercial plastic samples (NE110, Pilot B, Pilot F and Pilot Y), such as efficiency to muons, decay time, absorption length, etc., are subject to wide variations, the relative scintillator saturation curves (i.e., the energy to light conversion efficiency as a function of projectile charge and velocity) are identical within an experimental error of several percent.

b) Negligible variation of the shape of the saturation curves was observed as the fluor concentration was varied. This rules out fluor depletion models for scintillator saturation.

c) For a given energy loss, the light output increases with increasing charge. For ΔE = 2 GeV, Fe output is 30% greater than Ar output which in turn is 50% greater than Ne output. This indicates the importance of the role of high energy delta rays in determining the scintillation efficiency.

d) The conversion efficiency for scintillation in Pilot 425 is not saturated in going from Ne to Fe.

e) When viewed with quartz phototubes, the Cerenkov light output of UVT acrylic is essentially the same as for Pilot 425 with a reduction by a factor of 2 of the scintillation level. This renders UVT acrylic a superior near-threshold particle speedometer.

More detailed analysis is currently in progress.

Footnote and Reference

*Presented at the 26th Annual Meeting of the Radiation Research Society, Toronto, 14 May 1978.

1. S. P. Ahlen, B. G. Cartwright and G. Tarlé, Nucl. Instr. and Methods 147, 321 (1977).

A NUCLEAR-TRACK-RECORDING POLYMER OF UNIQUE SENSITIVITY AND RESOLUTION*

B.G. Cartwright,† E.K. Shirk,† and P.B. Price

Nuclear-track-recording solids, in which tracks can be enlarged to visible size by chemical etching, can be used to identify energetic nuclear particles, because the rate of growth of the conical etch pit that develops at the intersection of the particle's trajectory and the surface is an increasing function of the rate of energy loss of the particle. The track etch rate is, in principle, nearly immune to the energy loss statistics that plague all other charged particle detectors, because it is controlled by the energy density deposited within a few tens of Angstroms of the center of the particle trajectory. An etched detector suffers only negligible fluctuations in response resulting from delta-ray generation and ought to provide the greatest resolution of any charged particle detection system yet developed. In practice, non-uniformities and inhomogeneities such as crystalline regions in the track-recording solids now being used (Lexan being the prime example) prevent their theoretical resolution from being attained.

Through a logical chain of reasoning developed in a recent paper, we have discovered that diethylene glycol bis(allyl carbonate), a thermosetting polymer known commercially as CR-39, records tracks that can be etched in NaOH solutions, as can tracks in Lexan, but is superior in three aspects: a) It has the highest sensitivity of any track-recording solid. Figure 1 compares the response of CR-39 and of Lexan. The half-angle of the cone-shaped etch pit is $\theta = \arcsin(V_B/V_T)$. Figure 2 shows that 42 MeV ^3He particles at normal incidence clearly record tracks in CR-39. b) It has potentially the highest resolution of any track-recording solid. Figures 3 and 4 show examples of the resolution of CR-39 under ideal conditions (monoenergetic beams at normal incidence in a small area). c) As the figures show, the optical clarity and contrast are superb, making automated image recognition and track parameter measurement feasible.

Commercially available sheets of CR-39 are generally extremely uniform in chemical reactivity in the plane of the sheet but vary with depth from a maximum at either surface to a flat minimum in the interior. For low-energy particles that do not penetrate deeply this may not be a problem,

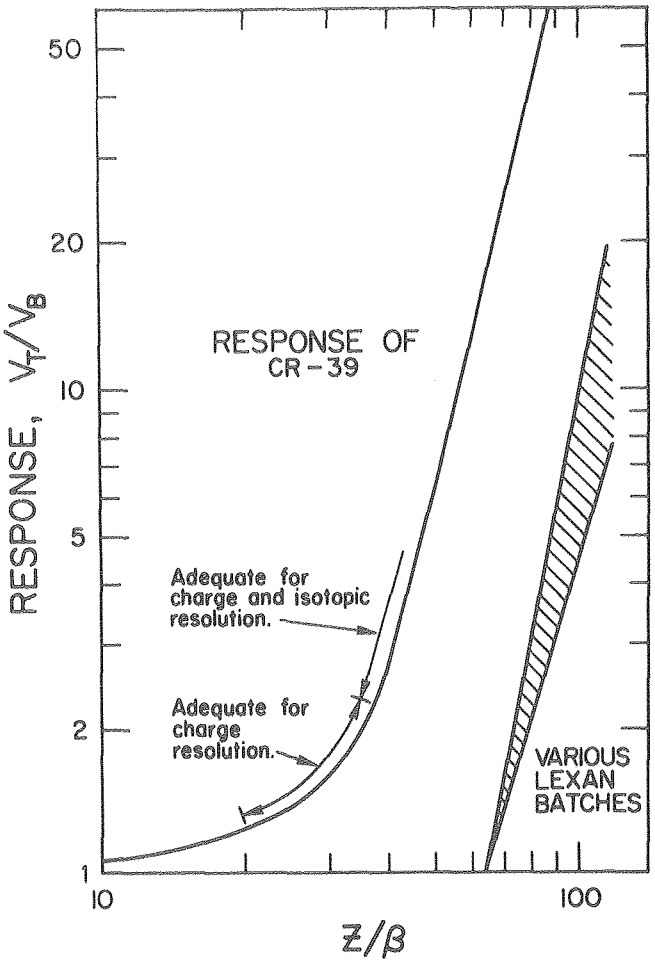

Fig. 1. Response of CR-39 and of Lexan as a function of the ratio of charge to velocity, Z/β. The response is defined as ratio of track etch rate to bulk etch rate. The higher sensivitity of CR-39 is obvious. (XBL 787-1278)

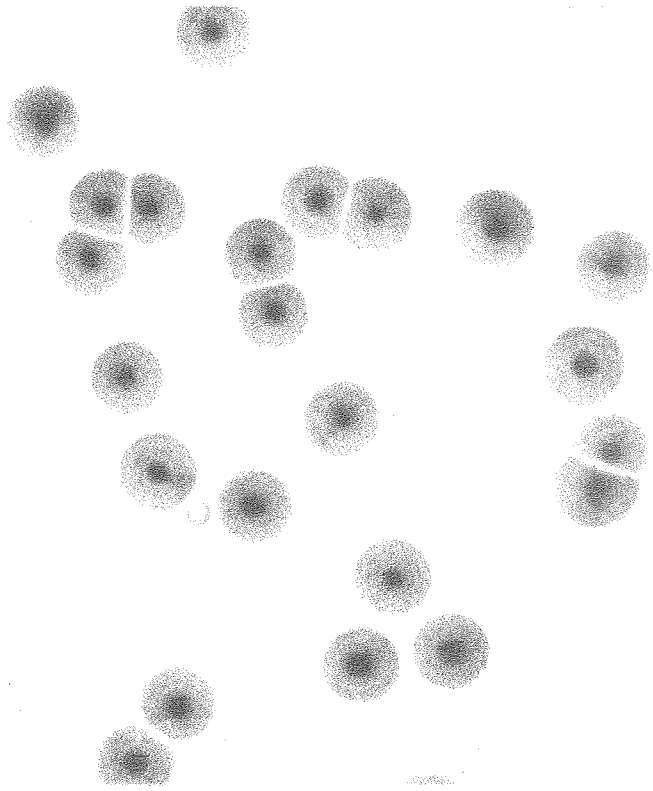

Fig. 2. Etch pits of ∿42 MeV ^{3}He particles ($Z/B \approx 10$) illustrating the high sensitivity of CR-39.

(XBB 787-8344)

but for applications of interest to us, such as the resolution of isotopes of energetic heavy nuclei, presently available sheets have disadvantages. We have begun to make our own sheets, with the goal of eliminating any depth dependence of the response. Results are encouraging.

The measurements of etch pit area in Fig. 4 were made with a vidicon camera that scanned a field of view and summed the number of pixels darker than a predetermined gray level. We are developing a semi-automatic scanning and measuring system that will eventually greatly speed up the rate of data acquisition with CR-39 detectors.

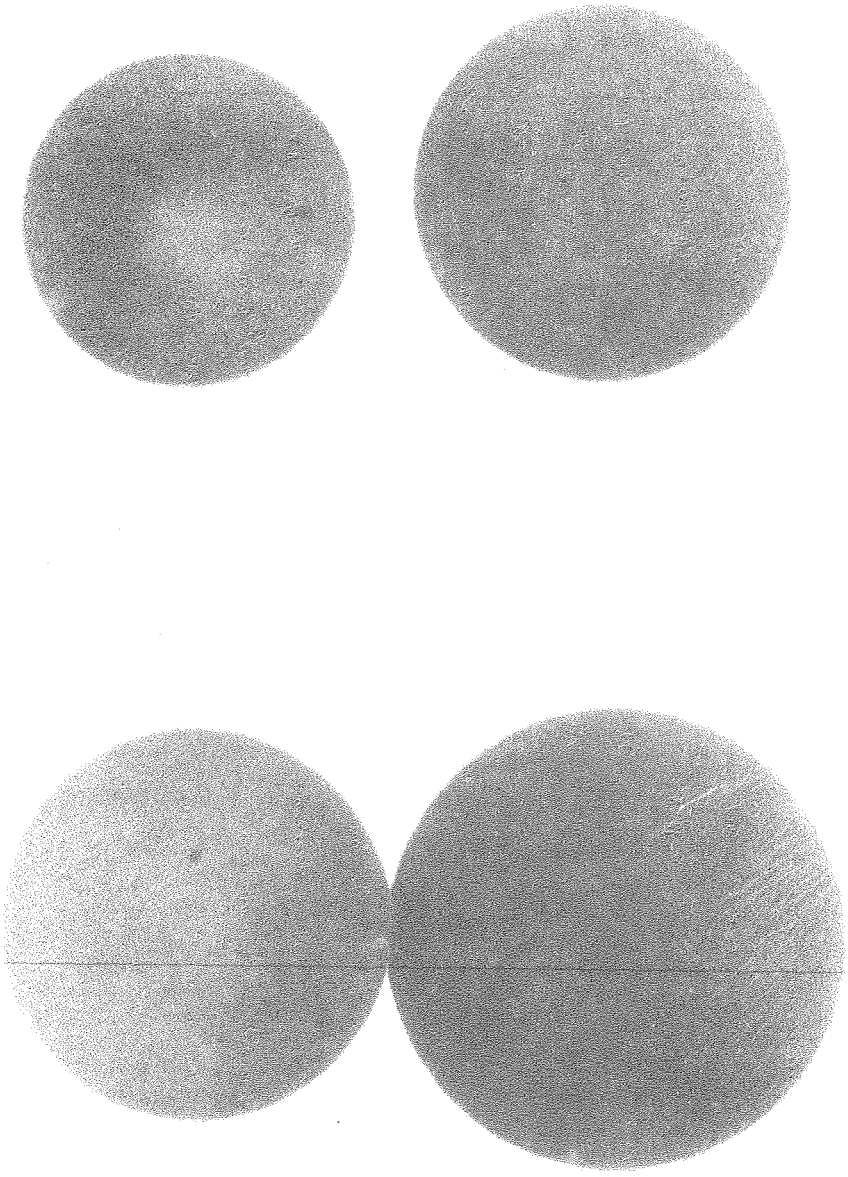

Fig. 3. Comparison of the etch pits of ^{12}C ions (left) and ^{14}N ions (right) in CR-39. At top they both have energies of 32 MeV/amu. At bottom they have passed through a 1.5-mm sheet of CR-39. Their clarity and contrast make automated measurements with a vidicon camera possible (see Fig. 4).
(XBB 787-8345)

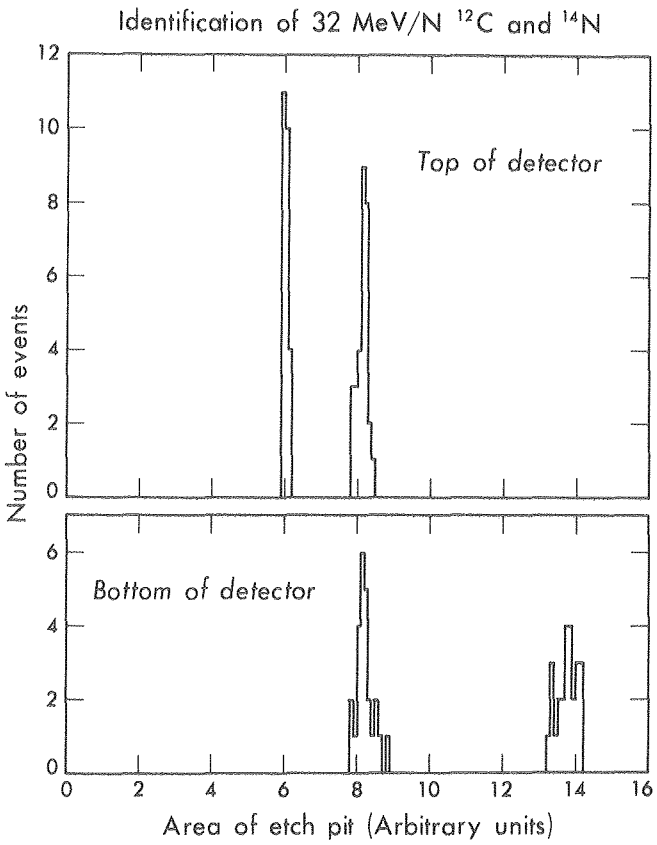

Fig. 4. Measurements of etch pit areas for events such as shown in Fig. 3, illustrating the high resolution of CR-39.
(XBL 7810-11752)

Footnotes

*Based in part on Nuclear Instruments and Methods 153, 457 (1978).

†Dept. of Physics, University of California, Berkeley, CA 94720.

ISOTOPE SHIFTS IN THE GROUND STATE OF SHALLOW, HYDROGENIC CENTERS IN PURE GERMANIUM*

E.E. Haller

Using photoelectric spectroscopy,[1] we have investigated a previously unexplained shallow donor D and a shallow acceptor A_2 in ultra-pure germanium. These shallow centers exhibit isotope shifts in their ground states when the germanium host crystal is grown in a pure deuterium atmosphere instead of the usual pure hydrogen atmosphere. This is the first time that an electronic isotope shift of shallow centers in semiconductors has been observed.

Ultra-pure germanium single crystals grown in our laboratory were investigated. We estimate hydrogen concentrations of 10^{13}-10^{14} cm^{-3} in the final crystal.

In addition to the known chemical residual impurities, a number of centers producing shallow energy levels have been discovered.[2] One acceptor (A_2) and one donor (D) are of special interest because we are able to link them to the presence of hydrogen in the Ge crystals.

The ground state energy of the centers A_2 and D have been determined to be $E_{gs}^{A_2}$ = 11.31 MeV and E_{gs}^{D} = 12.34 MeV.[2] By growing several crystals in a pure deuterium atmosphere (<0.03% H_2), we were able to demonstrate a large isotope shift in the ground state binding energies of both A_2 and D. The upper spectrum in Fig. 1 was obtained with a rapidly quenched sample of the hydrogen containing crystal No. 497-5.5. This sample is p-type ($N_A - N_D \simeq 10^{10}$ cm^{-3}) and all the acceptor related lines are positive while the donor lines have opposite polarity. The lower spectrum has been obtained with a deuterium containing sample from crystal No. 519-4.0. The residual chemical impurities make this crystal n-type ($N_D - N_A \simeq 10^{10}$ cm^{-3}) which is the reason that negative lines are produced by acceptors and positive lines by donors. The set of lines due to the donor D exhibit perfect "hydrogenic" spacing and are shifted towards lower energies in the lower spectrum by ΔE_{gs}^{D} = -51 ± 3 μeV. This corresponds to a shift of the ground state closer to the bottom of the conduction band. An opposite shift away from the top of the valence bands $\Delta E_{gs}^{A_2}$ = 21 ± 3μeV has been found for the acceptor A_2.

The isotope shift in the ground state of A_2 and of D is a direct proof for the presence of hydrogen in these two centers.

Taking into account the recent observations, we propose that the centers A_2 and D are complexes of hydrogen and other electrically nonactive impurities (the most likely candidate being oxygen). We cannot exclude the possibility that the donor D is due to atomic hydrogen in which case the "deep" donor model would have to be revised.

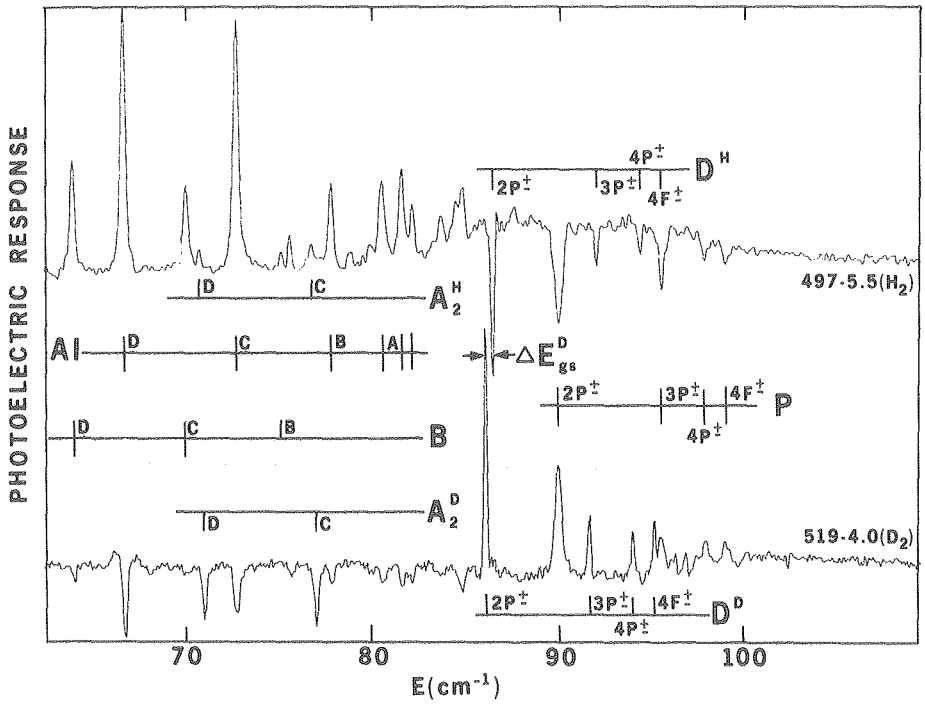

Fig. 1. Photoelectric spectra of hydrogen grown, p-type sample 497-5.5 (H_2) and deuterium grown, n-type sample 519-4.0 (D_2). Temperature T = 8.00K; Al = aluminum, B = boron, P = phosphorous, $D^{H,D}$ = hydrogen, deuterium related donor $A_2^{H,D}$ = hydrogen, deuterium related acceptor. The notation of Jones and Fisher[3] was used for the acceptor lines (B, Al).

(XBL 778-2792)

Footnote and References

*Condensed from LBL-6184.

1. T. M. Lifshitz and F. Ya. Nad., Sov. Phys. Doklady 10, 532 (1965). For a review see: S. Kogan and T. M. Lifshitz, Phys. Stat. Sol. (a) 39, 11 (1977).

2. E. E. Haller, First Seminar on Photoelectric Spectroscopy of Semiconductors (Moscow, May 1977), Izv. Acad. Nank. SSSR. Phys. Ser. 42, 1131 (1978).

3. R. L. Jones and P. Fisher, J. Phys. Chem. Solids 26, 1125 (1965).

ZONE REFINING HIGH-PURITY GERMANIUM*

G.S. Hubbard, E.E. Haller, and W.L. Hansen

High purity ($|N_A - N_D| \leq 2 \times 10^{10}$ cm^{-3}) single crystal germanium suitable for large volume radiation detectors has been produced in several laboratories for a number of years.[1,2] Once it was demonstrated by Haller et al.[3] that the zone refined germanium was the source of all but one (P) of the impurities found in these crystals, a program to investigate the zone-refining process was begun.

The zone-refining process for germanium as described by Pfann and others in the 1950's[4,5] depends for its effectiveness on the nature of the equilibrium between the solid and liquid phases of germanium in which impurities are dissolved. This relationship is usually expressed as the segregation or distribution coefficient k; a ratio between the impurity concentration in the solid phase to that in the liquid.

Evidence provided by zone refining and crystal growth has led us to construct a model of impurity behavior which involves binary and ternary complexes of silicon, oxygen, boron, and aluminum.

In Fig. 1, the total concentration of aluminum or boron in a melt or zone is considered to be

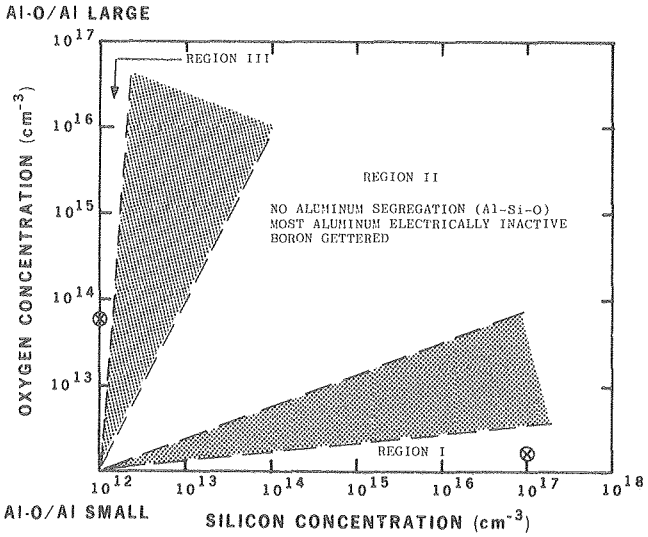

Fig. 1. Our tentative qualitative model of the effect of silicon and oxygen on aluminum and boron is shown. In Region I where silicon is dominant, the impurities segregate. Region II represents the conditions of crystal growth from quartz and silica zone refining. In Region III, oxygen is dominant and electrically active impurities segregate. As the amount of oxygen increases, more impurities become electrically inactive (Al-O, B-O).

(XBL 7710-10058)

constant. The material in contact with the germanium is not directly relevant; although, as we shall see, each container considered may be represented by one of the regions.

Region I is characterized by an increasing silicon concentration and low oxygen concentration. At even very high silicon concentrations, normal segregation of aluminum and boron occurs and almost all of the aluminum and boron is electrically active. In Region III, the concentration of silicon is low and the amount of oxygen increases. Here the behavior of aluminum and boron is more complex, but in general the electrically active impurities still segregate normally. At very high concentrations of oxygen, B and Al completely disappear due to the creation of electrically inactive Al-O, B-O complexes. This was demonstrated by the work of Edwards.[6] At intermediate levels of oxygen, both electrically active and inactive impurities exist. The electrically active form segregates normally, whereas the electrically inactive impurity-oxygen complex seems to have $k \approx 1$. Most high-purity germanium crystals are grown under the conditions of Region II. In this region, silicon and oxygen are present in approximately equal quantities, creating Si-O-(Al, B) complexes. Electrically active aluminum does not segregate and a large fraction of aluminum is in the form of electrically inactive complexes. Boron is largely gettered by complex formation.

One realization of this model of complex formation has been the use of silica smoke as a boat coating. Made by burning silane, the smoke consisted of Si and Si_xO_y. Most likely the Si/O ratio is slightly in favor of the silicon, i.e., the impurity behavior should be in Region II but nearer the x-axis and Region I.

Figure 2 shows a cast ingot (174) of intrinsic grade commercial germanium refined in a silica smoke-coated quartz boat for five zone passes. After removing the ingot and measuring the concentration it was etched, exposing a new surface. The ingot was returned to the same coating for five more passes and a further reduction of 2.5 in impurity concentration was achieved (Ingot 175). Ingot 179 was also a cast ingot of 40 Ω-cm germanium refined for five passes. The ingot was carefully removed but not etched and only the silica smoke coating replaced. By moving the position of zone start, enough of the initially refined germanium could be preserved to determine the profile after the first five passes. The balance of the ingot, unetched but in contact with a fresh coating, exhibited a dramatic five-fold drop in impurity concentration. Taken together, these two experiments demonstrate that a vigorous gettering by complex formation occurred at the germanium/silica coating interface. No change in the shape of the impurity profile was noted, as would be

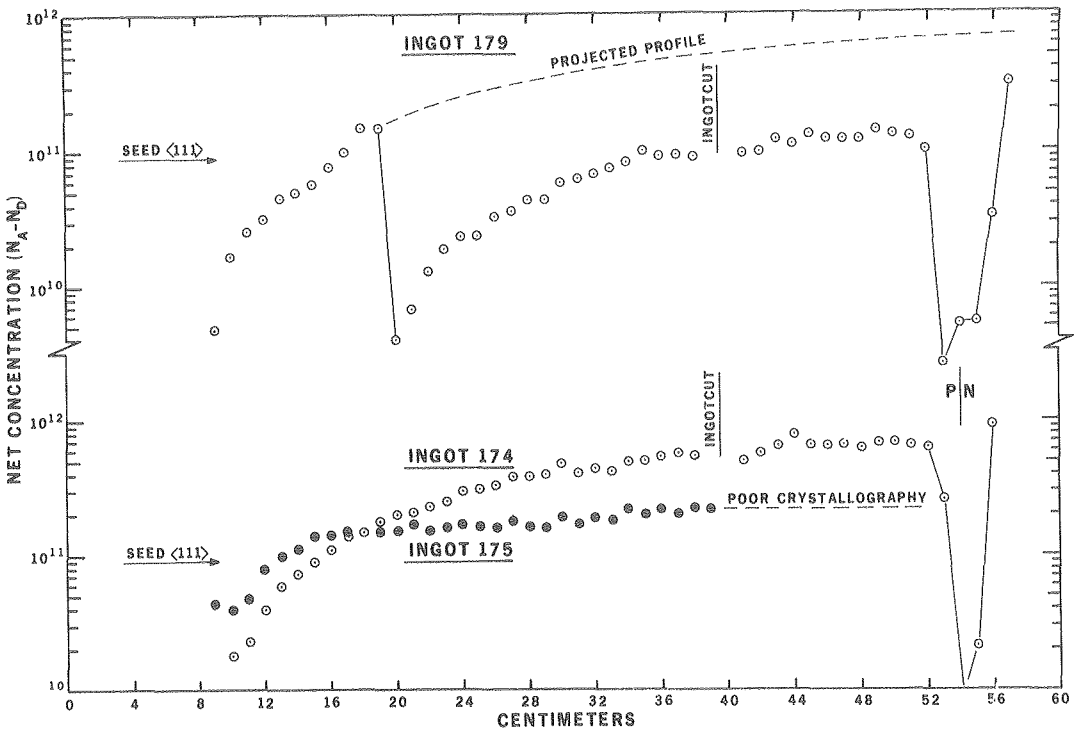

Fig. 2. All ingots are single crystals. ⊙ and ● both represent net acceptors. Ingot 179 was given five passes in a silica smoked boat, removed, the silica replaced and given five more passes from 20 cm to the end. Ingot 174 was given five passes in a silica smoked boat, removed, analyzed, etched, and replaced into the same silica coating. After five more passes, the ingot, now called 175, was removed and measured to the point where poor crystallography began to disturb the measurement.

(XBL 7710-10062)

the case with segregation, but etching the ingot and replacing the silica coating effected large reductions in the impurity concentration.

Using this gettering action, one can consistently produce germanium of sufficiently high purity for detector grade crystals to be made in a single pull. If one begins with intrinsic grade germanium, the process requires two separate refinings in which the ingot is etched and the silica coatings replaced. A final equilibrium between electrically active and complexed impurities appears to be established at a measured impurity concentration of 1 to 4 x 10^{10} cm^{-3}. As a result more etching and new coatings do not further improve the impurity concentration. If the ingot has been first refined in a graphite or pyrolitic carbon/carbon smoke environment, a subsequent refining in silica smoke usually removes the boron easily in a few passes.

A qualitative model (Fig. 1) involving ternary and binary complexes of silicon, oxygen, boron, and aluminum has been presented to account for most of the behavior of the impurities observed during single crystal growth and zone refining of high purity germanium. At least four different methods of refining commercial 40 Ω-cm germanium to sufficient purity for detector grade single crystals have been found:

a) Refining in a solid graphite boat followed by refining with amorphous carbon smoke on quartz.

b) Pyrolitic carbon/carbon smoke refining followed by silica smoke refining.

c) Silica smoke refining repeated.

d) Pyrolitic carbon/silica smoke refining alone.

Further areas for investigation involve reducing the oxygen content during refining so that higher levels of purity can be reached, and attempting to understand the nature of the new acceptors that have appeared in both zone-refined and single-crystal material. We feel that the understanding of high-purity germanium is now at the point where the consistent production of large amounts is feasible.

Footnote and References

*Condensed from LBL-6441

1. R. N. Hall, IEEE Trans. Nucl. Sci. NS-21 (1), 260 (1974).

2. W. L. Hansen and E. E. Haller, IEEE Trans. Nucl. Sci. NS-21 (1), 251 (1974).

3. E. E. Haller, W. L. Hansen, G. S. Hubbard, and F. S. Goulding, IEEE Trans. Nucl. Sci. NS-23 (1), 81 (1976).

4. W. G. Pfann, Zone Melting (John Wiley and Sons, New York, 1966).

5. H. E. Bridges, J. H. Scaff, and J. N. Shive, eds., Transistor Technology, Vol. I (D. Van Nostrand, 1958).

6. W. D. Edwards, J. Appl. Phys. 34, 2497 (1973).

A NEW METHOD TO DETERMINE THE CHEMICAL COMPOSITION AND STRUCTURE OF NON-ELEMENTAL ACCEPTOR AND DONOR CENTERS IN ULTRA-PURE GERMANIUM

E.E. Haller

A new approach towards the understanding of hitherto unknown, non-elemental acceptors and donors that can limit the purity of ultra-pure germanium has been explored for a specific pair of shallow centers, designated A_2 and D. Using photoelectric spectroscopy, we have demonstrated that an isotope shift in the ground-state binding energy occurs when the germanium crystals are grown in pure deuterium instead of in the usual pure hydrogen atmosphere. This isotope shift is the most direct proof of the presence of hydrogen atoms in the centers A_2 and D. Applying uniaxial stress to Ge samples containing A_2 and D, we show that the symmetry and structure of the centers can be explored. The knowledge of the chemical composition and the structure of the non-elemental centers will allow development of methods to reduce and keep their concentrations to acceptable levels.

In pure germanium the donor ground state is fourfold degenerate. The continuum corresponds to the four conduction band minimas along the <111> directions. The presence of a donor "core" splits the fourfold degenerate ground state into a triplet (T) and a singlet (S) state. The energy difference is called chemical split 4Δ. However, all the bound excited states remain fourfold degenerate. If a uniaxial stress is applied to the germanium crystal, the energies of the band edges and of the ground and excited states are changed. The four-fold lattice symmetry is broken and this affects the degeneracy of the donor states in the way illustrated in Fig. 1. The spectrum of the hydrogen related donor D does not follow the pattern described above. From spectra recorded at various values of stress (Fig. 2), we obtained the situation displayed in Fig. 3. The position of the lines does not change at all under stress. At a stress of 2.1×10^8 dyn cm^{-2} (0.981×10^6 dyn = 1 kg force) the intensity of the lines reduces rapidly and a new set of lines appear at 2.7 MeV lower energy. No further changes occur up to very large stresses.

Using the A_2/D pair as an example, we have demonstrated that isotope effects and uniaxial

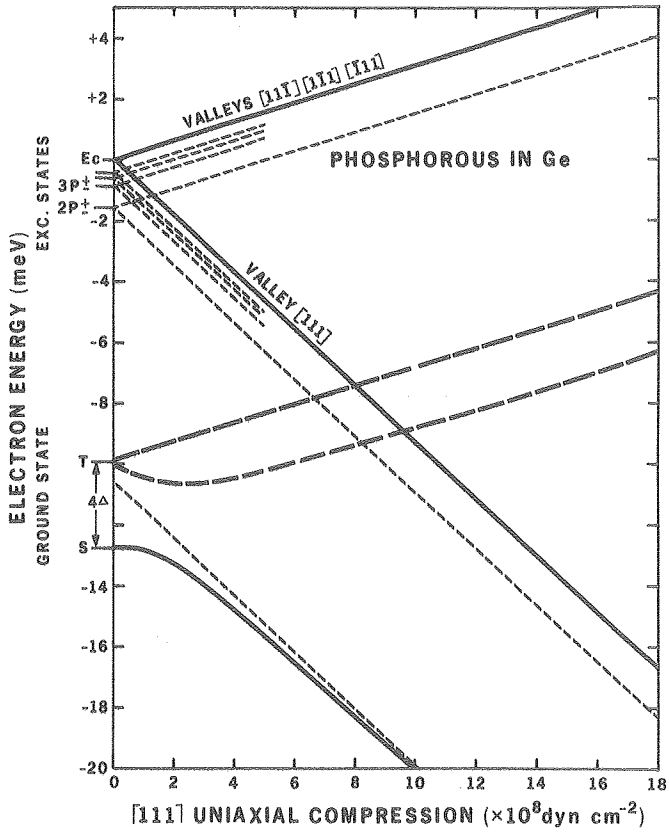

Fig. 1. Dependence of the energies of the ground- and excited-states and the conduction band minima (valleys) on uniaxial compression applied along the [111] direction. Whereas the four valleys and the excited states show perfectly linear dependences, the ground-state components exhibit quadratic terms resulting in changes in energy differences between ground- and excited-states. These changes cause the shift of the lines in photoelectric spectra under uniaxial compression. At the temperatures used in photoelectric spectroscopy (~7°K) only the lowest lying S-state is populated.

(XBL 7710-10009)

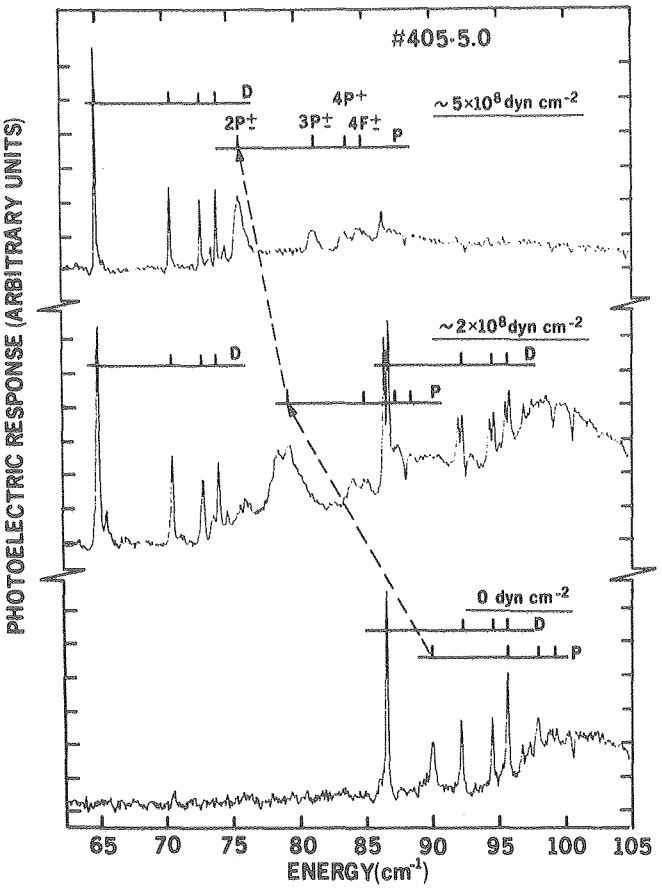

Fig. 2. Spectra of Ge-samples 405-5.0 recorded for three uniaxial stress values. The phosphorous spectra move to lower energies as illustrated in Fig. 1. The hydrogen-related donor D spectra exhibit two sets of exceptionally sharp lines which do not move but which change their intensities. Around 2.1 x 10^8 dyn cm^{-2} the ground state components cross and produce some interferences which result in a line splitting.

(XBL 7710-6740A)

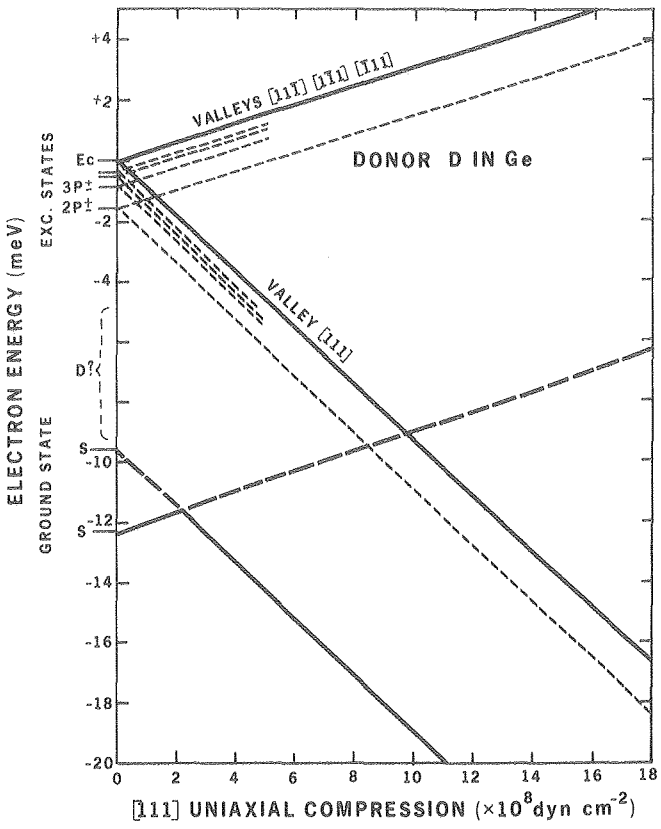

Fig. 3. Dependence of the energies of the ground-state components of the hydrogen related donor D on uniaxial compression along the [111] direction. The excited states and the <111> valleys are the same as in Fig. 1. Contrary to elemental substitutional donors the lines of the D spectrum do not move under uniaxial compression but their intensity drops rapidly around 2.1 x 10^8 dyn cm^{-2}. A new set of lines appears at 2.7 MeV lower energies. This behavior is explained by a crossing of two singlet states (S). A doublet (D) or two more singlet (S) components of the ground state must exist close to the conduction band minima, but they cannot be populated and are therefore not observed at the temperatures used.

(XBL 7710-10008)

stress can be successfully used to determine composition and structure of unknown acceptor and donor centers in germanium. The same technique will be applied to other unknown centers and also the case of lithium which has not been solved satisfactorily up to the present time.

THE LITHIUM-OXYGEN DONOR IN GERMANIUM: A DYNAMIC JAHN-TELLER SYSTEM*

E.E. Haller and L.M. Falicov†

Lithium is a fast diffusing, interstitial, shallow donor in germanium.[1] Lithium ions can get trapped in the Ge-lattice at low energy sites, e.g., acceptors,[2] point defects,[3] oxygen impurities, etc. The Li-O complex is, as lithium itself, a shallow donor and is used in the lithium precipitation technique to determine the oxygen concentration in germanium crystals.[4]

We have investigated the Li-O donor system using electron paramagnetic resonance (EPR) and high-resolution photoelectric[5] piezospectroscopy.

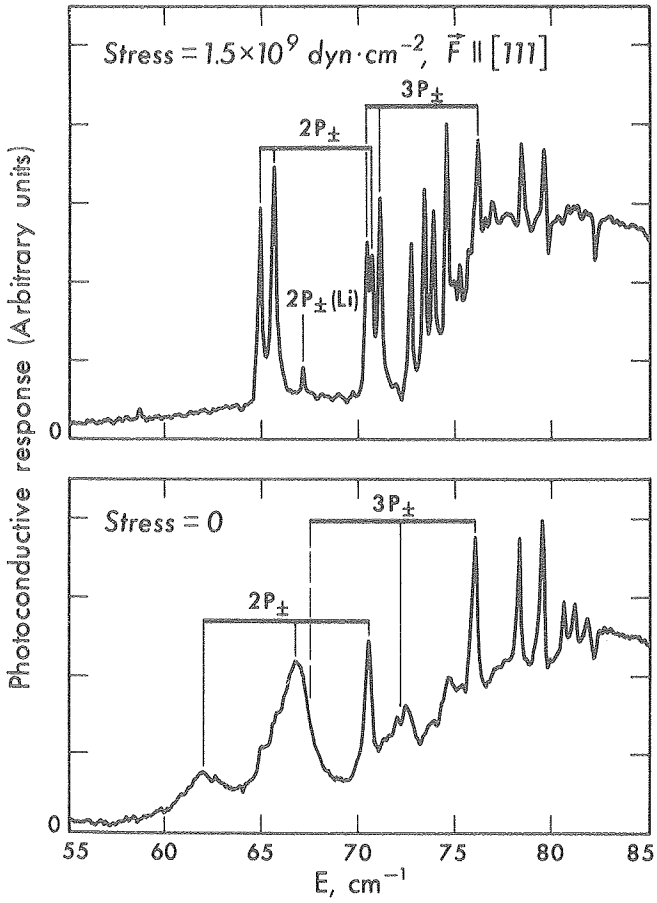

Fig. 1. Photoelectric spectrum of the Li-O donor in Ge at T = 6.5 K. (Lower figure) At zero stress. (Upper figure) At a stress of 1.5×10^9 dyn cm^{-2} applied along the <111> axis.

(XBL 7810-11902)

The EPR measurements were performed with cylindrical samples acting as a dielectric microwave cavity with high Q (axis along ⟨110⟩). The EPR spectrum shows four resonances which are magnetic-field-direction dependent. The dependence is very similar to the one reported[6] for the antimony donor in Ge. We find $g_{\parallel} = 0.85 \pm 0.05$ and $g_{\perp} = 1.91 \pm 0.03$. It follows that the Li-O donors have a symmetry axis along a ⟨111⟩ direction.

Photoelectric spectroscopy was performed using a Far Infrared Michelson Interferometer with a resolution of 8 μeV.

Two typical spectra obtained at T = 6.5 K are displayed in Fig. 1(a) and (b). The lines observed below the photoconductivity continuum are due to transition of an electron from the ground state manifold of the Li-O donor system to an excited state and subsequent promotion into the conduction band via absorption of a phonon.

The analysis of our data is based on the following observations:

The EPR experiment indicates four different but equivalent real-space orientations of the Li-O complex donor, all along ⟨111⟩ axes.

The experimental observation Figure 1 (b) shows unequivocally a singlet-doublet-singlet structure. Such a structure can only appear if the various equivalent orientations of the Li-O complex are coupled, i.e., there is tunneling between any two of the four equivalent orientations.

Under these circumstances one can write a 16 x 16 parameterized matrix which describes the ground state manifold.

The symmetry analysis of the matrix is straightforward and yields three representatives (Γ_1-singlet, Γ_2-singlet and Γ_3-doublet) for arbitrary stress, and five representations (singlets γ_1 and γ_2, doublet γ_3 and triplets γ_4 and γ_5) for the ε=0 case.

In conclusion we have observed by photelectric spectroscopy and for the first time an electronic effect which is caused by the dynamic Jahn-Teller tunneling of the nuclei of Li-O, a diatomic donor complex in a very pure semiconductor.

This tunneling effect gives rise to a fairly complex spectrum, which in itself explains most of the puzzling features discussed in previous papers and eliminates the discrepancies often encountered in interpreting the optical data of the Li and Li-O donors in Ge.

Footnotes and References

*Condensed from LBL-7545.

†Physics Department, University of California.
Work supported in part by the National Science Foundation through Grant DMR76-80561.

1. H. Reiss, C. S. Fuller, and F. J. Morin, Bell Syst. Tech. J 35, 535 (1956).

2. P. LoVecchio, "Lithium-Multivalent and Acceptor Impurity Interaction in Germanium," Ph.D. Thesis, Syracuse University (1972), University Microfilms 72-20, 352.

3. R. F. Konopleva and S. R. Novikov, Sov. Phys. Semicond. 7, 906 (1974).

4. R. J. Fox, IEEE Trans. Nucl. Sci. NS-13, 367 (1966).

5. Sh. M. Kogan and T. M. Lifshitz, Phys. Stat. Sol. (a) 39, 11 (1977).

6. R. E. Pontiner and T. M. Sanders, Phys. Rev. 152, 850 (1966).

AN INTERACTIVE COMPUTERIZED SYSTEM FOR THE ANALYSIS OF GAMMA RAY SPECTRA FROM HEAVY ION NUCLEAR REACTIONS*

D.J. Morrissey, R.J. Otto, D. Lee, J.O. Liljenzin,† I. Binder,‡ M.M. Fowler,‡ W. Loveland,§ and G.T. Seaborg

Gamma-ray spectrometric methods have been developed to deduce mass yield distributions for heavy-ion induced nuclear reactions at incident particle energies ranging from 5.0 MeV/A to 8.5 MeV/A and 0.4 to 2.1 GeV/A. These nuclear reactions produce radioactive, gamma-ray emitting nuclides that cover the entire chart of the nuclides. In a single heavy ion reaction, such as ~960 MeV ^{136}Xe + ^{238}U (Ref. 1) or 25.2 GeV ^{12}C + ^{238}U (Ref. 2) over 100 neutron-excessive and neutron-deficient nuclides ranging from ^{7}Be to ^{238}Np were produced and identified by their characteristic gamma-ray transitions between 40 keV and 2 MeV from spectrometric measurements of the target.

The object of the analysis is to translate the complicated gamma-ray spectra into a data set consisting of the partial cumulative and independent yield production cross sections from which isobaric mass yield distributions can be deduced.

The gamma-ray spectra are automatically recorded onto magnetic tape along with the start and stop times of the measurement and an alpha-numeric tag. A typical gamma-ray spectrum is shown in Fig. 1. The identification and analysis of photopeaks in the spectra is done with a modified version of the program SAMPO.[3] The modified automatic mode of this program, which was written for the CDC machine at Lawrence Berkeley Laboratory, has proved to be very successful. Desirable features that are built into this code include exact, energy-dependent calibration of the detector efficiency, polynomial energy calibrations, and particularly energy-dependent peak line shape calibration. The count rates for each identified peak, corrected for efficiency, are output on magnetic tape in blocks that are labeled with the spectrum tag and the time from the end of bombardment to the midpoint of the measurement.

After the SAMPO analysis is complete, the next step is to sort the observed gamma-ray peak areas so that decay curves can be constructed for each gamma ray. The code TAU1 was written to perform this sorting. The code starts with the magnetic tape output from SAMPO and searches first on the spectrum identification tag and then on gamma-ray energy. Throughout the analysis the chronological order of the original measurement schedule is preserved. Thus, the SAMPO analysis is performed on spectra in chronological order, which TAU1 preserves, thereby eliminating the need for any chronologic sorting in TAU1. The code is able to collect the data from up to 40 spectra for each of 10 samples. The code then generates a new magnetic tape as output that contains the gamma-ray intensities sorted by energy for each of the samples. The code also provides a printed output of all the accepted gamma rays for each sample along with the results of the least-square estimate of the half-life and the identity of the spectrum in which the gamma ray was observed.

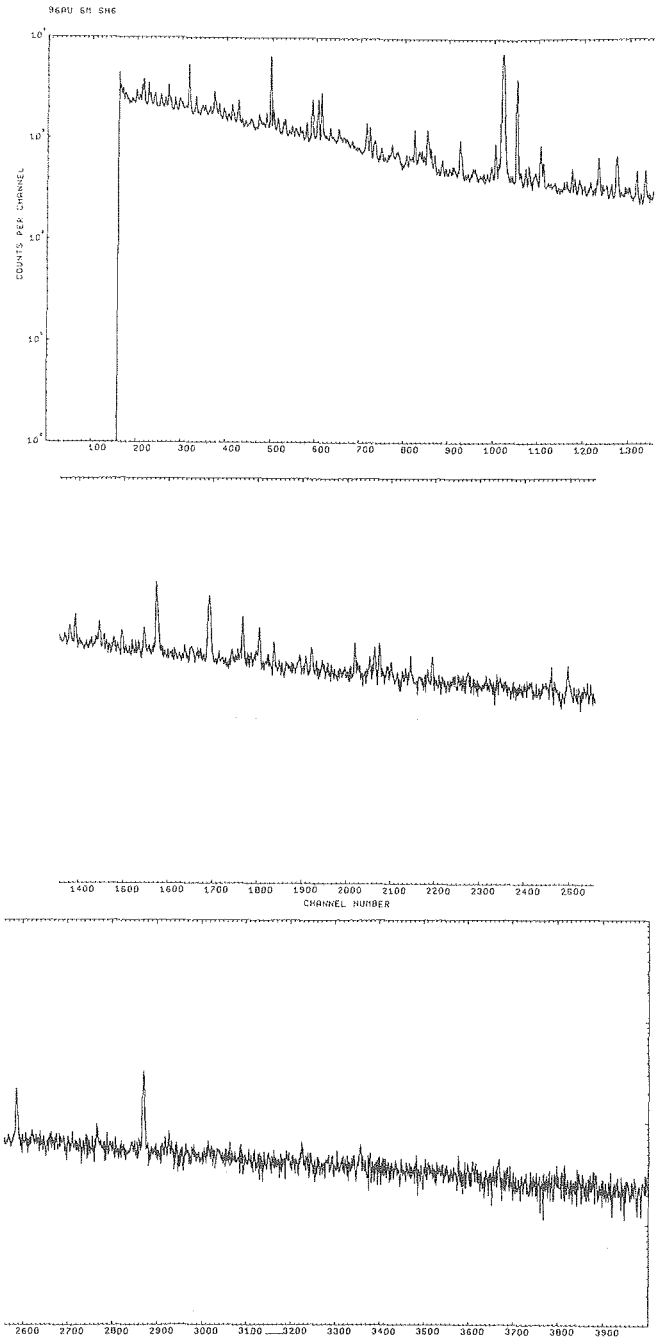

Fig. 1. Typical gamma-ray spectrum observed in this work. A gold target was irradiated with 1140-MeV ^{136}Xe ions and the gamma radiation measured directly with a range of 75 to 2000 keV in a 4096 channel spectrum.

(XBL 776-8998)

The next stage of the analysis is to bring the measured decay curves for each gamma ray together with a compilation of the known gamma-ray transitions in order to identify the radionuclides present in the sample. For this task we have written the computer code TAU2, which is an interactive decay-curves analysis program that constructs decay curves and also presents relevant data on the 20 nearest known gamma-ray transitions to facilitate the identification. The code has been designed to run on the CDC-6000 series machines at LBL with a Tektronix 4014 terminal. Input data for this code are the sorted gamma-ray data from TAU1 and a listing of the updated abridged compilation of Binder et al.[4] of the MacMurdo-Bowman gamma-ray tables,[5] both on magnetic tape. The code begins with the lowest energy gamma ray observed in the first sample and plots a semi-logarithmic decay curve (time unit of days) on the CRT of the terminal. Simultaneously, the code searches the gamma-ray table for a known gamma-ray transition nearest to the average measured gamma-ray energy. Finding the closest known gamma ray, the code presents the energy, isotope, half-life, relative intensity, and parents (if any) for the 20 gamma rays nearest to the measured energy. A typical display is shown in Fig. 2. The operator is then able to choose any single known line or combination of known lines to be least-squares fitted to the measured decay curve, or arbitrary half-lives may be fit to the data. When an acceptable identification of the decay curve has been made by the operator, the graphical display is recorded on microfiche; the A_0 value, along with its error, energy, and radionuclide identification, is output on a punched card. This A_0 value has the units of decays per minute corrected for the abundance of the gamma-ray transition and the branching ratio of the parent nuclide when necessary. Nuclear reaction cross sections are calculated on weighted average of all the observed gamma rays for each product nuclide after the identifications have been screened for duplicate or erroneous

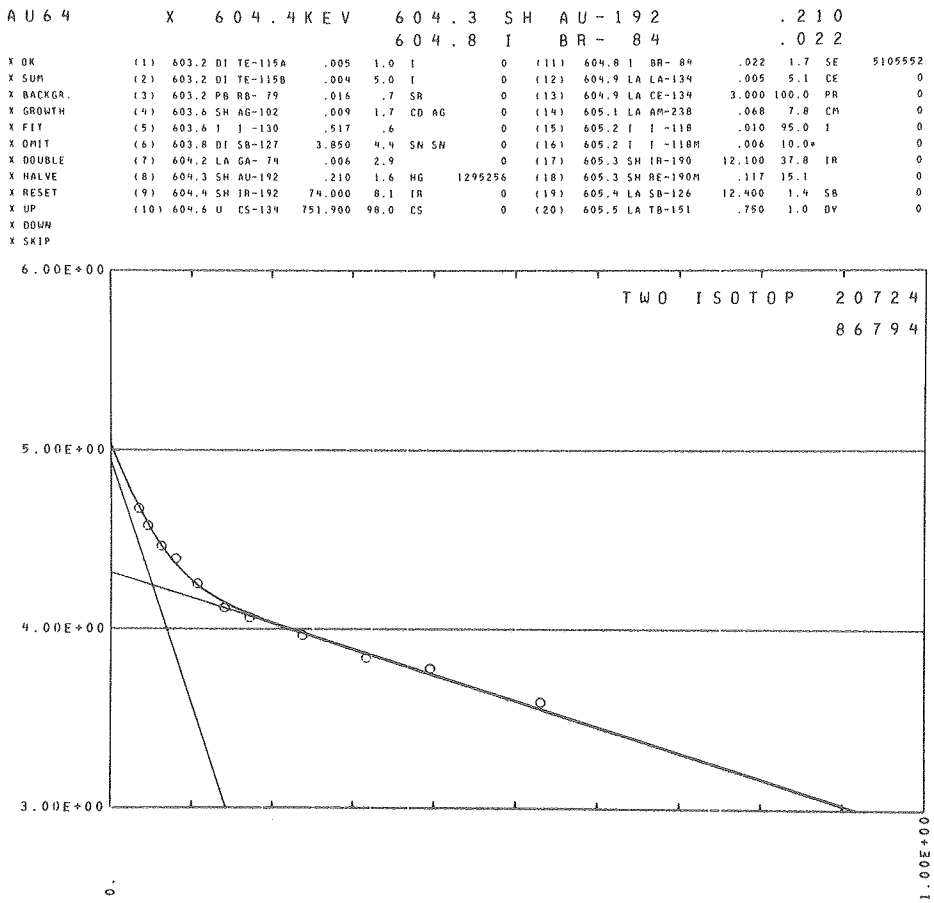

Fig. 2. Graphics terminal display showing the fit of two components (solid lines) to the measured decay curve of a 604.4-keV gamma ray (open circles). The ordinate is the logarithm of the count rate and the abscissa the time after the end of bombardment in days. Also shown on the CRT display are 20 gamma rays that are nearest in energy to the measured 604.4 keV from the Binder et al. gamma-ray catalogue.[4] These entries, numbered 1 to 20, contain information on the energy, chemical property, isotope, half-life in days, percent abundance of the transition, and chemical symbol of the parents, if any. (XBL 776-8887)

identifications and for self consistency. Once a set of partial cumulative and independent yield cross sections has been obtained, an iterative procedure is used to deduce the mass and charge distribution for the nuclear reaction under study.

We believe that the analysis system we have described represents a relatively unique combination of analytical methods and programs for the analysis of complex gamma-ray spectra. Because this system requires no prior knowledge of which radionuclides are contributing to the spectra, we hope that it may be applicable to a broad range of problems in the field of activation analysis and gamma-ray spectroscopy. Most important to this analysis system is the interactive graphics display program, which makes it possible to identify reaction products based on their half-lives and known gamma-ray transitions. Although this interactive program is presently run on a CDC 6000 machine with a Tektronix 4014 terminal, it could be easily adapted to a smaller computer such as the PDP 11.

Footnotes and References

*Condensed from LBL-7199.

†Present address: Department of Nuclear Chemistry, Chalmers University of Technology, Goteberg S., Sweden.

‡Present address: Los Alamos Scientific Laboratory, Los Alamos, New Mexico 87544.

§Present address: Oregon State University, Corvallis, Oregon 97331.

1. R. J. Otto, M. M. Fowler, D. Lee, and G. T. Seaborg, Phys. Rev. Lett. 36, 135 (1976).

2. W. Loveland, R. J. Otto, D. J. Morrissey, and G. T. Seaborg, Phys. Rev. Lett. 39, 320 (1977).

3. J. T. Routti and S. G. Prussin, Nucl. Inst. and Methods 72, 125 (1969).

4. I. Binder, R. Kraus, R. Klein, D. Lee, and M. M. Fowler, Lawrence Berkeley Laboratory Report No. LBL-6515 (1977).

5. W. W. Bowman and K. W. MacMurdo, Atomic and Nuclear Data Tables 13, 89-292 (1974).

HEAVY ION SPECTROMETER SYSTEM—CONCEPTUAL DESIGN REPORT*

P.J. Lindstrom, F. Bieser,† R. Wolgast, C. McParland, H. Crawford,† and D. Rothfuss

The document summarized here describes in detail the Heavy Ion Spectrometer System (HISS), which is designed as a multi-user facility to allow many different types of multiparticle experiments to be performed with minimum overhead.

The heart of the HISS facility is a large superconducting dipole magnet described to accommodate experiments that require good momentum and spatial resolution and a large solid angle. The basic magnet will be augmented by a versatile, automated beam preparation system, a powerful computer for experiment control, data taking, and on-line interactive monitoring, and a large cave and staging area to facilitate resource sharing. HISS will thus provide many of the major components essential to performing the new generation of high-energy heavy-ion multiparticle experiments.

The HISS facility will provide the basic workbench around which experiments can be performed and the structure necessary to coordinate resources for sophisticated experiments. Adequate manpower will be provided to help interface the user with the spectrometer system. A number of experimental groups within the Nuclear Science Division at LBL plan programs at HISS, which will make a wide-ranging pool of expertise available to the outside user.

The equipment used in the HISS project includes the following:

a) The superconducting dipole magnet, which has pole tips 2 m in diameter, with a 1-m gap, and a maximum central field of 3 T. The magnet yoke is of a window-frame type, mounted on a rotatable base. The magnet parameters are shown in Table 1.

b) A large VAX II/780 computer, which forms a fast back-end analysis system to couple to existing front-end data collection systems. Experimenter-oriented software will include a versatile graphics package and a real-time multiple trajectory ray tracing package.

c) An automated beam transport system consisting of two beam lines to allow multiple experimental setups. This system can deliver clean secondary beams to a number of different focal positions.

d) A large cave area with sufficient radiation shielding to accommodate high-intensity beams and floor space for multiple experiment staging (see Fig. 1).

e) Beam-line, dipole, and cave area controls and monitor equipment.

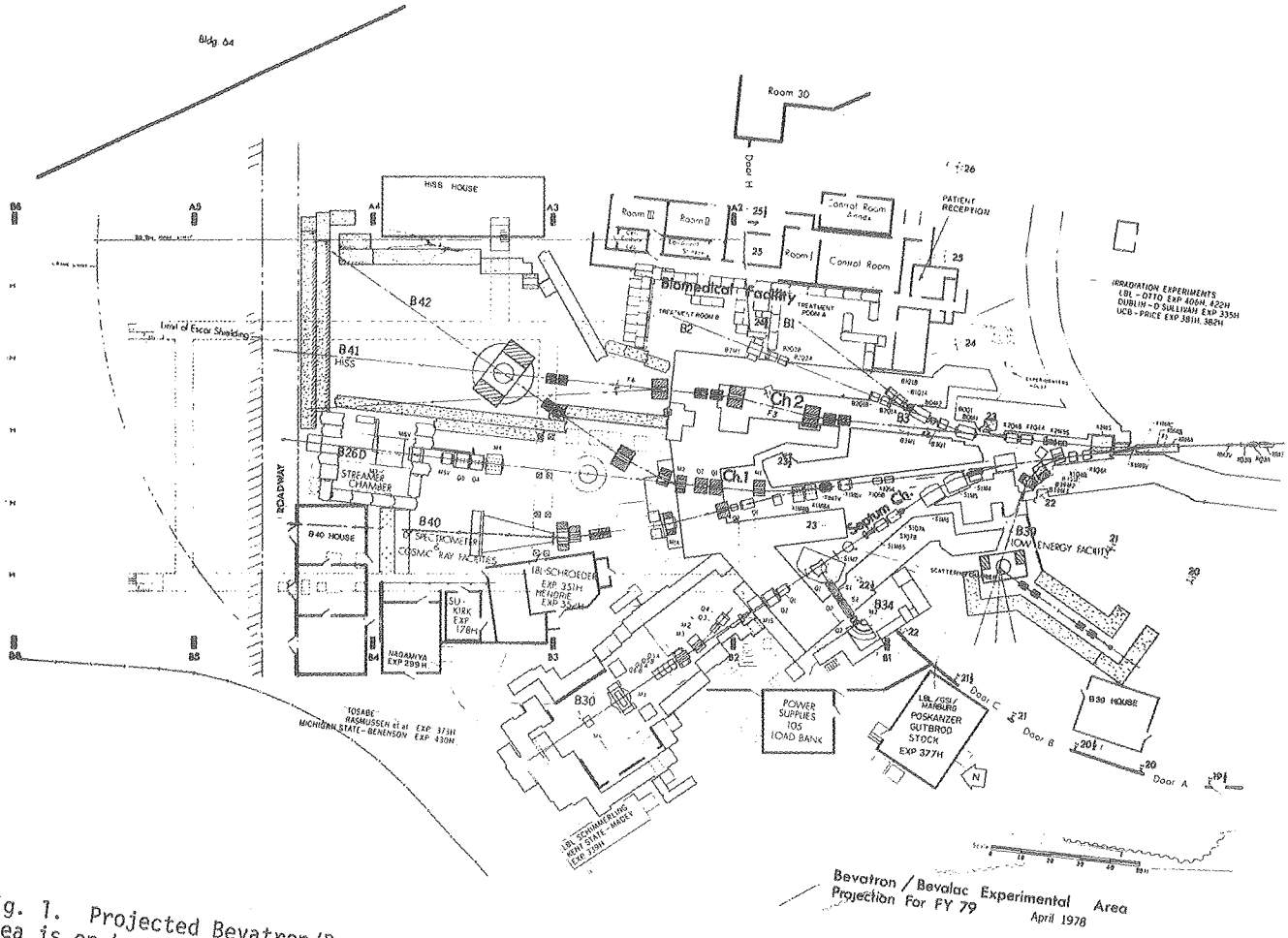

Fig. 1. Projected Bevatron/Bevalac experimental area for late 1979. HISS experimental cave area is on beam lines 41 and 42.

(XBL 787-9282)

Table 1. Magnet parameters (Ref. Dwg. 18H7966).

Central field:	3 T max., dc
Field in coil region:	4 T max.
Pole Diameter:	2 m (83 in.)
Magnet Gap:	1 m at 3 T 0.3 m (12 in.) at 3.6 T--obtained by adding pole pieces.
Yoke:	Window-frame type, total steel weight 511 tons (University of Michigan cyclotron steel at 300 tons, plus added yoke pieces).
Unobstructed azimuthal angle:	110° at the front and at the back.
Coil:	Superconducting Nb-Ti in copper matrix, 4.4°K, 4.6×10^6 ampere-turns two circular coils each with a cross section 33 cm radially by 30 cm axially, overall current density may be as low as 2400 A/cm^2.
Magnet energy:	50 MJ at 3 T, 40-in. gap.
Mounting:	Rotatable base

Table 2. HISS Cost Summary.

Engineering (Design liaison, engineering)	$ 172,000
Tech management and administration	-
Construction costs Magnet	1,073,000
Facility Implementation	482,000
U. Mich. cyclotron iron at crane hook	-
Contingency (10% of engineering and construction costs)	173,000
Total estimated cost	$1,900,000

The project will take 19 months to complete. Approximately 67% of the construction costs for this project will be spent for outside fabrication or purchase and 33% for use of LBL facilities. The project is expected to utilize 3.6 man years of engineering and 10 man years of fabrication, installation, and testing--all provided by LBL personnel. The manpower effort is distributed among the various LBL facilities and is expected to have only a modest impact on LBL staffing.

The total cost of the HISS project is summarized in Table 2. The facility will be operational in early 1980.

Footnotes

*Condensed from LBL publication PUB-5004.

†Space Sciences Laboratory, University of California, Berkeley, California 94720.

EVIDENCE AGAINST COPIOUS THRESHOLD PION PRODUCTION IN HEAVY ION COLLISIONS*

P.J. Lindstrom, H.J. Crawford,† D.E. Greiner, R. Hagstrom, and H.H. Heckman

In a recent publication, McNulty et al.[1] reported a charged-pion multiplicity of 2.1 pions/interaction in the reactions of 280-100 MeV/nucleon ^{20}Ne in Ilford G.5 nuclear emulsion. Bertsch[2] has made a theoretical calculation of the charged-pion multiplicity expected in nucleus-nucleus collisions based on an independent particle model, which includes the effects of Fermi motion; his model predicts a pion multiplicity less than 2% of that claimed by McNulty et al. Thus, if the multiplicity of 2.1 pions/interaction were true, it would represent strong evidence for the existence of a new cooperative effect in nuclear interactions. We have attempted to verify this result, but find that in the region we scanned the stopping pion multiplicity, at the 95% confidence level, is less than 0.06 of that claimed by McNulty et al. We shall show that the discrepancy can be resolved since the results of McNulty et al.[1] were based on a misidentification of fast protons as pions.

We were able to check their experimental results directly because we have on hand a stack

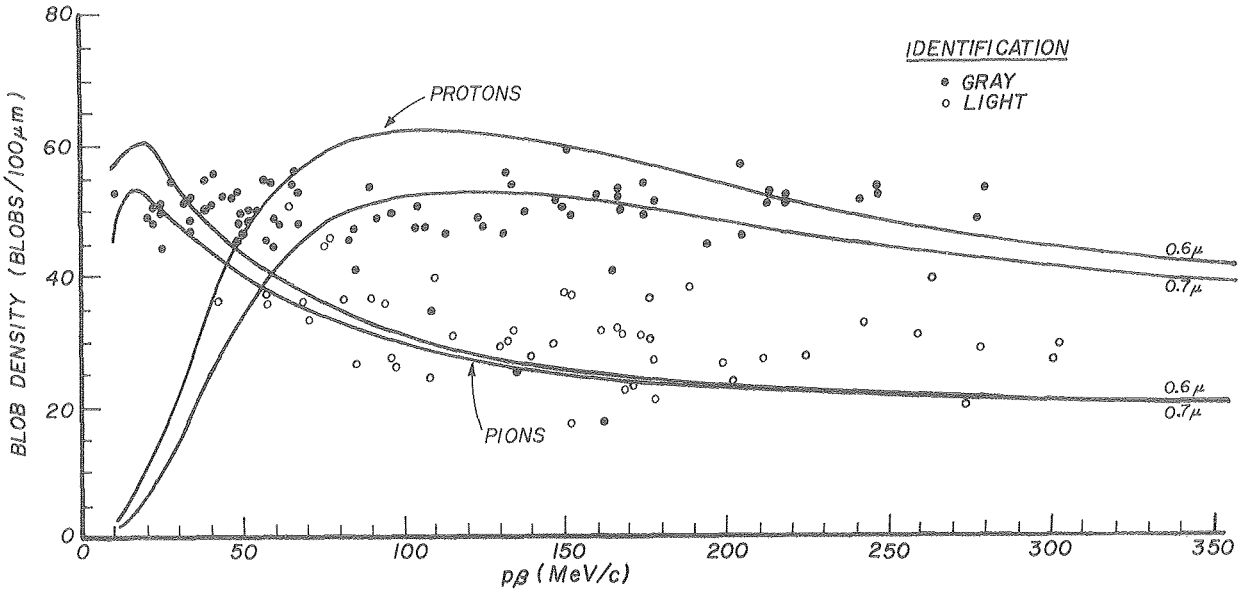

Fig. 1. Blob density vs. the product of momentum and velocity presented as Fig. 1 in McNulty et al.[1] Tracks identified by inspection as light tracks (pions) are represented as open circles and gray tracks (protons) by closed circles. As discussed in the text, values of p quoted here must be considered unreliable.

(XBL 778-2538)

of Ilford G.5 nuclear emulsion which had been exposed to 230 MeV/nucleon ^{20}Ne at the Bevalac. We checked the results of McNulty et al. by area scanning for stopping charged pions. Based on the pion production frequency as a function of ^{20}Ne energy, the pion energy spectrum, and the pion angular distribution claimed by McNulty et al.,[1,3] as well as on our measured ^{20}Ne beam profile, we calculated the stopping pion density as a function of distance into our emulsion stack.

We scanned for stopping pions and muons over a volume of 1 cm^3. We should have seen $\approx$ 50 stopping pions, according to our calculations using the data of McNulty et al., but instead we found no pions that traced back to a ^{20}Ne interaction. Because our scanning efficiency for stopping pions is above 90%, we can confidently state that the pion multiplicity, in the region of pion kinetic energies near 65 MeV, is consistent with zero and is, at the 95% confidence level, less than 0.06 of that claimed by McNulty et al.

To obtain a positive identification of the light tracks which McNulty et al. claim are pions, we quantitatively matched the types of tracks seen in the two experiments. We verified their event topology by scanning along a strip in our emulsion at a depth corresponding to a ^{20}Ne energy of 220 MeV/nucleon and analyzing the first 14 events we found. The light tracks in our emulsion are virtually identical to the light tracks McNulty et al. identified as pions.

From the calibration of our emulsion we can calculate the blob density for any particle of charge Z and velocity β. We find that any proton with energy greater than 100 MeV will give a blob density corresponding to a light track, that is, less than 40 blobs/100 μm. We also know that any proton emitted from a ^{20}Ne interaction with an energy less than 200 MeV (~31 blobs/100 μm) will stop in our emulsion. We returned to the ^{20}Ne events and found 10 light tracks whose blob densities were between 31 and 40 blobs/100 μm. The secondary tracks we followed from the ^{20}Ne interactions had blob densities indicating that they were caused by protons. If they were the tracks of pions their ranges would be ~1.5 cm; if they were the tracks of protons or heavier particles, their ranges would be ~10 cm or greater. None of these tracks were those of pions; all were consistent with protons or heavier. Therefore, most tracks classified as light tracks (and hence as pions in Ref. 1) were actually caused by protons.

In the work of McNulty et al., both the pion energy spectrum and the verification that light tracks were pions were extracted from their Fig. 1, which is reproduced here as Fig. 1. Both axes in Fig. 1 (the blob density, B, a function of velocity and charge, and the multiple-scattering parameter, $p\beta c/Z$ = momentum x velocity/charge) represent experimental measurements by McNulty et al. Their pion identification was extracted from Fig. 1 by noting that the gray and light tracks form distinct bands and the light track band is far from the computed curve of B versus $p\beta$ for protons, and is near the pion curve.

We must explain the bimodal nature of their data to completely resolve the conflicting results. The low correlation between $p\beta$ and ionization measurements shown in Fig. 1, the failure of

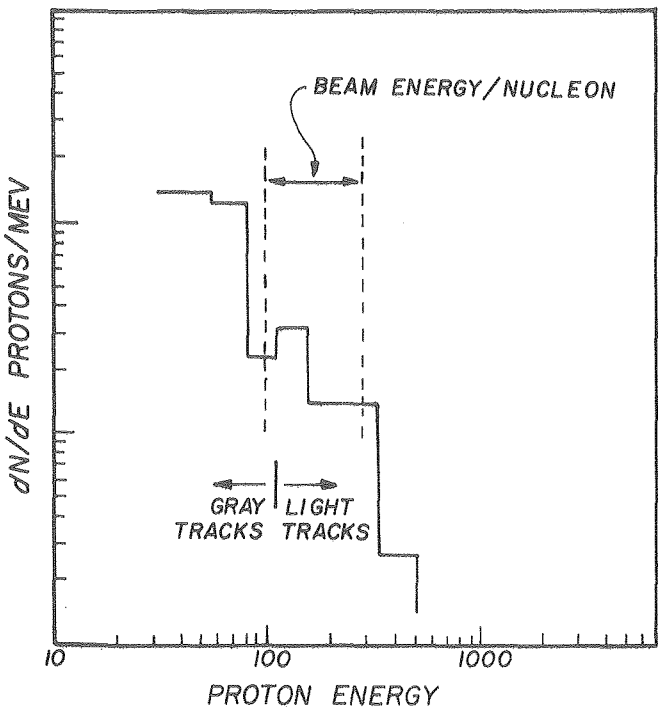

Fig. 2. The proton energy spectrum obtained from the blob density distribution assuming all tracks are protons. Note that the light tracks appear as protons whose velocities correspond to the beam velocities studied by McNulty et al.
(XBL 778-2539)

these data to predict our stopping pion density, and our observation that the bulk of the light tracks are protons lead us to examine the information contained in the blob density distribution alone. The bimodal feature of Fig. 1 is contained in the blob density distribution alone. If we assume that all the tracks are protons, we can convert the blob density distribution into a proton energy spectrum, as shown in Fig. 2. This conversion is done by using standard nuclear emulsion relations and the emulsion calibration values given in Ref. 1--minimum grain density g_{min} = 18.5 grains/100 μm and mean grain diameter, α = 0.6-0.7 μm. The low blob density events convert into a shoulder in the proton energy spectrum between 100 and 300 MeV, as shown in Fig. 2. Thus, the light tracks are compatible with beam velocity protons (fragments of the projectile). The bimodal feature of the blob density distribution is a consequence of the nonlinear relation between blob density and proton kinetic energy in nuclear emulsion.

Footnotes and References

*Condensed from Phys. Rev. Lett. 40, 93 (1978).

†Space Sciences Laboratory, University of California, Berkeley, California 94720.

1. P. J. McNulty, G. E. Farrell, R. C. Filz, W. Schimmerling, and K. G. Vosburgh, Phys. Rev. Lett. 38, 1519 (1977).

2. G. F. Bertsch, Phys. Rev. C 15, 713 (1977).

3. P. J. McNulty, private communication: pion angular distribution.

IV. THESIS ABSTRACTS

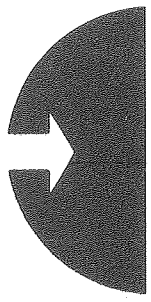

ATOMIC X-RAY PRODUCTION BY RELATIVISTIC HEAVY IONS

John G. Ioannou

(LBL-7133)

The interaction of heavy-ion projectiles with the electrons of target atoms gives rise to the production of K-, L- or higher shell vacancies in the target, which are in turn followed by the emission of characteristic x rays. The calculation of the theoretical value of the K- and k-shell vacancy production cross section has been carried out for heavy-ion projectiles of any energy.

It was found that the total vacancy production cross section for any inner shell could be subdivided into two parts--the longitudinal cross section and the transverse cross section. The longitudinal cross section comes from the instantaneous Coulomb interaction of the projectile-target system whereas the transverse cross section is due to the virtual photon or radiation field interaction of the same system. The longitudinal part is dominant at lower projectile energies whereas the transverse part contributes appreciably to the total cross section, especially for heavier elements, only at relativistic projectile energies. In this work the transverse component is calculated for the first time in detail and extensive tables of its numerical value as a function of its parameters are also given.

STUDY OF THE ROLE OF COMPLETE FUSION IN THE REACTION OF ^{48}Ca AND ^{56}Fe WITH CERIUM AND TERBIUM

David J. Morrissey

(LBL-7713)

^{48}Ca and ^{56}Fe beams from the SuperHILAC accelerator were used to irradiate thick metal foils of cerium and terbium. Product gamma-ray activities were detected offline and individual products were identified by half-life, gamma-ray energy and gamma-ray abundances. The production cross sections were iteratively fit to charge and mass dispersions to allow correction for parent decay and calculation of mass yields. From the mass yield curves, contributions from quasielastic transfer, deep inelastic transfer, and complete fusion reaction mechanisms were inferred. Complete fusion was made up of contributions from both evaporation residue and fusion-fission products for the ^{48}Ca-induced reactions. However, only fusion-fission products were detected in the ^{56}Fe-induced reactions.

Critical angular momenta for fusion were found to be 82 ± 8 h for $^{48}Ca + ^{159}Tb$ and 34 ± 5 h for $^{56}Fe + ^{140}Ce$, which can be compared with 53 ± 8 h for $^{12}C + ^{197}Au$ (Natowitz, 1970) and 86 ± 5 h for $^{40}Ar + ^{165}Ho$ (Hanappe, 1973). All of these reactions lead to essentially the same compound nucleus and seem to show the dramatic decline in complete fusion for heavy ions larger than ^{40}Ar. The prediction of this decline was found to be beyond the model calculations of Bass and the critical distance approach of Glas and Mosel.

EQUILIBRATION IN THE REACTION OF 175- AND 252-MeV ^{20}Ne WITH ^{197}Au

James B. Moulton

(LBL-7717)

The highly inelastic nuclear reaction of ^{197}Au with ^{20}Ne at 175- and 252-MeV laboratory energies is studied. Energy, elemental, and angular distributions for atomic numbers 5 to 30 (175 MeV) or 34 (252 MeV) are presented.

The means and widths of the kinetic energy spectra for detected elements are compared with a theoretical calculation. The calculation postulates thermalization of the incident projectile kinetic energy and includes one shape-vibrational degree of freedom and rigid rotation of the reaction complex. The effect of particle evaporation is considered. Good agreement of the experimental mean energies with the theory is obtained. Poorer agreement of the kinetic energy widths with the theory may be due to a low-temperature quantal effect.

The relative elemental yields are analyzed for their degree of equilibration, based on a model of diffusive nucleon exchange as described by the master equation. A similar degree of equilibration is observed for both reaction energies. The absolute elemental yields are reproduced qualitatively by employing an advanced diffusion code, coupled with calculation of the subsequent fission of heavy reaction products including the compound nucleus.

The angular distributions are analyzed with a simple model to estimate the reaction lifetime of selected elements.

THE DEPENDENCE OF DEEP-INELASTIC PROCESSES ON ENTRANCE CHANNEL ASYMMETRY AND EXCITATION ENERGY

Richard P. Schmitt

(LBL-7168)

The dependence of deep-inelastic processes on entrance channel asymmetry and on excitation energy has been investigated. Thin targets of ^{nat}At, ^{159}Tb, ^{181}Ta, and ^{197}Au have been bombarded with 620-MeV ^{86}Kr ions. Additional measurements have been performed on the reactions ^{nat}Ag + ^{86}Kr and ^{197}Au + ^{86}Kr at 506 and 732-MeV incident energy. Projectile-like fragments from these reactions were detected with particle telescopes consisting of gas ionization ΔE detectors and solid-state E detectors. The energy spectra, charge distributions, and angular distributions of these fragments were measured.

At 620 MeV, the energy spectra show that the distinction between quasi-elastic and deep-inelastic processes diminishes as the target mass is increased. The charge distributions, which are peaked at symmetry for ^{nat}Ag, tend to become increasingly asymmetric for the heavier systems. Likewise, the angular distributions exhibit a strong dependence on the entrance channel asymmetry. For the lightest system, ^{nat}Ag + ^{86}Kr, the angular distributions are essentially forward peaked, aside from a separable quasi-elastic component. For the heaviest system, ^{197}Au + ^{86}Kr, the angular distributions are side-peaked. The transition between these two regimes occurs smoothly with increasing target mass.

EMISSION OF HEAVY CHARGED PARTICLES IN RELATIVISTIC NUCLEUS-NUCLEUS COLLISIONS

John D. Stevenson

(LBL-7192)

The energy and angular distributions of nuclei produced in interactions of 500-MeV/nucleon ^{40}Ar projectiles with an Au target have been investigated. Nuclei with charge $3 \leq Z \leq 11$ were observed. Single particle inclusive spectra have been obtained at angles between 35^{o} and 85^{o}, in the energy range 20- to 60-MeV/nucleon.

The spectra decrease monotonically with the increasing energy, angle, and charge. The distributions are consistent with an isotropically emitting source recoiling with an average velocity of ~0.08 c in the beam direction. Thermal model fits to the data yield temperatures, τ, of about 60 MeV. The low recoil velocity and high temperature are shown to be in conflict with energy and momentum conservation. Two non-thermal models of emission involving expansion or rotation are explored. Although neither of these models gives good quantitative fits to the data, they do much better than the thermal model if it is constrained to be energy and momentum conserving.

The data for all energies, angles and species may be simply parameterized. When transformed into a recoiling source frame with $\beta_0 \approx 0.08$, all data points lie near ($\pm$4x) a common curve, for which the invariant cross section, $f \equiv 1/p\ d^2\sigma/d\Omega dE$, falls exponentially with increasing momentum, $f \propto e^{-p/pc}$, with a characteristic momentum $p_c \approx 340$ MeV/c.

THE NUCLEAR AND ATOMIC PHYSICS GOVERNING CHANGES IN THE COMPOSITION OF RELATIVISTIC COSMIC RAYS

Lance W. Wilson

(LBL-7723)

Many quantitative studies of relativistic cosmic ray propagation exist in which "standard" values for the input quantities are adopted in an uncritical manner. In contrast, the major emphasis of this study is on developing the proper set of formulae and error for each of the atomic and nuclear processes that govern the composition of the cosmic rays between lithium and nickel. In particular, it is shown that (1) errors of approximately a factor of two exist in the standard (Bohr) cross sections for stripping; (2) the correction function from high-energy photoionization needs to be introduced into the standard cross section for radiative attachment; and (3) because of the half-life of a neutral atom, several laboratory-based values need correction. The framework used to assemble and correct these quantities is a matrix formalism for the leaky box model similar to that used by Cowsik and Wilson in their "nested leaky box" model. It is shown that once the assumption of species-independent leakage is introduced, the matrix formalism becomes virtually identical with the standard exponential path length formalism.

V. PUBLICATIONS

PAPERS PUBLISHED AND LBL REPORTS ISSUED

1977-1978

AJZENBERG-SELOVE, F. (See KEKELIS, G. J., LBL-6557)

ALEONARD, M. M., G. J. Wozniak, P. Glässel, M. A. Deleplanque, R. M. Diamond, L. G. Moretto, R. P. Schmitt and F. S. Stephens
Evidence for Angular Momentum Fractionation in ^{86}Kr-Induced Reactions on ^{107,109}Ag, ^{165}Ho and ^{197}Au
LBL-6599, October 1977
Phys. Rev. Lett. 40, 622 (1978)

ALEONARD, M. M. (See DELEPLANQUE, M. A., LBL-7145)

ALSTER, J. (See GUTERMAN, A., LBL-7758)

ANHOLT, R.
On the Separated Atom Lorentzian Contribution to the Molecular Orbital Z-Ray Yield
LBL-4301, August 1975
J. of Phys. B. Atom. Molec. Phys. 9, 1249 (1976)

ANHOLT, R. and the TOSABE Group
K-Vacancy Production by 4.88 GeV Protons
LBL-4307, September 1975
Phys. Rev. A 14, 2103 (1976)

ANHOLT, R. (See SHIBATA, T., LBL-7189)

ARTZY, Michal, I. Perlman and F. Asaro
Imported and Local Bichrome Ware in Megiddo
LBL-4088, August 1975
J. Levant X (1978)

ASARO, F. (See ARTZY, Michal, LBL-4088)

ASCUITTO, R. J. (See MAGUIRE, C. F., LBL-7187)

ASHERY, D. (See GUTERMAN, A., LBL-7758)

BACHER, A. D. (See BRUGE, G., LBL-5823)

BAISDEN, P. A., R. E. Leber, M. Nurmia, J. M. Nitschke, M. Michel and A. Ghiorso
Isomeric States in ^{212}Bi
LBL-7708, April 1978
Phys. Rev. Lett.

BAISDEN, P. A., R. E. Leber, M. Nurmia, J. M. Nitschke, M. Michel, and A. Ghiorso
Isomeric States in ^{212}Bi
LBL-7708 Rev., June 1978

BALTZ, A. J., S. K. Kauffmann, N. K. Glendenning, and K. Pruess
Long Range Absorption in the Heavy-Ion Optical Potential
LBL-6581, August 1977
Phys. Rev. Lett. 40, 20 (1978)

BALTZ, A. J. (See P. Doll, LBL-7195)

BANASCHIK, M. V. (See SIMON, R. S., LBL-5827)

BAUER, R. (See DELEPLANQUE, M. A., LBL-7726)

BEHKAMI, A. N.
Statistical Description of Interacting Fermions and Limiting Angular Momentum
LBL-7175, January 1978

BEHKAMI, A. N. (See REGIMBART, R., LBL-7751)

BEHKAMI, A. N., and S. I. Najafi
Statistical Analysis of the Energy Level Widths in Charged Particle Induced Reactions
LBL-7752, June 1978

BIESER, F. S. (See GREINER, D. E., LBL-7163)

BINDER, I. (See OTTO, R. J., LBL-7199)

BINDER, Irwin
A Radiochemical Study of the Reactions of Heavy Ions With Gold
LBL-6526, October 1977

BINDER, I. (See MORRISSEY, D. J., LBL-7199)

BINI, M. (See GELBKE, C. K., LBL-6551)

BINI, M. (See GELBKE, C. K., LBL-6563)

BINI, M. (See DOLL, P., LBL-7195)

BINI, M. (See SCOTT, D. K., LBL-7729)

BIZARD, G. (See WOZNIAK, G. J., LBL-7158)

BIZARD, G. (See SCHMITT, R. P., LBL-6571)

BOISSON, J.-P. (See GUIDRY, M. W., LBL-4363)

BOWMAN, H. (See SHIBATA, T., LBL-7189)

BROKLOFF, R. (See CLARK, D. J., LBL-7143)

BRUGE, G., M. S. Zisman, A. D. Bacher, R. Schaeffer, C. J. Zeippen, and J. M. Loiseaux
Study of the (^{3}He,t) Reaction Mechanism via the ^{38}Ar(^{3}He,t)^{38}K Reaction at 40 MeV
LBL-5823, April 1978

BUENERD, M. (See OLMER, C., LBL-6553)

BURLEIGH, R. J., D. J. Clark and W. S. Flood
150 MeV Proton Medical Cyclotron Design Study
LBL-4085, 1975
Proc. 7th Intern. Conf. on Cyclotrons and their Applications (Birkhauser, Basel), 135, 1975

BURLEIGH, R. J., D. J. Clark, and L. R. Glasgow
Heavy Ion Booster Cyclotron Design Studies at Berkeley
LBL-4086, November 1977

Proc. 7th Intern. Conf. on Cyclotrons and their Applications (Birhauser, Basel, 604, 1975)

BUTLER, G. W. (See WESTFALL, G. D., LBL-6558)

BUTLER, P. A. (See Lee, I. Y., LBL-6512)

BYRSKI, TH. (See DELEPLANQUE, M. A., LBL-7726)

CARTWRIGHT, Brian G., Edward K. Shirk, and P. Buford Price
CR-39: A Nuclear-Track-Recording Polymer of Unique Sensitivity and Resolution.
LBL-7123, December 1977
Science

CAUVIN, B., R. P. Schmitt, G. J. Wozniak, P. Glässel, P. Russo, R. C. Jared, J. B. Moulton, and L. G. Moretto
Transitional Features Observed in the Charge and Angular Distribution of Deeply Inelastic Fragments Produced in the Reaction ^{181}Ta + 620 MeV ^{86}Kr
LBL-6506, April 1977
Nucl. Phys. A 294, 225 (1978)

CERNY, Joseph, and J. C. Hardy
Delayed Proton Radioactivities
LBL-5852, March 1977
Ann. Rev. Nucl. Sci. 27, 333 (1977)

CERNY, Joseph (See VIEIRA, D.J., LBL-6556)

CERNY, Joseph (See KEKELIS, G. J., LBL-6557)

CERNY, Joseph, D. M. Moltz, H. C. Evans, D. J. Vieira, R. F. Parry, J. M. Wouters, R. A. Gough and M. S. Zisman,
Initial Results with the Berkeley On-Line Mass Separator-RAMA
LBL-7156, November 1977
Proceedings of the On-Line Isotope Separators Workshop, Brookhaven National Laboratory, Upton, Long Island, NY, October 31-November 1, 1977

CERNY, Joseph (See JAHN, R., LBL-7157)

CERNY, Joseph and A. M. Poskanzer
Exotic Light Nuclei
1978
Sci. Amer. 238, 59 (1978)

CHARLTON, L. A., (See DELIC, G., LBL-5074)

CHIBA, J. (See SHIBATA, T., LBL-7189)

CLARK, D. J. (See BURLEIGH, R. J., LBL-4085)

CLARK, D. J. (See BURLEIGH, R. J., LBL-4086)

CLARK, D. J., R. A. Gough, W. R. Holley, and A. Jain
Systematics in the Control Settings of the Berkeley 88-Inch Cyclotron
LBL-6502, September 1977
Nucl. Inst. and Meth. 154, 1-7 (1978)

CLARK, D. J. (See STEPHENSON, E. J., LBL-6591)

CLARK, D. J., R. M. Richter, E. Zajec, R. Brokloff and J. E. Osher
Tests and Development of Duoplasmatron and Multi-aperture Heavy Ion Sources for an RF Linac
LBL-7143, November 1977

CLINE, D. (See LEE, I. Y., LBL-6512)

CONZETT, H. E. and F. Seiler
Extreme Values of Spin-Polarization Analyzing Powers in Nuclear Reactions: M-Matrix Conditions
LBL-5850, February 1977
Nucl. Phys. A 290, 93 (1977)

CONZETT, H. E. (See SEILER, F., LBL-5851)

CONZETT, H. E.
Tensor Analyzing Powers in Deuteron-Proton Elastic Scattering and the Breakup Reaction at 45.4 MeV
LBL-7799, August 1978
Presented at the International Conference on Few Body Systems and Nuclear Forces, Graz, Austria, August 24-30, 1978

CRAMER, J. G. (See DeVRIES, R. M., LBL-7103)

CRAWFORD, H. J. (See HECKMAN, H. H., LBL-6561)

DAS GUPTA, S.
An Examination of the Chemical Equilibrium Relations Used in the Fireball Model of Relativistic Heavy Ion Reactions
LBL-7734, June 1978
Comments and Addenda of Phys. Rev. C.

DAS GUPTA, S.
^{12}C on ^{12}C at 800 MeV/n; One Fireball or Two?
LBL-7749, June 1978

DELEPLANQUE, M. A. (See ALEONARD, M. M., LBL-6599)

DELEPLANQUE, M. A., I. Y. Lee, F. S. Stephens, R. M. Diamond and M. M. Aleonard
Nuclear Shapes at High Angular Momentum
LBL-7145, March 1978
Phys. Rev. Letters 40, 629 (1978)

DELEPLANQUE, M. A.
Multipolarity of Continuum γ Rays from Enhanced Angular Correlation Measurements
LBL-7726, May 1978
Phys. Rev. Letters

DELIC, G., K. Pruess, L. A. Charlton, and N. K. Glendenning
Effect of Polarization of Shell-Model States in Reaction Calculations for ^{40}Ca(^{16}O,^{15}N)^{41}Sc if$_{7/2}$

LBL-5074, October 1976
Phys. Lett. B 69, 20 (1977)

de MEIJER, R. J. (See JAHN, R., LBL-7157)

de SAINT-SIMON, M., R. J. Otto, and G. T. Seaborg
Relative Thresholds for Production of Iodine Isotopes from Fusion and Transfer-Induced Fission Reactions
LBL-7114, November 1977

DeVRIES, R. M., D. A. Goldberg, J. W. Watson, M. S. Zisman, and J. G. Cramer
The Transition Between Light- and Heavy-Ion Elastic Scattering
LBL-7103, October 1977
Phys. Rev. Lett. 39, 450 (1977)

DIAMOND, R. M. (See SIMON, R. S., LBL-5827)

DIAMOND, R. M. (See LEE, I. Y., LBL-6512)

DIAMOND, R. M. (See SIMON, R. S., LBL-6531)

DIAMOND, R. M. (See ALEONARD, M. M., LBL-6599)

DIAMOND, R. M. (See DELEPLANQUE, M. A., LBL-7145)

DIAMOND, R. M. (See DELEPLANQUE, M. A., LBL-7726)

DIAMOND, R. M. (See HUBEL, H., LBL-7750)

DIAMOND, R. M. (See KLEINHEINZ, P., 1978)

DOLL, P., M. Bini, D. L. Hendrie, S. K. Kauffmann, J. Mahoney, A. Menchaca-Rocha, D. K. Scott, T. J. M. Symons, K. Van Bibber, Y. P. Viyogi, H. Weiman, and A. J. Baltz
LBL-7195, March 1978
Phys. Lett. B

DOLL, P. (See SCOTT, D. K., LBL-7729)

DOLL, P.
Nuclear Hole States as a Probe of the Nuclear Many Body System
LBL-7790, August 1978

DONANGELO, R. (See GUIDRY, M. W., LBL-4363)

DONANGELO, R., L. F. Oliveira, J. O. Rasmussen, and M. W. Guidry
Classical-Limit Description of Rotation-Vibrational Band Excitation in Deformed Even-Even Nuclei
LBL-7720, May 1978

DONANGELO, Raul (See OLIVEIRA, Luiz F., LBL-7731)

EJIRI, H. (See SHIBATA, T., LBL-7189)

EVANS, H. C. (See CERNY, Joseph, LBL-7156)

FLOOD, W. S. (See BURLEIGH, R. J., LBL-4085)

FOWLER, M. M. (See OTTO, R. J., LBL-6529)

FOWLER, M. M. (See MORRISSEY, D. J., LBL-7199)

FRIEDLANDER, Erwin, M. and Richard M. Weiner
"Small," "Large," and "Very Large" Transverse Momenta in a Unified Hydrodynamical Description
LBL-7724, May 1978

FRIEDLANDER, Erwin M.
Statistical Inference from Inclusive Spectra in Multihadron Production: A Caveat
LBL-7733, May 1978

GARPMAN, Sten I. A., Norman K. Glendenning, and Yasha Karant
Thermodynamic Behavior of Non-Strange Baryonic Matter
LBL-7742, June 1978
Nucl. Phys.

GELBKE, C. K., C. Olmer, M. Buenerd, D. L. Hendrie J. Mahoney, M. C. Mermaz and D. K. Scott
Energy Dependence of Peripheral Reactions Induced by Heavy Ions
LBL-5826, June 1977
Phys. Reports 42, 311 (1978)

GELBKE, C. K., D. K. Scott, M. Bini, D. L. Hendrie, J. L. Laville, J. Mahoney, M. C. Mermaz, and C. Olmer
Influence of Intrinsic Nucleon Motion on Energy Spectra and Angular Distributions for ^{16}O-Induced Reactions at 20 MeV/A
LBL-6551
Phys. Lett. B 70, 415 (1977).

GELBKE, C. K. (See OLMER, C., LBL-6553)

GELBKE, C. K., M. Bini, C. Olmer, D. L. Hendrie, J. L. Laville, J. Mahoney, M. C. Mermaz, D. K. Scott, and H. H. Wieman
Particle-Particle Angular Correlations in Peripheral Heavy-Ion Reactions
LBL-6563
Phys. Lett. B 71, 83 (1977)

GELBKE, C. K. (See SCOTT, D. K., LBL-7729)

GELBKE, C. K. (See GUTERMAN, A., LBL-7758)

GHIORSO, A. (See NITSCHKE, J. M., LBL-6534 Rev.)

GHIORSO, A. (See Otto, R., LBL-7104)

GHIORSO, A. (See BAISDEN, P. A., LBL-7708)

GLASGOW, L. R. (See BURLEIGH, R. J., LBL-4086).

GLASSEL, P. (See CAUVIN, B., LBL-6506)

GLASSEL, P. (See WOZNIAK, G. J., LBL-6532)

GLASSEL, P. (See ALEONARD, M. M., LBL-6599)

GLASSEL, P. (See WOZNIAK, G. J., LBL-7158)

GLENDENNING, N. K. and Georg Wolschin
Indirect Transition in Two-Nucleon Transfer Reactions Between Heavy Ions
LBL-5052, July 1976
Nucl. Phys. A 281, 486-508 (1977)

GLENDENNING, N. K. (See DELIC, G., LBL-5074)

GLENDENNING, N. K. (See BALTZ, A. J., LBL-6581)

GLENDENNING, Norman K. and Yasha Karant
Can the Hadronic Mass Spectrum be Discovered Through High Energy Nuclear Collisions?
LBL-6590, August 8, 1977
Phys. Rev. Lett. 40, 374 (1978)

GLENDENNING, Norman K.
Nuclear Collisions at Very High Energy
LBL-6597, August 31, 1977
Invited paper presented at the Symposium on Future Accelerators, Bombay, India, September 19, 1977

GLENDENNING, Norman K.
Very High Energy Nuclear Collisions: The Asymptotic Hadron Spectrum, Anti-Nuclei, Hyper-Nuclei, and Quark Phase
LBL-7165, January 2, 1978
Invited paper presented at the Workshop on Gross Nuclear Properties of Nuclei and Nuclear Excitations, Hirschegg, Austria, January 16, 1978

GLENDENNING, Norman K.
Models of High Energy Nuclear Collisions
LBL-7739, June 1978
Presented at the NATO Advanced Study Institute on Theoretical Methods in Medium-Energy and Heavy-Ion Physics, Madison, WI, June 12-23, 1978

GLENDENNING, Norman (See GARPMAN, Sten I. A., LBL-7742)

GLENN, Rowe, Martin Salomon, Rubin H. Landau
An Energy-Dependent Phase Shift Analysis of Pion-Nucleon Scattering Below 400 MeV
LBL-7182, February 1978
Phys. Rev. C 18, 584 (1978)

GOLDBERG, D. A. (See DeVries, R. M., LBL-7103)

GOLDHABER, Alfred S., and Harry H. Heckman
High Energy Interactions of Nuclei
LBL-6570, March 1978
Ann. Rev. of Nucl. Sci.

GOLDHABER, Alfred S.
Large Baryon Densities Attainable in High Energy Nuclear Collisions
LBL-7123, November 1977
Phys. Rev. Lett.

GOLDHABER, Alfred S.
Volume Versus Surface Sampling of Maxwellian Distributions in Nuclear Reactions
LBL-7146
Phys. Rev. C 17, 2243 (1978)

GOSSET, J., J. I. Kapusta, and G. D. Westfall
Calculations with the Nuclear Firestreak Model
LBL-7139, April 1978

GOUGH, R. A. (See CLARK, D. J., LBL-6502)

GOUGH, R. A. (See VIEIRA, D. J., LBL-6556)

GOUGH, R. A. (See STEPHENSON, E. J., LBL-6591)

GOUGH, R. A. (See CERNY, Joseph, LBL-7156)

GREINER, D. E. (See HECKMAN, H. H., LBL-3656)

GREINER, D. E. (See HECKMAN, H. H., LBL-6561)

GREINER, Douglas, Andres Sandoval, Miklos Gyulassy
LBL-7141, November 1977
Proceedings of the Special Bevalac Research Meetings
November 1-3, 1977

GREINER, D. E., F. S. Bieser, and H. H. Heckman
LBL-7163, December 1977
ISEE-C HKH High Energy Cosmic Rays
IEEE Geoscience Elect.

GUIDRY, M. W., R. Donangelo, J. O. Rasmussen, and J.-P. Boisson
The Classical-Limit S-Matrix and Orbital Dynamics in Semiclassical Coulomb Excitation Theory
LBL-4363, July 13, 1977
Nucl. Phys. A 295, 482-512 (1978)

GUIDRY, M. W. (See DONANGELO, R., LBL-7720)

GUTBROD, H. H.
Single Particle Inclusive and Correlation Measurements
LBL-7730, May 1978
Presented at the Relativistic Heavy-Ion Physics Symposium, GSI, Darmstadt, West Germany
March 5-8, 1978

GUTERMAN, A., D. Ashery, J. Alster, D. K. Scott, M. S. Zisman, C. K. Gelbke, H. H. Wieman, and D. L. Hendrie
Excitation of Giant Resonances in ^{208}Pb by Inelastic Scattering of ^{16}O
LBL-7758, July 1978
Phys. Rev. Lett.

GYULASSY, M. and S. K. Kauffmann
Pion Multiplicity Distributions in Heavy Ion Collisions
LBL-6593, October 1977

GYULASSY, Miklos
Comparisons of Models of High Energy Heavy Ion Collisions
LBL-6594, September 1977

GYULASSY, Miklos (See GREINER, Douglas, LBL-7141)

GYULASSY, M. (See VAUTHERIN, D., LBL-7197)

GYULASSY, M. (See KAUFFMANN, S. K., LBL-7700)

GYULASSY, Miklos
Coherent Pion Processes in Nuclear Collisions
LBL-7704, April 1978

GYULASSY, Miklos (See LANDAU, R. H., LBL-7719)

HARDY, J. C. (See CERNY, Joseph, LBL-5852)

HECKMAN, H. H., D. E. Greiner, P. J. Lindstrom, and H. Shwe
Fragmentation of ^{4}He, ^{12}C, ^{14}N, and ^{16}O Nuclei in Nuclear Emulsion at 2.1 GeV/Nucleon
LBL-3656, July 1977
Phys. Rev. C 17, 1735 (1978)

HECKMAN, H. H., H. J. Crawford, D. E. Greiner, P. J. Lindstrom, and Lance W. Wilson
Central Collisions Produced by Relativistic Heavy Ions in Nuclear Emulsion
LBL-6561, July 1977
Phys. Rev. C 17, 1651 (1978)

HECKMAN, Harry H.
High Energy Interaction of Nuclei
LBL-6570, March 1978
Ann. Rev. of Nucl. Sci.

HECKMAN, H. H. (See GREINER, D. E., LBL-7163)

HECKMAN, Harry H.
High Energy Collisions of Nuclei: Experiments 1978
Fizika 9 Supplement 4, 595-622 (1977)
(Proceedings of the Int. Symp. on Nuclear Collisions and Their Microscopic Description, Bled, September 1977).

HENDRIE, D. L. (See GELBKE, C. K., LBL-6551)

HENDRIE, D. L. (See OLMER, C., LBL-6553)

HENDRIE, D. L. (See GELBKE, C. K. LBL-6563)

HENDRIE, David L.
Heavy Ion Reactions in the Transition Region
LBL-7167, November 1977
Invited Paper at the International Symposium on Nuclear Physics at Cyclotron Energies, Calcutta, India, September 14-16, 1977

HENDRIE, D. L. (See MAGUIRE, C. F., LBL-7187)

HENDRIE, D. L. (See P. DOLL, LBL-7195)

HENDRIE, D. L. (See SCOTT, D. K., LBL-7729)

HENDRIE, D. L. (See GUTERMAN, A., LBL-7758)

HERSKIND, B. (See DELEPLANQUE, M. A., LBL-7726)

HERSKIND, B. (See HUBEL, H., LBL-7750)

HOLLEY, W. R. (See CLARK, D. J., LBL-6502)

HOLLEY, W. R., (See STEPHENSON, E. J., LBL-6591)

HUBEL, H. (See DELEPLANQUE, M. A., LBL-7726)

HUBEL, H., U. Smilansky, R. M. Diamond, F. S. Stephens, and B. Herskind
Average Lifetimes of Collective Transitions in the Spin 30-50 Region
LBL-7750, June 1978
Phys. Rev. Lett.

HYDE, E. K. (See WESTFALL, G. D., LBL-6558)

IOANNOU, John G.
Atomic X-ray Production by Relativistic Heavy Ions
LBL-7133, December 1977
Ph.D. Thesis

IOANNOU, J. G. (See SHIBATA, T., LBL-7189)

JAHN, R (See KEKELIS, G. J., LBL-6557)

JAHN, R., D. P. Stahel, G. J. Wozniak, R. J. de Meijer, and Joseph Cerny
Survey of the (, ^{2}He) Reaction on 1p- and 2s1d-Shell Nuclei
LBL-7157, March 1978
Phys. Rev. C 18, 9 (1978)

JAHNKE, U. (See MAGUIRE, C. F., LBL-7187)

JAIN, A. (See CLARK, D. J., LBL-6502)

JAIN, A., (See STEPHENSON, E. J., LBL-6591)

JARED, R. C., (See CAUVIN, B., LBL-6506)

JARED, R. C. (See WOZNIAK, G. J., LBL-7158)

JELTEMA, B. D. (See STAHEL, D. P., LBL-6508)

KAPUSTA, J. I.
Particle Production in the Nuclear Fireball Model
LBL-6504, April 1977
Phys. Rev. C 16, 1493 (1977)

KAPUSTA, J. I., (See GOSSET, J., LBL-7139)

KAPUSTA, Joseph I.
Quantum Chromodynamics at High Temperature
LBL-7745, June 1978
Nucl. Phys. B

KARANT, Yasha (See GLENDENNING, N. K., LBL-6590)

KARANT, Yasha (See GARPMAN, Sten I. A., LBL-7742)

KAUFFMANN, S. K. (See BALTZ, A. J., LBL-6581)

KAUFFMANN, S. K.
Pion Multiplicity Distributions in Heavy Ion Collisions
LBL-6593, October 1977

KAUFFMANN, S. K.
Time Dependence of Interaction Picture Transition Amplitudes to all Orders of Perturbation Theory
LBL-7140, January 1978

KAUFFMANN, S. K. (See DOLL, P., LBL-7195)

KAUFFMANN, S. K. and M. Gyulassy
Multiplicity Distribution of Created Bosons: The Combinants Tool
LBL-7700, March 1978

KEKELIS, G. J., M. S. Zisman, D. K. Scott, R. Jahn, D. J. Vieira, Joseph Cerny, and F. Ajzenberg-Selove
Masses of the Unbound Nuclei ^{16}Ne, ^{15}F, and ^{12}O
LBL-6557, September 1977
Phys. Rev. C 17, 1929 (1978)

KLEINHEINZ, P., A. M. Stefanini, M. R. Maier, R. K. Sheline, R. M. Diamond, and F. S. Stephens
Different Structure Collective Bands in the N=87 Nuclei ^{149}Sm, ^{151}Gd and ^{153}Dy
Nucl. Phys. A 283, 189 (1977)

KUMAR, K. (See MAGUIRE, C. F., LBL-7187)

LANDAU, R. H.
The Connection Between Elastic and Quasi-Elastic Pion Scattering From Nuclei
LBL-7166, December 1977
Phys. Rev. Lett.

LANDAU, Rubin H.
Inclusive Pion Production in Relativistic Proton Collisions with Nuclei, A Reexamination
LBL-7169, January 1978
Phys. Rev. C 17, 2144 (1978)

LANDAU, Rubin H. (See ROWE, Glenn, LBL-7182)

LANDAU, R. H.
Scaling and Non-Scaling of Inclusive Pion Production in Nuclear Collisions
LBL-7719, April 1978
Phys. Rev. C

LAVILLE, J. L. (See GELBKE, C. K., LBL-6551)

LAVILLE, J. L. (See GELBKE, C. K., LBL-6563)

LAVILLE, J. L. (See SCOTT, D. K., LBL-7729)

LEBER, R. E. (See NITSCHKE, J. M., LBL-6534 Rev)

LEBER, R. E. (See YASHITA, S., LBL-6547)

LEBER, R. E. (See OTTO, R., LBL-7104)

LEBER, R. E. (See BAISDEN, P. A., LBL-7708)

LEBER, R. E. (See BAISDEN, P. A., LBL-7708 Rev.)

LEE, D. (See GHIORSO, A., LBL-7104)

LEE, D. (See MORRISSEY, D. J., LBL-7199)

LEE, D. (See MORRISSEY, D. J., LBL-7711)

LEE, I. Y. (See DELEPLANQUE, M. A., LBL-7145)

LEE, I. Y., D. Cline, P. A. Butler, R. M. Diamond, J. O. Newton, R. S. Simon, and F. S. Stephens
Determination of Softness in ^{192,194,196}Pt from Coulomb Excitation with ^{136}Xe Projectiles
LBL-6512, June 1977
Phys. Rev. Lett. 39, 684 (1977)

LICHTNER, P. (See PRUESS, K., LBL-6524)

LILJENZIN, J. O. (See MORRISSEY, D. J., LBL-7199)

LINDSTROM, P. J., (See HECKMAN, H. H., LBL-3656)

LINDSTROM, P. J. (See HECKMAN, H. H., LBL-6561)

LOISEAUX, J. M. (See BRUGE, G., LBL-5823)

LOVELAND, W., R. J. Otto, D. J. Morrissey, and G. T. Seaborg
Large Collision Residues and Nuclear Fission in Relativistic Heavy Ion Reactions
LBL-6513, April 1977
Phys. Rev. Lett. 39, 320 (1977)

LOVELAND, W., R. J. Otto, D. J. Morrissey, and G. T. Seaborg
Further Studies of Large Collision Residues in Relativistic Heavy Ion Reactions with Heavy Nuclei
LBL-6522, May 1977
Phys. Lett. B 69, 28 (1977)

LOVELAND, W. (See MORRISSEY, D. J., LBL-6539 Rev.)

LOVELAND, W. (See MORRISSEY, D. J., LBL-6579)

LOVELAND, W. D. (See OTTO, R. J., LBL-7188)

LOVELAND, W. (See MORRISSEY, D. J., LBL-7199)

LOVELAND, W. D. (See OTTO, R. J., LBL-7710)

MACFARLANE, M. H. (See OLMER, C., LBL-6553)

MAGUIRE, C. F., D. L. Hendrie, U. Jahnke, J. Mahoney, D. K. Scott, J. S. Vaagen, R. J. Ascuitto, and K. Kumar
Observation of Striking Shape Differences Between 2_1^+ Angular Distributions for Heavy-Ion Induced Two Neutron Stripping and Pickup Reactions in Transitional Samarium Nuclei
LBL-7187, February 6, 1978
Phys. Rev. Lett. 40, 358 (1978)

MAHONEY, J. (See GELBKE, C. K., LBL-6551)

MAHONEY, J. (See OLMER, C., LBL-6553)

MAHONEY, J. (See GELBKE, C. K., LBL-6563)

MAHONEY, J. (See MAGUIRE, C. F., LBL-7187)

MAHONEY, J. (See DOLL, P., LBL-7195)

MAHONEY, J. (See SCOTT, D. K., LBL-7729)

MAIER, M. R. (See KLEINHEINZ, P., 1978)

MANTZOURANIS, G.
The Statistics of the Fireball Model
LBL-7712, April 1978
Phys. Rev. C

MANTZOURANIS, G.
A Relation Between the Nuclear Dynamics and the Renormalization Group
LBL-6598, November 1977

MANTZOURANIS, G. (See MORETTO, L. G., LBL-7732)

MARSH, W. R. (See MORRISSEY, D. J., LBL-6579)

MASRI, Y. El, (See SIMON, R. S., LBL-6531)

MASSMANN, H. (See RING, P., LBL-6538)

MATHEWS, G. J., G. J. Wozniak, R. P. Schmitt, and L. G. Moretto.
Evidence for the Characterization of Heavy-Ion Reactions by the Ratio E/B
LBL-5812, November 1976
Z. Phys. A 283, 247-252 (1977)

MATHEWS, G. J. and V. E. Viola, Jr.
On the Light Element Abundances, Galactic Evolution, and a More Sensitive Indicator of the Universal Baryon Density
LBL-7709, April 1977
Astrophys. J.

MEKJIAN, A.
Explosive Nucleosynthesis, Equilibrium Thermodynamics, and Relativistic Heavy-Ion Collisions
LBL-6545, June 1977
Phys. Rev. C 17, 1051 (1978)

MEKJIAN, Aram
Correlations and Total Muon Capture Rates
LBL-7793, August 1978
Presented at the Banff Intern. Conf. on Medium-Energy Physics, Banff, Canada, August 21-31, 1978

MENCHACA-ROCHA, A. (See DOLL, P., LBL-7195)

MENCHACA-ROCHA, A. (See SCOTT, D. K., LBL-7729)

MERMAZ, M. C. (See GELBKE, C. K., LBL-6551)

MERMAZ, M. (See OLMER, C., LBL-6553)

MERMAZ, M. C. (See GELBKE, C. K., LBL-6563)

MERMAZ, M. C. (See SCOTT, D. K., LBL-7729)

MICHEL, M. (See BAISDEN, P. A., LBL-7708 Rev.)

MOLTZ, D. M. (See CERNY, Joseph, LBL-7156)

MORETTO, L. G. (See MATHEWS, G. J., LBL-5812)

MORETTO, L. G. (See CAUVIN, B., LBL-6506)

MORETTO, L. G. (See WOZNIAK, G. J., LBL-6532)

MORETTO, L. G. (See SCHMITT, R. P., LBL-6571)

MORETTO, L. G.
Charge and Angular Distributions as well as Sequential Decay and γ Ray Emission in Heavy Ion Collisions Viewed in the Light of the Diffusion Model
LBL-6587, October 1977

MORETTO, L. G., J. S. Sventek
Theoretical Correlation Between Energy Dissipation, Angular Momentum Transfer and Charge Diffusion in Deep Inelastic Reactions
LBL-6596, September 1977

MORETTO, L. G. (See ALEONARD, M. M., LBL-6599)

MORETTO, L. G. (See WOZNIAK, G. J., LBL-7158)

MORETTO, L. G., J. Sventek, and G. Mantzouranis
The Giant El Mode and Its Energy Broadening from the Charge Distributions in Heavy-Ion Reactions
LBL-7732, July 1978
Phys. Rev. Lett.

MORETTO, L. G. (See REGIMBART, R., LBL-7751)

MORETTO, Luciano
Angular Momentum Transfer in Deep Inelastic Scattering Experiment and Theory
LBL-7755, July 1978
South African J. Phys.

MORETTO, L. G. and R. P. Schmitt
Deep-Inelastic Processes: A Workbench for Large Scale Motion in Nuclear Matter
LBL-7757, July 1978
Presented at the Intern. Conf. on Nuclear Interactions, Australian Academy of Science, Canberra City, Australia, August 28-September 2, 1978

MORRISSEY, D. J. (See LOVELAND, W., LBL-6513)

MORRISSEY, D. J. (See LOVELAND, W., LBL-6522)

MORRISSEY, D. J., W. Loveland, R. J. Otto, and G. T. Seaborg
Lowered Fusion Cross Section in the Quadruply Magic Heavy Ion System, $^{48}Ca + ^{208}Pb$
LBL-6539 Rev., October 1977
Phys. Lett. B 74, 35 (1978)

MORRISSEY, D. J., W. R. Marsh, R. J. Otto, W. Loveland, and G. T. Seaborg
Calculation of Target Residue Mass and Charge Distributions in Relativistic Heavy Ion Reactions
LBL-6579, March 1978
Phys. Rev. C

MORRISSEY, D. J. (See OTTO, R. J., LBL-7188)

MORRISSEY, D. J., R. J. Otto, D. Lee, J. O. Liljenzin, I. Binder, M. M. Fowler, W. Loveland, and G. T. Seaborg
An Interactive Computerized System for the Analysis of Gamma Ray Spectra From Heavy Ion Nuclear Reactions
LBL-7199, March 1978

MORRISSEY, D. J. (See OTTO, R. J., LBL-7710)

MORRISSEY, D. J., D. Lee, R. J. Otto, and G. T. Seaborg
Measurement of the Product Mass Distributions from Heavy-Ion Induced Nuclear Reactions, I: Gamma-Ray Spectrometer Product Identification
LBL-7711, April 1978
Nuclear Instruments and Methods

MORRISSEY, David Joseph
Study of the Role of Complete Fusion in the Reaction of ^{48}Ca and ^{56}Fe with Cerium and Terbium
LBL-7713, May 1978
Ph. D. Thesis

MOULTON, J. B., E. J. Stephenson, R. P. Schmitt, and G. J. Wozniak
A New Method for Calibrating the Pulse Height Defect in Solid State Detectors
LBL-7101, October 1977

MOULTON, James Bennett
Equilibration in the Reaction of 175 and 252 MeV ^{20}Ne with ^{197}Au
LBL-7717, June 1978

MOULTON, J. B. (See CAUVIN, B., LBL-6506)

MYERS, WILLIAM D.
A Model for High Energy Heavy Ion Collisions
LBL-6569, August 1977
Nucl. Phys. A 296, 177 (1978)

NAGAMIYA, S. (See SHIBATA, T., LBL-7189)

NAJAFI, S. I. (See BEHKAMI, A. N., LBL-7752)

NAKAI, K. (See SHIBATA, T., LBL-7189)

NEWTON, J. O. (See SIMON, R. S., LBL-5827)

NEWTON, J. O. (See LEE, I. Y., LBL-6512)

NEWTON, J. O. (See SIMON, R. S., LBL-6531)

NITSCHKE, J. M., R. E. Leber, M. J. Nurmia, and A. Ghiorso
Observations in the Reaction of Two Magic Nuclei
LBL-6534 Rev., January 1978

NITSCHKE, J. Michael
Experimental Prospects for the Synthesis and Detection of Superheavy Elements
LBL-7705, March 28, 1978
Invited Talk Given at the Intern. Symp. on Superheavy Elements, Lubbock, TX, March 9-11, 1978

NITSCHKE, J. (See BAISDEN, P. A., LBL-7708)

NITSCHKE, J. M. (See BAISDEN, P. A., LBL-7708 Rev.)

NURMIA, M. J. (See NITSCHKE, J. M., LBL-6534 Rev.)

NURMIA, M. (See BAISDEN, P. A., LBL-7708)

NURMIA, M. (See BAISDEN, P. A., LBL-7708 Rev.)

OLIVEIRA, L. F. (See DONANGELO, R., LBL-7720)

OLIVEIRA, Luiz F., Raul Donangelo, and John O. Rasmussen
Abrasion-Ablation Calculations of Large Fragment Yields from Relativistic Heavy Ion Reactions
LBL-7731, May 1978
Phys. Rev. C

OLMER, C. (See GELBKE, C. K., LBL-6551)

OLMER, C., M. Mermaz, M. Buenerd, C. K. Gelbke, D. L. Hendrie, J. Mahoney, D. K. Scott, M. H. Macfarlane, and S. C. Pieper
Energy Dependence of Elastic Scattering and One-Nucleon Transfer Reactions Induced by ^{160} on ^{208}Pb - II.
LBL-6553, December 1977
Phys. Rev. C 18, 205 (1978)

OLMER, C. (See GELBKE, C. K., LBL-6563)

OLMER, C. (See SCOTT, D. K., LBL-7729)

OSHER, J. E. (See CLARK, D. J., LBL-7143)

OTTO, R. J. (See LOVELAND, W., LBL-6513)

OTTO, R. J. (See LOVELAND, W., LBL-6522)

OTTO, R. J., M. M. Fowler, and G. T. Seaborg
Recoil Range Distributions of Heavy Mass Products in Deep Inelastic Reactions with Gold and Uranium Targets
LBL-6529, October 1977
Phys. Rev. C 17, 1071 (1978)

OTTO, R. J. (See MORRISSEY, D. J., LBL-6539 Rev.)

OTTO, R. J. (See MORRISSEY, D. J., LBL-6579)

OTTO, R. J., A. Ghiorso, D. Lee, R. E. Leber, S. Yashita, and G. T. Seaborg
Search for Superheavy Elements Produced in the ^{136}Xe + ^{238}U Reaction and an Upper Limit Cross Section for the ^{nat}Gd(^{136}Xe,X)^{212}Pb Reaction
LBL-7104, October 1977
Radiochim. Acta 24, 3-7 (1977)

OTTO, R. J. (See de SAINT-SIMON, M., LBL-7114)

OTTO, R. J., D. J. Morrissey, G. T. Seaborg, and W. D. Loveland
Large Contribution of Deep Inelastic Processes to Reactions of ^{40}Ar and ^{48}Ca with ^{238}U
LBL-7188, February 6, 1978
Zeitschrift fur Physik A 287, 97 (1978)

OTTO, R. J. (See MORRISSEY, D. J., LBL-7199)

OTTO, R. J., D. J. Morrissey, G. T. Seaborg, and W. D. Loveland
New Experimental Insights into the Production of Superheavy Elements Using Heavy Ion Reactions
LBL-7710, April 1978
Presented at the International Symposium on Superheavy Elements, Lubbock, TX, March 9-11, 1978.

OTTO, R. J. (See MORRISSEY, D. J., LBL-7711)

PARRY, R. F. (See CERNY, Joseph, LBL-7156)

PERLMAN, I. (See ARTZY, Michal, LBL-4088)

PIEPER, S. C. (See OLMER, C., LBL-6553)

POSKANZER, A. M. (See WESTFALL, G. D., LBL-6558)

POSKANZER, Arthur M.
Central Collisions of Relativistic Nuclei
LBL-7762, July 1978
Invited paper for the International Conference on the Dynamical Properties of Heavy Ion Reactions, Johannesburg, S. Africa, 1-3 August, 1978

POSKANZER, Arthur M.
Relativistic Heavy Ion Reactions
J. Phys. 44, 760 (1978)
Invited paper presented at The International Conference on Nuclear Structure, Tokyo, Japan, September 5-10, 1977

PRICE, P. Buford (See CARTWRIGHT, Brian G., LBL-7123

PRICE, P. B., and J. Stevenson
Mass-Independent Correlation of Fragment Velocity and Source Velocity in Nucleus-Nucleus and Proton-Nucleus Collisions.
LBL-7702, March 14, 1978
Phys. Lett. B

PRUESS, K. (See DELIC, G., LBL-5074)

PRUESS, K, and P. Lichtner
Calculations of Single Particle Polarization Using a Realistic Two-Center Shell Model
LBL-6524, May 1977
Nucl. Phys. A 291, 475-509 (1977)

PRUESS, K. (See BALTZ, A. J., LBL-6581)

PRUESS, K.
Amplitude for Transitions Between Molecular (Two-Center) Channels
LBL-7747, June 1978
Phys. Rev. Lett.

RAD, F. N. (See SEILER, F., LBL-5851)

RADI, Hafez M. A., A. A. Shihab-Eldin, and J. O. Rasmussen
Configuration Mixed Shell Model Relative Alpha Decay Rate Calculations for Spherical Doubly Odd Nuclei (^{212}At and ^{212m}At)
LBL-5071, October 1976)
Phys. Rev. C 15, 1917 (1977)

RAICH, D. G. (See SOINSKI, A., LBL-6516)

RASMUSSEN, J. O. (See GUIDRY, M. W., LBL-4363)

RASMUSSEN, J. O. (See RADI, Hafez M., LBL-5071)

RASMUSSEN, J. O. (See SOINSKI, A., LBL-6516)

RASMUSSEN, J. O. (See RING, P., LBL-6538)

RASMUSSEN, J. O. (See DONANGELO, R., LBL-7720)

RASMUSSEN, J. O. (See SHIBATA, T., LBL-7189)

RASMUSSEN, John O. (See OLIVEIRA, Luiz F., LBL-7731)

RAUSCHER, E. A. (See SOINSKI, A., LBL-6516)

RAUSCHER, E. A. (See SHIBATA, T., LBL-7189)

REGIMBART, R., A. N. Behkami, G. J. Wozniak, R. P. Schmitt, J. S. Sventek, and L. G. Moretto
Ray Multiplicities from a Diffusion Model Incorporating One-Body Dissipation.
LBL-7751, June 1978
Phys. Rev. Lett.

RICHTER, R. M. (See Clark, D. J., LBL-7143)

RING, P., H. Massmann, and J. O. Rasmussen
On the Treatment of a Two-Dimensional Fission Model with Complex Trajectories
LBL-6538, June 1977
Nucl. Phys. A 296, 50-76 (1978)

ROWE, Glenn, Martin Salomon, and Rubin H. Landau
Energy-Dependent Phase Shift Analysis of Pion Nucleon Scattering Below 400 MeV
LBL-7182, February 1978
Phys. Rev. C. 18, 584, (1978)

ROY, R. (See SEILER, F., LBL-5851)

RUSSO, P., R. P. Schmitt, G. J. Wozniak, R. C. Jared, P. Glässel, B. Cauvin, J. S. Sventek, and L. G. Moretto
Evidence for Diffusive Relaxation along the Mass Asymmetry Coordinate in the Reaction ^{197}Au+620 MeV ^{86}Kr
LBL-5810, November 1976
Nucl. Phys. A 281, 509-532 (1977)

RUSSO, P. (See CAUVIN, B., LBL-6506)

SALOMON, Martin (See ROWE, Glenn, LBL-7182)

SANDOVAL, Andres (See GREINER, Douglas, LBL-7141)

SAWA, P. (See SIMON, R. S., LBL-6531)

SCHAEFFER, R. (See BRUGE, G., LBL-5823)

SCHMITT, R. P. (See RUSSO, P., LBL-5810)

SCHMITT, R. P. (See MATHEWS, G. J., LBL-5812)

SCHMITT, R. P. (See CAUVIN, B., LBL-6506)

SCHMITT, R. P. (See WOZNIAK, G. J., LBL-6532)

SCHMITT, R. P., G. Bizard, G. J. Wozniak and L. G. Moretto
Evidence for Energy Thermalization in Deep-Inelastic Processes: ^{63}Cu + ^{20}Ne
LBL-6571, August 1978

SCHMITT, R. P., (See ALEONARD, M. M., LBL-6599)

SCHMITT, R. P., (See MOULTON, J. B., LBL-7101)

SCHMITT, R. P. (See WOZNIAK, G. J., LBL-7158)

SCHMITT, Richard P.
The Dependence of Deep-Inelastic Processes on Entrance Channel Asymmetry and Excitation Energy
LBL-7168, May 1978
Ph.D. Thesis

SCHMITT, R. P., (See REGIMBART, R., LBL-7751)

SCHMITT, R. P. (See MORETTO, L. G., LBL-7757)

SCHROEDER, L. S.
Streamer Chambers--Their Use for Nuclear Science Experiments
LBL-7707, June 1978

SCOTT, D. K. (See GELBKE, C. K., LBL-6551)

SCOTT, D. K. (See OLMER, C., LBL-6553)

SCOTT, D. K. (See GELBKE, C. K., LBL-6563)

SCOTT, D. K. (See KEKELIS, G. J., LBL-6557)

STEPHENSON, E. J., D. J. Clark, R. A. Gough, W. R. Holley, and A. Jain
Heavy Element Mass Spectroscopy with the Berkeley 88-Inch Cyclotron
LBL-6591, August 1977
Nucl. Inst. and Meth. 152, 477-483 (1978)

STEPHENSON, E. J. (See MOULTON, J. B., LBL-7101)

STEVENSON, John David
Emission of Heavy Charged Particles in Relativsitic Nucleus-Nucleus Collisions
LBL-7192, March 17, 1978

STEVENSON, J. (See PRICE, P. B., LBL-7702)

SYMONS, T. J. M. (See DOLL, P., LBL-7195)

SYMONS, T. J. M. (See SCOTT, D. K., LBL-7729)

SVENTEK, J. S., and L. G. Moretto
Theoretical Correlation Between Energy Dissipation, Angular Momentum Transfer, and Charge Diffusion in Deep Inelastic Reactions
LBL-6596
Phys. Rev. Lett. 40, 697 (1978)

SVENTEK, J. (See MORETTO, L. G., LBL-7732)

SVENTEK, J. S. (See REGIMBART, R., LBL-7751)

THOMAS, A. W. and R. H. Landau
The Connection Between Elastic and Quasi-Elastic Pion Scattering From Nuclei
LBL-7166, December 1977
Phys. Rev. Lett.

TUGGLE, Dale Glenn
Decay Studies of a Long Lived High Spin Isomer of ^{210}Bi
LBL-4460, August 1976

VAAGEN, J. S. (See MAGUIRE, C. F., LBL-7187)

VAN BIBBER, K. (See DOLL, P., LBL-7195)

VAN BIBBER, K. (See SCOTT, D. K., LBL-7729)

VAUTHERIN, D., and M. Gyulassy
Nuclear Matter, PCAC and Pion Condensation
LBL-7197, April 1978
Phys. Rev. C.

VIEIRA, D. J., R. A. Gough, and Joseph Cerny
β-Delayed Proton Decay of ^{29}S
LBL-6556, May 1978
Phys. Rev. C.

VIEIRA, D. J. (See KEKELIS, G. J., LBL-6557)

VIEIRA, D. J. (See CERNY, Joseph, LBL-7156)

VIOLA, V. E., Jr. (See MATHEWS, G. J., LBL-7709)

VIYOGI, Y. P. (See DOLL, P., LBL-7195)

VIYOGI, Y. P., (See SCOTT, D. K., LBL-7729)

WATSON, J. W. (See DeVRIES, R. M., LBL-7103)

WESTFALL, G. D., R. G. Sextro, A. M. Poskanzer, A. M. Zebelman, G. W. Butler, and E. K. Hyde
Energy Spectra of Nuclear Fragments Produced by High Energy Protons.
LBL-6558, Phys. Rev. C 17, 1368 (1977)

WESTFALL, G. D. (See GOSSET, J., LBL-7139)

WEINER, Richard M. (See FRIEDLANDER, LBL-7724)

WIEMAN, H. H. (See GELBKE, C. K., LBL-6563)

WIEMAN, H. (See DOLL, P., LBL-7195)

WIEMAN, H., (See SCOTT, D. K., LBL-7729)

WIEMAN, H. H. (See GUTERMAN, A., LBL-7758)

WILSON, Lance W. (See HECKMAN, H. H., LBL-6561)

WOLSCHIN, Georg (See GLENDENNING, N. K., LBL-5052)

WOUTERS, J. M. (See CERNY, Joseph, LBL-7156)

WOZNIAK, G. J. (See MATHEWS, G. J., LBL-5812)

WOZNIAK, G. J., (See SCHMITT, R. P., LBL-6506)

WOZNIAK, G. J. (See STAHEL, LBL-6508)

WOZNIAK, G. J., R. P. Schmitt, P. Glassel, and L. G. Moretto
A Study of Diffusion Phenomena In the Rare Earth Region: The Reaction ^{159}Tb + 620 MeV ^{86}Kr
LBL-6532, September 1977
Nucl. Phys. A 298, 169 (1978)

WOZNIAK, G. J. (See SCHMITT, R. P., LBL-6571)

WOZNIAK, G. J. (See ALEONARD, M. M., LBL-6599)

WOZNIAK, G. J. (See MOULTON, J. B., LBL-7101)

WOZNIAK, G. J. (See JAHN, R., LBL-7157)

WOZNIAK, G. J., R. P. Schmitt, P. Glässel, R. C. Jared, G. Bizard and L. G. Moretto
Evidence for Angular Momentum Depolarization and for Enchanced Sequential Fission in the Reaction ^{197}Au (^{86}Kr, Z_3f).
LBL-7158, January 1978
Phys. Rev. Lett. 40, 1436 (1978)

WOZNIAK, G. J., (See REGIMBART, R., LBL-7751)

YASHITA, S., and R. E. Leber
Searching for Volatile Superheavy Elements
LBL-6547, July 1977

YASHITA, S., (See OTTO, R. J., LBL-7104)

ZAJEC, E. (See CLARK, D. J., LBL-7143)

ZEBELMAN, A. M. (See WESTFALL, G. D., LBL-6558)

ZEIPPEN, C. J., (See BRUGE, G., LBL-5823)

ZISMAN, M. S. (See BRUGE, G., LBL-5823)

ZISMAN, M. S. (See STAHEL, D. P., LBL-6508)

ZISMAN, M. S. (See KEKELIS, G. J., LBL-6557)

ZISMAN, M. S.
Exchange Interpretation of Anomalous Back Angle Heavy Ion Elastic Scattering
LBL-7102, October 1977

ZISMAN, M. S. (See DeVRIES, R. M., LBL-7103)

ZISMAN, M. S. (See CERNY, Joseph, LBL-7156)

ZISMAN, M. S. (See GUTERMAN, A., LBL-7758)

VI. AUTHOR INDEX

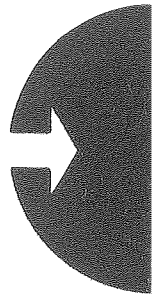

AUTHOR INDEX

U.S.GPO:1979-690-474/135